This is to certify that the

thesis entitled

PART I. NUCLEAR MAGNETIC RESONANCE STUDIES OF AMIDES

PART II. THEORETICAL STUDIES OF AMIDES

presented by

Biing-Ming Su

has been accepted towards fulfillment
of the requirements for

Ph.D. degree in Chemistry

Max T. Rogers
Major professor

Date Feb. 6, 1978

O-7639

PART I. NUCLEAR MAGNETIC RESONANCE STUDIES OF AMIDES
PART II. THEORETICAL STUDIES OF AMIDES

By

Biing-Ming Su

A DISSERTATION

Submitted to
Michigan State University
in partial fulfillment of the requirements
for the degree of

DOCTOR OF PHILOSOPHY

Department of Chemistry

1978

ABSTRACT

PART I. NUCLEAR MAGNETIC RESONANCE STUDIES OF AMIDES.
PART II. THEORETICAL STUDIES OF AMIDES.

By

Biing-Ming Su

A variety of nuclear magnetic resonance (NMR) techniques has been used to investigate various physical properties of a series of amides, N-substituted amides, and both symmetrically and unsymmetrically N,N-disubstituted amides. The results are presented in Part I in seven sections.

I. Anisotropic molecular reorientation in a series of N,N-disubstituted amides ($RCONR'_2$, R = H,CH_3,C_2H_5,C_3H_7 and R' = CH_3,C_2H_5,C_3H_7, etc.) has been studied by measuring ^{13}C spin-lattice relaxation times and NOE factors over a range of temperature. It is shown that the data can be satisfactorily treated on the basis of an approximate ellipsoidal model which leads to an axial diffusion tensor with $D_{||}$ associated with a preferred rotation axis in the molecular plane. Values of the diffusion constants, $D_{||}$ and $D_{\perp}$, the directions of the preferred rotation axes, the internal rotation rates of the N-methyl groups, the energy barriers associated with the motions of the various carbons,

and the effective quadrupole coupling constants for ^{17}O, have been obtained and their significance discussed.

II. The isomer ratios, and the ^{13}C nuclear spin-lattice relaxation times and NOE factors, have been measured for a series of N-monosubstituted amides and unsymmetrically N,N-disubstituted amides. The dipolar and other contributions to the ^{13}C T_1 values have been determined along with the correlation times for overall rotational motion of the molecules, τ_R, and for the internal motions of individual groups, τ_G. The anisotropic reorientational motions have been analyzed in terms of an approximate ellipsoidal model. The effects of structure and of intermolecular hydrogen bonding on the nuclear relaxation parameters have been evaluated. Effective quadrupole coupling constants for nitrogen have been estimated in four amides from the measured ^{14}N relaxation times.

III. The effects of phenyl substitution on the structures and molecular motions of amides have been investigated in a series of formanilides and acetanilides. The ^{13}C chemical shifts, T_1 values and NOE factors were measured for all carbons and the dipolar and other contributions to T_1 calculated, along with the correlation times for overall anisotropic rotational motion of the molecules. The effects of carbonyl and nitrogen

substituents on the tumbling ratios for the benzene ring (with C_2 the preferred axis) have been determined.

IV. Chemical shifts for ^{13}C, ^{14}N, ^{15}N and ^{17}O have been measured in a series of N,N-disubstituted amides and the effects of substituents on these shifts evaluated. A number of linear correlations among them have been discovered including relationships between the chemical shifts of ^{14}N (or ^{15}N) and both ^{17}O and the ^{13}C of the carbonyl group; linear correlations between these and the energy barriers E_a restricting rotation about the central C-N bonds have also been obtained. The γ and δ effects used in interpreting ^{13}C NMR spectra have been shown to have analogues in the ^{14}N, ^{15}N and ^{17}O NMR spectroscopy of the amides.

V. The assignment of proton and carbon NMR signals in several amides has been accomplished by the use of off-resonance proton-selectively decoupled ^{13}C NMR spectra along with ^{13}C T_1 measurements. From values of the residual one-bond ^{13}C-H coupling constants as functions of the separation between the applied decoupling frequency and the proton resonance frequency, the ^{13}C and ^{1}H NMR spectra were correlated for these amides and some errors in previous assignments of proton chemical shifts corrected.

VI. Concentration dependence of the chemical shifts of the carbons of DMF in benzene and DMA in cyclohexane and formamide have been used to investigate the

nature of the species present in these solution

VII. Solutions of Mn^{2+} in N,N-dimethylformamide have been studied by measuring the ^{13}C T_1 and T_2 values for all the carbons of DMF over a range of temperature. The paramagnetic shifts and hyperfine electron-^{13}C interaction constants have been evaluated, the relaxation mechanisms determined and the ^{13}C-Mn^{2+} distances calculated for each carbon. The results indicate that Mn^{2+} has coordination number eight in these solutions with weak bonding to the oxygens of four DMF dimers, which are tetrahedrally arranged about the metal ion.

In Part II calculations by the INDO method of the theoretical energy barriers for rotation about the central C-N bond in some selected amides are reported along with the bond orders for the C-N bonds. The variation of the partial charges on each atom in going from the ground equilibrium geometry to the transition state geometry was also studied. From the variation of the charges on the nitrogen and oxygen atoms, the observed decrease of the energy barrier resulting from the formation of hydrogen bonds to the carbonyl oxygen can be rationalized. The results obtained here for substituted amides using the INDO method are similar to those reported previously using the CNDO/2 method.

TO MY PARENTS

ACKNOWLEDGEMENTS

The author would like to express his appreciation to Professor M.T. Rogers for his patient guidance and encouragement throughout this research.

Gratitude is also extended to Dr. J.F. Harrison and Dr. W.G. Waller for allowing the author to use their INDO and MBLD programs.

Many thanks go to my wife, Shiu-Chin, and to my parents for their encouragement during these years.

Finally, the author wishes to acknowledge the financial support of the Department of Chemistry through these years as a graduate student.

TABLE OF CONTENTS

LIST OF TABLES

LIST OF FIGURES

List of Figures

PART I

NUCLEAR MAGNETIC RESONANCE STUDIES OF AMIDES

INTRODUCTION

Nuclear magnetic resonance spectroscopy has developed rapidly into a major spectroscopic technique during the last ten years or so. The applications of high-resolution NMR in chemistry are numerous and are growing at an almost exponential rate. In recent years NMR has undergone a revolutionary change in technique from swept continuous-wave to pulsed excitation. With the development of pulsed Fourier transform NMR techniques and the use of heteronuclear decoupling, the signal-to-noise of the observed nuclei can be increased by 2-3 orders of magnitude over the older methods. This increase in sensitivity has made ^{13}C NMR almost routine work in many laboratories. Recently, the quadrature detection and the phase-alternating pulse sequence techniques have also been used to increase the sensitivity of ^{15}N and ^{17}O signals so that these nuclei can now be observed routinely in natural abundance.

The properties of the amide bond have received considerable attention because of its importance in determining secondary and tertiary structure in peptides and proteins. In Part I of this dissertation, several

different properties of amides are studied by ^{13}C, ^{14}N, ^{15}N and ^{17}O NMR.

A theoretical section is presented first to familiarize the reader with the basic theories of pulsed and continuous-wave NMR, the nuclear Overhauser effect, double resonance experiments, and chemical shifts. The historical section covers the various known relaxation mechanisms and methods for extraction of the microscopic parameters of interest from the experimental measurements. A section describing the experimental techniques and methods for data interpretation follows. The main portion of Part I has been separated into seven sections. The first three sections comprise a study of the molecular motion of symmetrically N,N-disubstituted amides, of N-monosubstituted amides and unsymmetrically N,N-disubstituted amides, and of N-alkyl anilides, respectively. To this end, the ^{13}C spin-lattice relaxation times and NOE effects have been measured. In the fourth section, various correlations of the chemical shifts of ^{14}N, ^{15}N, ^{17}O and ^{13}C (of the carbonyl group) in the amido groups of N,N-dimethyl amides and N,N-diethyl amides are presented, as well as correlations between the energy barrier restricting rotation about the C-N partial double-bond and the ^{15}N and carbonyl group ^{13}C chemical shifts. The fifth section outlines the determination of proton chemical shifts by the ^{13}C off-resonance technique and the reassignment of proton and

carbon chemical shifts in some amides. The sixth section reports the solvent effects on some amides by ^{13}C NMR. The last section in this part describes a series of experiments designed to investigate the solvation of Mn^{2+} in N,N-dimethyl formamide.

Part two of the thesis consists of theoretical studies of some selected amides by the intermediate neglect of differential overlap (INDO) method. In this part, a brief description of molecular orbital theories and approximate molecular orbital theories are presented initially. An historical section presents the bond length, bond angles and dihedral angles used in these calculations, along with some results of the CNDO/2 and EHT methods. The calculated results relate the energy barrier for rotation about the C-N bond to the charge distribution in the amido group as the amide is twisted from the ground state goemetry to the transition state configuration.

NUCLEAR MAGNETIC RESONANCE THEORY

1. Introduction to NMR Theory

It is well known from elementary nuclear magnetic resonance theory[1] that the possession of both spin and charge confers on the nucleus a magnetic moment $\underline{\mu}$, given by

$$\underline{\mu} = \gamma \underline{I} \hbar = g \beta \underline{I}, \qquad (1)$$

where γ is the magnetogyric ratio, which is characteristic of each nucleus and is measured in radians sec^{-1} $gauss^{-1}$, g is the nuclear g factor and I is the nuclear spin quantun number . β is the nuclear magneton, which is equal to $e\hbar/2Mc$, where e and M are, respectively, the charge and mass of the proton, c is the velocity of light, and $\hbar$ is Planck's constant divided by 2π. When the nucleus is placed in an external magnetic field H_o, there are 2I+1 energy levels available, each corresponding to a different component of the angular momentum. The allowed components of angular momentum along H_o have the values m = I, I-1,...,-I (in units of $\hbar$) and its energy levels have the values $E = -\gamma\hbar m H_o$. The selection rule is $\Delta m = \pm 1$ so the energy difference ΔE between two levels is

$$\Delta E = \mu H_o/I = \gamma \hbar H_o. \qquad (2)$$

Nuclear magnetic resonance occurs when transitions take place between these levels. This can occur by the absorption of photons from an oscillating external field having the correct polarization and satisfying the frequency conditions in the above equation or

$$\nu_o = \gamma H_o/2\pi, \qquad (3)$$

where ν_o is the frequency of radiation from an external field which is absorbed by the nuclear spin system. Continuous irradiation by the rf field H_1 would cause all nuclei to precess around H_o, and no further absorption of energy would occur if there were no other process at work to restore the energetically favored orientation of the spins. In fact, continuous energy absorption from radiofrequency fields due to nuclear magnetic resonance is observed over a long period if the rf power is not too high. The processes responsible for this are referred to as relaxation.

At equilibrium, nuclei are distributed among the energy levels according to the Boltzmann distribution, which favors the lower state. For the two orientations relative to H_o of nuclei with $I = 1/2$, the spin populations may be symbolized N_α and N_β. The distribution N_α/N_β can be expressed by the Boltzmann factor, and recalling that $\Delta E = \mu H_o/I = 2\mu H_o$ $(I = 1/2)$,

$$N_\alpha/N_\beta = e^{\Delta E/kT} \approx 1 + \Delta E/kT = 1 + 2\mu H_o/kT \ . \qquad (4)$$

For carbon nuclei in an external magnetic field of about 20 kG at room temperature, N_α/N_β is of the order of 1.00000345. Consequently the populations of the two spin states differ by only 3.5 ppm and so the nuclear resonance absorption is very weak.

II. NUCLEAR RELAXATION - GENERAL THEORY

A. Spin-lattice relaxation

At resonance, the rf field H_1 causes the transfer of spins from the lower to the higher energy level. The equilibrium distribution of the spins in the static field H_o is disturbed. Following any process that disrupts this distribution, the nuclear spins will relax to equilibrium with their surroundings (the lattice) by a first-order relaxation process characterized by a time constant T_1, the spin-lattice relaxation time. Observed values of T_1 cover a range of about 10^{-4} to 10^{+4} sec. This constant reflects the efficiency of the coupling between the nuclear spin and its surroundings. The shorter this time, the faster equilibrium is attained and the more efficient this coupling is, and vice versa.

For liquids with rapid molecular motions, T_1 is a measure of the lifetime of a nucleus in a particular state. According to the Heisenberg uncertainty principle

$$\Delta E \times \Delta t = h(\Delta \nu_{1/2})T_1 \geq h \tag{5}$$

and the minimum width $\Delta \nu_{1/2}$ at half-maximum intensity of an NMR absorption line is

$$\Delta \nu_{1/2} \geq 1/T_1 \, . \tag{6}$$

If W_1 and W_2 are the transition probabilities of absorption and emission, respectively, and the total number of spins is N, then the approach to equilibrium is described by the following differential equations,

$$\begin{aligned} dN_\alpha/dt &= N_\beta W_2 - N_\alpha W_1 \\ dN_\beta/dt &= N_\alpha W_1 - N_\beta W_2 \, , \end{aligned} \tag{7}$$

and at equilibrium $dN_\alpha/dt = dN_\beta/dt = 0$. If n is the population difference between the two nuclear spin states then the following equation can be derived:

$$dn/dt = 2\, W_2 N_\beta - 2\, W_1 N_\alpha = N(W_2 - W_1) - n(W_1 + W_2). \tag{8}$$

This equation can be rewritten in the form

$$dn/dt = (n - n_o)/T_1, \tag{9}$$

if $n_o = N(W_2 - W_1)/(W_1 + W_2)$ and $1/T_1 = W_1 + W_2$. The solution to Equation (9) is

$$n = n_o(1 - \exp(-t/T_1)). \tag{10}$$

Equation (10) describes the return of the Z component of

the magnetization to equilibrium after it has been disturbed by the application of a pulse. This relaxation is a nonradiative transition between two energy levels.

B. Spin-spin relaxation

In solids and liquids with slowly tumbling molecules, internuclear dipole-dipole interactions become important. Furthermore, energy quanta $\Delta E = 2\mu H_o$ are exchanged between nuclei to a certain degree. Both factors tend to shorten the lifetime of spin states, again leading to line broadening. This second type of first-order relaxation process is called spin-spin relaxation and is characterized by a time T_2.

The spin-spin relaxation time reduces the lifetime of a nucleus in a particular spin state to $T_2 \leq T_1$. The linewidth at half-maximum intensity is expressed more precisely by $\Delta\nu_{1/2} = 1/\pi T_2$. The observed linewidth of an NMR signal depends additionally on the field inhomogeneity ΔH_o, which contributes to $\Delta\nu_{1/2}$ so that

$$\Delta\nu_{1/2(obs)} = 1/\pi T_2^* = \Delta\nu_{1/2} + \Delta\nu_{1/2(inhom)}$$

$$= 1/\pi T_2 + \gamma\Delta H_o/2\pi. \qquad (11)$$

Thus T_2^* includes contributions from both the natural linewidth $\Delta\nu_{1/2}$ and from the magnetic field inhomogeneity $\Delta\nu_{1/2(inhom)}$.

C. Comparison of spin-lattice and spin-spin relaxation times

(1) Spin-lattice relaxation of nuclei (e.g., ^{1}H, ^{13}C) in a molecule may be accelerated by interaction with (a) adjacent nuclei having spins $I \geq 1$ (e.g., ^{2}D, ^{14}N, ^{17}O), since the electric quadrupole moments of such nuclei result in additional fields in the tumbling molecule, and

(b) unpaired electrons in paramagnetic compounds (radicals or some metal chelates).

(2) Spin-spin relaxation of nuclei is accelerated when they are bonded to another magnetic nucleus (^{17}O-^{1}H, ^{14}N-^{1}H, ^{13}C-^{1}H). This relaxation, involving dipole-dipole interaction, is very effective in solids and in viscous liquids in which molecular motion is slow, since the magnetic fields caused by slowly tumbling dipoles change very slowly.

(3) Spin-lattice relaxation occurs via transitions which are stimulated by components of the local magnetic field seen by a particular nucleus and which fluctuate at its Larmor frequency. Fluctuations in the local magnetic field are generated by variations in $H_{dipolar}$ caused by changes in r and θ resulting from Brownian motion. $H_{dipolar}$ is given by

$$H_{dipolar} = \mu_z/4r^3(3\cos^2\theta - 1), \qquad (12)$$

where r is the distance of the first dipole from the second dipole and θ is the angle between the axis of the first dipole and the line joining their centers. This dipole-dipole effect, due to the term r^3, is a local one and the average value of the $H_{dipolar}$ field is zero. However, at any particular time, the dipolar field is not necessarily zero.

Spin-spin relaxation also occurs through local magnetic fields, but in a different way. If one nucleus undergoes a transition from one spin state to another, then changes of H_{loc} at the correct frequency will induce a transition in a second nucleus. If at this particular time a second nucleus of the same type and the opposite spin state is close by, then the two nuclei can in effect exchange energy. Such a process is not of the spin-lattice type as the total system energy is conserved. A process of this type, however, does affect the lifetime of the excited state, hence the resonance linewidth. Spin-spin relaxation is an entropy effect, as opposed to spin-lattice relaxation which is an energy effect. The spin-spin relaxation time can be defined as the lifetime or phase memory of the excited spin state. The relationship between T_1 and T_2 can be visualized by a vector model as shown in Figure 1. In this model the nuclei are considered as vectors. In the presence of only an external field H_z, the spin

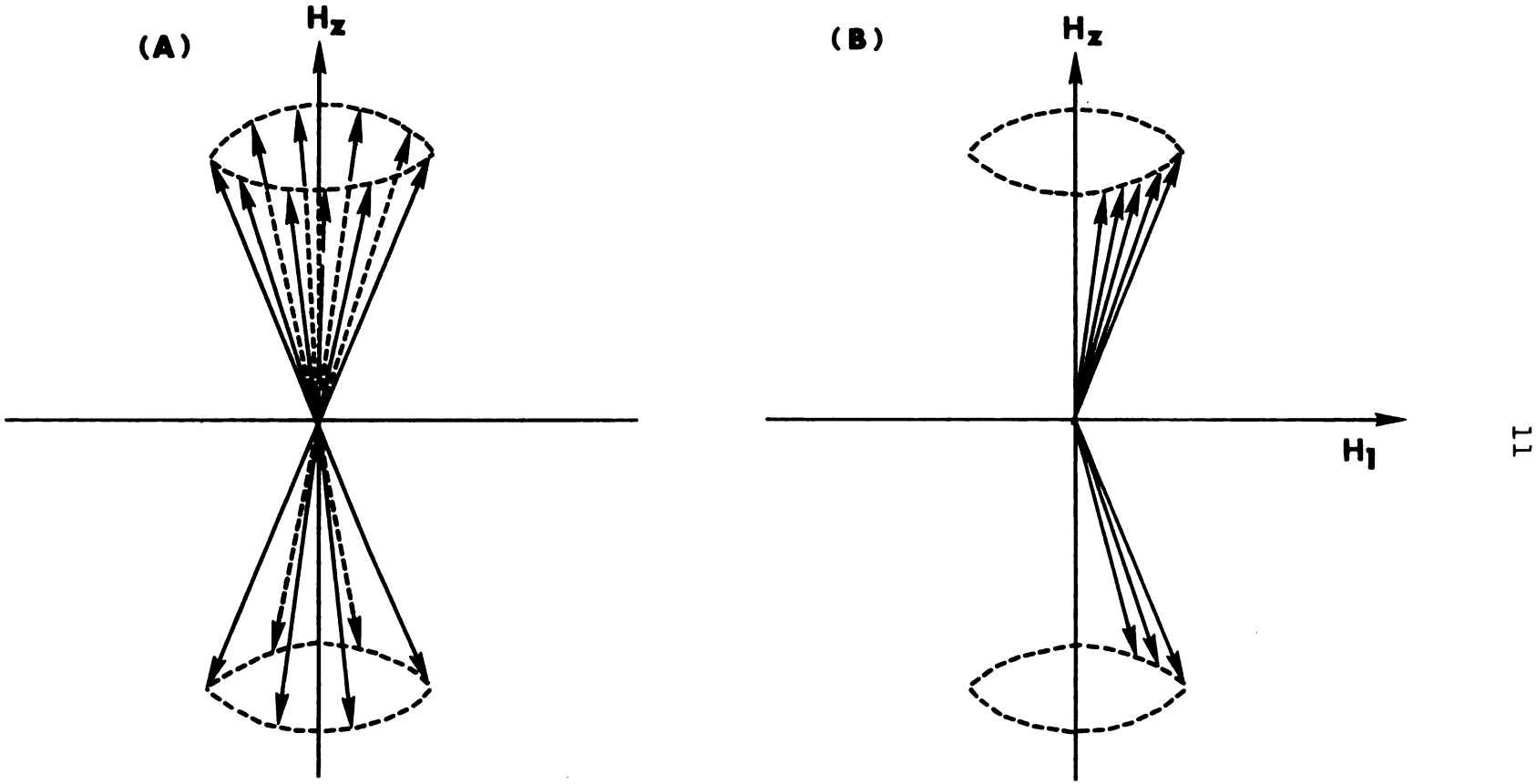

Figure 1. (A) Precession of an ensemble of vectors with random phases in the X'Y' plane produces a net magnetization only in the Z direction. (B) Application of an H_1 field, which rotates at the resonant frequency, causes the vectors to attain phase coherence and a net X', Y' magnetization results.

vectors precess about H_z with random phases (Figure 1-A) there being slightly more vectors parallel to the field than opposed to it, as was previously discussed. The average value of the magnetization in the x and y directions is zero, i.e., $\langle M_x \rangle = \langle M_y \rangle = 0$. If now an exciting field H_1 is applied precisely at the Larmor frequency of the nuclei, then resonance occurs and they attain phase coherence as shown in Figure 1-B. M_x and M_y become finite and M_z decreases appropriately.

An alternative description, and perhaps a similar one, can be given using the idea of a rotating frame of coordinates which will be discussed later. On the removal of H_1, M_z returns to its original value at the spin-lattice relaxation rate, however M_x and M_y relax exponentially at a different rate, responding to any process which changes phase coherence of the vectors but not the total energy of the system. The constant T_2 can thus be defined by the following equations:

$$dM_y/dt = -M_y/T_2 \quad \text{and} \quad dM_x/dt = -M_x/T_2. \tag{13}$$

Equations (9) and (13) illustrate the origin of the alternative names for T_1 and T_2 which are, respectively, the longitudinal and transverse relaxation times. So local magnetic fields fluctuating at the Larmor frequency can contribute to both T_1 and T_2 relaxation process. Static magnetic field, however, can only contribute to

transverse relaxation. It is thus not surprising that T_2 must be equal to, or shorter than, T_1. In normal liquids T_1 and T_2 are often equal, though this depends in detail on the molecular motions involved. In solids, however, particularly at low temperatures, T_1 may be very long due to the lack of any suitable molecular motion, while T_2 may be short due to static dipolar fields. In changing from liquids to solids there are changes in the absolute and relative values of T_1 and T_2.

Hahn[2] experimentally observed the effect of a single radiofrequency pulse applied to a spin system as had been suggested by Bloch[3]. The pulse experiment is basically quite different from the continuous wave (cw)[4] experiment, since it depends upon the behavior of the spin system monitored just after the application of a single rf pulse, rather than its being observed during the continuous application of low-level rf energy. Since pulse techniques are now used almost exclusively in sophiscated NMR instrumentation, the following discussion will mainly focus on the theory of pulse techniques.

III. Phenomenological Theory

A. The Bloch equations

(1) The motion of the magnetization vectors in a laboratory coordinate system

The earliest treatment of the magnetic resonance phenomenon is that of Bloch[3,4]. He used a vector model

and treated the assembly of nuclear spins in macroscopic terms. The starting point in his theory is the classical equation of motion of a magnetic field $\underline{H}_o$. Upon irradiation with a rf field H_1 at resonance, transitions between the nuclear magnetic energy levels occur. The nuclear spins change their directions relative to $\underline{H}_o$. The direction of the angular momentum $\underline{P}$ is now time dependent, as shown in the equation

$$d\underline{P}/dt = \underline{\mu} \times \underline{H}, \tag{14}$$

where H is the total field resulting from the static field H_o and the rf field H_1. By multiplying Equation (14) by the magnetogyric ratio γ, one obtains

$$d\underline{\mu}/dt = \gamma\, \underline{\mu} \times \underline{H}, \tag{15}$$

where $\underline{\mu} = \gamma\underline{P}$. If $\underline{M}$ is the vector sum of the $\underline{\mu}$'s, its time dependence is given by

$$d\underline{M}/dt = \gamma\, \underline{M} \times \underline{H}. \tag{16}$$

The vector product $\underline{M} \times \underline{H}$ can be expressed in terms of the components along the three Cartesian coordinates (x,y,z) and the unit vectors along these axes ($\underline{i}$,$\underline{j}$,$\underline{k}$),

$$\underline{M} \times \underline{H} = \begin{vmatrix} M_x & H_x & \underline{i} \\ M_y & H_y & \underline{j} \\ M_z & H_z & \underline{k} \end{vmatrix} = (M_y H_z - M_z H_y)\underline{i} + (M_z H_x - M_x H_z)\underline{j} + (M_x H_y - M_y H_x)\underline{k} \tag{17}$$

and the time derivative of $\underline{M}$ is

$$d\underline{M}/dt = dM_x/dt\ \underline{i} + dM_y/dt\ \underline{j} + dM_z/dt\ \underline{k}\ . \tag{18}$$

A comparison of Equations (17) and (18) yields

$$\begin{aligned} dM_x/dt &= \gamma\ (M_y H_z - M_z H_y) \\ dM_y/dt &= \gamma\ (M_z H_x - M_x H_z) \\ dM_z/dt &= \gamma\ (M_x H_y - M_y H_x)\ . \end{aligned} \tag{19}$$

The field components H_x, H_y, and H_z can be expressed in terms of the static field H_o and the alternating field H_1:

$$H_x = H_1 \cos \omega t,\ H_y = -H_1 \sin \omega t,\ H_z = H_o, \tag{20}$$

where ω is the angular velocity of the rf field H_1 in the xy plane. By combining Equations (19) and (20), one obtains Equations (21) describing the motion of the components of the magnetization vector produced by the fields H_o and H_1 (without considering relaxation)

$$\begin{aligned} dM_x/dt &= \gamma\ (M_y H_o + M_z H_1 \sin \omega t) \\ dM_y/dt &= \gamma\ (M_z H_1 \cos \omega t - M_x H_o) \\ dM_z/dt &= \gamma\ (M_x H_1 \sin \omega t + M_y H_1 \cos \omega t). \end{aligned} \tag{21}$$

In order to include spin-lattice relaxation and spin-spin relaxation, the Bloch equations in the final form are modified to give

$$dM_x/dt = \gamma\ (M_y H_o + M_z H_1 \sin \omega t) - M_x/T_2$$

$$dM_y/dt = \gamma\ (M_z H_1 \cos \omega t - M_x H_o) - M_y/T_2 \qquad (22)$$

$$dM_z/dt = -\gamma (M_x H_1 \sin \omega t + M_y H_1 \cos \omega t) - (M_z - M_o)/T_1 .$$

(2) The motion of the magnetization vector in the rotating coordinate system

The path of the magnetization vector $\underline{M}$ subjected to magnetic fields will be simplified in a coordinate system rotating at the angular velocity ω of the rf field H_1. In the rotating coordinate system Equation (16) becomes

$$(d\underline{M}/dt)_{rot} = \gamma\ \underline{M} \times \underline{H} - \underline{\omega} \times \underline{M}\ , \qquad (23)$$

where $\underline{\omega}$ is the angular velocity of the three unit vectors in the rotating coordinate system. Rearranging Equation (23), we obtain

$$(\delta\underline{M}/\delta t)_{rot} = \gamma\ \underline{M} \times \underline{H} + \gamma\ \underline{M} \times \underline{\omega}/\gamma$$

$$= \gamma\ \underline{M} \times (\underline{H} + \underline{\omega}/\gamma). \qquad (24)$$

The term $\underline{\omega}/\gamma$ has the dimensions of a magnetic field and can be treated as a "fictitious" field that arises from the effect of the rotation. If we define the effective field $\underline{H}_{eff} = \underline{H} + \underline{\omega}/\gamma$, then

$$(\delta\underline{M}/\delta t)_{rot} = \gamma\ \underline{M} \times \underline{H}_{eff}\ . \qquad (25)$$

Thus, in the rotating frame of reference the net magnetization $\underline{M}$ precesses about $\underline{H}_{eff}$.

B. NMR in the rotating frame of reference

Suppose the magnetization $\underline{M}$ precesses about the effective field $\underline{H}_{eff}$ in a coordinate system rotating with frequency $\omega = 2\pi\nu$ about the z axis and symbolized as the x',y',z' frame of reference with rotating unit vectors $\underline{i}'$, $\underline{j}'$, and $\underline{k}'$.

(A) In the absence of H_1, the magnetization vector $\underline{M}$ keeps its equilibrium value and orientation $\underline{M}_o$ in the z direction. $\underline{M}$ is thus time invariant in the rotating coordinate system, so that Equation (25) is equal to zero, and consequently $\underline{H}_{eff} = 0$ since $\underline{M} = \underline{M}_o \neq 0$. If the frame rotates at the Larmor frequency $\omega_o = 2\pi\nu_o$, then $\omega/\gamma = \omega_o/\gamma$, since the effective field is zero, and the Larmor equation is thus $\underline{H}_{eff} = (H_o + \omega_o/\gamma) = 0$, so that $\omega_o = -\gamma H_o$. This means that the rotational field ω/γ opposes $H_o \underline{k}'$ in the rotating coordinate system, Figure 2(A), finally cancelling $H_o \underline{k}'$ when the coordinates rotate at the Larmor frequency, ω_o.

(B) If an rf field $\underline{H}_1$, with $\omega_1 = 2\pi\nu_1$, is applied perpendicular to H_o along the z' axis, the effective field $\underline{H}_{eff}$ in the coordinate system rotating at ω_1 is

$$\underline{H}_{eff} = (H_o + \omega_1/\gamma)\ \underline{k}' + H_1\ \underline{i}' \ . \qquad (26)$$

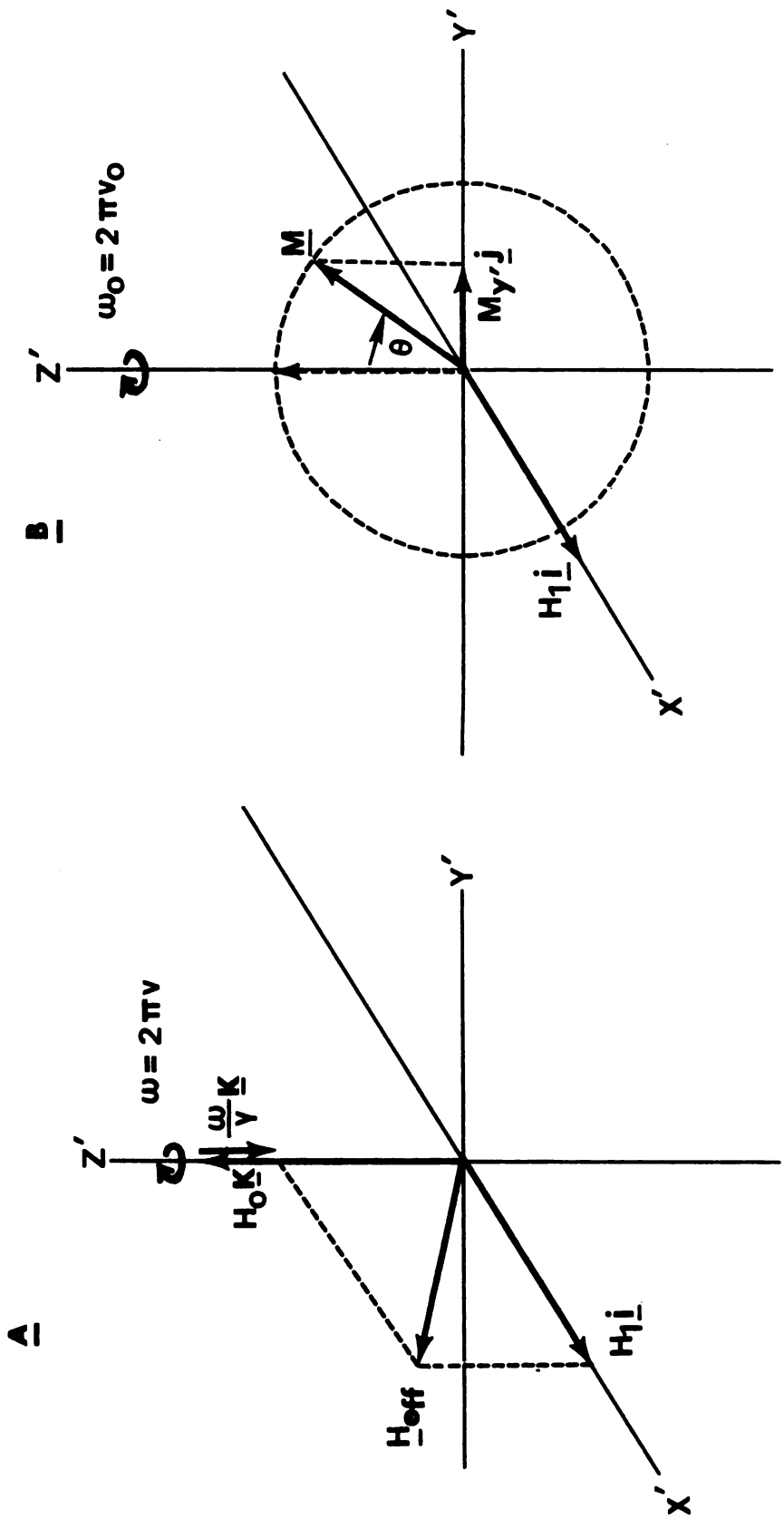

Figure 2. The effective field in the rotating coordinates: (A) off resonance, (B) at resonance.

If the coordinate system rotates at an rf frequency ν_1 matching the Larmor frequency ν_o, the term $(H_o + \omega_1/\gamma)\ \underline{k}'$ becomes zero. The remaining effective field at resonance is now $\underline{H}_{eff(res)} = H_1\underline{i}'$, so that Equation (25) becomes

$$(\delta\underline{M}/\delta t)_{rot} = \gamma\ \underline{M} \times H_1\ \underline{i}' \ . \qquad (27)$$

This relation tells us that at resonance the vector $\underline{M}$ precesses about the field vector $H_1\ \underline{i}'$, Figure 2(B).

Since the coordinate system and H_1 are chosen to rotate at the same frequency, H_1 lies along the rotating x' axis. According to Equation (27) the vector $\underline{M}$ will precess about the x' axis and the precession frequency ω_1 of $\underline{M}$ about the x' axis is $\omega_1 = \gamma\ H_1$. Thus, an rf field H_1 applied at resonance for t_p seconds, causes the vector $\underline{M}$ to precess about the x' axis by an angle θ, where

$$\theta = \omega_1\ t_p = \gamma\ H_1\ t_p \ (rad). \qquad (28)$$

If only H_o is applied, the nuclear moments will precess without any phase coherence. No resultant component of the magnetization in the x'y' plane will be observed and M_z will equal M_o, Figure 3(A). A radiofrequency H_1 applied perpendicular to H_o forces the nuclei to precess in phase, tipping the vector M_o by an angle θ toward the y' axis, Figure 3(B). A transverse magnetization $M_{y'}\underline{j}'$ in the x'y' plane arises and the magnitude of M_z, decreases. To restore equilibrium, the nuclei exchange

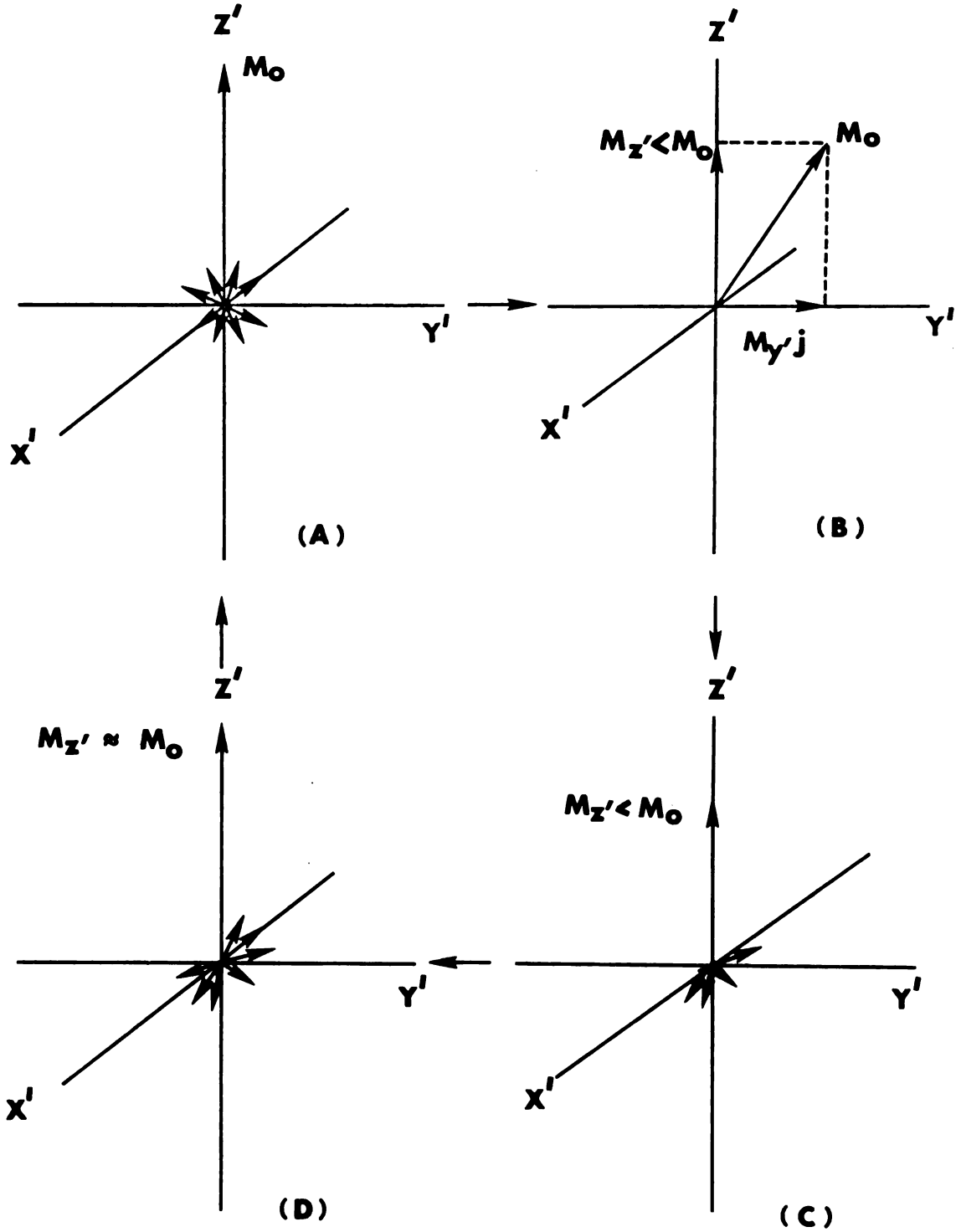

Figure 3. Relaxation in the rotating frame of reference. (A) only the external field H_o is applied; (B) a radiofrequency H_1 is applied perpendicular to H_o; (C),(D) dephasing of magnetic moments in the x'y' plane and restoration of magnetic moments in the z' direction.

energy with each other (spin-spin relaxation) and dephase, causing $M_y,\underline{j}'$ to spread out in the x'y' plane and finally decay to zero with time constant $1/T_2$, Figure 3(C,D). Dephasing may be accelerated by the field inhomogeneity so that $1/T^*_{2(inhom)}$ is greater than $1/T_2$. Moreover, the nuclear moments lose energy to their surroundings (spin-lattice relaxation), causing $M_z\underline{k}'$ to increase to M_o. The decay of the magnitude of transverse magnetization M_y, due to spin-spin relaxation (T_2) or due to field inhomogeneity (T^*_2) may be faster but cannot be slower than the spin-lattice relaxation time (T_1).

C. Nuclear induction

At resonance the magnetization vector $\underline{M}$ precesses about the vector $H_1\underline{i}'$ of the rf field according to Equation (27). As a result, a component of transverse magnetization $M_y,\underline{j}'$ rotates in the x'y' plane at the Larmor frequency ν_o. If a receiver coil is placed in the x'y' plane, the rotating magnetic vector $M_y,\underline{j}'$ induces an electromotive force measurable as an induced current. This process is called nuclear induction. The orientation of coil axis will affect the phase relative to $H_1\underline{i}'$ but not the magnitude of the induction current.

Following Equation (27), the magnetization vector $\underline{M}$ is rotated toward the y' axis by the oscillation of $H_1\ \underline{i}'$ in phase with the x' axis of the rotating frame. The current I_{ind} due to the induced EMF opposes the

inducing magnetization. At resonance, the magnetization vector rotates 90° behind H_1 $\underline{i}'$. The maximum induction current, however, is observed 90° ahead of H_1 $\underline{i}'$.

In practice it is usual to study a spin system which, in an external field H_o, contains chemically non-equivalent nuclei each with a different precession frequency. In a pulsed NMR experiment, the sample is irradiated by short, intense rf pulses. The rapid switching necessary to generate such pulses generates Fourier components over the range $\nu_o \pm 1/t_p$, where ν_o is the rf frequency of the instrument and t_p is the pulse width. Every frequency component in the range $\nu_o \pm 1/t_p$ is present and any nuclear spin which precesses at a frequency within the range is excited by the appropriate frequency. A short rf pulse is therefore equivalent to the simultaneous application of a wide range of rf frequencies to the spin system. According to Equation (28), the rf pulse width t_p seconds, Figure 4(A), rotates the magnetization vector by an angle θ, Figure 4(B). A transverse component of magnetization $M_{y'}$, results. The magnitude of $M_{y'}$, is given by $M_{y'} = M_o \sin \omega_1 t_p$ as can be seen in Figure 4(B). Following the rf pulse, the transverse magnetization $M_{y'}$, decays exponentially to zero via spin-spin relaxation, Figure 4(C).

At resonance the magnetization $M_{y'}$, always has a phase shift of $\pi/2$ relative to the rf field H_1 in the

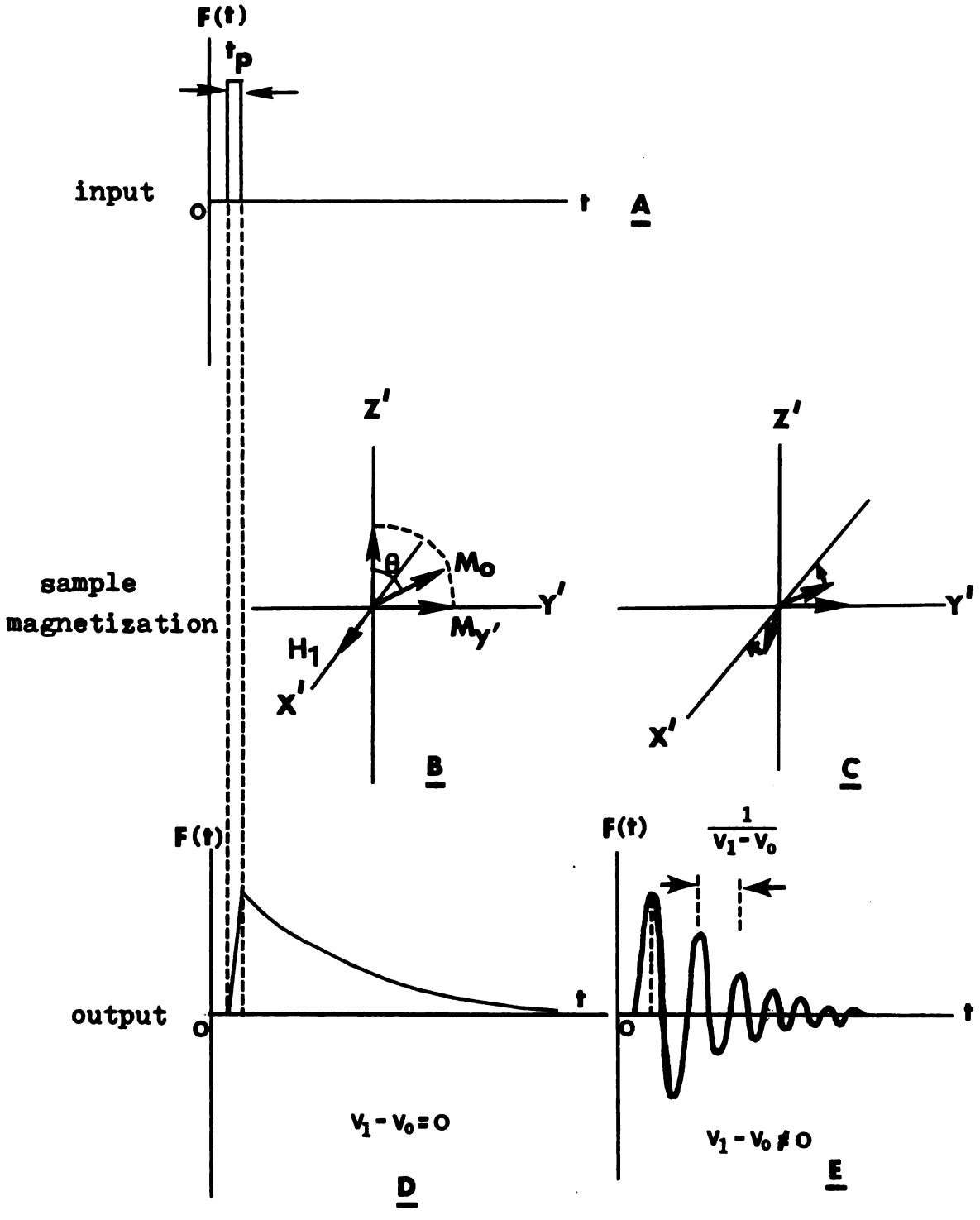

Figure 4. Free induction decay. (A) rf pulse as input signal; (B) sample magnetization during the rf pulse; (C) free induction decay following the rf pulse; (D) output for rf at resonance; (E) output for rf off resonance.

rotating coordinate system. This is due to the experimental arrangement and is not affected by pulsing. Thus, a nuclear induction current stemming from the decay of M_y, is built up in the receiver coil following the rf pulse, Figure 4(D).

If the rf frequency differs from the Larmor frequency of the nuclei to be investigated ("off resonance") the transverse magnetization M_y, is rotating relative to the coordinate system after the pulse has ended. M_y, and H_1 periodically rephase and dephase, Figure 4(E), leading to a response analogous to the wiggles observed in cw high-resolution NMR spectra. The spacing between two best peaks is the reciprocal of the difference between the frequency of the pulse and the Larmor frequency $1/(\nu_1 - \nu_o)$, Figure 4(E).

The time domain function F(t) arising from the relaxing spins following an rf pulse is called the free induction decay (FID) signal or the transverse relaxation function (5). Due to chemical shielding, each nucleus may come into resonance within a range of Larmor frequencies sw (sw = spectral width), $2\pi(sw) = \omega_o - \omega$, depending on its chemical environment. In order to rotate all nuclear spins within that range by the same angle θ, the strength of the rf pulse must be $\gamma H_1 >> 2\pi(sw)$. Furthermore, the pulse width must be shorter than the relaxation times, $t_p << T_1, T_2$, so that relaxation is negligible during the pulse.

For a liquid sample containing identical nuclei, the transverse magnetization M_y will arise from one Larmor frequency, which is actually the maximum of a very small frequency distribution caused by spin-spin relaxation and slight field inhomogeneity. The FID signal F(t) of this sample decays exponentially according to $F(t) = F(0)e^{-t/T_2}$, where F(0) is the amplitude of the FID signal at the time the pulse has stopped. If a sample contains equivalent nuclei A (e.g., ^{13}C) subject to spin-spin coupling with nuclei X (e.g., ^{1}H), the transverse magnetization will arise from two or more Larmor frequencies, depending on the multiplicity. The corresponding magnetization vectors periodically rephase and dephase with the field vector H_1 as in the off-resonance case. The FID signal is thus modulated by the frequency of the coupling constant J_{AX}.

Similarly, in a sample containing two non-equivalent nuclei A_1 and A_2, the transverse magnetization results from two components due to two Larmor frequencies. In this case, the FID signal is modulated by the chemical shift difference of Larmor frequencies, $\nu = \nu_1 - \nu_2$. FID signals caused by rf pulses and modulated by spin-spin coupling and chemically shifted Larmor frequencies are referred to as pulse interferograms. In most pulsed NMR experiments, the rf pulse is applied off resonance.

Modulated pulse interferograms arise because the vectors of transverse magnetization do not precess with a constant phase shift of $\pi/2$ relative to the vector H_1, as shown in Figure 5. The transverse magnetization is then the resultant of two components, $v(t)$ with a phase shift of $\pi/2$ relative to H_1, and $u(t)$ in phase with H_1, where

$$\begin{aligned} v(t) &= M_o \sin\theta \cos\omega t \\ u(t) &= M_o \sin\theta \sin\omega t \ . \end{aligned} \tag{29}$$

In mathematical treatments of FID and NMR signals, $F(t)$ and $F(\omega)$, it is convenient to use complex quantities. The time domain signal is then defined by

$$F(t) = v(t) + i\,u(t), \text{ where } i = \pm\sqrt{-1} \ . \tag{30}$$

Combining Equations (29) and (30) yields

$$F(t) = M_o \sin\theta\ (\cos\omega t + i \sin\omega t) \tag{31}$$

or, recalling that

$$e^{i\omega t} = \cos\omega t + i \sin\omega t, \tag{32}$$

$$F(t) = M_o \sin\theta\ e^{i\omega t}. \tag{33}$$

Since NMR spectra are not sequences of lines representing discrete Larmor frequencies but sequences of Lorentizian frequency distributions $f(\omega)$, Equation (33) must be replaced by

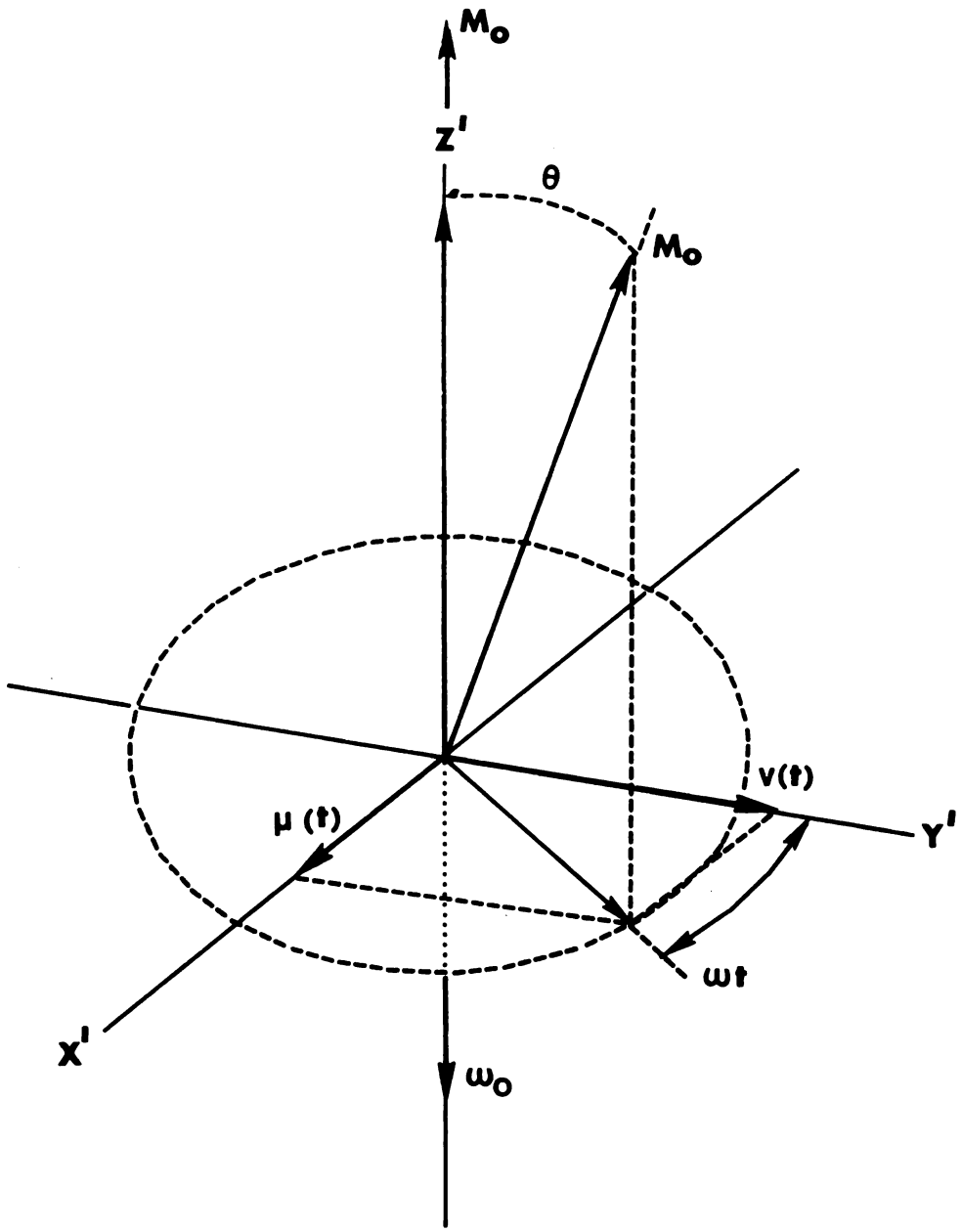

Figure 5. The components v(t) and u(t) of the transverse magnetization in the rotating coordinates for the off-resonance case ($\omega_1 - \omega_o = \omega \neq 0$).

$$F(t) = M_o \sin\theta \int_{-\infty}^{+\infty} f(\omega)\, e^{i\omega t}\, d\omega, \qquad (34)$$

where $M_o \sin\theta\, e^{i\omega t}$ is multiplied by the frequency $f(\omega)$, and ω represents the difference between ω_1 and the Larmor frequency distribution $\omega_o + \Delta\omega$, $\omega = \omega_1 - (\omega_o + \Delta\omega)$. Furthermore, $M_o \sin\theta\, f(\omega)\, e^{i\omega t}$ must be integrated over the Larmor frequency distribution with limits of integration $\pm\infty$. Equation (34) can be solved by developing it as a complex series of sines and cosines according to Equation (32). This is a Fourier series[6]. Thus, we can say that an exponential in the time domain, F(t) and a Lorentzian in the frequency domain f(ω) are Fourier transforms of each other[7,8,9].

Fourier transformations of pulse interferograms are normally performed in digital computers. Consequently, the FID analog signal must pass through an analog-to-digital converter (ADC). The sampling time during which FID data points must be collected in order to gain the true NMR spectrum after Fourier transformation depends on the spectral width (sw). According to information theory[10,11], the sweep time per data point, called the dwell time (dw), must satisfy the relation

$$dw \leq 1/2(sw). \qquad (35)$$

Multiplying the dwell time by the number of data points (dp) to be collected during the FID yields the acquisition time (AT) required for recording the interferogram

digitally,

$$AT = (dp) \times (dw) \leq (dp)/2(sw) \quad . \tag{36}$$

When several pulse interferograms must be accumulated in order to improve the signal-to-noise ratio (S/N), AT is the minimum repetition time between two pulses or the minimum pulse interval. Sometimes, Larmor frequencies not included in sw contribute to the FID signal. This occurs only when partial spectra are desired. All frequencies outside of the spectral width given by Equation (35) at a certain dwell time will be "folded back" within the range sw of the Fourier transformed FID. This is also true for high- and low-frequency noise. In order to avoid folding back peaks in FT NMR spectra, frequency components higher than sw must be filtered before digitization.

In order to optimize the pulse interferograms for Fourier transformation, the rf pulse frequency must be set outside the Larmor frequency range to be observed. This requirement is due to the experimental arrangement, which measures frequency difference relative to the rf field using phase sensitive detectors. Positive and negative frequencies relative to the rf frequency cannot be distinguished in the FID. Fourier transformation of an interferogram obtained by an rf pulse of frequency ν_1', which is within the spectral width sw, yields a distorted

NMR spectrum in which the frequencies on both sides of the rf pulse overlap. To optimize the FID signal, the pulse width t_p must be adjusted for a 90° pulse and the power must also be very strong without saturation, so that $\gamma H_1 << 2$ (sw). Combining this relation with Equation (28) gives

$$t_p << 1/4(sw). \tag{37}$$

Routine Fourier transformations of the FID are achieved in digital computers with a memory size of 4-20 K. The transformation program makes use of the Cooley-Tukey algorithm[12,13,14], which requires a minimum time for multiplications and efficiently uses the computer memory. This computation is called the fast Fourier transformation (FFT) and requires less than one minute for transforming an 8 K interferogram, depending upon the speed of the computer. FFT computation yields both real and imaginary FT NMR spectra, $v(\omega)$ and $iu(\omega)$, which are related to the absorption and dispersion modes of cw spectra. These two parts of the complex spectrum are stored in different blocks of the memory and can be displayed on an oscilloscope to aid in further data manipulations.

The real and imaginary spectra obtained by Fourier transformation of FID signals are usually mixtures of the absorption and dispersion modes. These phase errors

mainly arise from frequency independent maladjustments of the phase detector and from frequency dependent influences such as the finite pulse length, delays in the start of data acquisition, and phase shifts induced by filtering frequencies outside the spectral width sw. One method of phase correction assumes a linear dependence of the phase ϕ on the frequency,

$$\phi = \phi_a + \phi_b \nu, \tag{38}$$

where ϕ_a is the phase at frequency difference zero, and ϕ_b is the phase shift across the total spectral width from zero to sw Hz. Correction of the real part for absorption mode yields the dispersion mode in the imaginary part and vice versa. The S/N ratio, or resolution of the FID and its Fourier transformation, can be improved by digital filtering. This involves multiplication of the FID with an exponential $e^{\mp at}$.[15] Negative values of at will enhance the signal-to-noise ratio while causing some artificial line broadening. Positive values of at improve the resolution at the expense of sensitivity. For a dwell time (dw) limited by the spectral width according to Equation (35), the resolution dv of a FT NMR spectrum depends on the number of data points (dp) constituting the digitized FID signal to be transformed,

$$d\nu = 1/(dp)(dw) = 2(sw)/(dp) \text{ Hz}. \tag{39}$$

For the S/N improvement of weak signals, FID's are accumulated many times. According to Equation (36) the minimum repetitive time of an 8 K ^{13}C interferogram at a spectral width 5 kHz is 0.82 sec. Spin-lattice relaxation times of some ^{13}C nuclei such as quaternary ^{13}C atoms are as long as 100 sec, so that T_1 is greater than At. These nuclei cannot relax within the pulse interval. Using the Bloch equations, a steady state will be reached in this case[16], the magnetization is attenuated and the signal strength depends on the ratio of $AT/2T_1$. The S/N ratio of the FID and its Fourier transform will decrease as a result. An obvious way to avoid this attenuation is to add a pulse delay (> $5T_1$). However, accumulation of pulse interferograms becomes time consuming. A more practical way is to decrease the flip angle θ below 90° by reducing the pulse width. Restoration of the equilibrium magnetization then requires shorter periods. However, the transverse magnetization is also decreased by reducing the flip angle. The best way to optimize the S/N is to use the so-called driven equilibrium Fourier transform NMR (DEFT NMR). This method involves a three-pulse sequence, 90° - τ - 180° - τ - 90° with a repetition time t_r sec. This sequence refocuses the magnetization vector M_o into its equilibrium position within the repetition time[17,18,19].

D. Comparison between cw and FT NMR

As is true of any time-domain function F(t), a square-wave rf pulse of width t_p can be approximated by a Fourier series of sines and cosines with frequencies $n/2t_p$ $(n = 1,2,...)$[5,6]. A pulse of width t_p thus stimulates a multifrequency transmitter of frequency range $sw = 1/4t_p$. Thus, a t_p = 250 μsec pulse simultaneously rotates with M_o vectors of all nuclei with Larmor frequencies within a range of at least sw = 1000 Hz. It stimulates at least 1000 simultaneous transmitters, the resolution in the Fourier transform depending on the number of FID data points (Equation (39)), not the stimulating time, t_p. During the 250 μsec, only 0.5×10^{-6} of a 1 kHz scan is stimulated in a cw experiment using a 500 sec sweep to cover 1 kHz. A more realistic comparison takes into account the time required for the Fourier transformation and the sweep time in a cw experiment at a spectral width of 1 kHz: (1) Fourier transformation of a 2 K FID takes about 10-25 sec, (2) Using a sweep of 1 kHz/500 sec the cw experiment needs 500 sec. Furthermore, the 500 sec required for the cw experiment can be used to accumulate at least 1000 2 K FID signals. The S/N of FT NMR is thus increased by a factor $10\sqrt{10}$ over the cw experiment.

In summary, FT NMR is much more efficient for equivalent measuring time, and much less time consuming

for equivalent S/N ratio, in comparison to cw NMR. FT NMR follows the Fellgett principle[20,21]: The signal-to-noise ratio of any spectroscopic experiment increases if simultaneous multichannel excitation is applied. In the FT NMR technique, rf pulses stimulate multichannel transmitters. If m transmitters are stimulated simultaneously, the enhancement factor relative to one channel excitation (m = 1) is

$$(S/N)_m = (S/N)_1 \sqrt{m} \ . \qquad (40)$$

The minimum number of simultaneously exciting channels m required for resolving a spectrum of width sw at a resolution dv is

$$m = sw/dv \ . \qquad (41)$$

Combining Equations (39) and (41), the number of simultaneously exciting channels stimulated by a rf pulse is therefore m = dp/2, which depends only on the computer memory size, and yields an enhancement of factor $\sqrt{dp/2}$. Thus, according to the Fellgett principle, a FT NMR spectrum obtained from an 8 K FID should give a S/N enhancement factor of $\sqrt{4096} = 64$ relative to a cw spectrum of equal width, resolution and measuring time.

Due to this greatly enhanced sensitivity in comparison to cw NMR, the FT method has made ^{13}C NMR into a routine method of structure analysis for all molecules

containing ^{13}C in its natural abundance of 1.1%. Additionally, phase-corrected FT NMR spectra contain all spectral details without the line-skewing and ringing observed in cw spectra. Short-lived molecules can also be measured by FT NMR and sensitivity enhancement by accumulation of FID's before Fourier transformation requires much less time than the accumulation of cw NMR spectra due to the small time required for acquisition of FID signals.

IV. THEORY OF CHEMICAL SHIFTS

When a molecule with a fixed geometry is placed in an external magnetic field $\underline{H}_o$, the electrons will produce a secondary field $\underline{H}'$ at any nucleus, where $\underline{H}'$ is not necessarily parallel to $\underline{H}_o$. The relation between $\underline{H}'$ and $\underline{H}_o$ is given by the equation

$$\underline{H}' = -\underline{\underline{\sigma}}\, \underline{H}_o \ , \tag{42}$$

where $\underline{\underline{\sigma}}$ is a second-rank tensor which depends on the position of the nucleus in the molecule. In solution, molecules are rotating rapidly and randomly such that the chemical shift is determined by the mean component of $\underline{H}'$ along the direction of $\underline{H}_o$, averaged over many rotations. As a result of the averaging the tensor $\underline{\underline{\sigma}}$ can be replaced by a scalar σ, which is the mean value of the diagonal elements of the tensor,

$$\sigma = 1/3(\sigma_{xx} + \sigma_{yy} + \sigma_{zz}). \tag{43}$$

A general expression for the tensor components σ_{xx}, σ_{yy} and σ_{zz} has been derived by Ramsey[22] for the case of an isolated molecule

$$\sigma_{zz} = (e^2/2mc^2)\langle 0|\Sigma \frac{(x_a^2 + y_a^2)}{r_a^3}|0\rangle$$

$$-(e^2h^2/4m^2c^2) \sum_{n\neq 0} (E_n - E_o)^{-1}(\langle 0|\Sigma_a L_{a,z}|n\rangle\langle n|\Sigma_a \frac{2L_{a,z}}{r_a^3}|0\rangle$$

$$+ \langle 0|\Sigma_a \frac{2L_{a,z}}{r_a^3}|n\rangle\langle n|\Sigma_a L_{a,z}|0\rangle), \tag{44}$$

where $\langle 0|$ refers to the unperturbed electronic ground state wave function and $\langle n|$ to the excited state wave functions, with energies corresponding to E_o and E_n, respectively. r_a is the separation of the nucleus and electron(whose coordinates are x,y,z)and L_z is the z component of the electronic orbital angular momentum operator. The summation is over all the electrons in the molecule. The first term in Equation (44) is called the diamagnetic term σ^d, and the second term the paramagnetic term σ^p, so that

$$\sigma = \sigma^d + \sigma^p . \tag{45}$$

This equation, however, is difficult to apply and, except for the smallest systems, gives inaccurate results. To evaluate σ^p precisely it is necessary to have detailed

knowledge of the energies and eigenfunctions of all the excited states of the molecule including the continuum. The latter difficulty may be circumvented by replacing all excitation energies with an average value, ΔE_{av}. For the larger molecules σ^d and σ^p tend to become very large, and of opposite sign, hence σ becomes the relatively small difference between large terms and its value is highly uncertain. Saika and Slichter[118] have taken σ to consist of three components,

$$\sigma_j = \sigma_j^d + \sigma_j^p + \sum_{i \neq j} \sigma_{ij}, \qquad (46)$$

where σ_j^d and σ_j^p refer to the diamagnetic and paramagnetic contributions from the electrons associated with the atom containing the given nucleus and σ_{ij} represents the contribution from the other electrons in the molecule. In diamagnetic molecules the experimental range of nitrogen and carbon chemical shifts is about 900 ppm and 200 ppm, respectively. Contributions from σ_{ij} are usually not more than a few ppm and can sometimes be neglected when comparing the changes in electronic screening in a number of different molecules. Similarly, the effects of ring currents, solvents, neighboring electric fields and shielding anisotropy can sometimes be ignored when the sources of nuclear screening in nitrogen and carbon NMR are being compared in a related series of compounds.

Karplus and Pople[23] concluded from the results of their detailed LCAO-MO treatment of carbon and nitrogen shieldings that variations in σ^p are the dominant factor governing those chemical shifts. In the average excitation energy approximation (AEE), Pople[24] had shown that the resulting expression for σ_j^p is

$$\sigma^p = - \frac{e^2 h^2}{2m^2 c^2 \Delta E_{av.}} \langle r^{-3} \rangle_{2p} \sum_i Q_{ij} , \qquad (47)$$

where the summation over i includes atom j. Also,

$$\begin{aligned} Q_{ij} = {} & 4/3 \; \delta_{ij} \; (P_{x_i x_j} + P_{y_i y_j} + P_{z_i z_j}) \\ & - 2/3 \; (P_{x_i x_j} P_{y_i y_j} + P_{x_i x_j} P_{z_i z_j} + P_{y_i y_j} P_{z_i z_j}) \\ & + 2/3 \; (P_{x_i y_j} P_{x_i y_j} + P_{x_i z_j} P_{x_j z_i} + P_{y_i z_j} P_{y_j z_i}), \end{aligned} \qquad (48)$$

where δ_{ij} is the Kroenecker delta, $\langle r^{-3} \rangle_{2p}$ is the mean value of the reciprocal cube of the 2p orbital radius, called the orbital expansion term, and all P's are the elements of the bond order matrix for the atomic orbitals comprising the molecular orbitals. Thus,

$$P_{uv} = 2 \sum_s^{occ.} c_{su} \, c_{sv}, \qquad (49)$$

where c_{su} are the coefficients of the atomic orbitals χ_u in the linear combination of atomic orbitals (LCAO) description of the molecular orbital ϕ_s, i.e.,

$$\phi_s = \sum_u c_{su} \chi_u . \qquad (50)$$

In Equation (47) $\Delta E_{av.}$ is the average excitation energy. The usefulness of this approximation depends upon whether $\Delta E_{av.}$ may be assumed constant for a group of molecules. The subscripts x_i, x_j, y_i, y_j, z_i and z_j correspond to the various 2p orbitals of atoms i and j. The factor $\langle r^{-3} \rangle$ correlates the electron density around the carbon atom with the size of the 2p orbital. An increase in the electron density on the atom containing nucleus j leads to a decrease in the value of $\langle r^{-3} \rangle_{2p}$ and thus a decrease in the absolute magnitude of σ_j^p. Since the paramagnetic term make a negative contribution to the screening parameter the resultant effect is to increase the shielding and to shift the NMR signal to lower frequency, i.e., to higher field.

The total variation of the screening constant due to changes in σ^d was estimated by Pople[25] to be no greater than 20 ppm, so it was considered to be of secondary importance in determining the shielding tensor.

A. Substituent effects on ^{13}C chemical shifts

Organic molecules, except some highly strained compounds, can be viewed as derivable by substitution upon a simple molecular framework. Adopting this kind of broad view, substituent effects can call for a complete review of the relationship between ^{13}C chemical shifts and molecular structure.

To intrepret substituent effects on ^{13}C chemical shifts, the shielding parameter σ for ^{13}C can be expressed in terms of two components,

$$\sigma = \sigma_{intra} + \sigma_{inter}, \tag{51}$$

where σ_{inter} is the intermolecular term which is the induced magnetic field on the atoms of the medium surrounding the molecular species of interest. This term is expected to be small. The intramolecular term, σ_{intra}, which is an intrinsic property of the pertinent species under consideration, can be separated into two terms,

$$\sigma_{intra} = \sigma_{el} + \sigma_{A}. \tag{52}$$

Equation (52) is similar to Equation (46). σ_{el} is associated with the local electronic current about the nucleus. The second term, σ_{A}, is the so-called neighbor-anisotropy effect, which arises from the magnetic fields produced by the electronic currents of other atoms. The chemical shift due to a change in the electronic environment of the nucleus can be separated as follows:

$$\delta_{12} = -(\sigma_2 - \sigma_1) = -(\sigma_{el_2} - \sigma_{el_1} + \sigma_{A_2} - \sigma_{A_1} + \sigma_{inter_2} - \sigma_{inter_1}) \tag{53}$$

where the negative sign in front of parentheses is due

to the normal convention of designating a lower shielding by an algebraically higher chemical shift. Here

$$\delta_{12} = \delta_{el}^{12} + \delta_{A}^{12} + \delta_{inter}^{12} , \qquad (54)$$

where $-\delta_{el}^{12}$, $-\delta_{A}^{12}$ and $-\delta_{inter}^{12}$ are the changes of the chemical shifts due to variations in the local electronic environment, neighbor-anisotropy effect and the induced magnetic field on atoms of the solvent , as the system is changed from state 1 to state 2.

For the solvent effect, one must consider all three contributions on the right side of Equation (54). δ_{inter}^{12} can be expected to be small, since σ_{inter} is quite small, so a solvent effect would mainly depend on the intramolecular shielding contributions. Furthermore, except in cases where a medium change brings about marked alterations in conformation, or in conformational distributions of highly anisotropic structural groups, the effect of a medium change upon σ_A should be small and solvent effects on ^{13}C chemical shifts would mainly fall on δ_{el}^{12}.

The effects of structural or substituent changes on ^{13}C chemical shifts would generally be described in terms of δ_{el}^{12} and δ_{A}^{12}, unless the change can cause a marked alteration of the solvation or cage structure of the medium in the immediate vicinity of the pertinent species. The δ_{el}^{12} term can be further separated into four

contributions:

$$\delta_{el}^{12} = \delta_{E}^{12} + \delta_{FE}^{12} + \delta_{St}^{12} + \delta_{mis}^{12} \quad . \tag{55}$$

All these terms affect the local electronic distribution and shielding of the relevant nucleus. Here δ_{E}^{12} is due to the effect of the changes in the electronic bonding framework, δ_{FE}^{12}, an electronic field term, is associated with difference in through-space polarization of the two relevant species, δ_{St}^{12}, a so-called steric term, is due to the effects of close-range perturbations exerted by two closely spaced structural groups, and an additional term δ_{mis}^{12} is used to account for any difference between the local electronic distribution and shielding of the nucleus in species 1 and 2 due to miscellaneous electronic influences which are not properly included in the other terms of Equation (55).

The δ_{E}^{12} term includes the classical types of substituent effects that will be transmitted to the relevant atom via the electronic bonding network (i.e., inductive and mesomeric effects). The electronic field term δ_{FE}^{12} represents the interaction that has been discussed as the "field effect" in considering substituent effects on chemical reactivity. The steric term δ_{St}^{12} represents the kind of effect described by Grant and coworkers[26] to explain the increase in shielding which has been identified empirically with the occurrence of a strong 1-4

interaction between a given carbon and another carbon atom (or other "heavy" atom) that is separated from it by three bonds, the intensively studied "γ effect". The miscellaneous term δ^{12}_{mis} could include various types of electronic perturbations such as the intramolecular dispersion interaction proposed by Schaefer, Reynolds and Yonemots[27] or a weak transannular interaction between a carbonyl group and a nucleophilic site in the same molecule[28].

When a structural substitution is made, there will be a small change of geometry which further divides δ_E into two terms as follows:

$$\delta^{12}_{el} = \delta^{12}_{TE} + \delta^{12}_{GE} + \delta^{12}_{FE} + \delta^{12}_{St} + \delta^{12}_{mis} , \qquad (56)$$

where we have separated δ_E into a contribution δ_{TE} which is transmitted through the electronic bonding framework (associated with a fixed geometrical arrangement of atoms), and a contribution δ_{GE} that results from alterations in the local electronic environment of the nucleus due to perturbations in the geometry of the basic structural framework.

The partitioning of substituent effects according to Equations (54) and (56) leaves us with a rather large array of terms. So far, the various kinds of effects in Equation (56) have been discussed qualitatively in many articles; however, quantitative partitioning was not

successful. One of the main obstacles to this kind of partitioning is the generally unknown geometrical arrangements of the atoms in the flexible molecule. Another type of uncertainty that may complicate the task of detailed partitioning of substituent effects is the role of solvent effects, which may differ markedly from one sample to another sample, and significant solvent perturbation effects on δ_{intra} can occur.

V. DOUBLE RESONANCE IN NMR

The proton broadband decoupling experiment is the most important decoupling technique used in ^{13}C NMR. In this kind of decoupling experiment, the ^{13}C - ^{1}H coupling is removed.

In general, spin decoupling is achieved by irradiating an ensemble of nuclei not only with a rf field H_1 at resonance with the nuclei to be observed, but also with a second alternating field H_2 at resonance with the nuclei to be decoupled. NMR double resonance experiments are often symbolized by putting the nuclei to be decoupled in the brackets beside the nuclei to be observed: A-{X}. Using a coordinate system rotating at the angular velocity, $\omega_2 = 2\pi\nu_2$, of the irradiating rf frequency H_2, the effective field produced, in the double resonance experiment on an AX_n system, is given by

$$H_{eff} = H_o + \frac{\omega_2}{\gamma} + H_2 \ . \qquad (57)$$

If H_2 is applied at the resonance frequency of nuclei X, ω_2/γ will cancel H_o, so that $H_{eff} = H_2$. As a result, the magnetization vectors of X will precess perpendicular to H_o while the spins of the observed nuclei A are still quantized along H_o. Since the observed coupling between A and X is the scalar product of $\underline{I}_A$ and $\underline{I}_X$, the observed splitting $J_{AX(obs.)}$ will be zero in this case.

In a ^{13}C - {H} broadband decoupling experiment, all the ^{13}C - ^{1}H multiplets are completely decoupled. To achieve this, $\gamma_X H_2$ should be made considerably greater than $2\pi(sw)_X$ by modulation of the decoupling frequency by an audio frequency or white noise.

The proton broadband decoupling experiment can simplify ^{13}C NMR spectra and increase the sensitivity. However, information concerning the multiplicity of the ^{13}C signal is lost. To retain that information, proton off-resonance decoupling may be applied. Under these conditions, the residual one bond ^{13}C - ^{1}H coupling constant J_r is given by

$$J_r = [(\Delta\nu - 1/2\ J_o)^2 + (\gamma H_2)^2]^{1/2} - [(\Delta\nu + 1/2\ J_o)^2 + (\gamma H_2)^2]^{1/2}, \qquad (58)$$

where J_o is the splitting of an undecoupled multiplet in the observed spectrum, $\Delta\nu$ is the difference between the resonance frequency of the corresponding decoupled nuclei and the decoupling frequency, and γH_2 is the power of the

decoupling field. If H_2 is sufficiently strong that $\gamma H_2 >> |\Delta\nu|, |J_o|$, then Equation (58) reduces to

$$J_r = J_o \Delta\nu / \gamma H_2 \ . \qquad (59)$$

The off-resonance cw spin decoupling technique has been widely applied to the assignment of ^{13}C NMR signals and such experiments are reported in many articles[29].

For measuring ^{13}C - ^{1}H coupling constants, broad-band decoupling and off-resonance techniques cannot be applied. However, the S/N ratio of coupled ^{13}C NMR spectra is much lower due to signal splitting and lack of nuclear Overhauser effects. It is possible to achieve NOE signal-to-noise enhancements without decoupling effects by applying the decoupling power H_2 only between H_1 pulses (i.e., not decoupling during acquisition time). Coupling constants can then be measured without much loss of sensitivity.

Intensities of ^{13}C signals are affected to a varying extent in ^{13}C - {H} NMR spectra due to different NOE and T_1 values, so that the relative numbers of non-equivalent carbons cannot be determined by integration in ^{13}C - {H} NMR spectra. To prevent this error, there are three ways to remedy the problem of different T_1 values: (1) Set a long enough delay time between pulses to result in the complete repolarization of all nuclei, (2) Use a very short pulse which perturbs the populations of the

spin states very little, or (3) Add a small amount of paramagnetic material to make all T_1 values short compared to the pulse repetition rate. There are also three ways of dealing with the problem of variable NOE effects: (1) Operate without proton noise-modulated decoupling. This has the disadvantage that the reappearance of the multiplicities will cause severe overlap of ^{13}C spectra. Furthermore, the usual gain in signal-to-noise due to NOE will not be realized, (2) Gate the decoupler on during the acquisition time and off during the rather long delay time, and (3) Add a small amount of a paramagnetic species which can quench the NOE for all of the carbons without unduly broadening the lines.

VI. NUCLEAR OVERHAUSER EFFECT

The nuclear Overhauser effect (NOE) is the change in the integrated intensity of the NMR absorption for one nuclear spin as a result of the concurrent saturation of another NMR resonance. The term "Overhauser effect" originally referred to the dynamic polarization of nuclei in a metal[30] when the electron spin resonance was saturated. The first application of this effect in a system containing only nuclear spins was made by Solomon and Bloembergen[31] in their study of chemical exchange in HF. Thereafter, the nuclear Overhauser effect found many applications such as the analysis of complex nuclear magnetic resonance spectra[32], the study of chemical

exchange[33], the study of nuclear relaxation[34], and signal-to-noise improvement in NMR spectra[35].

The nuclear Overhauser effect is commonly observed in ^{13}C - {H} experiments and arises from an intramolecular dipole-dipole relaxation mechanism. Any nucleus with a spin is a magnetic dipole. Two such nuclei A and X in a molecule having intermolecular and intramolecular mobilities (rotations, vibrations, translations) give rise to fluctuating fields. Energy transfers between A and X may occur via fluctuating fields. In an A - {X} experiment, the transitions of nuclei X are irradiated while the resonance of nuclei A is observed. Since the irradiating field is very strong, the homonuclear relaxation processes are not adequate to restore the equilibrium population of the nuclei X. The nuclei X may transfer their energy to the nuclei A via the internuclear dipole-dipole interaction. The nuclei A, receiving these transferred amounts of energy, behave as if they have been irradiated themselves and relax. By way of these additional heternuclear relaxation processes of the nuclei A, induced by double resonance, the population of the lower A level increases. As a result, the intensity of the A signal is enhanced.

To consider mathematically how the NOE enhancement occurs, let us start with a system of two nuclei of spin 1/2 (e.g., I = ^{13}C, S = ^{1}H), without J coupling, in

an external magnetic field H_o along the Z direction. The energy level diagram for this two-spin system is shown in Figure 6. If the spins are labelled as I and S, then the energy levels can be designated as follows:

spin I is α, spin S is α ———— ++

spin I is α, spin S is β ———— +-

spin I is β, spin S is α ———— -+

spin I is β, spin S is β ———— -- .

The W's are the transition probabilities, which are:

W_{1I} : the single quantum transition probability that spin I will go from α to β (or β to α) while the state of spin S remains unchanged.

W_{1S} : the single quantum transition probability for spin S when I remains unchanged.

W_2 : the two-quantum transition probability for the two spins to relax simultaneously in the same direction, i.e., -- to ++ or ++ to --.

W_o : the zero-quantum transition probability for a mutual spin flip, i.e., +- to -+ or -+ to +-.

The Hamiltonian for this system of two nuclei of spin 1/2 (I and S) is[36]

$$H = H_M - \hbar \gamma_I H_o I_z - \hbar \gamma_S H_o S_z + H' , \qquad (60)$$

where H_M is the Hamiltonian operator for the motion of the two nuclei I and S, and commutes with the spin

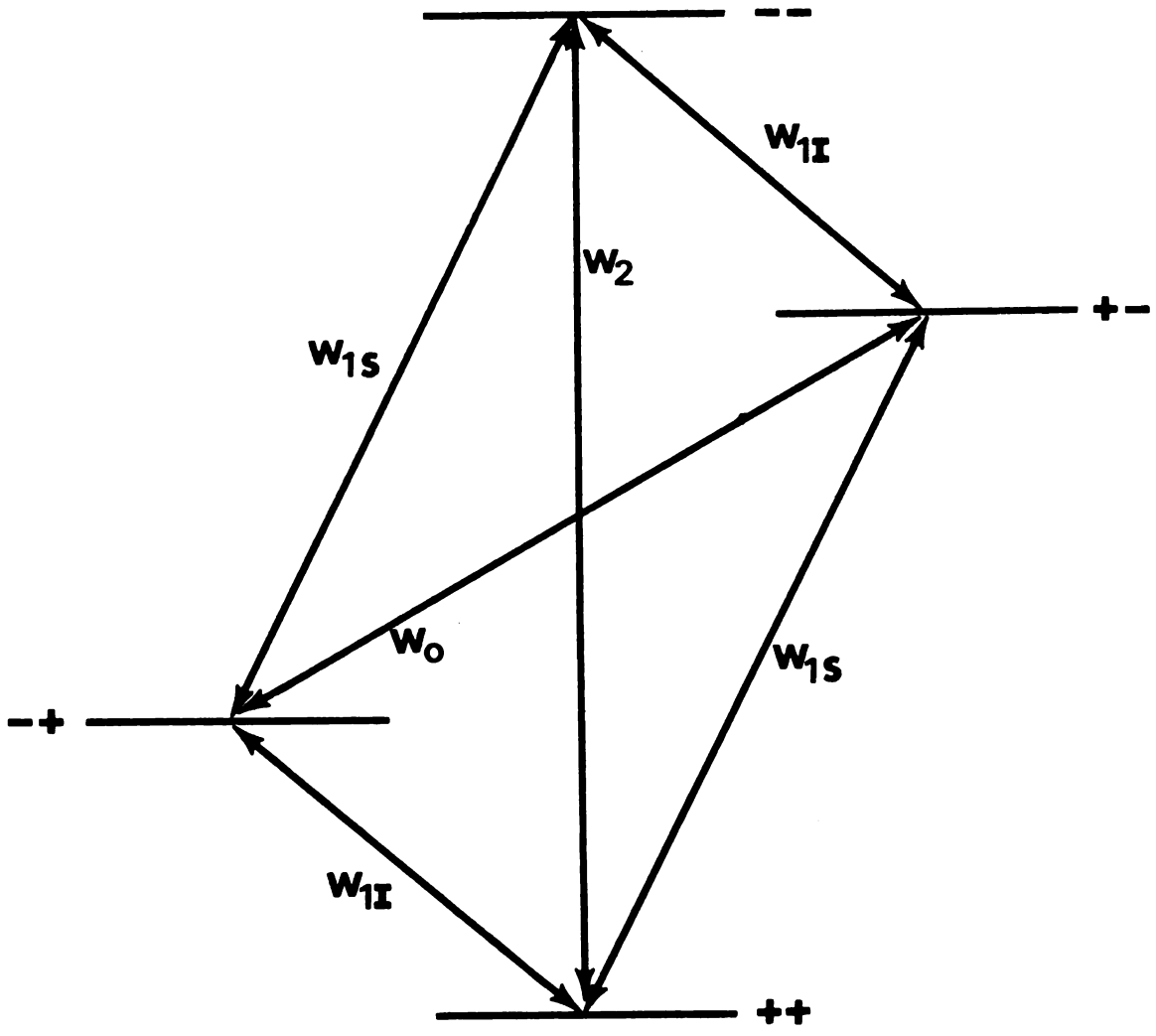

Figure 6. Energy level diagram and transition probabilities for a two-spin system without J coupling.

operators. The next two terms are the Zeemann energies of the spins in the constant magnetic field H_o. H' is the dipolar interaction term of nuclei I and S, which is considered as a perturbation,

$$H' = -\left(\frac{\hbar^2 \gamma_I \gamma_S}{r^3}\right)[3(\underline{I} \cdot \underline{r})(\underline{S} \cdot \underline{r}) - \underline{I} \cdot \underline{S}] \ . \qquad (61)$$

If the populations in each energy level are designated as N_{++}, N_{+-}, N_{-+} and N_{--}, then the following rate laws can be written:

$$\frac{dN_{++}}{dt} = -(W_{1I} + W_{1S} + W_2)N_{++} + W_{1I}N_{-+} + W_{1S}N_{+-} + W_2N_{--} + \text{const.}$$

$$\frac{dN_{+-}}{dt} = -(W_{1I} + W_o + W_{1S})N_{+-} + W_oN_{-+} + W_{1S}N_{++} + W_1I_{N--} + \text{const.}$$

$$\frac{dN_{-+}}{dt} = -(W_{1I} + W_o + W_{1S})N_{-+} + W_oN_{+-} + W_{1S}N_{--} + W_1IN_{++} + \text{const.} \qquad (62)$$

$$\frac{dN_{--}}{dt} = -(W_2 + W_{1I} + W_{1S})N_{--} + W_{1I}N_{+-} + W_{1S}N_{-+} + W_2N_{++} + \text{const.}$$

The constants are obtained by considering the system at temperature equilibrium and inserting the proper Boltzmann factors, and are unimportant in the

computation of the relaxation times. The experimentally observable quantities are the macroscopic magnetic moments $\langle I_z \rangle$ and $\langle S_z \rangle$, which are given by

$$\begin{aligned} (N_{++} + N_{+-}) - (N_{-+} + N_{--}) &= K \langle I_z \rangle \\ (N_{++} + N_{-+}) - (N_{+-} + N_{--}) &= K \langle S_z \rangle \, . \end{aligned} \tag{63}$$

Combining Equations (62) and (63) yields

$$\begin{aligned} \frac{d\langle I_z \rangle}{dt} &= -(W_o + 2W_{1I} + W_2)\langle I_z \rangle - (W_2 - W_o)\langle S_z \rangle + \text{const.} \\ \frac{d\langle S_z \rangle}{dt} &= -(W_2 - W_o)\langle I_z \rangle - (W_o + 2W_{1S} + W_2)\langle S_z \rangle + \text{const.} \end{aligned} \tag{64}$$

With respect to the equilibrium values I_o and S_o we may write

$$\begin{aligned} \frac{d\langle I_z \rangle}{dt} &= -(W_o + 2W_{1I} + W_2)(\langle I_z \rangle - I_o) \\ &\quad - (W_2 - W_o)(\langle S_z \rangle - S_o) \\ \frac{d\langle S_z \rangle}{dt} &= -(W_2 - W_o)(\langle I_z \rangle - I_o) \\ &\quad - (W_o + 2W_{1S} + W_2)(\langle S_z \rangle - S_o) \, . \end{aligned} \tag{65}$$

Equation (65) shows that the decay of the observed magnetizations $\langle I_z \rangle$ and $\langle S_z \rangle$ is not a simple exponential, but a linear combination of two exponentials. If we apply an intense rf field at the resonance frequency of

spin S, so that the populations in states $|+\rangle$ and $|-\rangle$ are equalized ("saturation"), we will have $\langle S_z \rangle = 0$ and the decay of $\langle I_z \rangle$ becomes

$$\frac{d\langle I_z \rangle}{dt} = -(W_o + 2W_{1I} + W_2)[\langle I_z \rangle - I_o(1 + \eta)]. \qquad (66)$$

Here η is defined by

$$\eta = \frac{W_2 - W_o}{W_o + 2W_{1I} + W_2} \frac{\gamma_S}{\gamma_I}, \qquad (67)$$

where γ_S and γ_1 are the gyromagnetic ratios of spins S and I, respectively. It follows from Equation (66) that $\langle I_z \rangle$ decays exponentially with a time constant $1/T_1$ given by

$$1/T_1 = W_o + 2W_{1I} + W_2 . \qquad (68)$$

Equation (66) also tells us that saturation of the S nucleus changes the equilibrium value of $\langle I_z \rangle$ to $(1 + \eta)\langle I_o \rangle$, giving rise to the familiar nuclear Overhauser enhancement (NOE)[37,38]

$$\text{NOE} = \frac{I_{\text{decoupled}}}{I_{\text{coupled}}} = (1 + \eta), \qquad (69)$$

where $I_{\text{decoupled}}$ and I_{coupled} are the integrated intensities of the decoupled and coupled spectra, respectively.

Calculation of the transition probabilities shows that the maximum enhancement occurs when the relaxation

mechanism of the I spin is dominated by dipole-dipole coupling to the S spin. Consider the interaction between two nuclear spins (I = 1/2, S = 1/2) acting as magnetic dipoles with the internuclear vector having polar coordinates, r, θ, and ϕ, with respect to space-fixed axes. The dipole-dipole interaction term in Equation (61) can be rewritten as[39]

$$H' = \sum_m Y_{2,m} A_m r^{-3} , \tag{70}$$

where $Y_{2,m}$ are second-order spherical harmonics normalized to unit root-mean-square averages,

$$\begin{aligned} Y_{2,0} &= (5/4)^{1/2} (1 - 3\cos^2\theta) \\ Y_{2,\pm1} &= \pm(15/2)^{1/2} \cos\theta \sin\theta \exp(\pm i\phi) \\ Y_{2,\pm2} &= -(15/8)^{1/2} \sin^2\theta \exp(\pm 2i\phi) . \end{aligned} \tag{71}$$

In the expressions for these functions, θ and ϕ are time dependent due to molecular motions in the liquid. The spin operators A_m in the dipolar Hamiltonian are

$$\begin{aligned} A_o &= (4/5)^{1/2} K[I_z S_z - 1/4(I_+ S_- + I_- S_+)] \\ A_{\pm1} &= -(3/10)^{1/2} K[I_\pm S_z + I_z S_\pm] \\ A_{\pm2} &= -(3/10)^{1/2} K I_\pm S_\pm , \end{aligned} \tag{72}$$

where the spins are designated I and S, and $K = \hbar\gamma_I\gamma_S$. According to time-dependent perturbation theory the probability per unit time of a transition being induced

between states ϕ_1 and ϕ_j (energies are E_i and E_j, respectively) by a stationary random interaction is

$$W_{ij} =$$

$$\int_{-\infty}^{\infty} \langle\langle \phi_i | H'(t) | \phi_j \rangle \langle \phi_j | H'(t+\tau) | \phi_i \rangle\rangle_{av.} \exp(-i\omega_{ij}\tau) d\tau, \quad (73)$$

where $\langle\ \rangle_{av.}$ indicates that an average is taken over a statistical ensemble. The transition frequency, $\omega_{ij} = \frac{E_i - E_j}{\hbar}$, is expressed in radians sec^{-1}. Substitution of the dipolar Hamiltonian in Equation (73) leads to

$$W_{ij} =$$

$$\sum_m [\langle \phi_i | A_m | \phi_j \rangle^2 \int_{-\infty}^{+\infty} \langle Y_{2,m}(t) Y_{2,m}(t+\tau) r^{-6} \rangle_{av.} \exp(-i\omega_{ij}\tau) d\tau], \quad (74)$$

since the autocorrelation function $G_m(\tau)$ is defined as

$$G_m(\tau) = \langle Y_{2,m}(t) Y_{2,m}(t+\tau) r^{-6} \rangle_{av.} . \quad (75)$$

The spectral density function $J_m(\omega)$ of $Y_{2,m} r^{-3}$, which is a measure of the spectral power available at angular frequency ω from the fluctuating interaction, is also defined as

$$J_m(\omega) = \int_{-\infty}^{+\infty} G_m(\tau) \exp(-i\omega\tau) d\tau = 2\int_{-\infty}^{+\infty} G_m(\tau) \cos(\omega\tau) d\tau. \quad (76)$$

It may be noted that J is the Fourier transform of G. The transition probability may then be written as

$$W_{ij} = \sum_m \langle \phi_i | A_m | \phi_j \rangle^2 \, J_m(\omega_{ij}). \tag{77}$$

It can be seen from the form of the operators that a given term A_m allows transitions of the type W_m only. It can also be shown that $W_m = W_{-m}$. Then evaluation of integrals $\phi_i \, A_m \, \phi_j$ gives

$$\begin{aligned} W_o &= (1/20) \, K^2 \, J_o(\omega_S - \omega_I) \\ W_{1I} &= (3/40) \, K^2 \, J_1(\omega_I) \\ W_{1S} &= (3/40) \, K^2 \, J_1(\omega_S) \\ W_2 &= (3/10) \, K^2 \, J_2(\omega_I + \omega_S). \end{aligned} \tag{78}$$

Introducing Equations (78) into Equations (67) yields

$$NOE = 1 + \eta = 1 + \frac{\gamma_S}{\gamma_I} [6J_2(\omega_S + \omega_I) - J_o] \Omega^{-1} \tag{79}$$

and

$$1/T_1 = (1/20) \, K^2 \, , \tag{80}$$

where $\Omega = J_o(\omega_S - \omega_I) + 3J_1(\omega_I) + 6J_2(\omega_S + \omega_I)$.

A. Theory for several important cases

(1) Isotropic reorientation

If the molecular motion can be described by means of a single rotational correlation time τ_R (i.e., reorientation is isotropic), then $G_m(\tau_R)$, the spectral density function, becomes

$$J_m(\omega) = 2\tau_R (1 + \omega^2 \tau_R^2)^{-1} \, r^{-6}, \tag{81}$$

where r is the distance between I and S. Introducing Equation (81) into Equations (79) and (80) yields

$$NOE = 1 + \frac{\gamma_S}{\gamma_I \chi} \left(\frac{6\tau_R}{1+(\omega_S+\omega_I)^2\tau_R^2} - \frac{\tau_R}{1+(\omega_S-\omega_I)^2\tau_R^2} \right) \tag{82}$$

and

$$1/T_1 = (1/10)\ K^2\ r^{-6} \chi, \tag{83}$$

where

$$\chi = \frac{\tau_R}{1+(\omega_S-\omega_I)^2\tau_R^2} + \frac{3\tau_R}{1+\omega_I^2\tau_R^2} + \frac{6\tau_R}{1+(\omega_S+\omega_I)^2\tau_R^2} \quad .$$

It should be noted that even though T_1 is strongly dependent on the I-S distance, the NOE is not a function of r, so that even for non-protonated carbons the NOE effect may be predicted by Equation (82). In the extreme narrowing limit, i.e., $(\omega_S + \omega_I)^2\tau_R^2 << 1$, all the J values in the above spectral densities are independent of the radiofrequencies under consideration and can be replaced by a single constant J_D, where the subscript D indicates that only the dipolar interaction is important. In this case, the ratio of the transition probabilities is, $W_o:W_{1I}:W_{1S}:W_2 = 2:3:3:12$ and the nuclear Overhauser effect is

$$\eta_{max} = \frac{\gamma_S}{2\gamma_I} , \tag{84}$$

which is independent of the actual value of J_D. For the

^{13}C - {H} experiments, $\gamma_H/\gamma_C = 3.976$ so $\eta_{C-\{H\}} = 1.988$ and NOE = 2.988. When other relaxation mechanisms contribute to the relaxation of ^{13}C the observed NOE value is decreased, since only the dipolar mechanism contributes to W_2 and W_o while other mechanisms will contribute only to W_1. The effect of these other mechanisms can be illustrated by separating W_1 into a dipolar component and a term W_{1C}^* expressing the effect of all other mechanisms. Thus, for a two-spin system

$$\eta_{I-\{S\}} = \left(\frac{\gamma_S}{2\gamma_I}\right)\left(\frac{K^2 J_D}{K^2 J_D + 4W_{1I}^*}\right). \qquad (85)$$

Equation (85) shows that when $K^2 J_D \approx W_{1I}^*$ the enhancement depends on the contribution of these other relaxation mechanisms relative to the dipolar term.

(2) ^{13}C-{all H} double resonance

An important case is that of more than two spins, where the resonance of one type of nucleus is observed while those of all other types of nuclei in the sample are saturated, e.g., ^{13}C-{all H}. This technique is very important in ^{13}C NMR because of (a) the common occurrence of CH_3 and CH_2 groups, and (b) the desirability of eliminating all indirect ^{13}C - ^{1}H spin-spin couplings by irradiation of the entire proton spectrum for the molecule.

Consider a spin system consisting of a spin I of one species and n spins or another species, S(i) (i = 1,2,3,...,n), where all spins are supposed to have a quantum number 1/2. It has been shown that $\langle I_z \rangle$ will not depend on which S spin is considered so we assume that the final expression for the multi-spin system differs from that for a single S spin merely by being a summation over independent contributions from each S spin:

$$\eta_{I-\{\text{all S}\}} = \frac{\gamma_S}{2\gamma_I} \left(K^2 \sum_i^n J_{Di} / \left(K^2 \sum_i^n J_{Di} + 4 W_{1I}^*\right)\right), \qquad (86)$$

where $\sum_i$ is the summation over all S nuclei being saturated. No distinction has been made in the above derivation between intramolecular and intermolecular dipole-dipole interactions. Clearly if dipole-dipole interaction in the $^{13}C-\{\text{all H}\}$ case is dominant, i.e., $4W_{1C}^* << K^2 \sum_i J_{Di}$, then Equation (86) reduces to Equation (84). In such cases the number of protons involved is irrelevant. Thus, if dipole-dipole relaxation between directly bonded carbon and hydrogen atoms provides the dominant mechanism, the same NOE value (i.e., 2.988) will be seen for all ^{13}C nuclei of CH, CH_2 or CH_3 groups. However, if contributions from other relaxation mechanisms are appreciable the number of nearest protons can lead to variations in the values of $\eta_{C-\{H\}}$.

It is of interest to consider the spin-lattice relaxation time of the decoupled ^{13}C nuclei. If it is assumed that all the protons are saturated, then

$$\frac{d\langle I_z\rangle}{dt} = -\left(\frac{1}{2} K^2 \sum_i J_{Di} + 2W^*_{1I}\right)[\langle I_z\rangle - (1 + \eta_{I-\{S\}})I_o] \quad (87)$$

and

$$\frac{1}{T_1} = \frac{1}{2} K^2 \sum_i J_{Di} + 2 W^*_{1I} . \quad (88)$$

Measurement of T_1 is thus a valuable complement to Overhauser effect measurement. Combination of Equations (86) and (88) leads to separate solutions for W^*_{1C} and $K^2 \sum_i J_{Di}$:

$$K^2 \sum_i J_{Di} = 4 \gamma_C \eta_{C-\{H\}} / (\gamma_H T_1) \quad (89)$$

$$W^*_{1C} = (2T_1)^{-1}[1 - 2(\gamma_C/\gamma_H)\eta_{C-\{H\}}] . \quad (90)$$

Equation (88) tells us that if the dipolar interaction is dominant among the relaxation mechanisms then the relaxation rate is proportional to the number of hydrogens bonded to ^{13}C. Combining Equations (84), (86) and (88), we derive

$$\frac{T_{1(obs)}}{T_{1(DD)}} = \frac{\eta_{obs}}{\eta_{max}}, \quad (91)$$

where $T_{1(obs)}$ and $\eta_{(obs)}$ are the experimentally

determined spin-lattice relaxation time and NOE effect, and $T_{1(DD)}$ and $\eta_{(max)}$ are the corresponding values contributed from the dipolar interaction alone.

(3) Anisotropic rotation or groups with internal rotation

If the rotational motion is anisotropic (39), or if internal motion must be considered, the relaxation times and NOE values will depend on all components of the rotational diffusion tensor. Equations (78)-(80) are still valid but the spectral densities are functions of the various components of the rotational diffusion tensor. The only case we will consider here is that of a rotating group attached to a molecule undergoing isotropic reorientation with τ_G and τ_R being the correlation times for internal motion and overall molecular motion, respectively. If the internal rotation is a stochastic diffusion process, i.e., there are a large number of equilibrium positions, Woessner[40] has shown that the spectral densities are given by

$$J_m(w) = 2r^{-6} f(\tau_R, \tau_G, \omega) \tag{92}$$

and

$$f(\tau_R, \tau_G, \omega) = A \frac{\tau_R}{1+\omega^2\tau_R^2} + B \frac{\tau_B}{1+\omega^2\tau_B^2} + C \frac{\tau_C}{1+\omega^2\tau_C^2}, \tag{93}$$

where

$$\tau_B^{-1} = \tau_R^{-1} + (6\tau_G)^{-1}$$

$$\tau_C^{-1} = \tau_R^{-1} + 2(3\ \tau_G)^{-1}$$

$$A = \frac{1}{4}\ (3\cos^2\theta - 1)^2 \qquad (94)$$

$$B = 3\ \sin^2\theta\ \cos^2\theta$$

$$C = \frac{3}{4}\ \sin^4\theta$$

θ = the angle between C-H vector and the axis of internal rotation.

Introducing Equations (92)-(94) into Equations (79) and (80) yields:

$$NOE = 1 + R(A\phi_R + B\phi_B + C\phi_C)(AX_R + BX_B + CX_C)^{-1} \qquad (95)$$

and $$1/T_1 = AT_{1R}^{-1} + BT_{1B}^{-1} + CT_{1C}^{-1}\ , \qquad (96)$$

where $1/T_{1j} = \frac{1}{10}\ K^2 r^{-6} X_j$, $R = \gamma_H \gamma_C^{-1}$ and

$$X_j = \frac{\tau_j}{1+(\omega_H-\omega_C)^2\tau_j^2} + \frac{3\tau_j}{1+\omega_C^2\tau_j^2} + \frac{6\tau_j}{1+(\omega_H+\omega_C)^2\tau_j^2}$$

$$\phi_j = \frac{6\tau_j}{1+(\omega_H+\omega_C)^2\tau_j^2} - \frac{\tau_j}{1+(\omega_H-\omega_C)^2\tau_j^2}\ . \qquad (j = R,B,C)$$

Rearranging Equation (96) yields

$$T_{1R}/T_1 = A + B(X_B/X_R) + C(X_C/X_R)\ . \qquad (97)$$

It should be noted that T_{1R} and $(1 + R\phi_R/X_R)$ are the T_1 and NOE, respectively, in the absence of internal

rotation. In the extreme narrowing limit, $(\omega_H + \omega_C)^2\tau_j^2 << 1$, $X_j = 10\tau_j$. If we introduce this relation and Equation (94) into Equation (97) we obtain

$$T_{1R}/T_1 = A + B[\frac{6\tau_G}{6\tau_G+\tau_R}] + C[\frac{3\tau_G}{3\tau_G+2\tau_R}]. \quad (98)$$

Thus, in the extreme narrowing limit $T_1 > T_{1R}$, since $A + B + C = 1$. If the internal rotation is much faster than the overall reorientation ($\tau_G << \tau_R$), Equation (98) becomes

$$T_{1R}/T_1 = A + (6B + 3/2)\tau_G/\tau_R . \quad (99)$$

If θ is appreciably different from the magic angle (for which $A = 0$) then Equation (99) becomes

$$T_1 = T_{1R}/A . \quad (100)$$

The above equation gives the maximum increase in T_1 from fast internal rotation when the overall reorientation satisfies the extreme narrowing condition. When the angle between the CH vector and the axis of rotation is tetrahedral, $\cos^2\theta = 1/9$, and $T_1 = 9\ T_{1R}$. A tetrahedral methine carbon with one degree of internal motion has a T_1 value up to nine times that of a methine carbon which is part of the rigid backbone in a large molecule undergoing isotropic reorientation. In the very common case of a methyl group directly attached to a rigid backbone,

one must correct for the presence of three hydrogens. In this case the upper limit to the T_1 of methyl carbon will be three times that of the T_1 of a methine carbon on the backbone. This behavior has been confirmed experimentally[41].

HISTORICAL REVIEW OF NUCLEAR RELAXATION STUDIES

I. STATISTICAL MECHANICAL THEORY

The rapidly increasing use of ^{13}C NMR has generated considerable interest in ^{13}C relaxation mechanisms. The information derivable from ^{13}C relaxation measurements is generally unobtainable from the chemical shifts, spin-spin couplings and peak area (integration) parameters. Relaxation data are related closely to overall and local molecular geometry, bonded and nonbonded interactions, and other factors controlling molecular motion. From relaxation data, together with the nuclear Overhauser effect observed on proton decoupling of ^{13}C NMR spectra, the ^{13}C relaxation mechanisms in a liquid can be obtained. Differences between the T_1 values measured for the ^{13}C nuclei of a molecule can help in the assignment of ^{13}C NMR spectra, particularly in cases of signal crowding and multiplet overlapping. In this section, the details of several relaxation mechanisms will be discussed.

The relaxation processes occur by the interaction of the nuclear spin system with fluctuating local magnetic fields. These fields are generated by other molecules in the sample and their fluctuation is governed by the motion

of these molecules. If the locally induced magnetic fields, which act as microscopic radiofrequency fields, have components at the appropriate Larmor frequency, they can interact with the given nuclei and cause spin relaxation. The larger such a component is, the quicker relaxation can occur. The frequency components of these motions in the MHz region are important for ^{13}C relaxation; fast motions, e.g., electronic motions and molecular vibrations, are thus going to have components of insufficient magnitude and so of little importance. However, Brownian motion (rotational and diffusional) is important for ^{13}C relaxation, as are certain molecular torsional and rotational motions.

Since molecular motion is effectively a random process in solution, any property generated from it, e.g., h(t), will have zero average,

$$\langle h_{loc}(t) \rangle = 0 \ ; \tag{101}$$

its mean square average, however, will not be zero,

$$\langle h^{*}_{loc}(t) \cdot h_{loc}(t) \rangle \neq 0 \ . \tag{102}$$

Thus, this latter average will be a useful property to describe molecular motion. If the Fourier transform of $h_{loc}(t)$ is $H_{loc}(\nu)$, then $H_{loc}(\nu)$ is itself random with a zero average but a non-zero square average. $|H_{loc}(\nu)|^2$ represents the total energy available at frequency ν, and would be infinite unless one limited the time under

consideration (t). We can thus define a power spectrum

$$J(\nu) = \lim_{t=-\infty} \frac{\pi}{t} H^{*}_{loc}(\nu) \cdot H_{loc}(\nu) \qquad (103)$$

$J(\nu)$ is called the spectral density function and tells us the power (energy/unit time) available in the molecular motion as a function of ν.

A useful property in describing random molecular motion is the correlation time τ_C which can be defined as the average time for a molecule to rotate by one radian in reorientational motion. If a molecule is in one state of motion for τ_C sec, one would expect there to be frequency components of the motion spread around τ_C^{-1}.

The correlation time of a molecule in solution will depend on many factors such as molecular size, symmetry and solution viscosity. If the molecule is small (M.W. < 100), then in solutions of normal viscosity τ_C is about 10^{-12} - 10^{-13} sec; for larger molecules (M.W. = 100-300) τ_C may increase to as much as 10^{-10} sec. Molecular geometry will obviously have an effect on the correlation time; a symmetrical molecule, causing less disordering of the solvent as it rotates, will move faster than an asymmetric one. Viscosity describes the ease with which reordering can be achieved in the solution and depends on both the solute and solvent. The correlation time for molecular reorientation used here is equal to one third of the dielectric correlation time τ_D of the Debye

theory of liquids and can thus be expressed, using that theory, in terms of the solution viscosity η and the molecular radius a:

$$\tau_C = (1/3)\tau_D = 4\pi\eta a^3/3kT. \tag{104}$$

By using the concept of a correlation time, one can set up a reasonable model for the auto-correlation function by assuming that the effect of molecular collisions decays exponentially with a time constant τ_C. The auto-correlation function will have the form

$$G(\tau) = \int_{-\infty}^{\infty} h^*(t) \cdot h(t) \exp(|\tau|/\tau_C)dt \ . \tag{105}$$

Rewriting the above equation one obtains

$$G(\tau) = \overline{h^2_{loc}} \exp(|\tau|/\tau_C). \tag{106}$$

Fourier transformation of Equation (106) leads to

$$J(\nu) = \overline{h^2_{loc}} \frac{2\tau_C}{1 + (2\pi\nu)^2\tau_C^2} \ . \tag{107}$$

It is evident that $J(\nu)$ is a maximum at $\nu = 0$ and begins to fall off with increasing frequency as $2\pi\nu$ becomes comparable to $1/\tau_C$. Any relaxation process can be represented by an equation which has the general form

$$R = \overline{H^2_{loc}} f(\tau_C) \ . \tag{108}$$

The value and origin of $\overline{H}_{loc}$ and τ_C will depend on the mechanisms under consideration.

II. RELAXATION MECHANISMS

Local magnetic fields in solution can be generated in many ways. Six possible relaxation mechanisms will be discussed here.

A. Dipole-dipole relaxation (DD)

The principal source of nuclear relaxation for spin-1/2 nuclei is via dipole-dipole interactions. Consider the relaxation of a nucleus I by a magnetic particle S (an unpaired electron or a nucleus). The local field generated at I by S is given by the classical equation

$$H_{loc}^{DD} = \pm\mu_S(3\cos^2\theta - 1)r_{IS}^{-3} \qquad (109)$$

where H_{loc}^{DD} is the magnetic field produced at nucleus I by nucleus S, μ_S is the dipole moment of S, r_{IS} is the nuclear separation of I and S, and θ is the angle of the r_{IS} vector relative to the applied magnetic field H_o. Thus, both inter- and intra-molecular interactions are possible, except that the former will tend to be attenuated more readily as a result of the r^{-3} dependence. Local fields from this source may be as large as approximately 2 mT where $1T = 10^3G$. In a rigid system of intramolecular dipoles, θ shows a time dependence in liquids due to molecular tumbling while for intermolecular interactions r_{IS} and θ can both fluctuate with time owing to translational and rotational diffusion.

For the interaction of two spins I and S, the perturbing Hamiltonian is [42]

$$H'_D(t) = \hbar \underline{I} \quad \underline{H}_{loc}(t) = \hbar \underline{I} \cdot \underline{\underline{D}} \cdot \underline{S}, \tag{110}$$

where $\underline{\underline{D}}$ is the dipolar coupling tensor and contains the time dependence of the system. When I and S are both spin 1/2 nuclei but different nuclear species, the expression for dipolar relaxation can be derived from Equation (83) and is

$$\frac{1}{T_{1(DD)}} = \frac{1}{10} \frac{\hbar^2 \gamma_I^2 \gamma_S^2}{r_{IS}^6} \left[\frac{\tau_R}{1+(\omega_S-\omega_I)^2\tau_R^2} + \frac{3\tau_R}{1+\omega_I^2\tau_R^2} + \frac{6\tau_R}{1+(\omega_S+\omega_I)^2\tau_R^2}\right]. \tag{111}$$

Under the extreme narrowing approximation, $(\omega_I + \omega_S)^2\tau_R^2 << 1$, Equation (111) reduces to

$$\frac{1}{T_{1(DD)}} = \frac{\hbar^2 \gamma_I^2 \gamma_S^2}{r_{IS}^6} \tau_R, \tag{112}$$

where τ_R is the reorientational correlation time which varies exponentially with temperature as [43]

$$\tau_R = \tau_R^o \exp(E/RT). \tag{113}$$

Equation (113) shows that τ_R will decrease as the temperature increases and hence $T_{1(DD)}$ becomes longer. Equation (112) holds for isotropic rotational diffusion which is

characterized by a single correlation time constant τ_R.

To handle the case of multi-spin relaxation, Equation (112) can be modified to[38]

$$\frac{1}{T_{1(DD)}} = \sum_S \frac{\hbar^2 \gamma_I^2 \gamma_S^2}{r_{IS}^6} \tau_C \ , \qquad (114)$$

provided that $S \neq I$ and that an effective isotropic correlation time τ_C can be employed. This expression has often been utilized as a means of acquiring rough quantitative estimates of the correlated motion even though the motion may actually be anisotropic. Under such conditions, however, details of the motional features are obscured and care should be taken not to over interpret these approximate correlation times. Due to the rapid attenuation of the r_{IS}^{-6} term, a simplified form can be obtained by summing S only over the directly-bonded nuclei to yield

$$\frac{1}{T_{1(DD)}} = \frac{n_S \hbar^2 \gamma_I^2 \gamma_S^2}{r_{IS}^6} \tau_C \qquad (115)$$

where n_S is the number of directly bonded S nuclei. Most of the ^{13}C nuclei in organic molecules, especially those linked to hydrogens (i.e. CH_3, CH_2, CH), are relaxed mainly by internuclear dipole-dipole interactions and intermolecular dipolar relaxation has rarely needed to be considered since the carbons are in the backbone of the molecule.

B. Spin-rotation relaxation (SR)

Electron and nuclear currents associated with overall molecular rotation can give rise to correlated fluctuating magnetic fields which can lead to spin relaxation. These fluctuations in the local magnetic fields may result from a modulation of the magnitude (M-diffusion), or of both the magnitude and the direction (J-diffusion), of the angular momentum vector associated with the rotating molecular system[44]. Although currents arising from completely symmetrical negative and positive charge distributions can be expected to cancel one another, it is to be noted that any angular momentum possessed by electrons around a given nucleus, no matter how symmetrical the charge distribution may be, will on the average lead to a local magnetic field at that nucleus. The spin-rotation mechanism is usually important for small, symmetrical molecules or small segments of larger molecules (methyl groups).

The Hamiltonian for the spin-rotation interaction is:

$$H'_{SR}(t) = -\underline{I} \cdot \underline{\underline{C}} \cdot \underline{J}(t), \qquad (116)$$

where $\underline{I}$ is the spin angular momentum, $\underline{\underline{C}}$ is the spin-rotation interaction tensor, and J(t) is the time-dependent angular momentum associated with overall molecular rotation. Although the above equation is relatively easy to

employ in the gas phase, where a set of good J quantum numbers can be used characteristic of such systems, only an approximate solution for liquids is possible because the states are rendered indistinguishable by lifetime broadening resulting from extensive intermolecular interactions.[45] Thus, relatively simple ensemble averaging of J(t) over all possible angular momenta is employed to estimate the magnitude of $H'_{SR}(t)$ due to rotation. For spherically symmetric molecules $T_{1(SR)}$ for a magnetic nucleus at the center of symmetry (and under the extreme narrowing limit) is given by

$$\frac{1}{T_{1(SR)}} = \frac{2\ IkT}{\hbar^2}\ C^2\ \tau_{SR}\ , \tag{117}$$

where I is the moment of inertia, C is the isotropic spin-rotation interaction constant and τ_{SR} is the spin-rotation correlation time. If the nucleus lies in a cylindrically symmetric electronic environment, Equation (117) can be modified by replacing C^2 by the relation

$$C^2 = \frac{1}{3} \cdot (C_{||}^2 + 2\ C_{\perp}^2), \tag{118}$$

where the parallel direction is that of the principal vector of the rotation axis. It may be shown that the angular momentum correlation time τ_{SR} is related to the molecular reorientation time τ_R by

$$\tau_R \tau_{SR} = \frac{I}{6kT}\ , \tag{119}$$

where k is the Boltzmann constant and T is the absolute temperature. This relation holds only at temperatures well below the normal boiling point of a liquid.

The important distinction between τ_{SR} and τ_R is that τ_{SR} becomes longer as the temperature increases, whereas τ_R becomes shorter. As the temperature becomes very high and the sample becomes a gas, collisions become more infrequent and the molecule remains in a given angular momentum state for a longer period of time. On the other hand, the higher the temperature the faster a molecule reorients and the shorter τ_R becomes. The result of this is that for the spin-rotation interaction the relaxation time T_1 becomes longer as the temperature decreases. This behavior is opposite to that observed for the other relaxation mechanisms.

In general, the small, symmetric molecules with nuclei which have a large range of chemical shifts, i.e. ^{19}F, ^{13}C, ^{15}N, will have important spin-rotation interactions. This relation between spin-rotation and chemical shifts arises because both the chemical shift and the spin-rotation tensor components of any given molecule depend on the electron distribution in a molecule and a distribution which results in large chemical shifts will also lead to large spin-rotation interactions.

C. Chemical shift anisotropy relaxation (CSA)

Significant anisotropy in the shielding of a nucleus can give rise to fluctuating magnetic fields when the molecule tumbles in solution. As is well known, the local magnetic field at a nucleus in an external field H_o is given by

$$H_{loc} = (1 - \sigma)H_o \tag{120}$$

where σ is the chemical shielding tensor. If the electron screening around the nucleus is not isotropic, $\underline{\underline{\sigma}}$ will have directional components which vary with time as the molecules tumble relative to the H_o axis. The linear coupling between H_o and spin I is represented by the Hamiltonian

$$H'_{CSA}(t) = -\underline{H}_o \cdot h\,\underline{\underline{\sigma}} \cdot \underline{I}\ . \tag{121}$$

In the extreme narrowing approximation limit, this yields the following expression for $T_{1(CSA)}$, the chemical shift anisotropy relaxation time,

$$\frac{1}{T_{1(CSA)}} = \frac{\gamma_I^2 H_o^2}{5}(\sigma_{12}^2 + \sigma_{23}^2 + \sigma_{31}^2)\tau_R, \tag{122}$$

where the σ_{ij}'s represent the anisotropic magnitudes $(\sigma_i - \sigma_j)/3$ of the three principal terms in the diagonalized shielding tensor $\underline{\underline{\sigma}}$ and τ_R is the reordintational correlation time for the dipole-dipole relaxation mechanism. If $\underline{\underline{\sigma}}$ is axially symmetric (C_{3v} or higher symmetry),

Equation (122) reduces to

$$\frac{1}{T_{1(CSA)}} = \frac{2}{15} \gamma_I^2 H_o^2 (\sigma_{||} - \sigma_{\perp})^2 \tau_R \ , \qquad (123)$$

where $\sigma_{||}$, $\sigma_{\perp}$ are the components of $\underline{\underline{\sigma}}$ parallel and perpendicular to the symmetry axis. A contribution of the CSA mechanism is apparent when the measured T_1 values are proportional to the square of the applied magnetic field strength H_o. This contribution is usually negligible for ^{13}C nuclei of organic molecules.

D. Scalar coupling relaxation (SC)

If the spins of two proximate nuclei I and S in a molecule undergo coupling, and the lifetime of these nuclei in their nuclear magnetic energy states is sufficiently long, then the signals for I and S will be split (scalar coupling). The interaction Hamiltonian is of the form

$$H'_{SC}(t) = h \underline{I} \cdot \underline{\underline{A}} \cdot \underline{S} \ . \qquad (124)$$

To produce a contribution to the relaxation of nucleus I, there are two possibilities, (a) S is time dependent, or (b) A is time dependent. If nucleus S relaxes very much faster than nucleus I, i.e., $1/T_1^S < 1/A$, then no signal splitting is observed. However, the fast relaxation of nucleus S will generate fluctuating fields which in turn contribute to the relaxation of nucleus A. Quadrupolar

nuclei with $I \geq 1$, i.e., nuclei whose charge distribution is not spherically symmetrical, relax so fast that they accelerate the relaxation of neighboring nuclei. This is the so-called scalar relaxation of the second kind. The relaxation rate due to this mechanism is

$$\frac{1}{T_{1(SA)}^{I}} = \frac{2A^2}{3} S(S + 1) \frac{\tau_S}{1+(\omega_I-\omega_S)^2\tau_S^2}, \qquad (125)$$

where A is the spin-spin coupling constant expressed in rad sec^{-1} and τ_S is the relaxation time of nucleus S, i.e., $T_1^S = \tau_S$.

Scalar relaxation can also occur when $\underline{\underline{A}}$ becomes a function of time. This situation can arise when chemical exchange is present and is referred to as scalar relaxation of first kind. In this case the local magnetic field at I is $A(t)S/\gamma_I$, when I and S are covalently bound in the same molecule, and zero otherwise. If the chemical exchange rate is much larger than either the coupling A, or $1/T_1$ for either I or S, and if the time the nuclei are uncoupled is short compared with the time they are coupled, the multiplet structure disappears and only a single resonance line is observed. This is quite similar to scalar relaxation of the second kind, and Equation (125) is still valid but τ_S now becomes τ_e, the exchange time. The contribution of the scalar mechanism can be recognized from a frequency and temperature dependence of T_1 when the nuclei I and S precess with similar Larmor frequencies.

E. Quadrupole relaxation (Q)

Nuclei with spin I > 1/2, having an electric quadrupole moment, eQ, will interact with the field gradient, eq, produced by the surrounding electrons. This interaction provides a very efficient relaxation for the quadrupolar nuclei. The interaction Hamiltonian $H'_Q(t)$ is

$$\underline{H}'_Q(t) = \underline{I} \cdot \underline{Q} \cdot \underline{I} \ , \tag{126}$$

where $\underline{Q}$ is the quadrople coupling tensor. The quadrupole relaxation rate in the extreme narrowing limit is[42]

$$\frac{1}{T_{1(Q)}} = \frac{3}{40} \frac{2I + 3}{I^2(2I - 1)} (1 + \eta^2) \left(\frac{e^2Qq}{\hbar}\right)^2 \tau_R \ , \tag{127}$$

where η is the asymmetry parameter and (e^2Qq/h) is the quadrupole coupling constant. Since in mobile liquids the molecular correlation times τ_R are in range of 10^{-11} to 10^{-12} sec, the quadrupole relaxation rate is primarily determined by the magnitude of the quadrupole coupling constant. The quadrupole interaction is usually the dominant one for nuclei with spin I > 1/2 (unless, due to molecular symmetry, $e^2Qq/\hbar = 0$). Since it is almost entirely an intramolecular interaction, a measurement of the quadrupole relaxation time provides an excellent means for measuring the molecular correlation time τ_R, if the quadrupole coupling constant can be determined independently.

F. Electron-nuclear relaxation (e)

The electron is a magnetic dipole and an unpaired electron will therefore generate a local magnetic field, which in general will have a non-zero average value and so cause a Knight shift. This local field will be randomly modulated by molecular motion, providing a nuclear relaxation mechanism. The interaction is dipolar in nature and its efficiency therefore depends on the square of both the magnetic moment of the electron and of the nucleus. The electron's magnetic moment is about 10^3 times larger than that of the proton, which has the largest known nuclear moment. Electron-nulcear dipolar relaxation is thus a more efficient relaxation process by a factor of 10^6 than the nuclear dipolar relaxation discussed above. Against this, the increased efficiency is only partially offset by the larger characteristic mean inter-dipole distance. The efficiency of this form of relaxation means that it has detectable effects even at very low concentrations of the paramagnetic species. The most common example of this kind of interaction is that resulting from oxygen dissolved in the solution. Dissolved oxygen can lead to line broadening, particulary in proton spectra where linewidths below a few tenths of a Hertz normally cannot be achieved without degassing the sample. Even in ^{13}C spectra, where the mean distance of approach of oxygen to carbon is much larger than that to protons and

consequently the effects much weaker, oxygen still contributes significantly to the relaxation of quaternary carbons.

Electron-nuclear relaxation is often produced in NMR by the addition of small quantities of paramagnetic ions to the solution. If the paramagnetism of the ion comes purely from spin angular momentum, its magnetic moment is $\mu = \gamma_e \hbar (S(S+1))^{1/2}$. If there are other contributions, an effective magnetic moment μ_{eff} has to be used. As a rule the relaxation rates $1/T_1$ and $1/T_2$ are directly proportional to N_S, the concentration of paramagnetic species, and roughly proportional to μ_{eff}^2. A detailed analysis of this mechanism is given later, but basically it follows the approach used in analyzing nuclear dipolar relaxation. In the extreme narrowing limit[42], it is found that

$$\frac{1}{T_{1(e)}} = \frac{4S(S+1)\gamma_e^2\gamma_I^2}{3\hbar^2 r^6}\tau_C \qquad (128)$$

and

$$\frac{1}{T_{2(e)}} = \frac{1}{T_{1(e)}} + \frac{S(S+1)A^2}{\hbar^2}\tau_e \,, \qquad (129)$$

where A is the electron-nuclear hyperfine interaction constant. The correlation time τ_e is related to the electron (T_{2S}) relaxation time, and also to the exchange time τ_h of the molecular complex between the ion and the molecule being relaxed,[44]

$$\frac{1}{\tau_e} = \frac{1}{T_{2S}} + \frac{1}{\tau_h} \,. \qquad (130)$$

The effect of paramagnetic ions on nuclear relaxation has important applications in chemistry and biology, where they can be applied to the measurement of exchange reactions. The "relaxation reagents" used in ^{13}C NMR provide another example of the use of electron-nuclear relaxation. These reagents are usually transition complexes, the trisacetonylacetonates of chromium (Cr^{3+}) and iron (Fe^{3+}) being the most common, and their function is to dominate ^{13}C relaxation in the sample. In doing so they first shorten all the T_1's, thus speeding up a pulsed experiment, and secondly they eliminate the NOE effects. This is especially useful in quantitative ^{13}C work.

G. Additivity of relaxation rates

Since the relaxation rate $1/T_1$, depending on several possible relaxation mechanisms, can be assumed to be additive,

$$\frac{1}{T_1} = \frac{1}{T_{1(DD)}} + \frac{1}{T_{1(SR)}} + \frac{1}{T_{1(CSA)}} + \frac{1}{T_{1(SC)}} + \frac{1}{T_{1(Q)}} + \frac{1}{T_{1(e)}} + \ldots \quad (131)$$

the contribution from each mechanism can give different chemical information. Consequently, in order to gain the full value from a study of relaxation data, the contribution of each mechanism must be resolved. For carbon atoms bonded to one or more protons in medium and large molecules, relaxation is dominated by the dipolar interaction and

this contribution can be measured by determining the nuclear Overhauser effect, as shown in Equation (91).

III. SOME EXPERIMENTAL RESULTS FROM THE LITERATURE

A. Studies of Amides.

The data available on ^{13}C relaxation times is quite limited and detailed separations into the contributing mechanisms are even less available. The majority of such analyses are due to Grant and coworkers[38,48-53] on small molecules, and to Allerhand and coworkers[41] on large systems. The results of these investigations combine to provide a consistent overview of ^{13}C relaxation for molecules of diverse size at ambient temperatures and verify the anticipated result that ^{13}C T_1 values are controlled mainly by the C-H intramolecular dipolar relaxation process. Thus, the dynamical information on liquid systems obtained from ^{13}C relaxation studies has, for the most part, been extracted from the effective reorientational correlation time associated with the C-H dipolar mechanism.

A few ^{13}C relaxation data and NOE values for amides have been reported so far, and these are shown in Table 1. The anisotropic molecular motion of N,N-dimethylformamide has been studied by Huntress et al.[54] by measuring the quadrupolar relaxation rates of deteurium, nitrogen, and oxygen. The anisotropic molecular motion of some symmetric-top molecules, e.g., CH_3CN, CH_3I, CH_3Cl,

Table 1. ^{13}C Spin-lattice relaxation times and NOE data for some amides

Compound	T(°C)	Substituent	T_1 (sec)	NOE	T_1(DD) (sec)	$\tau_C \times 10^{12}$ (sec)
N,N-Dimethylformamide[a]	38.0	cis-NCH_3	18.6	2.3	28.6	
		trans-NCH_3	11.1	2.7	13.1	
		C = O	20.2	2.4	28.9	
	25.0	cis-NH_3	17.8			
		trans-NCH_3	10.5			
		C = O	19.5			
	72.0	cis-NCH_3	19.0	2.2	32.0	
		trans-NCH_3	18.0	2.3	28.0	
Acetamide[b] (in D_2O)	30.0	C = O	72.0	2.0	139	7.5
		CH_3	12.3	2.3	18.5	7.5
Acetamide[b,c] (in H_2O)	30.0	C = O	37.1	2.2	61.0	7.5
		CH_3	11.0	2.3	17.5	7.5
N,N-Dimethylacetamide[b]	30.0	C = O	44.2	2.3	65.6	11.1
		Carbonyl-CH_3	9.6	2.6	12.2	11.1
		N-CH_3	9.5	2.6	12.0	11.1
N,N-Di-n-butylformamide[a]	38.0	N-α-C	1.0(trans)			
			1.2(cis)			
		N-β-C	1.5(trans)			
			1.7(cis)			
		N-γ-C	2.4(trans)			
			2.3(cis)			
		N-δ-C	3.1(trans, cis)			

[a] Reference 58.

[b] 5.3 M, Reference 59.

[c] D_2O External lock.

have also been studied by measuring the ^{13}C and the quadrupolar relaxation times.[49,55-56]

Quantitative calculations of the diffusion tensors for asymmetric-top molecules have been carried out on trans-decalin and norbornane,[57] where symmetry now requires three diffusional parameters to diagonalize the diffusion tensor. Thus, ^{13}C $T_{1(DD)}$ data from carbons with different geometrical arrangements of the C-H vector relative to the principal axis of the molecule were required to solve the three simultaneous equations.

B. Methyl group rotation

Analysis of the internal reorientational effects upon dipolar relaxation have also been investigated. The methyl rotational barriers in some compounds[59] have been determined as shown in Table 2.

C. Anisotropic tumbling in monosubstituted benzenes

Levy et al.[47] have determined the anisotropic tumbling ratios of some monosubstituted benzenes as shown Table 3.

They found that T_1 for the para carbon is shorter than that for the meta and para carbons in all cases. This phenomenon results from anisotropic tumbling. The motional behavior of substituted benzenes can be used to facilitate resonance assignments. The ^{13}C T_1 values can also give a new view of solvent effects such as

Table 2. Methyl internal rotational barriers from ^{13}C dipolar relaxation rates

Molecule[g]	$Dx10^{-11}$ (sec^{-1})	$Rx10^{-11}$ (sec^{-1})	E_a (kcal/mole)
$(CH_3)_2SO$	0.35[h]	4.0[h]	2.2[a], 3.07[b], 2.87[c]
$(CH_3)_2CO$	1.6	29.9	0.92[a], 0.76[d], 0.78[c]
$(CH_3)CCl_3$	1.3	1.2	2.9[a], 2.91[c]
$(CH_3)_3C\text{-}Cl$	1.4	0.5	3.5[a], 4.3[c,e]
$(CH_3)COOCH_3$	1.4	49.4	0.67[a], 0.48[c]
$CH_3COO(CH_3)$	1.4	21.0	1.1[a], 1.19[c,f]

[a]Reference 57.

[b]Reference 60.

[c]Reference 61. Values represent gas phase data.

[d]Reference 62.

[e]Value for t-butyl fluoride.

[f]Value for OCH in methyl formate.

[g]The methyl group for which data are given is in parentheses.

[h]R is the tumbling rate (diffusion constant) for rotation of the methyl group about the C_{3V} axis and D is the diffusion constant for overall rotation of the molecules.

Table 3. Anisotropic tumbling in monosubstituted benzenes.[a]

Substituent	$T_{1(o,m)}/T_{1(p)}$	Approximate tumbling ratio (R/D)[b]	Reference
CH_3	1.3	2	47
$C(CH_3)_3$	1.8	3.5	47
C≡CH	1.7	3.2	47
Ph	1.8	3.5	47
C≡CPh	2.4	7	63
C≡CC≡CPh	4.9	17	63
NO_2	1.4	2.2	47
OH	1.5	2.5	47

[a] $T_{1(o,m)}$ is an average T_1 for ortho and meta carbons and $T_{1(p)}$ is for the para carbon.

[b] Tumbling ratio, R/D, where R is the tumbling rate for motion about the C_{2v} axis of the benzene ring and D is the diffusion constant for rotation about an axis perpendicular to C_{2v} in the plane (or for the overall molecular motion).

hydrogen bonding and strong solvation of organic ions. For example, when phenol is diluted with CCl_4, the phenol molecular aggregates begin to dissociate; this effect is reflected in the ^{13}C T_1 values of phenol by an increase in T_1 for the protonated ring carbons and a decrease in $T_{1(o,m)}/T_{1(p)}$.

EXPERIMENTAL

I. INSTRUMENTAL

A. ^{13}C NMR Spectrometer

A Varian CFT-20 high-resolution nuclear magnetic resonance spectrometer was used to obtain the ^{13}C spectra. The spectrometer is computer controlled. After initial set up procedures, data are accumulated, transformed and plotted by entering commands through the console keyboard. There are three resonance experiments involved in the observation of ^{13}C nuclear resonances: (1) The excitation and resonance detection of ^{2}D nuclei (lock channel), (2) The excitation and resonance detection of ^{13}C nuclei (observe channel), and (3) The excitation of ^{1}H nuclei (decouple channel). At a constant field of 18.7 kG, the resonance frequency of ^{2}D is 12.0 MHz, ^{13}C is 20 MHz, and ^{1}H is 80 MHz. All these frequencies are derived from a master oscillator (18 MHz) and are phase-locked to each other. The ^{13}C and ^{2}D frequencies generated in the spectrometer are not applied in a continuous wave, but transmitter and receiver are pulsed on and off to achieve optimum operating efficiency. The rate of pulsing is regulated by the computer and by the parameters entered.

The decoupler transmitter frequency may be applied either as a continuous wave or as a pulsed wave depending on the parameters entered. The power of the RF pulse is constant for the ^{13}C transmitter but may be varied by the operator for the ^{2}D and ^{1}H transmitters.

The CFT-20 is composed of separate magnet and operating consoles and a probe; all are connected by a harness containing various wires for signal generation, data transportation, and control of operational parameters.

The magnet console contains a 6" electromagnet with a self-contained power supply and cooling system. The magnet is further regulated by flux stabilizing circuits in the operating console which control and stabilize the magnetic field through pick-up and buck-out coils located around the poles. Shim coils, mounted on the poles caps, adjust the homogeneity of the magnetic field at the sample. Adjustment of the current through the shim coils is controlled with the homogeneity controls on the operating console.

The operating console contains all of the operating electronics including the Varian 620L-computer, the data displaying devices (X-Y plotter and oscilloscope), computer keyboard, and various controls for homogeneity adjustments, field stabilization, and decoupling.

The 12K computer controls most operations of the spectrometer by the use of CFT-20 T_1 program tape. This

tape uses 4096 words of computer memory, leaving 8192 words for data storage. The keyboard provides the operator/computer interface for entering commands and parameters. The alphanumeric oscilloscope, X-Y plotter, and optional printer provide the computer/operator interface for data and parameter display. An analog-to-digital converter (ADC) converts the electrical signal (analog) from parameters, commands, and data to the digital information for computer storage. Alternatively, a digital-to-analog converter (DAC) allows the stored digital information to be transmitted in analog form to the display devices mentioned above.

The computer has two modes of operation: the Executive mode in which it is performing an instruction or routine, and the Waiting mode in which it is waiting for an instruction. The programmed 4K consists of a series of routines for: 1) Control of accumulation of data, 2) Transformation of data by several methematical functions including Fourier transformation, phasing and integrating, 3) Transmission of data to several devices, 4) Referencing of data to internal standards, and 5) T_1 and NOE determination.

In order to select one of these operations or routines, the operator communicates with the computer via the keyboard in the operating console. The communication

consists of one and two letter mnemonics which may stand for either a command, a parameter, a flat or an interrupt.[79]

The temperature at the 8 mm sample tube may be varied from -80°C to +200°C by use of the NMR variable temperature accessory. The sample is placed in a temperature-controlled nitrogen gas stream which maintains the selected operating temperature at the sample. During operation below ambient temperature, the nitrogen gas is cooled by liquid nitrogen, then the gas is heated to the selected temperature by a heater in the probe. When operating at ambient temperature and above, the air flows directly into the probe and is heated to the selected temperature.

The ^{13}C NMR spectrometer functional block diagram is shown in Figure 7.

B. Calibration of Temperature for CFT-20 NMR Spectrometer

(1) Calibration of the temperature was accomplished by using the chemical shift thermometers, (A) TMS:CH_3I = 1:3, v/v, for -60°C to +20°C, and (B) Cyclooctane:CH_2I_2 = 1:5, v/v, for +20°C to +100°C.[64] Temperatures in the low temperature range were found from the expression

$$1/T = 0.0161165 - 0.000570057 \times \Delta\delta_{(TMS:CH_3I = 1:3,\ v/v)},$$

where $\Delta\delta_{(TMS:CH_3I = 1:3,\ v/v)}$ is the chemical shift difference between the ^{13}C chemical shifts of TMS and CH_3I at

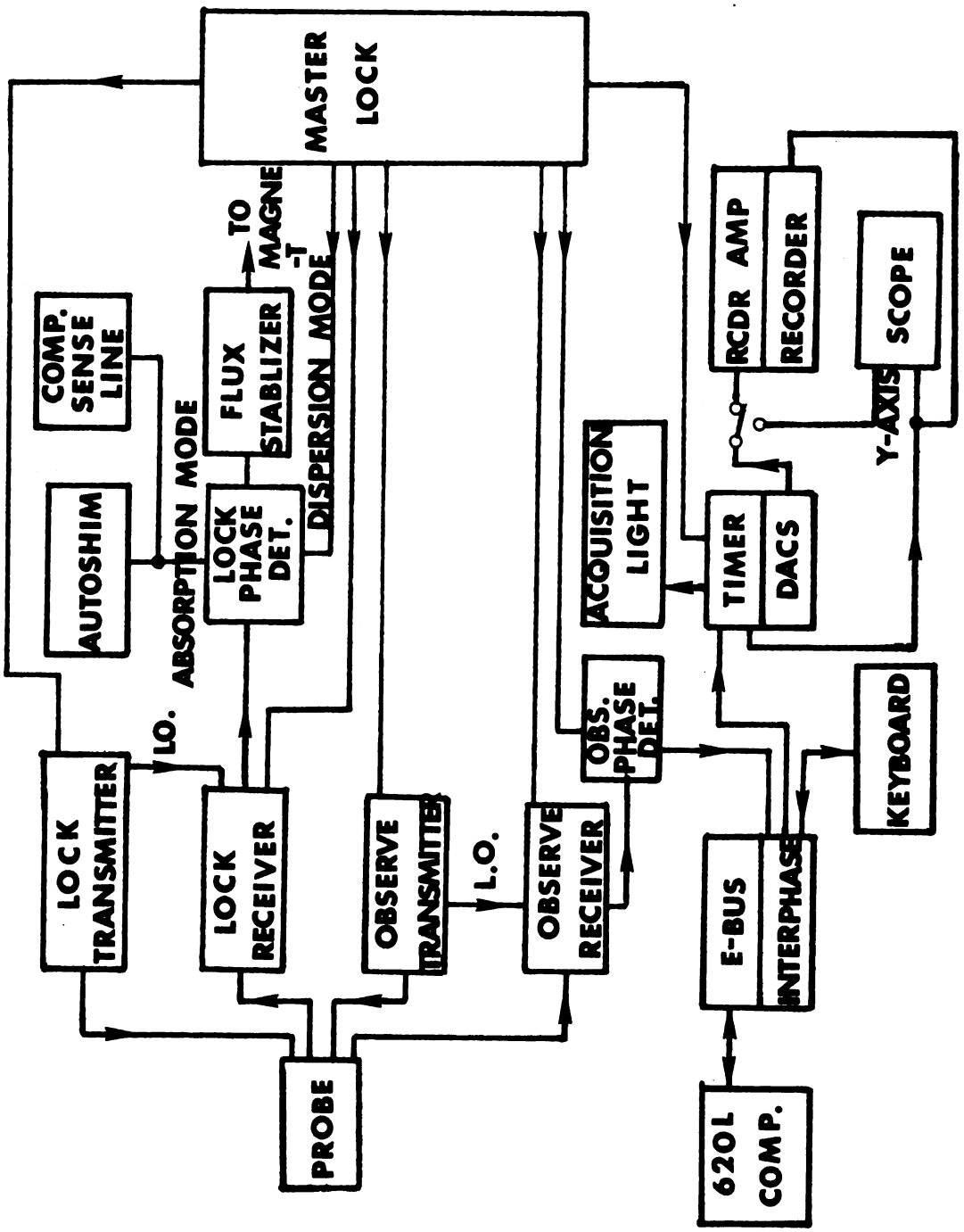

Figure 7. CFT-20 FUNCTIONAL BLOCK DIAGRAM.

20 MHz and T is the absolute temperature. In the high temperature range, +20°C to +100°C, the calibration equation is

$$1/T = 0.0220027 - 0.000223362 \times \Delta\delta_{(\text{cycoct.}:CH_2I_2 = 1:5,\ v/v)},$$

where $\Delta\delta_{(\text{cycoct}:CH_2I_2 = 1:5,\ v/v)}$ is the chemical shift difference between the ^{13}C chemical shifts in cyclooctane and CH_2I_2.

(2) In measuring the spin-lattice relaxation time, the spectral width used is sometimes smaller than the chemical shift difference of the chemical shift thermometers, so temperature measurement was accomplished by using a copper-constantan thermocouple to determine the temperature at the start and at the end of each experiment. It usually takes about 30 to 50 minutes to obtain temperature equilibrium in the probe. Temperature measurements were obtained by use of the set-up shown in Figure 8.

C. ^{13}C Spin-Lattice Relaxation Time Measurement

Four techniques are used with the 16 K CFT-20 T_1 program and these are summarized in the following paragraphs.

(1) The Inversion-Recovery Method

The inversion-recovery method[65] uses the pulse sequence (Figure 9)

$$-(PD - P1 - t - P2 - AT)_n- ,$$

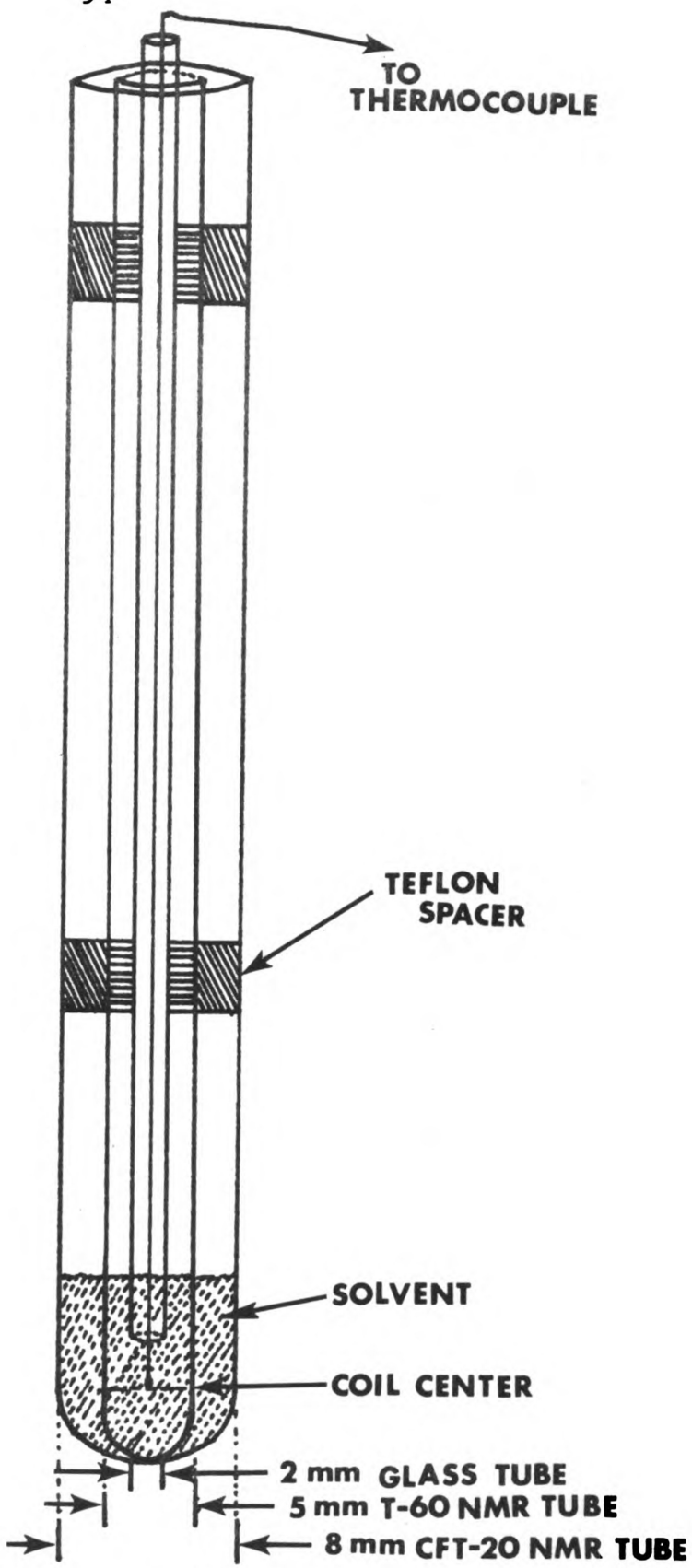

Figure 8. SET-UP FOR TEMPERATURE MEASUREMENT IN THE CFT-20 NMR SPECTROMETER.

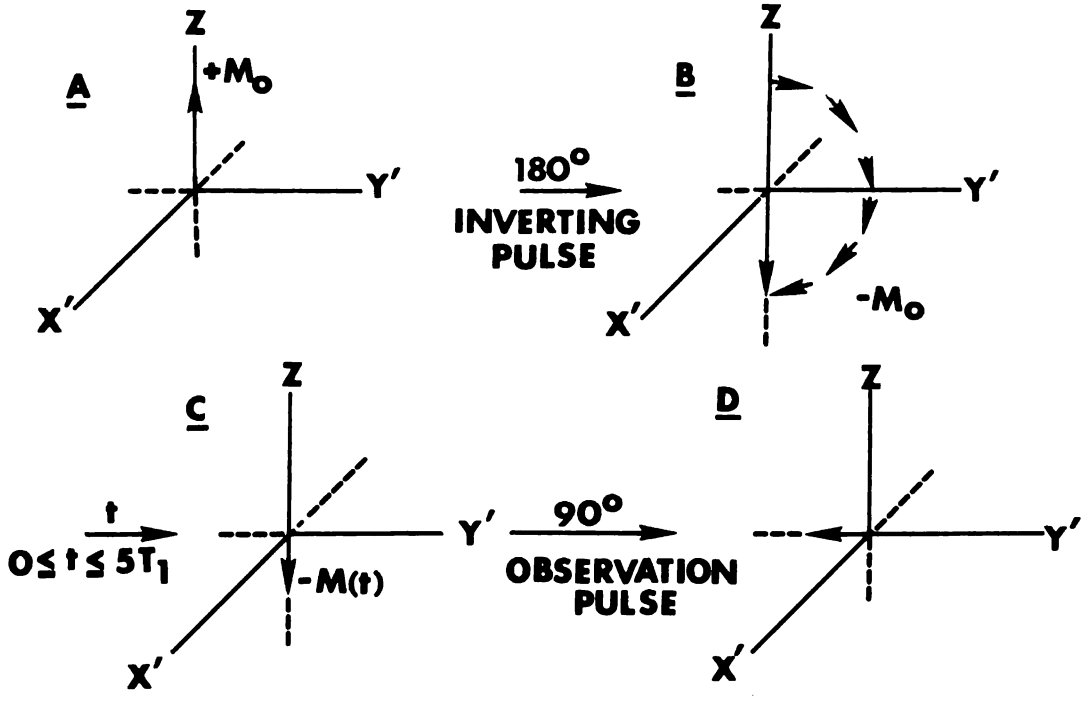

Figure 9. **INVERSION-RECOVERY SEQUENCE.**

where PD is the pulse delay time, P1 is the first RF pulse, t is a delay time which is experimentally varied, P2 is the RF pulse, AT is the acquisition time, and n is the number of times this sequence is repeated. In this method P1 is a 180° pulse and P2 is 90° pulse, PD should be at least greater than five times the longest T_1 value to be measured. In order to get more accurate T_1 values, the value of t is usually varied from 0 to $2T_1$.[66] The Bloch equation for the Z component of the magnetization vector is

$$\frac{dM_z(t)}{dt} = - \frac{[M_o - M_z(t)]}{T_1}$$

and integration of this equation will give

$$M_z(t) = M_o[1 - 2 \exp(-t/T_1)] \ .$$

Rearranging the above equation and taking the logarithm gives

$$\ln[M_o - M_z(t)] = \ln(2M_o) - t/T_1 \ .$$

A plot of $\ln[M_o - M_z(t)]$ versus t gives a line of slope $1/T_1$ (Figure 10).

(2) The Homospoil Sequence (or Saturation Recovery Sequence)

The homospoil sequence[67,68] uses the pulse sequence (Figure 11)

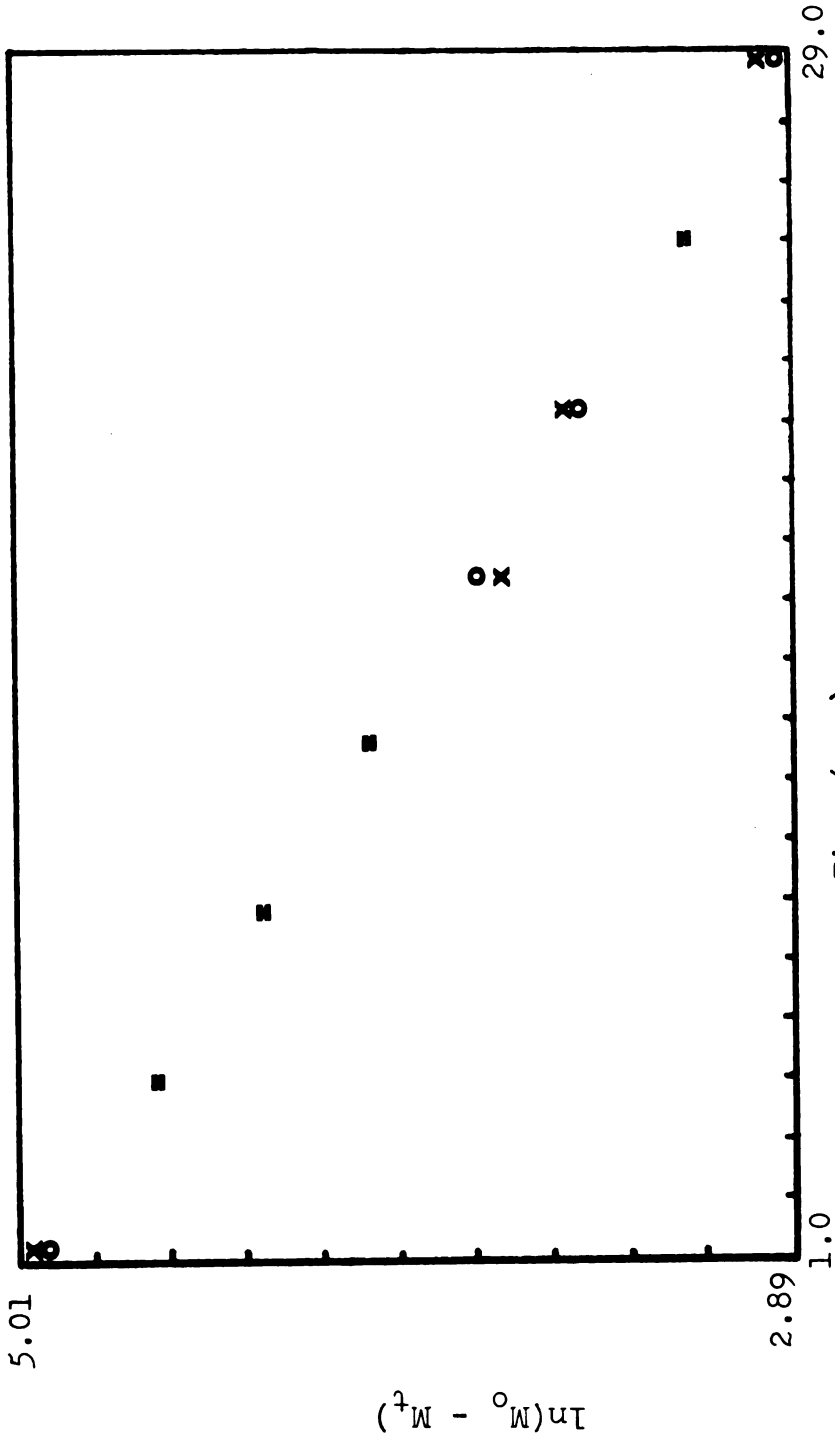

Figure 10. Computer fit of data for determining the ^{13}C T_1 of the trans-NCH_3 in N,N-dimethylformamide by the inversion-recovery method; x means an experimental point, o means a calculated point, = means that an experimental and calculated point are in the same delta x by delta y.

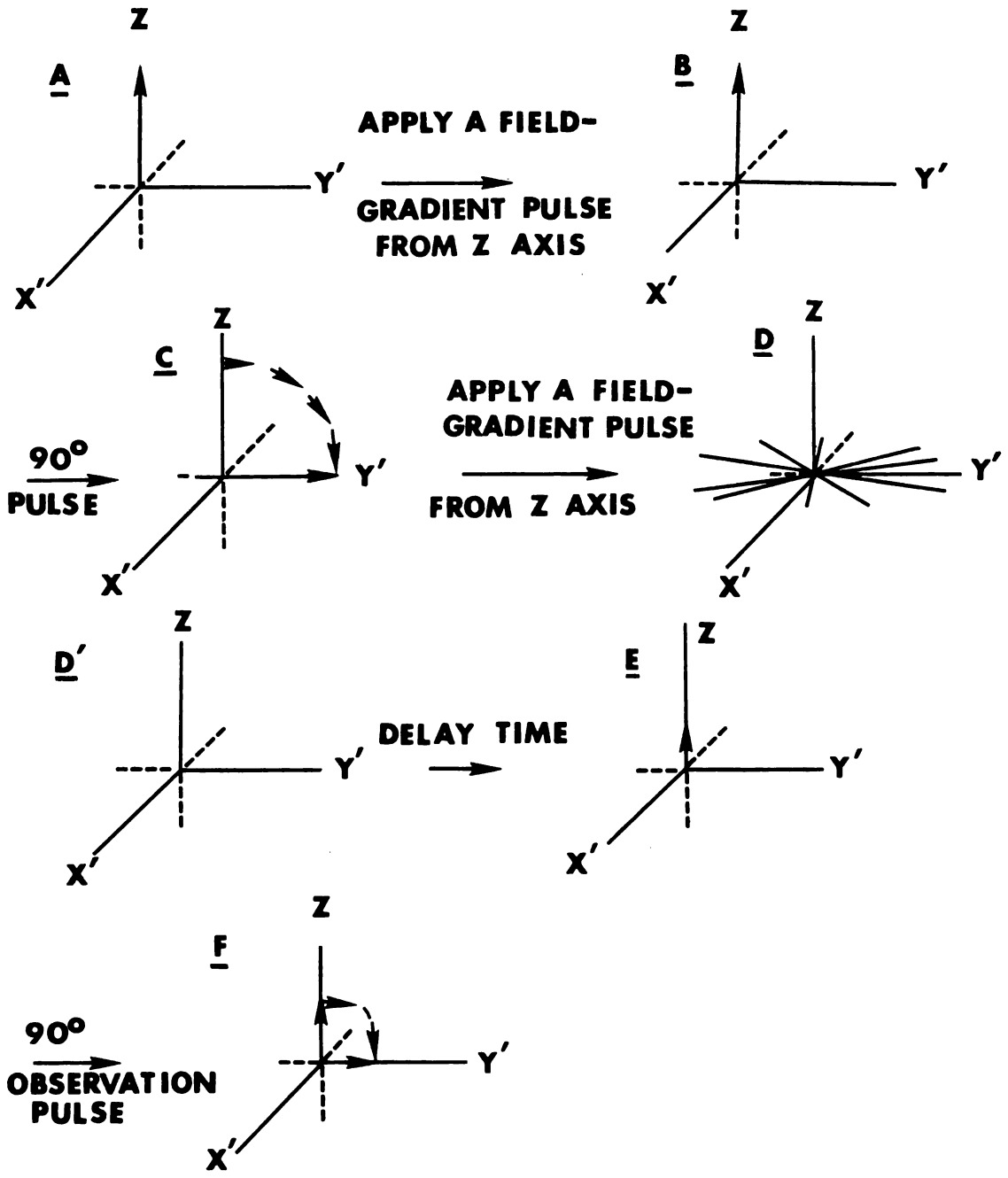

Figure 11. HOMOSPOIL PULSE SEQUENCE.

$$-(PD - HS - P1 - HS - t - P2 - AT)_n- \ ,$$

where HS is the homospoil pulse applied to the Z-axis shim coil and all other symbols are the same as those for the inversion-recovery method. In this sequence, PD is set equal to HS. For this sequence to work properly, it is essential that the net magnetization in the x'y' plane be zero. Using this method, there is no wait for the establishment of thermal equilibrium. Therefore, this sequence has the potential of being a very fast method for the determination of spin-lattice relaxation times. By using the equation $\ln[M_o - M_z(t)] = \ln(M_o) - t/T_1$, a semi-log plot similar to that used for the inversion-recovery data will yield the T_1 value.

(3) The Progressive Saturation Sequence

The progressive saturation sequence[69] uses the pulse sequence

$$-[P1 - (AT + t)]_n-$$

If the sample is subjected to a series of 90° pulses more frequently spaced than $3T_1$, the line intensities are detectably reduced by saturation. By studying line intensities as a function of the interval between the 90° pulses, T_1 can be extracted by use of the equation

$$\ln[M_o - M_z(t)] = \ln(M_o) - (AT + t)/T_1.$$

The main limitation of this sequence is that the smallest interval between pulses which can be chosen is limited by the data acquisition time.

(4) The variable-nutation-angle Sequence

This method[70] uses the pulse sequence

$$-(PD - HS - \overset{\text{variable nutation}}{\underset{\text{rf pulse}(\theta)}{\quad}} - AT)_n - ,$$

where the rf pulse angle is varied manually and n should be a big number (> 100). The spin system is subjected to rapid repetitive pulses of nutation angle θ, with a constant T between pulse cycles ($T = AT + PD$). A steady state of magnetization is achieved after about the first four pulses.[71] The resulting steady-state NMR signal obtained by Fourier transformation is lower in amplitude than the equilibrium value M_o, due to incomplete recovery of magnetization, as in the progressive saturation method. The amplitude of this steady-state signal is a function of T, θ, and T_1 as shown below

$$\frac{M_\theta}{\sin\theta} = e^{-T/T_1}\frac{M_\theta}{\tan\theta} + M_o(1 - e^{-T/T_1}) .$$

By systematically varying θ, the pulse nutation angle, in the range 20° to 110° at an appropriately chosen constant interval between pulse cycles, T_1 can be evaluated by a linear regression analysis. A linear plot of $M_\theta/\sin\theta$ versus $M_\theta/\tan\theta$ will give a line of slope equal to e^{-T/T_1}. Knowing T, the time interval between pulse cycles, T_1 can

be calculated. In an actual experiment, T is chosen approximately equal to $0.5T_1$.

Due to the restriction of data memory size (8K), spectral widths used were 500 Hz or 1000 Hz. When larger widths were required, separate experiments were run on each spectral region. For each experiment, 7-14 sets of measurements were taken. Some determinations were run two or three times. All the T_1 values were calculated by use of the KINFIT program[72] by using appropriate equations. Reproducibility of T_1 values was better than 5%. T_1 values of the C = O group carbon, and of the α-carbon of the N-N-butyl group in ^{15}N-n-butylformamide were determined by taking the average value of the pair of signals split by $J_{^{15}N-^{13}C}$. One set of the partially relaxed Fourier transform spectra (PRFT) obtained by application of each of the four methods is shown in Figures 12-16 and the results obtained by each method are given in Table 4.

(4) Nuclear Overhauser Effect Measurement

The NOE is determined by using the NOE-suppress procedure. Two pulse sequences are recorded, one with the decoupler on all the time, the other with the decoupler on only during the 90° pulse and acquisition time, as shown in Figure 17.

Due to the decoupling of protons during the acquisition time in both sequences, the final results are that there is only one peak for each carbon. This prevents

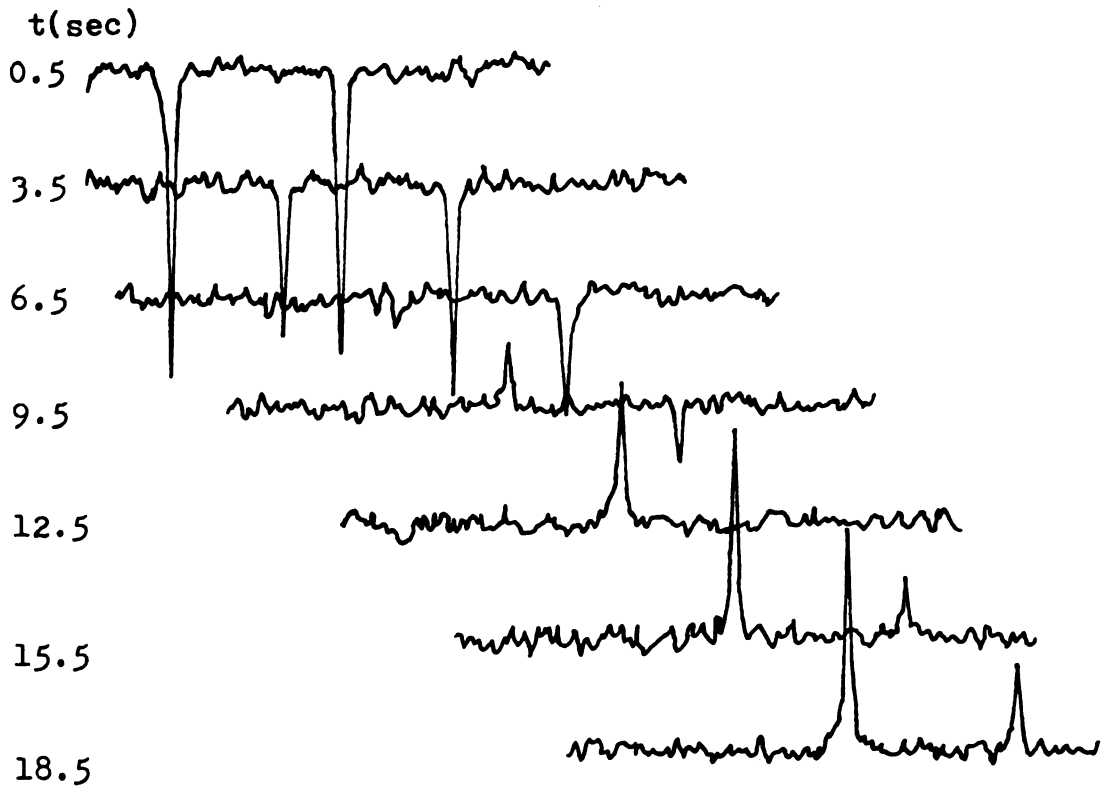

Figure 12. Measurement of T_1 for ^{13}C in the $-NCH_3$ groups of N,N-dimethylformamide by the inversion-recovery method.

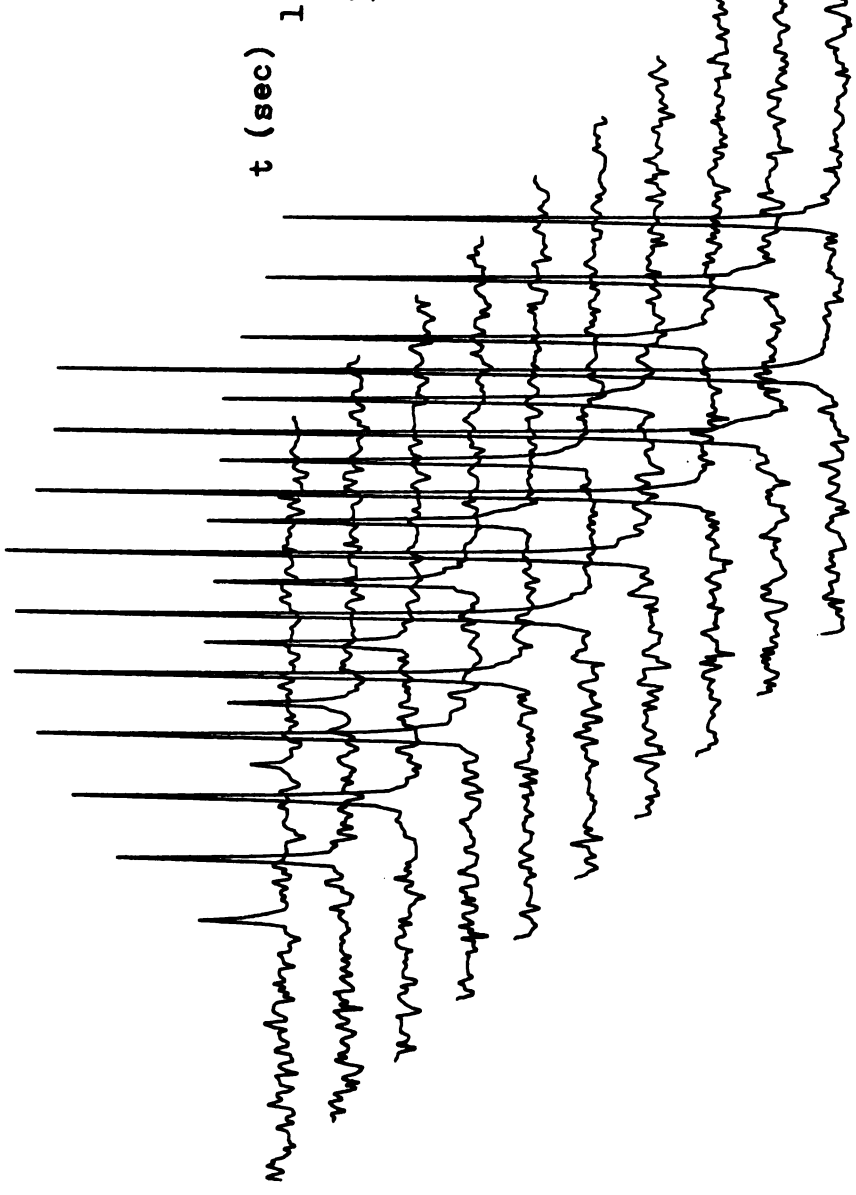

Figure 13. Measurement of ^{13}C T_1 values for the NCH_3 groups in N,N-dimethylformamide by the homospoil pulse sequence.

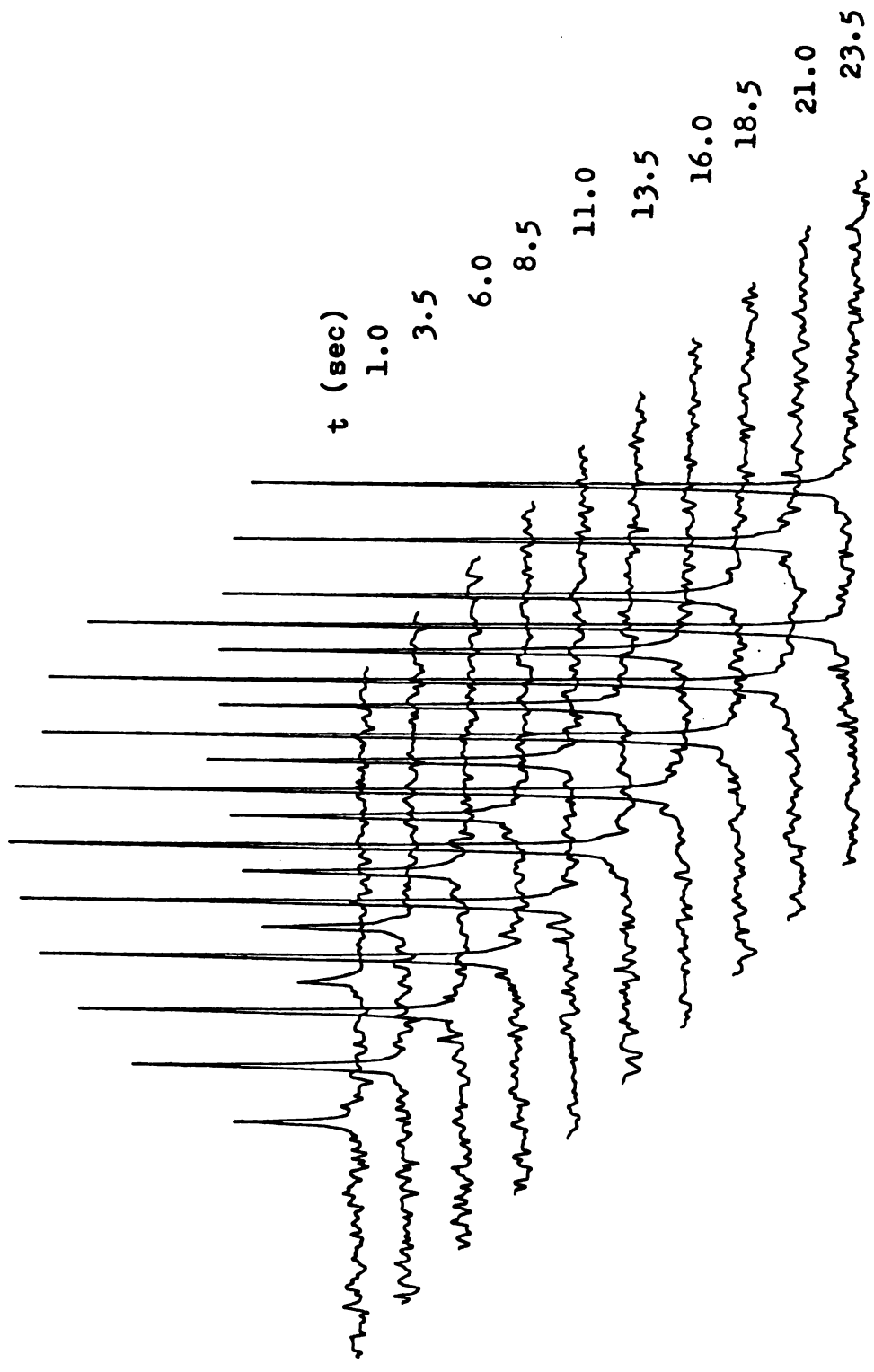

Figure 14. Determination of the ^{13}C T_1 relaxation times for the $N\underline{C}H_3$ groups in N,N-dimethylformamide by the progressive saturation method. Acquisition time is 0.512 sec.

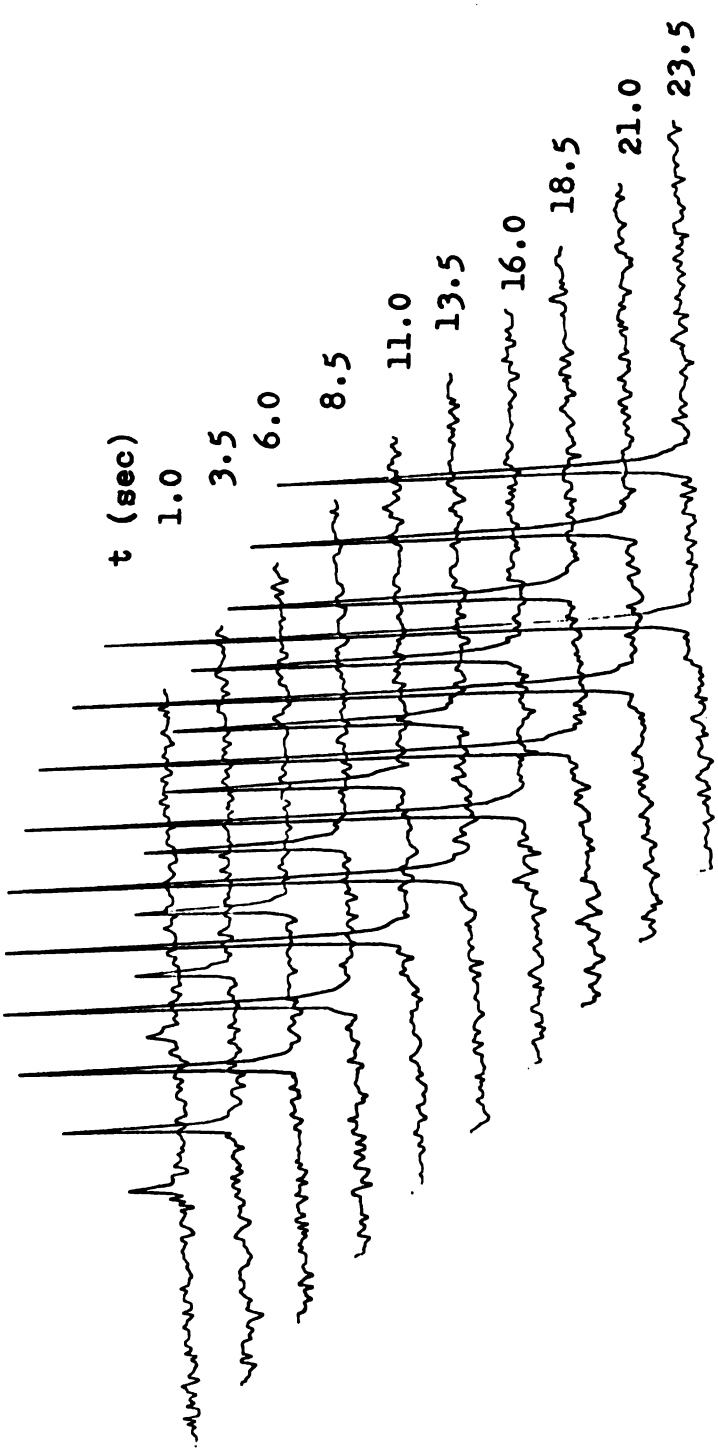

Figure 15. Determination of the ^{13}C T_1 relaxation times for the $N\underline{C}H_3$ groups in N,N-dimethylformamide by the -[90°- t - 90°- AT]- pulse sequence.

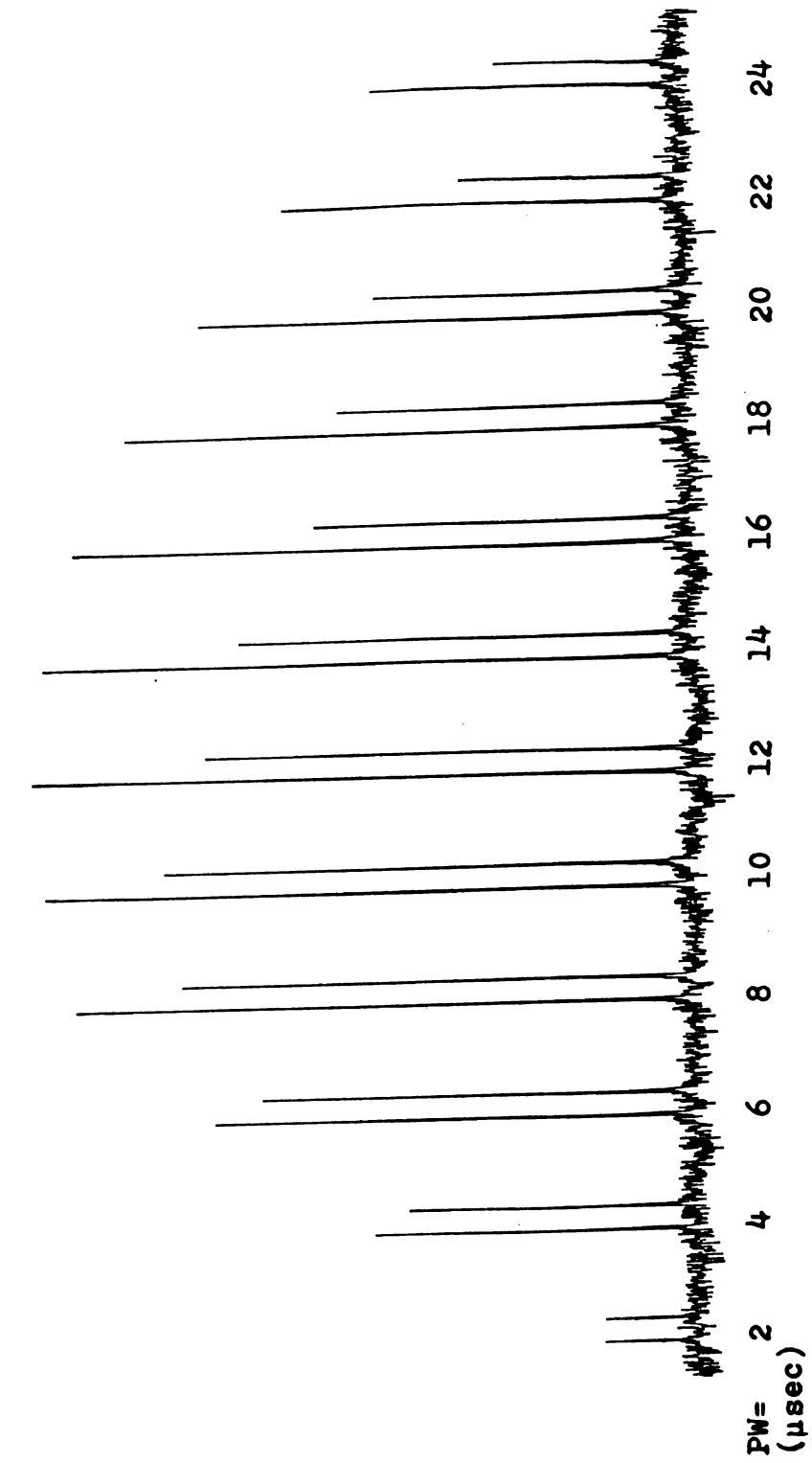

Figure 16. Measurement of the ^{13}C relaxation times T_1 for the N-CH_3 groups of N,N-dimethylformamide by the variable-nutation-angle method.

Table 4. Results of the determination of ^{13}C spin-lattice relaxation times in N,N-dimethylformamide by different methods.

Substituent	Inversion-Recovery[a] (sec)	Homospoil[b] sequence (sec)	Progressive[c] saturation (sec)	Saturation[d] Recovery without homospoil (sec)	Variable-nutation angle[e] (sec)
trans-NCH_3	11.64±0.34	11.92±0.29	10.39±0.20	12.59±0.15	10.16± .19
cis-NCH_3	19.38±0.49	18.80±0.25	16.48±0.39	19.45±0.32	18.99±1.13
C = 0	21.19±0.68	18.17±0.39	20.08±0.40	21.36±0.49	17.30±1.81

[a] -(PD - 180° - t - 90° - AT)$_n$-

[b] -(PD - HS - P1 - HS - t - P2 - AT)$_n$-

[c] -[P1 - (AT + t)]$_n$-

[d] -(P1 - t - P2 - AT)$_n$-

[e] -(PD - HS - variable nutation rf pulse(θ) - AT)$_n$-

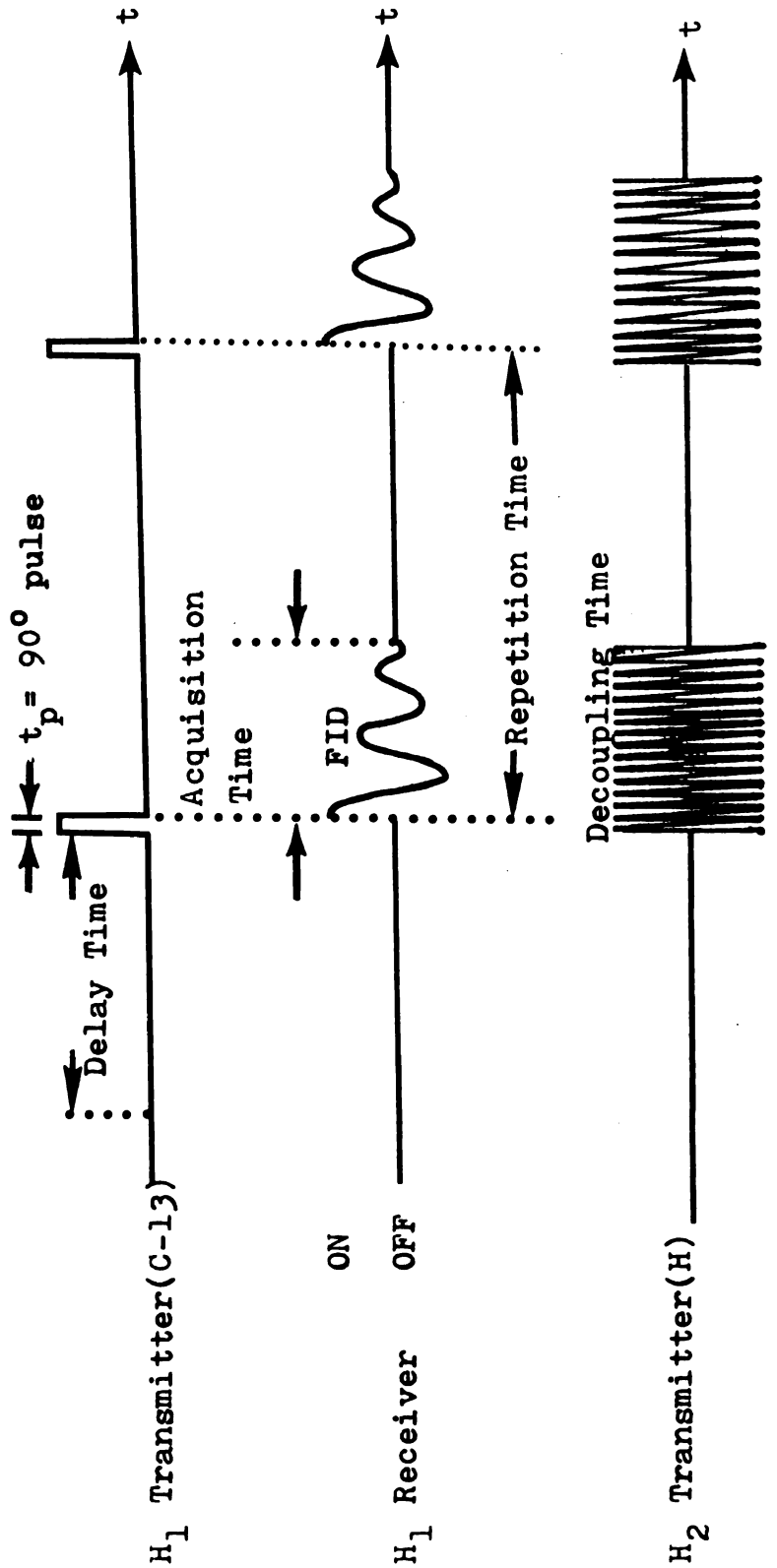

Figure 17. Nuclear Overhauser enhancement of coulped spectra by the gating technique.

overlap of the coupled spectra which might occur in some complicated spectra. In the NOE determination, the pulse delay should be ten to twelve times that of the longest relaxation time of the carbon being measured.[73,74] The NOE value is determined by the ratio of the integrals of the signals. The accuracy of the NOE values is ± 10 to 15%. One set of the PRFT spectra is shown in Figure 18.

D. ^{14}N NMR Spectrometer (DA-60)

A homemade DA-60 multinuclear NMR spectrometer was used to obtain the N-14 chemical shifts and T_1 values. The spectrometer consists of a modified NMR Specilities MP-1000 spectrometer, a Nicolet 1083 computer, and an interface built in this laboratory.

The frequency source of the RF unit is a 56.4 MHz crystal-controlled oscillator. By using the mixing network shown in Figure 19, any desired nuclear resonance frequency can be obtained by changing the synthesizer frequency instead of changing the magnetic field. The preamplifier and receiver were also standard components, tuned to 56.4 MHz.

In the T_1 measurements, the program Relax2 was used.[75] This employs the inversion-recovery sequence

$$-(6T_1 - P1 - nt - P2 - \text{measure signal})- .$$

Due to the quadrupole moment of N-14 (I = 1), most of the T_1 values are very short (0.1-0.001 sec), so this method

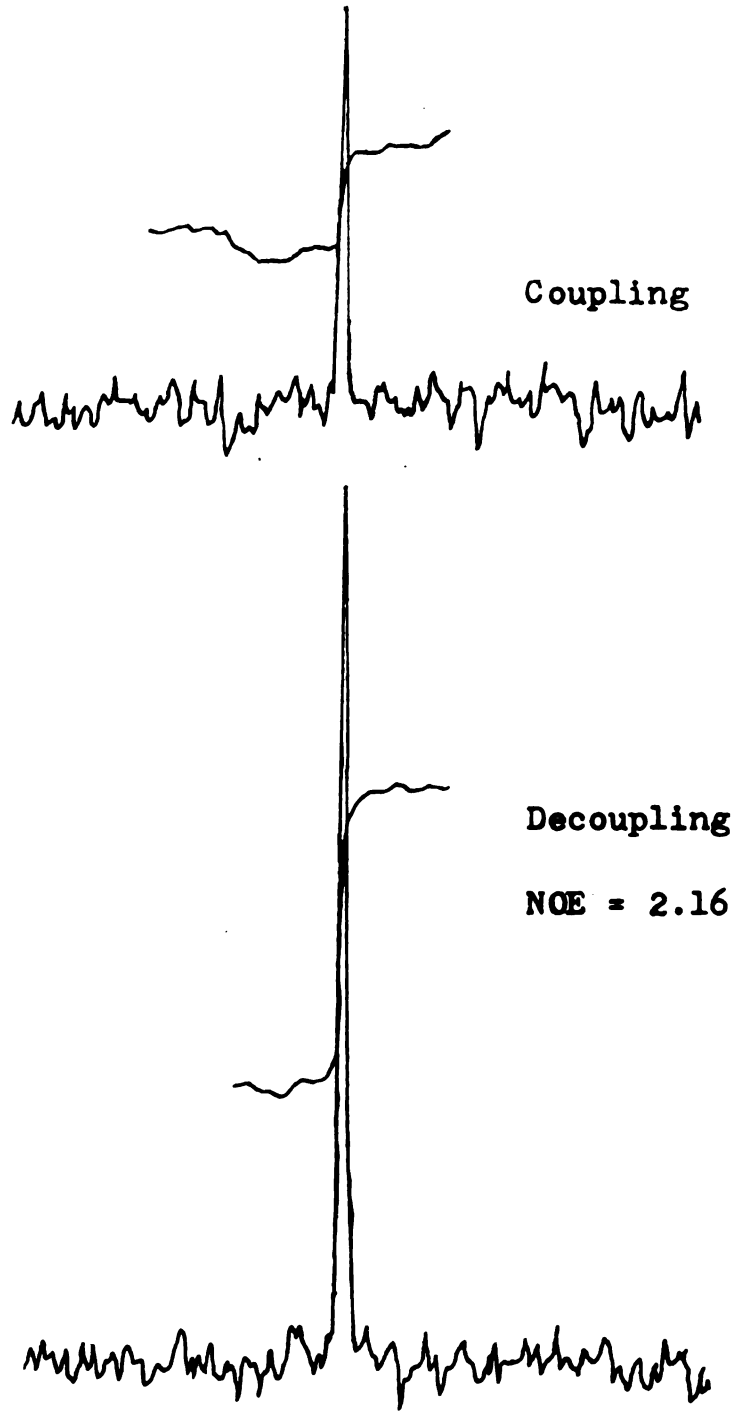

Figure 18. NOE measurement for ^{13}C of the C=O group in N,N-dimethyl-n-butyramide.

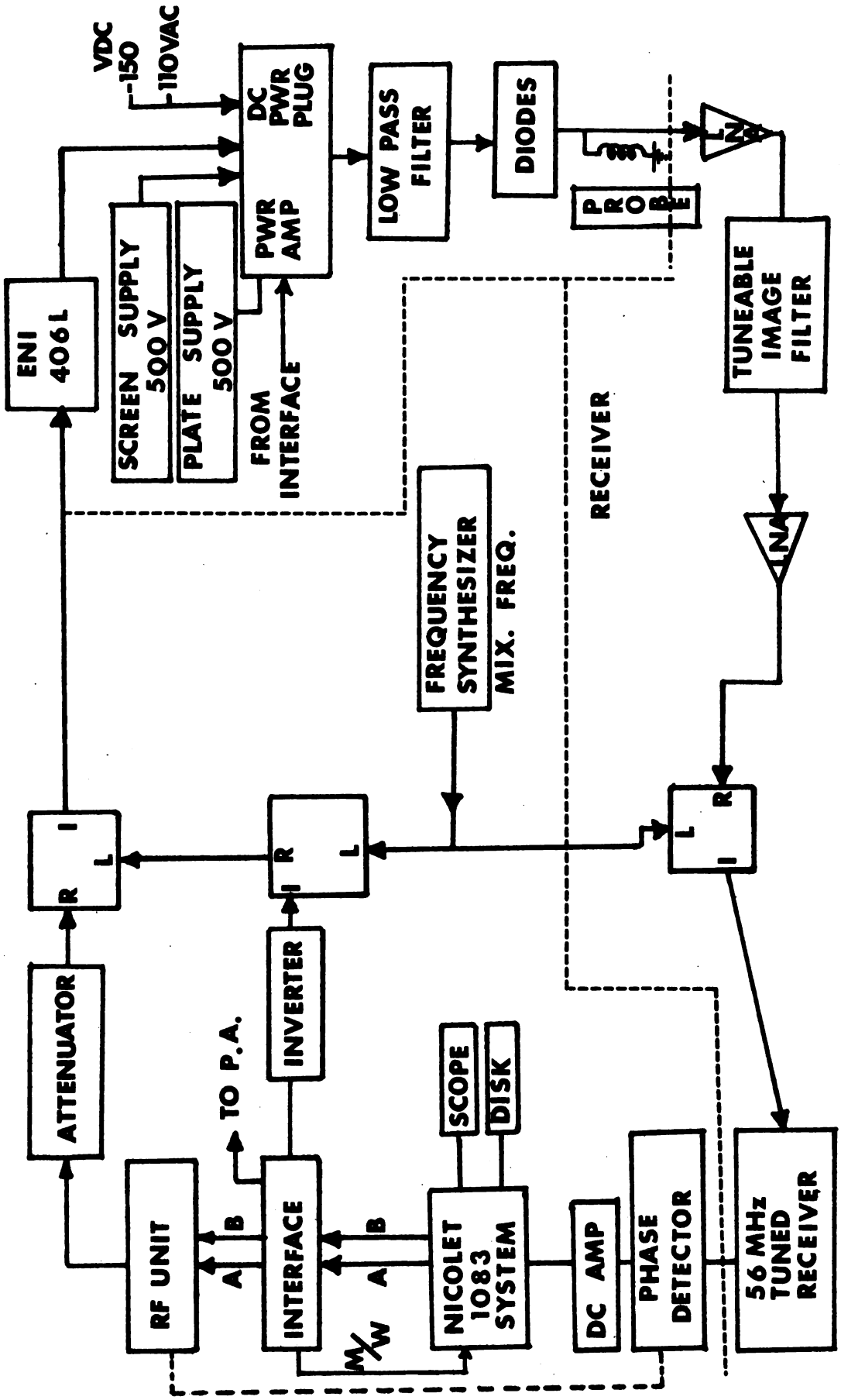

Figure 19. Block diagram of the DA-60 multi-nuclear NMR spectrometer.

is very useful. In this sequence, T_1 is the estimated spin-lattice relaxation time, entered via the teletype, P1, P2 are the 180° and 90° pulses, which are varied from 1-100 μsec in two ranges by three-turn potentiometers, n is an integer varied by the program from $1 \leq n \leq NP$, $t = 4T_1/NP$, and NP is the number of data points desired. Before the experiments, the probe and image filter were carefully tuned to the N-14 resonance frequency. The homogeneity was also maximized. The magnetic field is fixed by the proton external lock at the H_2O upfield sideband.

The temperature was regulated by the heater-sensor and V-4343 variable temperature controller and the temperature was determined using a copper-constantan thermocouple. During the experiments the temperature is very stable.

E. WH-180 NMR Spectrometer

A Bruker WH-180 multinuclear NMR spectrometer was used to obtain the ^{15}N and ^{17}O chemical shifts and the T_1 values of ^{17}O. The spectrometer consists of a superconducting solenoid, a Nicolet 1180 computer, and the necessary accessories such as plotter, disk system, etc. The spectrometer is computer controlled as are the CFT-20 and DA-60. Like the CFT-20, there are three RF frequencies involved in the observation of the desired nucleus (e.g., ^{15}N, ^{17}O): (1) The lock channel frequency-^2D(45 MHz), (2) The decouple channel frequency-^1H (180 MHz), and (3) The observe channel frequency-the resonance frequency for the observed nucleus

(e.g., ^{15}N or ^{17}O). The ^{15}N (or ^{17}O) and ^{2}D frequencies are pulsed on and off instead of using continuous waves. The observe or lock channel receiver is gated off during each pulse and then on for phase-sensitive detection between each pulse. This technique can (1) eliminate the leakage between transmitter and receiver, (2) eliminate the field modulation and unwanted side bands, (3) optimize lock and observe channel separately for improved sensitivity, and (4) improve efficiency in the decouple channel since power is not dissipated in side bands.

In order to improve the sensitivity for ^{15}N and ^{17}O spectra in our experiments, the phase-alternating-pulse-sequence (PAPS) and quadrature-detection techniques are employed. Conventional time-averaging techniques (e.g., those used on the CFT-20 and DA-60) normally will result in a reduction of incoherent noise but are ineffective in removing coherent noise. Such coherent noise usually comes from the computer, A/D converter and pulse generator. In the WH-180 NMR spectrometer, all such effects can be removed by the PAPS technique which employs phase alternation of the observe RF pulses (180° phase shift). The input signals produced will then have alternating phases (+ and -); the + signals are added to memory and the - signals are subtracted. In this manner the desired signal is coherently added, coherent (phase-independent) noise is cancelled out, and incoherent noise is

averaged. In addition, the PAPS technique can prevent spin-echoes, which occur when the pulse repetition rate is faster than the time required for complete free induction decay. This effect will produce phase and intensity distortion in transformed spectra.

In conventional FTNMR, a single phase-sensitive detector (such as used on the CFT-20 and DA-60) can only determine the magnitude of the frequency difference between the signal and the rf pulse, but not the sign of this difference, so the rf pulse is usually set at one end of the spectral region to avoid folding back of the resonance. This gives rise to two problems: (1) The power bandwidth of the rf pulse must be equal to twice the total spectral width (i.e., $\gamma H_1 > 2\pi(sw)$), and (2) Noise from the unused side of the carrier frequency is folded into the spectral region decreasing S/N by 40% (a factor of $\sqrt{2}$). Quadrature detection can solve both of these problems directly. The incoming sample signal is fed to two identical phase-sensitive detectors whose reference signals differ by 90°. The resultant audio signals are passed through identical low-pass filters digitized by a multiplexed A/D converter, and stored in separate data memory blocks. Quadrature Fourier transformation produces a real and imaginary spectrum in a manner analogous to normal detection with the exception that now + and - frequencies (relative to the RF carrier) can be carried. Thus, the rf pulse may be

applied at the center of the spectral region with the following advantages: (1) Audio filters can be optimized at half the bandwidth necessary for normal detection giving a S/N improvement of $\sqrt{2}$, or a time saving factor of 2, and (2) The transmitter power is now symmetrically distributed about the center of the spectral region, allowing twice the normal usable spectral width at any given pulse width. Since the rf power requirement varies as the square of the spectral width, quadrature techniques bring an effective gain of a factor 4. Switching from normal to quadrature detection is performed by a single program command.

In addition to the above two advanteges, the WH-180 can also perform a wide variety of experiments: (1) Homonuclear decoupling experiments for proton FTNMR, including cw and gated decoupling, and (2) Heteronuclear decoupling including broadband, single-frequency on- or off-resonance, gated decoupling and inverse-gated decoupling.

The Nicolet-1180 computer is incorporated into the spectrometer with the 8K program FTQUAD located in 400-17777 with starting address 1000; FTQUAD includes a sophisticated microprogram. The data memory available in this computer is 16K. With the FTQUAD program the following experiments can be carried out by entering the commands through the teletypewriter: (1) T_1 experiments, (2) NOE determination, (3) Solvent peak suppression and sample homodecoupling experiment, etc.

The FTQUAD program can also leave the central processor of the computer free to perform any calculations and output commands while the spectrometer performs the automated experiments.

In the ^{17}O T_1 experiments, the inversion-recovery procedure is used. The 180° pulse is about 72 μsec. Due to the quadrupole moment of ^{17}O (I = 3/2), the spin-lattice relaxation times of most amides are rather short so it is convenient to use this pulse sequence.

II. MATERIALS

A. Compound Preparation

All of the amides used in this work are listed in Table A (symmetrically N,N-disubstituted amides), Table B (unsymmetrically N,N-disubstituted amides) and Table C (N-monosubstituted amides). Boiling points are also given in these tables.

(1) N-Methyl-N-t-butylacetamide

In order to prepare this amide, N-methyl-N-t-butylamine was first prepared[76] by adding t-butylamine (73.14 g; 1.0 mole) to ice cold formic acid (160 g; 3.0 mole, 85% purity) in a three-neck flask. The three-neck flask was then equipped with a reflux condenser, a thermometer and a separatory addition funnel and the contents were stirred with a magnetic stirrer. The reaction mixture was brought to 50°C by means of a heating mantle. Formaldehyde solution (1.25 mole) was added dropwise (2 drops per

Table A. Physical properties of symmetrically N,N-disubstituted amides.

Amide	B.P (°C/mm)	Source
N,N-Dimethylformamide	31.5-34.0°/25 mm	A
N,N-Dimethylacetamide	44.0-45.0/3	B
N,N-Dimethylpropionamide	51.0-52.0/3	C
N,N-Dimethyl-n-butyramide	47.0-47.5/0.5	C
N,N-Dimethylacrylamide	46./3	D
N,N-Diethylformamide	177-179/760	E
N,N-Diethylacetamide	60.5-61.5/2	C
N,N-Diethylpropionamide	53.0-54.0/1.5	C
N,N-Diethyl-n-butyramide	61.0-64.0/1.0	C
N,N-Diethylacrylamide	106-107/?	D
N,N-Di-n-propylformamide	60.5-61.5/2.5	F
N,N-Diisopropylpropionamide	6.20-62.5/0.5	C
N,N-Diphenylacetamide	M.P. = 103°C	C
3-Methyl-2-phenylbutyramide	M.P. = 111-112°C	B

A: Fisher Scientific Company, Fair Lawn, N.J.

B: Aldrich Chemical Co., Milwaukee, Wisconsin.

C: Eastman Organic Chemicals, Rochester, New York.

D: The Borden Chemical Co., Philadelphia, Pennsylvania.

E: Matheson Coleman and Bell, East Rutherford, N.J.

F: Prepared by L.A. Laplanche in this laboratory.[78]

Table B. Physical properties of unsymmetrically N,N-disubstituted amides

Amide	B.P. (°C/mm)	Source
N-Methyl-N-n-butylformamide	55.0-56.0/1.0	A
N-Methyl-N-ethyltrimethylacetamide	62.0-65.0/5.0	A
N-Methyl-n-butyltrimethylacetamide	75.0-76.0/2.0	A
N-Methylformanilide	M.P. = 8-13 B.P. = 243-244	B
N-Ethylformanilide		C
N-methylacetanilide	M.P. = 102-104 B.P. = 258/731	B
N-Ethylacetanilide	M.P. = 55 B.P. = 266/712	B
N-n-Propylacetanilide	M.P. = 49 B.P. = 266/712	D
N-n-Butylacetanilide	M.P. = 24.5 B.P. = 281/760 or 141/10	C
N,N'-Diphenylurea	M.P. = 238 262/760 (decomp)	B
N-Methyl-N-t-butylacetamide	56.5/5	E

A: Prepared by L.A. Laplanche is this laboratory.

B: Eastman Organic Chemicals, Rochester, New York.

C: Aldrich Chemical Co., Milwaukee, Wisconsin.

D: City Chemical Corporation, New York, New York.

E: Prepared in this work as described in the text.

Table C. Physical properties of N-monosubstituted amides

Amide	B.P. (°C/mm)	Source
N-Methylformamide	56°/6 mm	A
N-Ethylformamide	63.2-64.0/1.0	A
N^{15}-n-Butylformamide	-	B
N^{14}-n-Butylformamide	81/5	C
N-t-Butylformamide	67/1.5	B
N-Methylacetamide	80.0-81.0/2 204-206/760	C
N-Ethylacetamide	80-83/1.5	A
N-Methylpropionamide	89.0-90.3/2.0	A
N-Ethylpropionamide	78.5-79.5/2.5	B
Thioacetamide	M.P. = 76-79	A

A: Eastman Organic Chemical Co., Rochester, New York.

B: Prepared by L.A. Laplanche in this laboratory (Reference 78).

C: Aldrich Chemical Co., Milwaukee, Wisconsin.

minute) through the separatory addition funnel to the mixture. The reaction mixture was then treated with 50 ml concentrated hydrochloric acid and 100 ml of liquid was distilled from the mixture. The residue was made strongly basic with a 50% NaOH solution and this mixture was fractionally distilled through a 3-foot Vigreux condenser. The purity of N-methyl-N-t-butylamine was checked by proton NMR until no impurity signal existed in the distillate.

A solution of NaOH (8g (0.2 mole) in 25 ml water) was added slowly to N-methyl-N-t-butylamine (17.4g) in 35 ml of water.[77] The resulting solution was cooled in an ice bath for about 3 hours, then 0.2 mole of acetyl chloride was added at such a rate as to keep the temperature below 10°C. The mixture was then allowed to come to room temperature and the amide layer was decanted. The aqueous layer was extracted three to four times with 12.5 ml portions of ether. The ether extract and the product were combined and dried over potassium carbonate and the ether was evaporated. The amide was collected by vacuum fractional distillation.

B. Purification of Compounds

(1) Liquid Amides

All the amides which were liquid at room temperatute were dehydrated by 4A molecular sieves (Matheson Coleman and Bell, Norwood, Ohio) for about 2-3 days then distilled under vacuum.

(2) N,N-Dimethylformamide

N,N-dimethylformamide was mixed with potassium metal (a small piece) to dehydrate it and then distilled under vacuum.

(3) Solid Amides

These were purified as follows:

N,N-Diphenylacetamide, N-methylacetanilide, N-ethylacetanilide, thioacetanilide and benzamide were recrystallized from hot distilled water three times and then dried under vacuum. The crystals were sublimed and collected on a cold finger. The pure crystals are colorless.

N-n-Propylacetanilide was recrystallized from a mixture of ligroin and ether (50:50,v/v) three times and then dried under vacuum. The pure crystals are colorless.

Thioacetamide was sumblimed onto a cold finger. The pure crystals are pale yellow.

C. Purification of Solvents

(1) Dimethylsulfoxide was dehydrated by 4A molecular sieves for about 1 week, then distilled under vacuum.

(2) Carbon tetrachloride was passed through an activated alumina column, then mixed with $KMnO_4$ (solid) and distilled at atmospheric pressure.

(3) Deuterated chloroform was purchased from Merck, Sharp and Dohme of Canada Limited, Montreal, Canada,in a sealed, coated vial and was not further purified.

(4) Deuterium oxide for NMR use was purchased from Mallinckrodt Chemical Co., St. Louis, Missouri, and was fractionally distilled.

(5) Cyclohexane was distilled over potassium and benzophenone to remove water and oxygen. All these procedures were carried out under nitrogen.

(6) Benzene was distilled over sodium, and benzophenone under nitrogen, to remove water and oxygen.

D. Sample preparation

(1) ^{13}C Samples

All the ^{13}C NMR chemical shifts, T_1 values and NOE data were obtained by placing the amides in a 5 mm inner tube with the deuterated compound in the outer tube as the external lock, as shown in Figure 20. The restriction at point A serves both to reduce diffusion at the liquid-vapor interface,[43] which provides an additional source of relaxation through spin-rotation in the vapor phase, and also to restrict the sample to the most homogeneous region of the magnetic field. The oxygen in the samples was removed by bubbling N_2 through the solutions for 1-5 minutes and then degassing by the freeze-pump-thaw cycle at least 5 times until no gas bubbles were visible. The samples were sealed off in vacuo.

The ^{13}C chemical shifts of the pure liquid amides were determined by using TMS as a reference in the outer tube, and $CDCl_3$ as an external lock. In order to measure

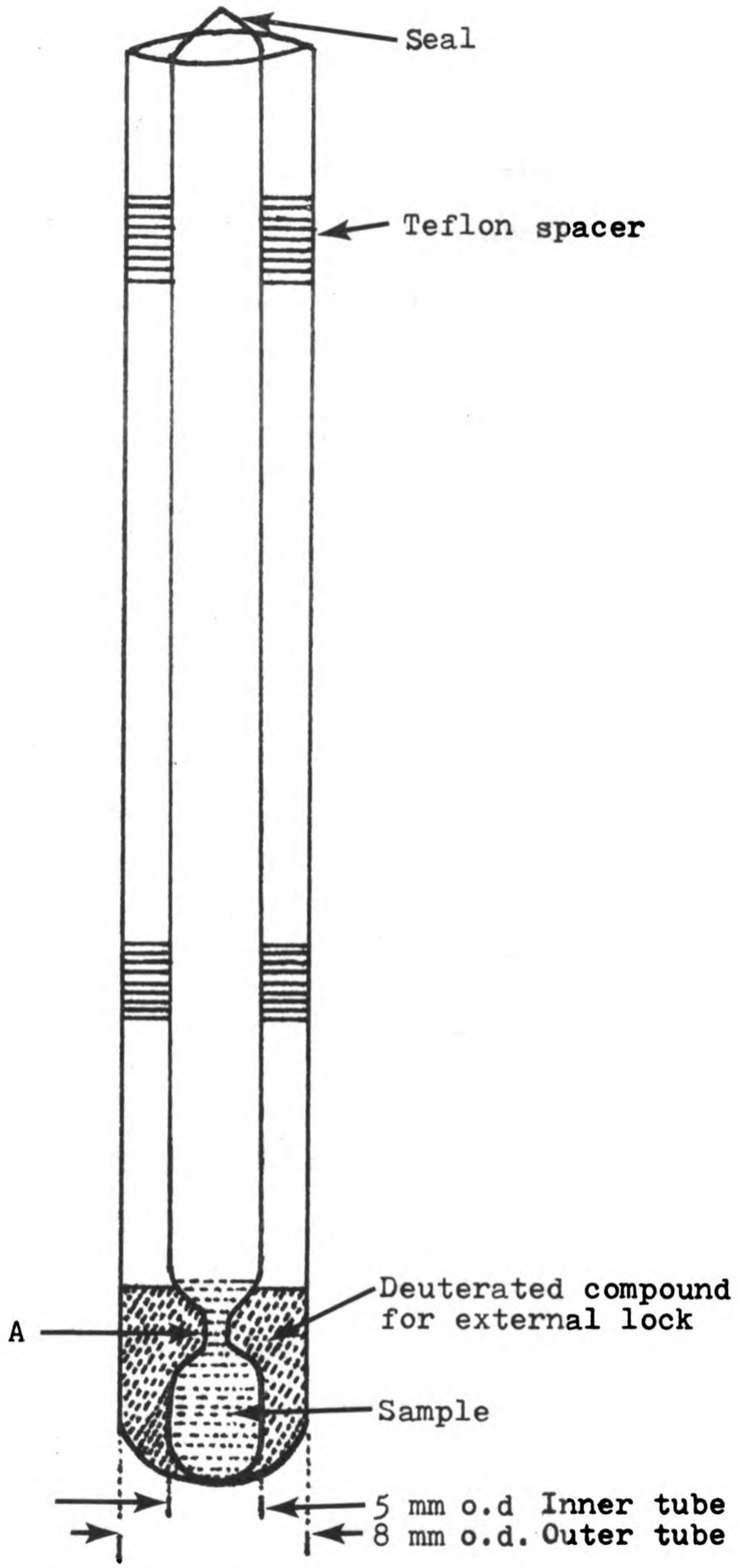

Figure 20. Sample tubes for CFT-20 NMR spectrometer.

the relative amounts of the trans and cis forms in some amides, a 90° pulse and a sufficient pulse delay were used. The corrections to the chemical shifts due to the bulk diamagnetic susceptibilities of the liquids are about 0.1-0.2 ppm. Since most of the susceptibilities of the amides were not known, this correction was neglected.

In the variable temperature studies of T_1 the external lock signals used were as follows:

$CDCl_3$ for low temperatures: 10°C to -60°C

D_2O for medium temperatures: 10°C to 80°C

DMSO-d_6 for high temperatures: 80°C to 150°C.

(2) ^{14}N Samples

The ^{14}N chemical shifts and T_1 values were determined in a 15 mm NMR tube. The samples were not degassed.

(3) ^{15}N and ^{17}O Samples

The ^{15}N and ^{17}O chemical shifts were determined in 25 mm and 20 mm NMR tubes, respectively. The samples were not degassed.

(4) ^{13}C Samples with added paramagnetic salt

To prepare the solutions containing different amounts of $MnCl_2$ in N,N-dimethylformamide, the $MnCl_2 \cdot 4H_2O$ had been dehydrated under vacuum, at a temperature over 300°C, for 3-4 days. Then the solutions were carefully prepared, degassed and sealed.

(5) ^{13}C Samples for solvent-effect measurements

In the preparation of samples of N,N-dimethylacetamide

in formamide, N.N-dimethylformamide in benzene, and N,N-dimethylacetamide in cyclohexane, the solutions were all degassed and sealed.

SECTION 1. NMR STUDIES OF MOLECULAR MOTION IN SYMMETRICALLY N,N-DISUBSTITUTED AMIDES

I. BACKGROUND

Amides have been studied more extensively by NMR spectroscopy than any other class of compounds. The substantial stimulus arises from the importance of the amide linkage in the peptide chain and in proteins.

For the last twenty years or so, most of the NMR studies of the amides have been concerned with determination of the energy barrier for rotation about the central C-N bond and its relationship to the C-N partial double-bond character. However, only a few papers have been reported concerning investigation of the overall molecular motion in amides [39,54,58,59,80,81]. The difficulties arose from the complicated molecular motion in amides, including overall anisotropic molecular reorientation, internal rotation, and segmental motion.

Several studies of anisotropic molecular motion using quadrupolar relaxation have been made[82,83]. Nuclei with spin I > 1/2 will possess an electric quadrupole moment, which can be relaxed by the interaction of the quadrupole moment with the molecular electric field gradient at the nucleus. The electric field gradient at the nucleus results from the distribution of electrons in the

molecule and fluctuates in orientation in the space-fixed axis system owing to molecular tumbling. Translational motion does not affect the orientation or magnitude of the electric field gradient at the nucleus and thus does not contribute to the relaxation. Furthermore,the quadrupole interaction is so large that it is usually the dominant relaxation mechanism. The complication of including several mechanisms for relaxation, and accounting for relative translation, in an expression for the relaxation time can thus be neatly avoided. By using quadrupolar relaxation, Huntress et al.[39,54], have studied the anisotropic molecular motion of N,N-dimethylformamide in the liquid. However, some disadvantages have arisen, since most of the quadrupolar nuclei have very low natural abundance and their NMR linewidths are very broad. As a result, enriching of the isotope is necessary in some cases and the measurement of T_1 by pulse sequences is more difficult due to the broad signals.

Since natural abundance ^{13}C NMR spectra have become available, there are several advantages to using ^{13}C NMR to investigate the molecular motions: (1) The intermolecular interactions can usually be neglected since the carbons are in the backbone of the organic molecules, (2) The main relaxation mechanism for ^{13}C is the dipole-dipole interaction, which can be separated from other mechanisms by measurement of the NOE effect,and (3) T_1 data for several

carbons in the molecule can be determined simultaneously.

In 1962, Woessner[40] developed an expression for T_1 in a symmetric-top molecule with no internal rotation in terms of the two unique parameters $D_{||}$ and $D_{\perp}$. These specify, respectively, the rotational diffusion about the C_3 axis and about the two perpendicular axes perpendicular to C_3:

$$\frac{1}{T_{1(DD)}} = \frac{n_S \hbar^2 \gamma_I^2 \gamma_S^2}{r_{IS}^6} \left(\frac{A}{6D_{\perp}} + \frac{B}{5D_{\perp} + D_{||}} + \frac{C}{2D_{\perp} + 4D_{||}}\right). \quad (132)$$

Here A,B, and C are geometrical constants

$$A = \frac{1}{4}(3\ell^2 - 1)^2$$

$$B = 3\ell^2(1 - \ell^2)$$

$$C = \frac{3}{4}(\ell^2 - 1)^2 ,$$

ℓ is the direction cosine of the angle between the C-H vector and the C_{3v} axis, γ_I and γ_S are the gyromagnetic ratios of nuclei I and S, n_S is the number of S nuclei bonded to I, r_{IS} is the distance between I and S, and $\hbar$ is Planck's constant divided by 2π.

Treatment of internal rotation by a methyl group attached to a rigid symmetric-top molecule has also been developed by Woessner et al.[84] giving

$$\frac{1}{T_{1(DD)}} = \frac{n_S \hbar^2 \gamma_I^2 \gamma_S^2}{r_{IS}^6} \left(\frac{A_1}{6D_{\perp}} + \frac{A_2 + A_3}{6D_{\perp} + R} + \frac{B_1}{5D_{\perp} + D_{||}} + \frac{B_2 + B_3}{5D_{\perp} + D_{||} + R} + \frac{C_1}{2D_{\perp} + 4D_{||}} + \frac{C_2 + C_3}{2D_{\perp} + 4D_{||} + R}\right). \quad (133)$$

In this equation

$$A_1 = \frac{1}{8}(1 - 3\cos^2\alpha)^2(1 - 3\cos^2\Delta)^2$$

$$A_2 + A_3 = \frac{9}{16}(\sin^2 2\alpha)(\sin^2 2\Delta) + \frac{9}{16}(\sin^4\Delta)(\sin^4\alpha)$$

$$B_1 = \frac{3}{8}(\sin^2 2\alpha)(3\cos^2\Delta - 1)^2$$

$$B_2 + B_3 = \frac{3}{4}(\cos^2 2\alpha + \cos^2\alpha)(\sin^2 2\Delta) + \frac{3}{4}(\sin^2\alpha + \frac{1}{4}\sin^2 2\alpha)\sin^4\Delta$$

$$C_1 = \frac{3}{8}(3\cos^2\Delta - 1)^2\sin^4\alpha$$

$$C_2 + C_3 = \frac{3}{16}[(1 + \cos^2\alpha)^2 + 4\cos^2\alpha]\sin^4\Delta + \frac{3}{4}(\sin^2\alpha + \frac{1}{4}\sin^2 2\alpha)(\sin^2 2\Delta),$$

where Δ is the angle between the C-H vector and the internal rotation axis, α is the angle between the internal rotation axis and the symmetry axis of the ellipsoidal molecule (as shown in Figure 21), R is the internal rotation rate of methyl group, and all the other symbols have the same meaning as in Equation (132). However, the expression for an internal top attached to a completely asymmetric rigid molecule has not been developed yet.

The symmetric-top formulation, Equation (132), for dipole-dipole spin relaxation has already received attention in ^{13}C studies[49,50,52,85]; however, Equation (133) for a methyl group attached to an ellipsoidal tumbler has not yet been utilized to interpret ^{13}C relaxation data. To be precisely applicable, this formulation requires that the D_{2h} symmetry group of the diffusion ellipsoid holds and that

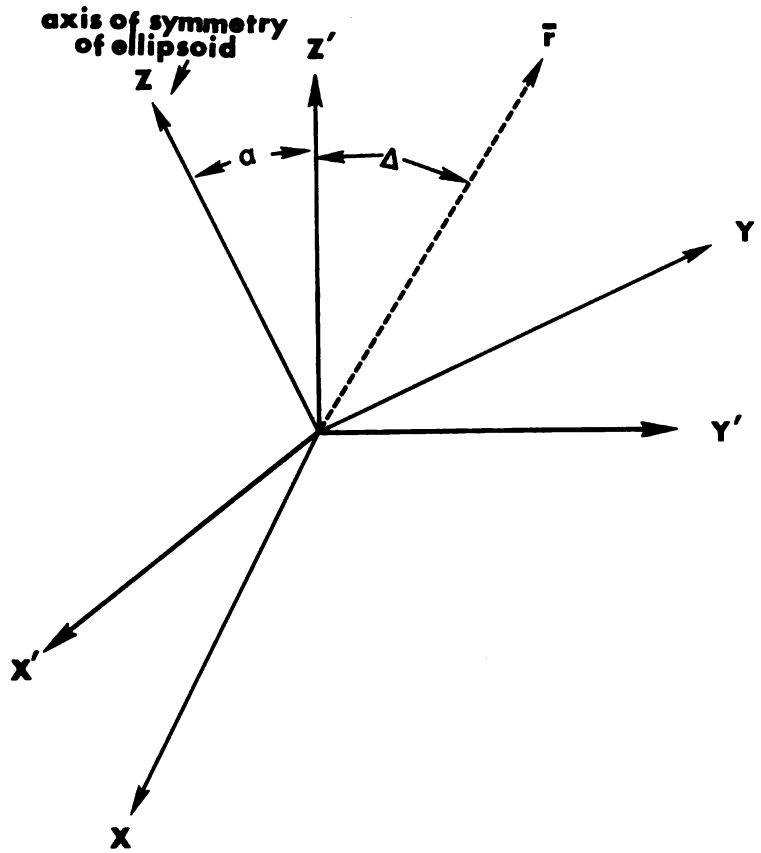

Figure 21. Coordinates for the orientation of the relaxation vector $\bar{r}$ in the diffusion ellipsoid. X, Y, and Z are the principal axes of the ellipsoid while X', Y', and Z' are the internal rotation axes, α is the angle between the Z and Z' axes, and Δ is the angle between the $\bar{r}$ vector and Z' axis.

the molecule possesses three uniquely different carbon atoms with attached protons whose C-H vectors manifest linearly independent sets of directional cosines. Such conditions allow diagonalization of the rotational diffusional tensor and provide sufficient data to specify its three diagonal components. Unfortunately, these conditions are so restrictive as to eliminate any extensive application of the theory, and, therefore, we have used the equations to give an approximate treatment of molecules with slightly lower symmetry.

Levy et al.[57,63,86-88] have utilized the symmetric-top equation for planar molecules, such as substituted benzenes, and have estimated the approximate tumbling ratio for the benzene ring rotating about the preferred rotation axis and about the other two perpendicular axes. In their systems, the molecules are treated as being axially symmetrical, although all the nuclei in the benzene ring are in one plane. Most of the macromolecules in proteins may also treated as ellipsoids (as shown in Figure 22).

Since amides are planar in the ground state, due to the C-N partial double-bond character, and their properties are like proteins, an ellipsoidal molecular model may also be assumed if a preferred rotation axis in the molecular plane can be found in the amides.

Equation (133), treating the methyl group relaxation in an ellipsoidal molecule, has never been utilized

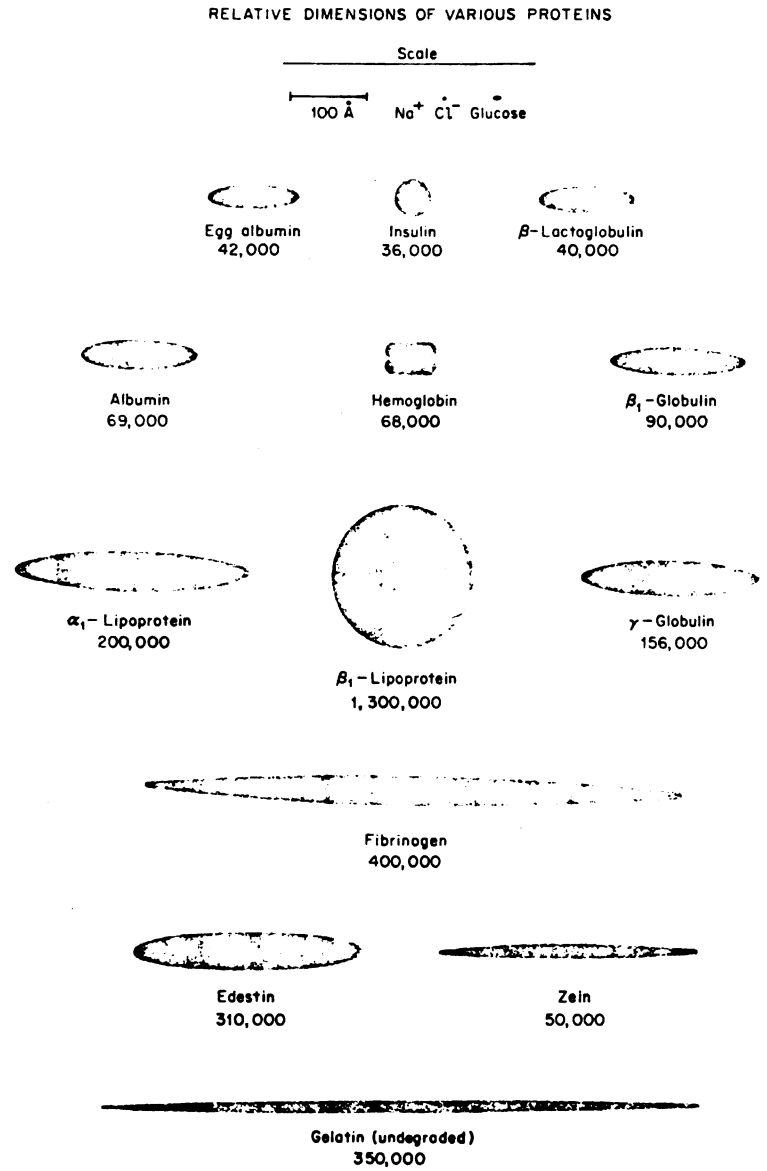

Figure 22. Estimated dimensions of various protein molecules as seen in projection. Most of the proteins are represented as ellipsoids of revolution. β-lipoprotein is a sphere [J. L. Oncley, Harvard University]. The molecular weight M_w is given under each name.

since it was published. In order to apply Equation (133) to the amides, an ellipsoidal molecular model should be assumed, and to further simplify the problem, the condition $R >> D_{||}, D_{\perp}$ is assumed. We also define $\rho = \frac{D_{||}}{D_{\perp}}$, so that Equation (133) can be reduced to

$$\frac{1}{T_{1(DD)}} = \frac{n_S \hbar^2 \gamma_I^2 \gamma_S^2}{r_{SI}^6} \cdot \frac{1}{D_{\perp}} \left(\frac{A_1}{6} + \frac{B_1}{5+\rho} + \frac{C_1}{2+4\rho}\right) . \qquad (134)$$

If there are two methyl groups whose C_{3v} axes make different angles with the preferred rotation axis, then the tumbling ratio for rotation around the preferred rotation axis relative to rotation about the perpendicular axis can be obtained from the ratio of their relaxation rates, as shown by the following equation:

$$\frac{\left(\frac{1}{T_{1(DD)}}\right)_a}{\left(\frac{1}{T_{1(DD)}}\right)_b} = \frac{\left(\frac{A_{1a}}{6} + \frac{B_{1a}}{5+\rho} + \frac{C_{1a}}{2+4\rho}\right)}{\left(\frac{A_{1b}}{6} + \frac{B_{1b}}{5+\rho} + \frac{C_{1b}}{2+4\rho}\right)} , \qquad (135)$$

where subscripts a and b denote the methyl groups in the a and b positions and A_{1a}, B_{1a}, C_{1a}, A_{1b}, B_{1b}, and C_{1b} are all defined as in Equation (133).

The effect of the motional anisotropy resulting from the shape of the molecule, approximated as an axially symmetrical ellipsoid, has been given by Woessner[40], who compared the relaxation rates corresponding to rotation about the principal axes of an ellipsoid to that for a

sphere of the same volume (Figure 23). It can be seen from Figure 23 that in an ellipsoidal molecule with $\rho = b/a < 1$, the C-H vector having a larger angle with the principal symmetry axis of the ellipsoid will have a smaller relaxation rate. This effect is especially enhanced in a rod-shaped molecule ($\rho << 1$), as shown in the left part of Figure 23.

II. RESULTS

A. Studies of the anisotropic molecular motion in N,N-dimethylamides by an approximate ellipsoidal model

Table 5 shows the ^{13}C chemical shifts, spin-lattice relaxation times T_1, nuclear Overhauser enhancements NOE, dipolar relaxation times $T_{1(DD)}$, effective correlation times τ_c, and the relaxation times due to other mechanisms $T_{1(O)}$ for several N,N-dimethylamides.

The different ^{13}C relaxation times for the trans- and cis-NCH_3 group carbons, relative to that for the C = O group, indicate that the overall molecular reorientation of the N,N-dimethylamides is anisotropic. This anisotropic effect is especially important in N,N-dimethylformamide, as compared with other N,N-dimethylamides, as shown in Figure 24. To describe this anisotropic motion, we will assume that there are two axes in the molecular plane, one the preferred rotation axis, as shown in Figure 25 and 26, the other perpendicular to this preferred rotation axis but still in the molecular plane. The third axis is perpendicular to the molecular plane, and

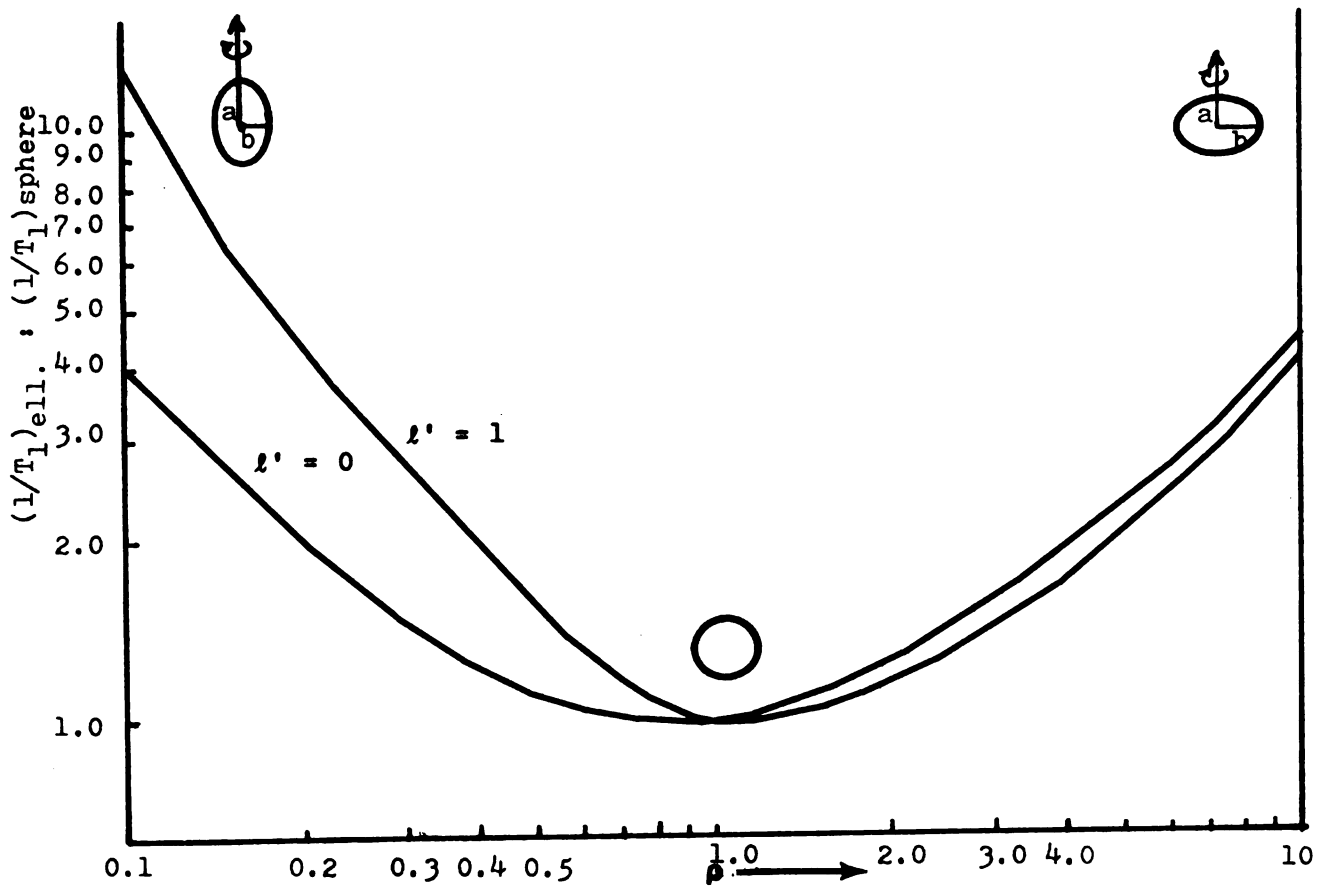

Figure 23. The relaxation in an axially symmetric ellipsoid compared to that in a sphere of the same volume as a function of the axial ratio ρ = b/a for particles obeying the Stokes approximation (evaluated at $\ell' = 0$ and $\ell' = 1$, where ℓ' is the direction cosine of the angle between the internuclear vector and the ellipsoid symmetry axis).

Table 5. ^{13}C Chemical shifts, spin-lattice relaxation times (T_1), and nuclear Overhauser enhancements (NOE), of several N,N-dimethylamides.*

Compound	Substituent	Chemical Shift (ppm)	T_1 (sec)	NOE	$T_{1(DD)}$ sec	$T_{1(O)}$ sec	$\tau_c \times 10^{12}$ sec
(A)							
N,N-dimethyl formamide	N-methyl(t)	35.09	11.64 ± 0.34	2.67	13.86	72.67	1.06
	N-methyl(c)	29.99	19.38 ± 0.49	2.35	28.54	60.39	0.52
	C = O	161.88	21.19 ± 0.68	2.67	25.22	132.47	1.75
(B)							
N,N-dimethyl acetamide	N-methyl(t)	37.25	13.37 ± 0.19	2.21	21.97	34.16	0.67
	N-methyl(c)	34.19	14.28 ± 0.46	2.31	21.67	41.87	0.68
	Carbonyl-CH_3	20.62	10.79 ± 0.29	2.67	12.85	67.45	1.14
	C = O	170.53	63.89 ± 2.70	2.04	122.23	133.98	-
(C)							
N,N-dimethyl propionamide	N-methyl(t)	36.43	14.40 ± 0.68	2.06	27.01	30.85	0.54
	N-methyl(c)	34.52	12.66 ± 0.60	2.24	20.30	33.65	0.72
	Carbonyl-sub -α-C**	25.89	5.96 ± 0.15	2.94	6.11	> 200	3.61
	Carbonyl-sub -β-C	8.84	6.61 ± 0.12	2.75	7.51	55.21	1.96
	C = O	173.25	56.08 ± 1.34	2.07	104.19	121.45	-

Table 5 (cont'd.)

Compound	Substituent	Chemical Shift (ppm)	T_1 (sec)	NOE	$T_{1(DD)}$ sec	$T_{1(O)}$ sec	$\tau_c \times 10^{12}$ sec
(D) N,N-dimethyl -n-butryamide	N-methyl(t)	36.36	12.83 ± 0.39	1.97	26.29	25.06	0.56
	N-methyl(c)	34.25	12.22 ± 0.72	2.09	22.29	27.05	0.66
	Carbonyl-sub-α-C	34.51	5.06 ± 0.15	2.59	6.33	25.27	3.48
	Carbonyl-sub-β-C	18.16	6.19 ± 0.24	2.55	7.94	28.10	2.78
	Carbonyl-sub-γ-C	13.39	7.29 ± 0.21	2.38	10.50	23.84	1.40
	C = O	171.68	53.78 ± 2.17	2.16	92.17	129.12	-
(E) N,N-dimethyl acrylamide	N-methyl(t)	36.56	17.61 ± 1.05	2.13	30.98	40.80	0.47
	N-methyl(c)	34.78	16.51 ± 1.43	2.00	32.82	33.22	0.45
	Carbonyl-sub-α-C	128.61	11.50 ± 0.85	2.60	14.29	58.92	3.08
	Carbonyl-sub-β-C	126.21	6.24 ± 0.24	2.90	6.53	140.97	3.37
	C = O	165.40	86.71 ± 5.52	1.97	177.71	169.33	-
(F) Formamide	C = O	165.56	9.11 ± 0.18	2.70	10.65	63.07	4.14

*Chemical shifts are relative to TMS, + indicates downfield. All the compounds were purified. The measurements were made 35°C. c = cis, t = trans relative to the C = 0 group. The probable errors in chemical shift are ± 0.02 ppm.
**Carbonyl-sub-α-C indicates the α carbon of the alkyl substituent on carbonyl Carbon.

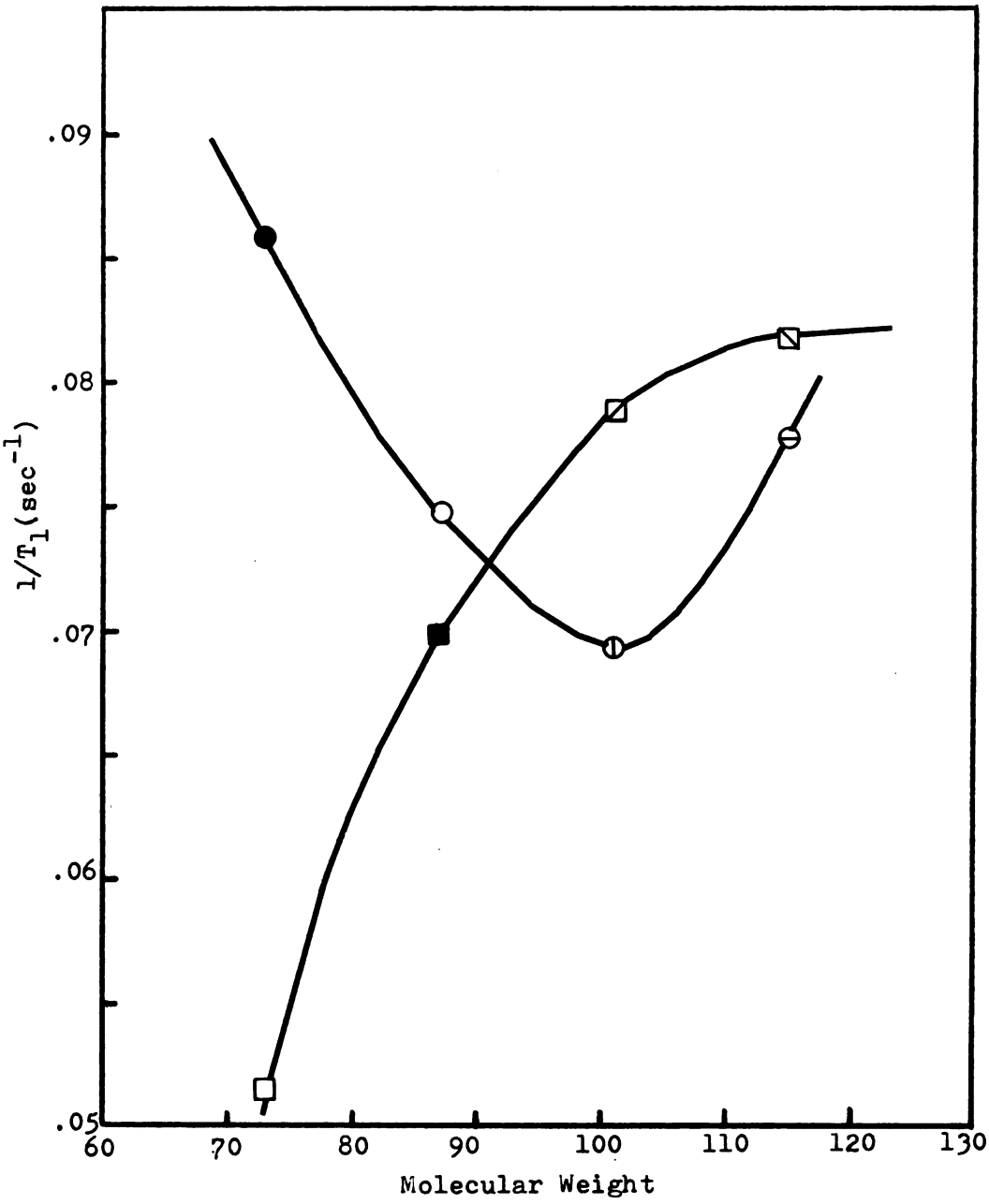

Figure 24. Relaxation rates of ^{13}C in the <u>trans</u>- and <u>cis</u>-NCH_3 groups of N,N-dimethylformamide (●)(□), N,N-dimethylacetamide (○)(■), N,N-dimethylpropionamide (⦶)(⧄), and N,N-dimethyl-n-butyramide (⊖)(⧅), plotted versus the molecular weight of the amides.

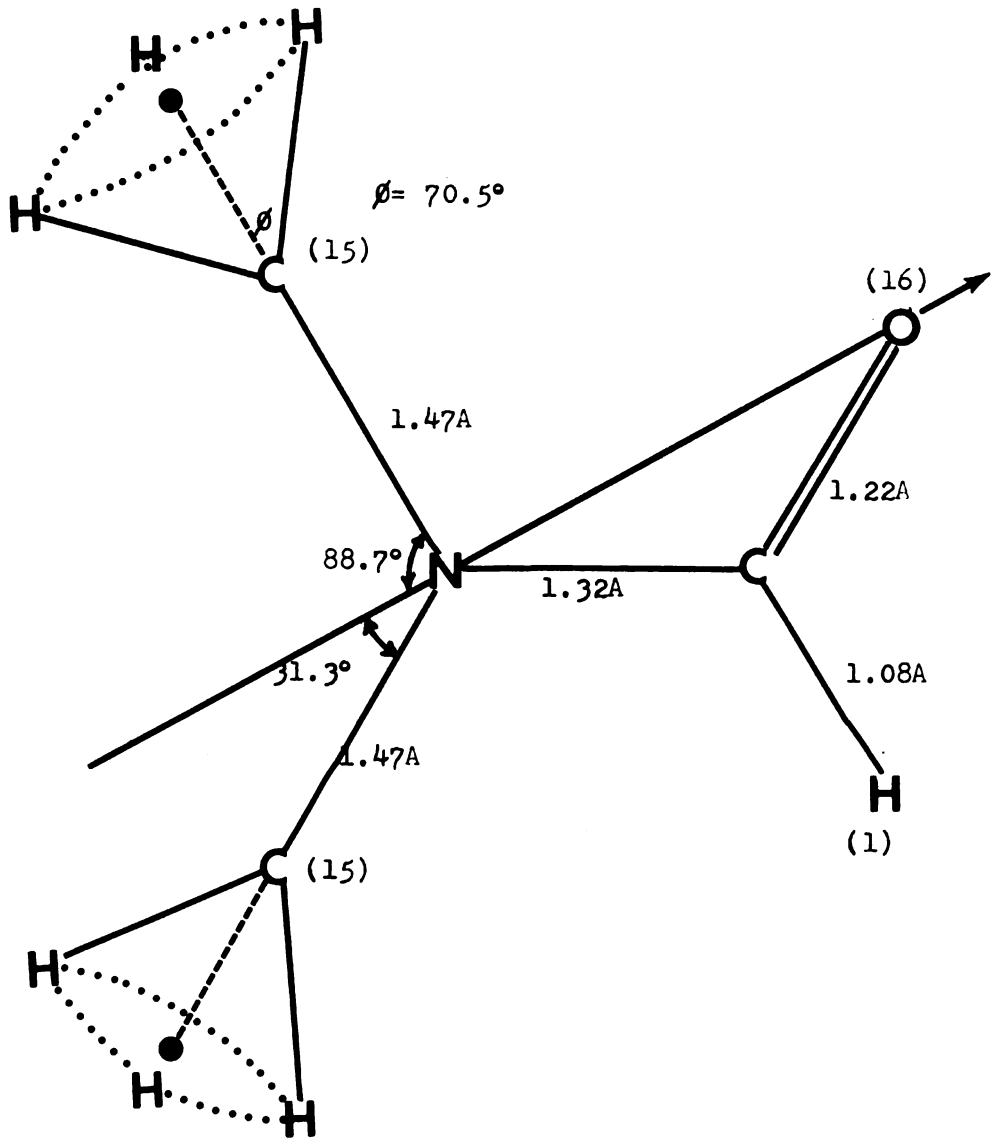

Figure 25. The preferred rotation axis for molecular motion in N,N-dimethylformamide(arrow). The bond angles and internuclear distances used in the calculations are shown.

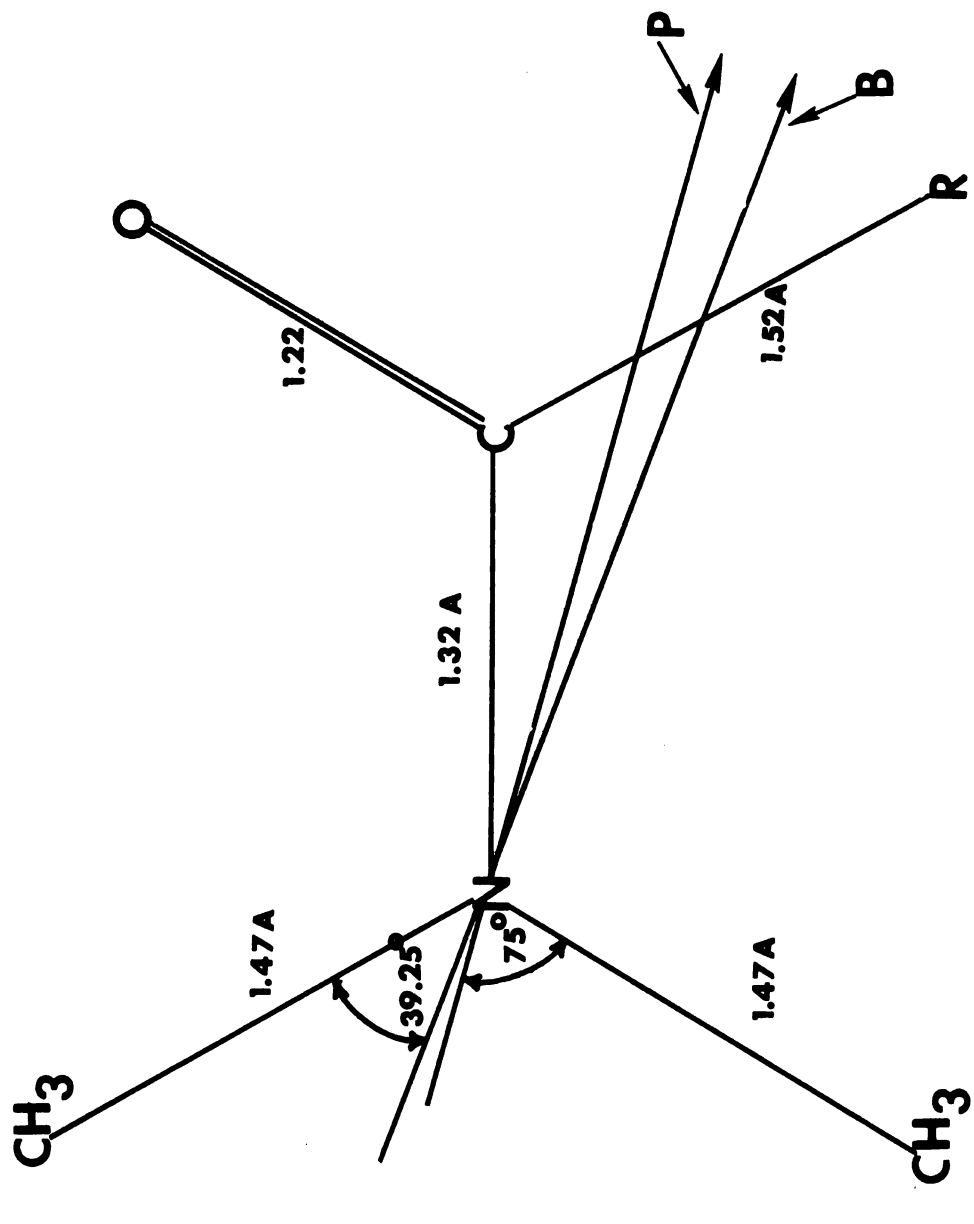

Figure 26. Preferred rotation axes for molecular motion of N,N-dimethylpropionamide and N,N-dimethyl-n-butyramide. For R = CH_3CH_2-, P is the preferred axis; for R = $CH_3CH_2CH_2$-, B is the preferred axis.

rotation about this axis will not affect the difference between the relaxation rate of the trans- and cis-N-methyl groups, since it makes the same angle (90°) with both N-methyl groups. Thus, the difference between the relaxation rates for the trans- and cis-N-CH_3 groups is attributed to rotation of the molecules around the axes in the molecular plane. However, in N,N-dimethylamides, the diffusion rate around the preferred rotation axis will be much faster than that about the other axis in the molecular plane, since rotation around the preferred axis will affect the neighboring molecules less than rotation about the other axis in the molecular plane. Therefore, the relaxation rate of trans- and cis-NCH_3 groups will be mainly dependent on the direction of the preferred rotation axis in the molecular plane. For the approximate ellipsoidal model, we will assume that the symmetry axis of the ellipsoid is along the preferred rotation axis in the molecular plane. Thus, on the ellipsoidal model, the considerably larger relaxation rate of the trans-NCH_3 group in N,N-dimethylformamide (DMF) is attributed to the angle between the preferred rotation axis and the N-C bond of the trans-N-CH_3 group being considerably smaller than the angle between the preferred rotation axis and the N-C bond of the cis-N-CH_3 group (Figure 23). In N,N-dimethylacetamide (DMA) the difference in the relaxation rates between the carbons of the trans- and cis-NCH_3 groups is greatly reduced, which

shows that the preferred rotation axis has been shifted until it is approximatly parallel to the central C-N bond of the amide. However, in N,N-dimethylpropionamide (DMP) and N,N-dimethyl-n-butyramide (DMB), the ^{13}C relaxation rate of the cis-NCH_3 carbon is greater than that of the trans-NCH_3 group, indicating that the preferred rotation axis makes a larger angle with the N-C bond of the trans-NCH_3 group. These results show that the preferred overall molecular reorientation axis has been shifted from being nearly parallel to the N-O direction in N,N-dimethylformamide to the direction shown in Figure 25 in N,N-dimethyl-n-butyramide. Since the variation of the ^{13}C spin-lattice relaxation rates for trans- and cis-NCH_3 groups in going from N,N-dimethylformamide to N,N-dimethyl-n-butyramide is mainly attributed to the change of the substituents on the carbonyl group (from -H to $-C_3H_7$), we can see that the change in the direction for the preferred rotation axis in the molecular plane is mainly determined by the relative masses of oxygen and of the carbonyl substituent (R). This means that the inertial effect is an important factor in determining the direction of the preferred rotation axis. In N,N-dimethylformamide the atomic weight of oxygen is sixteen times that of hydrogen,so we can assume that the preferred rotation axis is along the N-O direction, as shown in Figure 25. However, in N,N-dimethylpropionamide and N,N-dimethyl-n-butyramide, the

masses of the carbonyl substituents are greater than that of oxygen, so the preferred rotation axes are shifted to the directions indicated in Figure 26. The directions of the preferred rotation axes in our models are determined by the ratios of the masses of the carbonyl substituents (R) and oxygen. In order to apply Equation (132) to (135) to our compounds, the bond lengths and bond angles for the amides are required, and the standard values[89] for the amides shown in Figures 25 and 26 were used. The ^{13}C relaxation rates for the carbons of the nonequivalent trans- and cis-NCH_3 groups can be used to calculate the ratio $\rho = D_{||}/D_{\perp}$ of the diffusion constants. From Equations (135) and the molecular dimensions given in Figure 25, the relationship between ρ and the ratio of the ^{13}C relaxation rates for the cis- and trans-NCH_3 groups in DMF was obtained and is plotted in Figure 27. Similar relationships were obtained for DMP and DMB by use of Equation (135) and the information in Figure 26; the results are plotted in Figure 28.

From the experimental values of $T_{1(DD)}$ for the methyl ^{13}C's of DMF, DMP and DMB given in Table 1, the values of ρ were calculated and are shown in Table 6. These ρ values can be used as an estimate of the anisotropy of the overall molecular motion -- the larger ρ, the more anisotropic the motion. Also, once the values of ρ have been determined, the absolute values of $D_{||}$ and $D_{\perp}$ can be

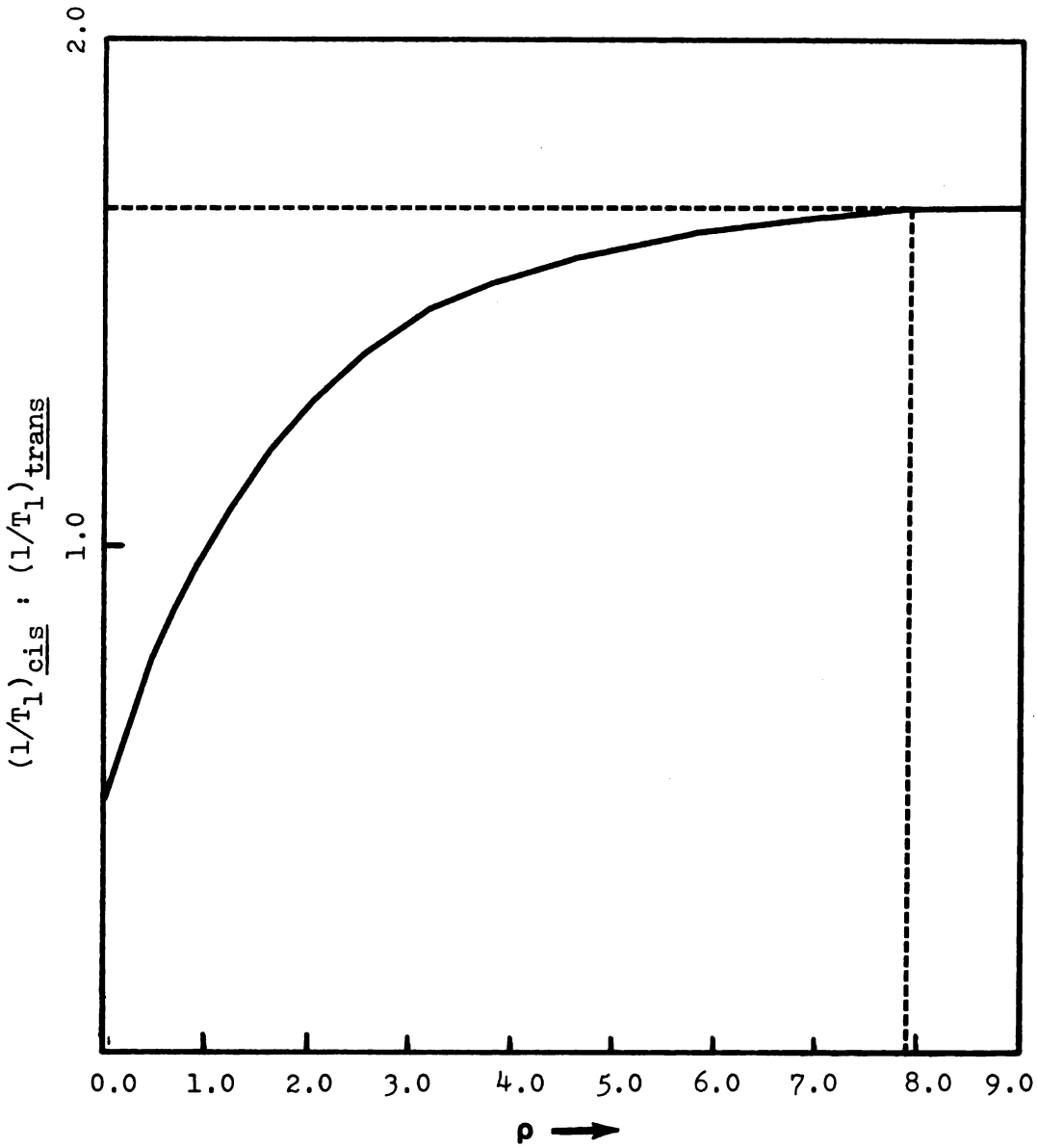

Figure 27. Calculated ratio of the relaxation rates for ^{13}C in the cis- and trans-NCH_3 groups plotted versus $\rho = D_{\parallel}/D_{\perp}$ for DMF.

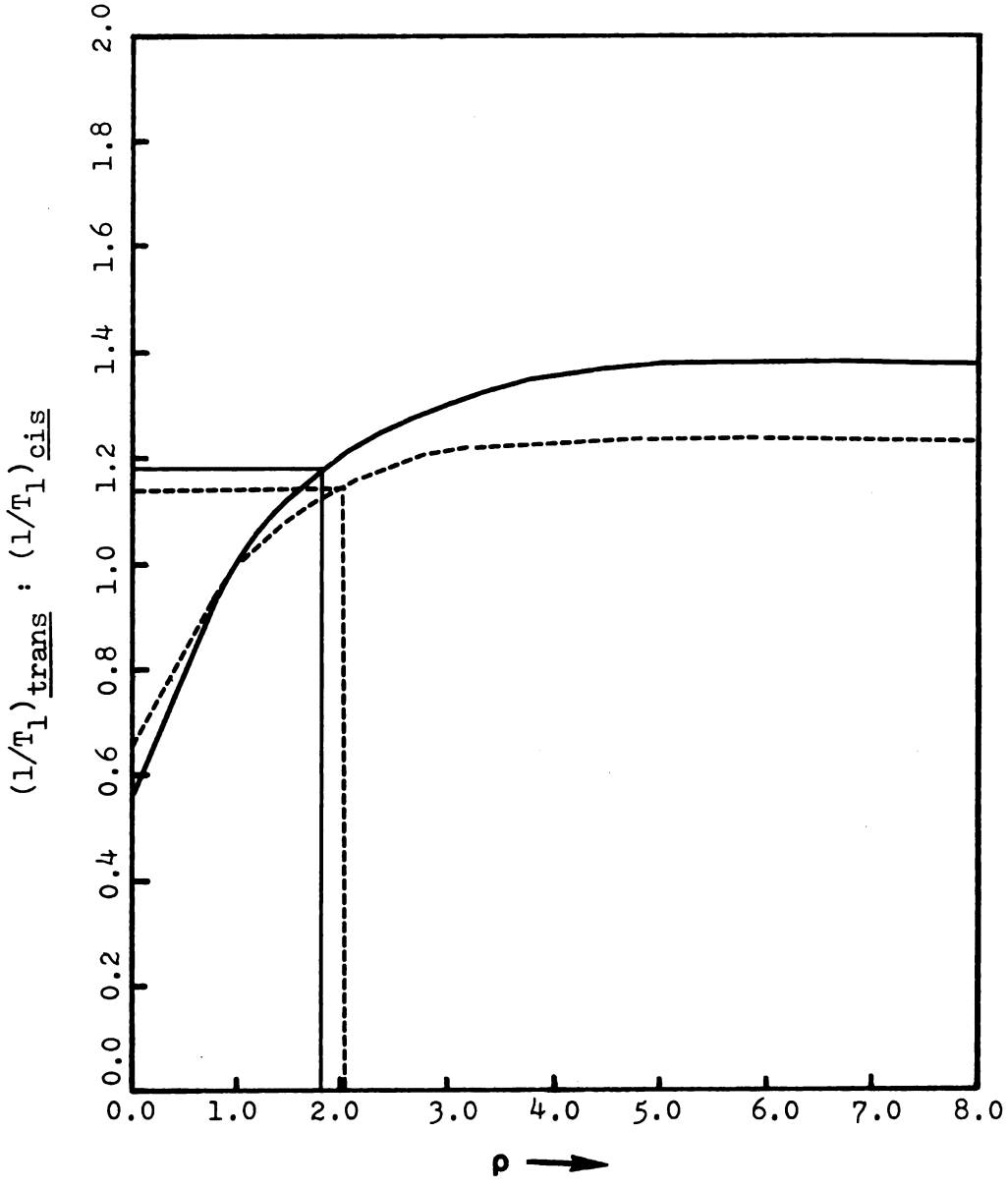

Figure 28. Calculated ratio of the relaxation rates for ^{13}C in the cis- and trans-NCH_3 groups of N,N-dimethylpropionamide (——) and N,N-dimethyl-n-butyramide (----) plotted versus $\rho = D_{\parallel}/D_{\perp}$.

Table 6. The calculated diffusion constants $D_{||}$, $D_{\perp}$ and internal rotation rates for <u>trans</u>- and <u>cis</u>-N-methyl groups in some N,N-dimethylamides.[a]

Compound	$1/T_1(DD)$ ratio[b]	ρ	$D_{||}$ (sec^{-1})	$D_{\perp}$ (sec^{-1})	$R_{\underline{cis}}$ (sec^{-1})	$R_{\underline{trans}}$ (sec^{-1})
N,N-dimethylformamide	1.66(c/t)	7.9	2.91×10^{11}	3.64×10^{10}	4.1×10^{12}	3.3×10^{12}
N,N-dimethylacetamide	1.01(t/c)	1.0	5.20×10^{10}	5.10×10^{10}	4.7×10^{12}	4.9×10^{12}
N,N-dimethylpropionamide	1.14(t/c)	2.0	7.54×10^{10}	3.77×10^{10}	4.8×10^{12}	5.4×10^{12}
N,N-dimethyl-n-butyramide	1.18(t/c)	1.8	7.50×10^{10}	4.17×10^{10}	3.9×10^{12}	4.9×10^{12}

[a]All the amides were measured at 35°C. $D_{||}$ and $D_{\perp}$ are the overall molecular diffusion constants parallel and perpendicular to the symmetry axis of the axially symmetric ellipsoid assumed in the model. R is the internal rotation rate of an N-methyl group.

[b]The notation c/t indicates the ratio $(1/T_1)_{\underline{cis}} / (1/T_1)_{\underline{trans}}$ and $\rho = D_{||}/D_{\perp}$.

obtained from Equation (132) and the experimental relaxation rates of the non-spinning carbons, i.e., the formyl carbon in DMF and either the carbonyl carbon or the α carbon in DMP and DMB. The internal rotation rates for the N-methyl groups can then be obtained by use of Equation (133). These values were calculated for DMF, DMP and DMB and are shown in Table 6.

Since the masses of the four substituents (oxygen and the three methyl groups) on the central C-N bond of DMA are nearly equal, its overall motion is almost isotropic[3] as seen from the ratio of the relaxation rates of the methyl carbons. Since there are no non-spinning carbons in N,N-dimethylacetamide, Equation (132) cannot be used. If Equation (133) is used for the three methyl groups in DMA, then difficult and tedious work is required to solve for the three unknowns from the three equations. In order to avoid this problem, we used an interpolation method shown in Figure 29 to find the internal rotation rate of the trans- and cis-NCH_3 groups in DMA, and then calculated the diffusion constants by Equation (133).

So far, only N,N-dimethylformamide has been studied in detail[54]. The reported diffusion constants[54] at 280°K are $D_x = 2.0 \pm 0.4 \times 10^{11}$ sec^{-1}, $D_y = 6 \pm 3 \times 10^{9}$ sec^{-1}, and $D_z = 2.90 \pm 0.7 \times 10^{10}$ sec^{-1}; the reported D_x value is very close to our $D_{||}$ value (Table 6). This is reasonable,

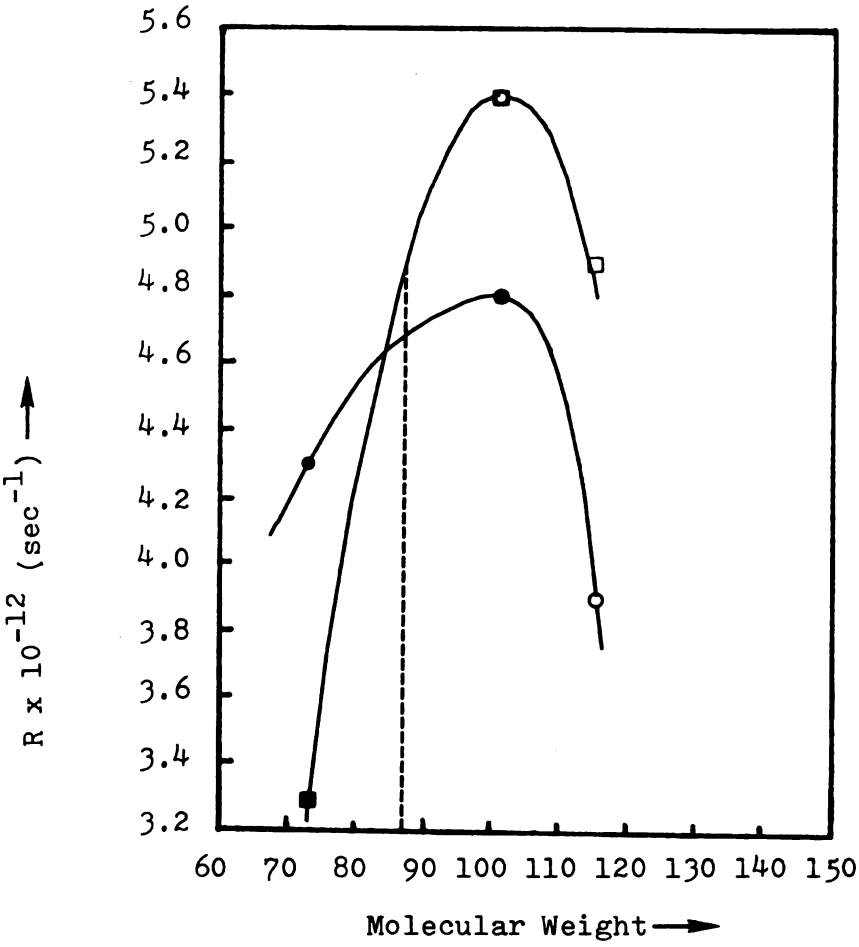

Figure 29. Internal diffusion constants R for the trans- and cis-NCH_3 groups of N,N-dimethylformamide (◙) (•), N,N-dimethylpropionamide (◙) (●), and N,N-dimethyl-n-butyramide (□) (o). The dotted line gives the interpolated values of R for DMA.

since the x axis chosen by Huntress corresponds to our preferred overall molecular rotation axis. The $D_{\perp}$ value in our result is an effective diffusion constant perpendicular to the preferred overall molecular rotation axis and is some average of the D_y and D_z values (which have been reported in Reference 54). Although individual values of D_y and D_z are not obtained using our approximations, we believe that the $D_{\perp}$ value obtained by our method should be closer to the larger of the two values D_y, D_z. In the case of N,N-dimethylformamide, $D_{\perp}$ is found to be closer to D_z. It might also be expected that the $D_{\perp}$ values for DMA, DMP and DMB would be closer to D_z at room temperature since rotation about D_z, which corresponds to spinning of the molecule in its molecular plane, should be easier than rotation about D_y.

These results show that the ^{13}C dipole-dipole spin-lattice relaxation rate provides as powerful a method for investigating anisotropic motion as the quadrupolar relaxation method used by Huntress[54].

In calculating the diffusion constants of N,N-dimethylpropionamide and N,N-dimethyl-n-butyramide, the relaxation rates of α carbons on the carbonyl substituents have been used and this may introduce some experimental error due to the segmental motion of the carbonyl substituents. The choice of the direction for the preferred rotation axis may also introduce about 10% error by introducing an uncertainty in the angle of about 10°.

B. Determination of the energy barriers for the internal rotation of the NCH_3 groups and for the segmental motion of the carbonyl substituents

The energy barriers for the internal rotation of NCH_3 groups and for the segmental motion of the carbonyl substituents in N,N-dimethylamides have been determined from the experimental values of the ^{13}C spin-lattice relaxation times. ^{13}C T_1 values for the cis- and trans-$N-CH_3$ groups and the C = O group of DMF are shown in Table 7. Values of $\ell n(1/T_1)$ are plotted versus reciprocal temperature in Figure 30 for the three carbons and the energy barrier corresponding to each was determined from the slope of the linear portion of the curve by use of the Arrhenius relationship

$$1/T_1 = Ae^{Ea/RT} \quad . \tag{136}$$

The temperature dependence of the ^{13}C spin-lattice relaxation for each carbon of DMA, DMP and DMB is given in Tables 8-10, respectively, and the values of $\ell n(1/T_1)$ are plotted versus reciprocal temperature for each in Figures 31-33, respectively. The values of E_a obtained from the slopes of the curves are also given in Figures 31-33.

The energy barriers for internal rotation about the threefold axes of the trans- and cis-NCH_3 groups are consistent with the internal rotation rates R_{trans} and R_{cis} in Table 6, except in the case of the high value

Table 7. Temperature dependence of the ^{13}C spin-lattice relaxation times of the carbons of N,N-dimethylformamide.

T(°C)	trans-N-methyl (T_1) sec	cis-N-methyl (T_1) sec	T(°C)	C = O (T_1) sec
-51.2	2.782±0.128	6.507±0.302	-52.4	3.136±0.106
-30.0	4.384±0.160	10.149±0.171	-36.0	7.324±0.129
-14.6	5.281±0.150	12.151±0.212	-21.0	11.180 ± .423
+ 2.2	8.183 ± .193	16.655 ± .261	- 4.0	17.204 ± .980
+23.5	11.107 ± .378	19.519 ± .332	14.0	16.706 ± .838
+34.5	13.080 ± .368	19.119 ± .320	+34.0	20.262 ± .364
+50.4	17.278 ± .651	18.755 ± .550	+52.2	25.510 ± .927
+66.2	21.680±1.070	20.104 ± .433	+70.3	27.269 ± .621
+83.3	21.532±1.680	25.757±1.460	88.6	20.262 ± .364
+98.0	20.814 ± .540	19.071 ± .585	101.5	19.790±1.120
+116.0	22.703±1.410	18.965±1.060	120.7	25.333±1.900

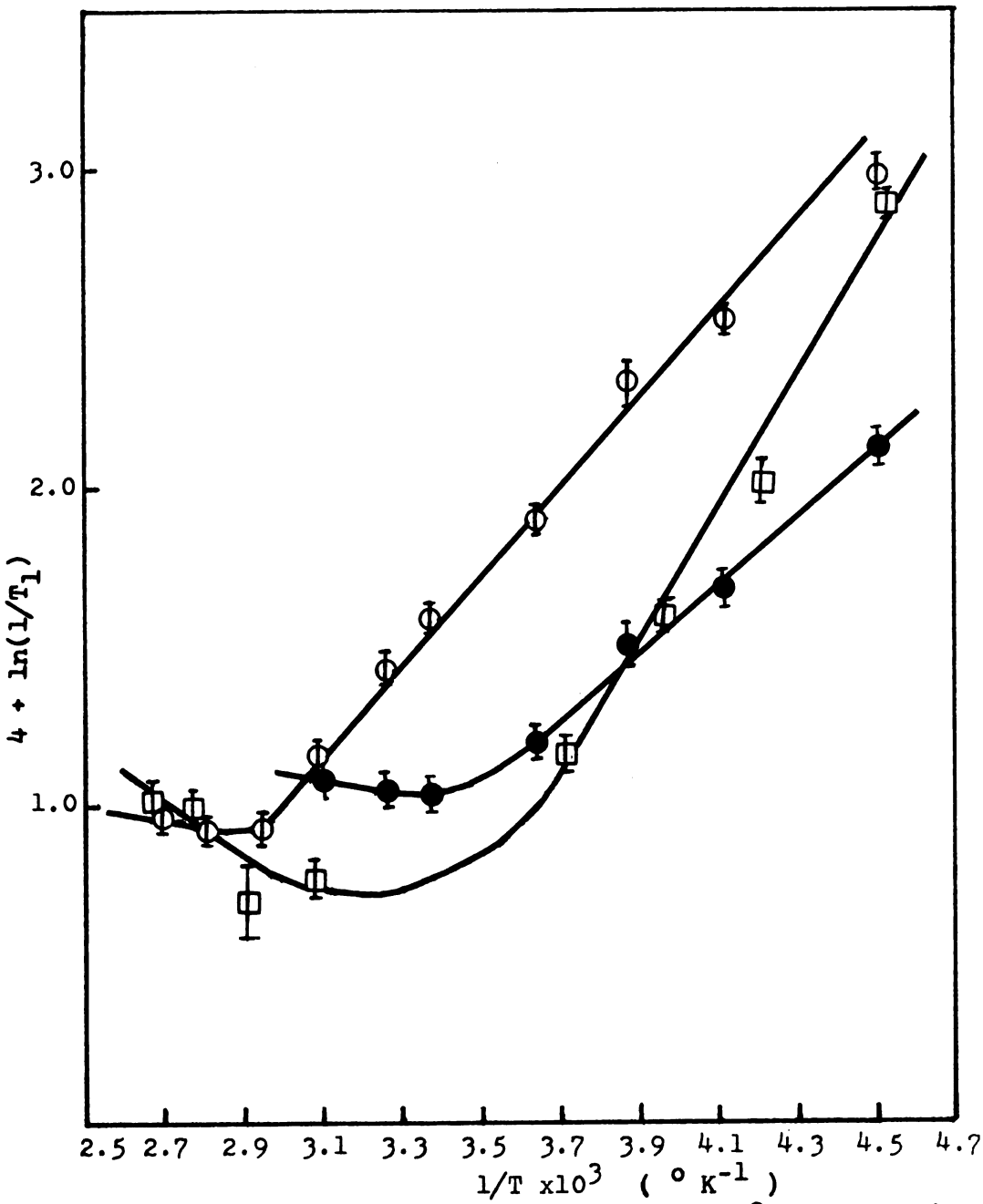

Figure 30. Plot of $\ln(1/T_1)$ versus $1/T \times 10^3$ for each ^{13}C of N,N-dimethylformamide: ○ denotes trans-NCH_3, □ denotes the C=O group, and ● denotes cis-NCH_3; $E_a(t\text{-}N\underline{C}H_3)$ = 2.60 kcal/mol, $E_a(c\text{-}NCH_3)$ = 2.12 kcal/mol, and $E_a(\underline{C}{=}O)$ = 4.10 kcal/mol.

Table 8. Temperature dependence of the ^{13}C spin-lattice relaxation times of each alkyl carbon of N,N-dimethylacetamide.

T(°C)	trans-N-methyl T_1(sec)	cis-N-methyl T_1(sec)	Carbonyl-$\underline{C}H_3$ T_1(sec)
-16.2	-	10.318 ± 0.277	-
-15.9	12.747 ± 0.414	10.554 ± 0.234	6.507 ± 0.289
- 4.6	-	15.595 ± 1.480	8.430 ± 0.155
+ 1.7	15.180 ± 0.185	-	11.800 ± 0.785
+18.1	18.575 ± 0.371	20.597 ± 0.789	12.286 ± 0.275
+17.3	18.653 ± 0.571	18.588 ± 0.829	11.925 ± 0.444
+26.8	23.168 ± 1.860	-	16.461 ± 1.160
+55.0	24.624 ± 2.490	21.489 ± 1.930	18.290 ± 0.690

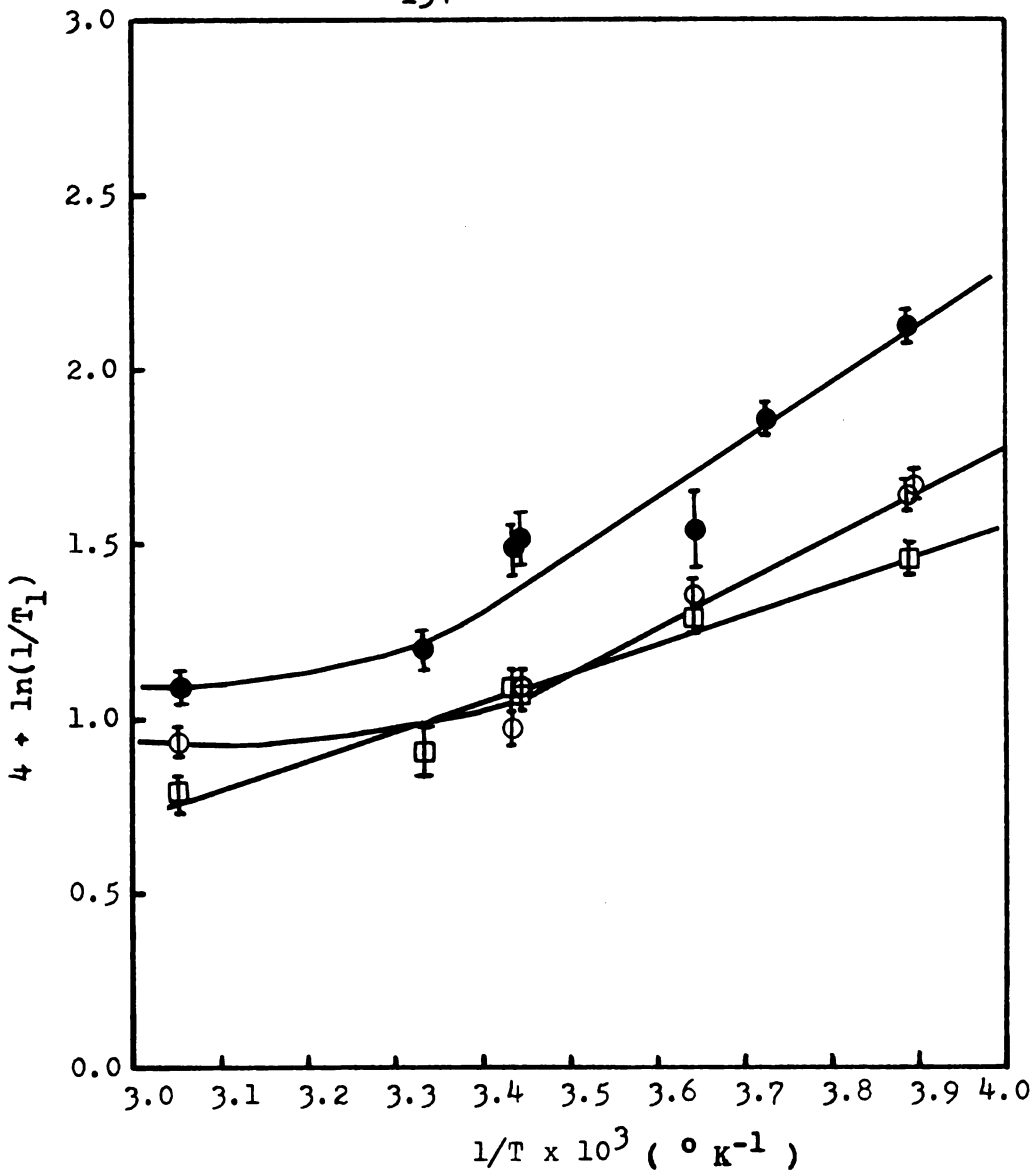

Figure 31. Plot of $\ln(1/T_1)$ versus $1/T \times 10^3$ for each alkyl ^{13}C of N,N-dimethylacetamide: ● denotes carbonyl-$\underline{C}H_3$, ○ denotes <u>cis</u>-N$\underline{C}H_3$, □ denotes <u>trans</u>-N$\underline{C}H_3$; E_a(t-N$\underline{C}H_3$) = 1.66 kcal/mol, E_a(c-N$\underline{C}H_3$) = 2.55 kcal/mol, and E_a(O=C-$\underline{C}H_3$) = 3.27 kcal/mol.

Table 9. Temperature dependence of the ^{13}C spin-lattice relaxation times of each alkyl carbon of N,N-dimethylpropionamide.

T(°C)	trans-N-methyl T_1 (sec)	cis-N-methyl T_1 (sec)	Carbonyl substituent α-C T_1 (sec)	β-C T_1 (sec)
-58.7	.502±.013	.451±.025	.124±.005	.332±.016
-42.6	1.198±.045	.989±.092	.404±.020	.777±.074
-30.2	2.600±.150	3.056±.142	.723±.036	1.549±.063
-13.8	4.408±.233	5.997±.249	1.576±.027	2.477±.132
1.0	7.290±.301	6.845±.315	2.530±.161	3.116±.171
+17.5	10.514±.476	10.104±.480	4.778±.220	5.456±.159
+34.0	14.400±.680	12.660±.600	5.96 ±.150	6.610±.120
+51.5	18.672±2.220	15.641±.888	12.618±.625	9.428±.499
+66.5	19.323±.508	19.482±.456	11.700±.287	11.030±.321

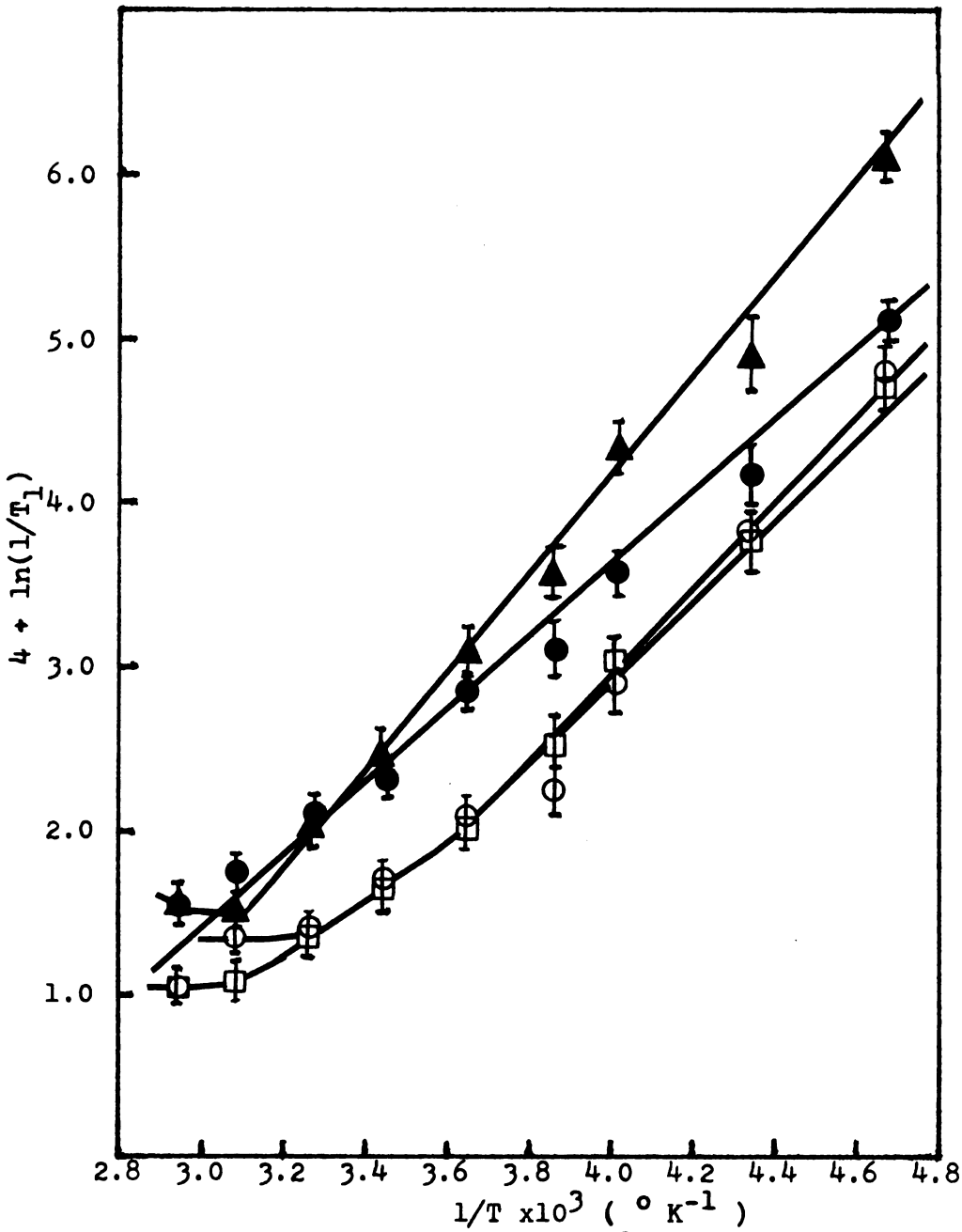

Figure 32. Plot of $\ln(1/T_1)$ versus $1/T \times 10^3$ for each alkyl carbon of N,N-dimethylpropionamide: ▲ denotes O=C-α-C, ● denotes O=C-β-C, ○ denotes cis-NCH_3, and □ denotes trans-NCH_3; E_a(O=C-α-C) = 5.97 kcal/mol, E_a(O=C-β-C) = 4.37 kcal/mol, E_a(t-NCH_3) = 4.38 kcal/mol, and E_a(c-NCH_3) = 5.19 kcal/mol.

Table 10. Temperature dependence of the ^{13}C spin-lattice relaxation times of each alkyl carbon of N,N-dimethyl-n-butyramide.

Temperature (°C)	trans-N-methyl T_1 (sec)	cis-N-methyl T_1 (sec)	Carbonyl substituent α-C T_1 (sec)	β-C T_1 (sec)	γ-C T_1 (sec)
-32.6	0.928±0.073	1.432±0.080	0.418±0.013	0.649±0.042	0.867±0.038
-21.2	1.800±0.136	2.491±0.123	0.566±0.025	0.808±0.043	1.277±0.057
- 7.9	4.529±0.381	4.478±0.184	1.925±0.171	1.749±0.132	1.974±0.107
+ 6.9	7.778±0.356	4.565±0.950	2.749±0.063	2.173±0.005	2.841±0.182
22.4	6.962±0.605	6.864±0.130	3.083±0.283	2.455±0.187	4.525±0.295
+34.2	12.830±0.390	12.220±0.720	5.060±0.160	6.190±0.240	7.970±0.480
+52.9	17.384±0.491	22.610±1.520	7.960±0.145	5.956±0.271	7.916±0.276

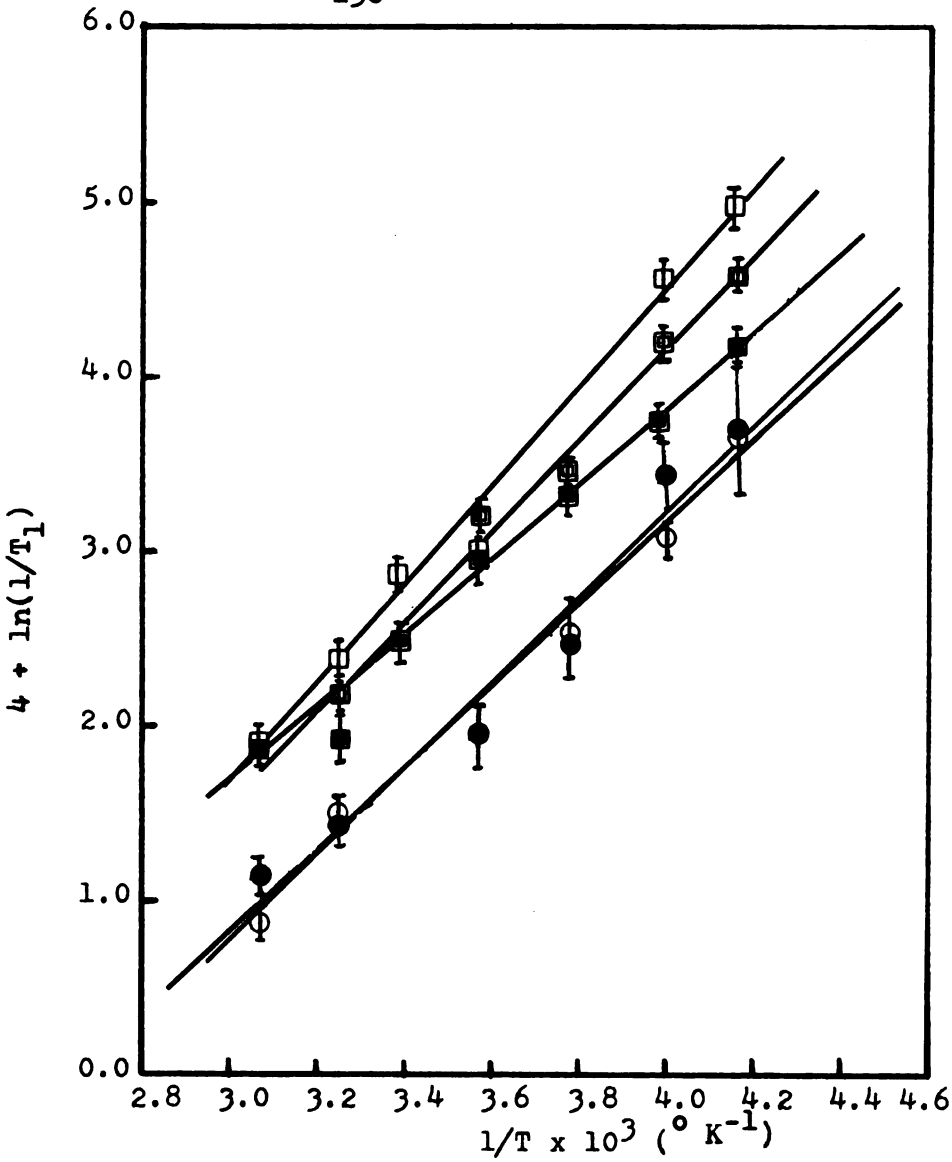

Figure 33. Plot of $\ln(1/T_1)$ versus $1/T \times 10^3$ for each alkyl ^{13}C of N,N-dimethyl-n-butyramide: □ denotes the α carbon of the carbonyl substituent, ◘ denotes the β carbon of the carbonyl substituent, ■ denotes the γ carbon of the carbonyl substituent, ● denotes trans-$N\underline{C}H_3$, and ○ denotes cis-$N\underline{C}H_3$; $E_a(O{=}C\text{-}\alpha\text{-}\underline{C})$ = 5.71 kcal/mol, $E_a(O{=}C\text{-}\beta\text{-}\underline{C})$ = 5.21 kcal/mol, $E_a(O{=}C\text{-}\gamma\text{-}\underline{C})$ = 4.30 kcal/mol, $E_a(t\text{-}N\underline{C}H_3)$ = 5.20 kcal/mol, and $E_a(c\text{-}N\underline{C}H_3)$ = 4.72 kcal/mol.

E_a = 5.20 kcal/mole for the trans-NCH_3 group of DMB. This value may be attributed to the strong steric effect of the n-C_3H_7 group, as has been found also in the INDO calculations (Part II).

The values of E_a for the carbons on the carbonyl substituents decrease in going from the α to the β or γ carbon. This is the expected behavior since the motion becomes freer toward the end of the chain. In the case of the formyl carbon of DMF, and the α carbons of the carbonyl substituents of DMP and DMB, the E_a values may be mainly attributed to the overall molecular motions since the internal rotations for those carbons are not important.

The theoretical values of E_a for the N-CH_3 groups of DMF and DMA have been calculated and show the same trends as the experimental values, as seen in Table 11.

For N,N-dimethylformamide, the ratio of $R_{trans}/D_{||}$ is equal to 11.34, Table 6. By using the experimental energy barriers of the trans-NCH_3 group and the formyl carbon, the calculated $\exp[E_{a,||}/RT]/\exp[E_{a,trans}/RT]$ is equal to 11.9, which is close to 11.34, indicating that the energy barrier determined for the trans-NCH_3 group is mainly due to the internal rotation of -CH_3 while that for formyl carbon (C = O) is mainly contributed from the anisotropic overall molecular motion around the preferred rotation axis (if the frequency factor is assumed to be the same). This assumption is reasonable since the trans-NCH_3

Table 11. Energy barriers for rotation about the internal rotation axes of the N-methyl groups and of the carbonyl substituents in N,N-dimethylamides

Compound	Substituent	E_a (kcal/mol)[+]	E_a (kcal/mol)[*]	A (sec^{-1})
N,N-Dimethyl formamide (DMF)	trans-NCH_3	2.60	2.07	0.0247
	cis-NCH_3	2.12	1.40	0.0178
	C=O	4.10		0.00745
N,N-Dimethyl acetamide (DMA)	trans-NCH_3	1.66	2.03	0.0097
	cis-NCH_3	2.55	2.99	0.0128
	Carbonyl-CH_3	3.27	4.69	0.0114
N,N-Dimethyl propionamide (DMP)	trans-NCH_3	4.38		0.0182
	cis-NCH_3	5.19		0.0166
	Carbonyl-α-C	5.97		0.0302
	Carbonyl-β-C	4.37		0.0474
N,N-Dimethyl n-butyramide (DMB)	trans-NCH_3	5.20		0.0212
	cis-NCH_3	4.72		0.026
	Carbonyl-α-C	5.71		0.050
	Carbonyl-β-C	5.21		0.0498
	Carbonyl-γ-C	4.30		0.0623

[*]Calculated values from Reference 90, obtained by the EHT method.

[+]The probable errors in E_a are ± 0.5 kcal/mol.

group is nearly parallel to the preferred rotation axis, as seen in Figure 25. However, the ratio of $R_{\underline{cis}}/D_{||}$ is equal to 26, and the calculated value of $\exp[E_{a,||}/RT]/\exp[E_{a,\underline{cis}}/RT]$ is equal to 14.1, which indicates that the frequency factors for the cis-NCH_3 group and for overall anisotropic molecular motion are different. The energy barrier for the cis-NCH_3 group is contributed from its internal rotation and the overall molecular motion. The frequency factor for the cis-NCH_3 group is about twice that of the trans-NCH_3 group as can be seen from Figure 25, where the cis-NCH_3 group is almost perpendicular to the preferred rotation axis.

In N,N-dimethylacetamide, N,N-dimethylpropionamide, and N,N-dimethyl-n-butyramide, the calculated values of $R_{\underline{trans}}/D_{||}$ and $R_{\underline{cis}}/D_{||}$ are quite different from those of $\exp[E_{a,\alpha\text{-}c}/RT]/\exp[E_{a,\underline{trans}}/RT]$ and $\exp[E_{a,\alpha\text{-}c}/RT]/\exp[E_{a,\underline{cis}}/RT]$, which indicates that the measured energy barriers for the trans- and cis-NCH_3 groups contain contributions from both the internal rotation and the overall molecular motion. This can be seen from the values of ρ and of the diffusion constants $D_{||}$ and $D_{\perp}$ for these three amides, which indicate that the overall molecular motions about the three principal axes are each important.

C. Separation of the total spin-lattice relaxation rate into components

Once the internal rotation rates of the trans- and cis-NCH_3 groups have been obtained, the spin-lattice

relaxation rates ($1/T_1$) can be separated into several contributions:

$$\frac{1}{T_{1(obs)}} = \frac{1}{T_{1(DO)}} + \frac{1}{T_{1(DI)}} + \frac{1}{T_{1(SR)}} \qquad (137)$$

where $1/T_{1(DO)}$ is the dipole-dipole relaxation due to the overall molecular motion, $1/T_{1(DI)}$ is the dipole-dipole relaxation due to the internal rotation of the methyl group and $1/T_{1(SR)}$ is the spin-rotation relaxation. These were separated by calculating the second term using

$$1/T_{1(DI)} = [n_H \hbar^2 \gamma_C^2 \gamma_H^2 / r^6] \tau_C ,$$

with $\tau_C = 1/6R$, and obtaining the first term as the difference $1/T_{1(DO)} = 1/T_{1(DD)} - 1/T_{1(DI)}$, with $1/T_{1(DD)}$ values taken from Table 5. Values of $1/T_{1(DD)}$ are obtained from the experimental spin-lattice relaxation times and NOE values using the relationship

$$T_{1(DD)} = T_{1(exp)} \frac{\eta_{max}}{\eta_{exp}} .$$

Finally, values of $1/T_{1(SR)}$ were obtained from Equation (137) by difference. Values of $1/T_{1(obs)}$, $1/T_{1(DI)}$, $1/T_{1(DO)}$ and $1/T_{1(SR)}$ are plotted versus molecular weight for four N,N-dimethylamides in Figure 34.

The results show that the variation of the total spin-lattice relaxation rate for the N,N-dimethylamides can be mainly attributed to the variation of the dipolar overall molecular reorientation relaxation rate. The contribution of spin-rotation relaxation due to the internal

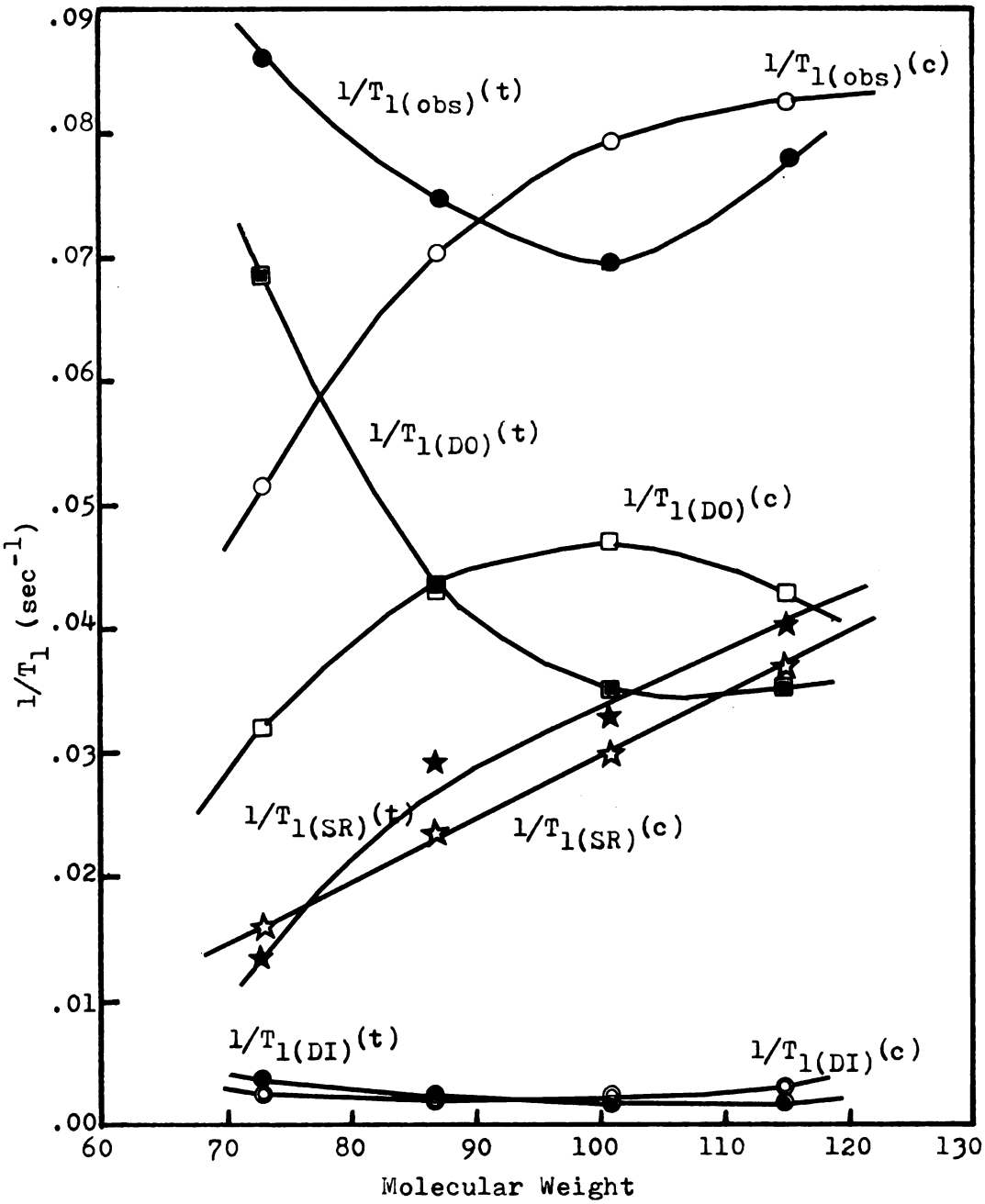

Figure 34. Various components of the total ^{13}C relaxation rates for the $-NCH_3$ groups of N,N-dimethylamides plotted versus molecular weight; obs: observed total relaxation rate; DO and DI are the dipolar relaxation rates due to overall molecular motion and to internal rotation of the methyl groups, SR is the spin-rotation relaxation rate. (All at 35° C)

Table 11a. Contributions of the internal rotation (DI), overall molecular reorientation to the total intramolecular ^{13}C dipolar relaxation rates $R_{1(DD)}$ and spin-rotation (SR) mechanism of some carbons in various N,N-dimethylamides[a,b]

Compound	Substituent	$R_{1(DD)}$	$R_{1(DI)}$	$R_{1(DO)}$	$R_{1(SR)}$
DMF	trans-NCH_3	0.0859	0.00235	0.0689	0.0138
	cis-NCH_3	0.0516	0.00262	0.0324	0.0166
DMA	trans-NCH_3	0.0748	0.00219	0.0433	0.0293
	cis-NCH_3	0.0700	0.00229	0.0439	0.0239
DMP	trans-NCH_3	0.0694	0.00199	0.0350	0.0297
	cis-NCH_3	0.0790	0.00224	0.0470	0.0324
DMB	trans-NCH_3	0.0779	0.00219	0.0427	0.0399
	cis-NCH_3	0.0818	0.00275	0.0353	0.0370

[a]These values are plotted in Figure 34.

[b]All values are in sec^{-1} and were determined at 35° C.

rotation of NCH_3 groups is also important but the contribution of the dipolar relaxation resulting from internal rotation of the NCH_3 groups is small. The narrowing of the difference between the relaxation rates $1/T_{1(obs)}$, for the trans- and cis-NCH_3 groups in N,N-dimethylpropionamide and N,N-dimethyl-n-butyramide, compared with the dipolar overall molecular relaxation $1/T_{1(DO)}$, is attributed to the contribution of the spin-rotation relaxation, as may be seen from Figure 34.

^{17}O Spin-lattice relaxation times and quadrupole coupling constants in some N,N-dimethylamides

The ^{17}O spin-lattice relaxation times for formamide, N,N-dimethylformamide, N,N-dimethylacetamide, and N,N-dimethylpropionamide were determined by the inversion-recovery method, as shown in Table 12. One set of partially relaxed FTNMR spectra for N,N-dimethylformamide is shown in Figure 35. Comparing the T_1 data with the T_2^* values calculated from the linewidths, we find that they are almost equal within the experimental error. Table 12 shows that the ^{17}O T_1 values decreased in the order DMF > DMA > DMP. This decrease is mainly due to changes in the overall molecular reorientation, since the larger the molecule the more difficult the overall molecular motion will be. The ^{17}O spin-lattice relaxation time of formamide is shorter than that for N,N-dimethylformamide, although its molecular weight is smaller than that of DMF. This can be rationalized by

Table 12. ^{17}O Spin-lattice relaxation times (T_1) and the quadrupole coupling constants of some amides

Compound	T_1[a] (sec)	Linewidth (Hz)	T_2^*[b] (sec)	(e^2qQ/h) (MHz)
Formamide	0.002356 ± 0.000144	145.8	0.002183	-
N,N-Dimethylformamide	0.005419 ± 0.000182	55.5	0.005741	8.17
N,N-Dimethylacetamide	0.003043 ± 0.000116	98.2	0.003242	10.34
N,N-Dimethylpropionamide	0.001984 ± 0.000194	205.6	0.001553	13.10

[a] T_1 was measured by the inversion-recovery method.

[b] T_2^* was calculated by use of the equation $T_2^* = \frac{1}{\pi\ (\text{linewidth})}$, where the linewidth was measured at 1/2 height.

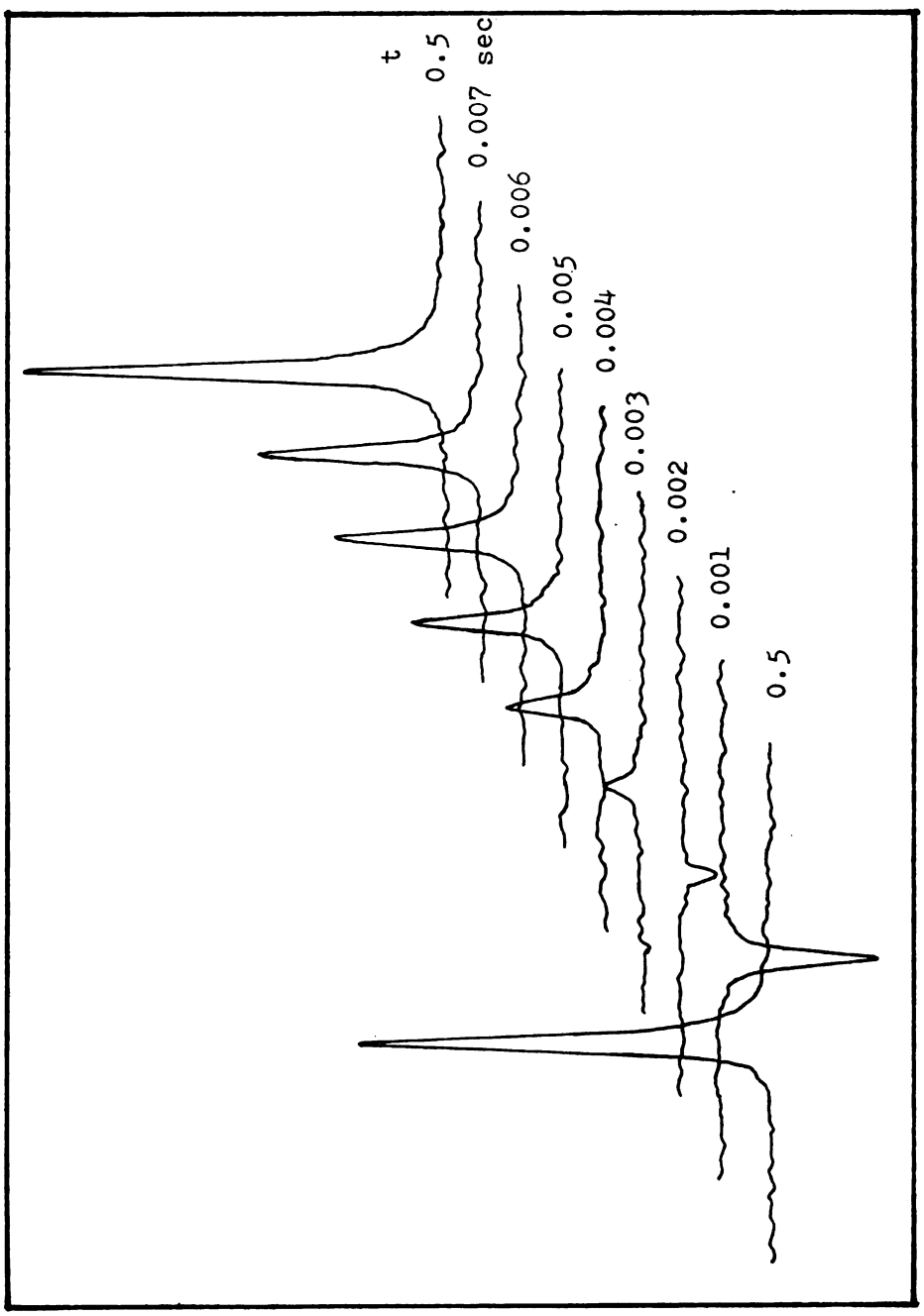

Figure 35. Determination of T_1 for ^{17}O in N,N-dimethylformamide by the inversion-recovery method; T_1 = 0.00542 ± 0.00018 sec..

postulating the formation of hydrogen-bonded polymers in liquid formamide, which give it a longer effective correlation time than that of DMF. By using the ^{17}O relaxation time and the equation for the quadrupolar relaxation in an ellipsoid[83,114], the effective quadrupole coupling constant (e^2qQ/h) can be obtained by use of the equation

$$\frac{1}{T_1} = \frac{1}{80}\left[\frac{2I+3}{I^2(2I-1)}\right](e^2qQ/\hbar)^2 \frac{1}{D_\perp}\left[1 + \frac{3(D_\perp - D_{||})}{(5D_\perp + D_{||})}\sin^2\theta(1 + \frac{3(D_\perp - D_{||})}{2(D_\perp + D_{||})}\sin^2\theta)\right], \quad (138)$$

where θ is the angle between the preferred rotation axis and the C = O bond, assuming that principal axis of the field gradient tensor at oxygen is along the C = O bond[54]. The calculated effective quadrupole coupling constants for some amides are assembled in Table 12. The values are close to the effective quadrupole coupling constant for gaseous formaldehyde, 9.42 MHz, obtained by microwave spectroscopy[91]. No experimental measurements of the ^{17}O quadrupole coupling constants in amides have been reported.

Comparison of the ^{13}C spin-lattice relaxation times for N,N-dimethylamides, N,N-diethylamides and N,N-di-n-propylamides.

The ^{13}C chemical shifts and values of T_1, $T_{1(DD)}$, τ_c, and $T_{1(O)}$ for the N,N-diethylamides and N,N-di-n-propylamides are shown in Tables 13 and 14. Examining the ^{13}C T_1 values for the trans and cis carbons in the

Table 13. ^{13}C Chemical shifts, spin-lattice relaxation times (T_1) and nuclear Overhauser enhancements (NOE) of N,N-diethylamides.

Compound	Substituent	Chemical* Shift(ppm)	T_1(sec)	NOE	$T_{1(DD)}$ sec	$T_{1(O)}$ sec	$\tau_c x10^{12}$ sec
(A) N,N-diethyl-formamide	N-sub -α-C(t)	41.28	4.31±0.15	3.00±0.20	4.31	>200	5.12
	N-sub -α-C(c)	36.07	4.37±0.32	2.30±0.09	6.68	12.63	3.30
	N-sub -β-C(t)	14.42	4.59±0.08	2.72±0.19	5.31	34.06	2.77
	N-sub -β-C(c)	12.36	4.30±0.54	2.09±0.17	7.85	9.53	1.87
	C = O	161.98	5.91±0.15	2.42±0.06	8.27	20.67	5.34
(B) N,N-diethyl-acetamide	N-sub -α-C(t)	42.92	4.39±0.24	2.53	5.70	19.06	3.87
	N-sub -α-C(c)	39.94	5.95±0.61	2.52	7.78	25.27	2.84
	N-sub -β-C(t)	14.35	4.59±0.24	2.47	6.21	17.62	2.37
	N-sub -β-C(c)	13.17	4.13±0.05	2.12	7.33	12.34	2.00
	Carbonyl-CH_3	21.39	11.13±0.31	2.46	15.16	41.91	0.97
	C = O	169.43	59.39±4.20	2.10	107.33	132.96	-

Table 13 (cont'd.)

Compound	Substituent	Chemical* Shift(ppm)	T_1(sec)	NOE	$T_{1(DD)}$ sec	$T_{1(O)}$ sec	$\tau_c x 10^{12}$ sec
(C) N,N-diethyl-propionamide	N-sub -α-C(t)	41.33	2.95±0.10	2.39	4.22	9.81	5.22
	N-sub -α-C(c)	39.49	2.24±0.18	2.52	2.93	4.78	7.52
	N-sub -β-C(t)	13.97	3.66±0.14	2.04	6.99	6.77	2.10
	N-sub -β-C(c)	12.72	3.44±0.10	2.21	5.65	8.79	2.60
	Carbonyl-sub -α-C	25.55	4.74±0.08	2.77	5.32	43.23	4.14
	Carbonyl-sub -β-C	9.04	5.99±0.18	2.32	9.02	17.83	1.63
	C = O	171.23	41.46±0.89	2.33	61.97	125.26	-
(D) N,N-diethyl--n-butyramide	N-sub -α-C(t)	41.40	1.89±0.07	2.56	2.41	8.78	9.14
	N-sub -α-C(c)	39.44	2.05±0.13	2.76	2.32	17.87	9.50
	N-sub -β-C(t)	14.07	3.02±0.20	2.48	4.06	11.82	3.62
	N-sub -β-C(c)	12.77	3.12±0.21	2.37	4.53	10.04	3.24
	Carbonyl-sub -α-C	34.28	3.44±0.12	3.00	3.44	> 200	6.41
	Carbonyl sub -β-C	18.44	3.85±0.08	2.93	3.97	131.96	5.55
	Carbonyl sub -γ-C	13.42	4.34±0.16	3.00	4.34	> 200	3.39
	C = O	170.25	34.69±1.31	2.21	56.99	88.64	-

Table 13 (cont'd.)

Compound	Substituent	Chemical* Shift(ppm)	T_1(sec)	NOE	$T_{1(DD)}$ sec	$T_{1(O)}$ sec	$\tau_c x10^{12}$ sec
(E) N,N-diethyl-acrylamide	N-sub -α-C(t)	41.60	1.86±0.08	2.46	2.53	7.00	7.71
	N-sub -α-C(c)	40.29	2.17±0.10	3.00	2.17	> 200	10.16
	N-sub -β-C(t)	14.73	2.78±0.11	2.35	4.09	8.66	3.59
	N-sub -β-C(c)	12.83	2.86±0.18	1.95	5.98	5.48	2.46
	Carbonyl-sub -α-C	128.60	4.21±0.10	2.56	5.37	19.55	8.21
	Carbonyl sub -β-C	126.02	2.22±0.08	3.00	2.22	> 200	9.93
	C = O	164.31	42.35±2.06	2.35	62.36	131.96	-

*Chemical shifts are relative to TMS and + indicates down field. All the compounds were purified. The measurements were made at 35°C.

Table 14. ^{13}C Chemical shifts, spin-lattice relaxation times (T_1) and nuclear Overhauser enhancements (NOE) of other symmetrically N,N-disubstituted amides

Compound	Substituent	Chemical* Shift(ppm)	T_1(sec)	NOE	$T_{1(DD)}$ sec	$T_{1(O)}$ sec	$\tau_c x10^{12}$
(A) N,N-di-n-propyl-formamide	N-sub -α-C(t)	48.37	3.23±0.24	2.44	4.46	11.72	4.94
	N-sub -α-C(c)	43.19	2.64±0.20	2.76	2.98	23.02	7.40
(neat)	N-sub -β-C(t)	21.76	2.71±0.15	2.52	3.54	11.51	6.23
	N-sub -β-C(c)	20.48	2.78±0.10	2.80	3.07	29.40	7.18
	N-sub -γ-C(c)	10.88	6.55±0.59	2.42	9.17	22.93	1.60
	N-sub -γ-C(t)	10.33	4.48±0.29	2.46	6.10	16.87	3.61
	C = O	162.18	3.56±0.14	2.83	3.87	44.79	5.69
(B) N,N-diisoproyl-propionamide	N-sub -α-C(t)	47.65					
	N-sub -α-C(c)	44.86					
(neat)	N-sub -β-C(t,c)	20.38	3.16±0.38	2.74	3.61	25.33	6.10
	Carbonyl-sub.-α-C	27.61	4.35±0.59	3.00	4.35	> 200	5.07
	Carbonyl-sub.-β-C	9.21	4.50±0.36	2.83	4.89	56.62	3.00
	C = O	170.82	27.50±0.50	2.18	46.33	67.66	-

*Chemical shifts are relative to TMS and + indicates downfield. The measurements were made at 35°C. t = trans, c = cis.

N-methyl substituents of these two series of amides, we find that a preferred rotation axis still exists, although the effect of anisotropy is greatly reduced. Since in these two series of amides the choice of preferred rotation axis becomes more difficult, only a qualitative discussion will be presented.

Several general properties of the T_1 data can be deduced from these three series of symmetrically N,N-disubstitued amides (i.e., the N,N-dimethyl-, N,N-diethyl- and N,N-di-n-propyl- amides):

1. The ^{13}C T_1 values of the non-protonated $\underline{C}$ = O groups are normally longer than those of the protonated carbons. Their values range from 25 to 87 sec, depending upon the size of the molecule. Since the ^{13}C relaxation is mainly attributed to the dipole-dipole interaction between ^{13}C and ^{1}H, in the non-protonated C = O groups this dipolar interaction can only come from the nonbonded protons and will be very small because the dipolar interaction is inversely proportional to r^6. In this case, spin-rotation interaction may become an important mechanism for the relaxation of the $^{13}\underline{C}$ = O group as seen in the NOE values, which are around 2.0.

Variation of the relaxation rates with molecular weight for the non-protonated C = O groups in N,N-dimethylamides and N,N-diethylamides is shown in Figure 36. Both curves show that the relaxation rate is increased as the

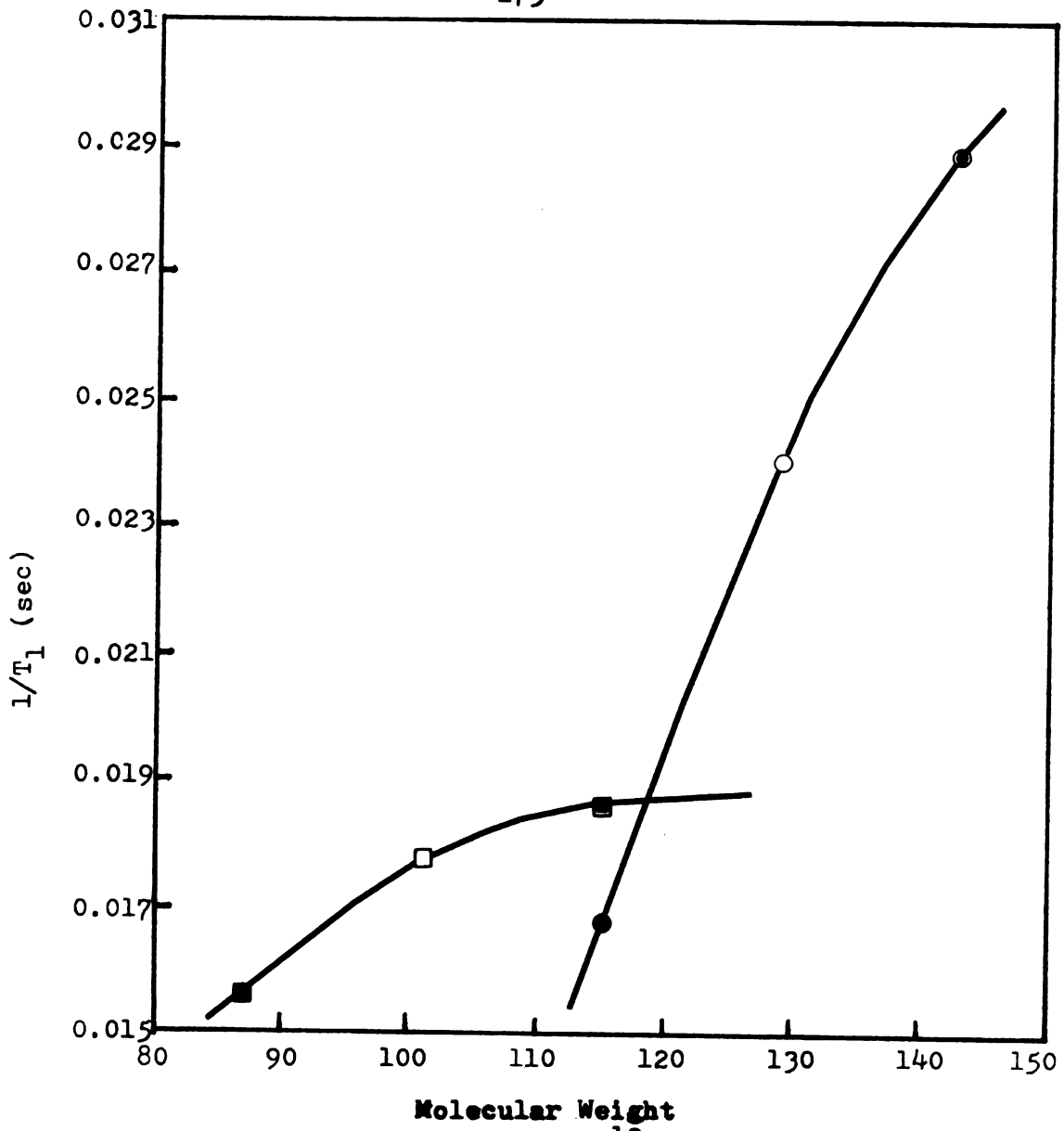

Figure 36. Relaxation rates of ^{13}C in the C=O group of N,N-dimethylacetamide (■), N,N-dimethylpropionamide (□), N,N-dimethyl-n-butyramide (■); N,N-diethylacetamide (●), N,N-diethylpropionamide (○), and N,N-diethyl-n-butyramide (●) plotted versus molecular weight.

carbonyl substituent is changed from $-CH_3$ to $-C_3H_7$. This is understandable since the relaxation rate is inversely proportional to the mobility of the molecule; thus, the larger the molecule the faster the relaxation rate will be. The variation of the $\underline{C}$ = O relaxation rate for N,N-diethylamides is more sensitive to change of the carbonyl substituent than is that for the N,N-dimethylamides. This is attributed to the larger size of the ethyl group, which introduces a larger moment of inertia for the overall molecular motion of N,N-diethylamides.

The relaxation rates of the carbons of C = O groups in the propionamides are also increased as the nitrogen substituents are varied from $-CH_3$ to $-CH(CH_3)_2$, as shown in Figure 37. Again, this is due to the increase in the moment of inertia when the size of the nitrogen substituents become larger.

2. The ^{13}C T_1 values for the prononated C = O groups in these three series of amides are usually smaller than those for the non-protonated C = O groups, since there is one hydrogen directly bonded to them. Their values range from 1.0 to 21 sec. The variation of the ^{13}C relaxation rate for these protonated C = O groups is almost inversely proportional to molecular weight, as depicted in Figure 38. The ^{13}C spin-lattice relaxation time of the C = O group in formamide is shorter than in DMF. This is again attributed to the formation of hydrogen-bonded polymers in liquid formamide, as was postulated in discussing the ^{17}O relaxation times.

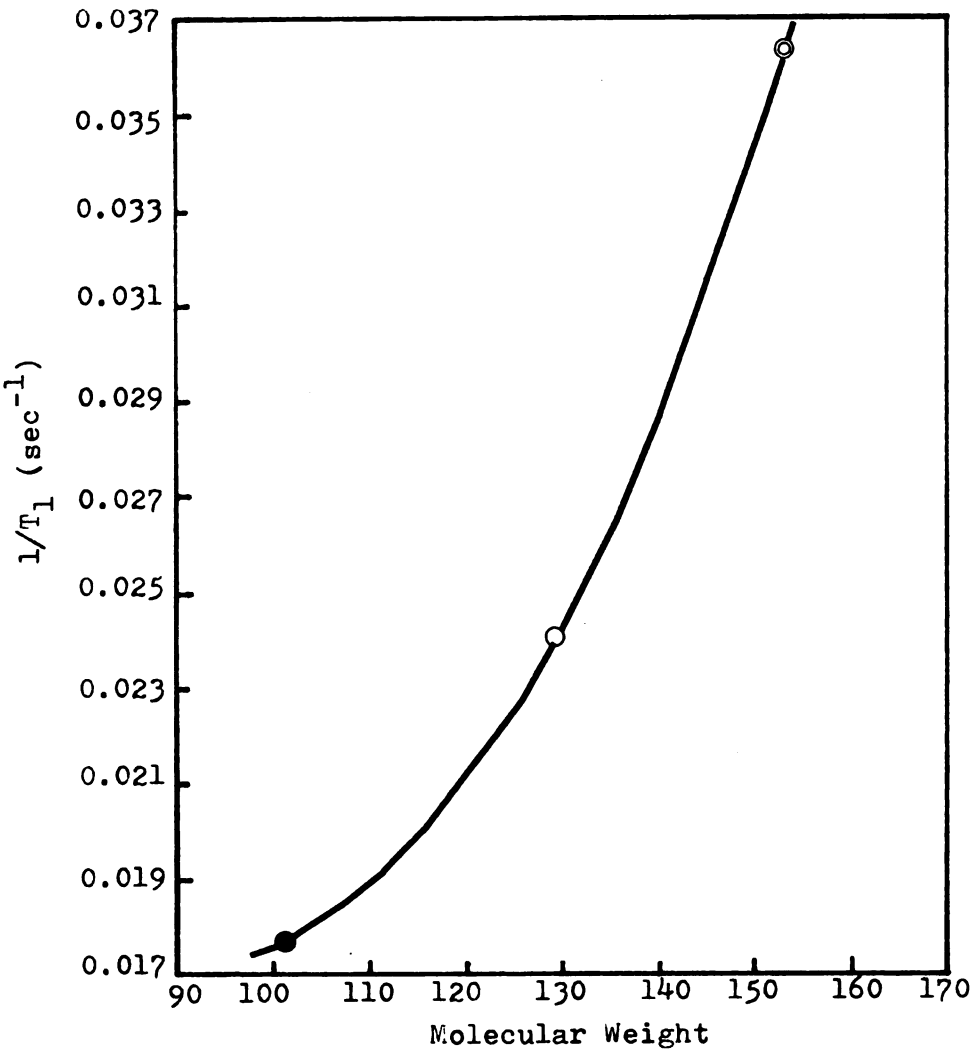

Figure 37. Relaxation rates of ^{13}C in the C=O groups of N,N-dimethylpropionamide (●), N,N-diethylpropionamide (○), and N,N-diisopropylpropionamide (⊙) plotted versus molecular weight.

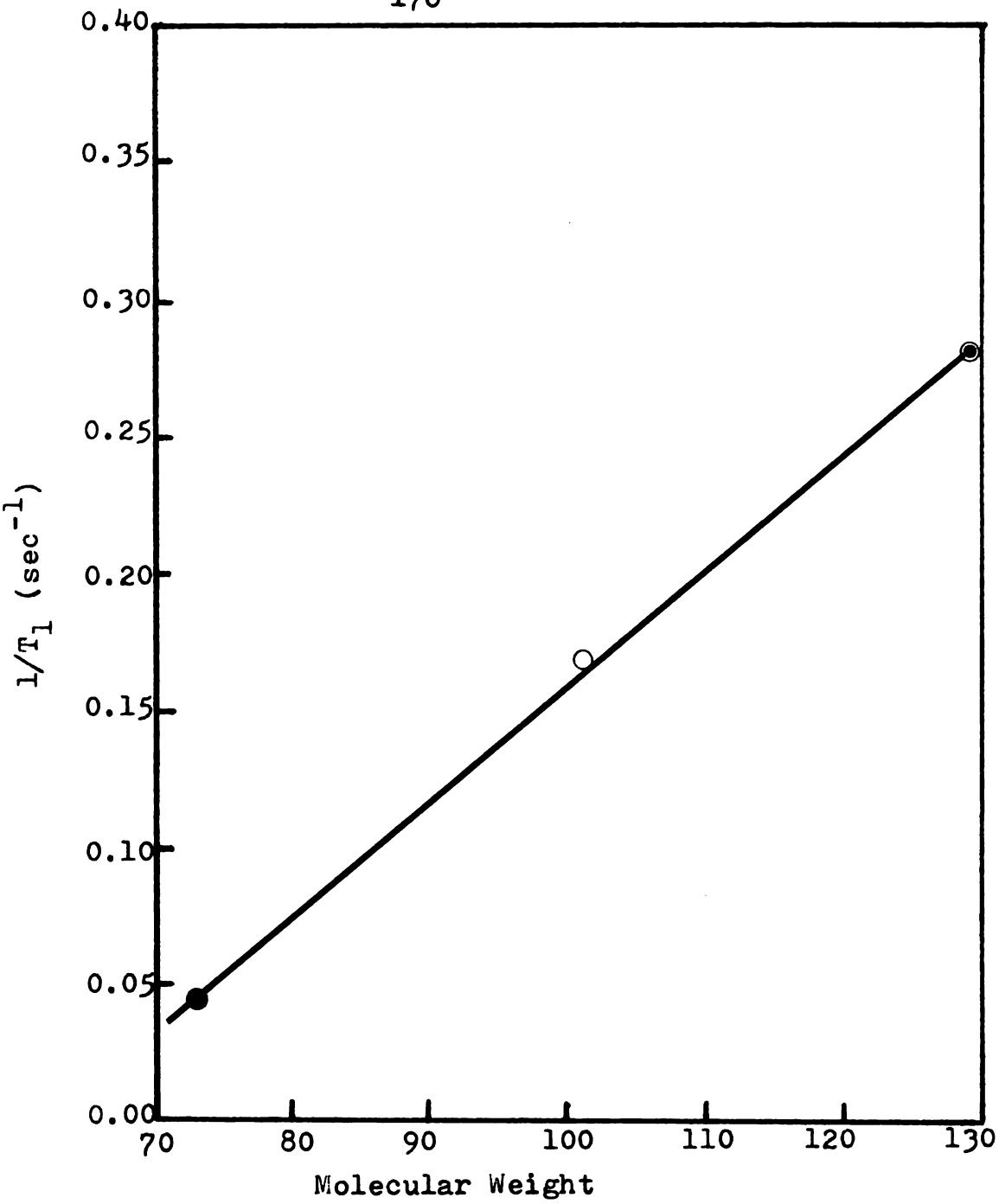

Figure 38. Relaxation rates of ^{13}C in the C=O groups of N,N-dimethylformamide (●), N,N-diethylformamide (○), and N,N-di-n-propylpropionamide (●) plotted versus molecular weight.

3. Values of the ^{13}C relaxation times for the trans- and cis-N-substituents are usually determined by the relative directions of the preferred rotation axes (if they exist). The predictable result is that the larger the angle between the preferred rotation axis and the N-substituent, the longer its relaxation time will be. This effect of motional anisotropy can sometimes be used to distinguish the chemical shifts of the trans- and cis-N-substituents if their T_1 values are determined. As we have already seen, the overall molecular motion will become more isotropic[41] as the molecular weight (or size) of the amides becomes larger, and thus this anisotropic effect will be diminished.

4. In the nitrogen substituents of N,N-diethyl and N,N-di-n-propyl amides, the ^{13}C T_1 values increase in going from an α carbon to a β or γ carbon. This is a result of a combination of the segmental motion of the methylene carbons and the internal rotation of the methyl carbons. These motions are also reflected in the NOE values and those of the effective correlation time τ_c.

The same segmental motion is also observed for the carbonyl substituents of N,N-disubstituted propionamides and n-butyramide in that T_1 increases from the α carbon outward. Although their ^{13}C T_1 values vary widely, they are normally shorter than those for non-protonated C = 0 groups or quarternary carbons. Due to the internal rotation of the $-CH_3$ group, and the segmental motion of $-CH_2-$ in the

substituents, their NOE values are usually below the maximum value, 2.988, since spin-rotation begins to make an important contribution.

5. In N,N-dimethylacrylamide and N,N-diethylacrylamide, the T_1 value for the α carbon on the carbonyl substituent is about twice the value of T_1 for the β carbon, and so is nearly inversely proportional to the number of directly bonded hydrogens, indicating that the overall molecular motions of these two unsaturated amides are nearly isotropic.

6. Due to steric effects, the NOE values for the carbons of the nitrogen substituents in N,N-di-n-propionamide tend to be random.

7. The relaxation rates of the α and β carbons in the carbonyl substituents of N,N-disubstitued propionamides, as shown in Figure 39, also increase as the size of the nitrogen substituent groups becomes bigger. This is, again, due to a decrease in the molecular mobility as the molecule becomes larger. The variation of the α-carbon relaxation rate is more sensitive than that of β carbon since its motion is only dependent on the overall molecular motion. However, that of the β carbon is also dependent on the internal rotation of methyl group.

8. The direction of the preferred rotation axis in the plane of N,N-dimethylamides is mainly determined by the masses of the carbonyl substituents and of oxygen, which indicates that the inertial effect is an important factor

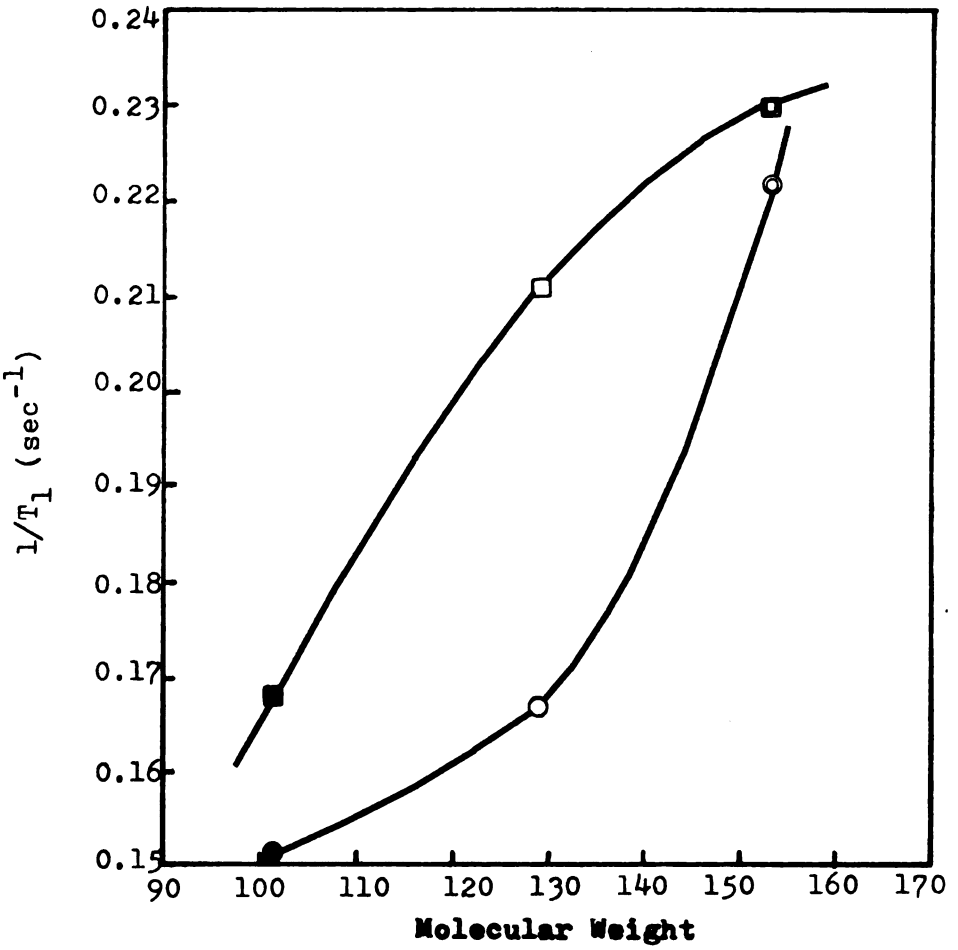

Figure 39. Relaxation rates of the α carbons of the carbonyl substituents of N,N-dimethylpropionamide (■), N,N-diethylpropionamide (□), and N,N-diisopropylpropionamide (◘) plotted versus molecular weight; (●), (○), and (⊙) are for the β carbons of the corresponding amides.

in determining the direction of the preferred rotation axis. The effect of the anisotropic motion will be greatly reduced as the size (or mass) of the molecule is increased. In N,N-diethylamides and N,N-di-n-propylamides, the difference between the relaxation times of the trans- and cis-carbons is greatly reduced, although some effects of anisotropy are still observed. Anisotropic molecular motion is also observed in unsymmetrically N,N-disubstituted amides and will be discussed in next section.

SECTION 2. NMR STUDIES OF N-MONOSUBSTITUTED AND UNSYMMETRICALLY N,N-DISUBSTITUTED AMIDES

I. RESULTS

The ^{13}C chemical shifts, spin-lattice relaxation times T_1, and NOE values determined experimentally for a series of N-monosubstituted and unsymmetrically N,N-disubstituted amides are presented in Tables 15-17. The dipolar contributions to the spin-lattice relaxation times $T_{1(DD)}$, the total contributions of the remaining mechanisms $T_{1(O)}$, and the effective correlation times τ_C are also given along with the cis-trans isomer ratios as determined from the integrated intensities.

A. Studies of cis-trans isomer ratios

N-monosubstituted amides may exist as the cis (I-A) or trans (I-B) isomers in which the nitrogen substituent R_2 is cis or trans to carbonyl oxygen. If an amide in solution

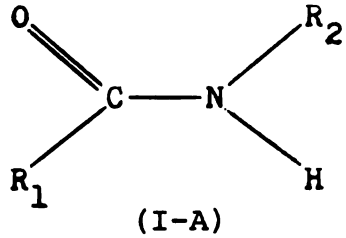

(I-A)

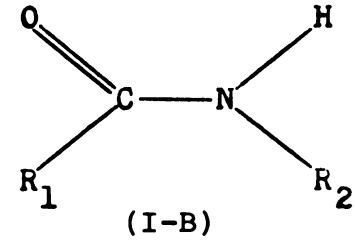

(I-B)

occurs as a mixture of cis and trans isomers, separate signals will be observed for the isomers if rotation around the C-N bond is slow, i.e., if $\tau_A >> \sqrt{2}/2\pi(\nu_A - \nu_B)$, where

τ_A is the mean lifetime at site A and ν_A and ν_B are the resonance frequencies at sites A and B, respectively. If separate cis and trans resonances can be observed, cis/trans isomer ratios can be determined. However, if only one set of signals is observed, it does not necessarily indicate that rapid rotation around the C-N bond is occurring, or that only one isomer is present, since other factors may cause chemical shift degeneracy of the trans and cis signals.

By using the relative integrated intensities of the ^{13}C NMR lines, the ratios of cis to trans isomers for some amides were obtained and are shown in the first column of each table.

Some of the cis/trans ratios for these amides have been determined by proton NMR and the values reported (as percentages) are as follows: N-methylformamide[93], 92%; N-ethylformamide[93], 88%; N-t-butylformamide[93], 70-82%; N-methylacetamide[94], 97%; N-ethylacetamide[93], 100%; N-methylpropionamide[93], 100%; N-ethylpropionamide[93], 100%; N-methyl-N-n-butylformamide[95], 39%. These are close to the values reported in Tables 15 and 16, except for N-ethylpropionamide. No values had been obtained by proton NMR for ^{14}N-n-butylformamide or ^{15}N-n-butylformamide. For N-alkylformamides the percentage of trans isomer increases as the size of the N-alkyl substituent increases[93], as shown by the values for N-methyl-N-ethylformamide and N-t-butylformamide

Table 15. ^{13}C Chemical shifts, spin-lattice relaxation times (T_1), cis-trans isomer ratios and nuclear Overhauser enhancements of N-monosubstituted amides. Derived values of the effective correlation times τ_c, and of the dipolar ($T_{1(DD)}$) and other ($T_{1(O)}$) contributions to T_1, are included.

Compound	Substituent	Chemical* Shift(ppm)	T_1(sec)	NOE	$T_{1(DD)}$ sec	$T_{1(O)}$ sec	$\tau_c x10^{12}$ sec
(A)							
N-methyl-	N-methyl	27.19(t)					
formamide		23.72(c)	14.58±0.37	1.96±0.05	30.18	28.21	0.49
cis/trans	C = O	165.99(t)					
= 10:1		162.65(c)	11.48±0.32	2.41±0.03	16.18	39.53	2.72
(B)							
N-ethyl-	N-sub -α-C	36.37(t)					
formamide		32.47(c)	6.15±0.13	2.63±0.04	7.50	34.23	2.94
	N-sub -β-C	16.15(t)					
cis/trans		13.97(c)	6.72±0.24	2.26±0.24	10.60	18.37	1.39
= 7:1	C = O	165.14(t)					
		161.84(c)	4.88±0.18	2.43±0.03	6.78	17.41	6.50
(C)							
N-t-butyl-	N-sub -α-C	49.91(t)	11.42±0.66	2.39±0.04	16.32	38.01	-
formamide		50.40(c)	10.67±0.93	2.52±0.15	13.95	45.40	-
	N-sub -β-C	30.47(t)	1.37±0.05	2.31±0.02	2.08	4.02	7.06
		28.65(c)	1.31±0.01	2.70±0.00	1.53	9.07	9.60
cis/trans							
= 3:1	C = O	163.21(t)	1.50±0.06	2.69±0.31	1.76	10.04	25.03
		161.05(c)	1.15±0.02	2.74±0.06	1.31	9.25	33.63

Table 15 (cont'd.)

Compound	Substituent	Chemical* Shift(ppm)	T_1(sec)	NOE	$T_{1(DD)}$ sec	$T_{1(O)}$ sec	$\tau_c \times 10^{12}$ sec
(D) N-methyl-acetamide	N-methyl	25.10	6.58±0.17	2.44±0.12	9.08	23.90	1.62
	Carbonyl-CH_3	21.52	7.12±0.19	2.68±0.12	8.42	46.08	1.74
	C = O	170.94	17.43±0.34	2.72±0.02	20.14	129.71	-
(E) N-ethyl-acetamide	N-sub -α-C	33.79	4.07±0.64	2.43±0.08	5.66	14.52	3.89
	N-sub -β-C	21.92	4.47±0.38	2.88±0.02	4.72	83.01	3.11
	Carbonyl-CH_3	14.01	7.61±0.89	2.44±0.12	10.50	27.64	1.40
	C = O	170.20	12.64±0.46	2.38±0.07	18.20	41.38	-
(F) N-methyl-propionamide	N-methyl	25.05	5.85±0.21	2.58±0.09	7.36	28.56	2.00
	Carbonyl-sub-α-C	28.54	3.77±0.17	2.28±0.10	5.85	10.60	3.77
	Carbonyl-sub-β-C	9.29	6.46±0.50	2.23±0.09	10.44	16.96	1.41
	C = O	174.42	14.89 0.27	2.27±0.11	23.30	41.26	-

Table 15 (cont'd.)

Compound	Substituent	Chemical* Shift(ppm)	T_1(sec)	NOE	$T_{1(DD)}$ sec	$T_{1(O)}$ sec	$\tau_c \times 10^{12}$ sec
(G) N-ethyl-propionamide	N-sub -α-C	33.54(t) 33.68(c)	1.47±0.12	2.56±0.09	1.87	6.84	11.78
	N-sub -β-C	14.07(t,c)	2.35±0.10	2.22±0.07	3.83	6.09	3.83
	Carbonyl-sub -α-C	28.35(t) 28.79(c)	1.55±0.04	2.82±0.07	1.69	18.44	13.03
	Carbonyl-sub -β-C	9.37(t) 9.46(c)	3.21±0.09	2.58±0.07	4.04	15.67	3.63
	C = O	176.82(t) 173.82(c)	6.64±0.83 8.51±0.23	2.18±0.18 2.24±0.05	11.18 13.64	16.35 22.64	- -

*Chemical shifts are relative to TMS and + indicates downfield. The measurements were made at 35°C. All the compounds were pure and degassed. c = cis, t = trans, and N-sub-α-C indicates the α carbon of the nitrogen substituent.

Table 16. ^{13}C Chemical shifts, spin-lattice relaxation times (T_1), cis/trans isomer ratios and nuclear Overhauser enhancements (NOE) of N^{14}-n-butylformamide and N^{15}-n-butylformamide. Derived values of the effective correlation times τ_c, and of the dipolar ($T_{1(DD)}$) and other ($T_{1(O)}$) contributions to T_1, are included.

Compound	Substituent	Chemical* Shift(ppm)	T_1(sec)	NOE	$T_{1(DD)}$ sec	$T_{1(O)}$ sec	$\tau_c \times 10^{12}$ sec
(A)							
N^{14}-n-butyl-formamide	N-sub -α-C	41.25(t) 37.33(c)	1.70±0.03	2.80±0.08	1.88	18.06	11.72
	N-sub -β-C	33.19(t) 31.34(c)	2.19±0.07	2.60±0.04	2.72	11.24	8.10
cis/trans = 9:1	N-sub -γ-C	19.33(t) 19.79(c)	3.43±0.13	2.51±0.08	4.51	14.29	4.88
(neat)	N-sub -δ-C	13.21(t,c)	4.52±0.17	2.34±0.14	6.70	13.88	2.19
	C = O	164.98(t) 161.56(c)	1.82±0.06	2.69±0.03	2.13	12.11	20.68
(B)							
N^{15}-n-butyl-	N-sub -α-C	41.64(t) 41.16(t) 37.68(c) 37.20(c)	1.22±0.08	2.77±0.10	1.37	11.17	16.08
cis/trans = 10:1	N-sub -β-C	33.10(t) 31.27(c)	1.94±0.12	2.74±0.10	2.22	15.61	9.92
(neat)	N-sub -γ-C	19.34(t) 19.80(c)	2.78±0.09	3.30±0.10	4.25	8.04	5.18
	N-sub -δ-C	13.23(t,c)	4.34±0.13	2.27±0.10	6.79	12.03	2.16
	C = O	165.69(t) 165.00(t) 162.34(c) 161.66(c)	1.52±0.05	2.90 0.02	1.59	34.33	27.71

given in Table 15. This trend has been explained in terms of simple steric interactions between the N-alkyl group and the carbonyl oxygen. However, no satisfactory explanation has been given[93] for the predominance of the cis isomer in N-alkylformamides, such as N-methylformamide, in which no steric interactions favoring the cis isomer are present, or in amides in which steric interaction would seem to favor the trans form, such as N-t-butylformamide[93].

B. ^{13}C Chemical shifts of amides and the ^{15}N-^{13}C coupling constants in ^{15}N-n-butylformamide

The ^{13}C chemical shifts of the trans isomers in N-monosubstituted amides are normally downfield relative to the cis isomers just as in the symmetrically N,N-disubstituted amides. However, exceptions are observed in the case of the α carbon of the N-t-butyl group in N-t-butylformamide and the α carbons of both the N-ethyl group and the carbonyl substituent in N-ethylpropionamide. The reason for these results is not clear. Due to the ^{13}C γ effect[96] and δ effect[31], the ^{13}C chemical shifts of the cis γ and δ carbons are usually downfield relative to the trans[97], as seen in ^{14}N-n-butylformamide, ^{15}N-n-butylformamide, and N-methyl-N-n-butylformamide. The coupling constants between ^{15}N and ^{13}C in the trans and cis forms are the same. The results are $J_{^{15}N,\ C=O}$ = 13.8 Hz and $J_{^{15}N,\ N\text{-}\alpha\text{-carbon}}$ = 9.6 Hz.

C. ^{13}C Relaxation studies and nuclear Overhauser effects

Most of the N-monosubstituted amides exist as trans and cis isomers at room temperature. However, the percentages of the trans isomer at room temperature are so low that measurement of their ^{13}C T_1 values become impossible. Thus, only the T_1 values for the cis isomers are reported, except in certain cases where the peaks for the trans isomers are intense enough to be measured, such as N-methyl-N-n-butylformamide, N-t-butylformamide and the carbonyl group of N-ethylpropionamide.

(1) N-monosubstituted amides

Comparing the T_1 data of N-monosubstituted amides with those of the corresponding N,N-disubstituted amides in Tables 11-13, we find that the ^{13}C relaxation times of C = O groups in N-monosubstituted amides are shorter than those of the corresponding N,N-disubstituted amides even though the molecular weights of N-monosubstituted amides are smaller than those of the corresponding N,N-disubstituted amides, as seen in the pairs N-methylformamide, N,N-dimethylformamide; N-methylacetamide, N,N-dimethylacetamide; N-methylpropionamide, N,N-dimethylpropionamide; N-ethylformamide, N,N-diethylformamide; N-ethylpropionamide, N,N-diethylpropionamide; and N-n-butylformamide, N-n-butyl-N-methylformamide. This effect is especially enhanced in the ^{13}C T_1 data for non-protonated C = O groups, i.e., all but

the substituted formamides. All of these results indicate that hydrogen bonds are formed in N-monosubstituted amides, which become impossible in the N,N-disubstituted amides.

The internal rotational rates of N-methyl groups in N-monosubstituted amides are still very fast, as seen in the NOE values, since this internal rotation is not affected by the hydrogen bonding very much. The segmental motion of the long chain substituents on nitrogen and on the C = O groups is also reflected in the T_1 values, which show increases in going from the heavy end to the free end. Let us assume that[98]

$$1/\tau_C = 1/\tau_R + 1/\tau_G \qquad (139)$$

where τ_R is the correlation time for the overall reorientation of the molecule and is approximately equal to the effective correlation time of the C = O group in N-alkylformamide; τ_G is an effective correlation time for the internal motion of some group in the molecule. It follows that the τ_G value for the N-methyl group in N-methylformamide is 0.59×10^{-12} sec, while the τ_G values for the α and β carbons of the N-ethyl group in N-ethylformamide are 5.38×10^{-12} sec and 1.77×10^{-12} sec, for the α, β, γ, and δ carbons of the N-n-butyl group in ^{14}N-n-butylformamide and ^{15}N-n-butylformamide are 27.05×10^{-12} sec, 13.32×10^{-12} sec, 6.39×10^{-12} sec, 2.45×10^{-12} sec and 38.31×10^{-12} sec, 15.45×10^{-12} sec, 6.37×10^{-12} sec, and 2.34×10^{-12} sec,

respectively. The effective correlation times τ_G increased about 11 to 17 times in going from the α to the δ carbon in N-n-butylformamide.

In ^{15}N-n-butylformamide and ^{14}N-n-butylformamide, the gyromagnetic ratios of ^{15}N and ^{14}N are very small compared with that of the proton, so the relaxation of the carbon of the C = O group, and of the α carbon on the N-n-butyl group, due to the dipolar interaction with the nitrogen, is not important and can be neglected. The ^{13}C T_1 values for ^{14}N-n-butylformamide are a little longer than those for ^{15}N-n-butylformamide, presumably due to the difference in the atomic weights of ^{15}N and ^{14}N.

In N-t-butylformamide, the T_1 values for the carbons in both the <u>trans</u> and <u>cis</u> isomers have been measured and it is seen that the T_1 values for the <u>trans</u> carbons are longer than those for the <u>cis</u> carbons. This effect is believed to result from the direction of the preferred overall molecular rotation axis which, for the <u>trans</u> form, lies roughly along the direction of a line joining carbonyl oxygen and the tertiary carbon of the t-butyl group (structure II-A). The τ_G value for the <u>cis</u> β carbon is

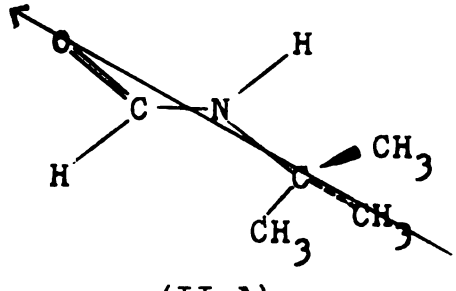

(II-A)

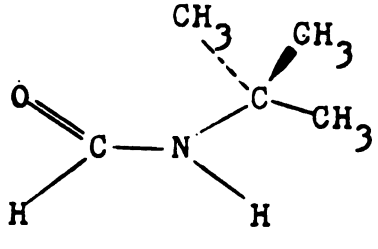

(II-B)

13.44×10^{-12} sec, which is considerably longer than that of the β carbon in N-ethylformamide (5.38×10^{-12} sec) indicating that the steric effect and mass effect are both important for the β carbon of N-t-butylformamide. In the cis isomer (Structure II-B) the motion is more nearly isotropic.

In the series of N-alkyl formamides (compounds A, B, C in Table 11 and compounds A, B in Table 16), N-alkyl acetamides (compounds D, E in Table 15) and N-alkyl propionamides (compounds F, G in Table 15), the relaxation rate of the carbon of the C = O group increases as the molecular weight of the amides increases. This mass effect is also shown by the relaxation rates for the carbons of the N-methyl groups of N-methylformamide, N-methylacetamide and N-methylpropionamide (as shown in Figure 40), and for the α and β carbons of the N-ethyl groups in N-ethylformamide, N-ethylacetamide, and N-ethyl propionamide. Again, the relaxation rate of the α carbon is more sensitive than that of the β carbon (Figure 41), since the α carbon is more dependent on the overall molecular motion.

The T_1 values for the carbons of the C = O groups in N-alkylformamides are considerably smaller than those of the corresponding N-alkyl acetamide or propionamide, since there is one hydrogen directly bonded to the C = O group in N-alkylformamides.

(2) Unsymmetrically N,N-disubstituted amides

Only four unsymmetrically N,N-disubstituted amides were studied, as shown in Table 17.

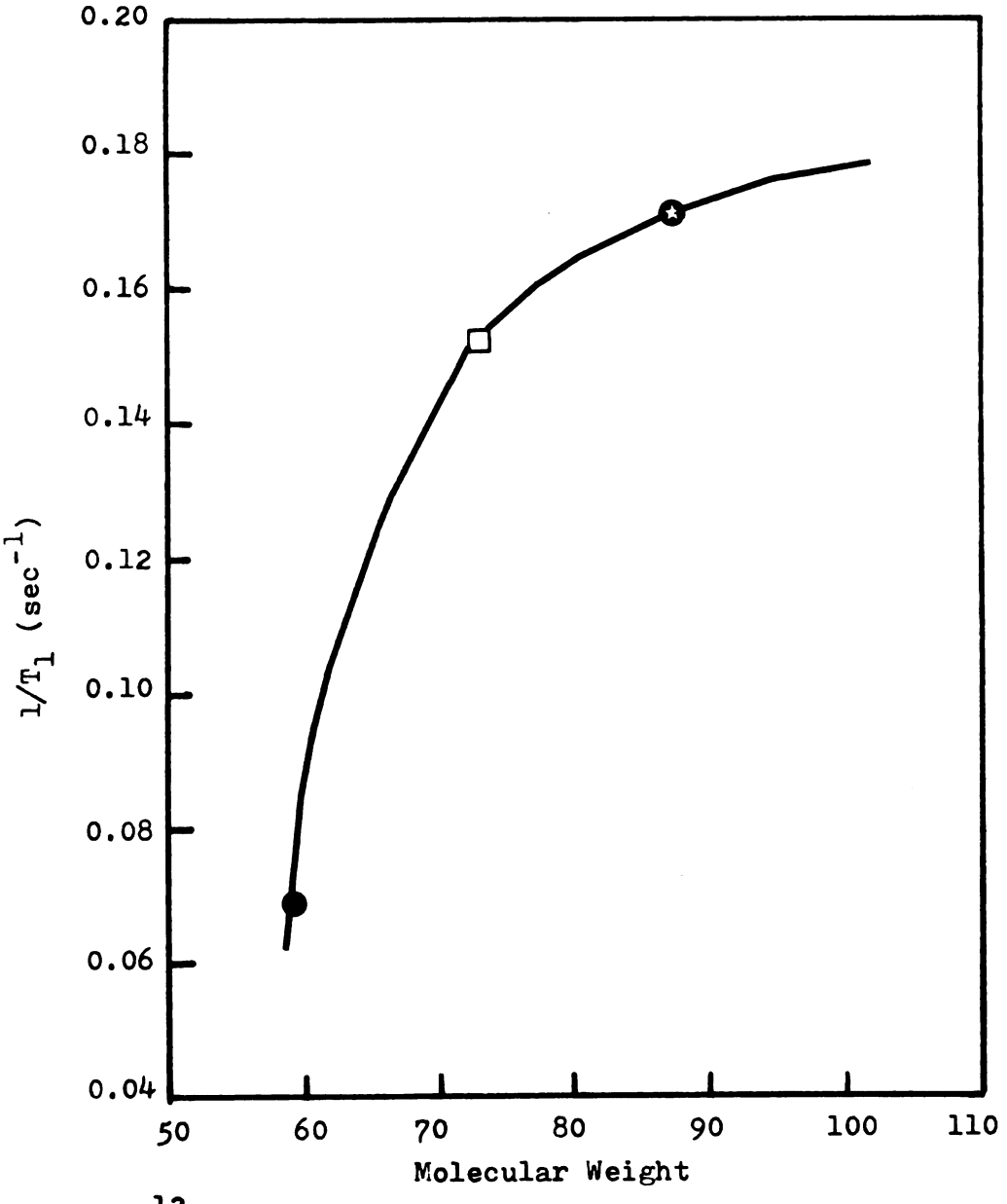

Figure 40. ^{13}C relaxation rates for the carbons of the N-$\underline{C}H_3$ groups of N-methylformamide (●), N-methylacetamide (□), and N-methylpropionamide (✪) plotted versus molecular weight.

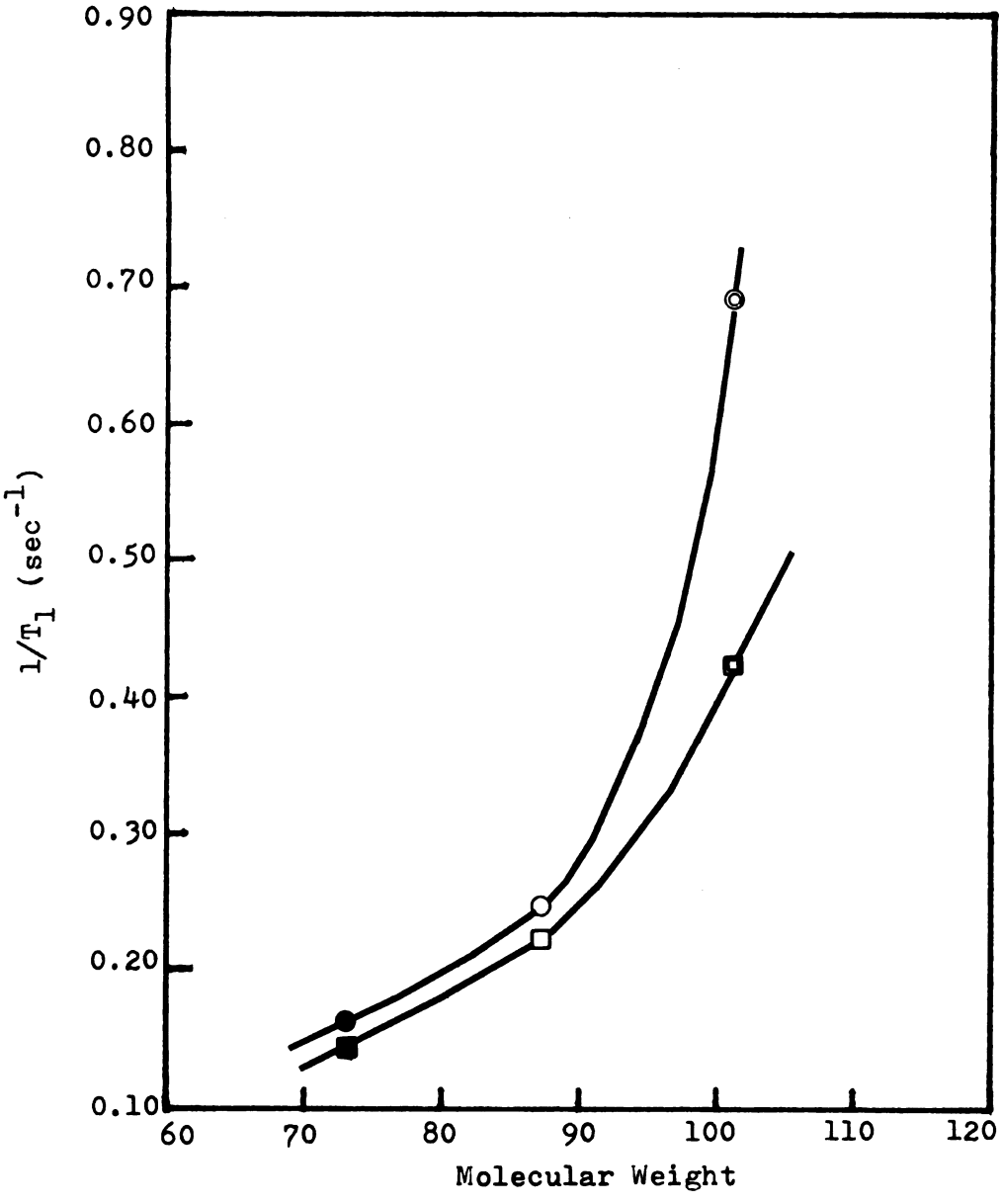

Figure 41. Relaxation rates of the α-carbon and β-carbon of the N-ethyl group of N-ethylformamide (●) (■), N-ethylacetamide (○)(□), and N-ethylpropionamide (◎)(◘) plotted versus molecular weight.

Table 17. ^{13}C Chemical shifts, spin-lattice relaxation times (T_1) and nuclear Overhauser enhancements of unsymmetrically N,N-disubstituted amides

Compound	Substituent	Chemical Shift (ppm)	T_1 (sec)	NOE	$T_{1(DD)}$ sec	$T_{1(O)}$ sec	$\tau_c \times 10^{12}$ sec
(A)							
N-methyl-N--n-butyl-formamide	N-methyl	33.40(t)	7.10±0.54	2.97±0.11	7.16	> 200	2.05
		28.26(c)	11.74±0.58	2.00±0.05	23.33	23.63	0.63
	N-n-but-α-C	48.28(t)	3.95±0.37	2.48±0.03	5.30	15.48	4.16
		42.94(c)	4.37±0.52	2.48±0.03	5.87	17.13	3.75
cis/trans = 0.76:1	N-n-but-β-C	29.95(t)	4.04±0.13	2.38±0.10	5.82	13.22	3.78
		28.59(c)	5.08±0.05	2.10±0.01	9.18	11.38	2.40
	N-n-but-γ-C	19.23(t)	5.96±0.26	2.33±0.08	8.90	18.03	2.47
		19.66(c)	6.15±0.41	2.22±0.11	10.02	15.93	2.20
	N-n-but-δ-C	13.28(c)					
		13.20(t)	4.92±0.27	2.79±0.02	5.46	49.62	2.69
	C = O	161.89(t,c)	5.81±0.23	2.49±0.03	7.75	23.23	7.58
(B)							
N-methyl-N-t-butyl-acetamide	N-methyl	32.46	11.92±0.51	1.82±0.07	28.89	20.28	0.51
	Carbonyl-CH_3	24.94	6.20±0.26	2.21±0.03	10.19	15.85	1.44
	N-t-but-α-C	55.75	33.34±2.00	2.31±0.11	50.59	97.75	-
	N-t-but-β-C	27.92	3.39±0.05	3.00±0.18	3.39	> 200	4.34
	C = O	170.01	21.34±0.55	1.57±0.08	74.45	29.93	-

Table 17 (cont'd.)

Compound	Substituent	Chemical* Shift(ppm)	T_1 (sec)	NOE	$T_{1(DD)}$ sec	$T_{1(O)}$ sec	$\tau_c \times 10^{12}$ sec
(C) N-methyl-N-ethyl-trimethylacetamide	N-methyl	34.90	7.72±0.41	2.59±0.09	9.65	38.64	1.52
	N-n-et-α-C	44.17	2.16±0.09	2.97±0.09	2.18	200	10.10
	N-n-et-β-C	12.38	3.47±0.14	2.54±0.05	4.48	15.42	3.28
	0=C-sub-α-C	38.26	24.54±1.49	2.15±0.17	42.40	58.26	-
	0=C-sub-β-C	28.06	3.20±0.04	2.60±0.10	3.97	16.43	3.70
	C = O	175.37	48.91±1.74	2.00±0.05	97.18	98.46	-
(D) N-methyl-N-n-butyl-trimethylacetamide	N-methyl	35.65	5.79±0.25	2.29±0.03	8.92	16.51	1.65
	N-n-but-α-C	49.29	1.20±0.07	2.64±0.01	1.45	6.87	15.19
	N-n-but-β-C	29.53	1.66±0.05	2.67±0.07	1.98	10.41	11.12
	N-n-but-γ-C	19.83	2.43±0.05	2.47±0.05	3.28	9.34	6.72
	N-n-but-δ-C	13.67	3.26±0.08	2.35±0.05	4.80	4.92	3.06
	0=C-sub-α-C	38.26	30.09±1.49	1.98±0.02	61.01	59.37	-
	0=C-sub-β-C	28.11	2.28±0.04	2.59±0.05	2.85	11.41	5.15
	C = O	175.12	27.81±0.67	2.14±0.03	48.47	65.24	-

*Chemical shifts are relative to TMS. The measurements were made at 35°C using purified compounds. Only the cis form could be detected for compounds C and D.

In N-methyl-N-n-butylformamide, all the carbons in both the trans and cis isomers are observed except those in the C = O group. The T_1 value of the cis-N-methyl group carbon (Structure III-A) is longer than that of the trans-NCH_3 group (Structure III-B), indicating that an anisotropic molecular rotation axis approximately along a line joining the C = O group and the N-n-butyl group may exist in the molecular plane, as shown in Structure III-A. However, when the NCH_3 group is trans to the C = O group, as shown in Structure III-B this preferred rotation axis will not exist and the motion will be nearly isotropic.

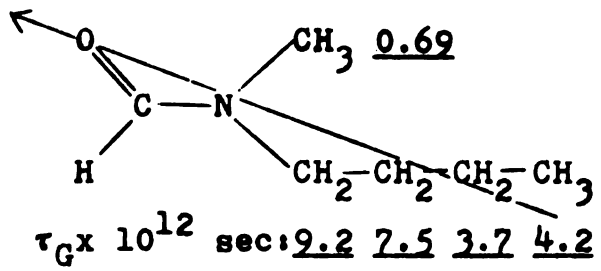

(III-A)

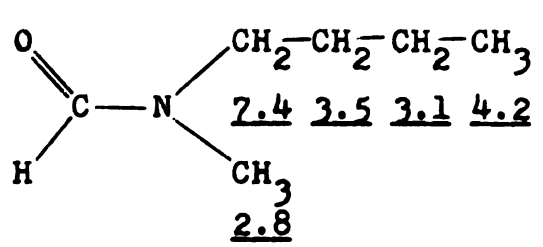

(III-B)

Based on the INDO calculations of N-ethyl-N-methylformamide (see Part II of thesis), we predict that the most stable conformation of Structure E for N-n-butyl-N-methylformamide is that shown in Figure 42. Using the approximate ellipsoidal molecular model, the diffusion constant along the preferred rotation axis $D_{||}$ is approximately 1.82×10^{10} sec^{-1}, and the diffusion constant $D_{\perp}$ for motion around the axis perpendicular to the molecular plane is about 4.23×10^{10} sec^{-1}, which is about equal to the $D_{\perp}$

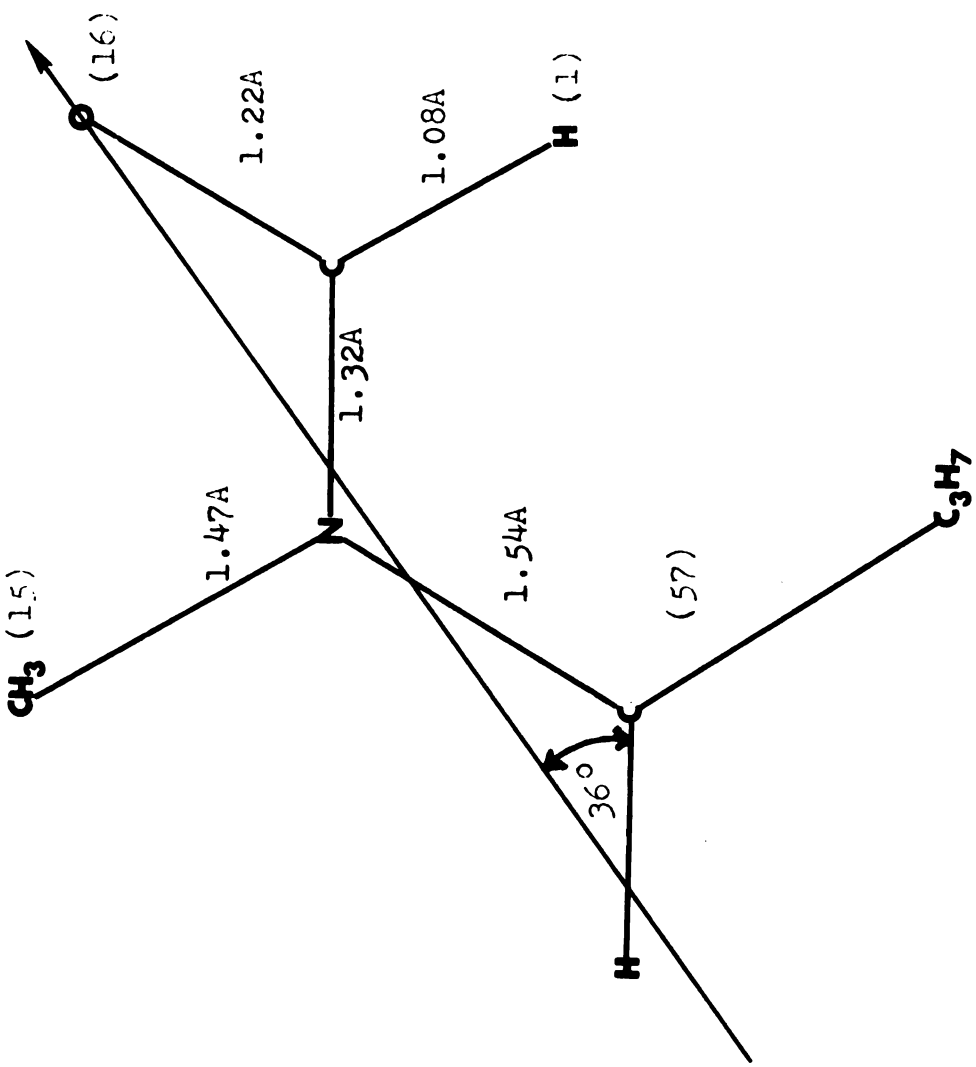

Figure 42. Preferred rotation axis for the molecular motion of N-n-butyl-N-methyl-formamide in the conformer with the n-butyl group trans to the C=O group.

value (4.17×10^{10} sec^{-1}) for N,N-dimethyl-n-butyramide. The molecular weights of N-n-butyl-N-methylformamide and N,N-dimethyl-n-butyramide are the same, this indicates that the overall molecular rotation around the axes perpendicular to the molecular planes are about the same, since their sizes are nearly equal. The T_1 values for the carbons of the trans-N-n-butyl group are shorter than those for the cis-N-n-butyl group, which we attribute to this anisotropic molecular motion. In the carbons of the N-n-butyl group of N-methyl-N-n-butylformamide, the T_1 values also increased from the α carbon to γ carbon. However, the T_1 value for the δ carbon is shorter than that for the γ carbon, which may be due to a steric effect as shown by the very high NOE for the δ carbon. The τ_G values calculated by use of Equation (139) are also shown in Structure (III-A) and Structure (III-B). The ratio of the τ_G value of the γ carbon to the α carbon is about three in the N-n-butyl group of N-methyl-N-n-butylformamide, and so is considerably smaller than the ratio of τ_G values for the γ and α carbons in the N-n-butyl group of ^{15}N- or ^{14}N-n-butylformamide. This is mainly a result of hydrogen bonding in N-n-butylformamide which is impossible in N-methyl-N-n-butylformamide.

In N-methyl-N-t-butylacetamide, N-n-butyl-N-methyltrimethylacetamide, and N-n-ethyl-N-methyltrimethylacetamide, the T_1 values of the non-protonated C = O carbon and of the quarternary carbons are very long, as expected. Their

NOE values are also very low since no hydrogen is directly bonded to them. The increase in T_1 values in going from the α carbon to the δ carbon in the N-n-butyl group of N-methyl-N-n-butyltrimethylacetamide is greater than that in N-methyl-N-n-butylformamide, but less than that in the N-n-butylformamide. This is due to having a heavier substituent group, the t-butyl group, on the C = O group of N-methyl-N-n-butyltrimethylacetamide, than the hydrogen on the C = O group of N-methyl-N-n-butylformamide. However, the variation of T_1 values in going along the chain of the n-butyl group in N-methyl-N-n-butyltrimethylacetamide is still less than that for N-n-butylformamide since hydrogen bonding does not exist in N-methyl-N-n-butyltrimethylacetamide.

Due to the mass effect, the T_1 values of the C = O group carbon and the NCH_3 group carbon in N-methyl-N-ethyltrimethylacetamide are longer than those in N-methyl-N-n-butyltrimethylacetamide. Since there is no hydrogen bonding in unsymmetrically N,N-disubstituted amides and symmetrically N,n-disubstituted amides, the T_1 values of the carbons of the C = O group will be comparable if their molecular weights are the same.

D. ^{14}N relaxation times and quadrupole coupling constants in some amides

Some ^{14}N relaxation times for the amides were measured and are shown in Table 18.

Due to hydrogen bonding, the ^{14}N relaxation times of N-alkylformamides are shorter than found for N,N-dimethylformamide. Quadrupole coupling constants may be estimated from the NMR data using the approximate equation[5]

$$\frac{1}{T_1} = \frac{3\pi^2}{2} \left(1 + \frac{\eta^2}{3}\right) \left(\frac{e^2qQ}{h}\right) \tau_c \quad , \qquad (140)$$

where η is the asymmetry parameter, e^2qQ/h is the quadrupole coupling constant, and τ_c is the effective correlation time of the molecular motion, which can be derived from the correlation time of the $\underline{C}$ = O carbon of each amide. The calculated quadrupole coupling constants are shown in Table 18. In the calculations, the asymmetry parameter used for each amide was the same as that reported for formamide since they tend not to vary much in a series, as shown by the values reported for hydrazine and its derivatives[100,101].

Our results show that the calculated quadrupole coupling constant of ^{14}N in formamide is very close to the value (2.274 MHz) reported in Reference 99(a). However, it is a little bit lower than the value (3.67 MHz) reported in Reference 99(b). The quadrupole constant obtained here for ^{14}N in N,N-dimethylformamide is also lower than the value (4.37 MHz) reported in Reference 99(b).

Table 18. ^{14}N Spin-lattice relaxation times (T_1) and quadrupole coupling constants in some amides

Compound	T_1[a] (sec)	τ_c (sec)	η%	(e^2qQ/h) (MHz)
Formamide	0.002104 ± 0.000100	4.14×10^{-12}	37.8[b]	2.61
N-methyl-formamide	0.002021 ± 0.000100	2.72×10^{-12}	37.8	3.29
N-ethyl-Formamide	0.000784 ± 0.000047	6.50×10^{-12}	37.8	3.41
N,N-dimethyl-formamide	0.003568 ± 0.000178	1.75×10^{-12}	37.8	3.08

[a] T_1 was measured by the inversion-recovery method.

[b] The asymmetry parameter for formamide is from Reference 99(a) and is in percent. The same value is assumed for the remaining amides in the table.

E. Energy of the hydrogen bond in N-ethylformamide

In order to estimate the energy of the hydrogen bond in liquid N-ethylformamide, the variation of the ^{14}N relaxation rate with temperature was measured, as shown in Table 19 and Figure 43. The energy barrier for the overall molecular motion of N-ethylformamide is about 5.58 kcal/mol, which compares with the value 4.10 kcal/mol for N,N-dimethylformamide which has the same molecular weight as N-ethylformamide. The estimated energy of the hydrogen bond is the difference between these values, approximately 1.48 kcal/mol

The enthalpy of formation of the hydrogen bond for N-methylformamide in benzene is 3.4 kcal/mol[102]. Klotz and Franzen[103] found that the energy of the hydrogen bond in N-methylacetamide decreased as the solvent became more polar. Davis and Thomas[102] also found that the formation constant of the hydrogen bond will decrease as the N-alkyl group becomes more bulky. All these results indicate that our value of 1.48 kcal/mol for N-ethylformamide is very reasonable.

Table 19. Temperature dependence of the ^{14}N spin-lattice relaxation time in N-ethylformamide[a].

Temperature (°C)	$T_1(^{14}N)$[b] (sec)
28.0	7.84×10^{-4}
30.0	8.58×10^{-4}
40.0	1.00×10^{-3}
51.0	1.40×10^{-3}
62.0	1.63×10^{-3}
70.0	1.87×10^{-3}
83.0	2.19×10^{-3}
95.0	2.43×10^{-3}
104.0	2.78×10^{-3}

[a]The sample was purified but not degassed.

[b]The T_1 value at each temperature is the average of at least five measurements. The probable errors of T_1 values are within 5 %.

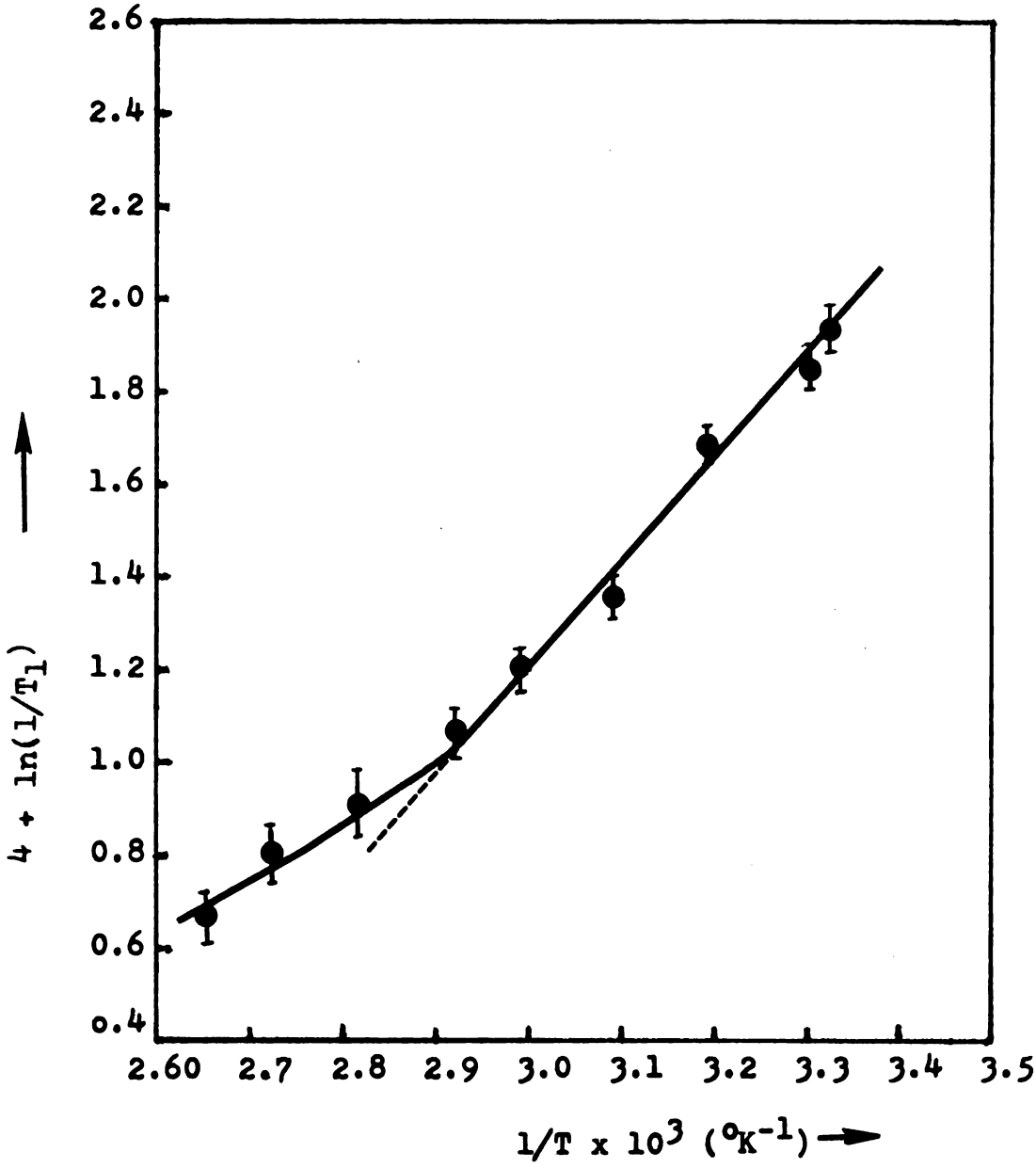

Figure 43. Plot of $\ln(1/T_1)$ versus $1/T \times 10^3$ for ^{14}N in N-ethylformamide; E_a = 5.58 kcal/mol for the overall molecular motion. The probable error is ± 0.5 kcal/mol.

SECTION 3. NMR STUDIES OF THE ANISOTROPIC MOLECULAR MOTION IN N-ALKYL ACETANILIDES AND FORMANILIDES

I. BACKGROUND

Many small molecules tumble anisotropically in the liquid phase or in solution. Preferential tumbling modes occur, resulting from the inertial, frictional, and electrostatic effects, as well as from the intramolecular and intermolecular interactions. Anisotropic molecular motion may also occur with large molecules, although localized electrostatic and inertial effects tend to cancel out in these systems. For large polycyclic molecules,[41] the central molecular framework may orient isotropically, while peripheral molecular fragments have shorter effective correlation times τ_c resulting from internal motions that are comparable with, or faster than, overall molecular reorientation.

The effect of the anisotropic overall, or internal, motion on T_1 values for the different carbons in a molecule which are bonded to hydrogen depends on the angular relationships between each C-H vector and the preferred rotation axis.

Anisotropic molecular motion of monosubstituted benzenes around the C_2 axis has been thoroughly

studied[47,63,88,104]. Levy et al.[47] found that, if the substituent is large and heavy, or highly polar, rotation around the C_2 axis may be 20 to 50 times faster than rotation around the remaining two perpendicular axes. Rotation around the C_2 symmetry axis does not lead to any modulation of the dipole-dipole interaction for the para ^{13}C and its directly attached hydrogen. However, such a rotation does lead to the relaxation of the ortho and meta carbons since the C-H vectors in these two positions make angles 60° and 120° with the C_2 axis. Therefore, the relaxation times of ortho and meta carbons are longer than those of para carbon. The steric effect of the ortho or para alkyl substituent on the rotation of biphenyls has also been studied[105] and it was found that the relaxation times of meta and para carbons are nearly equal, indicating that the rotation around the C_2 axis in 2,2', 6,6'-tetramethylbiphenyl is more difficult than that in biphenyl. Levy[86] also studied the internal motion of the five-membered rings in monosubstituted ferrocenes and found that a substituent can effectively reduce the rotation rate of the substituted ring, simultaneously allowing relatively free spinning of the unsubstituted ring.

Allerhand, Doddrell, and Komorowski[41] have developed the relaxation equation for a group ($-CH_3$, benzene ring, etc.) attached to a rigid isotropic tumbler and undergoing internal rotation.

$$\frac{1}{T_{1(DD)}} = \frac{n_S \hbar^2 \gamma_I^2 \gamma_S^2}{r_{IS}^6} \left(\frac{A}{6D} + \frac{B}{5D + R} + \frac{C}{2D + 4R}\right). \qquad (141)$$

Here, R is the internal rotational diffusion constant and D is the overall molecular diffusion parameter. The above equation is similar to Equation (132) except that $D_{||}$ is replaced by R and $D_{\perp}$ replaced by D. All the other symbols are the same as for Equation (132) except that ℓ is now the direction cosine of the angle between the C-H vector and the internal rotation axis. Replacing R/D by ρ in in Equation (141), Equations (134) and (135) will be obtained.

II. ANALYSIS OF THE ^{13}C CHEMICAL SHIFTS IN N-ALKYLACETANILIDES AND N-ALKYLFORMANILIDES

The experimental ^{13}C chemical shifts, relaxation times T_1, and NOE values are shown in Tables 20 and 21 along with the derived values of the dipolar and other contributions to the spin-lattice relaxation times ($T_{1(DD)}$ and $T_{1(O)}$), and the effective correlation times, τ_C, for N-alkylacetanilides and N-alkylformanilides. At room temperature, most of the N-alkylacetanilides and N-alkylformanilides exist predominantly as the <u>exo</u> isomers[106-111], i.e., the phenyl group is <u>trans</u> to the C = O oxygen.

In order to compare the ^{13}C chemical shifts with those for previously studied amides, the following series of amides are examined:

(1) N-Methylacetanilide, N-methylacetamide, N,N-dimethyl acetamide, N-methyl-N-t-butylacetamide.

Table 20. Experimental ^{13}C chemical shifts, spin-lattice relaxation times T_1, and nuclear Overhauser enhancements NOE, in the N-alkylacetanilides. The derived values of the dipolar and other contributions to the spin-lattice relaxation times, $T_{1(DD)}$ and $T_{1(O)}$, and of the effective correlation times, are also given.

Compound	Substituent	Chemical Shift* (ppm)	T_1 (sec)	NOE	$T_{1(DD)}$ sec	$T_{1(O)}$ sec	$\tau_c \times 10^{+12}$ sec
(A)							
N-Methyl-	Carbonyl-CH_3	22.25	7.80±0.33	2.18±0.06	13.14	19.19	1.12
acetanilide	N-methyl	36.95	6.89±0.55	2.27±0.06	10.79	19.08	1.36
	N-phenyl-o-C	127.01	3.74±0.13	2.19±0.10	6.25	9.32	7.05
(3.7M in $CDCl_3$)	N-phenyl-p-C	127.52	2.36±0.12	2.94±0.10	2.42	97.74	18.20
	N-phenyl-m-C	129.66	3.84±0.07	2.49±0.10	5.12	15.33	8.60
	N-phenyl-q-C	144.62	47.76±8.16	1.71±0.10	133.73	74.29	-
	C = O	169.90	51.88±6.45	1.91±0.10	113.34	95.67	-
(B)							
N-Ethyl-	Carbonyl-CH_3	22.44	6.38±0.47	2.65±0.13	7.69	37.52	1.91
acetanilide	N-ethyl-α-C	43.53	2.01±0.14	2.99±0.04	2.01	> 200	10.96
	N-ethyl-β-C	12.93	2.89±0.14	2.52±0.11	3.78	12.28	3.88
(4.1M in $CDCl_3$)	N-phenyl-o-C	128.10	2.83±0.10	2.50±0.08	3.75	11.53	11.75
	N-phenyl-p-C	127.57	1.48±0.12	3.00±0.14	1.48	> 200	29.77
	N-phenyl-m-C	129.51	2.26±0.05	2.47±0.07	3.06	8.67	14.40
	N-phenyl-q-C	142.91	32.36±0.89	1.98±0.05	65.64	68.82	-
	C = O	168.92	38.07±1.87	1.88±0.03	86.00	68.31	-

Table 20 (cont'd.)

Compound	Substituent	Chemical Shift (ppm)	T_1 (sec)	NOE	$T_{1(DD)}$ sec	$T_{1(O)}$ sec	$\tau_c \times 10^{+12}$ sec
(C)							
N-n-Propyl-	N-n-propyl-α-C	50.29	0.79±0.09	3.00±0.21	0.79	> 200	27.88
acetanilide	N-n-propyl-β-C	22.39	1.52±0.08	2.61±0.06	1.88	7.99	11.72
	N-n-propyl-γ-C	10.99	2.27±0.10	2.35±0.16	3.34	7.07	4.40
(4.1M in	Carbonyl-CH_3	20.86	3.95±0.15	2.55±0.16	5.07	17.93	2.90
$CDCl_3$)	N-phenyl-p-C	127.46	1.03±0.07	2.99±0.02	1.03	> 200	42.77
	N-phenyl-o-C	127.98	1.60±0.06	2.49±0.10	2.13	6.39	20.68
	N-phenyl-m-C	129.44	1.69±0.06	2.30±0.01	2.58	4.88	17.08
	C = O	169.06	20.98±1.25	2.45±0.06	28.76	77.52	-
	N-phenyl-q-C	143.21	16.68±0.21	2.01±0.09	32.83	33.91	-
(D)							
N-n-Butyl-	N-n-butyl-α-C	48.16	0.43±0.03	2.98±0.03	0.43	> 200	51.23
acetanilide	N-n-butyl-β-C	29.85	0.82±0.09	2.79±0.02	0.91	8.23	24.21
	N-n-butyl-γ-C	19.76	1.05±0.04	2.37±0.03	1.52	3.38	14.49
(4.1M in	N-n-butyl-δ-C	13.49	2.73±0.21	2.65±0.08	3.29	16.06	4.46
$CDCl_3$)	Carbonyl-CH_3	22.26	1.72±0.06	2.33±0.09	2.57	5.20	5.71
	N-phenyl-p-C	127.31	0.43±0.02	2.85±0.05	0.47	6.19	95.77
	N-phenyl-o-C	128.14	0.51±0.01	2.73±0.05	0.59	3.93	74.64
	N-phenyl-m-C	129.46	0.61±0.03	2.91±0.08	0.64	15.55	68.84
	N-phenyl-q-C	143.48	8.04±0.38	1.91±0.05	17.56	14.83	-
	C = O	168.23	8.54±0.32	2.26±0.07	13.47	23.32	-

*Chemical shifts are relative to TMS, and + indicates a downfield shift. The measurements were made at 35°C.

Table 21. ^{13}C Chemical shifts, spin-lattice relaxation times(T_1) and nuclear Overhauser enhancements(NOE) of N-alkylformanilides.

Compound	Substituent	Chemical shift* (ppm)	T_1 (sec)	NOE	$T_{1(DD)}$ sec	$T_{1(O)}$ sec	$\tau_c \times 10^{12}$ sec
(A)							
N-methyl-formanilide	N-methyl	30.87	6.38±0.34	2.53±0.13	8.29	27.69	1.77
	N-phenyl-o-C	121.44	2.60±0.09	2.06±0.12	4.88	5.57	9.03
(neat)	N-phenyl-p-C	125.55	1.36±0.04	2.55±0.05	1.74	6.17	25.32
	N-phenyl-m-C	129.39	2.46±0.14	2.50±0.03	3.26	10.02	13.51
	N-phenyl-q-C	142.31	22.70±0.91	1.75±0.17	60.17	36.45	-
	C = O	161.68	3.50±0.12	2.73±0.10	4.02	26.97	10.96
(B)							
N-ethyl-formanilide	N-Ethyl-α-C	39.16	1.35±0.03	2.60±0.05	1.68	6.92	13.11
	N-Ethyl-β-C	12.75	2.23±0.23	2.51±0.04	2.94	9.27	4.99
(neat)	N-phenyl-o-C	123.38	1.99±0.21	2.44±0.02	2.75	7.22	16.02
	N-phenyl-p-C	126.08	0.83±0.08	2.68±0.03	0.98	5.36	44.95
	N-phenyl-m-C	129.48	1.89±0.09	2.59±0.04	2.36	9.44	18.67
	N-phenyl-q-C	141.02	23.23±0.70	2.48±0.14	31.20	90.91	-
	C = O	161.21	1.91±0.15	2.99±0.09	1.91	> 200	23.07

*Chemical shifts are relative to TMS, and + indicates a downfield shift. The measurements were made at 35°C.

(2) N-Ethylacetanilide, N-ethylacetamide, N,N-diethylacetamide.

(3) N-n-Butylacetanilide, N-n-butyl-N-methylacetamide.

(4) N-Methylformanilide, N-methylformamide, N,N-dimethylformamide, N-methyl-N-n-butylformamide.

(5) N-Ethylformanilide, N-ethylformamide, N,N-diethylformamide.

We find in each series that the ^{13}C chemical shifts of the carbons of the C = O groups in N-alkyl acetanilides and formanilides are normally at higher fields compared with their analogs. This is atrributed to the cross conjugation of the C = O group with the nitrogen lone pair electrons and the benzene ring π electrons, as shown in Structure (IV).

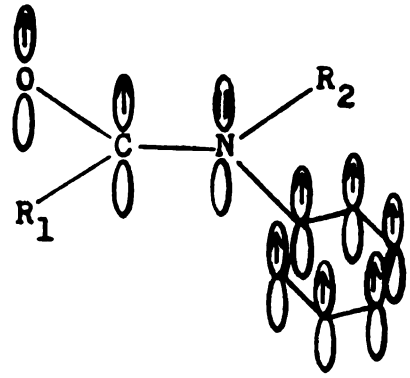

(IV)

However, the ^{13}C chemical shifts of the carbons of the carbonyl-CH_3 groups in N-alkylacetanilides and formanilides are normally to lower field, relative to their analogs in each series. Since the carbonyl-CH_3 group in N-alkyl acetanilides and formanilides is in the deshielding

zone of the benzene ring, a downfield shift would be expected due to the ring-current effect. A similar ring-current effect is also observed for the N-alkyl group carbons of the N-alkylacetanilides and N-alkylformanilides thus introducing a downfield shift relative to that of ^{13}C in the cis-N-alkyl groups of their analogs without the phenyl substituent.

The quaternary carbons in the benzene rings of the N-alkyl acetanilides and formanilides are usually at lower field relative to the ortho, meta, and para carbons, as expected. The ^{13}C chemical shift of the para carbon in the N-phenyl group can be distinguished from those of the meta and ortho carbons by measuring their ^{13}C spin-lattice relaxation times, since the relaxation time of the para carbon is usually shorter than that of ortho or meta carbons. The ^{13}C chemical shifts of the para carbons in the N-alkylacetanilides change only very slightly as the N-alkyl group is varied from N-methyl to N-n-butyl since the resonance effect remains about the same. Spiesecke and Schneider[113] have found that the ^{13}C chemical shifts of meta carbons in aniline and N,N-dimethylaniline are normally at lower field due to resonance involving the nitrogen lone pair electrons and the benzene ring. They also found that the meta carbon chemical shift changed very slightly, even the properties of the substituent group are quite different. Thus, they concluded that the

contribution to the ^{13}C chemical shift of the meta carbons from the magnetic anisotropy and inductive effects of the substituent is negligible. Since acetanilides and formanilides are analogous to aniline and N,N-dimethyl-aniline, we have determined the ^{13}C chemical shifts of meta and ortho carbons by comparing our values with those of Spiesecke and Schneider[113], as shown in Table 16. The ^{13}C chemical shifts of the ortho and meta carbons in N-methylacetanilide have been assigned,[112] and their assignment agrees with ours.

III. RELAXATION TIMES AND NOE EFFECTS

The T_1 values of the para carbons in the phenyl groups of the N-alkyl acetanilides and formanilides are shorter than those of the meta and para carbons, since the preferred rotation axis passes through C-1 and the para carbon of the benzene ring and so will not lead to any modulation of the dipolar interaction between the para carbon and C-H vector. The NOE value for the para carbon is very close to the maximum value of 3.0, indicating that dipolar relaxation makes a very important contribution to its relaxation.

The relaxation times of the N-alkyl group carbons in these two series of anilides increase in the order $\alpha < \beta < \gamma < \delta$ due to the segmental motions and internal rotations.

Due to the inertial effect, the ^{13}C relaxation rates of the carbons of the benzene ring, the carbonyl-CH_3 group and the C = O group in N-alkylacetanilides and N-alkylformanilides increase as the N-alkyl group is varied from CH_3 to N-n-butyl, as shown in Figures 44, 45, and 46.

The relaxation times of the carbons of the C = O group, and of the quaternary carbon of the phenyl group, are very long, since there is no hydrogen directly bonded to them. The variation of the relaxation rates for these C = O group carbons nearly parallels that for the quaternary carbons of the N-phenyl group, as shown in Figure 44, indicating that the relaxation of these carbons is governed by nearly the same overall molecular motion. The variation of the relaxation rates for the meta carbons is nearly identical with that for the ortho carbons, since both are dependent on the overall molecular motion and on the internal rotation of benzene ring. However, the relaxation rate of the para carbon is quite different from that of meta and ortho carbons, since it is almost independent of the internal rotation of the benzene ring.

According to Equations (141), (134), and (135), the relationship between the ratio of the relaxation time of the ortho or meta carbon to the para carbon and $\rho = R/D$ is shown in Figure 47. Since some deviation between the

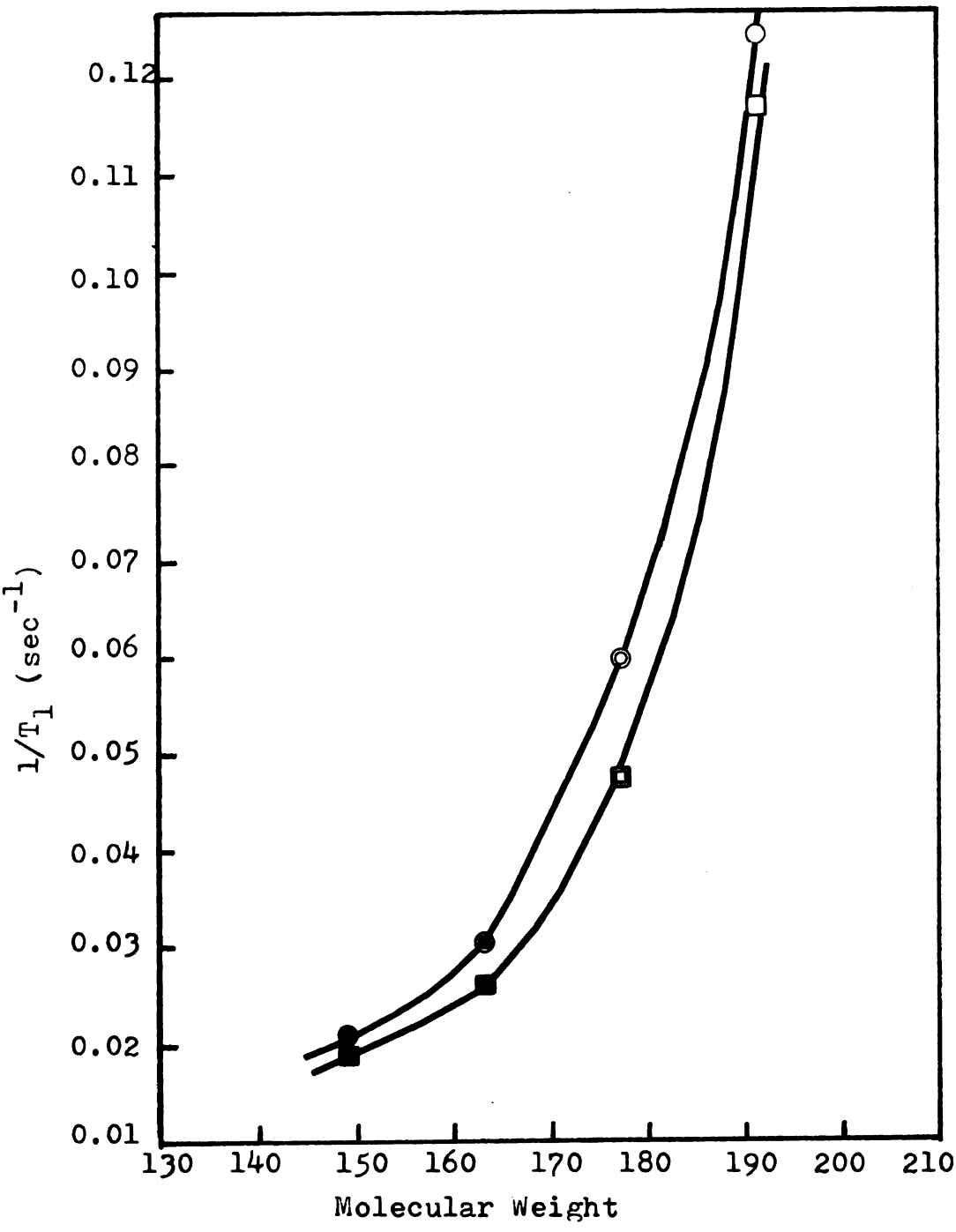

Figure 44. Relaxation rates of the quaternary carbon on the N-phenyl group and the carbon of the C=O group in N-methylacetanilide (●)(■), N-ethylacetanilide (●)(■), N-propylacetanilide (◎)(◘), and N-n-butylacetanilide (○)(□), plotted versus molecular weight.

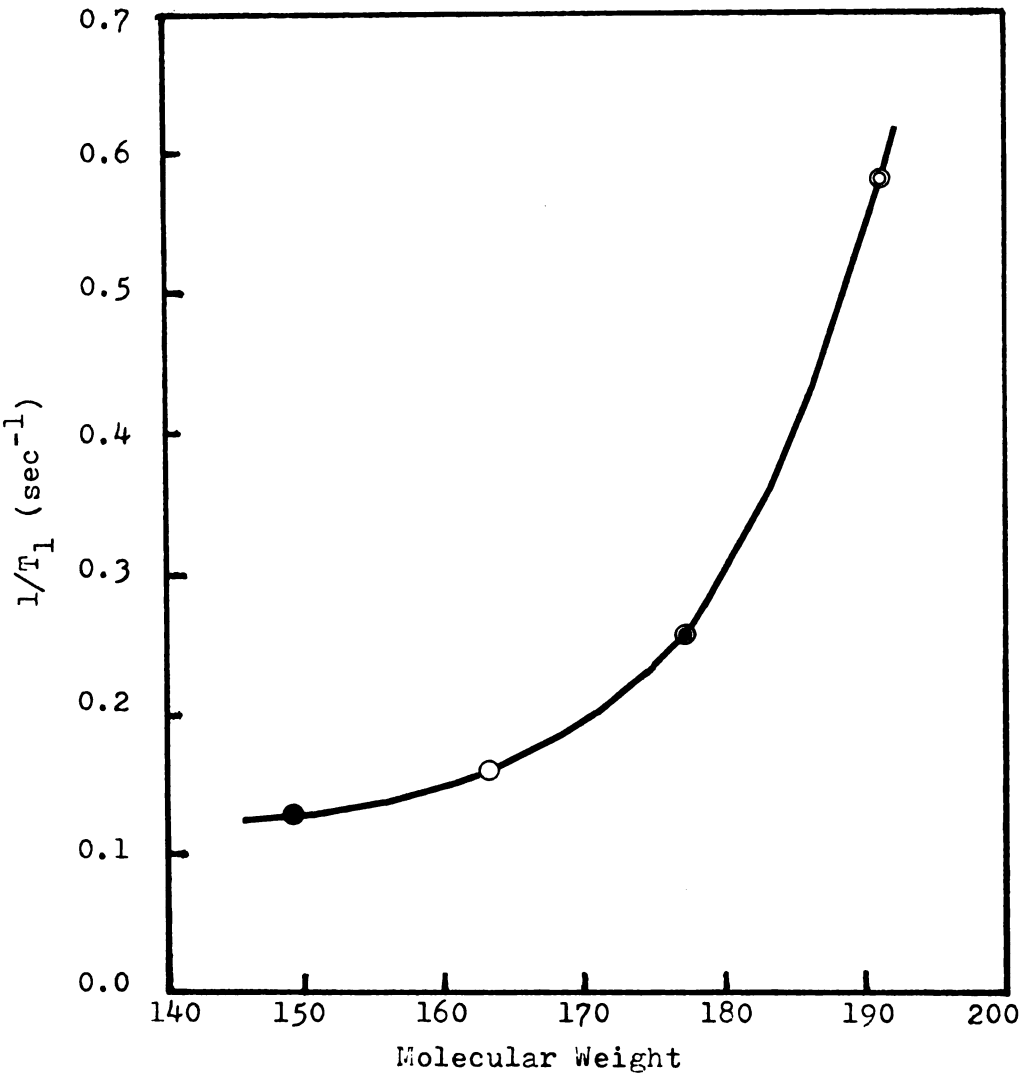

Figure 45. Relaxation rates of the carbonyl-$\underline{C}H_3$ carbon in N-methylacetanilide (●), N-ethylacetanilide (○), N-propylacetanilide (●), and N-n-butylacetanilide (◎), plotted versus molecular weight.

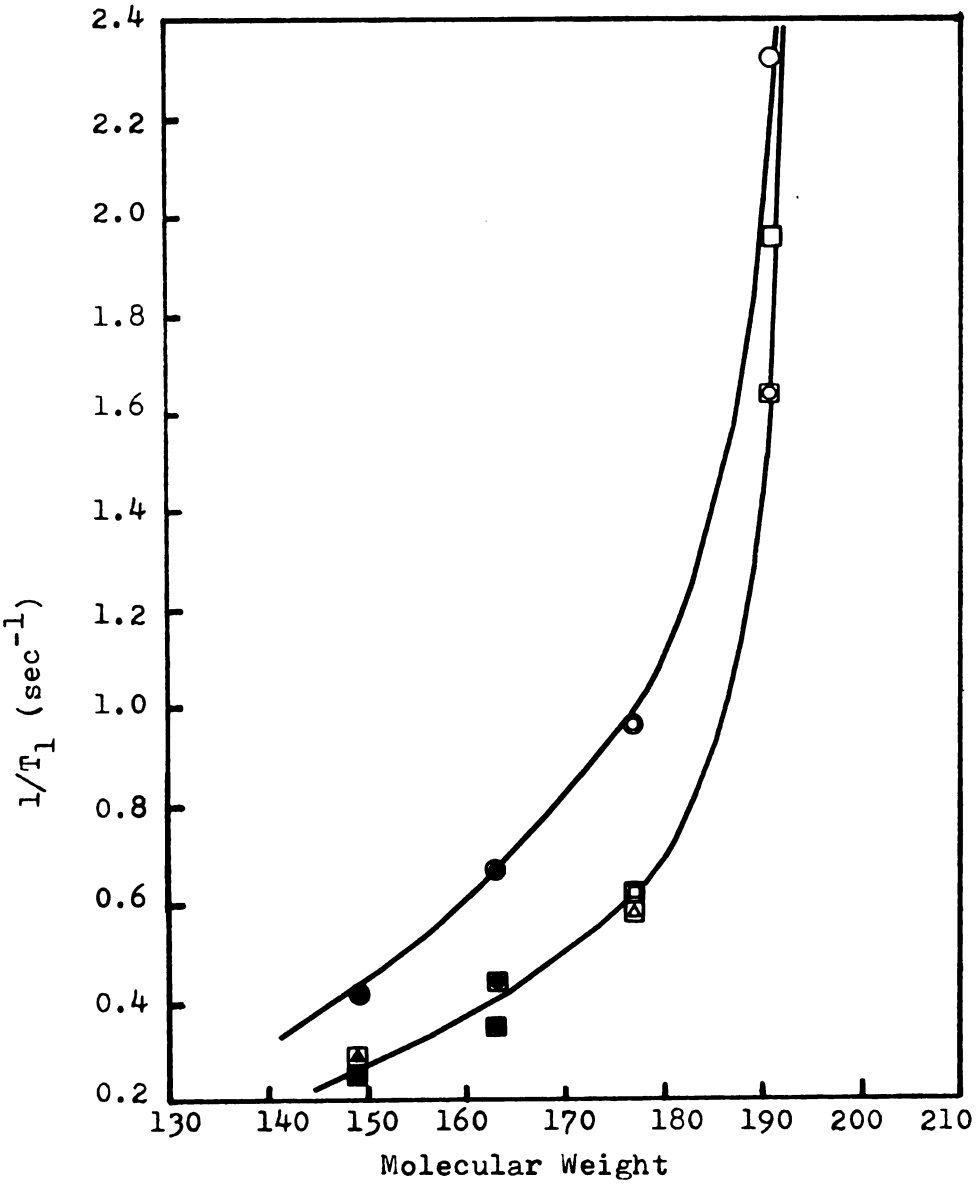

Figure 46. Relaxation rates of the meta, ortho, and para carbons of the N-phenyl groups of N-methylacetanilide (■)(▲)(●), N-ethylacetanilide (◙)(■)(◉), N-propylacetanilide (▲)(■)(◎), and N-n-butylacetanilide (▣)(□)(○), plotted versus molecular weight.

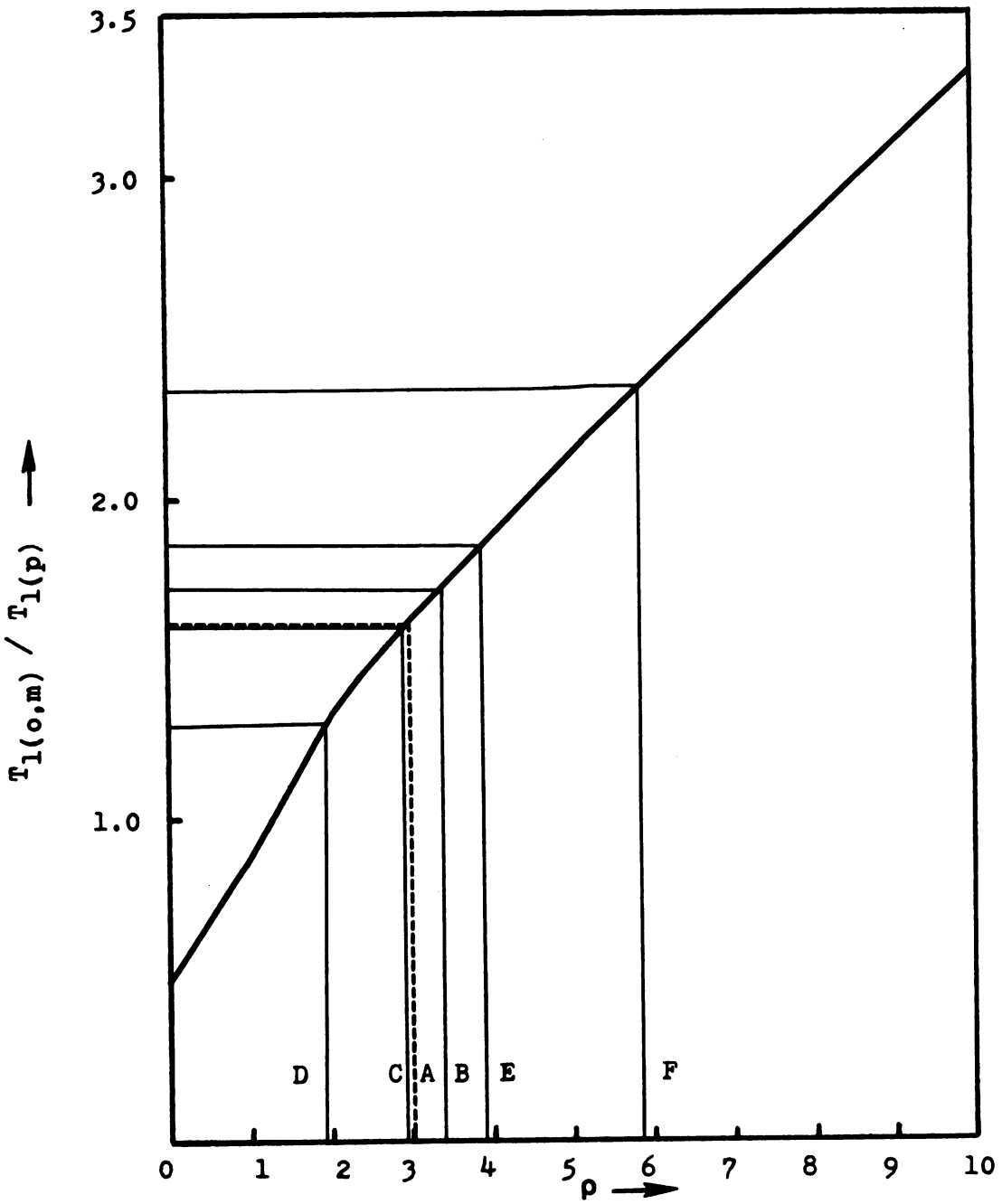

Figure 47. Calculated ratios $T_{l(o,m)} / T_{l(p)}$ versus $\rho = R/D$. (for benzene ring geometry with $\theta = 60^{o}$). A-F are the compounds listed in Table 22.

relaxation times of meta and ortho carbons is observed, the average value of the relaxation times for these two carbons is used for the $T_{1(o,m)}$ value. From the value of $T_{1(o,m)}/T_{1(p)}$, the tumbling ratios ρ of the diffusion constant R of the benzene ring around its C_2 axis (relative to D) in N-alkyl acetanilides and formanilides were calculated and are shown in Table 22.

In monosubstituted benzenes, Levy has found that the tumbling ratio increases as the substituent group becomes larger or heavier. However, Imanari et al.[105] also found that the tumbling ratio decreases as the steric effect becomes important, as in the case of 2,2', 6,6'-tetramethylbiphenyl. In N-alkylacetanilides and formanilides, these two effects, i.e., the inertial effect and the steric effect, will compete with each other.

In N-methylacetanilide, N-ethylacetanilide, N-methylformanilide, and N-ethylformanilide, the inertial effect will be more important than the steric effect, since the sizes of the N-ethyl and N-methyl groups are not large enough to overcome the inertial effect. However, in N-n-propylacetanilide and N-n-butylacetanilide, the steric effect becomes more important than the inertial effect, and thus a lower tumbling ratio results. The tumbling ratios of N-methylformanilide and N-ethylformanilide are also larger than those of N-methylacetanilide and N-ethylacetanilide and this may also be attributed to the steric effect of the carbonyl methyl group.

Table 22. Anisotropic rotation of the N-phenyl group in N-alkyl acetanilides and formanilides

Compounds	$T_{1(o,m)}/T_{1(p)}$ [a]	ρ [b]	D (x 10^{10} sec^{-1})	R (x 10^{10} sec)
A. N-Methylacetanilide	1.61	3.00	0.887	2.66
B. N-Ethylacetanilide	1.72	3.40	0.558	1.90
C. N-n-Propylacetanilide	1.60	2.90	0.391	1.14
D. N-n-Butylacetanilide	1.30	1.95	0.161	0.34
E. N-Methylformanilide	1.86	3.90	0.516	2.01
F. N-Ethylformanilide	2.34	5.85	0.319	1.87

[a] $T_{1(o,m)}$ is the average relaxation time of ortho and meta carbons in the N-phenyl group; $T_{1(p)}$ is the relaxation time of the para carbon.

[b] The tumbling ratio $\rho = R/D$, where D is the diffusion coefficient of the overall molecular motion and R is the diffusion coefficient of the benzene ring around the C_2 axis.

SECTION 4. CORRELATIONS AMONG ^{14}N, ^{15}N, ^{17}O, AND ^{13}C CHEMICAL SHIFTS, AND BETWEEN THESE AND THE ROTATIONAL ENERGY BARRIERS IN SYMMETRICALLY N,N-DISUBSTITUTED AMIDES

I. BACKGROUND

Relatively little work has been done so far on the systematic measurement of ^{14}N, ^{15}N, ^{17}O, and ^{13}C chemical shifts for amides. The reason for this lies in the low signal-to-noise ratio for these nuclei. Owing to a low nuclear moment, low natural abundance, or presence of a nuclear quadrupole moment, the signal strength for each of these nuclei is normally lowered by a factor of about 10^{-3} from that for the same number of protons in the same magnetic field. Moreover, in most compounds of oxygen and nitrogen there is a large electric field gradient at the ^{14}N nucleus (I = 1) or O^{17} (I = 5/2) nucleus and the interaction of this with the electric quadrupole moments of the ^{14}N and ^{17}O nuclei leads to considerable broadening of their NMR signals.

The variation of the ^{14}N chemical shifts in primary and secondary amides and thioamides had been qualitatively explained by Hampson and Mathias[115] in terms of the delocalization of the nitrogen lone pair. Siddall et al.[116] had failed to observe the predicted correlation between

^{14}N downfield shifts and the increase of barrier heights E_a to rotation about the central C-N bond in N-alkyl substituted amides and explained their results as arising from the dominant role of steric effects. However, Martin et al.[117] found that there is a good linear correlation between the energy barriers E_a hindering rotation about the central C-N bond and the ^{15}N chemical shifts in N,N-dimethylamino derivatives (amides, thioamides, and related compounds). Unfortunately, they were unable to correlate the ^{15}N and carbonyl ^{13}C chemical shifts in the amido groups of amides. However, since amides are generally considered to be resonance hybrids of the two structures (V-A) and (V-B), there should be some relationships

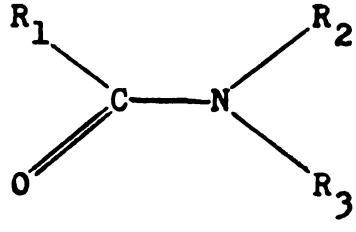

(V-A)

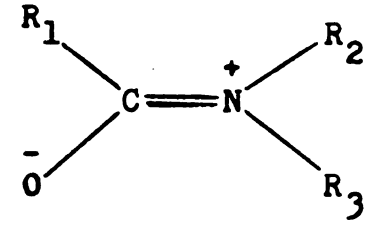

(V-B)

among the chemical shifts of nitrogen, carbon, and oxygen in the amido groups of amides. In order to probe these relationships, two series of symmetrically N,N-disubstituted amides were studied: (1) Formamide, N,N-dimethylformamide (DMF), N,N-dimethylacetamide (DMA), N,N-dimethylpropionamide (DMP), and N,N-dimethyl-n-butyramide (DMB); and (2) N,N-Diethylformamide (DEF), N,N-diethylacetamide (DEA),

N,N-diethylpropionamide (DEP), and N,N-diethyl-n-butyramide (DEB).

The ^{13}C chemical shifts were determined by use of the CFT-20 NMR spectrometer. This has a very stable magnetic field and the variation of the ^{13}C chemical shifts was less than 0.02 ppm per month. The ^{14}N chemical shifts were measured by use of the DA-60 NMR spectrometer with an external lock; the variation of the ^{14}N chemical shifts was about 3-5 ppm, which is mainly a result of the large linewidth of the ^{14}N signals. The determination of the ^{15}N and ^{17}O chemical shifts was carried out on the WH-180 NMR spectrometer which, like the CFT-20, has a very stable magnetic field so the variation of the ^{15}N shifts was less than 0.05 ppm. However, the variation of the ^{17}O shifts was about 1.0 ppm as a result of the broad ^{17}O signals.

Saika and Slichter[118] had proposed that chemical shieldings (with respect to isolated nuclei) can be broken down into three components: σ_D, due to the diamagnetic effect of the electrons on the nucleus concerned, σ_P due to the paramagnetic effect caused by asymmetries in the electronic distribution about the nucleus produced by the bonding in the molecule, and σ_A due to long-range effects produced by other atoms or groups in the molecule. In the ^{14}N, ^{15}N, ^{17}O, and ^{13}C cases, contributions to the chemical shifts due to σ_A can be considered too small for consideration at present. Since the s electrons will dominate σ_D

in these nuclei, and these electrons are affected little by chemical bonding, σ_D will not be the main factor controlling the variation of the chemical shifts in a series of related compounds such as the amides. The experimental evidence support the dependence of the chemical shifts of these nuclei upon the remaining term σ_P.

The overall variations of the chemical shifts of these nuclei can be understood qualitatively from the nature of the bonding involved. The results for the ^{15}N, ^{14}N, ^{17}O, and $^{13}\underline{C}$ = ⊙ chemical shifts for the symmetrically N,N-disubstituted amides are shown in Table 23. Various relationships among these chemical shifts have been obtained in the amides and will be discussed in detail separately below.

II. RELATIONSHIP BETWEEN ^{14}N AND ^{15}N CHEMICAL SHIFTS

There is an almost linear relationship between ^{15}N and ^{14}N chemical shifts for N,N-dimethylamides and N,N-diethylamides, as shown in Figure 48. These results further support the equivalence of ^{14}N and ^{15}N chemical shifts, which had been proposed before for various other nitrogen-containing compounds.[119,120] The relationship between the ^{14}N and ^{15}N chemical shifts can be expressed by the following equation:

$$\delta_{^{15}N} = 0.8487 \quad (\pm\ 0.0456)\ \delta_{^{14}N} + 46.1536 \text{ (ppm)}. \quad (142)$$

Table 23. Chemical shifts of ^{14}N, ^{15}N, ^{17}O and $^{13}C = O$ in some symmetrically N,N-disubstituted amides. Experimental values of the energy barriers (E_a) restricting rotation about the central C-N bonds of these amides are also shown[a,b,d]

Compound	Chemical Shift (ppm)				Energy Barrier	
	^{14}N	^{15}N	^{17}O	$^{13}C{=}O$	E_a ($\frac{kcal}{mol}$)	References
Formamide	262.0	268.69	157.2	165.56	-	
N,N-Dimethylformamide	271.0	276.98	138.9	161.88	22.85	131,132,121,134 135,136
N,N-Dimethylacetamide	281.7	283.00	119.7	170.53	20.40	131,135,136,137
N,N-Dimethylpropionamide	281.7	285.01	128.9	173.25	18.83	131,135,125
N,N-Dimethyl-n-butyramide	277.8	283.78	128.8	171.68	20.00	135
N,N-Diethylformamide	241.2	247.62	143.9	161.98	19.6	138
N,N-Diethylacetamide	248.5	255.24	116.3	169.43	16.9	138
N,N-Diethylpropionamide	245.7	256.92	126.1	171.23	16.31[c]	This work
N,N-Diethyl-n-butyramide	244.5	256.05	124.5	170.25	16.62[c]	This work

[a]The chemical shifts of ^{14}N, ^{15}N, and ^{17}O are all relative to CH_3NO_2, with + values indicating shifts upfield relative to CH_3NO_2; the NMR tubes used for these observations were 15 mm, 20 mm, and 25 mm o.d., respectively. The measurements were made at 28°C.

[b]The $^{13}C = O$ chemical shifts are relative to TMS, with + values indicating shifts downfield from TMS; the NMR tubes used were 5 mm o.d. and the measurements were made at 34.5°C.

[c]See text.

[d]The probable errors in $\delta(^{14}N)$, $\delta(^{17}O)$ are ±1 ppm and in $\delta(^{15}N)$, $\delta(^{13}C)$ are ±0.02 ppm.

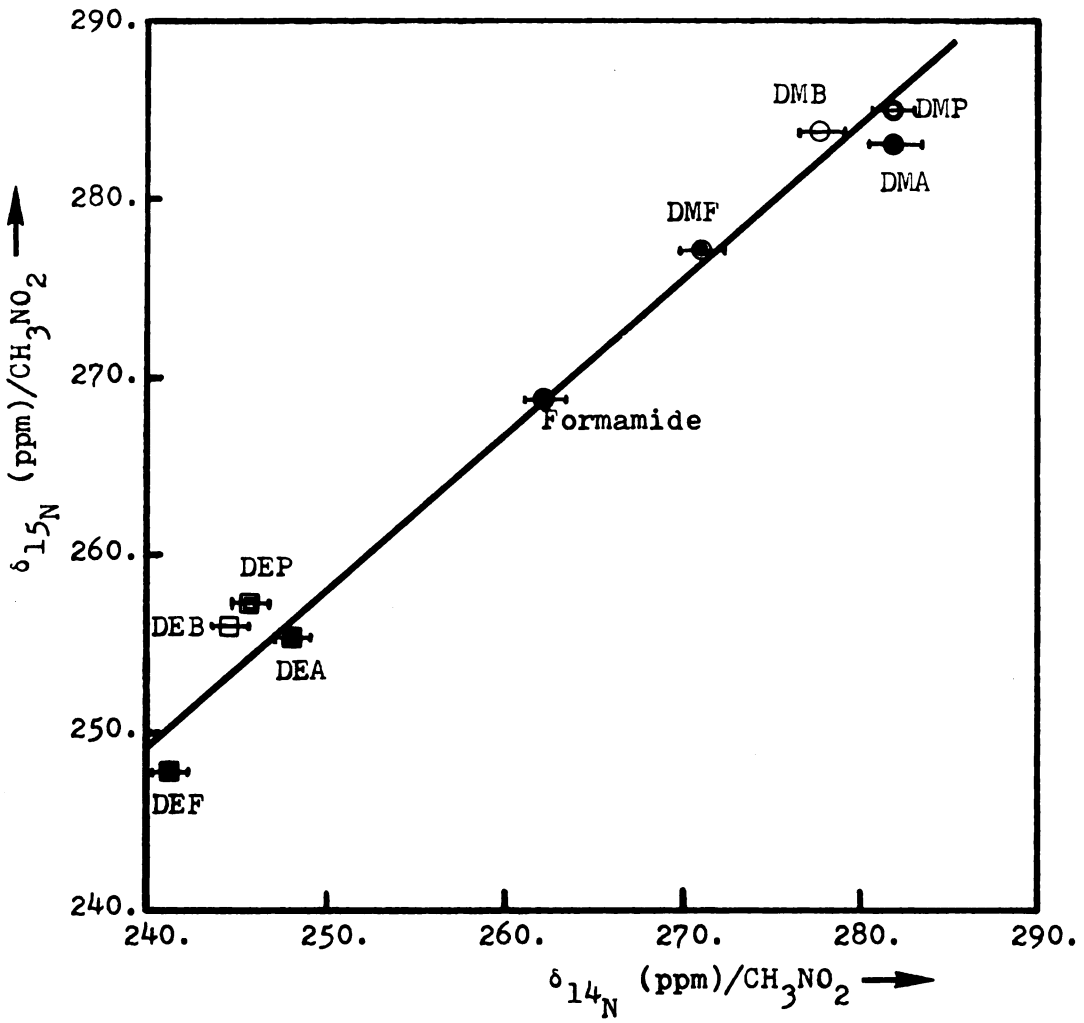

Figure 48. Correlations between the chemical shifts δ_{15_N} and δ_{14_N} for N,N-dimethylamides and N,N-diethylamides.

The above relation is obtained by use of the KINFIT program, where $\delta_{^{15}N}$ and $\delta_{^{14}N}$ are the chemical shifts of ^{15}N and ^{14}N in amides, with respect to the reference CH_3NO_2. The linear relationship between ^{14}N and ^{15}N chemical shifts indicates that there are no intrinsic differences of any importance between the electron distributions and that the deviations from Equation (142) are the result of experimental errors. The qualitative description of the variations in the nitrogen chemical shifts among the amides can then be based on either $\delta_{^{15}N}$ or $\delta_{^{14}N}$ values but, since the ^{15}N chemical shifts have smaller experimental errors, the discussion of nitrogen chemical shifts will be mainly based on ^{15}N chemical shifts.

The ^{14}N and ^{15}N chemical shift range is known to cover about 800-1000 ppm. The variations can be understood on the basis of the nature of the bonding involved. Normally, as the bonds to nitrogen become stronger (i.e., increasing partial double bond character of the C-N bond), the contribution of the paramagnetic term will become more important and a downfield shift of ^{14}N and ^{15}N resonances will result. In the case of amides, the change of σ_p for nitrogen is governed largely by the effect of substituents on the nitrogen lone pair electrons.

According to resonance theory, the barrier hindering internal rotation in amides is due to the contribution of resonance form (V-B) to the ground state of the system. As seen from examination of the resonance structures, the

^{15}N and ^{14}N chemical shifts of form (V-B) would be expected to occur at lower field than those of form (V-A). Richards[121] noted that low-field shifts are found when the nitrogen lone pair electrons become involved in bonding. Fraenkel and Franconi[122] have shown that protonation takes place preferentially on the oxygen and the larger internal rotational barriers found for protonated DMF, compared with the non-protonated species, indicate that there is appreciable contribution of canonical form (VI) in acid solution.

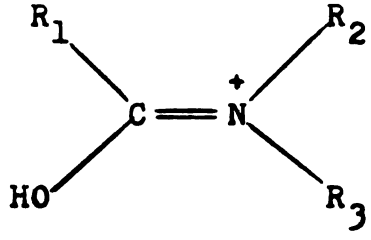

(VI)

Table 23 shows that all the ^{14}N and ^{15}N chemical shifts in the N,N-diethylamides examined are shifted downfield relative to the corresponding N,N-dimethylamides by about 30-36 ppm, which is about twice the shift in N-ethylformamide relative to N-methylformamide, 15.4 ppm.[115] This is reasonable since there are two substituent groups in the N,N-diethylamides. These big downfield field shifts can be reasonably explained[123] by the structural changes which occur involving an increase in π bonding of the nitrogen atom through its lone pair electrons when either a stronger electron donor is introduced (Me → Et) or the π-orbital

system is extended over the R_2 and R_3 groups. These structural changes should result in an increase in the absolute value of the paramagnetic term, inducing a down-field shift of the nitrogen resonance.

By examining the ^{14}N and ^{15}N chemical shifts within the series of N,N-dimethylamides and of N,N-diethylamides, we find that a similar trend in the variation of the ^{14}N and ^{15}N chemical shifts is observed as the substituent group on the carbonyl carbon is varied from -H to $-C_3H_7$. The nitrogen chemical shift moves to higher field as the group α to carbonyl group is changed from -H to $-C_2H_5$, then to lower field as it is varied from $-C_2H_5$ to $-C_3H_7$. This type of variation is attributed to the steric effect. Microwave studies of formamide[124] indicate that there is an angle of 12° between the planes defined by the H_1-C-O bonds and the H_2-N-C bonds. If this twist increases, the overlap between nitrogen lone pair electrons and those of the C = O group would decrease, and the increased localization of the nitrogen lone pair would be expected to produce an upfield shift in the ^{14}N and ^{15}N resonances. The upfield shifts found in the series of N,N-dimethylamides and N,N-diethylamides with larger R_1 groups could therefore be due to such an effect. These conclusions are supported by the lower energy barriers observed for rotation about the central C-N bonds in the series of N,N-dimethylamides[125] as the size of the R_1 group is increased. Models also show

that increased twisting about the N-CO bond might be expected in order to facilitate normal rotation about the bond between the α-carbon and the carbonyl carbon in these larger molecules.

In N,N-dimethyl-n-butyramide and N,N-diethyl-n-butyramide the ^{14}N chemical shift is to slightly lower field than that in their analogs, N,N-dimethylpropionamide and N,N-diethylpropionamide. The actual reason for this result has never been reported. However, in studies of ^{13}C NMR spectra, a downfield δ "steric effect" has been extensively probed[126-128], although its actual cause is still unknown. The downfield shift for the ^{14}N and ^{15}N chemical shifts in N,N-dimethyl-n-butyramide and N,N-diethyl-n-butyramide may be due to a similar δ effect on the nitrogen atom, since in these two compounds we have introduced a δ methyl group (structure VII). This appears to be the first

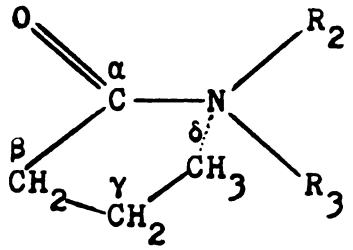

(VII)

example of a downfield δ "steric effect" which has been observed in the NMR spectra of nuclei other than ^{13}C.

This δ effect is also observed in the ^{14}N spectra of the compounds n-$C_3H_7CONH_2$ and i-$C_3H_7CONH_2$, which had been reported by Hampson and Mathias but not explained[115]

by them. The ^{14}N chemical shift of i-$C_3H_7CONH_2$ is slightly upfield relative to that in n-$C_3H_7CONH_2$, since there is no δ methyl group in i-$C_3H_7CONH_2$ but there is a δ methyl group in n-$C_3H_7CONH_2$.

The large low field ^{14}N chemical shift in formamide can be attributed to the formation of hydrogen bonds which stabilize structure (V-B).

III. RELATIONSHIP BETWEEN THE ^{15}N AND $^{13}\underline{C}(=O)$ CHEMICAL SHIFTS

Since structure(V-B) corresponds to overlap between the C = O group and nitrogen lone pair electrons, we expect to find a relationship between the ^{13}C chemical shift of the C = O group carbon and the nitrogen chemical shifts in these two series of amides. A completely linear relationship between the ^{13}C = O chemical shift and ^{15}N chemical shift is indeed obtained, as shown in Figure 49. The relation between ^{15}N chemical shifts and ^{13}C = O chemical shifts for N,N-dimethylamides and N,N-diethylamides can be expressed by the following two equations:

$$\delta_{^{15}N}(\text{p.p.m.}) = 0.6997 \quad (\pm\ 0.0100)\ \delta_{^{13}\underline{C}=O} + 163.7070 \tag{143}$$

for N,N-dimethylamides, and

$$\delta_{^{15}N}(\text{p.p.m.}) = 1.0126 \quad (\pm\ 0.0111)\ \delta_{^{13}\underline{C}=O} + 83.6074 \tag{144}$$

for N,N-diethylamides. Here $\delta_{^{13}\underline{C}=O}$ is the ^{13}C chemical

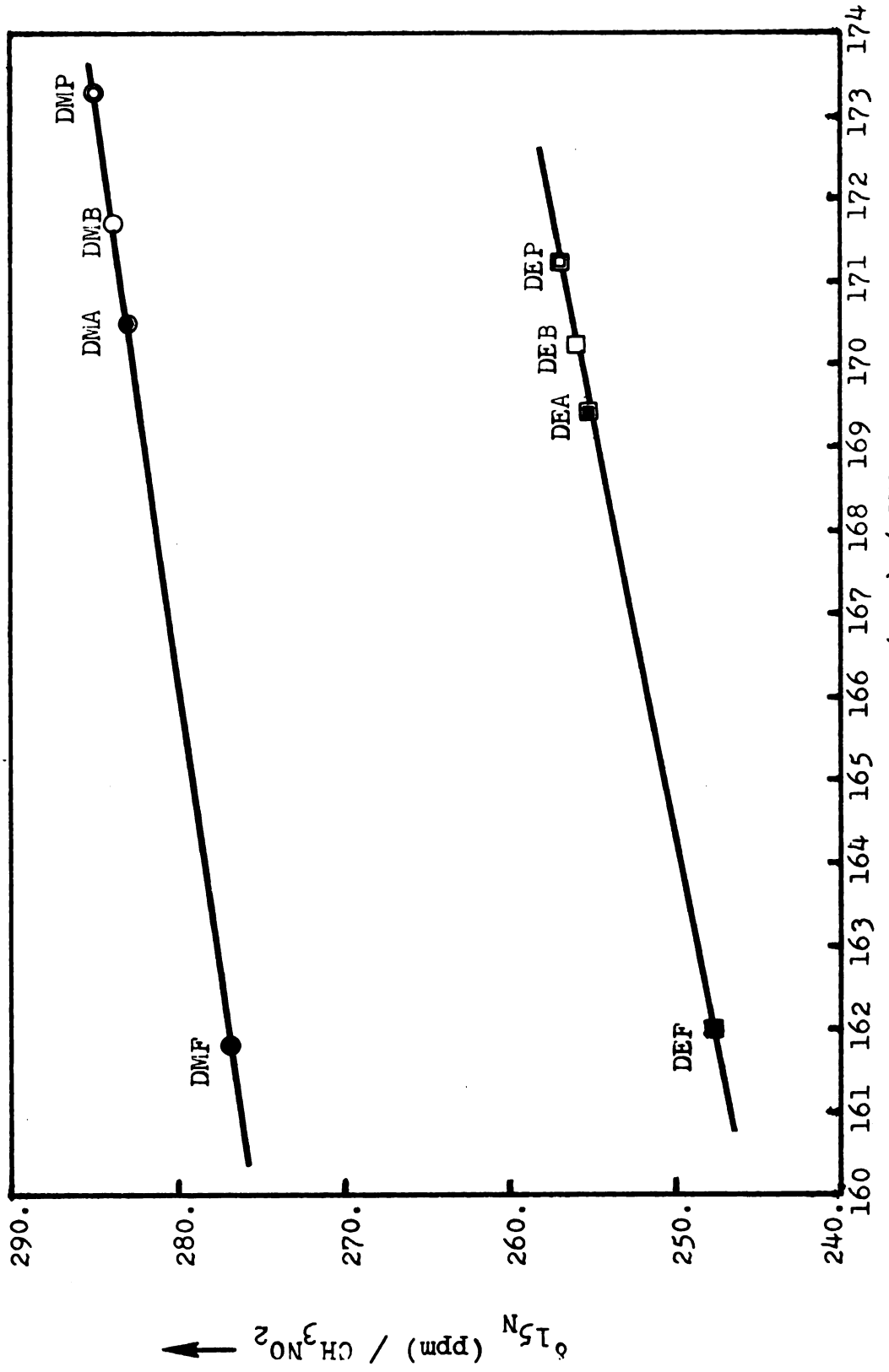

Figure 49. Correlations between the chemical shifts δ_{15_N} and $\delta_{13_{\underline{C}(=O)}}$ for the series of N,N-dimethylamides and N,N-diethylamides.

shift for the C = O group in ppm with respect to TMS. By using Equations (143) and (144), the analogous relations between $\delta_{^{14}N}$ and the carbonyl $\delta_{^{13}C}$ can also be obtained.

IV. RELATIONSHIP BETWEEN THE ^{15}N and ^{13}C δ VALUES AND E_a

Martin et al.[117] were unable to find a relationship between the ^{15}N and ^{13}C chemical shifts in N,N-dimethylamino derivatives; the main reason for that may be due to the quite different properties of the carbonyl substituents in their systems. Using the saturated alkyl groups as the carbonyl substituents, we do find a linear relation between ^{15}N and $^{13}\underline{C}$ = O chemical shifts, since these substituents (-H,-CH_3,-C_2H_5, and -C_3H_7) have similar properties.

Using the series of N,N-dimethyl- and N,N-diethylamides, we also sought a relation between the barriers to rotation about the C-N bonds, E_a, and the ^{15}N chemical shifts. Since the values of E_a for the amides reported over the last two decades have varied considerably, average values for these have been taken. The correlation between E_a and $\delta_{^{15}N}$ for N,N-dimethylamides is shown in Figure 50. This relation can be expressed by the equation

$$E_a(\text{kcal/mole}) = -0.4670 \ (\pm 0.0582)\ \delta_{^{15}N} + 152.2930 \quad (145)$$

For the N,N-diethylamides, only the energy barriers of N,N-diethylformamide and N,N-diethylacetamide had been reported. By using these two values, the following

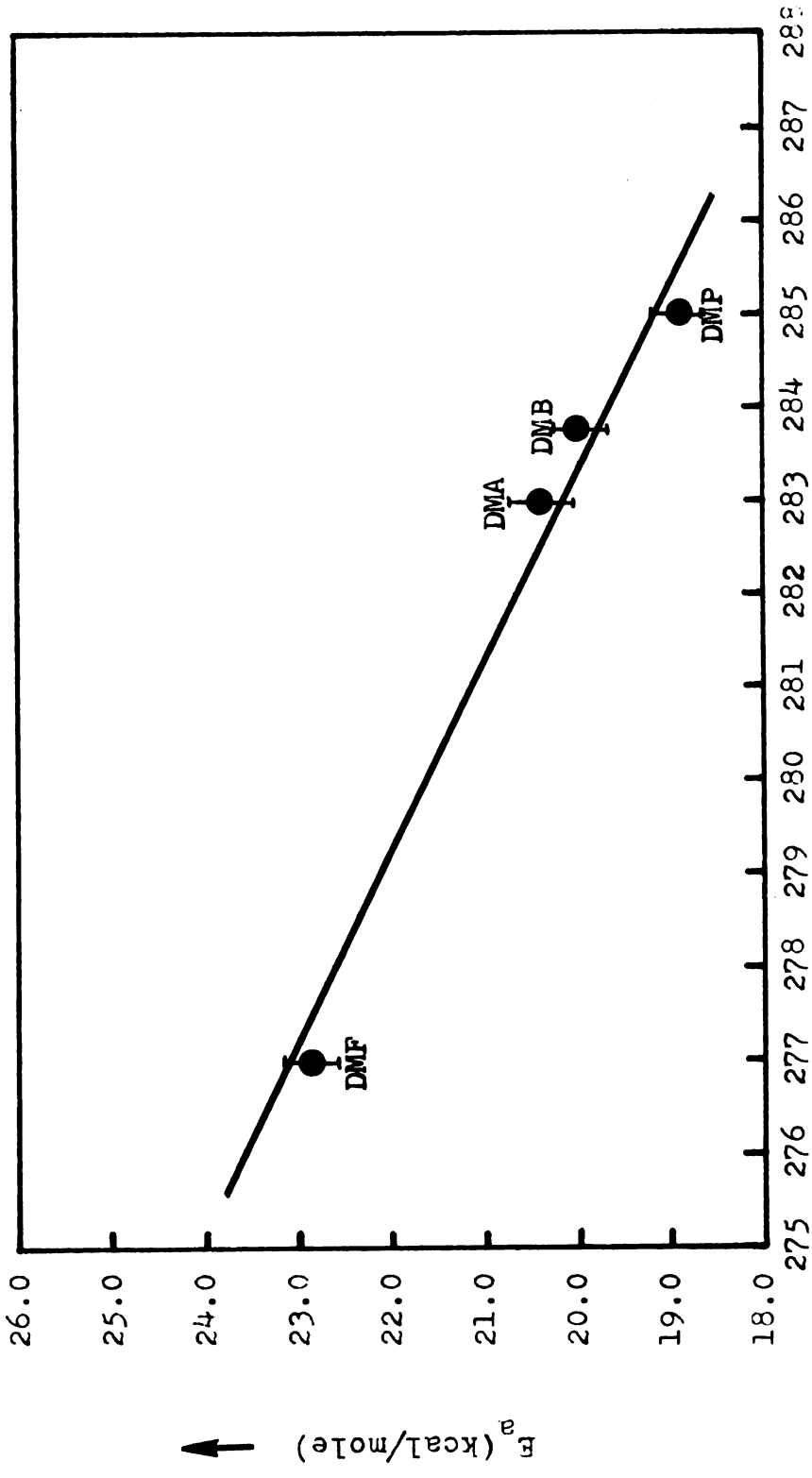

Figure 50. Correlation between E_a and $\delta^{15}N$ for N,N-dimethylamides.

approximate relation between E_a and $\delta_{^{15}N}$ for N,N-diethylamides is obtained,

$$E_a(\text{kcal/mol}) = -0.3541 \quad \delta_{^{15}N} + 107.2700 \qquad (146)$$

From the above relation, the approximate activation energies for N,N-diethylpropionamide and N,N-diethyl-n-butyramide are predicted to be 16.31 kcal/mol and 16.62 kcal/mol , respectively.

Since ^{13}C NMR is more popular than ^{15}N NMR, we would also like to write the relations between E_a and $\delta_{^{13}C=O}$ for these two series of amides. The equations which we have obtained are

$$E_a(\text{kcal/mol}) = -0.3267 \quad (\pm 0.0411) \quad \delta_{^{13}C=O} + 75.8458 \qquad (147)$$

for N,N-dimethylamides, and

$$E_a(\text{kcal/mol}) = -0.3585 \quad (\pm 0.0039) \quad \delta_{^{13}C=O} + 77.6686 \qquad (148)$$

for N,N-diethylamides. By using the above equations, we can evaluate the energy barriers in cases where dynamic NMR methods (lineshape analysis or Forsén-Hoffmann double resonance studies) are not applicable.

From the linear relations between $\delta_{^{15}N}$ and $\delta_{^{13}C=O}$ for N,N-dimethylamides and N,N-diethylamides, we see that the mechanisms for the ^{15}N and $^{13}C=O$ chemical shifts must be closely related to each other. This would

be expected since the variation of their chemical shifts arises in each case from the paramagnetic term which results from the overlap of the nitrogen lone pair electrons with those of the C = O group.

The $^{13}\underline{C}$ = O chemical shifts in the N,N-diethylamides (Table 23) are only slightly upfield relative to those in the N,N-dimethylamides. This is reasonable since the C = O group is far away from the nitrogen substituents. This slight upfield ^{13}C shift of 1-2 ppm in the N,N-diethylamides may be attributed to the well-known upfield "γ" steric effect[126] illustrated in structure (VIII). In the

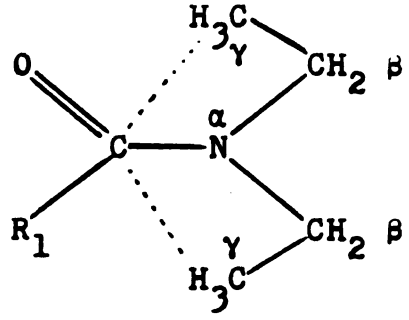

(VIII)

N,N-dimethylamides, no such effect is possible.

Within both the series of N,N-dimethylamides and the series of N,N-diethylamides, the same trends for variation of the $^{13}\underline{C}$ = O chemical shifts are also observed. The $^{13}\underline{C}$ = O chemical shifts move to lower fields as the group α to the carbonyl group is varied from -H to $-C_2H_5$, then move upfield when it is changed from $-C_2H_5$ to $-C_3H_7$. This upfield shift may also be due to the upfield "γ" steric

effect as illustrated by structure (IX). The downfield

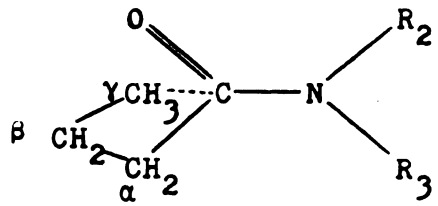

(IX)

shift for $^{13}\underline{C}(=O)$ in formamide, compared with the values in DMF and DEF, is mainly due to the effect of hydrogen bonding.

V. RELATIONSHIP BETWEEN ^{17}O AND ^{15}N CHEMICAL SHIFTS

The variation of ^{17}O chemical shifts also arises from changes in the paramagnetic term. Examining the chemical shifts of ^{17}O in the N,N-dimethylamides and N,N-diethylamides, we see that they are all in the same region. This is expected since the substituent groups on nitrogen are far away from oxygen, as in the $^{13}\underline{C} = O$ case.

However, a slight downfield shift of 3-4 ppm is observed for ^{17}O in N,N-diethylamides relative to N,N-dimethylamides. This downfield shift could be due to the twisting of the $-NR_2$ group out of the molecular plane as the nitrogen substituent groups are changed from methyl to ethyl. In that case the overlap of the C=O group electrons with the nitrogen lone pair electrons would be decreased, i.e., structure (V-A) will make a larger contribution, and a downfield shift of the oxygen resonance will be introduced.

The δ effect, as illustrated by structure (X), may also contribute to the downfield shift. The ^{17}O chemical shifts

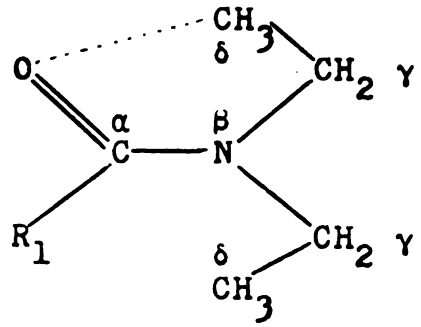

(X)

show the same trend of variation with carbonyl substituent in both the series of N,N-dimethylamides and the series of N,N-diethylamides. The ^{17}O chemical shift moves downfield as the group α to the C = O group is varied from -H to $-CH_3$, since a big structure change is introduced and the molecule may be twisted from the planar form. Structure (V-A) would then make a larger contribution and a downfield shift would be expected. However, when the group α to the C = O group is varied from $-CH_3$ to - C_2H_5, the effect will be less than for the change from H to $-CH_3$. However, an upfield γ steric effect (structure (XI)) begins to produce an upfield ^{17}O

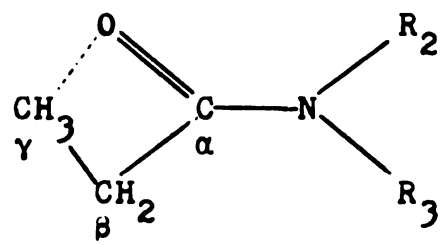

(XI)

chemical shift in N,N-dimethylpropionamide and N,N-diethylpropionamide relative to their analogs with a methyl

substituent on carbonyl carbon, N,N-dimethylacetamide and N,N-diethylacetamide. In going from N,N-disubstituted propionamides to N,N-disubstituted-n-butyramides, the ^{17}O chemical shifts move downfield again, since a downfield δ steric effect of the terminal methyl group has been introduced. This is also the first example of a δ downfield effect in oxygen NMR spectroscopy.

An approximate linear relation between the ^{15}N and ^{17}O chemical shifts is also observed, as shown in Figure 51. The small deviations from linearity may be attributed to experimental errors in the ^{17}O chemical shifts, since quite broad signal are obtained in ^{17}O NMR spectra. These linear relations can be expressed by the following two equations:

$$\delta_{^{15}N}(\text{p.p.m.}) = -0.4451 \quad (\pm 0.0952)\ \delta_{^{17}O} + 339.4430 \qquad (149)$$

for N,N-dimethylamides, and

$$\delta_{^{15}N} = -0.3172 \quad (\pm 0.131)\ \delta_{^{17}O} + 294.4710 \qquad (150)$$

for N,N-diethylamides.

VI. ^{14}N CHEMICAL SHIFTS OF SOME OTHER AMIDES MEASURED AT HIGH TEMPERATURES

Some of the ^{14}N NMR resonances are so broad at room temperature that measurements of their ^{14}N chemical shifts are impossible. In order to circumvent this problem, the temperature was raised to a constant high temperature.

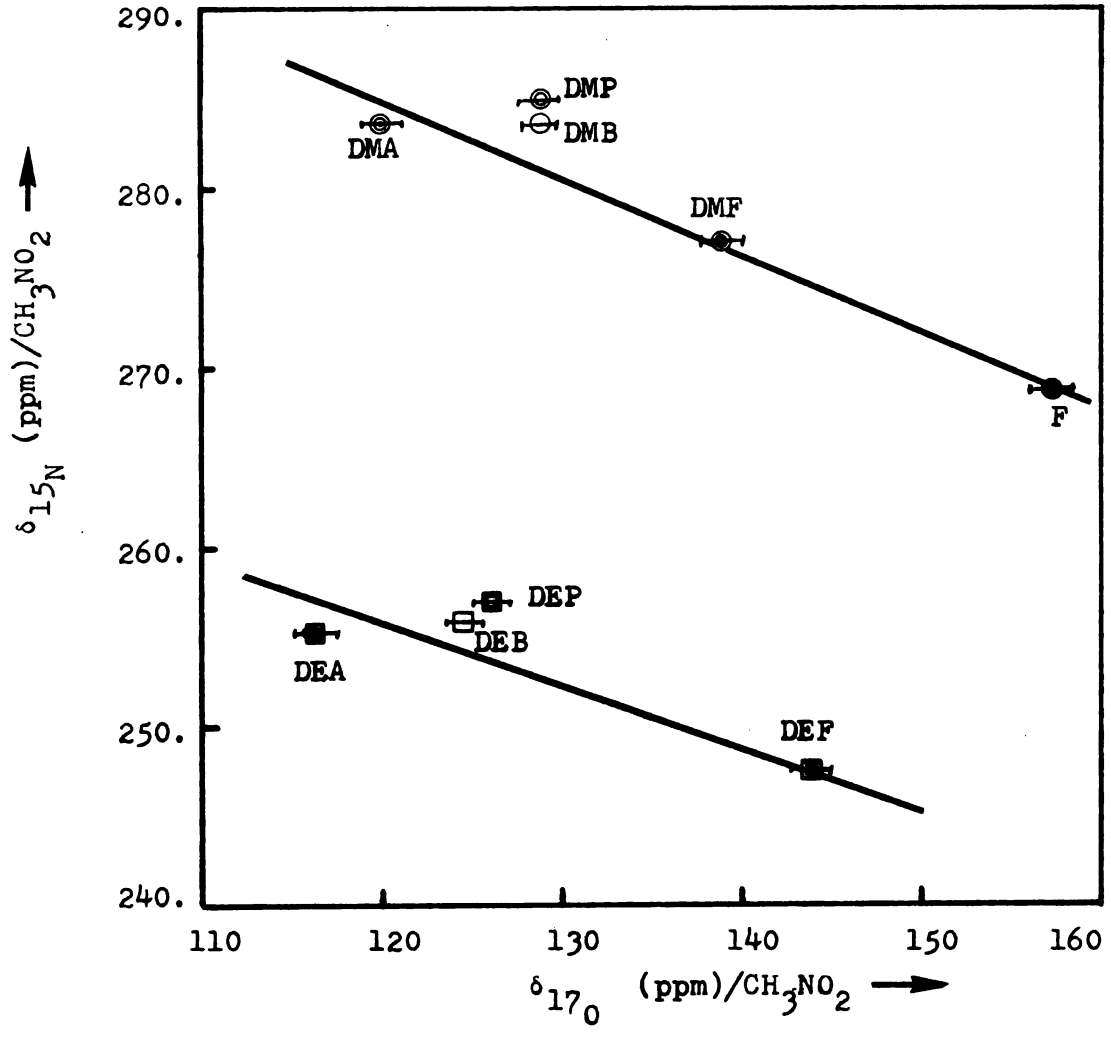

Figure 51. Correlations between the chemical shifts δ_{15_N} and δ_{17_O} for a series of N,N-dimethylamides and a series of N,N-diethylamides.

The signal then became sharper, although the linewidths remained quite broad, as shown in Table 24. For the amides listed in Table 24, only a qualitative discussion of the ^{14}N chemical shifts will be presented.

The ^{14}N chemical shifts for N,N-dimethylacrylamide and N,N-diethylacrylamide are at higher fields relative to those of their analogs with alkyl substituents on carbonyl carbon in the series of N,N-dimethylamides and N,N-diethylamides, as shown in Table 23. This is attributed to "cross conjugation" in these two acrylamides which results from additional contributions of resonance structures of the type of structure (XII). As a consequence, the contribution

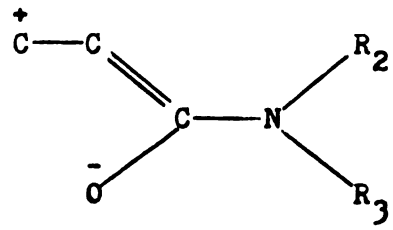

(XII)

of structure (V-A) will be lowered, the nitrogen lone pair electrons will become more localized and the observed ^{14}N chemical shifts for these two compounds will be at higher field. Rogers and Woodbrey[127], had suggested this effect to account for the lowering of the energy barrier in N,N-dimethylacrylamide. The downfield shift of ^{14}N in N,N-diethylacrylamide relative to that in N,N-dimethylacrylamide is about 35 ppm, which is in the range observed for their analogs, the saturated N,N-dimethylamides and N,N-diethylamides, 30-36 ppm.

Table 24. ^{14}N Chemical shifts for some other amides[+]

Compound	Temperature (°C)	Chemical Shift* (ppm)	Linewidth (Hz)
N,N-Dimethylacrylamide	96.0	289.6	-
N,N-Diethylacrylamide	97.0	254.7	350.0
N,N-Di-n-propylacetamide	97.0	260.3	540.4
N,N-Diisopropylpropionamide	97.0	236.7	489.2
N-Methylformanilide	97.0	246.8	411.0
N-Ethylformanilide	98.0	232.1	459.9
N-n-Butylacetanilide	135.0	224.8	1314.4
N-Methyl-N-n-butyl-trimethylacetamide	96.0	273.7	855.4
N-Methyl-N-n-butyl-isobutyramide	97.0	271.5	540.5
N-Methylformamide	28.0	270.5	245.0
N-Ethylformamide	28.0	252.4	372.0
N-n-Butylformamide	28.0	173.0	1199.6
N-n-Butylformamide	98.0	256.9	350.0
N-t-Butylformamide	97.0	241.2	347.2
N-Methylacetamide	28.0	269.3	532.2
N-Methylpropionamide	96.0	277.2	347.6
N-Ethylpropionamide	96.0	261.4	-

*The chemical shifts are relative to CH_3NO_2, with + values indicating shifts upfield relative to CH_3NO_2. The NMR tubes used were 15 mm o.d. All compounds were purified.

[+]Measured at 4.335 MHz on the DA-60. The probable errors in ^{14}N chemical shifts are ± 4 ppm.

The ^{14}N chemical shift for N,N-di-n-propylacetamide is between that of N,N-dimethylacetamide and that of N,N-diethylacetamide. This is a result of the upfield γ steric effect in N,N-di-n-propylamide, illustrated in the conformation of Structure (XIII). So the ^{14}N chemical

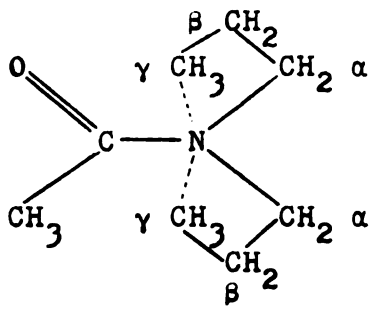

(XIII)

shift of N,N-di-n-propylacetamide is upfield relative to N,N-diethylacetamide.

The ^{14}N chemical shift in N,N-diisopropylpropionamide is at lower field than in N,N-diethylpropionamide, since there are two β carbons in each nitrogen substituent and so isopropyl is a stronger electron donor group.

The ^{14}N chemical shifts for N-methylformanilide, N-ethylformanilide, and N-n-butylacetanilide are at rather low fields compared with those for N-methylformamide, N-ethylformamide, and N-n-butylformamide. This is because the N-phenyl substituent in these compounds gives rise to contributions of additional resonance forms of the type of Structure (XIV).

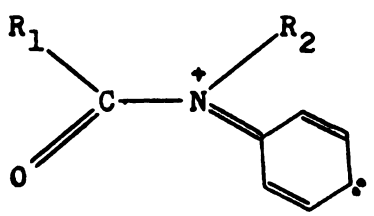

(XVI)

This leads to a decrease in the double-bond character for the central C-N bond and a lowering of the energy barrier for internal rotation about that bond.

The ^{14}N chemical shift in N-methyl-N-n-butyltrimethylacetamide is at higher field than that in N-methyl-N-n-butylisobutyramide, since there are three γ methyl groups in N-methyl-N-n-butyltrimethylacetamide. The strong steric effect of the tertiary butyl group substituent on C = O may also force the molecule out of the planar form, which would increase the localization of the nitrogen lone pair electrons and cause an upfield ^{14}N chemical shift.

At room temperature (28°C) the ^{14}N chemical shifts for N-methylformamide, N-ethylformamide, and N-n-butylformamide are lower, as expected. However the very low chemical shift for N-n-butylformamide may be due to an unusually large experimental error, since the linewidth of 1199 Hz is unusually large.

The downfield shift of ^{14}N in N-ethylformamide relative to that in N-methylformamide is 15 ppm, which is just half of the downfield shift in going from N,N-dimethylformamide to N,N-diethylformamide.

At 98°C, the chemical shift of ^{14}N in N-n-butylformamide is 256.9 ppm, which is at higher field than the ^{14}N resonance in N-t-butylformamide (241.2 ppm). This is attributed to the tertiary butyl group being a stronger electron donor group, which would shift the ^{14}N resonance in N-t-butylformamide to lower field.

The downfield shift of ^{14}N in N,N-dimethylacetamide relative to that in N-methylacetamide is about 12 ppm, which is considerably greater than the downfield shift in N-methylacetamide relative to that in acetamide, 0.9 ppm.

Comparing the ^{14}N chemical shifts in N-methylpropionamide and N-ethylpropionamide, we find that the ^{14}N chemical shift in N-ethylpropionamide is at lower field, since the ethyl group is a stronger electron donor than the methyl group. This downfield shift is about 15 ppm, which is half the value obtained for N,N-diethylpropionamide relative to N,N-dimethylpropionamide.

From the above results we can conclude that the linear relationships between the ^{14}N, ^{15}N, ^{17}O, and $^{13}\underline{C} = O$ chemical shifts in the amido groups of amides actually exist. The reason that Martin et al. did not find a linear relationship between E_a and the $^{13}C = O$ chemical shift was because the carbonyl substituent groups in their system, which included unsaturated groups, changed the properties of the $^{13}C = O$ group. However, in our system the carbonyl substituents are all saturated alkyl groups so the variations in the chemical shifts of $^{13}\underline{C} = O$, ^{15}N, ^{14}N, and ^{17}O mainly arise from overlap of the nitrogen lone pair electrons with those of the C = O groupl conditions are therefore favorable for the existence of linear relationships between the chemical shifts of those nuclei. The reason that Martin et al. were able to find a linear

relation between E_a and the ^{15}N chemical shift is that the nitrogen is far away from the carbonyl substituents so their effect on the nitrogen chemical shift is small. We can predict that if an amide system has the same carbonyl substituent, and the same number of substituents on the nitrogen, then the energy barrier for rotation about the C-N bond will be related linearly to the $^{13}\underline{C}(=O)$ and ^{17}O chemical shifts as the nitrogen substituent groups are changed. However, a linear relation between E_a and $\delta_{^{15}N}$ may not exist. The second result obtained in these studies of the ^{14}N chemical shifts is that when one of the nitrogen substituents is varied from $-CH_3$ to $-C_2H_5$ a 15 ppm downfield shift will result, and this shift is additive when two nitrogen substituent groups are introduced. However, in going from primary amides to the corresponding N-methyl secondary amides, the variation in ^{14}N chemical shifts is small.

SECTION V. OFF-RESONANCE PROTON-SELECTIVELY DECOUPLED ^{13}C NMR SPECTRA AND SPIN-LATTICE RELAXATION TIMES AS TOOLS FOR ASSIGNING THE ^{13}C AND ^{1}H CHEMICAL SHIFTS OF AMIDES

I. BACKGROUND

The use of the heteronuclear off-resonance decoupling technique, and of the application of graphical and other methods, in the interpretation of ^{13}C and ^{1}H NMR spectra has been extensively demonstrated.[69,139,140] Not only can the chemical shifts of quaternary carbons, CH-, CH_2-, and CH_3- be determined but also the residual one-bond ^{13}C-^{1}H coupling constant J_r measured in these partially decoupled spectra may be used to interrelate carbon and proton chemical shifts. The relation between $\Delta\nu$, the separation of the proton signal from the applied decoupling frequency, and J_r is[141]

$$\Delta\nu = \frac{\gamma H_2}{J_o} J_r \qquad (151)$$

at very strong decoupling fields, i.e., for $|\gamma H_2| >> |J_o|$ and $|\Delta\nu|$. Here J_o is the coupling constant of the undecoupled multiplet in the observed spectrum, and γH_2 is the decoupling field strength.

In ^{13}C - {H} experiments, a plot of the proton irradiation frequency versus the corresponding residual coupling constant J_r will yield a straight line with a

slope equal to $\gamma H_2/J_o$, and the exact position of the decoupling field H_2 in the proton spectrum corresponds to $J_r = 0$.

Therefore, if the chemically different protons or carbons have already been assigned from the proton or ^{13}C NMR spectra, then corresponding carbons or protons can be readily assigned.

This method is particularly useful for assigning closely spaced ^{13}C and ^{1}H signals.[29,142-147] Any wrong assignments of carbon resonances will result in deviations from the straight line relationship of Equation (151). Since the range of ^{13}C NMR chemical shifts is larger than that of proton NMR shifts, the ^{13}C NMR spectra usually can be easily assigned by simply comparing spectra of similar compounds[97] whereas the corresponding proton NMR spectra may be broad, highly split, or overlapped. For some ^{13}C NMR spectra with closely spaced lines, the spin-lattice relaxation times may be very helpful in assigning the signals, in case they have quite different T_1 values.[148]

By using these two techniques, off-resonance cw proton decoupling and ^{13}C T_1 determination, the ^{13}C and proton chemical shifts of N,N-dimethylformamide (DMF), N,N-dimethylacetamide (DMA), N,N-dimethylpropionamide (DMP), N,N-dimethyl-n-butyramide (DMB), and N-n-butyl-N-methylformamide (NnBNMF) have been assigned.

II. RESULTS

The ^{13}C chemical shifts of the carbons in these five compounds have been determined before,[131] as shown in Table 25, where the ^{13}C chemical shifts have been measured at 0°C with TMS as the reference. The proton chemical shifts have also been reported (Table 26). Using the assignments of the ^{13}C chemical shifts from Reference 131 (Table 25), we have determined the spin-lattice relaxation times of each of the carbons in the amides and these are shown in Table 25. The T_1 values for DMF, DMA, and DMP are very reasonable, while those for DMB and NnBNMF are abnormal in the case of certain carbons.

In DMB, the ^{13}C chemical shifts of the cis-N-methyl group carbon and the α carbon of the carbonyl substituent (35.5 and 35.2), and in NnBNMF, of the cis-N-methyl group carbon and of the β carbon of the cis-n-butyl group (29.5 and 29.1), are so close that they have been incorrectly assigned in the literature. Following the scheme of ^{13}C spin-lattice relaxation times in Table 25, we find that if the chemical shifts in the above pairs of carbons in DMB and NnBNMF are exchanged, then the spin-lattice relaxation time data can be explained in a reasonable manner. Due to the segmental motion of the long chain substituents in organic molecules, the spin-lattice relaxation times of methylene carbons usually increase in going from the heavier end to the free end[149,150], i.e., from the α

Table 25. ^{13}C Chemical shifts and spin-lattice relaxation times of some amides as assigned in the literature.

Amide	Substituent[c]	Chemical Shift[a] (ppm)	T_1 (sec)[a]
N-N-Dimethyl-formamide	N-methyl(t)	36.2	11.64±0.34
	N-methyl(c)	31.2	19.38±0.49
	C = O	162.8	
N,N-Dimethyl-acetamide	N-methyl(t)	38.0	13.37±0.19
	N-methyl(c)	34.9	14.28±0.46
	Carbonyl-CH_3	21.9	10.79±0.29
	C = O	170.2	63.89±2.70
N,N-Dimethyl-propionamide	N-methyl(t)	37.3	14.40±0.68
	N-methyl(c)	35.4	12.66±0.60
	Carbonyl-sub -α-C	26.8	5.96±0.15
	Carbonyl-sub -β-C	9.8	6.61±0.12
	C = O	173.8	56.08±1.34
N,N-Dimethyl--n-butyramide	N-methyl(t)	37.3	12.83±0.39
	N-methyl(c)	35.5	5.06±0.15
	Carbonyl-sub -α-C	35.2	12.22±0.72
	Carbonyl-sub -β-C	19.2	6.19±0.24
	Carbonyl-sub -γ-C	14.6	7.29±0.20
	C = O	172.6	53.78±2.17
N-n-Butyl-N-methyl-formamide	N-methyl	34.4(t) 29.5(c)	7.10±0.54 5.08±0.05
	N-n-butyl-α-C	48.9(t) 43.8(c)	3.95±0.37 4.37±0.52
	N-n-butyl-β-C	30.8(t) 29.1(c)	4.04±0.13 11.74±0.58
	N-n-butyl-γ-C	20.6(t) 20.2(c)	5.96±0.26 6.15±0.41

Table 25 (cont'd.)

Amide	Substituent	Chemical Shift[a] (ppm)	T_1 (sec)[a]
	N-n-butyl-δ-C	14.4(t,c)	4.92±0.27
	C = O	163.3(t,c)	5.81±0.23

[a]From Reference 131.

[b]This work.

[c]Carbonyl-sub-α-C = carbonyl-substituent α carbon.

Table 26. Proton chemical shifts in some amides

Amide	H(C=O)	Substituent N - CH_3 trans	N - CH_3 cis	R(C = O) α-C	β-C	γ-C	N-n-butyl
N,N-Dimethyl-formamide[a]	7.90	2.98	2.81				
N,N-Dimethyl-acetamide[b]		3.01	2.83	1.98			
		3.01	2.83	1.98			
N,N-Dimethyl-propionamide[c]		3.01	2.95	2.37	1.15		
N,N-Dimethyl-n-butyramide[d]		3.11	2.94	2.41	1.59	0.96	
N-n-Butyl-N-methyl-formamide[e]	8.02	2.96	2.81				

[a]Solvent CCl_4, Sadtler 9287M.

[b]Solvent CCl_4, Sadtler 8875M.

[c]Solvent $CDCl_3$, Sadtler 19929M.

[d]Solvent D_2O, Sadtler 19021M.

[e]Only a partial set of proton chemical shifts is reported in Reference 95.

to the β, γ,... carbons. After exchanging the assignments of the chemical shifts in the pairs of carbons in DMB and NnBNMF discussed above, the new ^{13}C chemical shift assignments shown in Table 27 are obtained. The spin-lattice relaxation times of the carbons of the carbonyl substituent in N,N-dimethyl-n-butyramide and of the carbons of the N-n-butyl group in N-n-butyl-N-methylformamide now increase in going from the α carbon to the γ or δ carbon in the correct order. And the expected longer T_1 values for the carbons of the cis-N-methyl groups compared to the methylene carbons of the n-butyl groups in both compounds may also be rationalized by assuming that there is free internal rotation of the methyl groups plus segmental motion of the n-butyl chain.[85] The observed T_1 value for the carbon of the cis-N-methyl group is shorter than that of the carbon of the trans-N-methyl group in DMB while the opposite result is observed for NnBNMF. All these results are expected since there is a preferred rotation axis in each molecule which governs the overall anisotropic molecular motion.

In order to prove that the ^{13}C chemical shifts of all these five compounds are actually assigned correctly in Table 27, the off-resonance decoupling technique was used to calculate the corresponding proton chemical shifts, since the experimental hydrogen NMR spectra have been correctly assigned before. By using graphical methods and

Table 27. Chemical shifts and spin-lattice relaxation times of some amides[a,b] measured in this work.

Amide	Substituent	Chemical Shift (ppm)	T_1 (sec)
N,N-Dimethyl-formamide	N-methyl	35.09(t) 25.99(c)	11.64±0.34 19.38±0.49
	C = O	161.88	21.19±0.68
N,N-Dimethyl-acetamide	N-methyl	37.25(t) 34.19(c)	13.37±0.19 14.28±0.46
	Carbonyl-CH_3	20.62	10.79±0.29
	C = O	170.53	63.89±2.70
N,n-Dimethyl-propionamide	N-methyl	36.43(t) 34.52(c)	14.40±0.68 12.66±0.60
	Carbonyl-sub -α-C	25.89	5.96±0.15
	Carbonyl-sub -β-C	8.84	6.61±0.12
	C = O	173.25	56.08±1.34
N,N-Dimethyl--n-butyramide	N-methyl	36.36(t) 34.25(c)	12.83±0.39 12.22±0.72
	Carbonyl-sub -α-C	34.51	5.06±0.15
	Carbonyl-sub -β-C	18.16	6.19±0.24
	Carbonyl-sub -γ-C	13.39	7.29±0.21
	C = O	171.68	53.78±2.17
N-n-Butyl-N-methyl formamide	N-methyl	33.40(t) 28.26(c)	7.10±0.54 11.74±0.58
	N-n-butyl-α-C	48.28(t) 42.94(c)	3.95±0.37 4.37±0.52
	N-n-butyl-β-C	29.95(t) 28.59(c)	4.04±0.13 5.08±0.05
	N-n-butyl-γ-C	19.23(t) 19.66(c)	5.96±0.26 6.15±0.41

Table 27 (cont'd.)

Amide	Substituent	Chemical Shift (ppm)	T_1 (sec)
	N-n-butyl-δ-C	13.28(c) 13.20(t)	4.92+0.27
	C = O	161.89(t,c)	5.81±0.23

[a]All the chemical shifts are relative to TMS. The measurements were made at 35°C.

[b]The assignments differ from those in Table 25 in some cases based on the arguments given in the text.

the KINFIT program, the proton chemical shifts of all these five amides have been determined in this work as shown in Figures 52-56. The proton chemical shifts calculated using Equation 151 are also shown in Table 28. Comparing the proton chemical shifts of all the symmetrically N,N-dimethyl-substituted amides - DMF, DMA, DMP, and DMB - we find that all the calculated results are matched with the experimental values, Tables 26 and 28. The chemical shift deviations between calculated and experimental results are mainly attributed to the bulk susceptibility factor (since our compounds were placed in an inner tube and the reference TMS in the outer tube, as described in Experimental Section). The matching of all the proton chemical shifts provides further proof that the ^{13}C chemical shifts of DMF, DMA, and DMP are correctly assigned in Table 27. In addition, the matching of the proton chemical shifts in DMB tells us that our assignment of ^{13}C resonances for the cis-N-methyl group and the α carbon of the carbonyl substituent in N,N-dimethyl-n-butyramide is correct.

Some of the proton chemical shifts for N-n-butyl-N-methyl formamide had been reported a long time ago and are given in Table 26. The reported proton NMR spectra of N-n-butyl-N-methylformamide and N-n-butyl-N-methylacetamide are also shown in Figures 57-A and B. Since the chemical shifts of the trans and cis γ protons in the N-n-butyl group are so close to the limit of the resolving

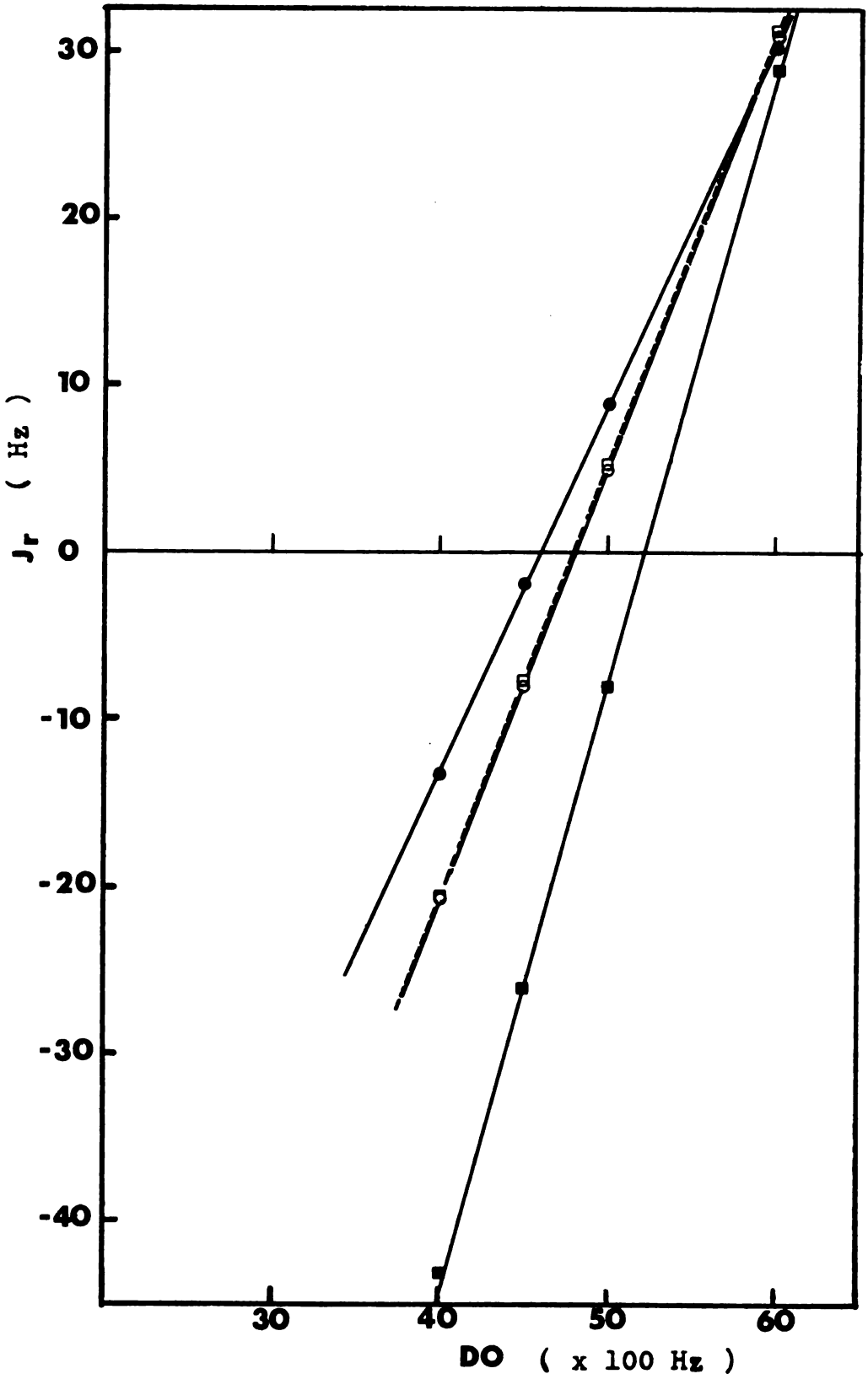

Figure 52. The dependence of the residual C-H coupling constants J_r on the decoupler offset frequency DO in N,N-dimethylformamide: TMS (●), NCH_3(<u>cis</u>) (□), NCH_3(<u>trans</u>) (○), and C=O (■).

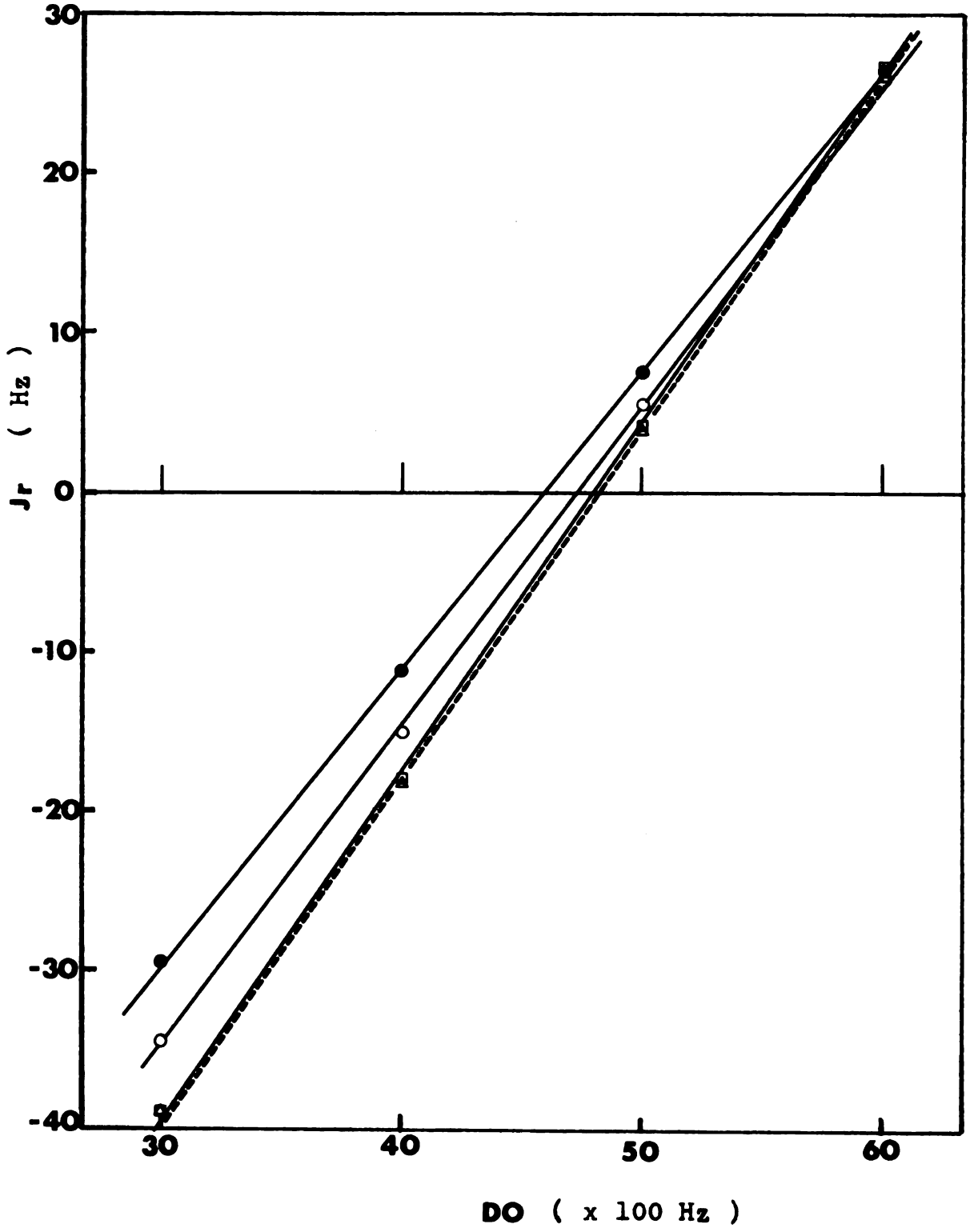

Figure 53. The dependence of the residual C-H coupling constants J_r on the decoupler offset frequency DO in N,N-dimethylacetamide: TMS (•), NCH_3(<u>trans</u>) (△), NCH_3 (<u>cis</u>) (□), and carbonyl-CH_3 (○).

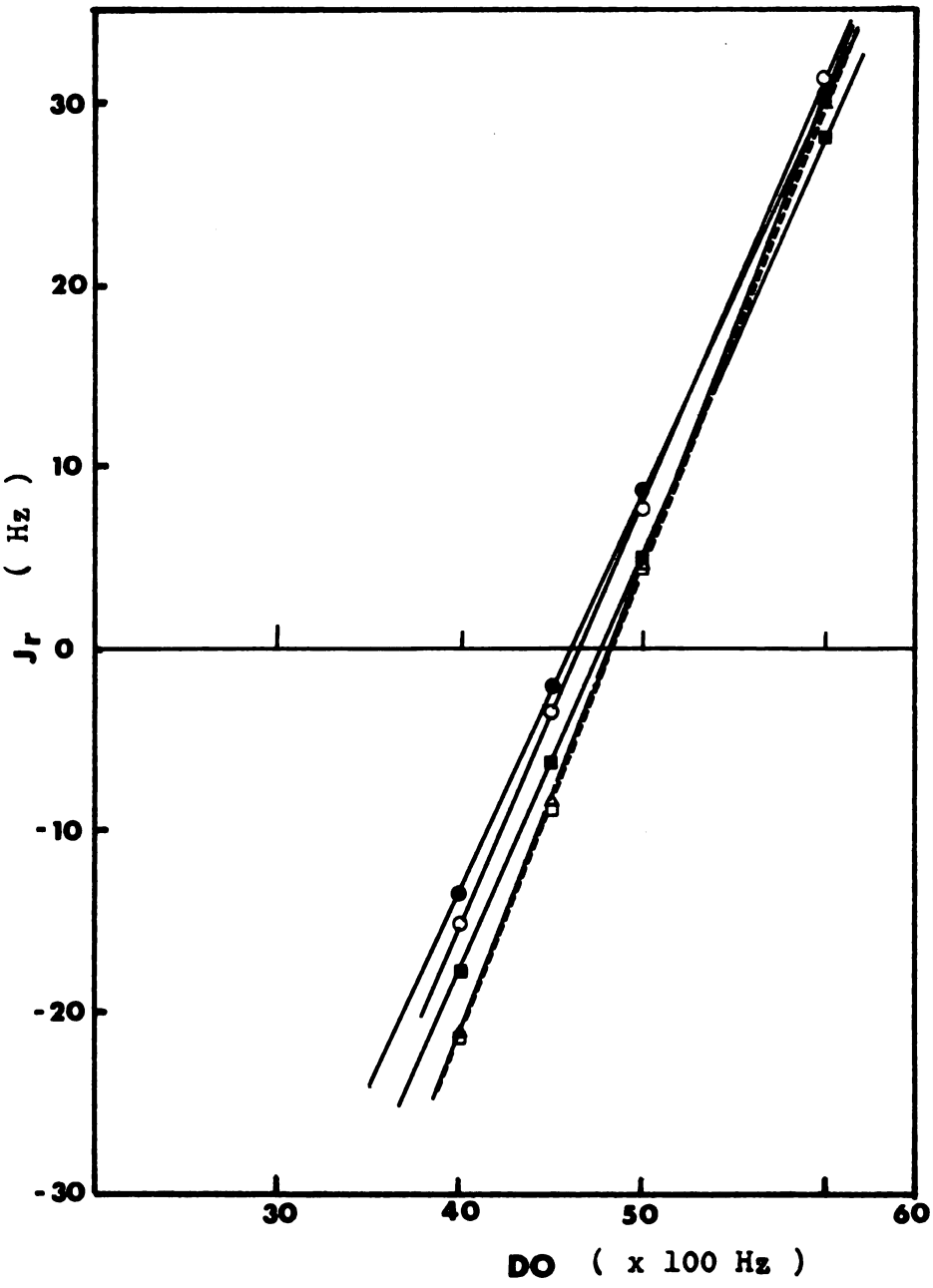

Figure 54. The dependence of the residual C-H coupling constants J_r on the decoupler offset frequency DO in N,N-dimethylpropionamide: TMS (●), NCH_3(<u>trans</u>) (□), NCH_3(<u>cis</u>) (△), α carbon of the carbonyl substituent (■), and β carbon of the carbonyl substituent (○).

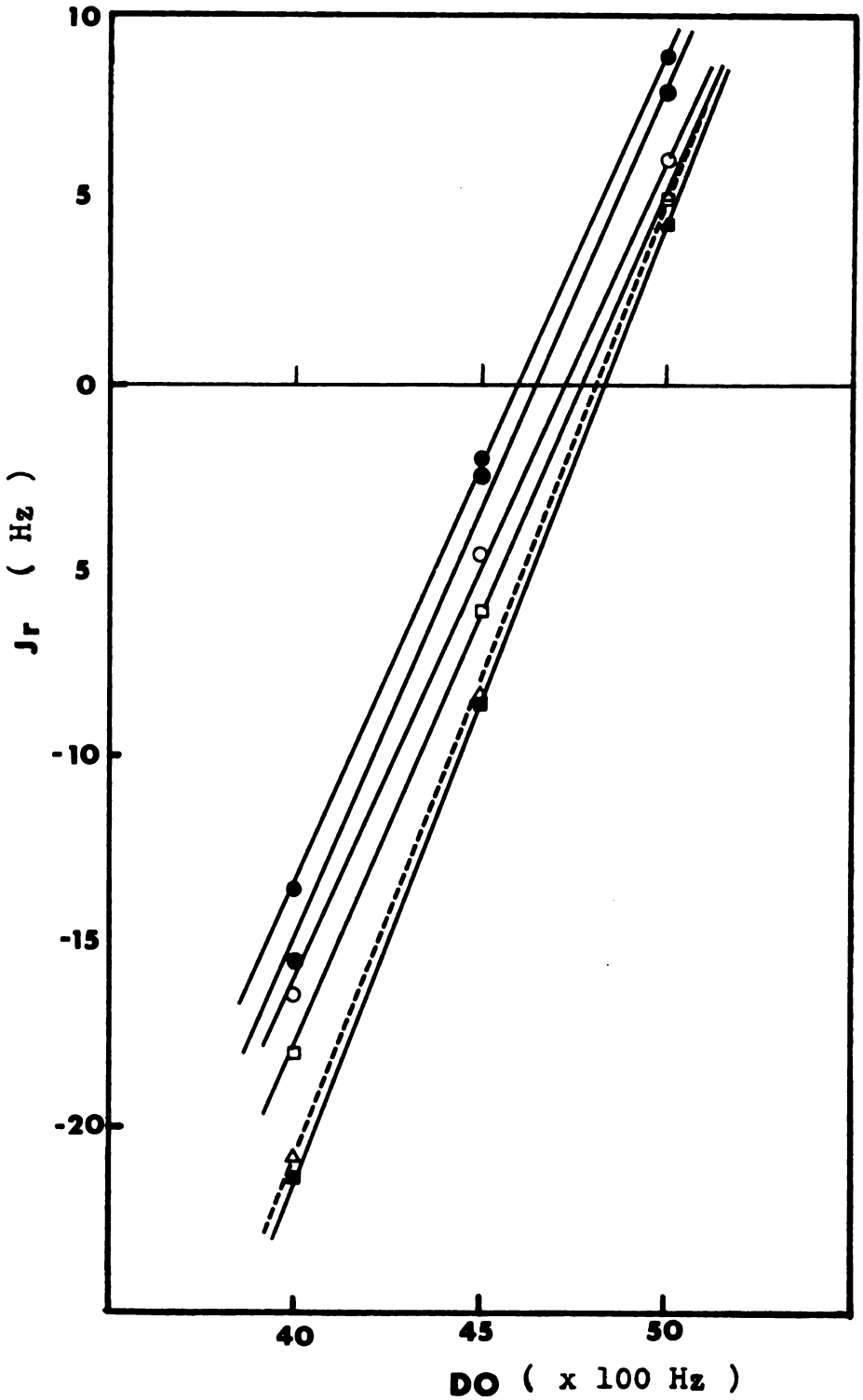

Figure 55. The dependence of the residual C-H coupling constants J_r on the decoupler offset frequency DO in N,N-dimethyl-n-butyramide: TMS (●), NCH_3(<u>trans</u>) (■), NCH_3(<u>cis</u>) (△), α carbon of the carbonyl substituent (□), β carbon of the carbonyl substituent (○), and γ carbon of the carbonyl substituent (●).

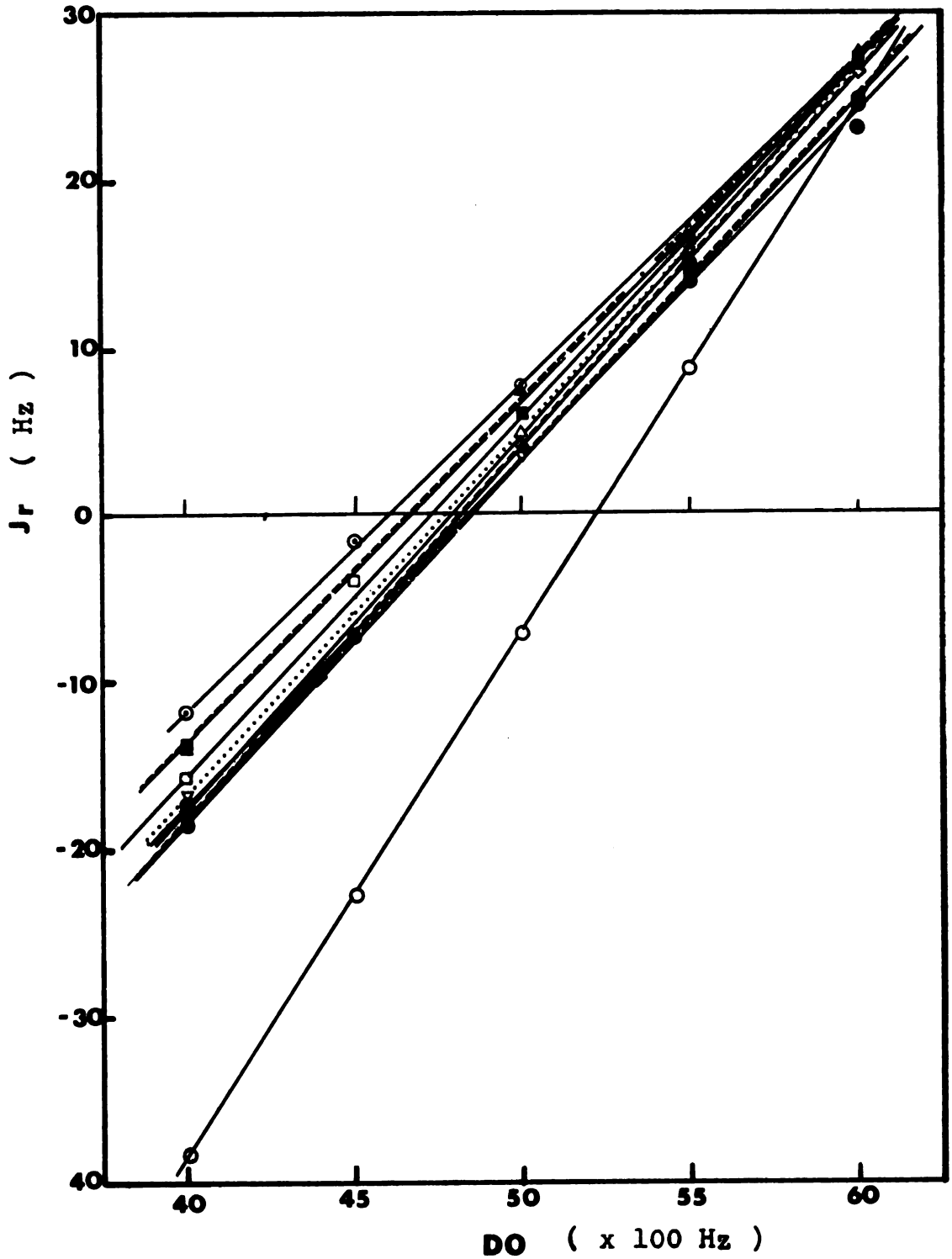

Figure 56. The dependence of the residual C-H coupling constants J_r on the decoupler offset frequency DO in N-n-butyl-N-methylformamide: TMS (⊙), trans- and cis-NCH_3 groups (◇)(---), α carbons of the trans and cis N-n-butyl groups (●)(■), β-carbons (⊙)(□), γ-carbons (△)(▽), and δ-carbons (▲)(▣), C=O (○).

Table 28. The dependence of residual C-H coupling constants J_r on the decoupler offset frequency, and the calculated hydrogen chemical shifts δ_H in some amides[a,b].

Amide	Substituent	J_r (Hz)						DO'(calculated) (x 100 Hz)	DO" (x 100Hz)	δ_H[c] (ppm)
		DO=30	DO=40	DO=45	DO=50	DO=55	DO=60			
DMF	TMS		-13.37	- 1.90	8.80		30.30	46.0127±0.079	0.00	0.00
	N-CH_3(t)		-20.77	- 8.17	4.80		30.83	48.1027±0.0362	2.09	2.61
	N-CH_3(c)		-20.77	- 7.60	5.30		31.37	47.9534±0.0153	1.94	2.43
	C = O		-43.00	-26.0	-8.1		28.90	52.0353±0.0944	6.02	7.53
DMA	TMS	-29.4	-11.3		7.6		26.4	45.8925±0.0696	0.00	0.00
	N-CH_3(t)	-38.7	-18.2		3.9		26.2	48.0892±0.161	2.20	2.75
	N-CH_3(c)	-38.7	-17.9		4.2		26.5	47.9735±0.133	2.08	2.60
	Carbonyl-CH_3	-34.3	-15.1		5.4		25.7	47.2813±0.116	1.39	1.74
DMP	TMS		-13.43	- 2.00	8.83		30.43	46.0263±0.0687	0.00	0.00
	N-CH_3(t)		-21.27	- 8.70	4.43		30.30	48.2894±0.0347	2.26	2.83
	N-CH_3(c)		-21.13	- 8.33	4.83		30.47	48.1847±0.0250	2.16	2.70
	Carbonyl-sub-α-C		-17.65	- 6.10	5.00		28.15	47.7224±0.0397	1.70	2.13
	Carbonyl-sub-β-C		-15.15	- 3.53	7.70		31.17	46.5684±0.0445	0.54	0.68

Table 28 (cont'd.)

Amide	Substituent	J_r (Hz)						DO' (calculated)	DO"	δ_H^c
		DO=30	DO=40	DO=45	DO=50	DO=55	DO=60	(x 100 Hz)	(x 100Hz)	(ppm)
DMB	TMS		-13.57	- 1.90	8.93			40.9684±0.0904	0.00	0.00
	$N-CH_3$ (t)		-21.37	- 8.60	4.33			48.3255±0.0189	2.36	2.95
	$N-CH_3$ (c)		-20.9	- 8.30	5.15			48.0763±0.0963	2.11	2.64
	Carbonyl-sub-α-C		-18.15	- 6.15	5.00			47.7784±0.108	1.81	2.26
	Carbonyl-sub-β-C		-16.45	- 4.55	6.05			47.2124±0.155	1.24	1.55
	Carbonyl-sub-γ-C		-15.45	- 2.40	7.93			46.4080±0.289	0.44	0.55
NnBNMF	TMS		-11.7	- 1.5	7.63	17.20	26.43	45.9933+0.084	0.00	0.00
	$N-CH_3$ (t)		-18.27	- 7.25	3.97	15.43	26.45	48.1868+0.0272	2.19	2.74
	(c)		-17.9	- 7.1	4.5	15.6	26.85	48.0438±0.0392	2.05	2.56
	N-n-butyl-α-C (t)		-18.4	- 7.25	-	13.95	24.95	48.4579+0.00483	2.47	3.08
	(c)		-18.3	- 7.1	-	14.35	24.8	48.4036±0.0637	2.41	3.01
	N-n-butyl-β-C (t)		-17.2	-	-	14.7	22.8	48.3404+0.455	2.35	2.93
	(c)		-15.7	- 3.9	-	15.6	26.85	47.2727±0.207	1.28	1.60

Table 28 (cont'd.)

Amide	Substituent	J_r (Hz) DO=30	DO=40	DO=45	DO=50	DO=55	DO=60	DO'(calculated) (x 100 Hz)	DO" (x 100Hz)	δ_H [c] (ppm)
	N-n-butyl-									
	γ-C (t)		-17.5	-	4.9	15.7	26.9	47.8674±0.0375	1.87	2.34
	(c)		-16.7	-	3.5	15.7	26.8	47.8953±0.229	1.90	2.38
	N-n-butyl-									
	δ-C (c)		-13.6	-	6.1	16.6	27.2	46.7969±0.119	0.80	1.00
	(t)		-13.65	-	7.8	17.2	27.6	46.5173±0.151	0.52	0.66
	C = O (t,c)		-38.1	-22.7	-6.9	8.7	24.5	52.2030±0.0181	6.21	7.76

[a] DO is the decoupler offset frequency in Hz x 10^{-2} and DO' is the intercept at $J_r = 0$ (Figures 52-56).

[b] t and c indicate groups trans or cis relative to the C = O group.

[c] δ_H = DO"/0.8 is the proton chemical shift relative to TMS and DO" = DO' (amide signal) - DO'(TMS).

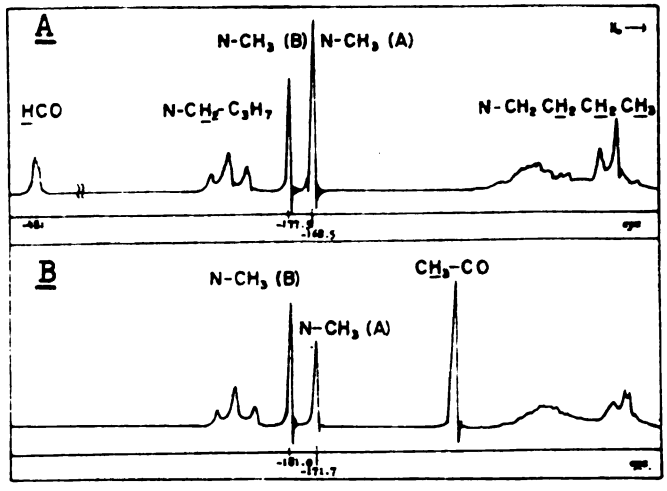

Figure 57. ^{1}H-NMR spectra (ν_o = 60 MHz) of N-n-butyl-N-methylformamide (A) and N-n-butyl-N-methylacetamide (B). The internal reference is TMS. The $NC\underline{H}_3$ at higher field (A) is the methyl group cis to the C=O group.

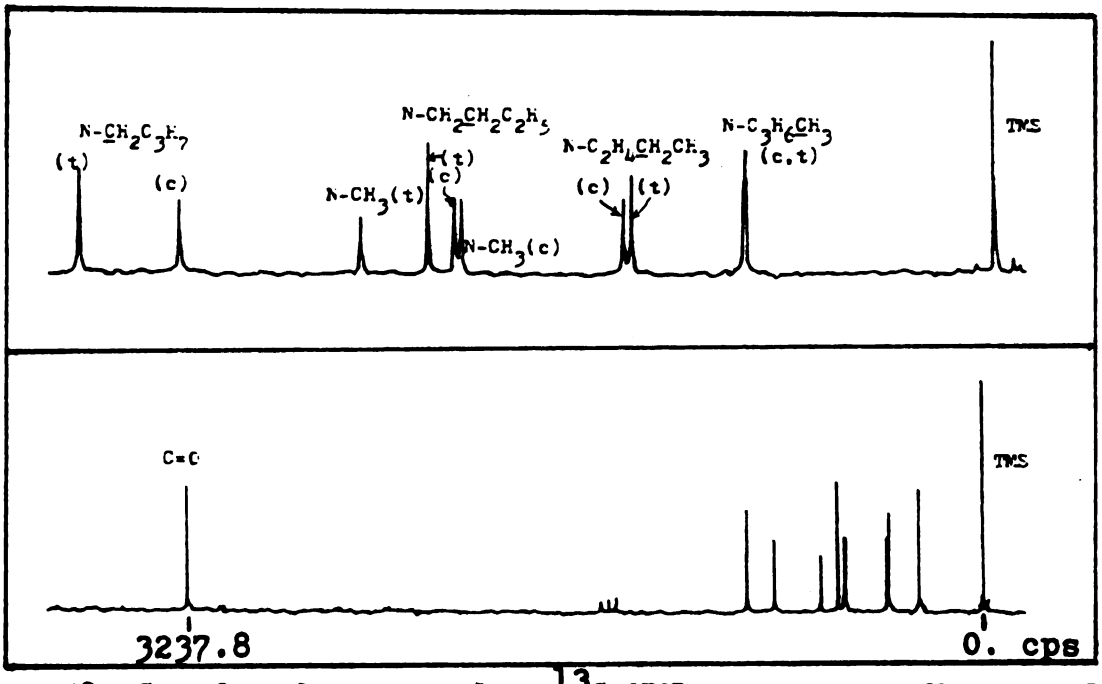

Figure 58. Completely decoupled ^{13}C NMR spectra of N-n-butyl-N-methylformamide (bottom, full spectrum, sw = 4000 Hz and (top) the region of upfield signals expanded).

power of the instrument, the signals for the $N-CH_2-CH_2-CH_3$ protons observed in the proton NMR spectrum form a single broad line. The three signals observed in the $N-C\underline{H}_2-C_3H_7$ region also have not been explained. Since the ^{13}C chemical shifts of N-n-butyl-N-methylformamide are well resolved, as shown in Figure 58, and had been assigned by us by comparison with the ^{13}C NMR spectra in similar compounds and by use of spin-lattice relaxation data, it is worth using the off-resonance decoupling method to assign all the proton chemical shifts in this compound. The off-resonance decoupled ^{13}C NMR spectra of N-n-butyl-N-methylformamide are shown in Figure 59. The residual C-H coupling constants are plotted versus decoupler off-set in Figure 56 and the values of the proton chemical shifts calculated from the ^{13}C data are given in Table 28. As shown in Table 28, the three signals observed in the $N-C\underline{H}_2C_3H_7$ region are assigned to <u>trans</u>-N-n-butyl-α-H, the <u>cis</u>-N-n-butyl-α-H, and the <u>trans</u>-N-n-butyl-β-H, respectively (from low field to high field). Within the broad bump, there are two protons, the <u>trans</u>-N-n-butyl-γ-H and the <u>cis</u>-N-n-butyl-γ-H. The calculated chemical shift for the <u>cis</u>-N-n-butyl-β-H is rather low (1.60 ppm), and was assigned to the second signal in the spectrum (Figure 57(A)) as counted from the high field. The signal at highest field is attributed to the <u>trans</u>- and <u>cis</u>-N-n-butyl-δ-H's, as shown by the signal intensity, which is about twice

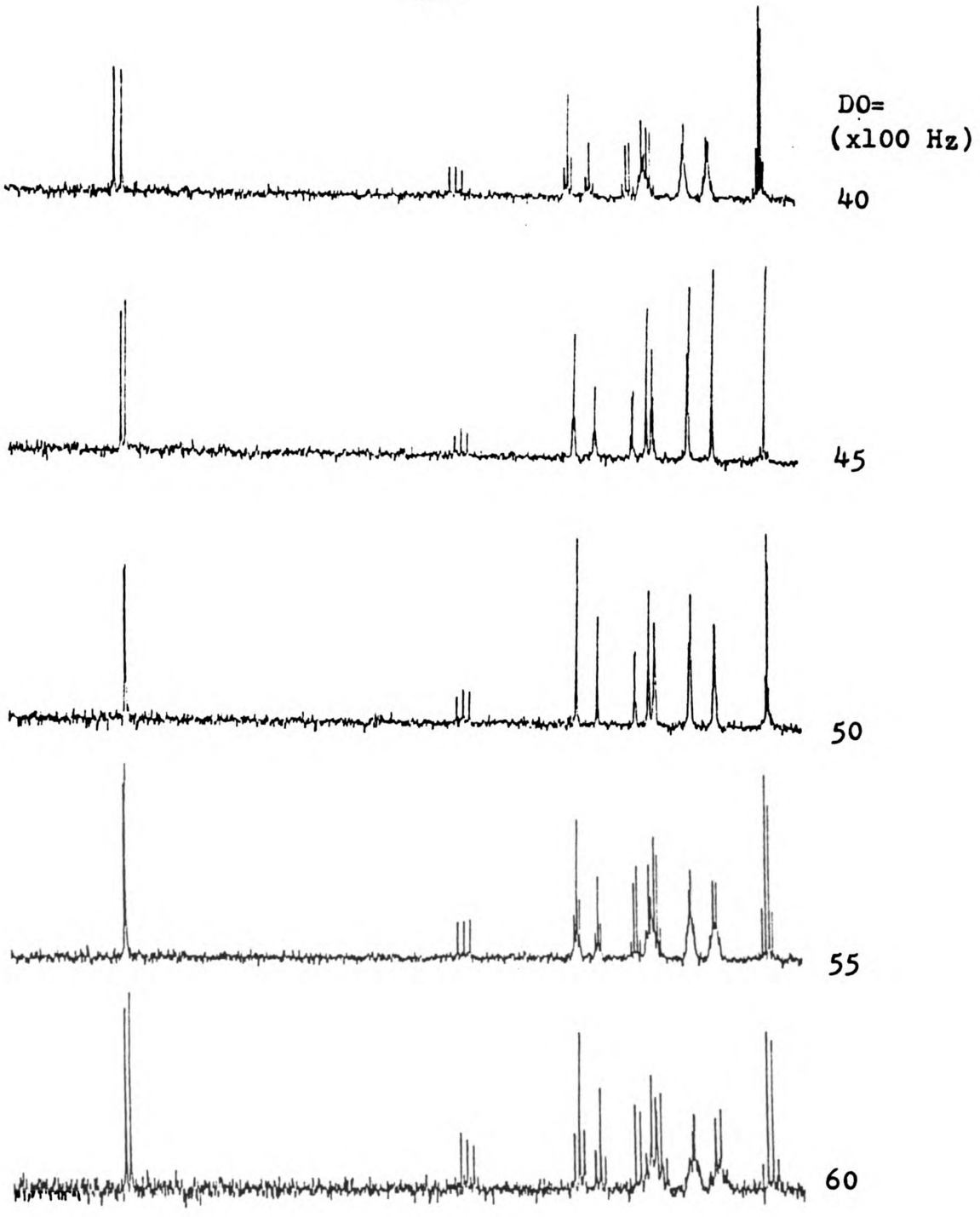

Figure 59. Off-resonance decoupled ^{13}C NMR spectra of N-n-butyl-N-methylformamide. The assignments and the scale are the same as in Figure 58.

that for the cis-N-n-butyl-β-H. In N-n-butyl-n-methylacetamide, Figure 56(b), the trans- and cis-δ-hydrogens of the N-n-butyl group are separated; this further indicates that there are actually two protons in the peak at highest field in the N-n-butyl-N-methylformamide spectrum (Figure 57(a)).

All the above results show that the off-resonance decoupling technique, and the use of T_1 measurements, are really powerful methods in solving the difficulties met in the assignment of ^{13}C and ^{1}H chemical shifts, especially when the signals in the spectra are complex, broad, or overlapped.

One point that should be mentioned is that if the condition $|\gamma H_2| >> |\Delta\nu|$ is not met, then the linear relationship between $\Delta\nu$ and J_r will break down at values of $\Delta\nu/\gamma H_2 \approx 0.5$. Under those conditions it has been suggested[29] that the equation

$$\Delta\nu = \frac{\gamma H_2 \, J_r}{(J_o^2 - J_r^2)^{1/2}} \qquad (152)$$

be used instead of the previous equation (Equation (151)). The symbols in the above equation have the same definitions as those in Equation (151). A plot of $J_r/(J_o^2 - J_r^2)^{1/2}$ versus $\Delta\nu$ will therefore yield the exact decoupling field H_2 in the proton spectrum corresponding to $J_r(J_o^2 - J_r^2)^{1/2} = 0$.

SECTION 6. SOLVENT EFFECT STUDIES OF N,N-DIMETHYLFORMAMIDE AND N,N-DIMETHYLACETAMIDE BY ^{13}C NMR

I. BACKGROUND

Hindered rotation around the central C-N bond in amides is a well-known phenomenon. It was detected by proton NMR and first reported in 1955 by Phillips[151] and by Gutowsky[152] for N,N-dimethylformamide. At sufficiently low temperatures, most N,N-dimethylamides show a doublet in the proton NMR spectrum and at higher temperatures this coalesces to a single line permitting measurement of rotation rates about the central C-N bond. Several proton NMR studies of this type had been carried out on N,N-dimethylformamide and N,N-dimethylacetamide.[153-161] Although the studies were made primarily for the purpose of making spectral assignments, concentration dependence of the chemical shifts of the amide protons in different solvents was noted.[162] It has been reported that when the pure amide is diluted with a nonpolar solvent, coupling across the C-N bond decreases[154] and the energy barrier E_a for rotation around the C-N bond decreases.[162] In N,N-dimethylamides, dilution produces a larger downfield shift of the *cis* proton signal than of the *trans*,[154] where *cis* and *trans* are taken relative to the C = O group. These results have been interpreted as indicating that in the

pure liquid the dipolar resonance form V-B is stabilized by head-to-tail dipolar association.[154,162] In dilute CCl_4 solution, ΔH^o and ΔS^o values of -6 kcal/mole and -14.5 eu, respectively, have been reported for the dimerization equilibrium.[153] Hydrogen-donating solvents also increase the contribution of the dipolar form by hydrogen bonding to the amide through the amide oxygen.[156]

Several workers have extended the studies of Hatton and Richards of the interaction between amides and aromatic solvents.[163-167] Sandoval and Hanna studied the complexes of DMF with benzene, toluene, p-xylene, mesitylene, and durene and obtained equilibrium quotients for association and the chemical shifts of the N-methyl groups in the pure complex. They found, in agreement with earlier work, that the proton $N-CH_3$ upfield shifts decreased as the number of aromatic methyl groups was decreased. However, since the equilibrium quotient for association increased in the same order, they concluded that the decrease in chemical shifts was due to a reduction in the aromatic ring current rather than to a weakening of the complex of amide with aromatic solvent. Matsuo has studied the effects of the solvent cyclohexane upon the chemical shifts of the protons in some N-substituted imides.[166]

As a result of the appearance of FT NMR spectrometers, ^{13}C NMR has become a popular tool for probing the interaction between solutes and different solvents. However,

only a few papers have been reported in which solvent effects of amides are investigated by ^{13}C NMR.[168] Here, we have studied the solvent effects in three different systems by use of ^{13}C NMR: (A) N,N-Dimethylacetamide in cyclohexane, (b) N,N-Dimethylacetamide in formamide, and (C) N,N-Dimethylformamide in benzene.

II. RESULTS

A. The N,N-dimethylacetamide-cyclohexane system

The concentration dependence of the chemical shifts for each carbon of N,N-dimethylacetamide and of cyclohexane in solutions of various concentrations are shown in Table 29 and Figures 60-62. From Figure 60 we see that the variation of the chemical shift for carbonyl carbon with the concentration of DMA is strongest, and that this resonance is shifted to low field as the concentration of DMA is increased. The chemical shifts at concentrations below 30% are not observed because the signals are too weak to be observed. The chemical shift of the carbon of the carbonyl methyl group as shown in Figure 61, is also strongly dependent on the concentration of DMA. The downfield chemical shift for carbonyl methyl group from infinite dilution to 100% DMA is about 0.64 ppm. The chemical shifts of the carbons of the trans and cis-N-methyl groups are also moved downfield, but their variations are smaller than those of the carbons of the C = O group and of the carbonyl methyl group. The variation of the chemical shifts

Table 29. ^{13}C Chemical shifts of the carbons in N,N-dimethylacetamide (DMA) and in cyclohexane for solutions of DMA in cyclohexane of various concentrations.

V/V Ratio of DMA to Cyclohexane	Chemical Shift (ppm)*					Chemical Shift Difference
	N,N-Dimethylacetamide				Cyclohexane	
	$\underline{C}=O$	$N-CH_3(t)$	$N-CH_3(c)$	$O=C-\underline{C}H_3$		$\Delta\omega_{CH_3}$**
100%	169.21	37.00	33.89	30.74	-	3.11
90%	169.14	36.98	33.88	20.72	26.56	3.10
80%	169.00	36.94	33.81	20.64	26.54	3.13
70%	168.91	36.90	33.78	20.59	26.58	3.12
60%	168.79	36.89	33.77	20.55	26.59	3.12
50%	168.72	36.85	33.74	20.52	26.57	3.11
40%	168.55	36.83	33.72	20.45	26.59	3.11
30%	168.43	36.80	33.67	20.41	26.59	3.13
20%	-	36.71	33.65	20.29	26.59	3.06
10%	-	36.64	33.63	20.21	26.63	3.01

*The chemical shifts are relative to TMS, the mixtures were degassed and the measurements were made at 35°C.

**$\Delta\omega_{^{13}C}$ denotes the chemical shift difference between the trans and cis-$N-CH_3$ carbons in DMA.

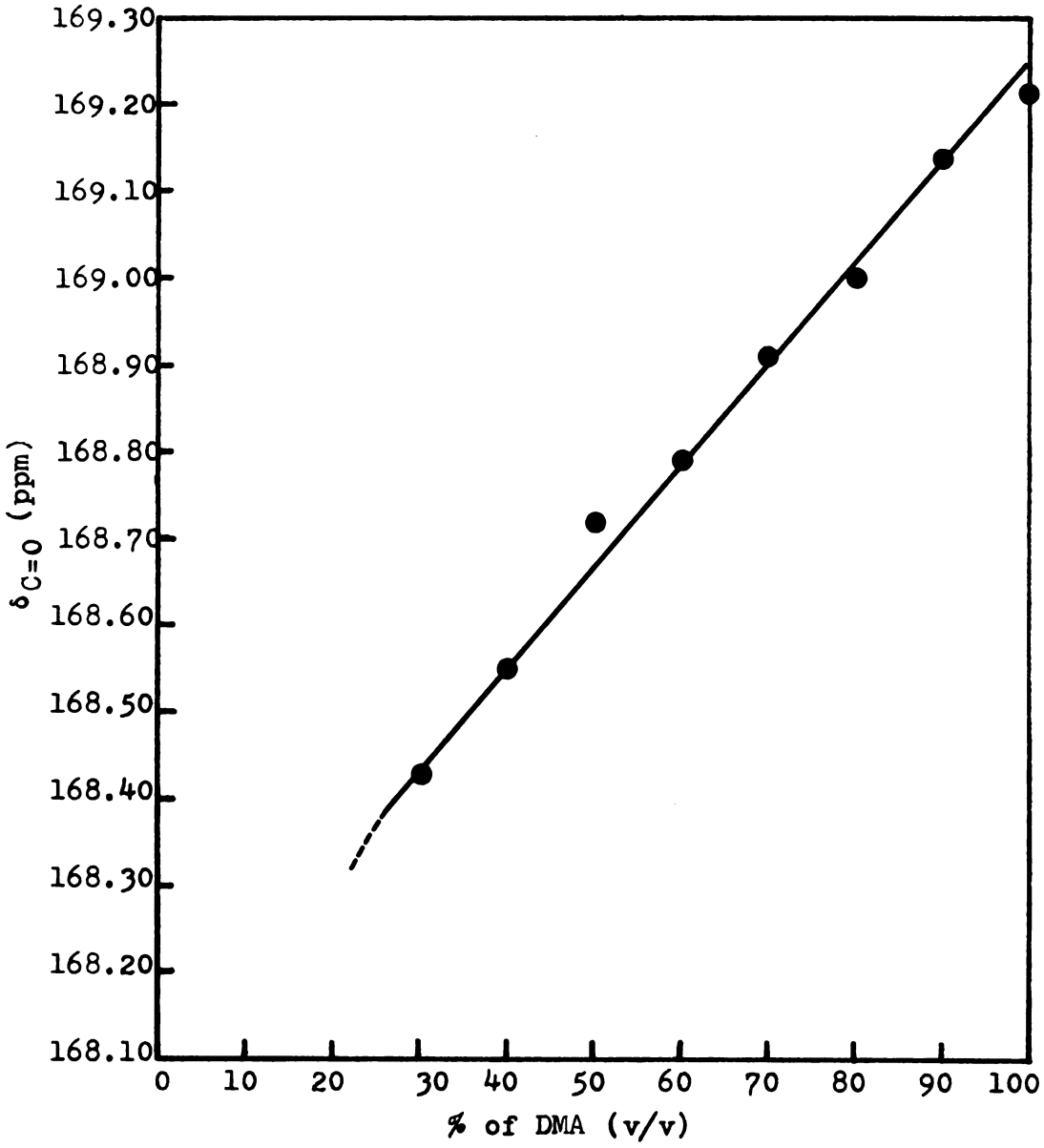

Figure 60. Concentration dependence of the ^{13}C chemical shift of the C=O group of DMA in cyclohexane solutions.

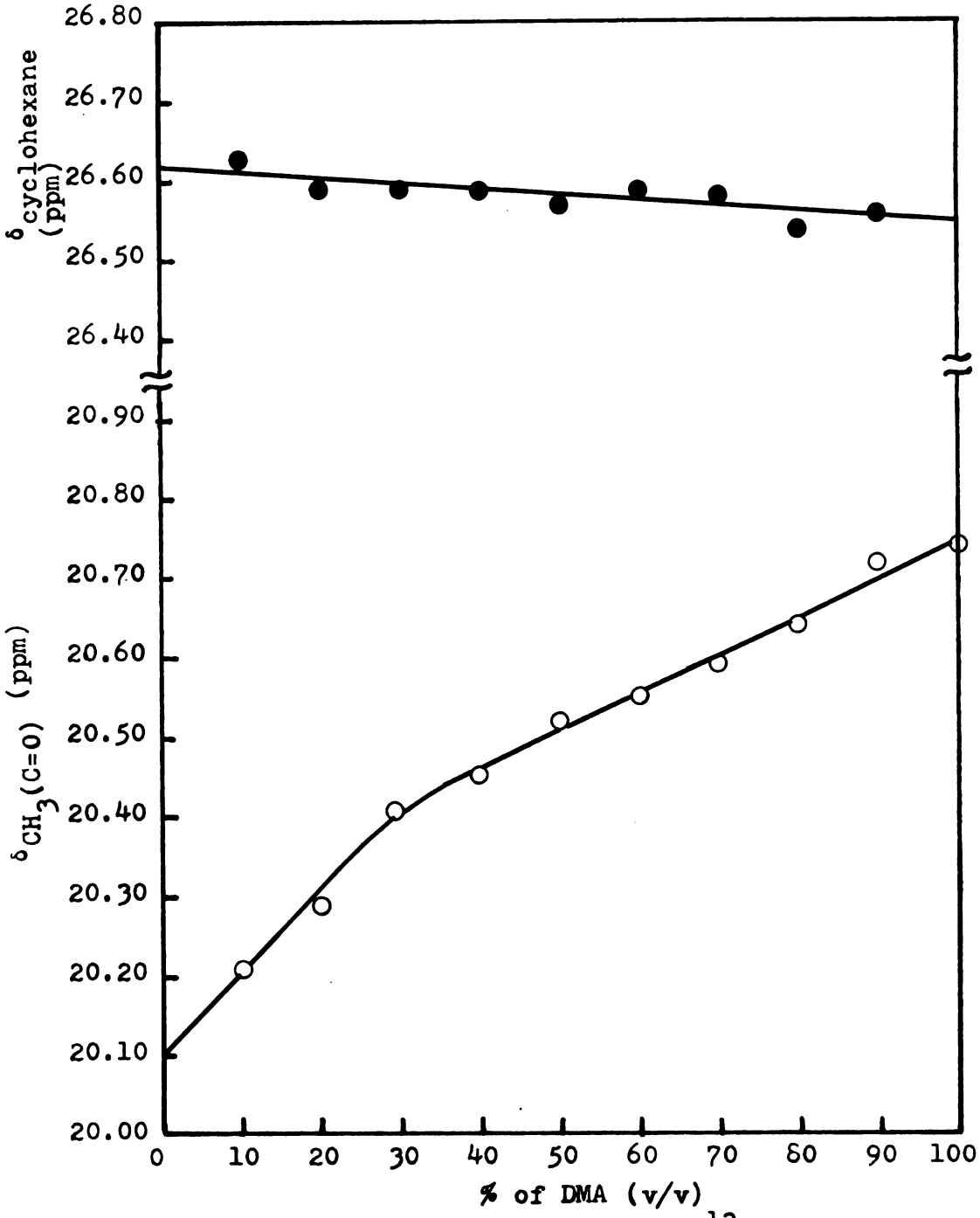

Figure 61. Concentration dependence of the ^{13}C chemical shifts of the cyclohexane carbons (top) and of the carbonyl-methyl carbon of DMA (bottom) in DMA-cyclohexane mixtures.

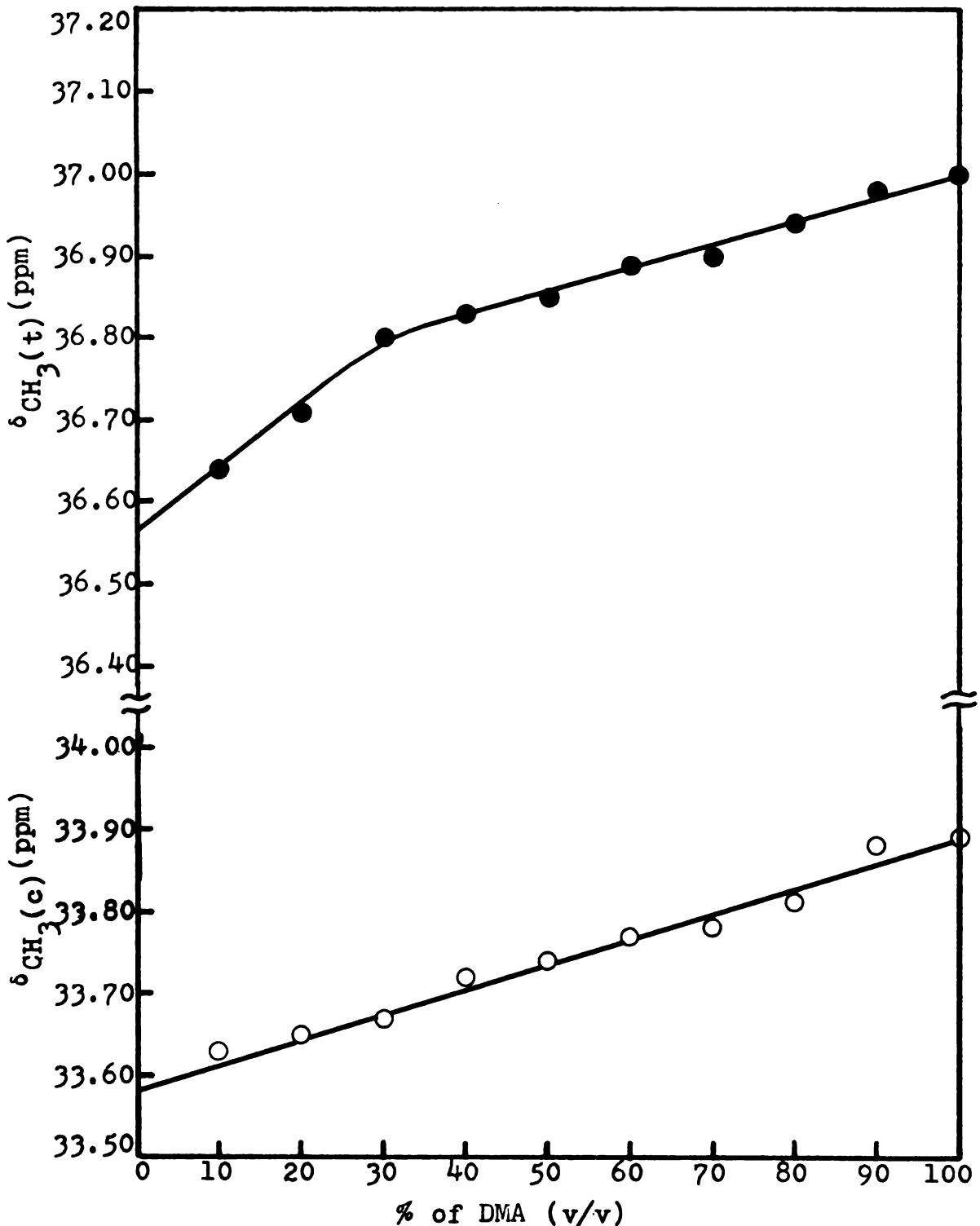

Figure 62. Concentration dependence of the ^{13}C chemical shifts for the carbons of the <u>trans</u>- and <u>cis</u>-NCH_3 groups of DMA in various DMA-cyclohexane mixtures.

for the cyclohexane carbons is only slight, which indicates that the intermolecular interaction between DMA and cyclohexane is not strong. This result is reasonable since cyclohexane is a nonpolar solvent. From the above results we see that the strong variation of the ^{13}C chemical shifts in DMA is mainly attributed to the interaction of DMA with itself, i.e., self-association. The chemical shift difference between the carbons of the trans- and cis-N-methyl groups is found to increase by about 0.18 ppm, as shown in Figure 63, as the concentration of DMA is increased from zero at infinite dilution to about 30% (by volume) and at concentrations above 30% the chemical shift only varied slightly. One would predict from these data that the energy barrier for rotation about the C-N bond would increase with an increase in the concentration of DMA up to about 30% (by volume) and then remain almost constant with further increases in DMA concentration.

A rapid increase within the range from 0 to 30% DMA corresponds to the rapid increase in the chemical shifts of the carbons of the carbonyl methyl and trans-N-methyl groups, which suggests that the solution structure changes rapidly in this concentration range and that it may be interpreted in terms of an association of the DMA molecules.[153,157] Woodbrey and Rogers[162] and Neuman and Young[169] suggested the cyclic structure (XV-A) for the dimer. The drawing (XV-B) of this dimer shows the regions of positive

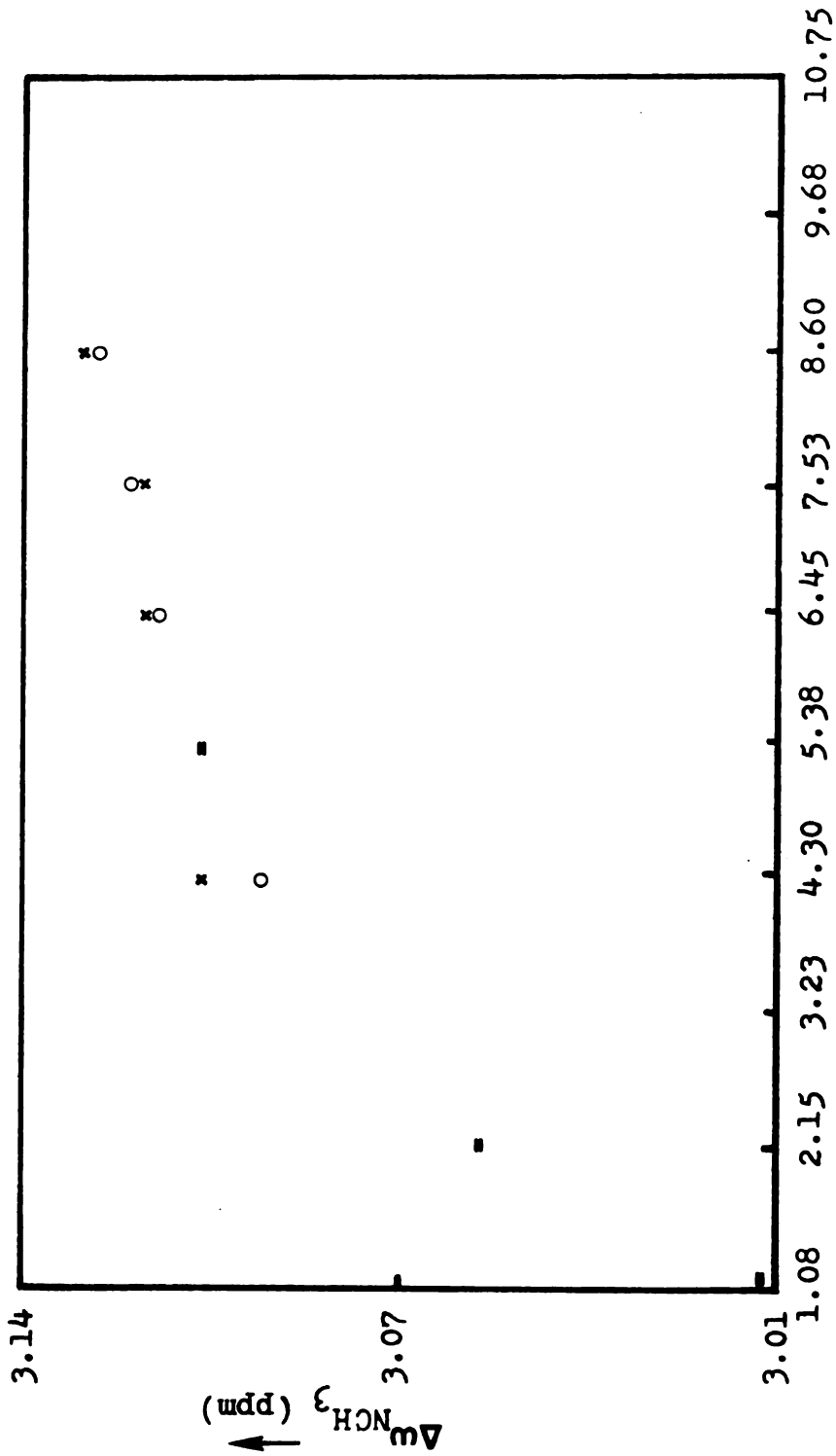

Figure 63. Concentration dependence of the calculated and experimental chemical shift differences ($\Delta\omega_{N\underline{C}H_3}$) between the two $N\underline{C}H_3$ ^{13}C signals of DMA in cyclohexane-DMA mixtures. x indicates an experimental point, o a calculated point, and = indicates that an experimental and calculated point are in the same delta x by delta y.

and negative shielding. Yonezawa[154,155] has used proton

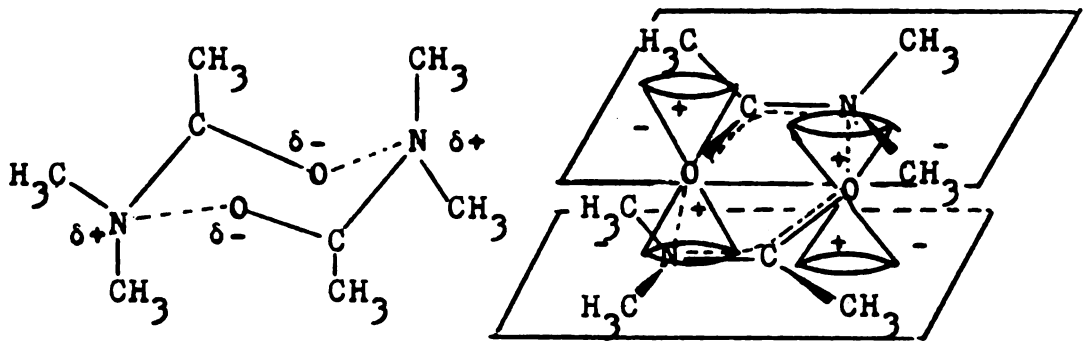

(XV-A) (XV-B)

NMR to show that the association shift of proton chemical shift in the dimer $(DMA)_2$ may be mainly attributed to the intermolecular long-range shielding effect of the carbonyl group (C = O) of the neighboring molecule instead of to the variation of the anisotropic shielding effect in the C = O group of the same molecule, i.e., an intramolecular effect.

Ando et al.[168] have reported that the ^{13}C chemical shifts of the three carbons of DMA in H_2SO_4 solution are shifted upfield as the concentration of DMA is increased. However, the ^{13}C chemical shifts of these three carbons for DMA in cyclohexane are shifted downfield when the concentration of DMA is increased (see Table 29).

Dipolar association, like hydrogen bonding at the carbonyl oxygen, will enhance the polarization of the C = O bond. If an intramolecular anisotropic shielding effect is an important factor, then the ^{13}C chemical shifts of the carbons in the dimer $(DMA)_2$ will be moved

upfield, as in the case of DMA in H_2SO_4 solution. The opposite results observed for DMA in cyclohexane solution indicate that the intermolecular shielding effect of the C = O group is more important than that of the intramolecular shielding effect illustrated in Structure (XV-B).

The variation of the ^{13}C chemical shift for the trans-N-methyl group with concentration is greater than that for the cis-N-methyl group. This can also be explained by the intermolecular shielding effect of a C = O group of one molecule of the dimer on the other one. Since the trans-N-methyl group is closer to the deshielding zone of the C = O group of the other molecule of the dimer, hydrogen bonding at the carbonyl oxygen will have a larger effect on it.

Neuman et al.[157] have reported that the concentration dependence, in carbon tetrachloride solution, of the chemical shift ($\Delta\omega_{CH_3}$) in the region of slow exchange between the two N-methyl resonances of DMA, as well as $\Delta\omega_{CH_3}$ for DMF and the corresponding thioamides, can be interpreted in terms of a monomer-dimer self-association equilibrium

$$2\ \mathrm{DMA} \underset{}{\overset{K}{\rightleftarrows}} (\mathrm{DMA})_2\ , \qquad (153)$$

where K is the equilibrium constant.

The dimer formed by self-association is held together by dipole-dipole interactions. Since cyclohexane, like CCl_4, is a nonpolar solvent, we expect that self-

association may also occur in amide solutions in cyclohexane. If such a monomer-dimer equilibrium exists, the values of $\Delta\omega_{NCH_3}$ may be described by the equation

$$\Delta\omega_{NCH_3} = (M(\Delta\omega_M) + 2D(\Delta\omega_D))/(M + 2D), \quad (154)$$

in which $\Delta\omega_M$ and $\Delta\omega_D$ are the chemical shifts in the region of slow exchange between the NCH_3 groups in pure monomer and dimer, respectively, and M and D are the respective molar concentrations.

From Equation (153) we may write

$$K = D/M^2 \quad (155)$$

and

$$C = M + 2D , \quad (156)$$

where C is the formal concentration of N,N-dimethylacetamide in the nonpolar solvent. From Equations (153) to (156), the following equation is obtained

$$\Delta\omega_{NCH_3} = \frac{(-1.0 + \sqrt{1.0 + 8KC})}{4KC} (\Delta\omega_M - \Delta\omega_D) + \Delta\omega_D . \quad (157)$$

By using the KINFIT program, the best-fit of the experimental data to Equation (157), which is based on the monomer-dimer model, was obtained. The resulting parameters K, $\Delta\omega_M$, and $\Delta\omega_D$ are given in Table 30 and the theoretical curve is compared with the experimental data in Figure 63. The calculated K value includes the activity coefficients.

Table 30. Calculated ^{13}C chemical shifts (in the slow exchange region) between the NCH_3 resonances in monomer and dimer, and the association equilibria, of some amides in nonpolar solvents.

Amide	Temperature (°C)	Solvent	$\Delta\omega_M$[b] (ppm)	$\Delta\omega_D$ (ppm)	K (ℓ mole^{-1})	References
DMA	34.5	Cyclohexane	2.61	3.21	2.78	This work
DMF[a]	36.	CCl_4	-	-	10.2	173
DMA[a]	36.5	CCl_4	-	-	0.37	157

[a]Only the proton chemical shifts were determined.

[b]$\Delta\omega_M$ is the ^{13}C chemical shift difference ($\delta_{trans} - \delta_{cis}$) for the N-methyl groups of the monomer and $\Delta\omega_D$ the difference for the dimer.

Comparing the experimental K values obtained by proton NMR in the DMA-CCl_4 and DMF-CCl_4 systems, as shown in Table 30,we find that our K value, 2.78, is within the range of K values reported by Neuman.[157] The ^{13}C chemical shift difference between the two NCH_3 groups in pure monomer and dimer is 2.61 ppm and 3.21 ppm, respectively.

B. The N,N-dimethylacetamide-formamide system

Rotation about the central C-N bond in the peptide link is restricted due to electron delocalization (Structure (XVI-A)) and this property imparts rigidity to proteins and polypeptides. An additional factor conributing to the secondary structure of these macromolecules is intramolecular hydrogen bonding between peptide linkages (Structure XVI-B). Such hydrogen bonding might be expected

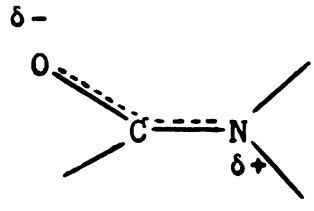

(SVI-A)

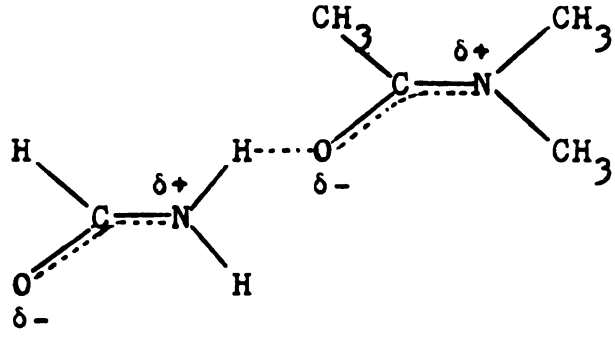

(XVI-B)

to increase the C-N rotational barrier over that for the non-hydrogen-bonded molecule by stabilizing the charge separation in the polar ground state.

Since the hydrogen bonding interaction between N,N-dimethylamide and formamide represents a

model for the hydrogen-bonding interaction between different peptide groups of a protein, we have investigated the variation of ^{13}C chemical shifts in this system as the concentration of DMA is changed. The results are shown in Table 31 and Figures 64-67. One main difference, compared with the chemical shifts of DMA in cyclohexane, is that the ^{13}C chemical shifts of all the carbons in this system are shifted upfield as the concentration of DMA is increased. This result is just the opposite of that obtained for the DMA-cyclohexane mixtures.

In addition, the curves showing the variation of chemical shift with concentration in these two systems are completely different, as shown in Figures 60-67, indicating that there is a specific interaction between solute and solvent for solutions of DMA in formamide. In the DMA cyclohexane system, the variation of the ^{13}C chemical shifts is interpreted in terms of a monomer-dimer self-association equilibrium. However, in the DMA-formamide system, there is an additional solute-solvent interaction which competes favorably with DMA self-association, i.e.,

$$DMA + F \rightleftarrows (DMA \cdot F).$$

Neuman et al. have investigated solutions of DMA in CCl_4 and in formamide by proton NMR[159] and obtained similar results to those obtained using ^{13}C chemical shift data for DMA-cyclohexane and DMA-formamide mixtures in

Table 31. ^{13}C Chemical shifts of the carbons of N,N-dimethylacetamide (DMA) and of formamide in solutions of different concentrations.

Mole Ratio of DMA in formamide	Chemical Shift* (ppm)					Chemical Shift Difference	
	N,N-Dimethylacetamide				Formamide		
	C = O	N-methyl(t)	N-methyl(c)	O=C-CH$_3$	C = O	$\Delta\omega_{CH_3}$**	$\Delta\omega_{C=O}$***
100%	170.53	37.25	34.19	20.62	-	3.06	-
80%	170.79	37.29	34.27	30.60	163.91	3.02	6.88
60%	171.09	37.33	34.37	20.58	164.34	2.96	6.75
50%	171.23	37.35	34.42	20.56	164.53	2.93	6.70
40%	171.29	37.35	34.45	20.56	164.59	2.90	6.70
30%	171.53	37.40	34.54	20.56	164.89	2.86	6.64
20%	171.68	37.43	34.61	20.56	165.09	2.82	6.59
10%	171.76	37.45	34.66	20.58	165.21	2.79	6.55

*The chemical shifts are relative to TMS. The mixtures were degassed and the measurements made at 35°C.

**$\Delta\omega_{CH_3}$ denotes the chemical shift difference between trans- and cis-N-CH_3 in DMA.

***$\Delta\omega_{C=O}$ is the chemical shift difference between C = O groups in DMA and formamide.

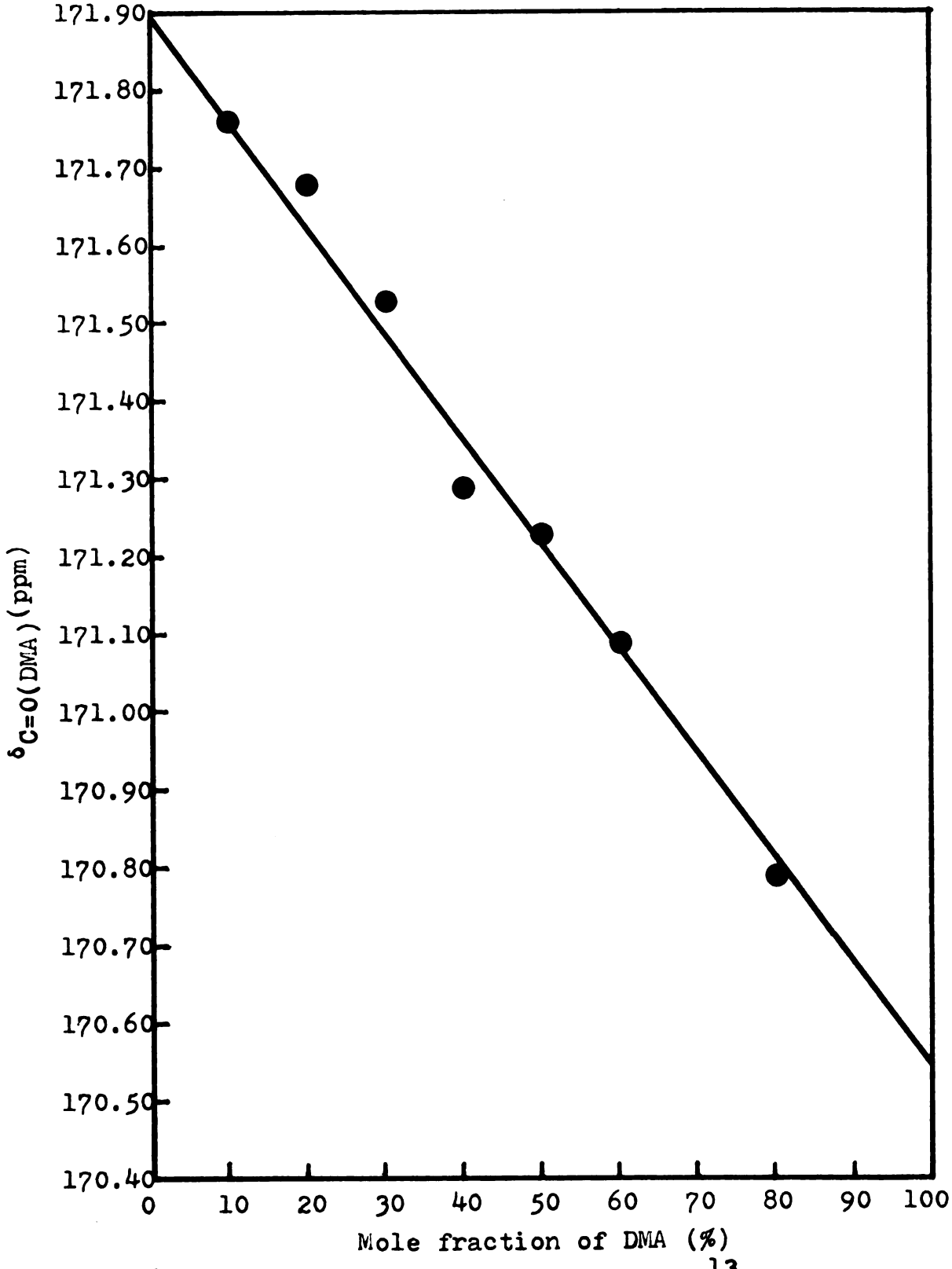

Figure 64. Concentration dependence of the ^{13}C chemical shift of the carbonyl carbon of DMA in DMA-formamide mixtures.

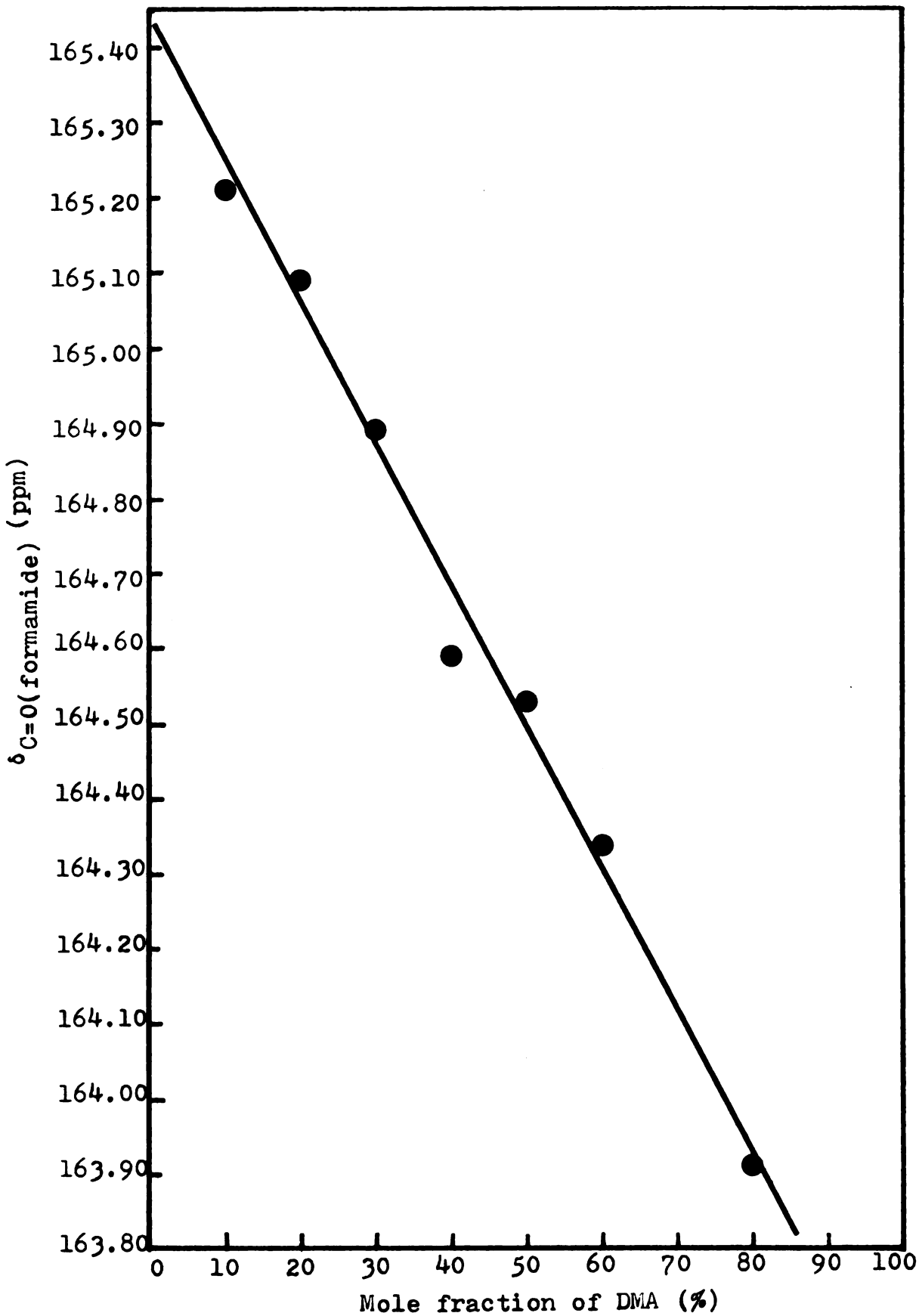

Figure 65. Concentration dependence of the ^{13}C chemical shift of the carbonyl carbon of formamide in DMA-formamide mixtures.

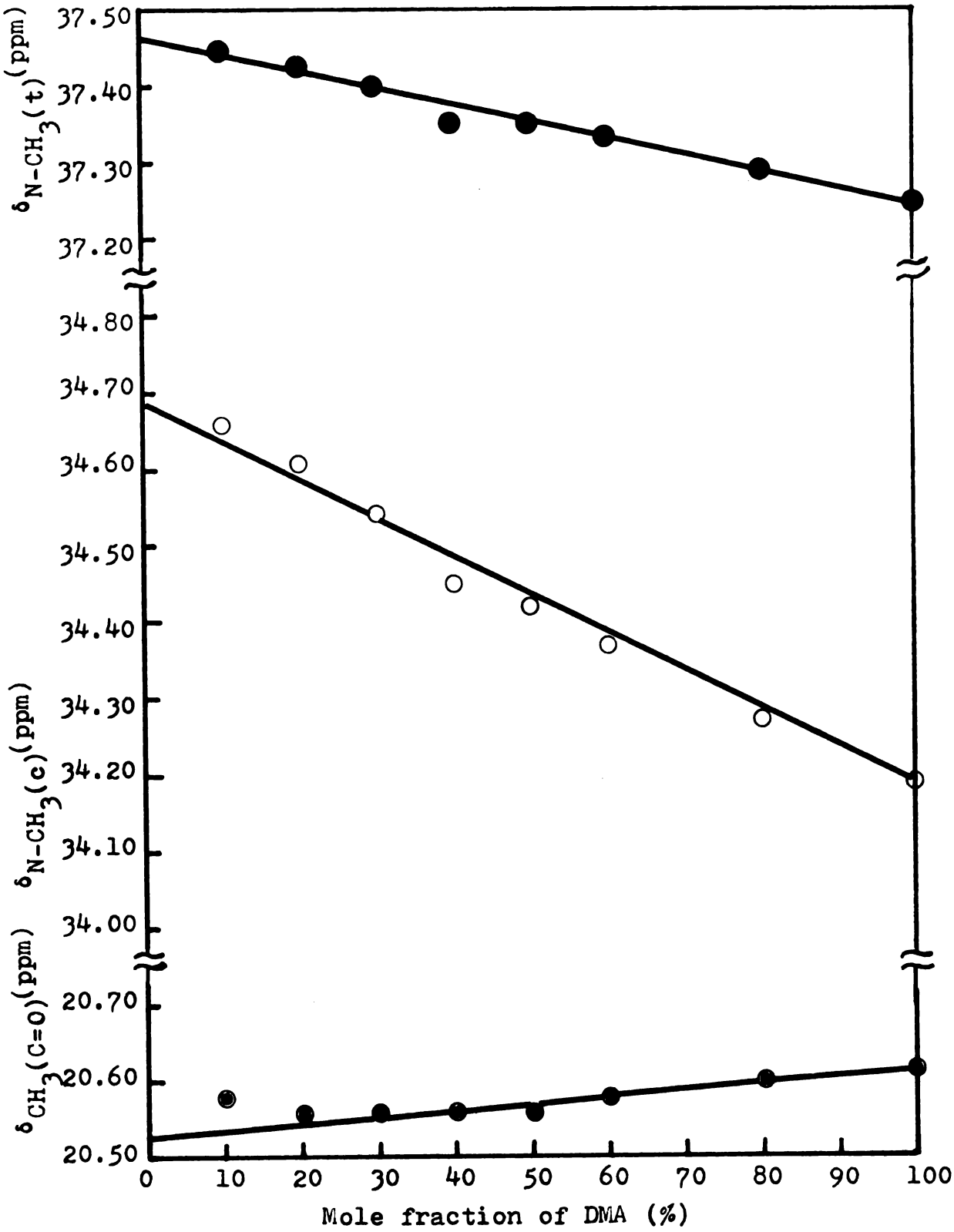

Figure 66. Concentration dependence of the ^{13}C chemical shifts of the carbons of the trans-$N\underline{C}H_3$ (top), cis-$N\underline{C}H_3$ (middle), and carbonyl-$\underline{C}H_3$ (bottom) groups of DMA in DMA-formamide mixtures.

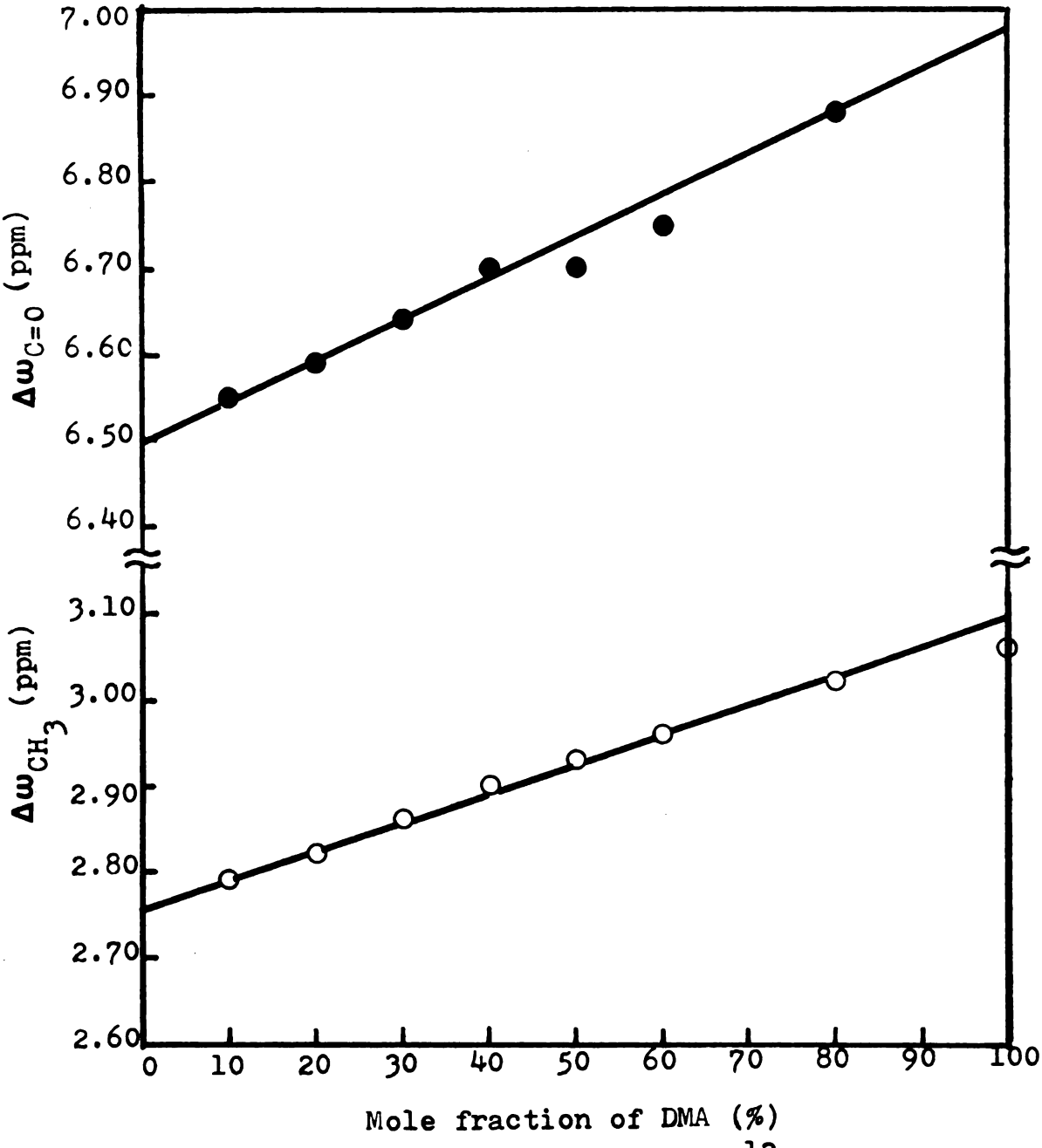

Figure 67. Concentration dependence of the ^{13}C chemical shift difference between the carbons of the C=O groups of DMA and formamide (top), and the chemical shift difference between the carbons of the <u>trans</u>- and <u>cis</u>-N<u>C</u>H_3 groups (bottom).

this work. Neuman et al. also have determined the energy barrier for internal rotation in DMA in formamide and find that it increases as the concentration of formamide increases.

From Figures 64 and 65 we find that the variation of the ^{13}C chemical shifts for the C = O groups of DMA and of formamide are sharp and almost linear, indicating that the intermolecular interaction between DMA and formamide is very strong. This is different from the concentration dependence of the carbonyl carbon in DMA-cyclohexane mixtures, since hydrogen bonding is important in the DMA-formamide system.

In the DMA-cyclohexane system, the dimers formed by the self-association of DMA are held together by dipole-dipole interactions. This type of interaction should also be possible between DMA and formamide molecules to form DMA·F complexes. However, we would expect that the ^{13}C chemical shifts in such a complex would be essentially similar to those for $(DMA)_2$, since the relative shielding of the two NCH_3 groups in DMA should be mainly a function of the respective positions of the two amide linkages. Such dipolar interactions should lead to little concentration dependence of the ^{13}C chemical shifts for DMA in formamide. However, a large dependence of ^{13}C chemical shifts in DMA is observed, so the structures of DMA·F and $(DMA)_2$ must be quite different. A hydrogen-bonded DMA·F linear complex (Structure (XVI-B)) would satisfy this criterion.

The variation of the ^{13}C chemical shift for carbon in the carbonyl-methyl group is only slight, which indicates that the carbonyl methyl group of DMA must be trans to the C = O group of formamide, as shown in Structure (XVI-B), instead of cis to the C = O group of formamide as suggested by Neuman.[159] The variation of the ^{13}C chemical shift of the carbon of the trans-N-methyl group is smaller than that observed for the cis-N-methyl group in DMA, which indicates that Structure (XVI-B), suggested here for DMA·F, is correct, since in this structure the trans NCH_3 group in DMA is far away from the C = O group of formamide.

Comparing the system DMA-formamide with the system DMA-H_2SO_4,[168] we find that the change of ^{13}C chemical shifts in both systems is similar. This provides further support for the hypothesis that hydrogen bonding between DMA and formamide is important.

The ^{13}C relaxation times for the carbons of DMA in various concentration solutions in formamide were also determined and are shown in Table 32. The results show that as the concentration of formamide increases, the relaxation times of the carbons in DMA decrease. This indicates that hydrogen bonds are formed between DMA and formamide.

Since the molecular weight of formamide is smaller than that of DMA, if only the DMA·F complex is formed in the DMA-formamide system, as suggested by Neuman,[159] then

Table 32. Concentration dependence of the ^{13}C relaxation times of the carbons of DMA in N,N-dimethylacetamide-formamide mixtures.

Substituent	Concentration (DMA) 100%	80%	60%	50%	30%
N-$\underline{C}H_3$ (trans)	13.28±0.46	13.23±0.55	-	12.76±0.44	10.91±0.80
N-$\underline{C}H_3$ (cis)	13.82±0.27	12.75±0.48	-	12.39±0.70	11.04±0.44
Carbonyl-$\underline{C}H_3$	10.95±0.23	-	10.14±0.28	10.04±0.36	8.75±0.22
$\underline{C}$ = O	63.89±2.70			41.83±3.08	
$\underline{C}$ = O (Formamide)	9.11±0.18			5.84±0.26	

*Concentrations are expressed as mole ratios. The measurements were made at 34.5°C.

the ^{13}C relaxation times of the carbons of DMA in this system should be almost equal to, or even longer than, those in neat DMA, which contains a high concentration of dimer, $(DMA)_2$, in the pure liquid state. This result then indicates that other species, such as $DMA \cdot F_n$, may exist in the DMA-formamide system. One possibility is the formation of DMA complexes containing more than one formamide molecule

$$DMA + F_n \rightleftarrows DMA \cdot F_n,$$

where n is greater than or equal to 2, and F_n can be cyclic dimers , chain dimers, or even trimers of formamide. The structure of such a complex might be written as in (XVI-C) additional molecules of formamide interacting with the first one by hydrogen bonding to the C = O group or by dipole-dipole interactions. Alternatively, additional molecules of formamide might interact with the DMA molecule of the DMA·F complex through dipole-dipole interactions as in Structure (XVI-B).

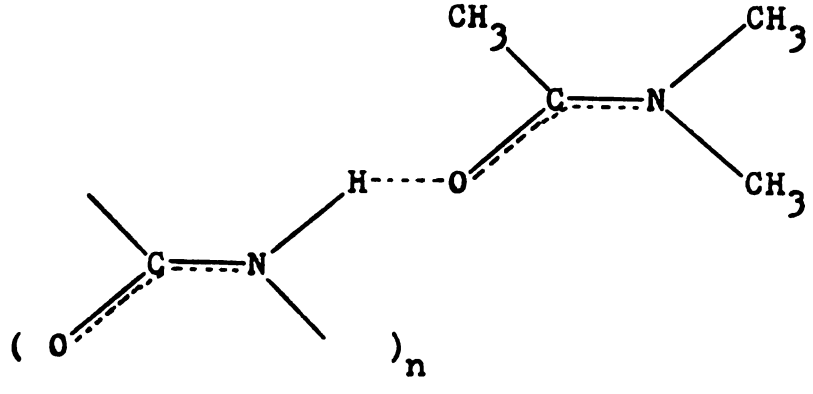

(XVI-C)

Because of the uncertainty concerning the actual species present in this system we have not attempted quantitative determination of constants.

C. The N,N-dimethylformamide-benzene system

The structure and chemistry of π molecular complexes have been extensively investigated in the last three decades. Information about the equilibrium between π complexes and their components, and about the structures of π complexes, has come from many different experimental methods[170-172] including visible, uv, and IR spectroscopic techniques.

Proton NMR studies of these complexes have also been carried out[95,161,164,173,174] and, by using proton NMR, some formation constants of the π complexes have been determined. The determination of the formation constant of the complex between DMF and benzene have been investigated by Hanna et al. and by Sandoval[174,161]. Hanna et al. were unable to determine the formation constants of the DMF-benzene and DMF-toluene complexes; however, Sandoval obtained these by the same method and the same equation.[161] Since Hanna's equation can only be applied under restricted conditions, i.e., the concentration of donor should be much greater than that of the acceptor, we tried to use ^{13}C NMR and develop a general equation to fit the experimental ^{13}C chemical shifts.

The results for the DMF-benzene system are shown in Table 33 and the ^{13}C chemical shifts are plotted

Table 33. ^{13}C Chemical shifts of the carbons of N,N-dimethylformamide in various DMF-benzene mixtures.

V/V Ratio of DMF to benzene (%)	Chemical Shift* (ppm) N,N-Dimethylformamide			Benzene	Chemical shift difference
	C = O	N-CH_3(t)	N-CH_3(c)		$\Delta\omega_{CH_3}$
100	161.92	35.13	30.03	-	5.10
95	161.89	35.11	30.04	128.06	5.08
90	161.86	35.10	30.04	128.02	5.07
85	161.83	35.09	30.03	128.02	5.06
80	161.80	35.08	30.03	128.03	5.05
75	161.77	35.07	30.04	128.02	5.03
70	161.71	35.04	30.02	128.00	5.02
65	161.66	35.02	30.02	127.97	5.00
55	161.59	34.95	29.99	127.94	4.96
50	161.52	34.92	29.99	127.92	4.93
45	161.49	34.88	29.97	127.91	4.91
40	161.50	34.90	30.01	127.92	4.89
35	161.41	34.82	30.01	127.90	4.81
30	161.42	34.84	29.98	127.91	4.86
25	161.26	34.70	29.93	127.83	4.77
20	161.17	34.61	29.89	127.78	4.72
15	161.11	34.54	29.84	127.76	4.70
10	161.02	34.44	29.83	127.72	4.61

*The chemical shifts are relative to TMS, the mixtures were degassed and the measurements were made at 35°C.

**$\Delta\omega_{CH_3}$ denotes the chemical shift difference between the trans-and cis-N-CH_3 carbons in DMF.

graphically as functions of concentration in Figures 68-70. We find that the variation with concentration of the ^{13}C chemical shift for the C = O group of DMF is again sharpest. The shapes of the curves are similar for each carbon and the chemical shifts are moved downfield as the concentration of DMF is increased, which is similar to the case of DMA in cyclohexane solutions. However, the change of the ^{13}C chemical shift of benzene is also relatively large. This indicates that the interaction between DMF and benzene is strong, which is opposite to the result obtained in the case of the DMA-cyclohexane system. As the concentration of DMF decreases, both the trans-and cis-NCH_3 carbon reasonances are shifted upfield but the trans signal shifts by a much larger amount.

These observations can be explained by assuming that the amide molecule associates with benzene in such a way that the nitrogen atom, with its fractional positive charge, is situated close to the region of high π electron density of the benzene ring and the negatively-charged oxygen atom of the carbonyl group stays as far from the center of the ring as possible. The DMF molecule presumably retains its planar configuration so that the planes of the solute and solvent molecules become parallel as in Structure (XVII).

In this arrangement the trans-NCH_3 group will be near the center of the ring and, consequently, the

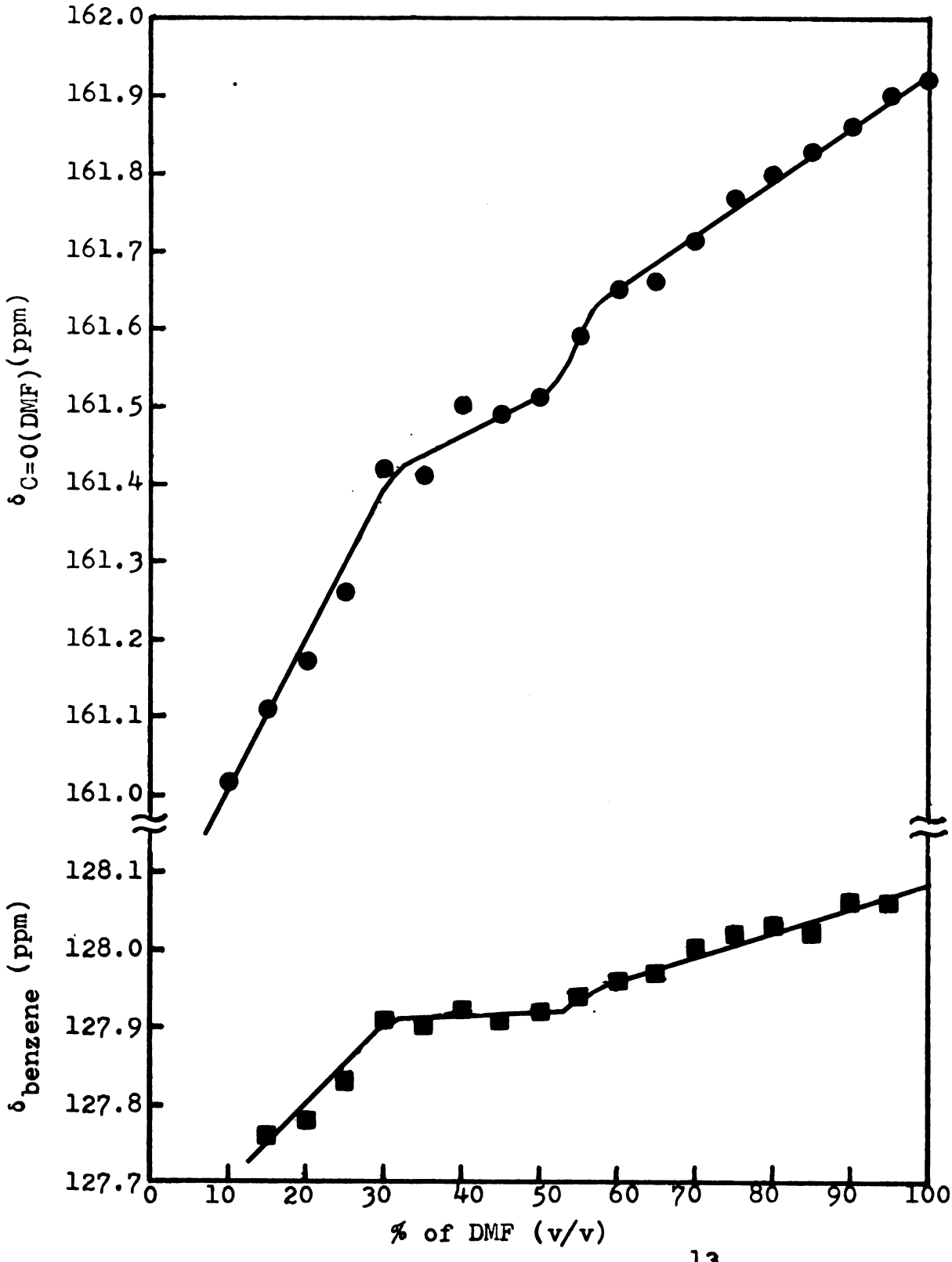

Figure 68. Concentration dependence of the ^{13}C chemical shifts of the carbon of the DMF C=O group and the carbons of benzene in DMF-benzene mixtures.

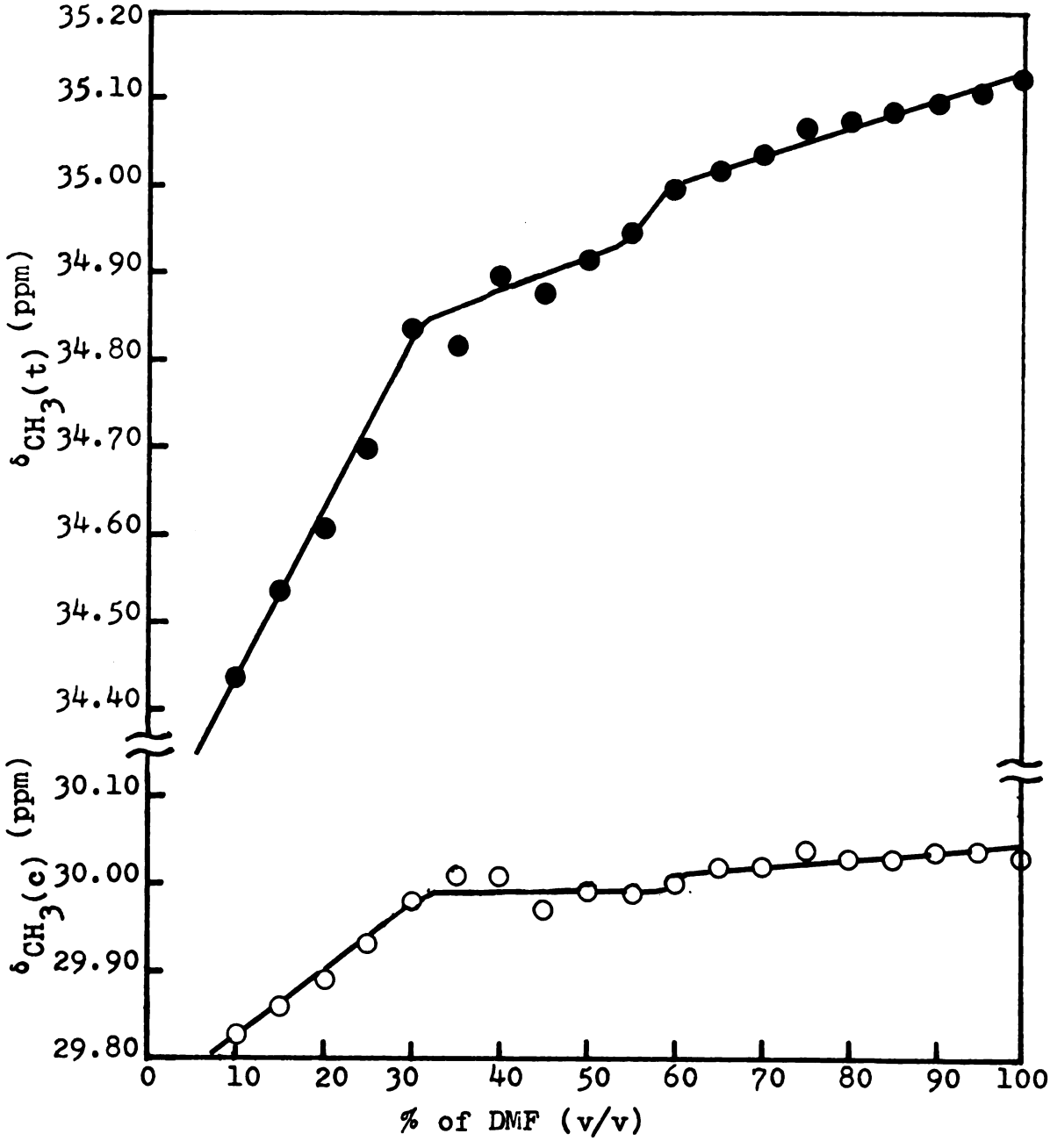

Figure 69. Concentration dependence of the ^{13}C chemical shifts of the carbons of the <u>trans</u>- and <u>cis</u>- $N\underline{C}H_3$ groups of DMF in DMF-benzene mixtures.

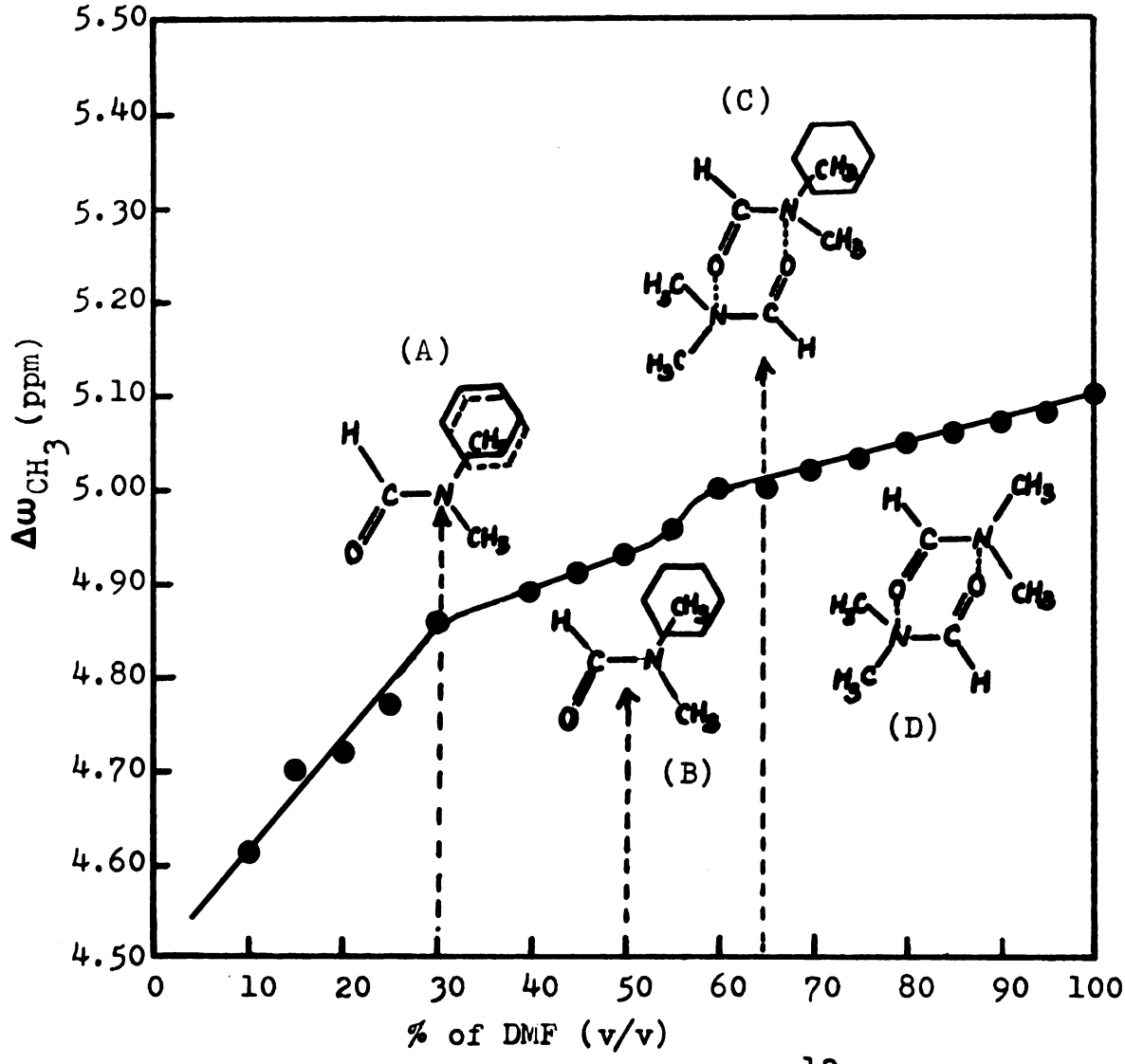

Figure 70. Concentration dependence of the ^{13}C chemical shift difference between the carbons of the trans- and cis-NCH_3 groups of DMF in DMF-benzene mixtures. The structures shown indicate the complexes which are postulated as the dominant species in the four concentration regions (A)-(D).

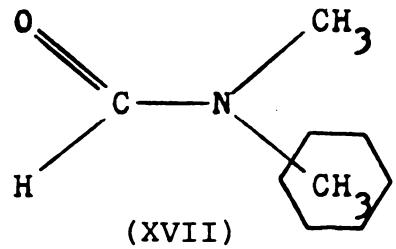

(XVII)

diamagnetic anisotropy of benzene will affect the trans-NCH_3 group more than the cis-NCH_3 group, tending to shift both the proton and ^{13}C resonance to higher magnetic field.

The formation of the π complex between DMF and benzene may be expressed by the equation

By using proton NMR, Hanna et al.[174] had developed an expression for calculating the formation constant of the π complex. Due to the limitations of that expression, i.e., that the concentration of benzene should be much greater than that of DMF, we have developed a general expression as outlined below.

Let us assume that A moles of DMF, B moles of benzene and C moles of 1:1 π complex are produced by mixing a total of 1 mole of DMF plus benzene, i.e., X moles of DMF and 1-X moles of benzene. Then the mole fraction of each species corresponds to A, B, and C divided by A + B + C, and hence the equilibrium constant K is given by

$$K = \frac{C(A + B + C)}{AB} \quad . \tag{158}$$

Since the total number of DMF and benzene molecules, including both free and complexed molecules, is constant before and after mixing, the following two equations hold:

$$X = A + C \tag{159}$$

$$1 - X = B + C \ . \tag{160}$$

The ^{13}C chemical shifts can be expressed as the weighted sum of the shifts in the free δ_f and complexed δ_c states

$$\delta_{cal} = (\frac{A}{X}\ \delta_f + \frac{C}{X}\ \delta_c) = \delta_f + \frac{C}{X}\ (\delta_c - \delta_f),$$

where δ_{cal} is the calculated ^{13}C chemical shift. From Equations 158 to 160, the following equation may be derived:

$$\delta_{cal} = \delta_f + (\delta_c - \delta_f)\ \frac{(K+1) + \sqrt{(K+1)^2 - 4K(K+1)(X-X^2)}}{2X(K+1)}. \tag{161}$$

The best fit of the experimental ^{13}C chemical shifts to Equation (161), which is based on the 1:1 π-complex model, was obtained by use of the KINFIT program.

One set of values calculated for the chemical shift difference δ_{NCH_3} between the two NCH_3 ^{13}C signals for DMF in benzene solution are shown in Figure 71 along with the experimental values of $\Delta\omega_{NCH_3}$. The calculated curve is based on the assumption that a 1:1 π complex is formed. The calculated chemical shifts of DMF in the free and complexed state, δ_c and δ_f, are also shown in

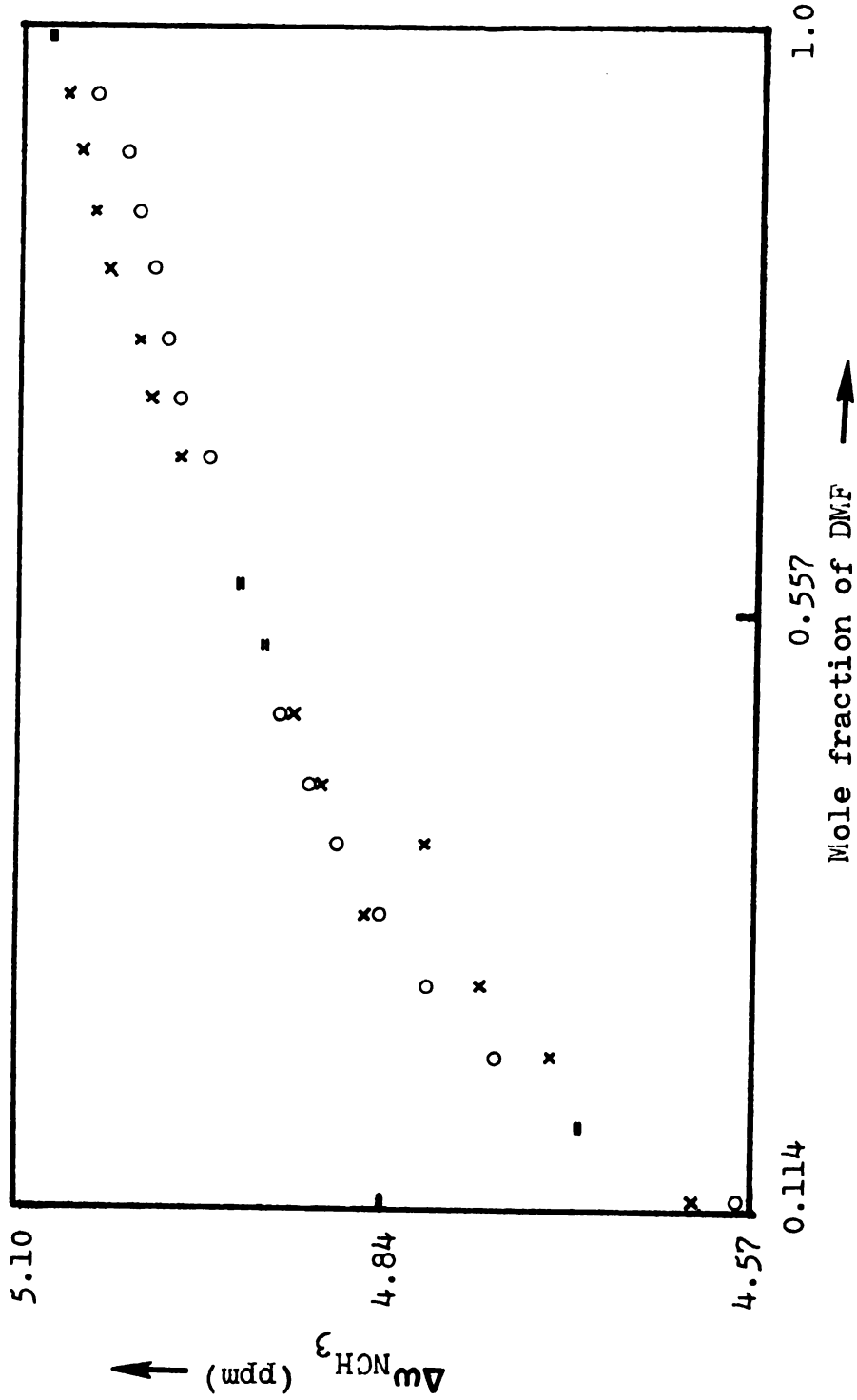

Figure 71. Concentration dependence of the calculated and experimental chemical shift difference ($\Delta\omega_{N\underline{C}H_3}$) between the two -$N\underline{C}H_3$ ^{13}C signal of DMF in DMF-benzene mixtures; x^3 indicates an experimental point, o a calculated point, and = indicates that an experimental and calculated point are in the same delta x by delta y.

Table 34. Unfortunately, the calculated formation constant is a negative number, -0.99. Hanna et al. were also unable to find the formation constant because a negative intercept was obtained by use of their equation. Sandoval obtained a value for the formation constant, 0.130, although it is a rather small number. The reason for the negative value of K obtained in our calculation may be the presence of species in our solutions other than the assumed 1:1 π complex, as shown in Figure 70. For example, we did not dilute the DMF-benzene mixtures with another solvent so the dimer of DMF may also have been present in the mixture. However, Hanna and Sandoval had diluted DMF-benzene mixtures with cyclohexane or dioxane so that most of the DMF molecules would be either present as monomer on in the 1:1 complex and the model would correspond better to the observations.

According to the 1:1 complex model, the ^{13}C chemical shifts should increase monotonically as the concentration of DMF is increased, as shown by the dotted lines in Figures 68-70. However, we find that there are deviations of between 30% and 60% from the monotonic increases represented by the dotted lines. At first we suspected that this might be attributed to experimental errors, so we carefully prepared the solutions again and redetermined all the ^{13}C chemical shifts. However, the same shaped curves were obtained. After examining these, we find that each curve

Table 34. Calculated ^{13}C chemical shifts for DMF-benzene mixtures[a]

Substituent	Chemical Shift	
	Free state δ_f	Complex δ_c
DMF		
NCH_3 (*trans*)[c]	35.1861±0.0135	35.1676±0.0241
NCH_3 (*cis*)	30.0681±0.0089	30.0456±0.0120
C = O	161.874 ±0.0292	161.850±0.0511
$\Delta\omega_{NCH_3}$	5.10505±0.0125	5.09041+0.0217
Benzene	128.060±0.0117	128.060±0.0249

[a] $K = -0.99$ is calculated by use of Equation (161) and these numbers, which are the parameters of Equation (161).

[b] Chemical shifts are relative to TMS and are in ppm.

[c] *cis* and *trans* are relative to the C = O group.

can be separated into several sections and the following set of equilibria is suggested in order to account for the complex shapes of the experimental curves of Figures 68-70. Between 10%-30% (v/v) of DMF, the principal equilibrium is

$$DMF + 2\,Bz \rightleftharpoons (DMF \cdot Bz_2),$$

from 30% to 48% DMF the additional equilibrium

$$(DMF \cdot Bz_2) + DMF \rightleftharpoons 2(DMF \cdot Bz),$$

becomes important, from 48% to 65% DMF the following equilibrium becomes important

$$(DMF \cdot Bz) + DMF \rightleftharpoons (DMF_2 \cdot Bz),$$

and from 65% to 100% DMF the dimer of DMF becomes the dominant species

$$(DMF_2 \cdot Bz) \rightleftharpoons DMF_2 + Bz.$$

The composition of the complexes in the above equations [$DMF.Bz_2$, DMF.Bz, DMF_2.Bz] correspond to the dotted lines in Figure 70 which are drawn approximately at the mole ratios DMF:Bz = 0.33, 0.50 and 0.67 [since the densities of DMF and benzene are about the same the mole ratios are nearly the same as the values of %DMF(v/v). The suggested structures of the complexes are also shown in Figure 70. Thus, between 10-30% DMF the favored complex

would be DMF.Bz_2 with a sandwich-type structure. In this species the ring current effect of both benzene rings would add and would result in the sharpest variation of chemical shift with concentration for the DMF carbons in this range. Beyond 30% DMF, the DMF molecules start to compete with benzene leading to the formation of the 1:1 complex in which the magnetic anisotropy of a single benzene ring affects the DMF carbons, leading to a greatly reduced effect of concentration on the ^{13}C chemical shifts. In the range 48% to 65% DMF, the complex of structure (C) in Figure 70 is gradually formed and, beyond 65% DMF, the ^{13}C chemical shifts of the carbons of DMF should approach those of the DMF dimer and so should be similar to those of DMF in cyclohexane solution where the dimer is an important species.

Mixtures of DMF and benzene, without any other added solvent, constitute a very interesting but complex system of a type which has never been studied before.

SECTION 7. NMR STUDY OF THE SOLVATION OF Mn^{2+} IN N,N-DIMETHYLFORMAMIDE SOLUTIONS

I. BACKGROUND

It is well known that nuclear magnetic relaxation in liquids is greatly enhanced by the presence of paramagnetic ions. This phenomenon has provided an important method for elucidating the structures of paramagnetic ions in solution since interatomic distances between protons and paramagnetic transition metal ions may be determined from the unpaired electron contribution to the relaxation times of the protons.[175-180] Recently, Mn^{2+} - ^{13}C distances have also been estimated from ^{13}C relaxation data.[181-184] Normally, the internuclear distances estimated in investigations of this type have been in agreement with those obtained by X-ray crystallography, when a comparison has been possible.

Similarly, structural information can also be obtained from changes in the ^{1}H or ^{13}C chemical shifts caused by paramagnetic ions of the lanthanide series.[185,186] However, a structural interpretation of the data obtained by this latter method is not always possible because of complexities in the interactions.

The first approach, the study of nuclear relaxation times, is usually straightforward due to the simple relation existing between the paramagnetic contribution to the relaxation rate of the nucleus and its distance from the paramagnetic ions. However, this method has certain inherent limitations when the magnetic nuclei are protons. First, the relatively narrow range of chemical shielding for protons, along with the broad lines often found in the presence of paramagnetic ions, may give seriously overlapping proton lines. This situation may prevent one from extracting separate relaxation parameters for individual proton resonances, especially when large molecules are studied. Second, protons generally are strongly spin coupled to other magnetic nuclei in the molecule, especially other protons, through the spin-spin interaction and this may complicate the extraction of parameters. Third, protons are often at the periphery of ion-solvent complexes, leading to proton-metal distances which are relatively long compared with the corresponding distances between the metal ion and the heavier atoms of the ligand such as C, N, or O. This tends to decrease the contribution of the paramagnetic ion to the relaxation and amplifies the uncertainties arising from additional interactions with the paramagnetic ions in neighboring molecules. These difficulties have restricted the application of the method, as far as protons are concerned,[175-180] mainly to water or methanol molecules,

which are directly attached to the paramagnetic ion, or to groups of equivalent protons in rather large molecules. Finally, in most cases only upper limits for the metal ion-ligand nucleus distances have been estimated because information on the effects of chemical exchange on the relaxation process is often lacking.

Using ^{13}C NMR, these disadvantages can be eliminated or significantly reduced, since the greater chemical shift range for ^{13}C tends to eliminate overlapping lines. Furthermore, proton decoupling usually collapses spin-spin multiplets to singlets leaving the relaxation of each of the ^{13}C nuclei governed by a single exponential time constant.[42] Also, ^{13}C nuclei are generally closer to the paramagnetic center and therefore not affected as greatly by intermolecular interactions. Despite these advantages, it is still necessary to unravel the relative importance of the different competing mechanisms contributing to the relaxation times of the ^{13}C nuclei in order to obtain the metal-carbon distances from the experimental relaxation values. To do this one has to determine the relaxation time of the paramagnetic electrons and the hyperfine coupling between metal ion and the observed ^{13}C nucleus, as well as the kinetics of the ligand exchange process. In this thesis a ^{13}C NMR investigation of Mn^{2+} in neat N,N-dimethylformamide solution will be presented. Mn^{2+} is known to have a nearly isotropic g tensor[187] and relatively long relaxation

times[188-191] for its unpaired electrons. Both of these features simplify the interpretation of the relaxation data and therefore increase the possibility of obtaining structural information.

A. Effects of paramagnetic ions on nuclear relaxation times

When coupling between the electron orbital and electron spin angular momenta can be neglected, which is generally the case for ions in the first transition series,[192] the electron paramagnetic contribution to the spin-lattice and spin-spin relaxation rates of an adjacent nuclear spin is given by the combined Solomon-Bloembergen equations, as shown below:[35,193,194]

$$1/T_{1M} = \frac{2}{15}\frac{S(S+1)\gamma_I^2 g^2 \beta^2}{r^6}\left(\frac{3\tau_c}{1+\omega_I^2\tau_c^2} + \frac{7\tau_c}{1+\omega_S^2\tau_c^2}\right) + \frac{2}{3}\frac{S(S+1)A^2}{\hbar^2}\left(\frac{\tau_e}{1+\omega_S^2\tau_e^2}\right) \quad (162)$$

$$1/T_{2M} = \frac{1}{15}\frac{S(S+1)\gamma_I^2 g^2 \beta^2}{r^6}\left(4\tau_c + \frac{3\tau_c}{1+\omega_I^2\tau_c^2} + \frac{13\tau_c}{1+\omega_S^2\tau_c^2}\right) + \frac{1}{3}\frac{S(S+1)A^2}{\hbar^2}\left(\tau_e + \frac{\tau_e}{1+\omega_S^2\tau_e^2}\right), \quad (163)$$

where S is the electron spin of the paramagnetic ion, γ_I is gyromagnetic ratio of the observed nucleus, g and β are the g value for the paramagnetic ion and the Bohr

magneton, respectively, r is the distance between the paramagnetic center and the observed nucleus, A is the hyperfine coupling constant between the paramagnetic electrons and the observed nucleus and τ_c and τ_e are the correlation times for the dipolar interaction and the hyperfine interaction, respectively. The latter are given by the equations[195]

$$1/\tau_c = 1/\tau_s + 1/\tau_M + 1/\tau_r \qquad (164)$$

$$1/\tau_e = 1/\tau_s + 1/\tau_M \ , \qquad (165)$$

where τ_r is the correlation time for the molecular rotational reorientation, τ_s is the electron spin-lattice relaxation time, and τ_M is the mean residence time of the nucleus in the first solvation sphere,[196] which characterizes the rate of ligand exchange.

At room temperature, for Mn^{2+} in various complexes which have been studied, the experimentally found values for the electron relaxation times τ_s are in the range 10^{-8} to 10^{-9} sec,[188-191] while the correlation time for the molecular rotational reorientation τ_r is approximately 10^{-10} to 10^{-11} sec for complexes with molecules of the size of N,N-dimethylformamide, therefore $1/\tau_s << 1/\tau_r$. Furthermore, for Mn^{2+} complexes it is observed that[187,197,198] $1/\tau_M < 1/\tau_s$ at room temperature or slightly above this temperature. Subject to these inequalities, the correlation time for the electron-^{13}C dipolar interaction τ_c

will be equal to τ_r. When one can use this effective correlation time, combined with the ratio $\omega_S/\omega_I \approx 2600$ between the Larmor frequencies ω_S and ω_I of the electron and ^{13}C nucleus, respectively, as well as the inequalities (all of which apply at the magnetic field strength used in this work, 18.7 kG for ^{13}C) $\omega_I^2\tau_r^2 << 1$, $\omega_S^2\tau_r^2 \sim 1$ and $\omega_S^2\tau_e^2 >> 1$, the Solomon-Bloembergen equations reduced to

$$1/T_{1M} = \frac{2}{15} \frac{S(S+1)\gamma_I^2 g^2 \beta^2}{r^6} \left(3\tau_r + \frac{7\tau_r}{1 + \omega_S^2\tau_r^2}\right) \qquad (166)$$

$$1/T_{2M} = \frac{1}{15} \frac{S(S+1)\gamma_I^2 g^2 \beta^2}{r^6} \left(7\tau_r + \frac{13\tau_r}{1 + \omega_S^2\tau_r^2}\right) + \frac{1}{3} \frac{S(S+1)A^2}{\hbar^2} \tau_e \, . \qquad (167)$$

We see that the scalar relaxation term contributes only to $1/T_{2M}$. This implies that the order of magnitude for the scalar coupling constant A for Mn^{++} in these complexes is not significantly larger than 10^6MHz, the same order of magnitude as found for similar couplings to protons.[175,190] The recently reported Mn^{2+} - ^{13}C coupling constants are in agreement with this assumption.[182-184] It has been shown that electron relaxation in dilute aqueous solutions of the paramagnetic ions is controlled by the modulation of the quadratic zero field splitting (ZFS) interaction. Therefore, for an aqueous Mn^{2+} complex, the correlation time for electron relaxation is given, to a good approximation,

by the equation

$$1/\tau_s = \frac{1}{25}\Delta^2(4S(S+1) - 3) \times \left(\frac{\tau_v}{1 + \omega_S^2\tau_v^2} + \frac{4\tau_v}{1 + 4\omega_S^2\tau_v^2}\right), \quad (168)$$

where Δ is the zero-field splitting parameter and τ_v is a time constant for the modulation of the ZFS interaction. For the Mn^{2+}-hexaaquo complex, where the Mn^{2+} ions are in an isotropic environment, it has been found[199] that the ZFS interaction, as well as its time modulation, results from collisions between the Mn^{2+} and the bulk solvent molecules. If the paramagnetic ions are in an asymmetric environment there will, in addition, be a static ZFS interaction. The temperature dependence of τ_v and τ_r can be approximated by the Arrhenius expression

$$\tau_i = \tau_i^o \exp(E_i/RT), \quad i = r \text{ or } v \quad (169)$$

while τ_M is usually given by the more elaborate Eyring equation

$$1/\tau_M = \frac{kT}{h} \exp\left(-\frac{\Delta H^*}{RT} + \frac{\Delta S^*}{R}\right). \quad (170)$$

B. Effects of Chemical Exchange

To observe the signal from the nuclei in the ligand, it is necessary to observe the resonance using a solution with a very low concentration of the paramagnetic ion relative to the ligand to avoid line broadening. In addition, a temperature must be selected to give a ligand exchange rate between the coordination sphere and the bulk

solution which is sufficiently fast on the NMR time scale to average the spectral features of the complex with those of the unbound ligand. Under these conditions, the following expressions[201,202] are appropriate for relating T_{1M}, T_{2M}, τ_M, ω_M, and pq to the experimental observables:

$$1/T_{1,obs} - 1/T_1^o = 1/T_{1P} = 1/T'_{1A} + \frac{pq}{T_{1M} + \tau_M} \qquad (171)$$

$$1/T_{2,obs} - 1/T_2^o = 1/T_{2P} = 1/T'_{2A} + \frac{pq}{\tau_M}\left[\frac{(1/T_{2M} + 1/\tau_M)^* 1/T_{2M} + \Delta\omega_M^2}{(1/T_{2M} + 1/\tau_M)^2 + \Delta\omega_M^2}\right] , \qquad (172)$$

where τ_M, T_{1M}, and T_{2M} have the same definitions as given previously, $\Delta\omega_M$ is the contact shift, p is the ratio of metal ions to ligand molecules and q is the number of coordinated ligands per metal ion. $1/T_1^o$ and $1/T_2^o$ are the relaxation rates of the nuclei in the free ligand while the adjusted rates $1/T_{1P}$ and $1/T_{2P}$ measure the paramagnetic contribution to the observed averaged relaxation rates $1/T_{1,obs.}$ and $1/T_{2,obs.}$. $1/T'_{1A}$ and $1/T'_{2A}$ are the contributions to the relaxation of the nuclei outside the first coordination sphere due to dipolar interaction with the paramagnetic ions. For protons[201] this contribution has been found to be less than 10% to $1/T_{1,obs}$, while it is a significantly smaller fraction of $1/T_{2,obs}$ when $1/T_{2M}$ is dominated by scalar relaxation. For ^{13}C relaxation,

these contributions are expected to be even smaller fractions of $1/T_{1,obs}$ and $1/T_{2,obs}$, and thus may be neglected. Assuming a Curie law of temperature dependence, and an isotropic g value for the system, the isotropic contact shift $\Delta\omega_M$ between the nuclei of the first coordination sphere and those of the bulk solution is given by[193,207]

$$\frac{\Delta\omega_M}{\omega_I} = \frac{\Delta H}{H} = \frac{S(S+1)g|\beta|}{3kT\gamma_I\hbar} A, \qquad (173)$$

where the symbols have their usual meanings. In case of chemical exchange, the experimental frequency shift $\Delta\omega_P$ is given by the equation [202]

$$\Delta\omega_P = \frac{pq}{\tau_M^2}\left[\frac{\Delta\omega_M}{(1/T_{2M} + 1/\tau_M)^2 + \Delta\omega_M^2}\right], \qquad (174)$$

where the symbols are the same as defined above. The experimental values of $T_{2,obs}$ were determined assuming Lorentzian line shapes and using the relationship

$$\Delta\nu_{1/2} = 1/(\pi T_2) . \qquad (175)$$

C. ^{13}C Relaxation data and isotropic contact shifts in Mn^{2+}-DMF mixtures

Each ^{13}C T_1 value was extracted from 7-10 partially relaxed Fourier transform spectra by fitting the data to the equation

$$\ln\left(\frac{M_\infty - M_t}{2M_\infty}\right) = -t/T_1 \qquad (176)$$

using the KINFIT program.[72] In this way values of $1/T_1^o$ and $1/T_{1,obs}$ were obtained for all three carbons of DMF from temperatures of about -60°C to +75°C and the results are given in Tables 7 and 35.

Due to extensive broadening of the ^{13}C signal from the C = O group, the Mn^{2+} concentration typically used was 2.77×10^{-4}M. To check the reliability of the final values of $1/T_{1P}$, the $1/T_{1P}$ values for the trans- and cis-NCH_3 carbons were measured at two concentrations at 34.5°C and the values obtained at 2.77×10^{-2}M Mn^{++} were divided by 100 for comparison with the values obtained in 2.77×10^{-4} M Mn^{++} solutions (Table 36). The agreement was within experimental error, as shown in Table 36, but the values used in later calculations were those obtained from the 2.77×10^{-4} M Mn^{++} solutions. The temperature variation of the $1/T_{1P}$ values for the carbons of the trans-NCH_3, cis-NCH_3 and C = O groups were also determined and are shown in Figures 72-74. Likewise, the temperature dependence of $1/T_{2P}$ and of $\Delta\nu_P$ for all three carbons was measured over the same temperature range and these results are given in Table 37 and Figures 75 and 76. Only the value of $1/T_{2P}$ for the C = O group is measured, since the uncertainties in the linewidth measurements of the carbons of the trans- and cis-NCH_3 groups lead to a wide variation in the values of $1/T_{2P}$ for those carbons.

Table 35. Temperature dependence of the ^{13}C spin-lattice relaxation times of the three carbons of DMF in a 2.77×10^{-4}M solution of $MnCl_2$ in N,N-dimethylformamide.[a]

T(°C)	trans-N-methyl T_1(sec)	cis-N-methyl T_1(sec)	T(°C)	C = O T_1(sec)
-59.0	1.63±0.093	2.358±0.115	-55.65	0.360±0.006
-41.95	2.855±0.149	3.642±0.086	-31.0	0.933±0.043
-29.2	3.317±0.059	4.523±0.065	-23.35	1.275±0.065
-17.9	4.013±0.081	6.242±0.178	- 9.6	2.220±0.085
11.95	7.129±0.320	10.222±0.224	5.05	2.501±0.146
35.0	9.432±0.131	13.033±0.202	20.1	3.346±0.118
54.2	11.964±0.281	15.263±0.358	35.0	6.005±0.278
70.5	16.793±0.664	17.297±0.693	50.5	7.850±0.386
			68.45	6.824±0.547
			88.3	12.222±1.16
			112.9	10.893±0.554

[a]N,N-dimethylformamide was purified and the sample degassed and sealed in the sample tube.

Table 36. Experimental ^{13}C spin-lattice relaxation rates for the carbons of DMF in N,N-dimethylformamide solutions of Mn^{++} at 34.5°C.

Substituent	$1/T_{1,obs}$ sec^{-1}	$1/T_1^o$ sec^{-1}	$1/T_{1P}$ sec^{-1}	$1/T_{1P}$ (normalized)[c] sec^{-1}
C = O [a]	0.167±0.008	0.049±0.001	0.118±0.008	0.118±0.008
NCH_3(t) [a]	0.106±0.001	0.076±0.002	0.030±0.002	0.030±0.002
NCH_3(t) [b]	2.306±0.110	0.076±0.002	2.230±0.110	0.022±0.001
NCH_3(c) [a]	0.076±0.001	0.0523±0.001	0.0237±0.001	0.024±0.001
NCH_3(c) [b]	2.508±0.150	0.052±0.001	2.455±0.150	0.0246±0.002

[a] $[Mn^{2+}] = 2.77 \times 10^{-4}$ M.

[b] $[Mn^{2+}] = 2.77 \times 10^{-2}$ M.

[c] Data normalized to $[Mn^{2+}] = 2.77 \times 10^{-4}$ M by dividing the values of $1/T_{1P}$ for the 2.77×10^{-2} M Mn^{++} solutions by 100.

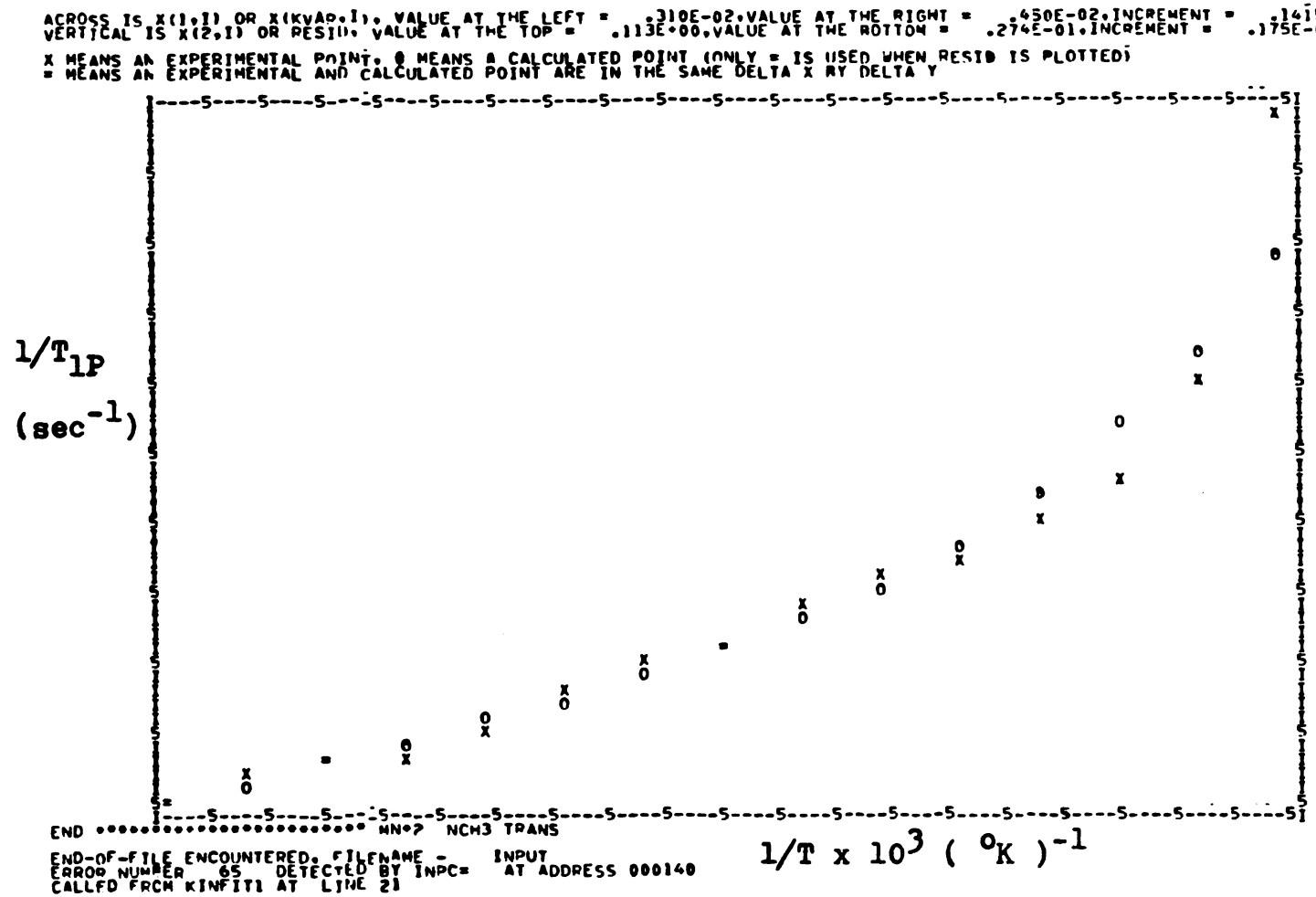

Figure 72. Computer fit of the temperature variation of the experimental relaxation rate T_{1P}^{-1} for the carbon of the <u>trans</u>-NCH_3 group in N,N-dimethylformamide. The solution was 2.77 x 10^{-4} M $MnCl_2$ in DMF.

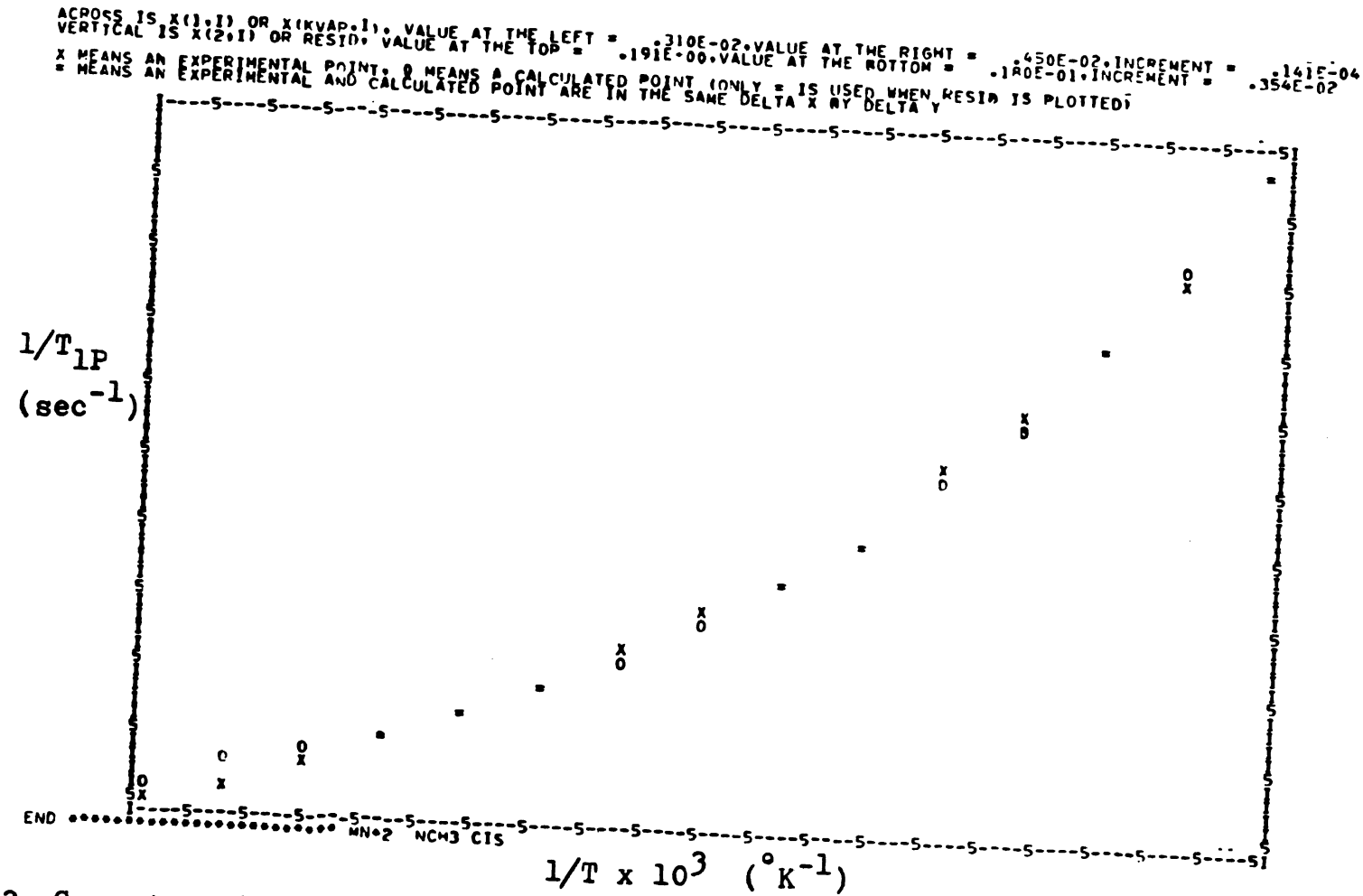

Figure 73. Computer fit of the temperature variation of the experimental relaxation rate $1/T_{1P}$ for the carbon of the <u>cis</u>-NCH_3 group in N,N-dimethylformamide. The solution was 2.77×10^{-4} M $MnCl_2$ in DMF.

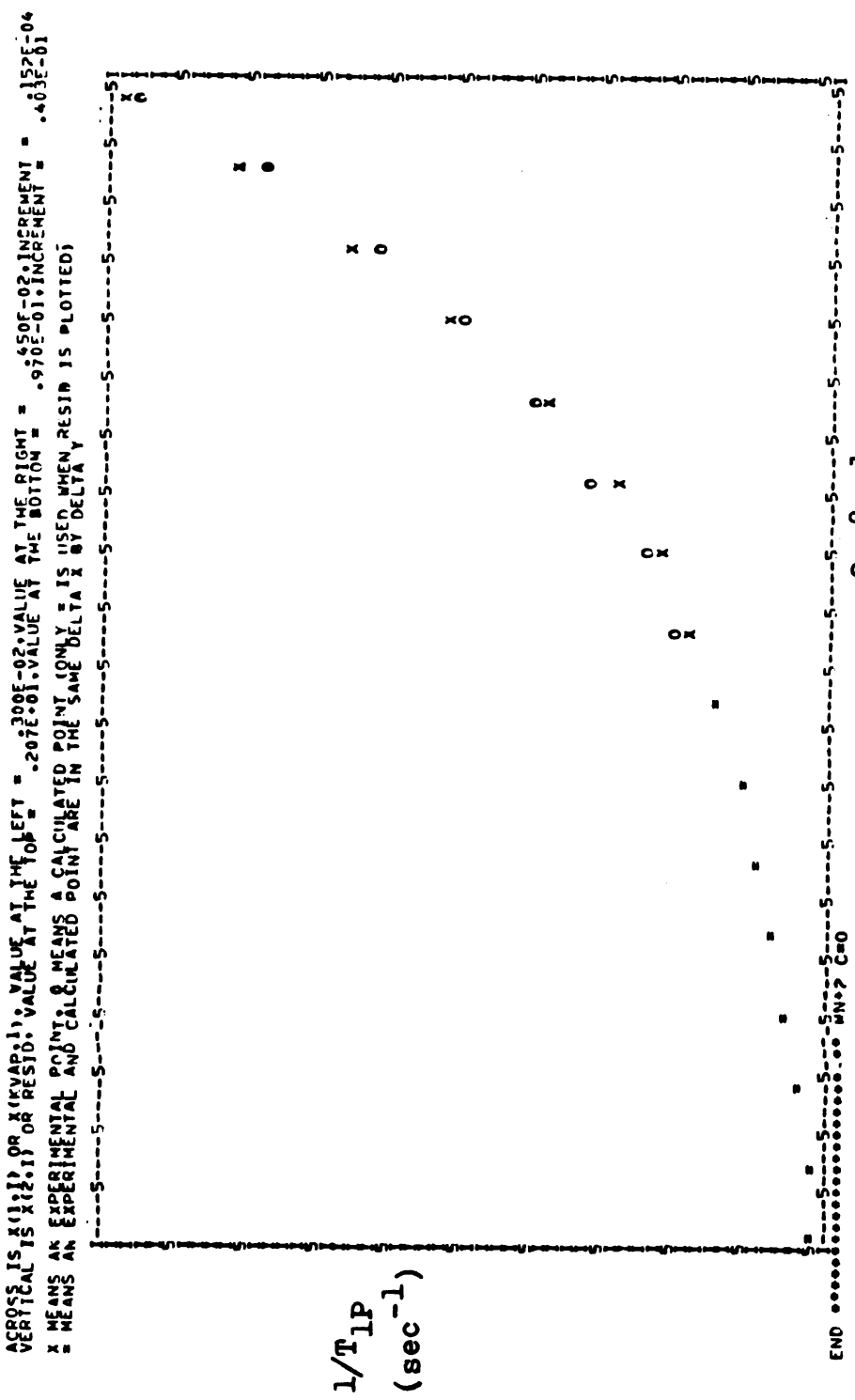

Figure 74. Computer fit of the temperature variation of the experimental relaxation rate T_{1P}^{-1} for the carbon of the carbonyl group in N,N-dimethylformamide. The solution was 2.77 x 10^{-4} M $MnCl_2$ in DMF.

Table 37. Temperature dependence of $\Delta\nu_P$ and $1/T_{2P}$ for the three carbons of DMF in a solution of $MnCl_2$ in N,N-dimethylformamide which is 2.77×10^{-4}M in Mn^{2+}.

T (°C)	$\Delta\nu_P$ (Hz)			T (°C)	$1/T_{2P}$
	$N\underline{C}H_3(t)$[a]	$N\underline{C}H_3(c)$[a]	$\underline{C}=O$		$\underline{C}=O$ (sec^{-1})
-56.0	0.1	0.1	0.1	-54.5	7.838
-46.1	0.1	0.2	0.3	-39.6	22.422
-35.3	0.2	0.3	1.9	-20.8	30.63
-17.0	0.1	0.0	1.8	2.7	19.635
2.2	0.3	0.1	1.0	18.0	16.808
12.5	-0.1	0.0	1.5	34.2	6.519
23.4	-0.2	-0.1	0.8	51.2	5.765
36.3	0.3	0.0	0.8	58.0	4.000
44.6	-0.1	-0.2	-	65.5	2.199
57.1	0.1	0.2	1.0		
72.3	0.0	0.0	0.9		
89.5	0.1	0.2	0.7		

[a] t and c Indicate groups that are <u>trans</u> or <u>cis</u> relative to the C = O group.

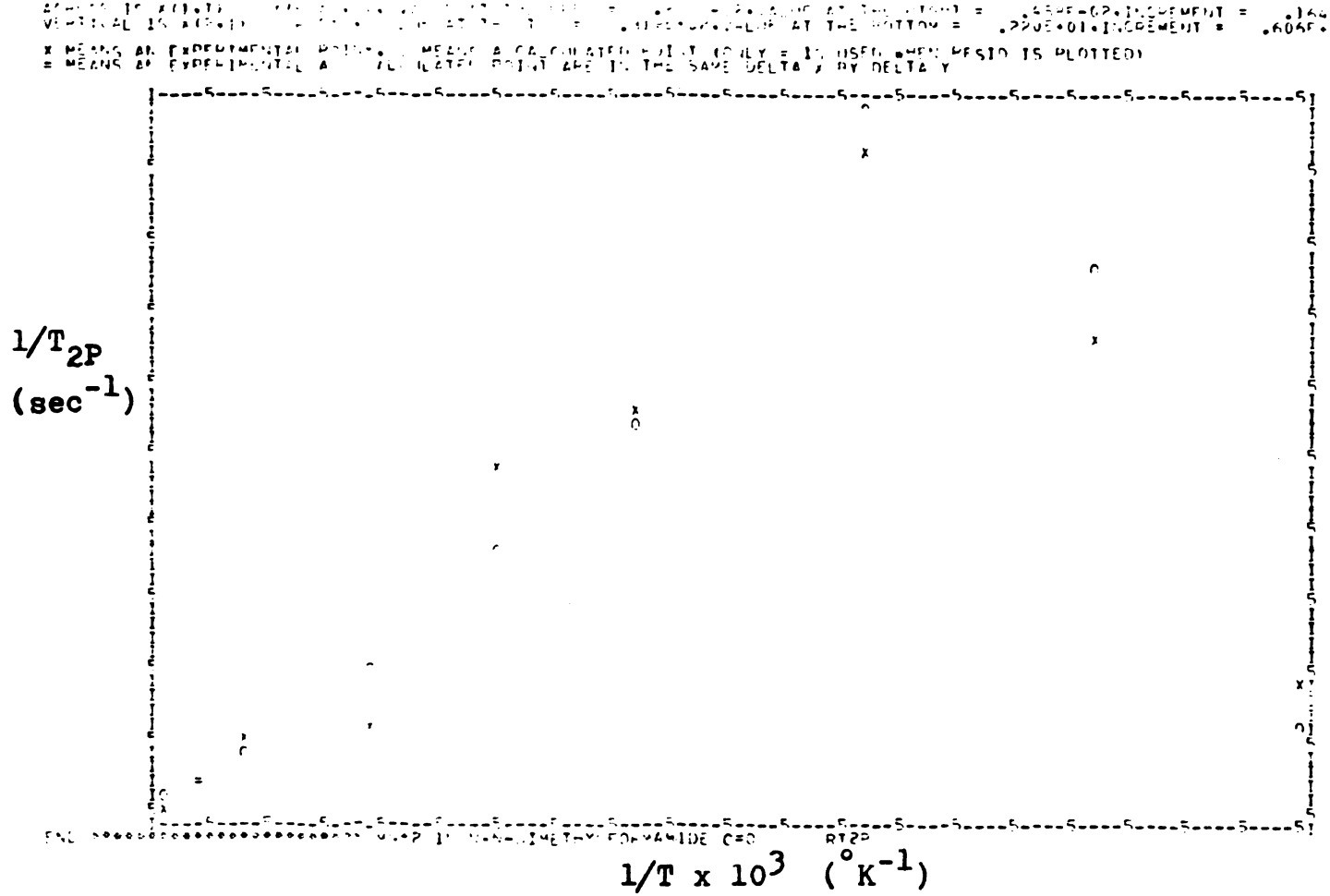

Figure 75. Computer fit of the temperature variation of the experimental relaxation rate T_{2P}^{-1} for the carbonyl carbon in N,N-dimethylformamide. The solution was 2.77×10^{-4} M $MnCl_2$ in DMF.

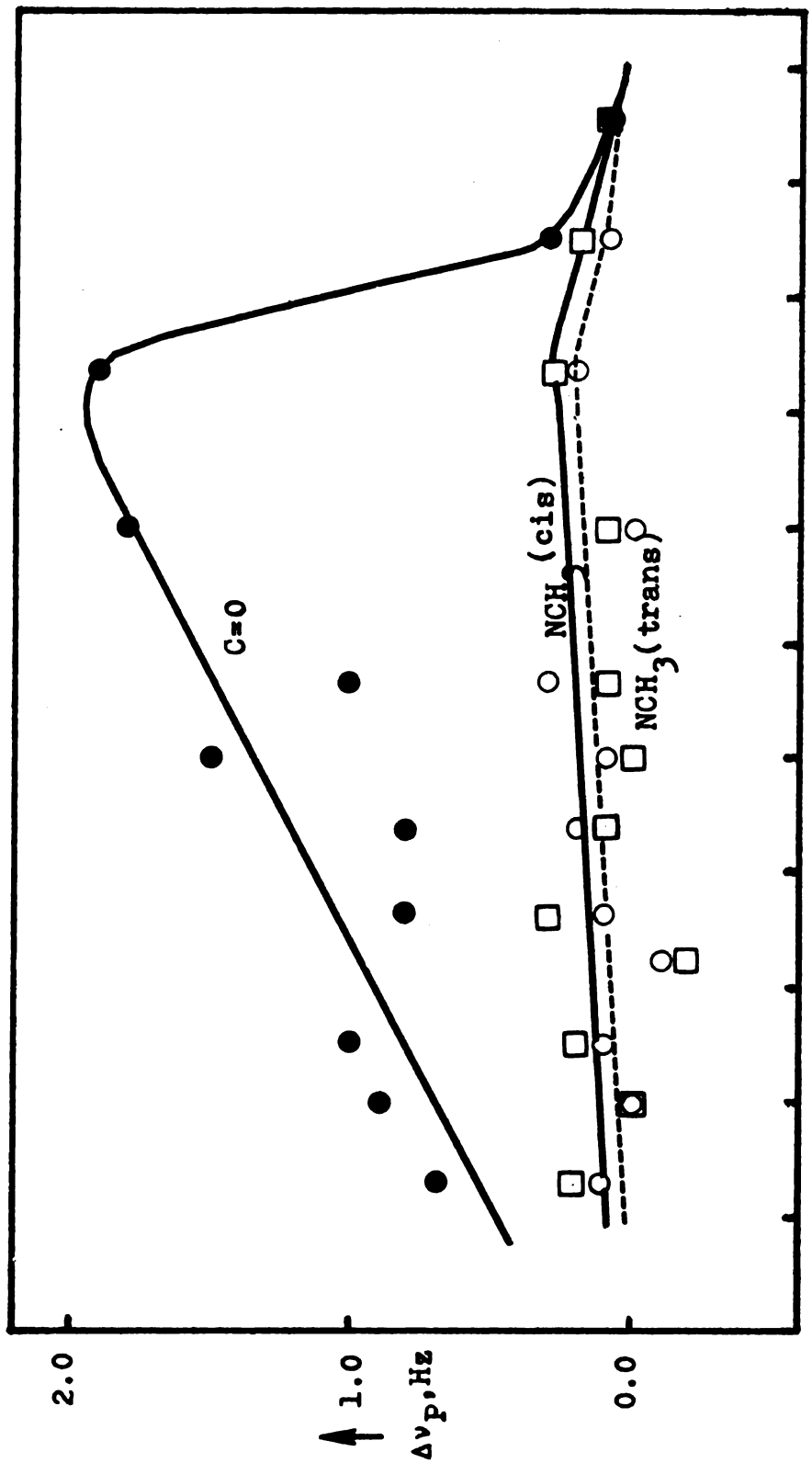

Figure 76. Temperature variation of the experimental contact shifts, $\Delta\nu_p$, of the carbons of N,N-dimethylformamide in a solution 2.77 x 10^{-4} M in Mn^{2+}.

D. The Dominant Mechanisms of Relaxation

To establish the relative importance of the different mechanisms discussed in Section A (above) which can influence the relaxation of the ^{13}C nuclei in the primary solvation sphere, a best fit of the $1/T_{1P}$, $1/T_{2P}$ and $\Delta\nu_P$ data to Equations (164)-(174) was made by use of the KINFIT program. The results are shown in Figures 72-75. The dipolar mechanism (Equation (166)) is dominant for $1/T_{1M}$ but both dipolar and scalar mechanism contribute to $1/T_{2M}$ (Equation (167)). The procedure used here depends on the reasonable assumption that in the exchange process the N,N-dimethylformamide molecules exchange as a whole in and out of the first coordination sphere of the Mn^{2+} ions and the assumption is strongly supported by the good agreement between calculated and observed curves in Figure 76.

II. RESULTS AND DISCUSSION

A. Determination of the Coordination Number, E_r, τ_r^o and the Structure of the Solvation Complex

The coordination number was determined by varying the value of q from 4 to 12, and it was found that when q was equal to eight, the best fit of the calculated curves to the experimental data for all three carbons could be obtained and that the number of iterations for the calculation to converge was less than fifteen. However, with other choices of coordination number, the fit of the experimental data for all three carbons only converged after 60 iterations,

and the deviation of the experimental data from the best fit curve was usually much greater than that obtained using coordination number eight. Thus, an assumed coordination number eight was accepted for later calculations.

From the parameters obtained by the fitting of the T_{1P}^{-1} data to the calculated curves for all three carbons, values of E_r and τ_r^o were calculated and the effective distances between Mn^{2+} and all three carbons obtained. These are shown in Table 38. The calculated E_r values for the carbons of the trans- and cis-NCH_3 groups are lower than that for the C = 0 group as a result of the internal rotation of the N-methyl groups. The E_r value for the C = O group (4.0 kcal/mole) is about the same as that for free DMF determined before (4.1 kcal/mole), since the overall molecular tumbling axis of DMF in Mn^{2+} solution is still apparently along the $Mn^{2+}...O = C$ direction which includes the carbon of the trans-N-CH_3 group. However, the τ_r value at 308°K for the DMF-Mn^{++} system is one order of magnitude larger than τ_r (= τ_c) for free DMF, since the solvation effect, which reduces the frequency factor, makes it more difficult for a DMF molecule to rotate in the Mn^{2+}-DMF system. The calculated r values for all three carbons are also shown in Table 38. They indicate that the distance between Mn^{+2} and the trans-NCH_3 carbon is shorter than that between Mn^{2+} and the carbon of the C = O group. To explain this result, the structure shown in Figure 77 for the solvation complex of Mn^{2+} in DMF is suggested.

Table 38. Parameters calculated from the experimental relaxation and contact shift data for Mn^{++} in DMF.

Parameter	Value	Parameter	Value
(A/h) [C = O], Hz	6.61×10^5	E_r (C = O), kcal/mol	4.00±0.09
(A/h) [NCH_3(c)],[a] Hz	$\approx 6.0 \times 10^4$	E_r(NCH_3,c), kcal/mol	2.90±0.12
(A/h) [NCH_3(t)],[a] Hz	$\approx 4.0 \times 10^4$	E_r(NCH_3,t), kcal/mol	3.11±0.12
r (C = O), A	3.82±0.30	ΔH^*, kcal/mol	12.67±0.60
r (NCH_3,c), A	6.20±0.50	ΔS^*, eu	20.97±2.00
r (NCH_3,t), A	3.44±0.04	τ_M(298°K), sec	8.20×10^{-9}
τ_r^o (C = O), sec	0.80×10^{-13}	Δ, G	≈ 800[b]
τ_r^o (NCH_3,c), sec	0.34×10^{-13}	τ_v^o, sec	$\approx 10^{-7}$
τ_r^o (NCH_3,t), sec	0.14×10^{-13}	E_v, kcal/mole	3.15
pq	1.71×10^{-4}	τ_r(308°K), sec	5.49×10^{-11}

[a] c and t Indicate groups cis and trans relative to the C = 0 group (see also the text, Section II-B).

[b] See text, Section II-C.

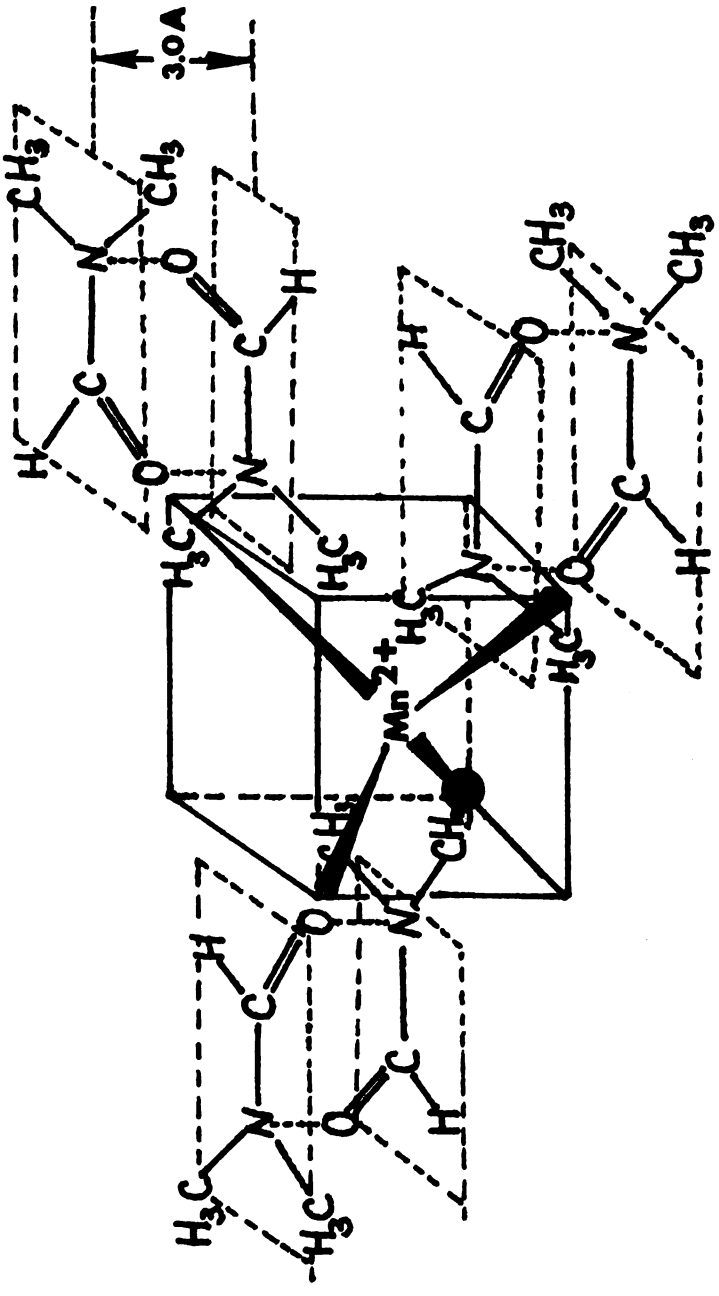

Figure 77. Structure of the solvation complex of Mn^{2+} in N,N-dimethylformamide; ● stands for a fourth dimer $(DMF)_2$ in the inner corner of the tetrahedron.

A tetrahedral structure for the ion-solvent complex is suggested, with two N,N-dimethylformamides (as a dimer, $(DMF)_2$) at each corner. From the distances found between Mn^{2+} and the trans-NCH_3 carbon and between Mn^{++} and the C = O carbon, the distance between the two DMF planes in the dimer $(DMF)_2$ may be estimated to be about 3.0 A, which is approximately equal to the sum of the van der Waals radii of oxygen (1.40A) and nitrogen (1.50A). The distance between the Mn^{2+} ion and the cis-NCH_3 carbon, 6.2 A, is also within experimental error of the value expected on the basis of the structure suggested Figure 77.

The distance between Mn^{2+} and the oxygen of the C = O group is estimated to be about 2.60 A, which is a little bit larger than the sum of the van der Waals radii of oxygen (1.40A) and Mn^{2+} (0.80A), indicating that the Mn-O "bond" is very weak. Also, this solvation complex is only stable at low temperatures (below -35°C) as seen from Figure 76. This is quite different from the case of Mn^{2+}-histidine where the ion-solvent complex is stable even at +15°C[9]. The reason that the distance between Mn^{2+} and carbonyl oxygen is so large in DMF may be that the $(DMF)_2$ dimers are rather bulky. Also, the interaction of the paramagnetic ion and the oxygen of the C = O group[181,183] may be weak as was found for Mn^{++} in pyruvate carboxylase and in histidine.

B. Determination of the Coupling Constants between Mn^{2+} and Carbon

At high temperatures, $(\tau_M)^{-2} >> (T_{2M})^{-2}$ and $(\Delta\omega_M)^{-2}$ so Equation (174) can be reduced to

$$\Delta\omega_P = pq\Delta\omega_M \qquad (177)$$

which, according to Equation (173), should follow the Curie law of temperature dependence. Figure 76 shows that the ^{13}C $\Delta\nu_P$ curves for all three carbons in DMF are given by Equation (177) over all of the experimental temperature range except at low temperatures. Using Equation (177), the coupling constants (hyperfine interaction constants) for all three carbons have been determined from the $\Delta\nu_P$ data in the high temperature range, as shown in Table 38.

All three electron-^{13}C hyperfine coupling constants, which correspond to isotropic contact shifts, tend toward lower field as the temperature increase and thus are positive. However, the temperature variations of the experimental $\Delta\nu_P$ for trans- and cis-NCH_3 carbons are of the same magnitude as the uncertainty in the measurements ($\pm$0.2Hz) so only the estimated values of A/h are presented. In the low temperature range of Figure 76 $\tau_M \sim T_{2M}$, which invalidates the approximations leading to Equation (177) and the curvatures should therefore be described by Equation (174).

Grant et al.[183] have found that the coupling constants for carbons forming π bonds are somewhat higher than those of the corresponding carbons forming only σ bonds, indicating a relatively smaller delocalization of the paramagnetic electrons. The measured electron-^{13}C coupling constant for C = O carbon is about the same order of magnitude as that in other complexes[181-183] but the A/h values for trans- and cis-NCH_3 carbons are about one order of magnitude smaller than those found for the singly bonded carbons of the Mn^{2+}-ATP complex.[182] This may be due to very weak "bonding" between Mn^{2+} and oxygen in the Mn^{2+}-DMF solvation complexes.

C. Determination of ΔH^*, ΔS^*, E_v, and τ_M

To obtain these values, a least-squares fit of the experimental $1/T_{2P}$ data to Equations (165), (167), (168), (169), (170), and (172) was made.

In order to obtain the best fit of the $1/T_{2P}$ data, a value of E_v = 3.16 kcal/mole is used, which is in the range 2.5-4.3 kcal/mole found for E_v in the case of the $Mn^{2+}(H_2O)_6$ complex.

The calculated values of ΔH^*, ΔS^*, E_v, and τ_M are shown in Table 38. The value ΔH^* = 12.67 kcal/mole obtained in this way is comparable in magnitude to the ΔH^* values of about 14 kcal/mole found for the Mn^{2+}-AMP[203] complex and about 11 kcal/mole found for the Mn^{2+}-histidine complex.[183] However, the value obtained for τ_M(298°K),

8.2×10^{-9} sec, is about two orders of magnitude smaller than that obtained in the complexes of Mn^{2+} with AMP, ATP, and histidine. This is due to the instability of the solvent complex of Mn^{2+} in pure DMF and to the very weak "bonding" between Mn^{2+} and oxygen, as reflected in the long distance between Mn^{2+} and $\underline{O}$ = C obtained in this work. The large value of ΔS^*, about 20.97 eu, is attributed to the solvation effect.

Using the parameters from the best fit of the $1/T_{2P}$ curve, the calculated values of τ_v^o and Δ are about 10^{-7} sec and 800 G, respectively, which are higher than those obtained for the Mn^{2+}-ATP, Mn^{2+}-AMP and Mn^{2+}-histidine complexes. However, the values τ_v^o and τ_M (298°K) obtained in this system are comparable to those obtained for the Mn^{2+}-RNA system,[191] 2.3×10^{-7} sec and 2.1×10^{-9} sec, respectively.

Using the values of τ_v calculated from Equation (169) and the τ_v, E_v values in Table 38 in Equation (168), it is seen that $1/\tau_s \cong 0$. Then $1/\tau_e \approx 1/\tau_M$ for Equation (165). This indicates that the ZFS factor does not make an important contribution to the scalar relaxation term.

III. CONCLUSION

This study shows the feasibility of using T_1 relaxation times of ^{13}C nuclei in the Mn^{2+}-DMF system to achieve information about the solvation structure. To a relatively high degree of accuracy, the paramagnetic

relaxation rate depends only on r^{-6} and not on the angle between the interatomic vector and a coordinate system fixed in the molecule. This makes the method simpler to employ and, therefore, more versatile than structural determination from the pseudo-contact shifts caused by lanthanide shift reagents.

This study has also shown that the contribution from the unpaired electrons of the Mn^{2+} ions to the T_2 relaxation time of the carbon of the C = O group is primarily due to a large scalar coupling term which, however, cannot be related to the structure in any simple way.

SUMMARY

A variety of nuclear magnetic resonance (NMR) techniques has been used to investigate various physical properties of a series of amides, N-substituted amides, and both symmetrically and unsymmetrically N,N-disubstituted amides. Measurements have been made of ^{13}C spin-lattice relaxation times, nuclear Overhauser enhancement (NOE) factors and chemical shifts for all the carbons in these compounds. In several cases ^{14}N, ^{15}N and ^{17}O chemical shifts and relaxation times have also been measured and several linear correlations among the various chemical shifts have been obtained. The results have been used to investigate various details of the electronic and geometrical structures of these amides, to obtain information concerning their conformations, to study their molecular motions in the liquid phase and to elucidate the nature of the complexes formed with solvent molecules or added paramagnetic ions.

PART II

THEORETICAL STUDIES OF AMIDES

INTRODUCTION

The electronic and molecular structures of amides, and particularly the barrier to internal rotation about the central C-N bond, has been the subject of numerous experimental and theoretical investigations during the past twenty years. Experimental determination of these barriers has been carried out by nuclear magnetic resonance methods, since they are at present the only techniques available for this purpose.[129-138] Theoretical estimates of the energy barriers have been made using various quantum mechanical methods.[209-211]

In this part of the thesis I report calculations of the energies of some selected amides in various conformations. The charge distributions, charge variations in going from ground state equilibrium geometry to the excited state geometry, energies for internal rotation and electron configurations will be presented. The molecules which have been studied are formamide, N,N-dimethylformamide, N,N-dimethylacetamide, N,N-dimethyltrifluoroacetamide, N-methylformamide, N-ethylformamide, N-methylacetamide, N-ethylacetamide, N-methyl-N-ethylformamide, and N-methyl-N-ethylacetamide. Calculations have been reported in the literature using extended Hückel theory (EHT) and the

complete neglect of differential overlap approximation (CNDO/2). In this work, the intermediate neglect of differential overlap approximation (INDO) has been employed and properties calculated by these different methods compared.

THEORETICAL

I. GENERAL SURVEY

The properties of amides were first discussed in terms of resonance among valence bond structures by Pauling, who suggested that in the ground state I and II would be the principal contributing resonance structures and that the resonance energy would be about 21 kcal/mole.

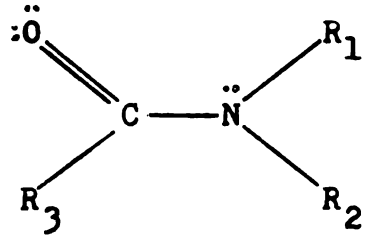

(I)

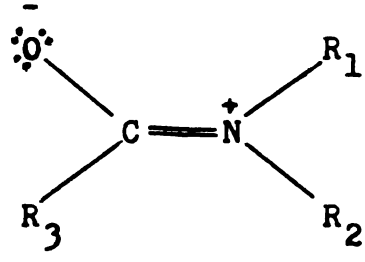

(II)

The large partial double-bond character predicted (about 50%) for the central C-N bond would then account for the short C-N distance observed, for the near coplanarity of the amide framework, and for the large barriers hindering rotation about the central C-N bond.

The development of molecular orbital (MO) theory has provided powerful methods for studying the electronic and geometrical structures of molecules and various approximate MO methods (CNDO/2, EHT, PPP, and ab initio) have been used to study the energy barriers[90] and various solvent effects[212,213] for substituted amides.

During the last decade, many different experimental methods (NMR, IR, UV, X-ray diffraction, electron diffraction and microwave spectroscopy) have been applied to the study of the molecular and electronic structures of amides. However, a theoretical approach should provide a more powerful method for looking into the variations in energy and charge distribution on going from the ground equilibrium geometry to the transition state geometry.

Formamide has been examined quite extensively by a number of theoretical methods[211,217-219] and the vibrational spectra and force constants discussed.[214-216] Some results of calculations of the electron distribution in formamide are shown in Table 39. N-Methylacetamide has also been studied[90] as the simplest model for the polypeptide chain and the data for the charge distribution in that molecule are shown in Table 40. In these studies the ground state geometry has been taken to be that in which the NCO fragment and all the atoms directly bonded to it form a plane. In the transition state, it has been assumed that the COR fragment is twisted out of this plane by 90°, the nitrogen atom and the three atoms bonded to it remaining in the original plane.

In these results,[214-219] it was found that the calculated quantities are very sensitive to variation in geometry and in the Slater orbital exponents. The results of all the CNDO/2 calculations are in reasonable agreement

Table 39. Calculated charge distributions for formamide (in electronic units)[a]

Atom	EHT[b-d]	ab initio[i,l]	ab initio[i,m]	ab initio[m,n]	CNDO/2[b-d]
O	-1.215	-0.41	-0.377	-0.429	-0.365
C	1.040	0.36	0.258	0.295	0.450
N	-0.312	-0.86	-0.758	-0.745	-0.409
H(C)	0.014	0.17	0.152	0.134	-0.039
H_1	0.236	0.37	0.368	0.383	0.188
H_2	0.237	0.37	0.357	0.362	0.174
	CNDO/2[b,e-g]	CNDO/2[e-h]	CNDO/2[b-e]	CNDO/2[f,g,i,j]	CNDO/2[f,g,j,k]
O	-0.338	-0.336	-0.373	-0.354	-0.306
C	0.358	0.356	0.441	0.348	0.367
N	-0.236	-0.237	-0.424	-0.223	-0.262
H(C)	-0.046	-0.046	-0.027	-0.044	-0.055
H_1	0.142	0.120	0.204	0.146	0.132
H_2	0.120	0.142	0.178	0.127	0.123

[a] H_1 and H_2 are the cis and trans hydrogens (relative to the C = O group).

[b] Reference 90.

[c] The exponent for the Slater orbital of H is 1.3.

[d] Reference 220. [e] Reference 221. [f] The exponent for the Slater orbital of H is 1.2.

[g] CNDO/2 population analysis. [h] Reference 221. [i] Reference 222. [j] Reference 223.

[k] Reference 224. [l] Reference 218. [m] Reference 217. [n] Reference 225.

Table 40. Calculated charge distributions in N-methylacetamide (in electronic units), a model for the peptide bond.

Atom	EHT[a,b]	CNDO/2[a,c]	CNDO/2[a,b]	Ooi. et al.[d]	Poland-Scheraga[e]	Brant et al.[f]	Schellman and Oriel[g]
C (C=O)	+1.08	+0.36	+0.47	+0.45	+0.32	+0.39	+0.43
O	-1.23	-0.36	-0.39	-0.42	-0.42	-0.39	-0.39
N	-0.32	-0.18	-0.34	-0.30	-0.20	-0.28	-0.30
H(N)	+0.24	+0.10	+0.16	+0.27	+0.20	+0.28	+0.26

[a]For N-methylacetamide, the N-methyl group is cis to the C = O group.

[b]Mulliken population analysis, reference 220.

with each other, while the charges calculated by the EHT and "ab initio" methods differ from those obtained by CNDO/2. In general, the EHT method tends to exaggerate the charge separation in polar molecules, while the charge distribution obtained in the "ab initio" method is significantly dependent on the size and quality of the basis set.

The calculated and experimental energy barriers of some amides are shown in Table 41. While the calculated results are in reasonable agreement with the experimental values, the experimental values for a given molecule show unusually wide variations as a result of the use of approximate formulas for characterizing the lineshapes of the exchange broadened signals and the use of different solvents. Comparisons with theoretical results must be made with this in mind.

II. STANDARD GEOMETRICAL MODELS

Normally, the calculations involve some attempt at energy minimization with respect to molecular geometry. However, this procedure becomes impractical as the size of the molecules under consideration increases. A set of standard geometrical models for commonly occurring structural parameters in polyatomic molecules has been established by Pople and Gordon.[221] The complete goemetry of molecules without closed rings can be defined by (a) the bondlengths for all bonds, (b) the bond angles specifying the

Table 41. Calculated energy barriers restricting rotation around the peptide bond (in kcal/mole).

Compounds	Barrier (EHT)	Barrier (CNDO/2)	Barrier (exptl)
Formamide	15.57[a] 20.66[a] 25.26[b]	20.29[b] 15.4 [c]	19.7±0.4[d] 19.2±0.4[e]
N,N-Dimethylformamide	21.13[a] 26.45[a] 25.81[b]	15.03[b]	20.5±0.2[f] 21.6±0.3[g] 19.8±0.5[k]
N,N-Dimethylacetamide	14.61[a] 18.93 20.52[b]	16.04[b]	16.85±0.41[h] 16.8[i] 19.7±0.5[k]
N,N-Dimethyl-propionamide	14.55[a] 18.63[a]		16.6±0.1[j] 18.9±0.4[k]
N,N-Dimethyl-pivaloylamide	6.68[a]		11.5[l]
N,N-Dimethyl-isobutyramide	13.36[a] 17.94[a]		16.4±0.2[m]
N-Methylformamide	25.60[b] 25.51[b]	18.05[b] 16.87[b]	19.0[n]
N-Methylacetamide	24.16[b] 21.24[b]	18.80[b] 18.89[b]	18.0[n]
Acetamide	24.01[b]	21.72[b]	16.7[o]
Benzamide		15.8[c]	

[a]Reference 125. Two different set of parameters are used.

[b]Reference 90. [c]Reference 230. [d]Reference 231. Solvent: diethylene glycol dimethyl ether. [e]Reference 231. Solvent: methyl propyl ketone. [f]Reference 160. Solvent: CCl_4. [g]Reference 125. Solvent: C_2H_6. [h]Reference 232. Solvent: CCl_4. [i]Reference 125. Solvent: cyclohexane. [j]Reference 162. Solvent: CCl_4. [k]Reference 233, neat. [l]Reference 234. Solvent: CH_2Cl_2. [m]Reference 125. Solvent: acetone. [n]Reference 235. Solvent: $C_2H_4Cl_2$. [o]Reference 242. Solvent: acetone.

stereogeometry of the neighboring atoms bonded to each atom in the molecule, and (c) the dihedral angles specifying the internal rotations about appropriate bonds.

The rule for using all these quantities is to use a notation X_n for an atom with elemental symbol X which is bonded to n neighbors, where n is the connectivity of X. For example, the carbon atoms in ethane and ethylene will be described as C4 and C3, respectively.

A. Bondlengths

There are four types of bond - single, double, triple, and aromatic (for benzene rings). The standard values used for the bondlengths of the H, C, N, O, and F atoms are shown in Table 42.

B. Bond Angles

Five types of local atomic geometry are distinguished. If the connectivity is 4, tetrahedral angles are used. For connectivity 3, the three bonds are either taken to be planar with bond angles of 120°, or pyramidal with bond angles of 109.47°. Atoms with connectivity 2 are taken as linear, or bent with a bond angle of 109.47°.

The nature of the local atomic geometry is dependent on the presence of unsaturation in a neighboring group. The rules adopted for selecting the atomic local geometry are given in Table 43.

Table 42. Standard bondlengths (in Angstrom units).

Bond	Length	Bond	Length	Bond	Length
		Single bonds			
H-H	0.74	C4-N2	1.47	C2-O2	1.36
C4-H	1.09	C4-O2	1.43	C2-F1	1.30
C3-H	1.08	C4-F1	1.36	N3-N3	1.45
C2-H	1.06	C3-C3	1.46	N3-N2	1.45
N3-H	1.01	C3-C2	1.45	N3-O2	1.36
N2-H	0.99	C3-N3	1.40[a]	N3-F1	1.36
O2-H	0.96	C3-N2	1.40	N2-N2	1.45
F1-H	0.92	C3-O2	1.36	N2-O2	1.41
C4-C4	1.54	C3-F1	1.33	N2-F1	1.36
C4-C3	1.52	C2-C2	1.38	O2-O2	1.48
C4-C2	1.46	C2-N3	1.33	O2-F1	1.42
C4-N3	1.47	C2-N2	1.33	F1-F1	1.42
		Double bonds			
C3-C3	1.34	C2-C2	1.28	N2-N2	1.25
C3-C2	1.31	C2-N2	1.32	N2-O1	1.22
C3-N2	1.32	C2-O1	1.16	O1-O1	1.21
C3-O1	1.22	N3-O1	1.24[b]		
Triple bonds				Aromatic bonds	
C2-C2	1.20			C3-C3	1.40
C2-N1	1.16			C2-N2	1.34
N1-N1	1.10			N2-N2	1.35

[a] 1.32 A used in the N - C = O group.

[b] Partial double bonds in the NO_2 and NO_3 groups.

Table 43. Standard atomic geometries and bond angles.

Atom	Total excess valence of neighbors[a]	Examples	Geometry	Bond angle (degrees)
C4	All values	CH_4	Tetrahedral	109.47
C3	All values	C_2H_4	Planar	120
C2	0,1	CH_2, CHO	Bent	109.47
	2,3,4	CO_2, HCN	Linear	180
N4	All values	NH_4^+	Tetrahedral	109.47
N3	0	NH_3	Pyramidal	109.47
	1,2,3,4	H_2N-CHO	Planar	120
N2	0,1,2	H_2CHN	Bent	109.47
	3,4	HNC	Linear	180
O3	0	H_3O^+	Pyramidal	109.47
	1,2,3,4		Planar	120
O2	All values	O_3, H_2O	Bent	109.47

[a]The excess valence is the normal valence minus the connectivity.

C. Dihedral Angles

In open chain molecules, dihedral angles have to be specified for each bond joining atoms with connectivity greater than 1. Values of 0°, 60°, and 180° will be used for the cis, gauche, and trans arrangements.

Rules used for dihedral angles are as follows: (a) Staggered configurations are used for bonds connecting atoms with tetrahedral angles, (b) For bonds between tetrahedral and trigonal atoms, as in propene, one of the other bonds on the tetrahedral atom is taken to be in the trigonal plane, the single bond being trans where appropriate, and (3) Neighboring trigonal atoms are taken to be coplanar.

With these conventions, we have calculated the coordinates for each of the atoms in the amides, which is a necessary starting point for the INDO calculations.

The program used to extract the cartesian coordinates from the bond lengths and bond angles (MBLD) was written by Waller[246] while the INDO program was written by Harrison[247].

THEORETICAL

I. MOLECULAR ORBITAL THEORIES

A. Roothaan Self-Consistent Field Procedure

The Hartree-Fock equation is an integro-differential equation in the three spatial coordinates of a single electron. When dealing with an isolated atom it is possible to separate this equation into equations in r, θ, and ϕ. The ϕ, θ equations are the same as those in the hydrogen atom problem; the r equation is quite different. As a consequence, the Hartree-Fock orbitals for atoms are described by the same n, l, m quantum numbers as were used in the hydrogen atom solution. In the early years of quantum mechanics the Hartrees, father and son, determined orbitals for many of the atoms in the periodic table.

In molecules there is no spherical symmetry and the electrons are attracted to more than one nucleus. Except for diatomic molecules, for which elliptical coordinates may be used, it is not practical to try to solve the Hartree-Fock differential equation directly. A better procedure was invented by Roothaan and is known as the Roothaan linear combination of basis orbitals, self-consistent field, molecular method (LCBO-SCF method).

The Roothaan procedure starts by writing the molecular orbitals (or atomic orbitals if the procedure is applied to an atom) as linear combinations of basis orbitals,

$$\phi_i(k) = \sum_{\mu=1}^{M} X_\mu(k)\ C_{\mu i}\ ,$$

where X_μ are judiciously selected basis orbitals and the $C_{\mu i}$ are to be determined. Hydrogen-like orbitals centered on the various nuclei are commonly used. If the LCBO expansion for the ϕ_i are substituted into the Slater determinant and the $C_{\mu i}$ varied to minimize the energy, it is found that the $C_{\mu i}$ are solutions of a series of equations called secular equations:

$$(F_{11}-E_iS_{11})C_{1i} + (F_{12}-E_iS_{12})C_{2i} +\ldots+ (F_{1M}-E_iS_{1m})C_{mi} = 0$$

$$(F_{21}-E_iS_{21})C_{1i} + (F_{22}-E_iS_{22})C_{2i} +\ldots+ (F_{2M}-E_iS_{2M})C_{mi} = 0$$

$$\vdots$$

$$(F_{M1}-E_iS_{M1})C_{1i} + (F_{M2}-E_iS_{M2})C_{2i} +\ldots+ (F_{MM}-E_iS_{MM})C_{Mi} = 0.$$

In this set of M equations with M unknowns,

$$S_{\mu\nu} = \int X_\mu^* X_\nu\ d\underline{r}$$

$$F_{\mu\nu} = h_{\mu\nu} + \sum_{\alpha=1}^{M}\sum_{\beta=1}^{M} P_{\alpha\beta}[2(\mu\alpha|\nu\beta) - (\mu\alpha|\beta\nu).]$$

$$h_{\mu\nu} = \int X_\mu(-\frac{\nabla^2}{2} - \frac{Z}{r})X_\nu\ d\underline{r}$$

$$P_{\alpha\beta} = 2 \sum_{i=1}^{N/2} C^{*}_{\alpha i} C_{\beta i}$$

$$(\mu\alpha|\nu\beta) = \int\int X_{\mu}(1)X_{\alpha}(2) \frac{1}{r_{12}} X_{\nu}(1)X_{\beta}(2) \, d\underline{r}_1 \, d\underline{r}_2 \, .$$

Once the set of different X_{μ} is selected, the integrals $S_{\mu\nu}$, $h_{\mu\nu}$, and $(\mu\alpha|\nu\beta)$ may be evaluated for all possible combinations of the basis orbitals. It is then possible to assume a set of $C_{\mu i}$ and compute $F_{\mu\nu}$. The secular equations are linear and homogeneous in the $C_{\mu i}$. This means that only ratios of the $C_{\mu i}$ to one of their number may be determined, and it requires that for a non-trivial solution to exist the secular determinant must vanish, or

$$\begin{vmatrix} (F_{11}-E_iS_{11}) & (F_{12}-E_iS_{12}) & \cdots & (F_{1M}-E_iS_{1M}) \\ (F_{21}-E_iS_{21}) & (F_{22}-E_iS_{22}) & \cdots & (F_{2M}-E_iS_{2M}) \\ & & & \\ (F_{M1}-E_iS_{M1}) & (F_{M2}-E_iS_{M2}) & \cdots & (F_{MM}-E_iS_{MM}) \end{vmatrix} = 0.$$

After expansion, this equation is a polynomial of degree M in the E_i. The M roots of the equation are the orbital energies of the M functions which approximate the Hartree-Fock orbitals. Each of the M orbital energies is then put back into the secular equations for determination of the ratios of the $C_{\mu i}$ which correspond to the particular E_i. The solutions are completed by normalizing the ϕ_i. Note that to determine the $F_{\mu\nu}$, it is necessary to know $C_{\mu i}$, which are the desired solution, and an iterative procedure is required. The Roothaan SCF procedure may be summarized

as follows:

(1) Select a set of M basis orbitals X_μ, calculate $h_{\mu\nu}$, $(\mu\alpha|\nu\beta)$, and $S_{\mu\nu}$.

(2) Choose a set of $C_{\mu i}$ for $\mu = 1$ to M, $i = 1$ to N/2, compute the $F_{\mu\nu}$.

(3) Find the roots E_i of the secular determinant and solve the secular equations for the $C_{\mu i}$.

(4) Compare the $C_{\mu i}$ from step (3) with those assumed in step (2). If the agreement is within the desired tolerance, stop. Otherwise use the new set of $C_{\mu i}$ and go back to step (2).

The procedure is iterated to self-consistency, after which the Roothaan-SCF energy may be computed by means of the equation:

$$E_{SCF} = 2 \sum_{i=1}^{N/2} E_i - \sum_{\mu}^{M} \sum_{\nu}^{M} \sum_{\alpha}^{M} \sum_{\beta}^{M} P_{\alpha\beta}[2(\mu\alpha|\nu\beta) - (\mu\alpha|\beta\nu)].$$

As $M \to \infty$, the Roothaan-SCF energy approaches the Hartree-Fock energy provided that the X_μ have been chosen to be independent functions.

The functions most commonly used for X_μ are

$$X(r,\theta,\phi) = f(r)\ Y_{lm}(\theta,\phi),$$

in which Y_{lm} are the usual spherical harmonics. Three types of functions are used for f(r):

(1) <u>Slater-type orbitals (STO's)</u>

$$f(r) = A_n\ r^{n-1}\ e^{-\zeta r},$$

where

$$A_n = \frac{(2)^{2N^*+1}}{(2N^*)!}, \quad \zeta = \frac{Z - S}{N^*},$$

$$N(N^*) = 1(1),\ 2(2),\ 3(3),\ 4(3.7),\ 5(4.0),\ 6(4.2).$$

The numerator Z - S may be considered as an effective nuclear charge, with S being a measure of the shielding effect of other electrons. It is determined by dividing electrons into the shells (1s), (2s,2p), (3s,3p), (3d), (4s,4p), (4d,4f), (5s,5p), (5d), each having a different shielding constant S. The shells are considered to be arranged from inside out in order named and the total value of S is built up from the following contributions:

(a) Nothing from any shell outside the one considered.

(b) 0.35 from each other electron in the same shell (except for 1s, where 0.30 is used instead).

(c) If the shell is an s, p shell, 0.85 from each electron with principal quantum number less by one, and an additional 1.00 for each electron further in.

(d) If the shell is d or f, 1.00 from each electron inside it.

(2) Gaussian-type orbitals (GTO's)

$$f(r) = A_k r^k e^{-\zeta r^2}.$$

The orbital exponents ζ in the STO's and GTO's are selected by trial calculations. The value of ζ for a given STO will not be the same as the ζ for the corresponding GTO. The

n and k in the orbital expressions are integers and the A's are normalization constants.

For atoms and diatomic molecules STO's are usually preferred because fewer STO's than GTO's are required to represent Hartree-Fock orbitals accurately. Since the number of $(\mu\alpha|\nu\beta)$ integrals that must be evaluated increases with M^4 (M = the number of basis functions), it is desirable to keep M as small as possible. For molecules with three or more centers, however, the calculation of the $(\mu\alpha|\nu\beta)$ integrals with basis orbitals centered on three or more nuclei becomes very tedious. On the other hand, these same integrals are easy to compute for GTO's. Thus, for larger molecules the choice between STO's and GTO's is essentially a choice between lengthy computation of a smaller number of integrals and quick computation of a larger number of integrals. Different choices have been made by different investigators.

(3) Gaussian-lobe functions

These are combinations of s-type GTO's located in space in such a way as to simulate s, p, d, etc. symmetry. For example, two spherically symmetrical GTO's centered on the Z axis at equal distance above and below a nucleus simulate a p_z orbital.

B. Approximate Molecular Orbital Theories

The application of the Roothaan-SCF method for calculating approximate ground state eigenfunctions and

eigenvalues for molecules has been hindered by two serious problems: (a) For a basis set consisting of M functions, the number of integrals of the type $(\mu\alpha|\nu\beta)$ which must be calculated increases with M^4. Doubling the size of the basis set increases the number of integrals by a factor of 16. (b) The $(\mu\alpha|\nu\beta)$ integrals are difficult to compute when the functions X_α, X_β, X_μ, and X_ν are centered on more than two nuclei. As a consequence of these computational difficulties, a number of approximate molecular orbital theories have been developed.[89,243,244]

Here, only a brief description of some of the approximate molecular orbital methods will be presented. Before describing the approximate methods, it is worth listing the kinds of approximations that have been employed and then writing down some criteria for approximate methods. The kinds of approximations that have been introduced include:

(a) Simplifications of the model. An example would be a calculation which treated only the valence electrons, or only the π electrons, by replacing the nuclei with nuclei surrounded by a spherical core of electrons.

(b) Simplifications of the Hamiltonian. An example would be replacement of the two electron terms $\sum_{i<j}\sum r_{ij}^{-1}$ with effective one-electron terms $\sum_i V(\underline{r}_i)$.

(c) Simplification of the calculations. An example would be the assumption that $(\mu\nu|\alpha\beta) = (\mu\nu|\mu\nu)\delta_{\mu\alpha}\delta_{\nu\beta}$. This

assumption, that many of the integrals are zero, eliminates all the difficult three- and four-center integrals and also reduces the number of electrons from M^4 to M^2.

(d) Replacement of integrals with empirical estimates. This assumption is at the heart of so-called "semi-empirical" theories. An example is the use of certain ionization potentials for some of the integrals.

Criteria for judging the value of the approximate methods are:

(a) The method should be simple enough to permit application to moderately large molecules without excessive computations.

(b) The approximations employed should not appreciably distort the physical features of the molecules.

(c) No preconceived ideas should be built into approximations; the calculations should be as unbiased as possible.

(d) The quantitative results should be useful for supporting, rejecting or suggesting hypotheses.

With this introduction, several approximate methods will be discussed.

1. Hückel Theory

This was a very early approximate molecular orbital method which assumes that the π electrons of a planar conjugated molecule may be described by an effective one-electron Hamiltonian

$$\hat{H} = \sum_k \hat{h}_{eff}(k), \quad \text{with} \quad \hat{h}_{eff}(k) = -\frac{\nabla_k^2}{2} + V(k),$$

where V(k) is the effective potential for the k^{th} electron. For a one-electron Hamiltonian, the assumption of a simple Hartree product for the wavefunction leads to the same energy as the antisymmetrized Hartree product. Therefore, we assume $\psi = \hat{A}\phi$ with $\hat{A} = \sum_{\hat{P}} (-1)^p \hat{P}$ ($\hat{P}$ is a permutation operator), where ϕ is a Hartree product which includes space orbitals ϕ_i, p is the order of the permutation and A is an asymmetric operator. These are linear expansions of p_z orbitals, one per atom, centered on the atoms in the π-electron system. Thus,

$$\phi_i = \sum_\mu X_\mu C_{\mu i} ,$$

where X_μ is a p_z orbital centered on atom μ. For this case,

$$E = \frac{\int \psi^* \hat{H} \psi d\underline{r}_1 \ldots d\underline{r}_N}{\int \psi^* \psi d\underline{r}_1 \ldots d\underline{r}_N} = \varepsilon_1 + \varepsilon_2 + \ldots + \varepsilon_N ,$$

where

$$\varepsilon_i = \frac{\int \phi_i^* \hat{h}_{eff} \phi_i d\underline{r}}{\int \phi_i \phi_i d\underline{r}} .$$

If X_μ and the $C_{\ i}$ are real, then

$$\varepsilon_i = \frac{\sum_\mu \sum_\nu C_{\mu i} C_{\nu i} h_{\mu\nu}}{\sum_\mu \sum_\nu C_{\mu i} C_{\nu i} S_{\mu\nu}} ,$$

where $h_{\mu\nu} = \int X_\mu \hat{h} X_\nu d\underline{r}$ and $S_{\mu\nu} = \int X_\mu X_\nu d\underline{r}$. To minimize the energy E, the energies ε_i of the occupied orbitals are minimized. This is accomplished by setting $\partial\varepsilon_i/\partial C_{\mu i} = 0$ for all μ and i, which leads to the secular equations

$$\sum_\nu (h_{\mu\nu} - \varepsilon_i S_{\mu\nu}) C_{\nu i} = 0,$$

one set for each ε_i. The ε_i are the roots of the secular determinant

$$|h_{\mu\nu} - \varepsilon S_{\mu\nu}| = 0 .$$

The Hückel method, as originally stated, also includes the approximations that $S_{\mu\nu} = \delta_{\mu\nu}$, that all $h_{\mu\mu} = \alpha_\mu$ (with one α_μ per atom) and that $h_{\mu\nu} = \beta_{\mu\nu}$ if atoms μ and ν are bonded neighbors, or $\beta_{\mu\nu} = 0$ otherwise. Hückel molecular orbitals have been calculated for an extremely large number of π-electron system.[245] The results have been correlated with many physical properties including spectra, overall stability, reactivity at various sites, and even carcinogenicity. However, the theory has many defects, the most glaring of which are:

(a) The use of the same α for each atom and the same β for each bond, which is unrealistic.

(b) The difficulty in choosing α's and β's for a π system which includes heteroatoms.

(c) The elimination of β's for non-bonded atoms eliminates the dependence of the energy on certain aspects of the

geometry. For example, cis- and trans-butadiene are predicted to have the same π-electron energy.

(d) The use of a one-electron Hamiltonian eliminates the energy difference between singlet and triplet states even though such differences are known to be large.

In spite of these difficulties, Hückel theory has played an important role in organic chemistry for many years and, more recently, also in inorganic chemistry.

2. Extended Hückel Theory (EHT)

The use of a one-electron Hamiltonian, as implied in the Hückel theory for π-electron systems, was extended to include the σ electrons by R. Hoffmann.[236] The extension involved making the following changes:

(a) Inclusion of s orbitals on C, N, O, and H.

(b) Direct calculation of the $S_{\mu\nu}$ integrals with the assumption of Slater-type orbitals.

(c) Approximation of $h_{\mu\nu}$ integrals by the negative of the ionization potentials of the atoms in the appropriate valence states.

(d) Approximation of the $h_{\mu\nu}$ integrals as

$$h_{\mu\nu} = K \frac{h_{\mu\mu} + h_{\nu\nu}}{2} S_{\mu\nu},$$

where K, called the Wolfsberg-Helmholz parameter, is taken to have a value between 1 and 3. The extended Hückel theory has had much wider application, and the results have found considerably wider acceptance, than the original Hückel theory.

3. Zero Differential Overlap Theories (ZDO)

The fundamental idea in ZDO theories is to set to zero any integrals of the type

$$\int f(\underline{r}_i)\, X_\mu(\underline{r}_i)\, X_\nu(\underline{r}_i)\, d\underline{r}_i \ ,$$

where X_μ and X_ν are different basis orbitals (i.e., $\mu \neq \nu$) and $f(\underline{r}_i)$ is any function of the position of electron i. Thus,

$$S_{\mu\nu} = \int X_\mu(\underline{r}_i) X_\nu(\underline{r}_i) d\underline{r}_i = 0 \quad \text{if } \mu \neq \nu$$

$$(\mu\alpha|\nu\beta) = \int X_\mu(1) X_\alpha(2) \frac{1}{r_{12}} X_\nu(1) X_\beta(2) d\underline{r}_1 d\underline{r}_2$$

$$= (\mu\alpha|\mu\alpha)\delta_{\mu\nu}\delta_{\alpha\beta} \ ,$$

where $\delta_{\mu\nu}$ and $\delta_{\alpha\beta}$ are Kronecker deltas, i.e., $\delta_{\mu\nu} = 0$ if $\mu \neq \nu$ and $\delta_{\mu\nu} = 1$ if $\mu = \nu$. In ZDO theories the integral

$$h_{\mu\nu} = \int X_\nu(1)\, \hat{h}(1)\, X_\nu(1)\, d\underline{r}_1$$

is not set equal to zero even if $\mu \neq \nu$ because it has been found that these integrals contain much of the information about the molecular bonding.

Application of ZDO to Roothaan theory for a closed shell system leads to the equation

$$F_{\mu\nu} = h_{\mu\nu} - \sum_\alpha \sum_\beta P_{\alpha\beta}\left[(\mu\alpha|\mu\alpha)\delta_{\alpha\beta}\delta_{\mu\nu} - \frac{1}{2}(\mu\alpha|\mu\alpha)\delta_{\mu\beta}\delta_{\alpha\nu}\right]$$

which, for $\mu = \nu$, becomes

$$F_{\mu\mu} = h_{\mu\mu} + \sum_\alpha P_{\mu\mu}(\mu\alpha|\mu\alpha) - \frac{1}{2} P_{\mu\mu}(\mu\mu|\mu\mu)$$

and for $\mu \neq \nu$, becomes

$$F_{\mu\nu} = h_{\mu\nu} - \frac{1}{2} P_{\mu\nu}(\mu\nu|\mu\nu).$$

It should be apparent that application of ZDO to Roothaan theory both greatly reduces the number of integrals that must be calculated and completely eliminates all integrals in which the basis orbitals are on more than two atoms. As a result of the ambiguity in obtaining the molecular orbitals that results from the fact that a determinantal wavefunction is unchanged if the orbitals are subjected to a linear transformation, the application of ZDO to molecular orbital calculations is more complex than appears at first sight. There are three common types of linear transformations that must be considered:

1. The mixing of equivalent orbitals (i.e., p_x and p_y) on the same atom that occurs whenever the coordinate system on an atom is rotated.
2. The mixing of orbitals on an atom that occurs when orbitals are hybridized.
3. The mixing of orbitals that occurs when orbitals are symmetry adapted.

Most ZDO theories are designed such that no important changes take place when linear transformations of types 1 and 2 occur.

4. Complete Neglect of Differential Overlap Approximation (CNDO)

This is one example of the application of ZDO theories. The following assumptions are made: (1) Only

valence electrons are treated, and (2) All of the integrals $(\mu\nu|\mu\nu)$ are set equal to γ_{AB} for any X_μ on atom A and any X_ν on atom B. This is done to retain invariance of the results to rotation about various axes. With this approximation,

$$F_{\mu\mu} = h_{\mu\mu} - \frac{1}{2} P_{\mu\mu}\gamma_{AA} + \sum_B P_{BB}\gamma_{AB}$$

for any X_μ on atom A. The sum over B is a sum over all the atoms (including A). Also, $P_{BB} = \sum_\mu P_{\mu\mu}$, where the sum extends over all X_μ on atom B. Ordinarily,

$$\hat{h}(1) = -\frac{\nabla_1^2}{2} - \sum_A \frac{Z_A}{r_{A1}} ;$$

however, in CNDO theory valence electrons are treated, so that

$$h(1) = -\frac{\nabla_1^2}{2} - \sum_B V_B ,$$

where $-V_B$ is an effective potential at atom B. Then we may write, for X_μ on atom A,

$$h_{\mu\mu} = U_{\mu\mu} - \sum_{B\neq A} V^B_{\mu\mu} ,$$

where $U^B_{\mu\mu} = \int X_\mu [-\frac{\nabla^2}{2} - V_A] X_\mu d\underline{r}$

and $V^B_{\mu\mu} = \int X_\mu V_B X_\mu d\underline{r}$ for X_μ on A. Now, the $F_{\mu\nu}$ for X_μ on A, X_ν on B reduces to

$$F_{\mu\nu} = h_{\mu\nu} - \frac{1}{2} P_{\mu\nu}\gamma_{AB} .$$

In the CNDO theory, it is usual to take

$$h_{\mu\nu} = \beta_{AB} S_{\mu\nu} \quad \text{for} \quad X_\mu \quad \text{and} \quad X_\nu \quad \text{on B}$$

and to take $h_{\mu\nu} = 0$ for X_μ and X_ν both on the same atom.

In summary, the parameters and integrals that are needed for the CNDO theory are $S_{\mu\nu}$, $U_{\mu\nu}$, V_{AB}, and β_{AB}. Two versions, CNDO/1 and CNDO/2, differ in the schemes used for the evaluation of these parameters and integrals. CNDO/2 differ from CNDO/1 in the way it handles the penetration integrals and the one-center atomic core integrals and as $Z_B\gamma_{AB} - V_{AB} = 0$ and $U_{\mu\mu} = -\frac{1}{2}(I + A)$, where I and A are ionization potential and electron affinity, respectively.

The CNDO theories suffer from an inability to account for the separation of an open-shell configuration into terms. As a result the important singlet-triplet energy separation is not obtained. To partially overcome this defect some of the approximations in CNDO theory have been eliminated in the INDO theory.

5. Intermediate Neglect of Differential Overlap Approximation (INDO)

The difference between the CNDO/2 and INDO approximations comes in the computation of the two-electron exchange integrals

$$(\mu\nu|\mu\nu) = \int\int X_\nu(1) X_\mu(2) \frac{1}{r_{12}} X_\nu(1) X_\nu(2)\, d\underline{r}_1 d\underline{r}_2, \quad \mu \neq \nu$$

where X_μ and X_ν are on the same atom. In CNDO theory such integrals are neglected, and all interactions between two electrons on atom A are replaced by γ_{AA} regardless of their spin. As a result, CNDO calculations are unable to give an account of the separation of states arising from the same configuration. In the INDO method, the monatomic differential overlap for one-center integrals is retained while in CNDO it is not.[89] Some examples for one-center integrals are shown below. By using the notation of Slater, and assuming that 2s and 2p orbitals have the same radial parts, we may write the nonvanishing integrals

$$(ss|ss) = (ss|xx) = (ss|yy) = (ss|zz) = F^0 = \gamma_{AA}$$

$$(xy|xy) = (xz|xz) = (yz|yz) = \frac{3}{25} F^{(2)}$$

$$(xx|xx) = (yy|yy) = (zz|zz) = \gamma_{AA} + \frac{4}{25} F^{(2)}$$

$$(sx|sx) = (sy|sy) = (sz|sz) = \frac{1}{3} G^{(1)}$$

$$(xx|yy) = (yy|zz) = (zz|xx) = \gamma_{AA} - \frac{2}{25} F^{(2)},$$

where x,y, and z stand for p_x, p_y, and p_z orbitals, respectively. In CNDO theory, $F^{(2)}$, and $G^{(1)}$ are zero. Hence,

$$F_{\mu\nu}(\text{INDO}) = F_{\mu\nu}(\text{CNDO/2}) + f(F^{(2)}, G^{(1)}).$$

The values for $F^{(2)}$ and $G^{(1)}$ are chosen semi-empirically.

Values for the monatomic core integrals $U_{\mu\mu}$ are again found semi-empirically by subtracting electron interaction terms from the mean of the ionization potential I and electron affinity A of appropriate average atomic states. However, details differ somewhat from those for the CNDO method because of the $F^{(1)}$ and $F^{(2)}$ constants.

RESULTS AND DISCUSSION

I. GENERAL PROCEDURE

The energy barriers to internal rotation about the N-C(O) bond in some selected amides, symmetrically or unsymmetrically substituted, were calculated by the intermediate neglect of differential overlap (INDO) method. Using the MBLD program, the coordinates of each of the atoms in the given amides were computed by employing the standard bondlengths and bond angles given in Tables 42 and 43. All these geometrical parameters remained the same for all amides in the calculations, to avoid a large increase in computational time, even though the results may be altered by this restriction. The orbitals used in the INDO program are those of the STO-3G basis set. The input parameters for the INDO program are shown in Table 44.

The choice of the transition state geometry is that formed by twisting the -COR fragment by 90° out of the plane of the -NCO fragment. The molecular structures, charges, and designations of dihedral angles for each of the amides are shown in Figure 78. All these conformations are designated as G-1 for each amide, the other conformations are defined in Table 45, column 2.

Table 44. INDO input parameters.

Atom	Slater exponents	α-s[a] (e.v.)	α-p[b] (e.v.)	$\beta/2$[c] (e.v.)	F[d]	G[d]
H	1.2	- 7.176	- 0.000	- 4.5	0.0000	0.000
C	1.625	-14.051	- 5.572	-10.5	0.17372	0.267708
N	1.950	-19.316	- 7.275	-12.5	0.219055	0.346029
O	2.275	-25.39	- 9.111	-15.5	0.266415	0.43423
F	2.60	-32.272	-11.08	-19.5	0.3158	0.532305

[a] $\alpha\text{-s} = -\frac{1}{2}(I_s + A_s)$, where I_s and A_s are the ionization potential and electron affinity of the 2s electron.

[b] α-p, the same definition as above except for the 2p electron.

[c] β is the bonding parameter.

[d] F and G are two-electron integrals as introduced in the Theoretical section.

Figure 78. Conformations of various amides (G-1) for INDO calculations[a]

(1) Formamide($\theta=0°$)

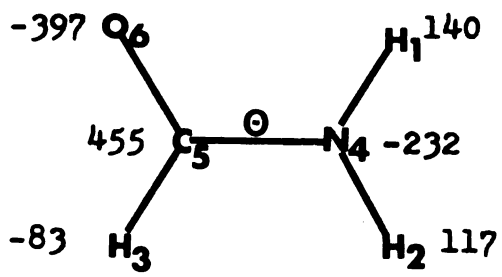

(2) N,N-Dimethylformamide($\theta=\phi_2=\phi_3=0°$)

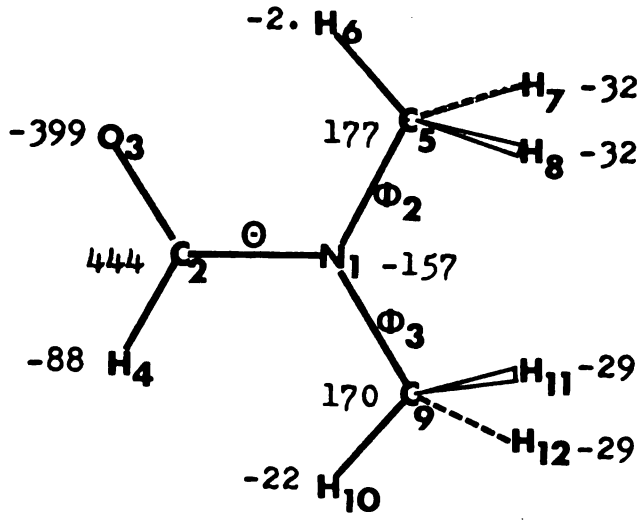

(3) N,N-Dimethylacetamide($\theta=\phi_1=\phi_2=\phi_3=0°$)

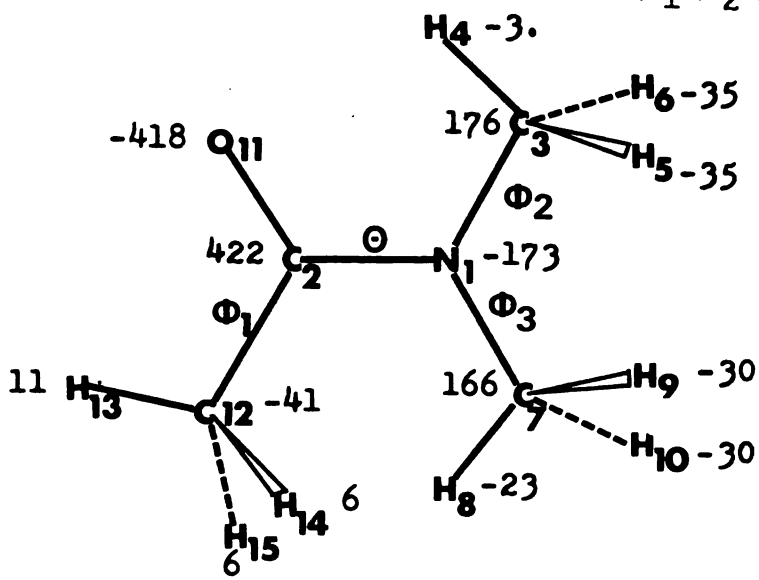

(4) N,N-Dimethyltrifluoroacetamide ($\theta=\phi_1=\phi_2=\phi_3=0°$)

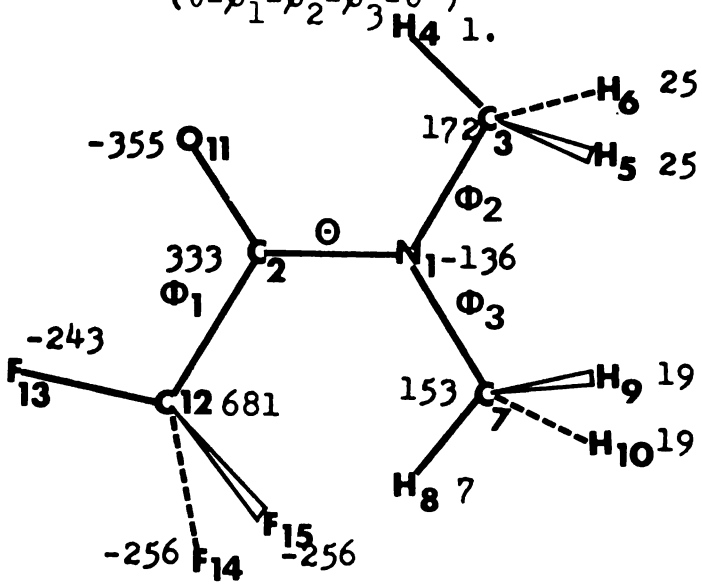

(continued)

(5) N-Methylformamide($\theta=\phi_3=0°$)

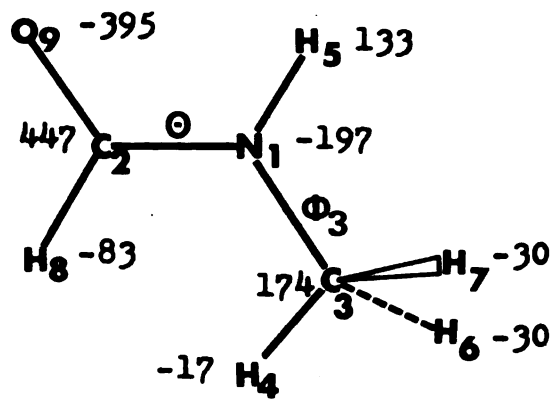

(6) N-Methylacetamide($\theta=\phi_1=\phi_2=0°$)

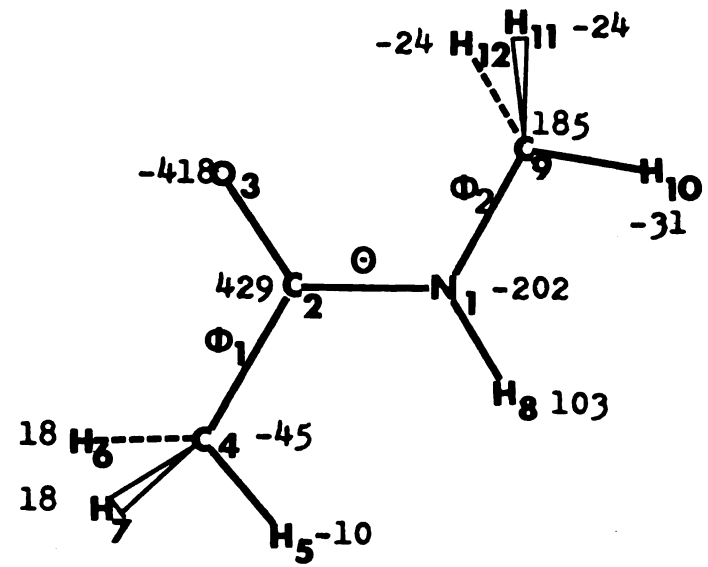

(7) N-Ethylformamide($\theta=\phi_3=\phi_4=0°$)

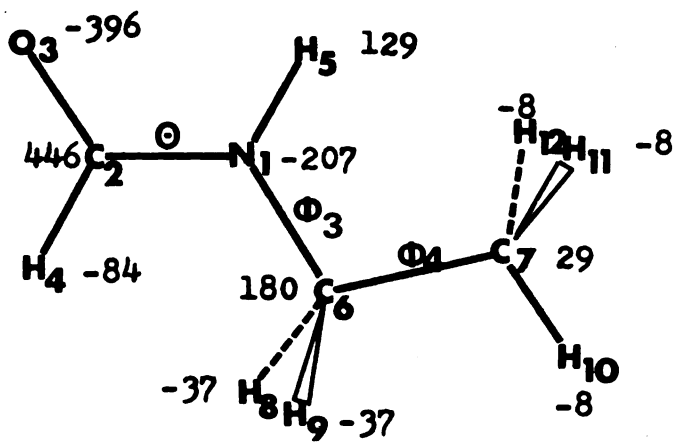

(8) N-Ethylacetamide($\theta=\phi_1=\phi_3=\phi_4=0°$)

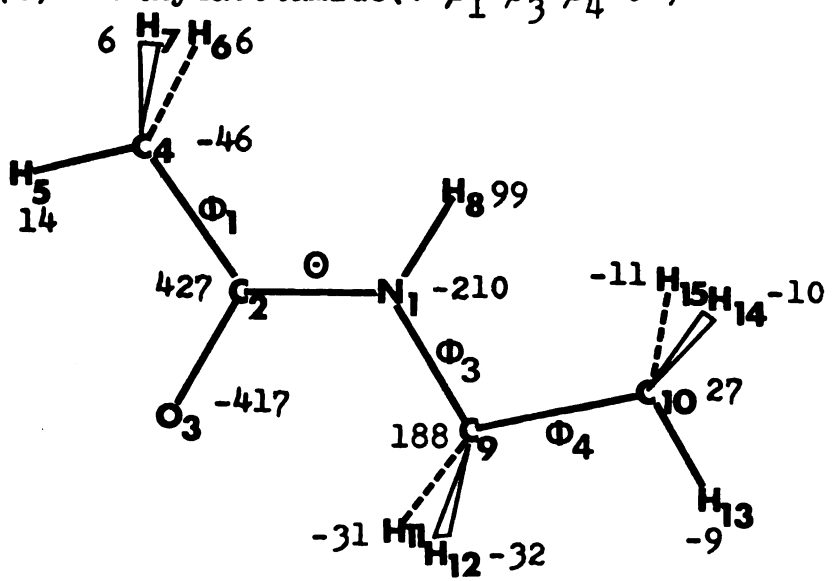

(continued)

(9) N-Methyl-N-Ethylformamide
($\theta=\phi_2=\phi_3=\phi_4=0°$)

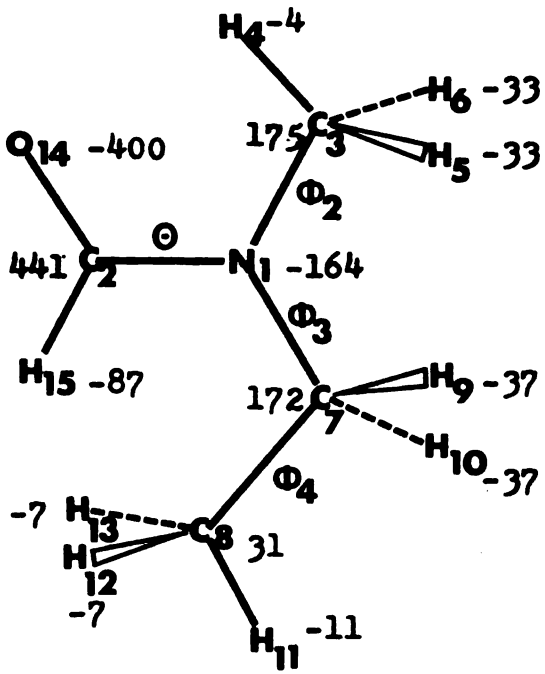

(10) N-Methyl-N-Ethylacetamide
($\theta=\phi_1=\phi_2=\phi_3=\phi_4=0°$)

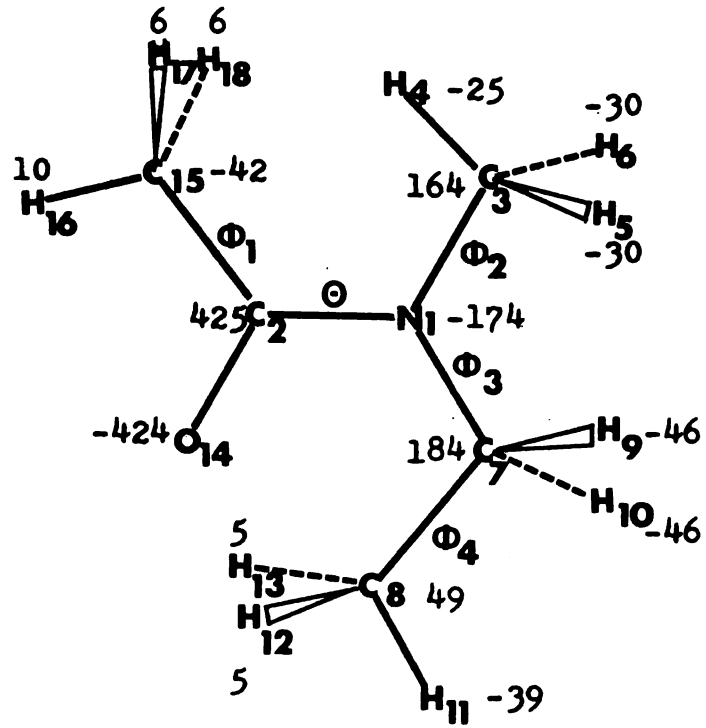

[a] The charge on each atom calculated by the INDO method is shown in units of 10^{-2} electrons.

Table 45. Total energies for various conformations of several amides by INDO method

Compounds	Structure Number	Dihedral Angle(°) θ	ϕ_1	ϕ_2	ϕ_3	ϕ_4	Total Energy (a.u.)	Relative Energy (kcal/mol.)	Bond Order for the N-C(O) Bond
Formamide	G-1	0					-37.72076809	0.00	1.45028
	E-1	90					-37.68744381	20.91	1.28659
N,N-Dimethyl formamide	G-1	0		0	0		-54.60917786	0.00	1.33582
	G-2	0		60	60		-54.60773433	0.91	1.33306
	G-3	0		60	0		-54.60897984	0.12	1.33517
	G-4	0		0	60		-54.60833906	0.53	1.33234
	E-1	90		0	0		-54.58477163	15.31	1.18688
	E-2	90		0	60		-54.58407294		1.18316
	E-3	90		60	60		-54.58304724		1.18919
N,N-Dimethyl acetamide	G-1	0	0	0	0		-63.05239379	0.00	1.30874
	G-2	0	60	0	0		-63.04168389	6.72	1.31146
	E-1	90	60	60	60		-63.02507940	17.14	1.11787
N,N-Dimethyl trifluoro acetamide	G-1	0	0	0	0		-140.10890632	0.00	1.33635
	G-2	0	60	0	0		-140.06010446	30.62	1.34779
	E-1	90	60	0	0		-140.0828723	17.96	1.16026
	E-2	90	60	60	60		-140.07890447	18.83	1.16441

(continued)

Compounds	Structure Number	Dihedral Angle(°) θ	ϕ_1	ϕ_2	ϕ_3	ϕ_4	Total Energy (a.u.)	Relative Energy (kcal/mol.)	Bond Order for the N-C(O) Bond
N-methyl formamide	G-1	0			0		-46.16301799	0.00	1.39965
	G-2	0			60		-46.16275153	0.17	1.39577
	G-3	0			30		-46.16288158	0.09	1.34028
	E-1	90			60		-46.13552259	17.25	1.20851
	E-2	90			0		-46.13579829	17.08	1.21233
N-Methyl acetamide	G-1	0	0	0			-54.60902996	0.19	1.29683
	G-2	0	30	0			-54.60916522	0.10	1.32054
	G-3	0	60	0			-54.60932957	0.00	1.31955
	G-4	0	60	30			-54.60922413	0.07	1.31799
	G-5	0	60	60			-54.60908005	0.16	1.31925
	G-6	0	0	30			-54.60893233	0.25	1.32079
	G-7	0	0	60			-54.60879702	0.33	1.32210
	G-8	0	30	30			-54.60905424	0.17	1.31895
	G-9	0	30	60			-54.60892398	0.25	1.30353
	E-1	90	60	30			-54.58063278	18.01	1.20184

(continued)

Compounds	Structure Number	Dihedral Angle(°) θ	ϕ_1	ϕ_2	ϕ_3	ϕ_4	Total Energy (a.u.)	Relative Energy (kcal/mol.)	Bond Order for the N-C(O) Bond
N-Ethyl formamide	G-1	0			0	0	-54.59962404	0.18	1.34002
	G-2	0			90	0	-54.59824691	1.05	1.34773
	G-3	0			30	0	-54.59926168	0.41	1.34461
	G-4	0			150	0	-54.59828892	1.02	1.33600
	G-5	0			180	0	-54.59991516	0.00	1.33948
	E-1	90			0	0	-54.57264174		1.21244
	E-2	90			90	0	-54.57056547		1.20866
	E-3	90			30	0	-54.57224976	17.36	1.21439
	E-4	90			150	0	-54.57558206		1.21382
	E-5	90			180	0	-54.57803027	13.73	1.20822
N-Methyl N-Ethyl formamide	G-1	0		0	0	0	-63.04482350	0.00	1.33474
	G-2	180		0	0	0	-63.04381338	0.63	1.40961
	E-1	90		0	0	0	-63.02578375	11.95	1.18280

(continued)

Compounds	Structure Number	Dihedral Angle(°)					Total Energy (a.u.)	Relative Energy (kcal/mol.)	Bond Order for the N-C(O) Bond
		θ	ϕ_1	ϕ_2	ϕ_3	ϕ_4			
N-Ethyl acetamide	G-1	0	0		0	0	-63.04702613	0.00	1.32083
	G-2	0	0		30	0	-63.04567516	0.85	1.32271
	G-3	0	0		90	0	-63.04478474	1.41	1.33205
	G-4	0	0		150	0	-63.04242927	2.88	1.33047
	G-5	0	0		180	0	-63.04467194	1.48	1.32829
	G-6	0	60		0	0	-63.04673212	0.18	1.32363
	E-1	90	0		0	0	-63.01554576	19.75	1.17701
	E-2	90	0		30	0	-63.01480022		1.17656
	E-3	90	0		90	0	-63.01277240		1.17353
	E-4	90	0		150	0	-63.01700040		1.17820
	E-5	90	0		180	0	-63.01953637	17.25	1.16689
N-Methyl N-Ethyl acetamide	G-1	0	0	0	0	0	-71.4869343	0.00	1.29290
	E-1	90	60	0	0	0	-71.4668792	12.58	1.11304

The output display from the INDO program includes (a) the overlap array, (b) the Hückel Hamiltonian, (c) the Coulomb matrix, (d) the core Hamiltonian, (e) the final Fock Hamiltonian, (f) the final vectors, (g) the initial density matrix, (h) the final density matrix, and (i) the partial charges on each atom.

Since calculations were made for many different conformations of each amide, it is possible to study the change of energy, and of partial charges on each atom, with the variations in the dihedral angles.

II. DEPENDENCE OF INDO RESULTS ON CONFORMATION

The results are to be presented in four sections: A. Variation of energy for rotation by angle θ about the N-C(O) bond, B. Energy variation with respect to the dihedral angles ø, C. Charge variation with rotation by angle θ about the peptide bond, and D. Charge variation with respect to dihedral angles ø.

A. Variation of energy with rotation about the N-C(O) bond

The variations in the energy barrier for rotation around the N-C(O) bond mainly arise from inductive, steric, and hyperconjugative interactions. However, it is still impossible to separate out the energy associated with any given type of interaction. To analyze the energy variations and bond orders for different conformations of a given amide, a listing of the absolute energies, relative energies, and bond orders is given in Table 45. The

calculated energy barriers for rotation about the N-C(O) bond for each amide are in reasonable agreement with the experimental data and the CNDO/2 data[212] shown in Table 41.

In order to look into the effect of the carbonyl substituent R(C = O) on the energy barriers in amides, some groups of amides are compared: (1) N,N-dimethylformamide, N,N-dimethylacetamide, and N.N-dimethyltrifluoroacetamide (DMTFA); (2) N-methylformamide, N-methylacetamide; (3) N-ethylformamide, N-ethylacetamide; and (4) N-methyl-N-ethylformamide, N-methyl-N-ethylacetamide.

The energy barriers of the first group are shown in Figure 79. The results show that as the substituent group R(C = O) changes from -H to $-CH_3$ (or $-CF_3$), the energy barrier about the N-C(O) bond is increased. This is attributed mainly to the steric effect. This result is similar to that obtained by CNDO/2[90] but opposite to that obtained by the EHT method.[90,125] In order to compare the calculated with the experimental results, which show a decrease as the substituent group R on the carbonyl group is changed from -H, $-CH_3$ to $-C_2H_5$ (though this tend is not unequivocally established), we must consider the solvent effect. Rabinovitz and Pines[160] have found that the energy barrier for rotation about the N-C(O) bond in N,N-dimethylformamide decreases with increasing dilution of the amide in CCl_4 and they proposed that this variation is the result of a change in amide-amide association equilibrium. The

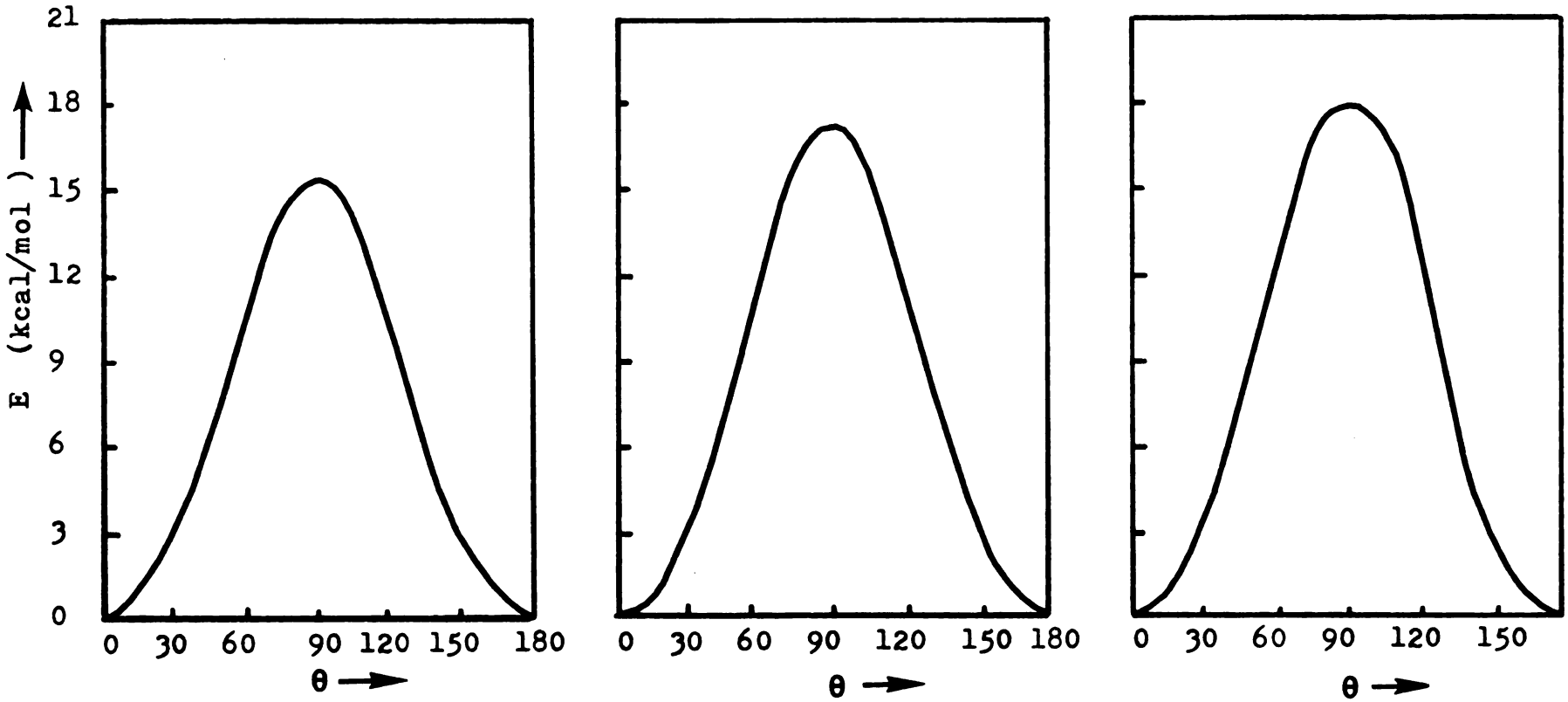

E_a = 15.31 kcal/mol E_a = 17.14 kcal/mol E_a = 17.96 kcal/mol

Figure 79. Comparison of the energy barriers for rotation about the peptide bond in N,N-dimethylformamide (left), N,N-dimethylacetamide (middle), and N,N-dimethyltrifluoroacetamide (right); θ is the angle of twist about the N-C(O) bond from the plannar form.

fact that the barrier decreases with increasing dilution indicates that the barrier in the monomer is lower than in the dimer.[162] This solvent effect has also been studied theoretically by Momany et al.[212] and experimentally by Kamei.[237] In the CNDO/2 results of Momany et al., they consider many different possible conformations of the formamide dimer and find that when hydrogen bonds are formed at the C = O group, the energy barrier of that amide for rotation about the N-C(O) bond is increased significantly (by about 2 kcal/mol). This effect was also observed in the NMR studies of Kamei. Normally, the amide-amide association in neat amides increases the barrier by ca. 1 kcal/mol , while hydrogen bonding can increase the barrier by ca. 2-3 kcal/mol , compared with the barrier in a dilute solution in a nonpolar solvent.[212] Using this model, with the same substituent group on nitrogen, the formation of the dimer for N,N-disubstituted acetamides will be more difficult than for N,N-disubstituted formamides since the size of $-CH_3$ group is quite a bit larger than that of hydrogen. Another possible factor affecting association may be the geometry of the ground state, since some amides are not actually planar in the liquid phase, especially when the substituent group becomes more bulky. The assumption that all amides, even those with bulky substituents, are planar will result in the calculated ground states being less stable than would be predicted for the

true, pyramidal ground state; the calculated energy barriers for rotation about N-C(O) would then be too low. Considering these two factors, the observed energy barrier for acetamide is almost equal to, or perhaps less than, that of formamide as seen in Table 46. This solvent effect will be described more clearly later. One very interesting pair of amides is N,N-dimethylacetamide and N,N-dimethyltrifluoroacetamide (DMTFA). Both the theoretical INDO energy barrier and the experimentally determined barrier[232] for DMTFA are greater than those for DMA. This difference is presumably the result of the different inductive effects of hydrogen and fluorine, since the atomic volumes for hydrogen and fluorine are similar (H: 13.1 ml/mol, F: 14.6 ml/mol), so the steric effect will not be very important.

To investigate the variation of the energy barrier in amides with different nitrogen substituents (i.e., -H, $-CH_3$ or $-CH_2CH_3$), and different substitution numbers (i.e., mono- or di- substituted), we compared the following groups of amides:

(a) <u>Those with different substituent groups but the same substitution number</u>:

(1) N,N-dimethylformamide, N-methyl-N-ethylformamide;

(2) N,N-dimethylacetamide, N-methyl-N-ethylacetamide;

(3) Formamide, N-methylformamide, and N-ethylformamide;

(4) N-methylacetamide and N-ethylacetamide.

Table 46. Energy barriers for rotation about various bonds in some amides.

Compound	Rotational energy of $-CH_3$ (or $-C[H_2CH_3]$) in the ground state (kcal/mol)						Barrier for rotation about N-C(O) bond (kcal/mol)	
	ϕ_1^i		ϕ_2^i		ϕ_3^i		θ^i	
	INDO	Exptl.	INDO	Exptl.	INDO	Exptl.	INDO	Exptl.
Formamide							20.91	19.7±0.4[a] 19.2±0.4[b]
N,N-Dimethyl-formamide (DMF)			0.12	2.12	0.53	2.60	15.31	20.5±0.2[c] 21.6±0.3[d] 19.8±0.5[e]
N,N-Dimethyl-acetamide (DMA)	6.72	3.26		2.55		1.66	17.14	16.85±0.41[f] 16.8[g] 19.7±0.5[e]
N,N-Dimethyltri-fluoroacetamide (DMTFA)	30.62						17.96	17.37±0.26[f]
N-Methylformamide					0.17		17.08	19.0[h]
N-Ethylformamide					1.05		13.73	
N-Methylacetamide	0.19		0.16				18.01	18.0[h]
N-Ethylacetamide	0.18				2.88		17.25	
N-Methyl-N-ethyl-formamide							11.95	

Table 46 (cont'd.)

Compound	Rotational energy of $-CH_3$ (or $-C[H_2CH_3]$) in the ground state (kcal/mol)						Barrier for rotation about N-C(0) bond (kcal/mol)	
	ϕ_1^i		ϕ_2^i		ϕ_3^i		θ^i	
	INDO	Exptl.	INDO	Exptl.	INDO	Exptl.	INDO	Exptl.
N-methyl-N-ethyl-acetamide							12.58	20.8 ± 0.5[a]

[a] Reference 231. Solvent: diethylene glycol dimethyl ether.

[b] Reference 231. Solvent: methyl propyl ketone.

[c] Reference 160. Solvent: CCl_4.

[d] Reference 125. Solvent: C_2H_6.

[e] Reference 233. Neat.

[f] Reference 232. Solvent: CCl_4.

[g] Reference 124. Solvent: cycloheane.

[h] Reference 235. Solvent: $C_2H_4Cl_2$.

[i] All angles are defined in Figure 78.

(b) Those with different substitution numbers:

(1) Formamide, N-methylformamide, and N,N-dimethylformamide;

(2) N-methylacetamide, N,N-dimethylacetamide;

(3) N-ethylformamide, N-ethyl-N-methylformamide.

The energy barriers for the first group of each set are shown in Figures 80 and 81. The results show that the barrier decreases as the substituent becomes larger or the substitution number is increased. Again, the INDO results are similar to those obtained by CNDO/2 and the experimental values also show this tendency (Table 41).

B. Energy variation with respect to the dihedral angle ϕ

The energy for rotation about either the N-methyl group or the carbonyl methyl group in N-methylacetamide has been studied by the INDO method. The results show that the rotational energy of either methyl group in cis-N-methylacetamide is varied slightly as the configuration of the other methyl group is changed, as shown in Figures 82-87; the variation is about 0.02 kcal/mol . Also shown in Figure 88 is the three-dimensional energy surface of cis-N-methylacetamide as a function of ϕ_1 and ϕ_2, with $\theta = 0°$. The most stable configuration of cis-N-methylacetamide is with $\phi_1 = 60°$ and $\phi_2 = 0°$. The average energy barrier restricting rotation about the N-methyl group is a little smaller than that for the carbonyl methyl group (ca. 0.03 kcal/mol). Momany et al., in their

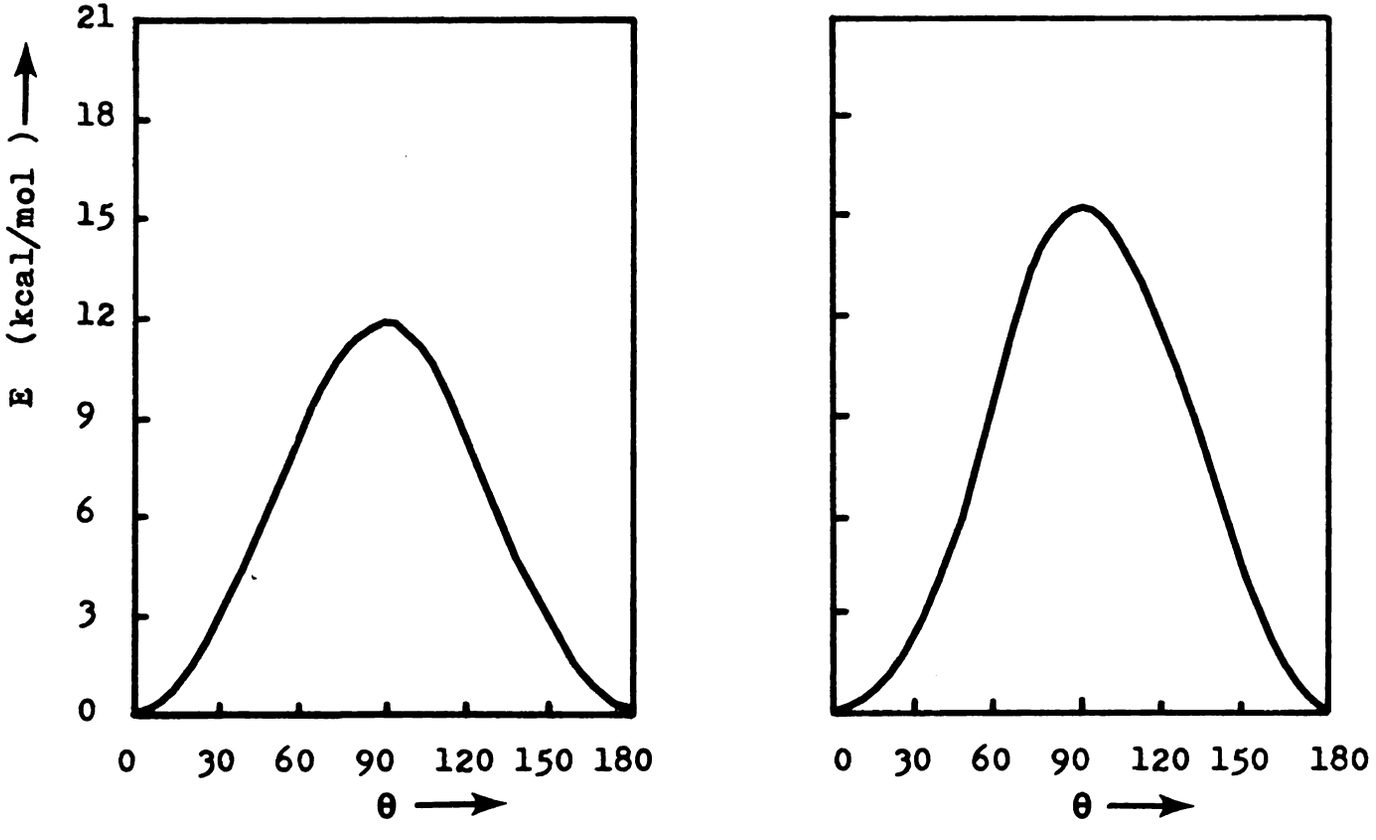

Figure 80. Comparison of the energy barriers for rotation about the peptide bond in N,N-dimethylformamide (right) and N-methyl-N-ethylformamide (left).

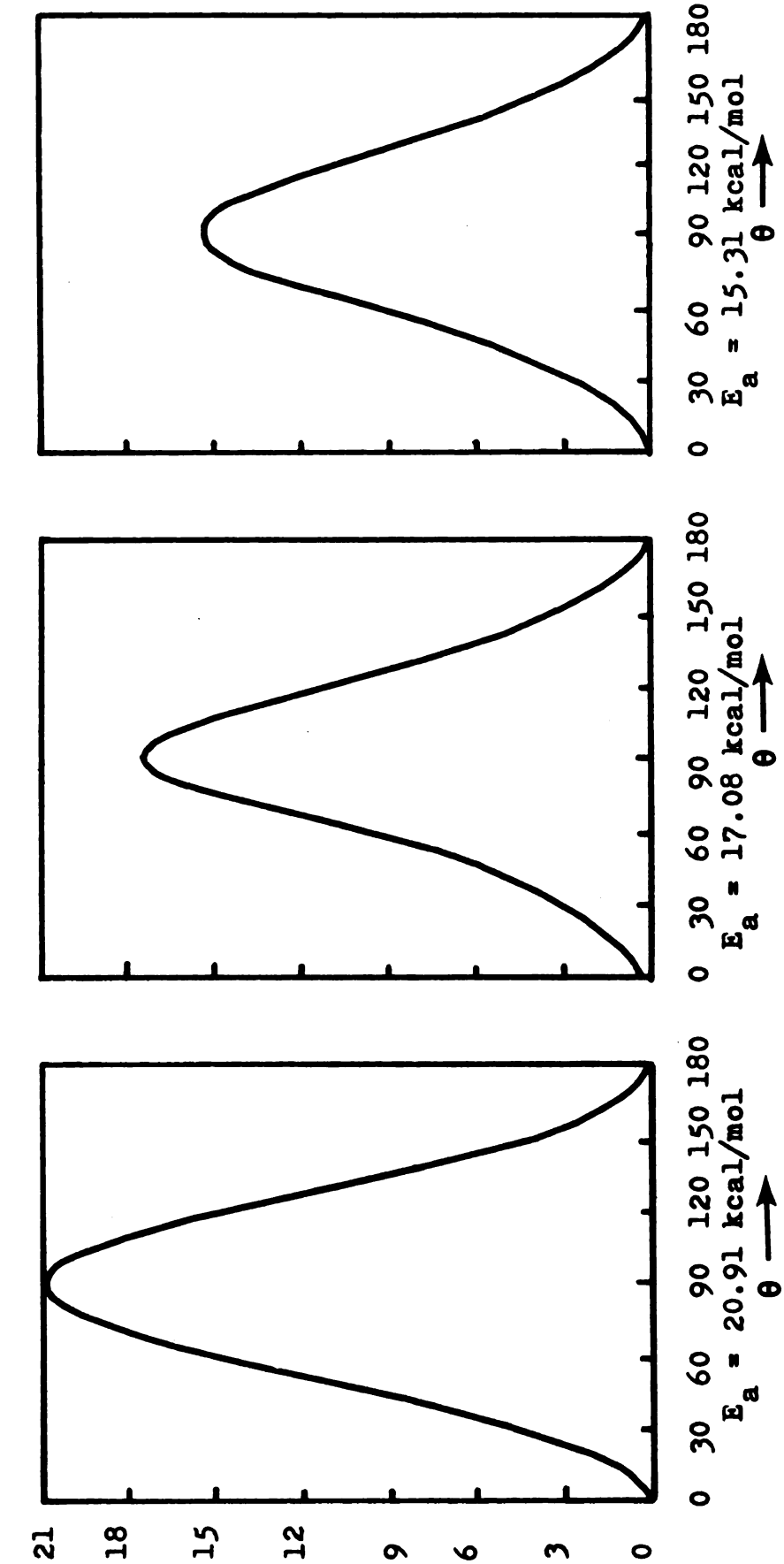

Figure 81. Comparison of the energy barriers for rotation about the peptide bond in formamide (left), N-methylformamide (middle), and N,N-dimethylformamide (right).

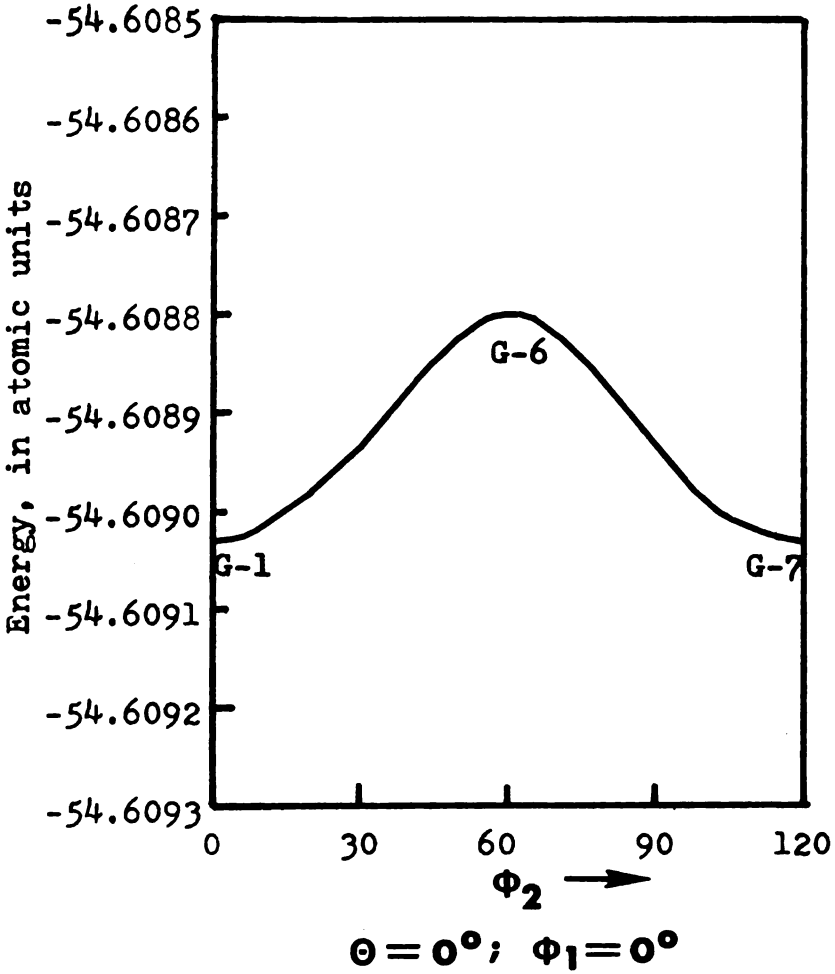

$\Theta = 0^\circ$; $\Phi_1 = 0^\circ$

Figure 82. Variation of the energy for rotation of $-CH_3$ in the $N-CH_3$ group of N-methylacetamide; E_a = 0.14 kcal/mol. The conformations G-1, G-6, and G-7 are defined in Table 45.

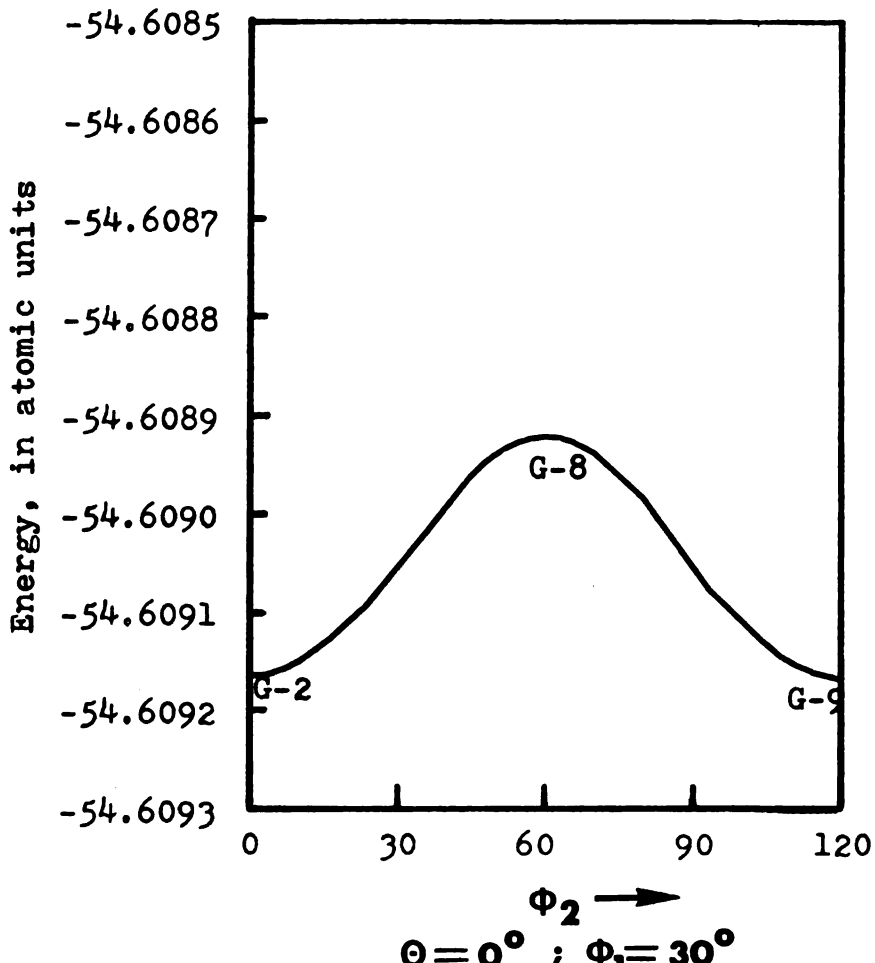

$\Theta = 0^\circ$; $\Phi_1 = 30^\circ$

Figure 83. Variation of the energy for rotation of $-CH_3$ in the $N-CH_3$ group of N-methylacetamide; E_a = 0.15 kcal/mol.

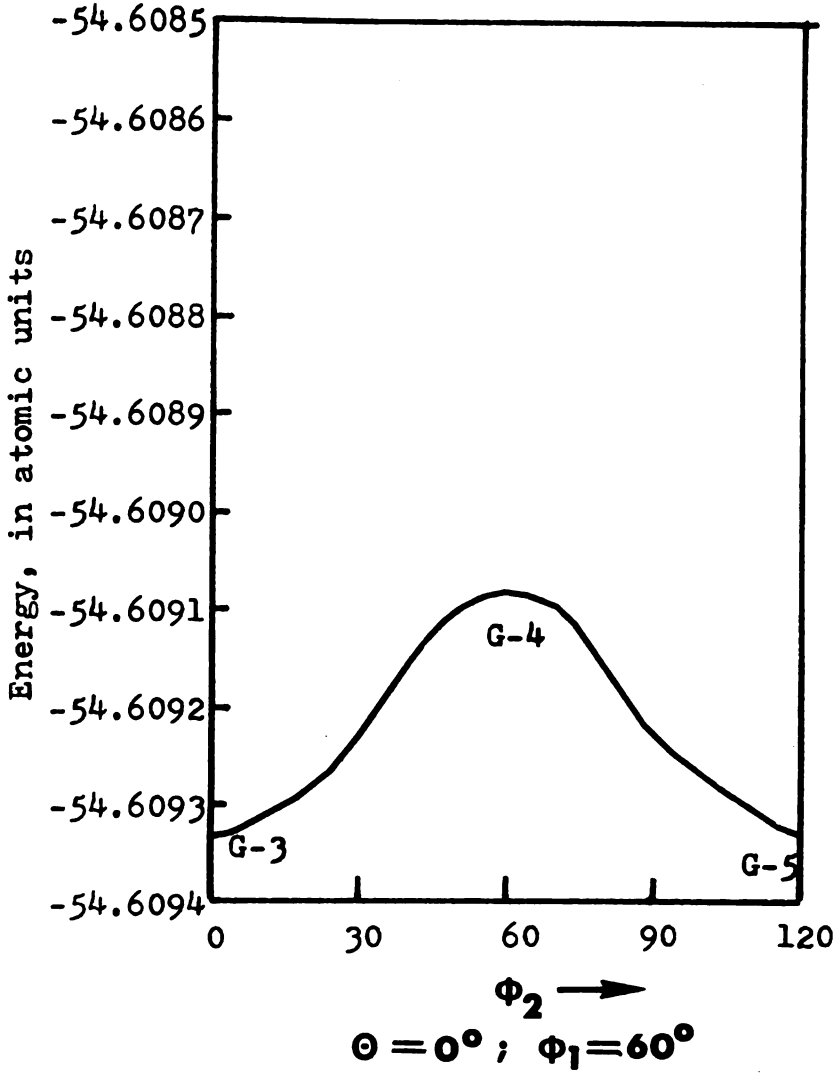

Figure 84. Energy variation for rotation of $-CH_3$ in the $N-CH_3$ group of N-methylacetamide; E_a = 0.16 kcal/mol.

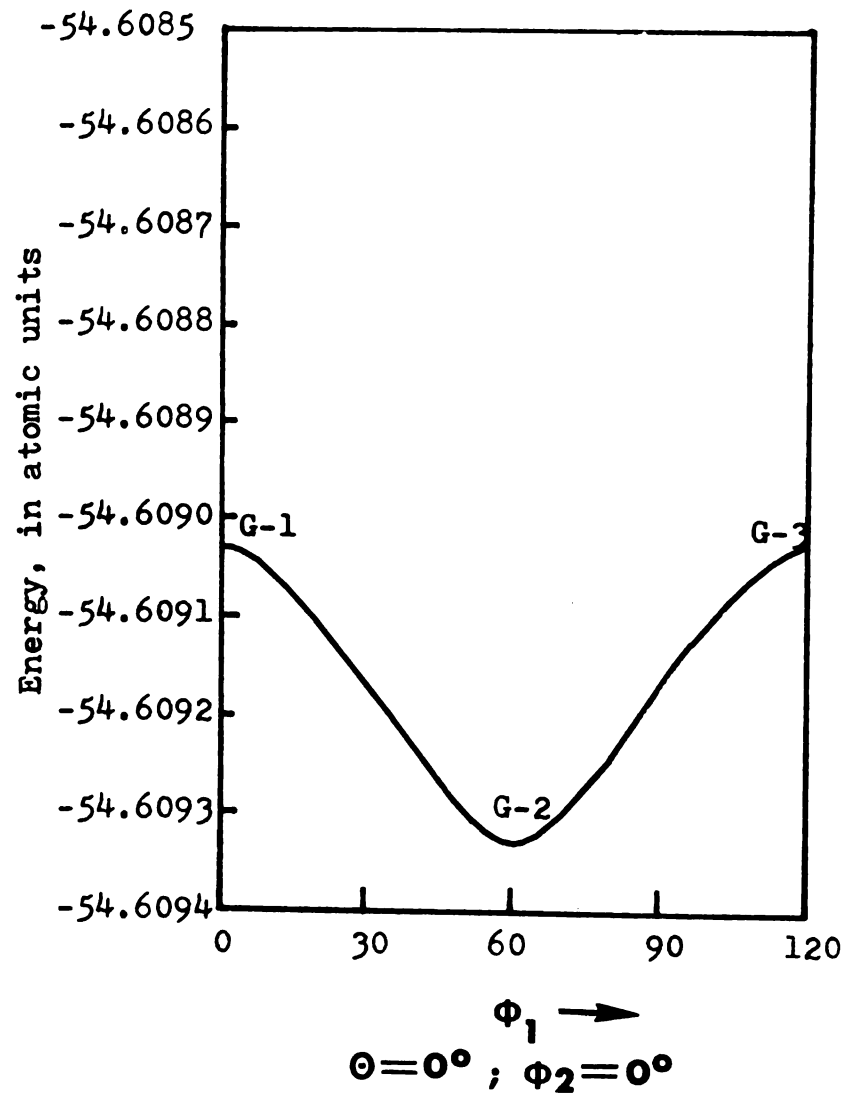

Figure 85. Energy variation for rotation of $-CH_3$ in the carbonyl-methyl group of N-methylacetamide; E_a = 0.19 kcal/mol.

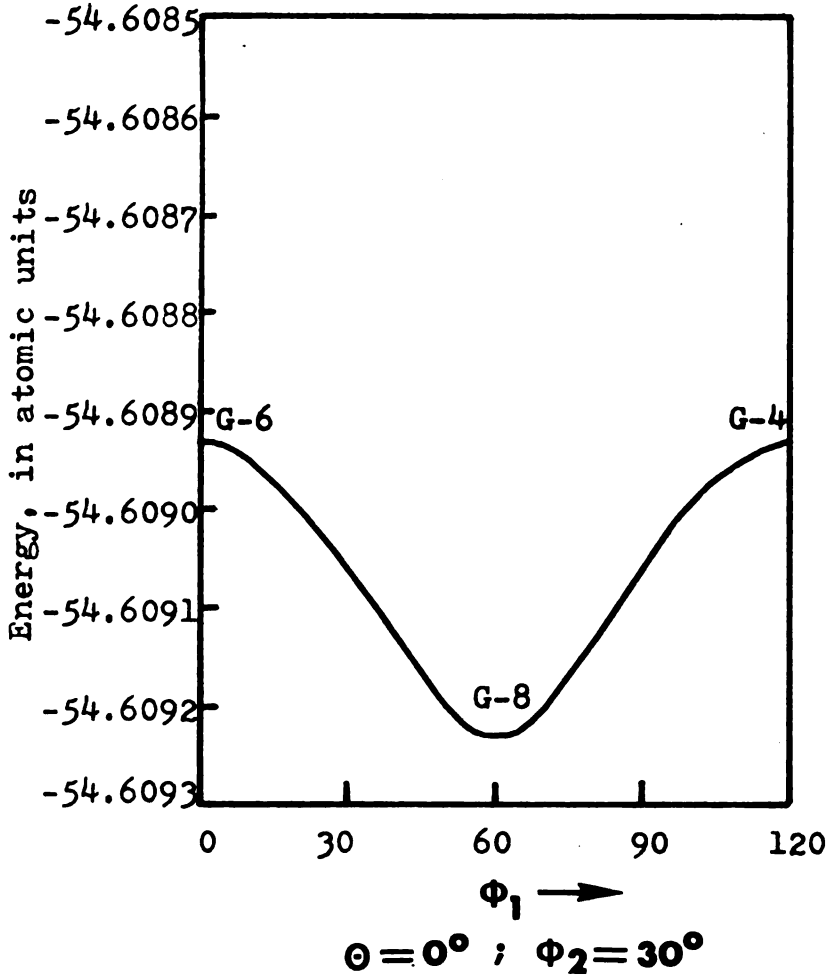

Figure 86. Energy variation for rotation of $-CH_3$ in the carbonyl-methyl group of N-methylacetamide; E_a = 0.18 kcal/mol.

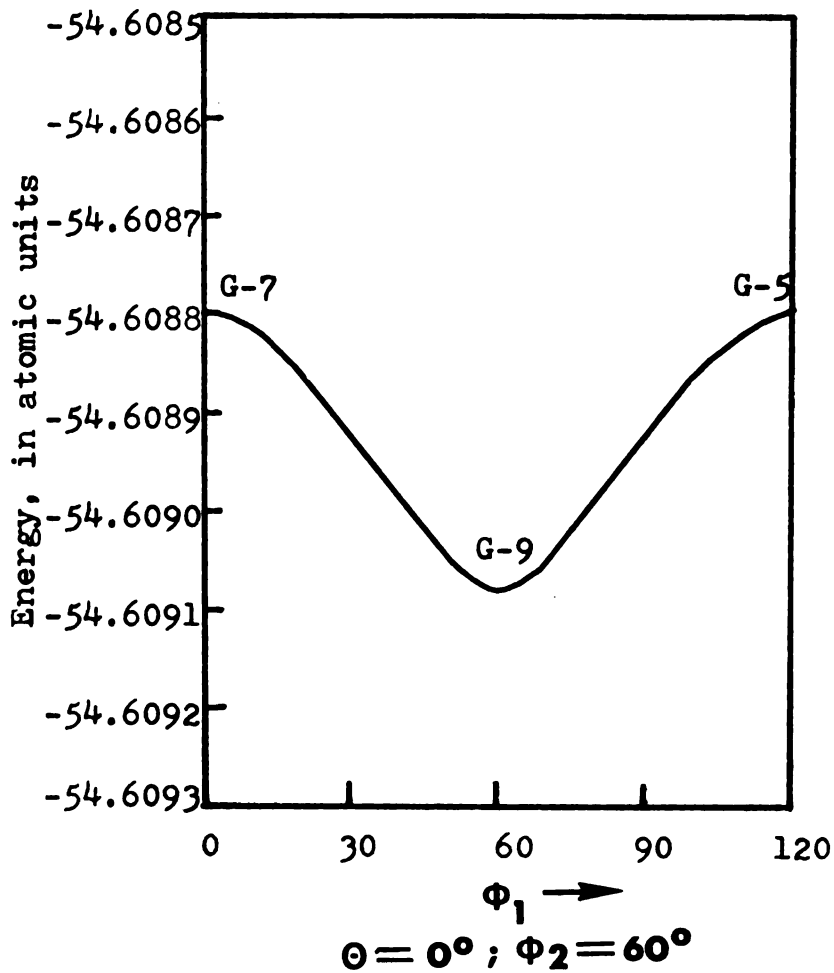

Figure 87. Energy variation for rotation of $-CH_3$ in the carbonyl-methyl group of N-methylacetamide; E_a = 0.17 kcal/mol.

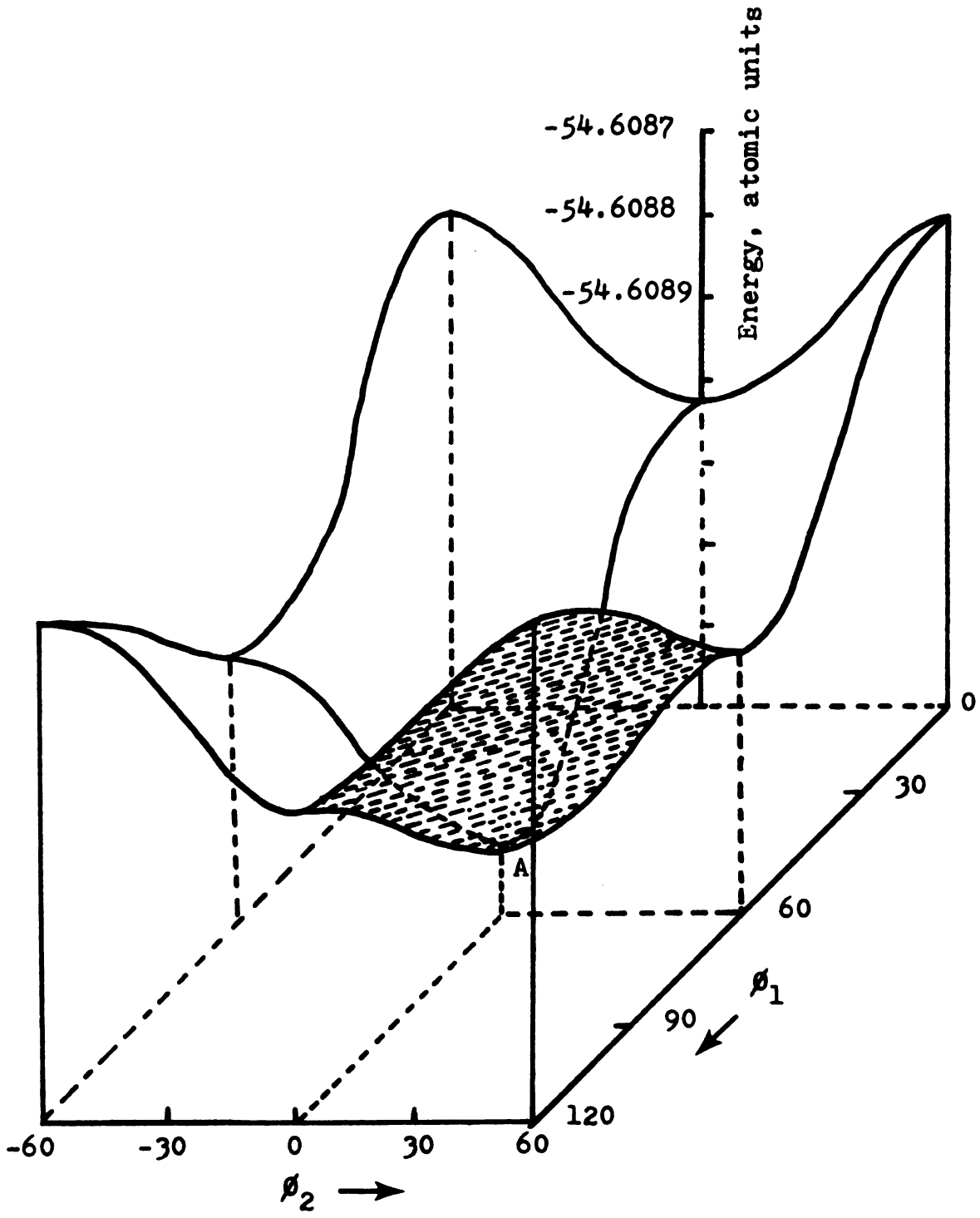

Figure 88. Three-dimensional energy surface for N-methylacetamide as a function of the dihedral angles of the N-methyl (ϕ_2) and the carbonyl-methyl (ϕ_1) groups. The lowest energy configuration is at point A with $\phi_1 = 60^\circ$ and $\phi_2 = 0^\circ$.

CNDO/2 calculation, find that when the peptide bond is twisted from the configuration in cis-N-methylacetamide to that in trans-N-methylacetamide (where cis or trans is relative to C = O group) by an angle θ greater than 120°, the rotational barrier of the N-methyl group rises sharply. This is highly indicative of a sharp increase in the potential due to steric repulsion.

Many different groups[238-241] had worked on the energy barrier for rotation about the C-X bond of the CH_3-XAB system, with X trigonal planar. They found that if A and B are equivalent the barrier will be sixfold, and such barriers are known to be small. When A and B are nonequivalent, a threefold component is introduced. While this will dominate the shape of the barrier its height will remain small as long as the trigonal planar configuration at X is preserved. This model can explain why most of the rotational energies for methyl groups in amides are so low. According to our INDO results, Table 46, most of the rotational energies for $-CH_3$ in amides lie between zero and 0.5 kcal/mol, except in some special cases such as DMA, DMTFA, N-ethylformamide, and N-ethylacetamide. The rather low rotational energies calculated for methyl groups are mainly a result of our assumption that the ground state is planar, which is consistent with the CH_3-XAB system which was assumed to be planar. We also measured the rotational energies for the

N-methyl groups in DMF and DMA by NMR T_1 experiments, and found that the barrier is usually more than 1.5 kcal/mol. These large experimental values are attributed to the solvent effect and to deviations from the planar structure in liquid amides.

Rotational energies of the carbonyl methyl group in DMA and DMTFA are considerably higher than those for the other methyl groups, as seen in Table 46. This is due to the presence of a trans-N-methyl group in both compounds. From the rotational energies of the carbonyl methyl group in N-methylacetamide and DMA, we find that some extra energy, ca. 5.53 kcal/mol, is needed for rotating the carbonyl methyl group in DMA over that in N-methylacetamide. This large steric interaction energy is completely consistent with the CNDO/2 results obtained by Momany et al. In N-methylacetamide, they found that when the N-methyl group is twisted from the cis configuration to the trans (relative to carbonyl oxygen), the rotational energy of the carbonyl methyl group is sharply increased. For DMTFA there is also a strong electronic interaction in addition to the steric interaction, as shown in Figure 113, where a sharp change of the electronic charge distribution on the carbonyl-methyl carbon is observed as compared with DMA. The calculated rotational energy of the carbonyl methyl group in DMTFA is 30.62 kcal/mol, which is higher than that calculated for DMA, 6.72 kcal/mol, as shown in

Figures 89 and 90. This strong electronic interaction energy makes the energy barrier for rotation of the $-CF_3$ group about its threefold axis even higher than that for rotation about the N-C(O) bond in DMTFA, so we expect that the $-CF_3$ group will stay in a fixed configuration at room temperature.

Rotational energies for the N-ethyl group about the N-C[H_2CH_3] bond in N-ethylformamide and N-ethylacetamide, Figures 91 and 92, are lower than calculated for the carbonyl methyl groups in DMA and DMTFA, but higher than obtained for the remainder of the methyl groups (Table 46). This is because the N-ethyl group in N-ethylacetamide considered here is cis to the C = O group, so the rotational energy of the N-ethyl group is mainly attributed to its greater mass. Comparing the rotational energies of the carbonyl methyl group in N-methylacetamide and N-ethylacetamide, both in the cis form, we find that they are nearly identical. That means that the rotational energies of carbonyl methyl groups are almost independent of the structure of the N-substituted group when these are trans to each other. From the rotational energies of the trans-N-methyl group in N-methylformamide (NMF) and N,N-dimethylformamide, Figures 93-95, we find that the steric effect energy due to replacing an N-H hydrogen in NMF by a cis-N-methyl group is about 0.36 kcal/mol. Comparing N-methylformamide and N-ethylformamide, we find that when one proton of the

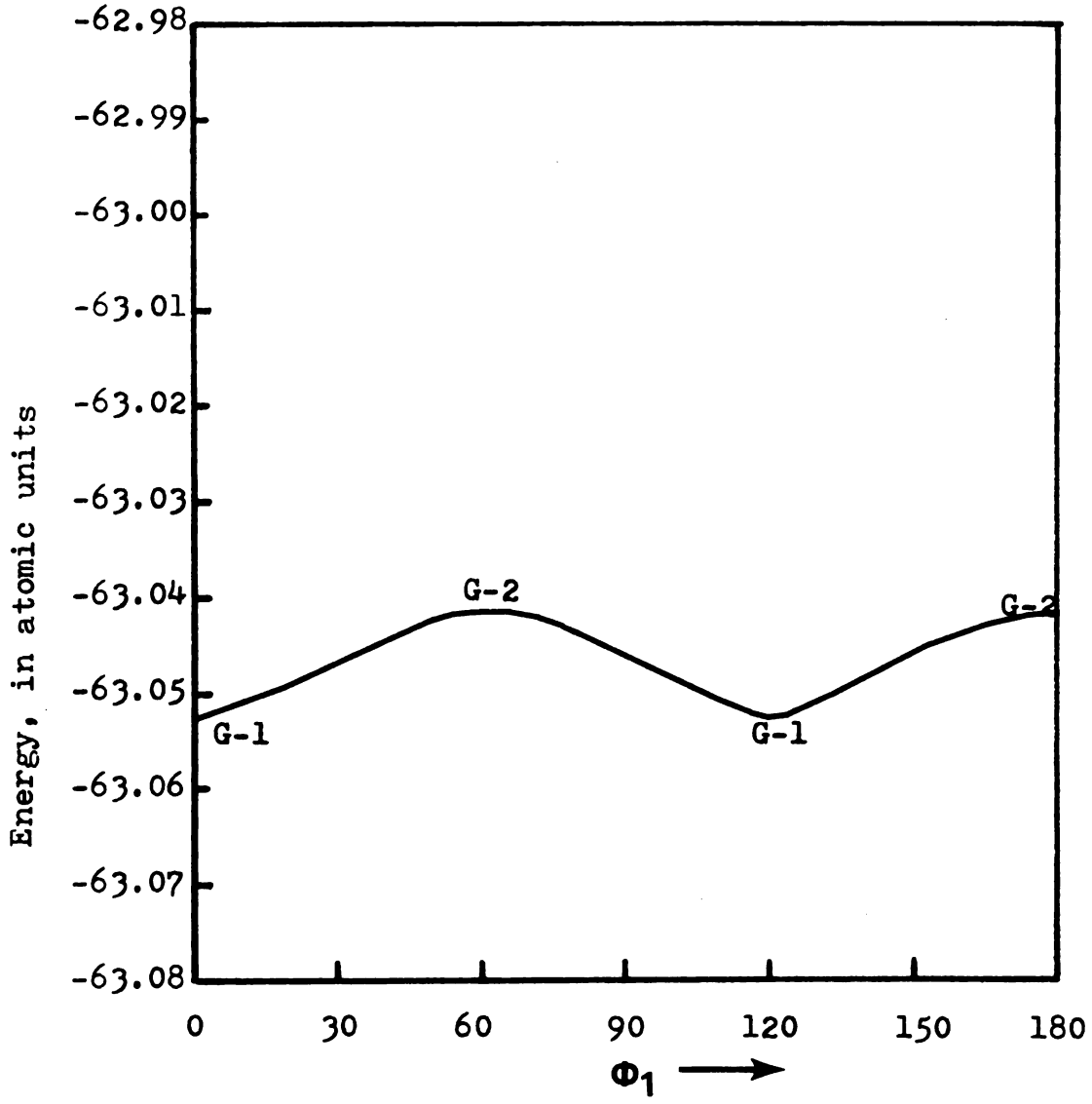

Figure 89. Variation of energy with rotation of the carbonyl-methyl group in N,N-dimethylacetamide; E_a = 6.72 kcal/mol. The notation G-1, G-2 refers to the configurations defined in Table 45; the values of the angle ϕ_1 corresponding to each configurations are also shown in Figure 79.

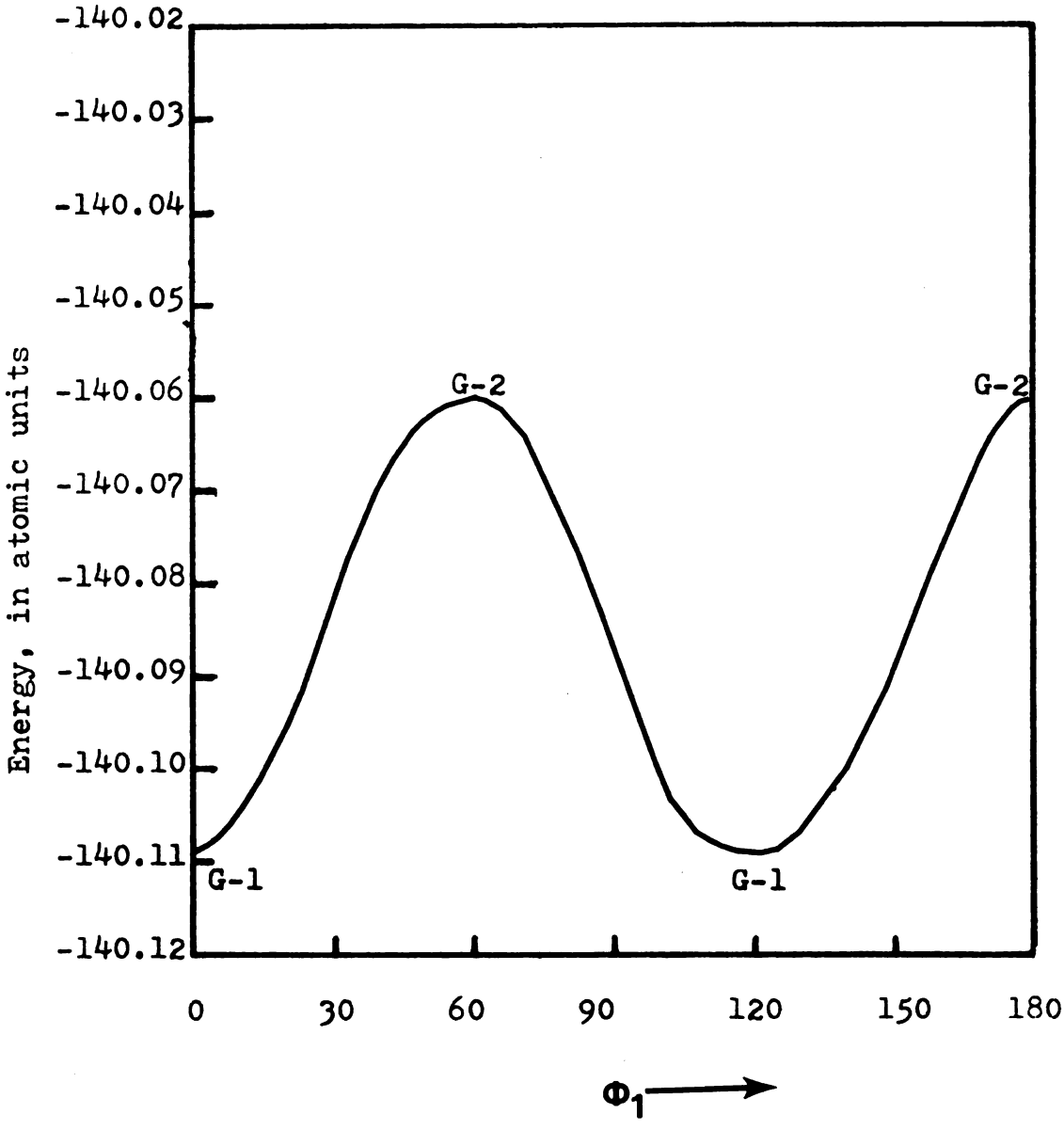

Figure 90. Energy variation for rotation of the carbonyl-CF_3 group in N,N-dimethyltrifluoroacetamide; E_a = 30.62 kcal/mol.

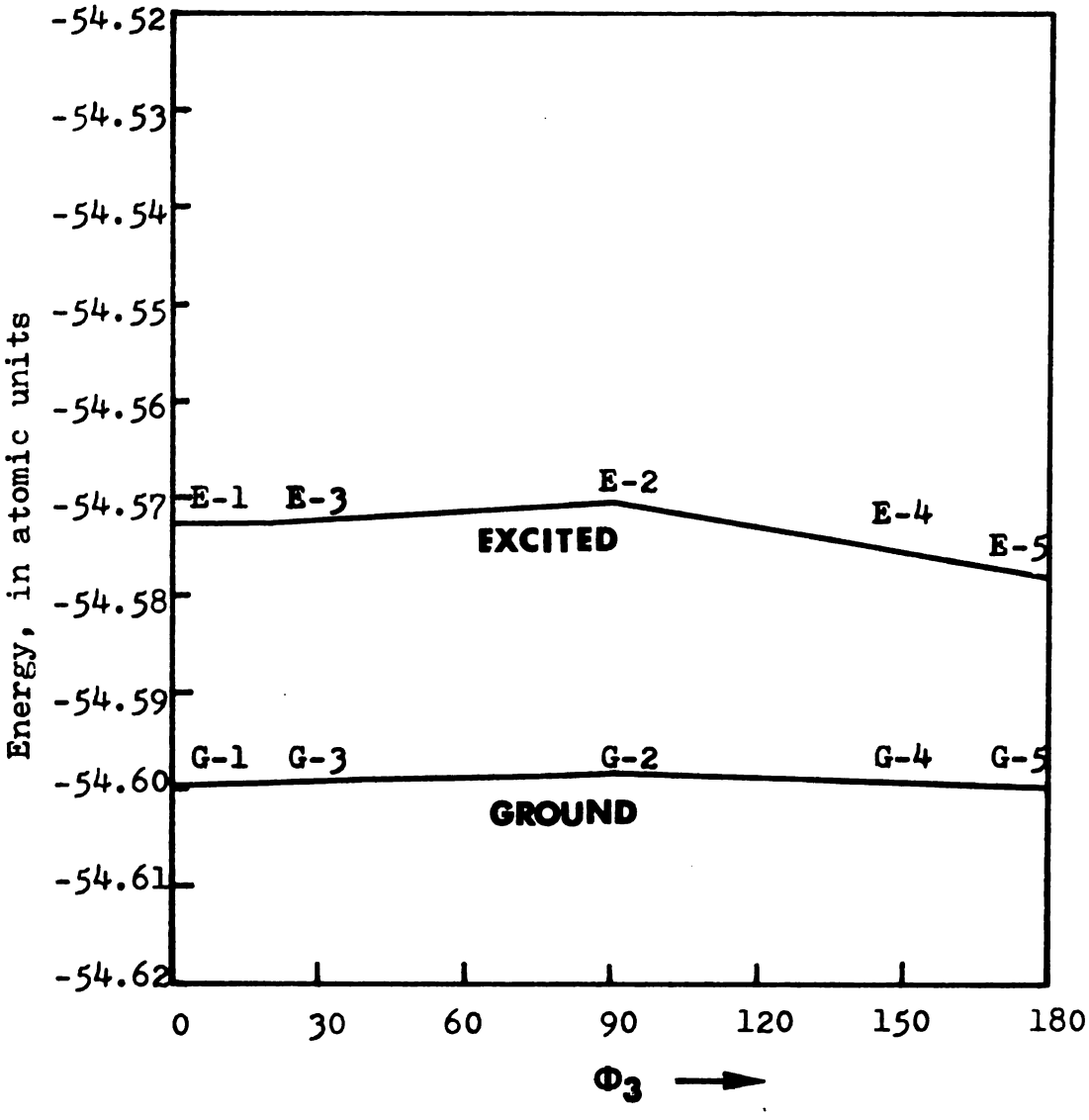

Figure 91. Energy variation for rotation of the N-ethyl group about the N-C(H_2) bond in N-ethylformamide in both the ground equilibrium geometry and transition geometry; E_a(ground) = 1.05 kcal/mol.

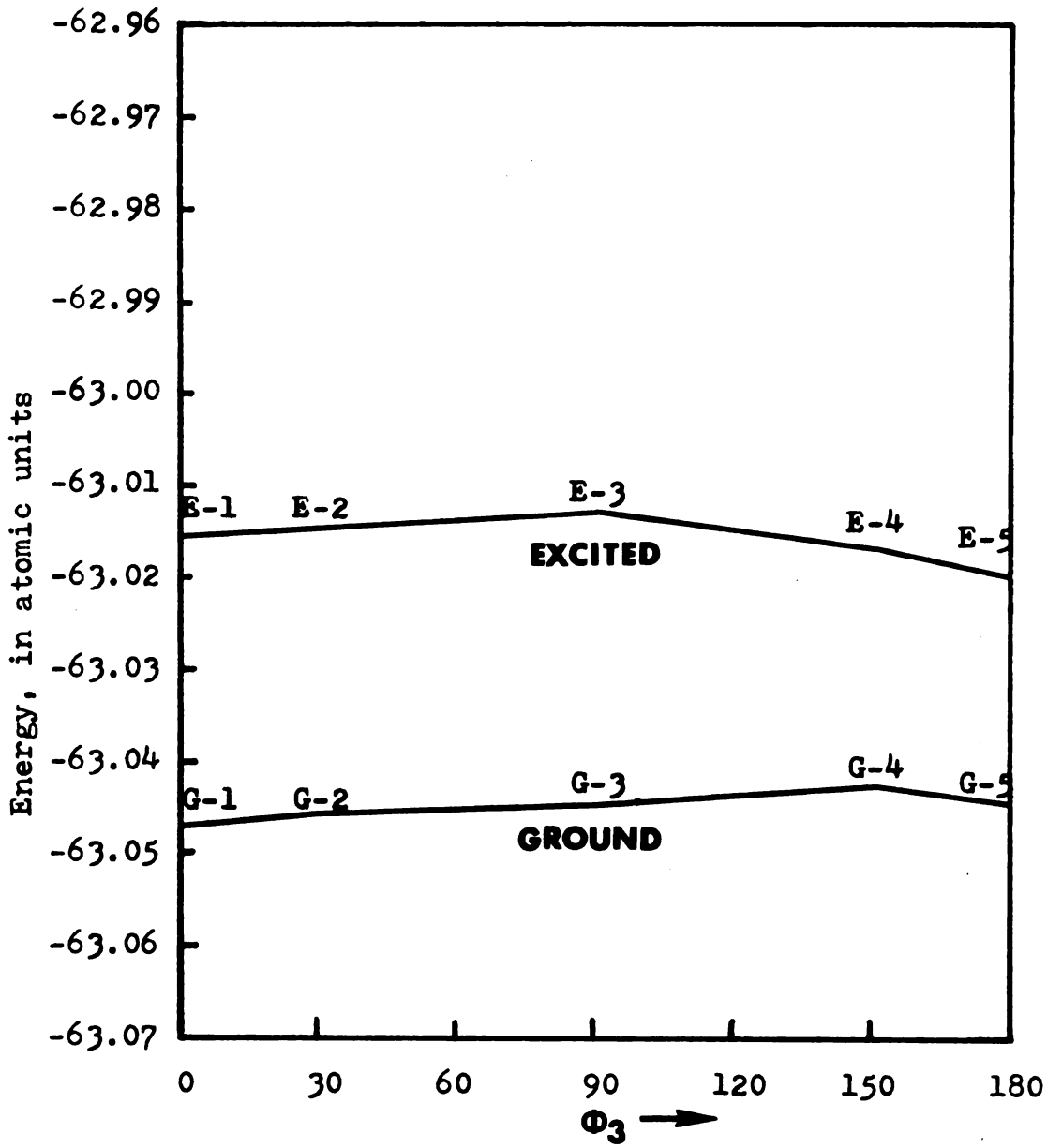

Figure 92. Energy variation for rotation of the N-ethyl group about the N-C(H_2) bond in N-ethylacetamide in both the ground equilibrium geometry and transition geometry; E_a(ground) = 2.88 kcal/mol.

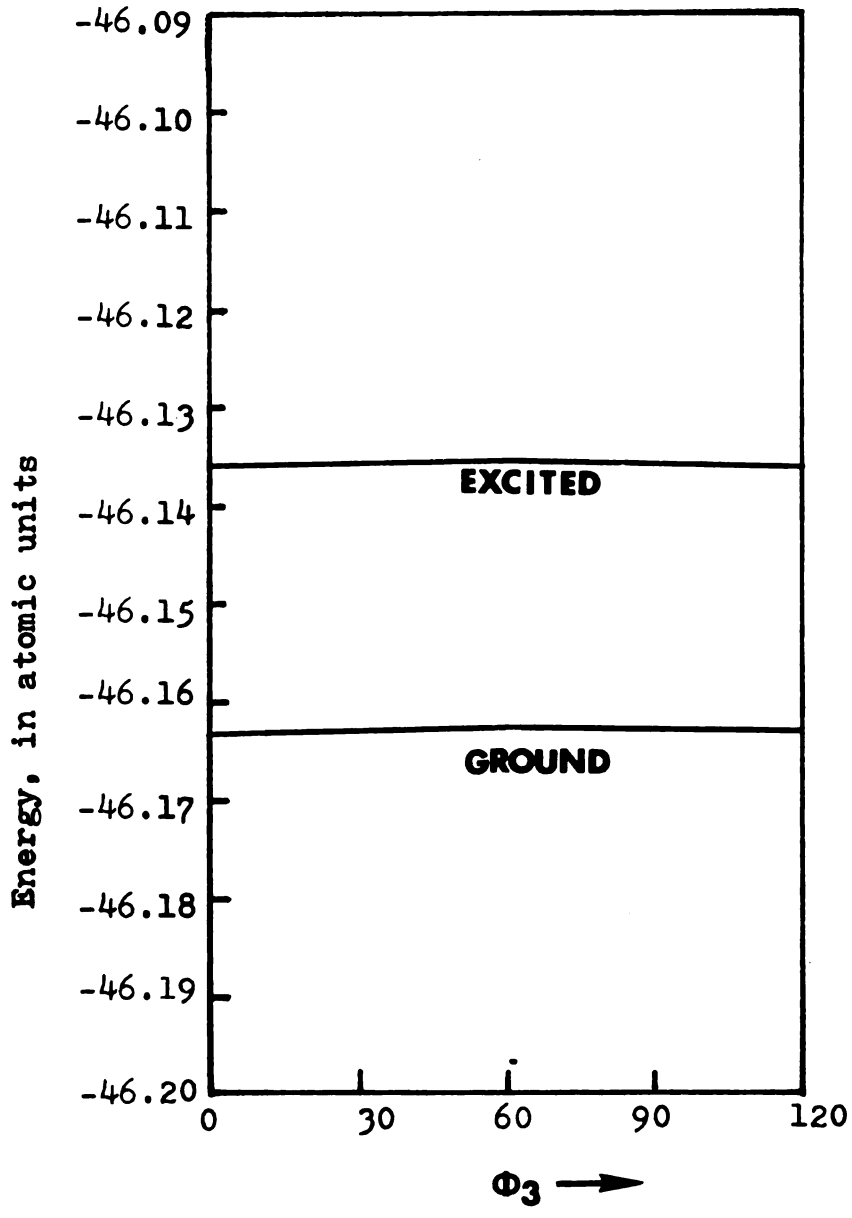

Figure 93. Energy variation for rotation of the N-methyl group about its threefold axis by angle ϕ_3 in N-methylformamide in the ground equilibrium geometry and in the transition geometry; E_a(ground) = 0.17 kcal/mol.

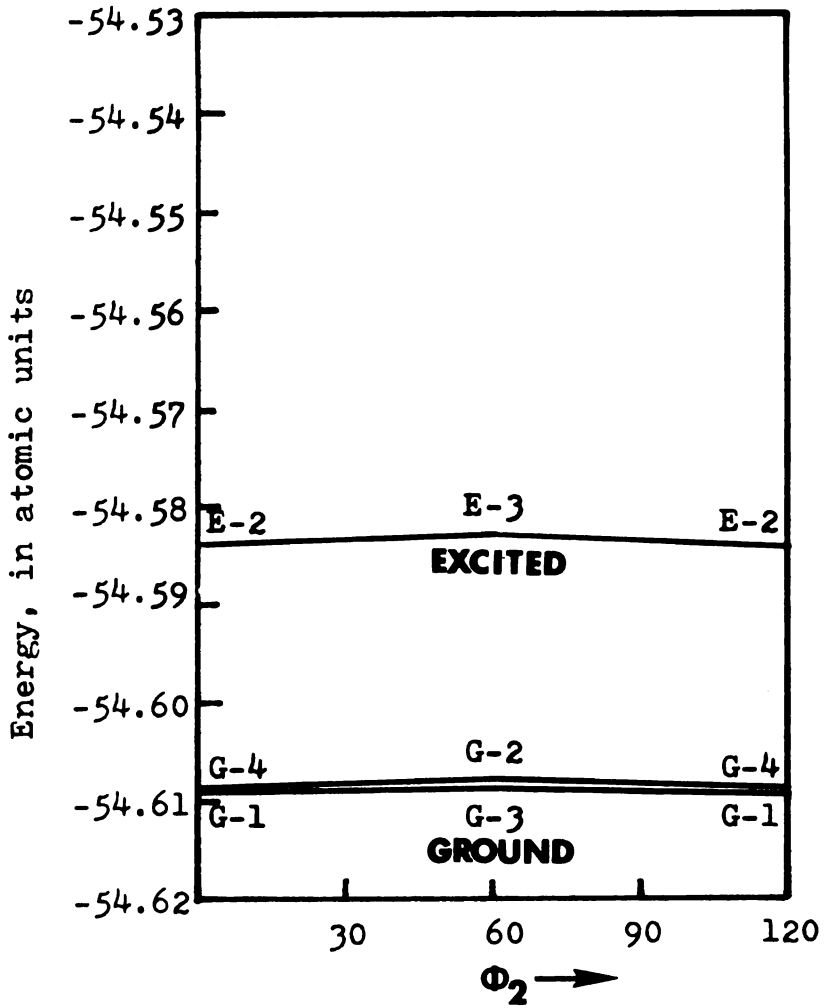

Figure 94. Energy variation for rotation of the N-CH_3 group in the transition geometry and in the ground equilibrium geometry of DMF.

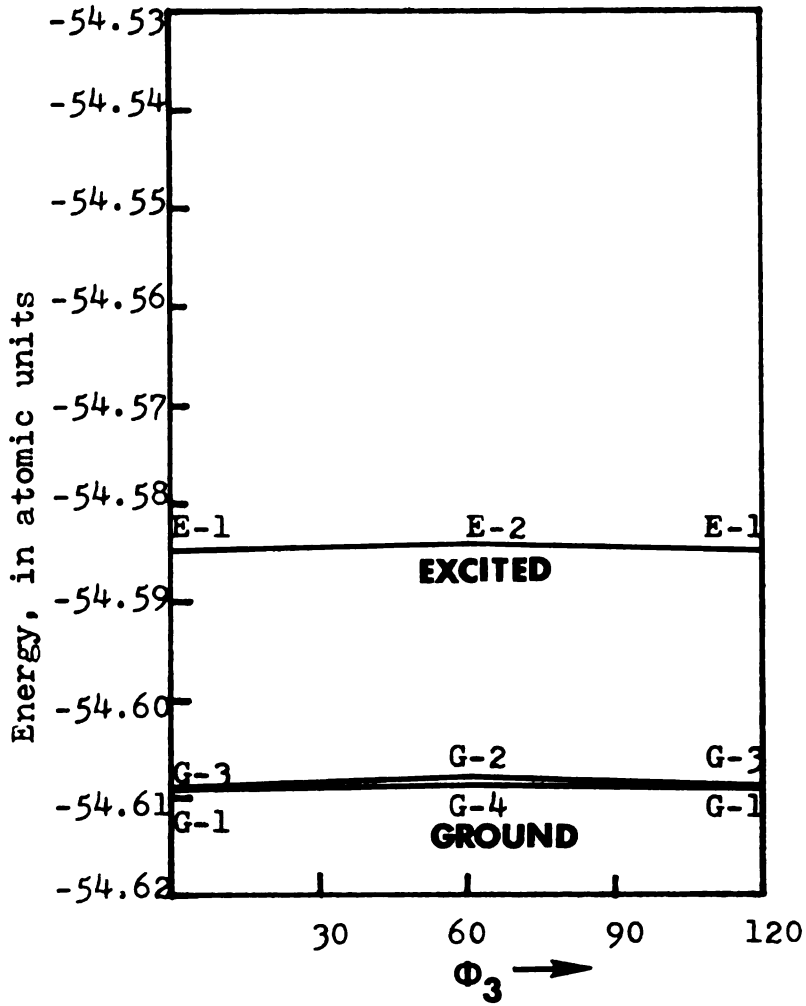

Figure 95. Energy variation for rotation of the N-CH_3 group in the transition geometry and in the ground equilibrium geometry of DMF.

N-methyl group in N-methylformamide is replaced by a $-CH_3$ group the energy for rotation about the (N-)C-R bond is increased by about 0.88 kcal/mol. This is the reason why the N-ethyl group rotational energy is usually greater than that for the N-methyl group.

C. Charge variation upon rotation about the N-C(O) bond

The computed charges on each atom for the selected amides in various conformations are shown in Figure 78 (all the charges on each atom have been multiplied by 100 in the figure).

Since formamide and N-methylacetamide have been treated by a number of theoretical approaches,[90,237] we will examine these two compounds more closely and compare the results with those obtained by other methods.

The charge distributions for formamide and N-methylacetamide obtained in the INDO calculations are shown in Table 47. The values are similar to those obtained by the CNDO/2 method.[90] The sum of charges on the atoms of the peptide group (i.e., the C and O atoms of the C = O group, N, the carbon atoms of the carbonyl substituent and the α carbons of the nitrogen substituents) is also negative, in agreement with the results of the CNDO/2 method. This produces a reasonable basis for the partial double-bond character postulated in resonance theory for the central C-N bond.

The variation of charges with θ, the dihedral angle for rotation about the peptide bond, in DMF,

Table 47. Charge distributions in formamide and N-methylacetamide (in electronic units) calculated by the INDO method.

Formamide		N-methylacetamide[b]	
Atom	Charge (electrons)	Atom	Charge (electrons)
O	-0.397	O	-0.418
C(O)	0.455	C(O)	0.429
N	-0.232	N	-0.202
H(C)	-0.083	H(N)	-.103
H_1(N)[a]	0.140		
H_2(N)[a]	0.116		

[a] H_1 and H_2 are hydrogen atoms *cis* and *trans* to the C = O group, respectively.

[b] For *cis*-N-methylacetamide, where the N-methyl group is *cis* to the C = O group. This is the same conformation as that in Reference 90, but designated there as the *trans* form.

formamide, DMA, DMTFA, and N-methyl-N-ethylformamide is shown in Figures 96-100. The variation of the charges is sharpest for the nitrogen and oxygen atoms of the peptide bond when the amides are twisted from the equilibrium geometry to that of the transition state. For symmetrically N,N-disubstituted amides, Figures 96-99, the partial charges on the atoms of the amido group are identical at $\theta = 0°$ and $\theta = 180°$, while for unsymmetrically N,N-disubstituted amides, e.g., N-methyl-N-ethylformamide, the partial charges on the amido group atoms are different at $\theta = 0°$ and $\theta = 180°$ (but the difference is negligible). For the remaining atoms, excluding those of the amido group, in symmetrically and unsymmetrically substituted amides, the variation of the partial charges is unsymmetrical since the electronic environment is completely different when $\theta = 0°$ and $\theta = 180°$. For the symmetrically N,N-disubstituted amides, the cis and trans atoms are exchanged, while for unsymmetrically substituted amides there is no relationship between the two forms.

As the peptide bond is twisted from the planar arrangement ($\theta = 0°$ or $180°$) to the transition state ($\theta = 90°$), we find that the charges on the carbonyl oxygen and carbon atoms are decreased, while the charge on nitrogen is increased. These results are consistent with the charges predicted on the basis of the resonance structures I and II suggested by Pauling[208] (discussed in

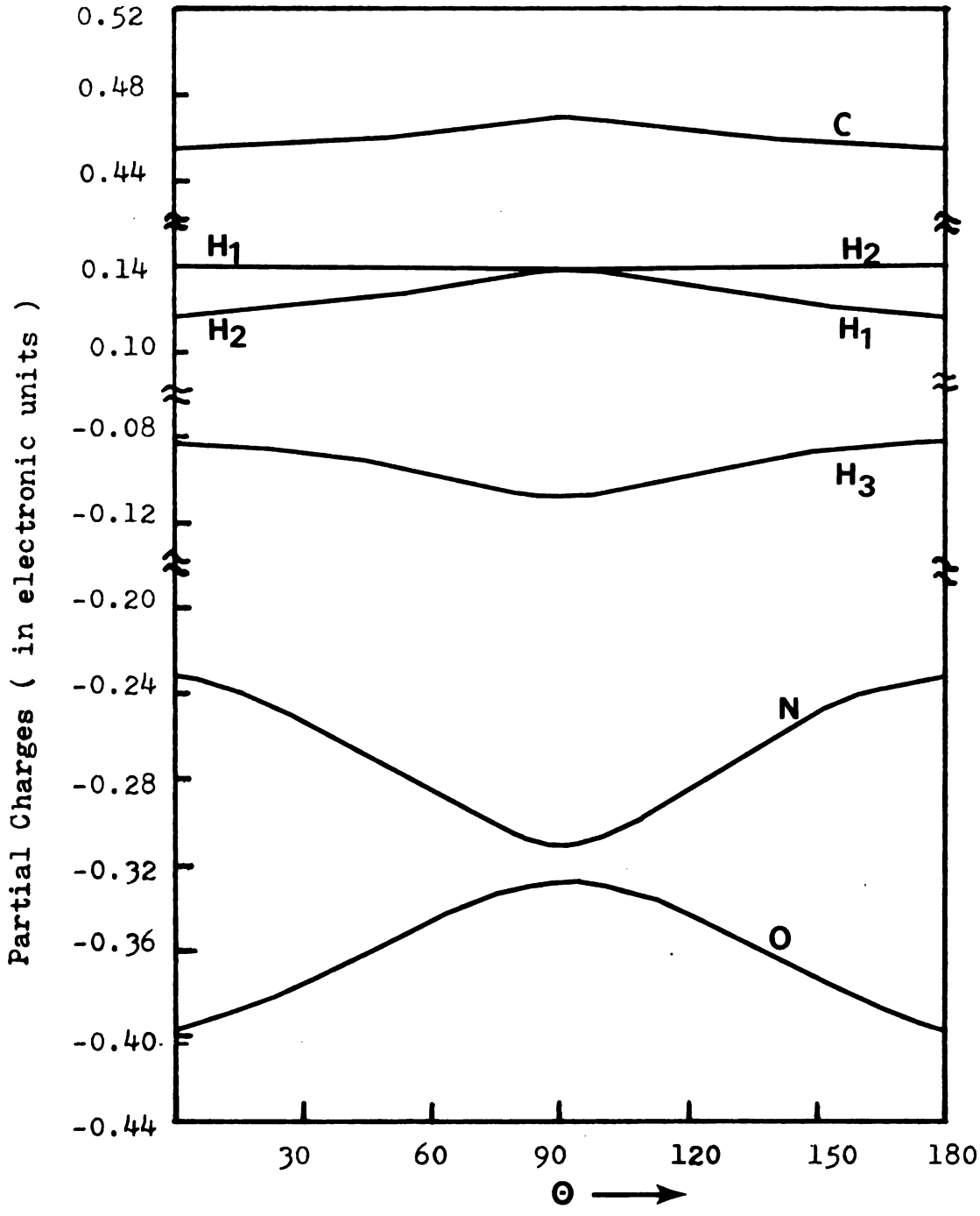

Figure 96. Variation with θ of the partial charges on the atoms of formamide. The numbering of the atoms corresponds to that in Figure 79.

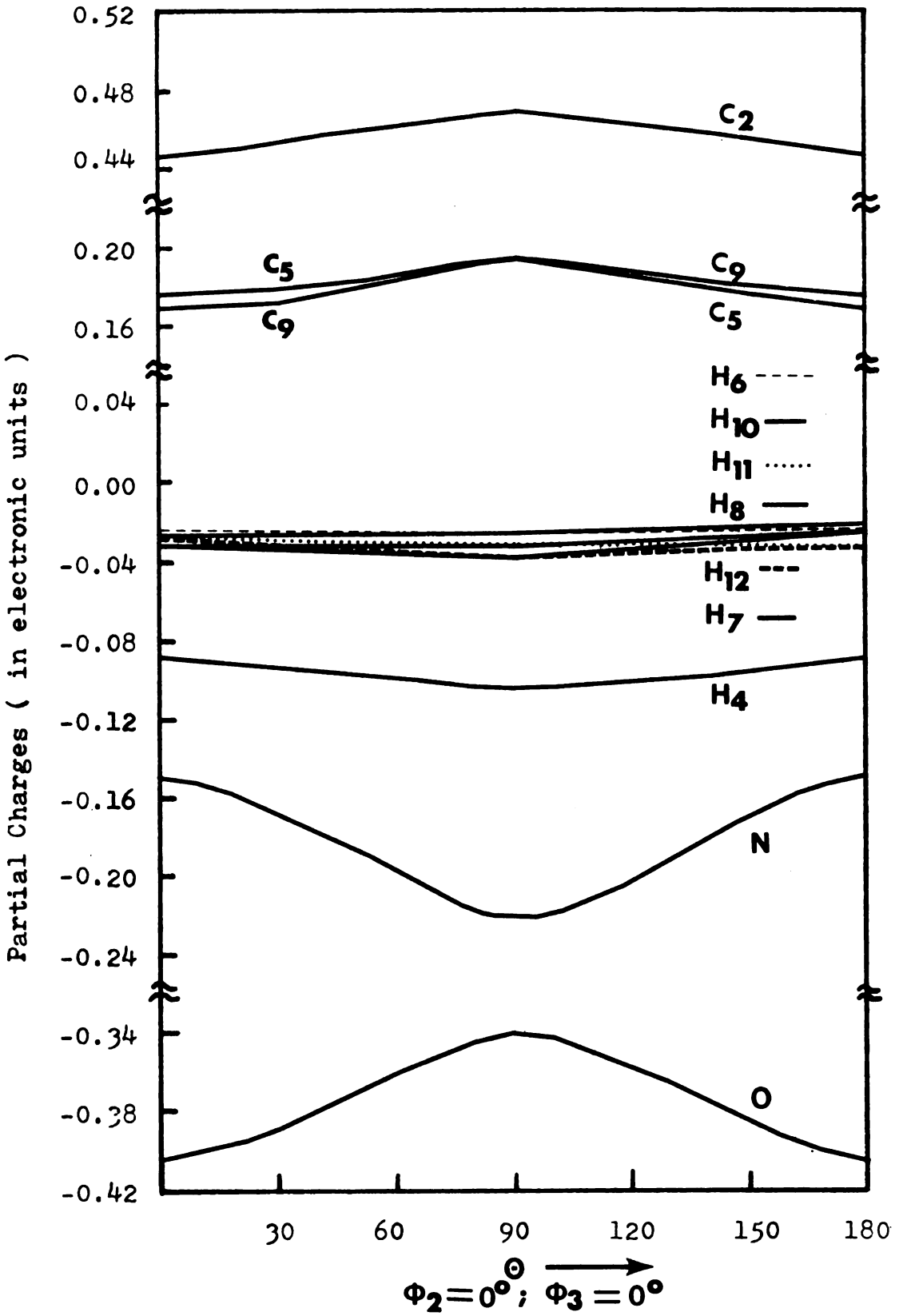

Figure 97. Variation with θ of the partial charges on the atoms of N,N-dimethylformamide.

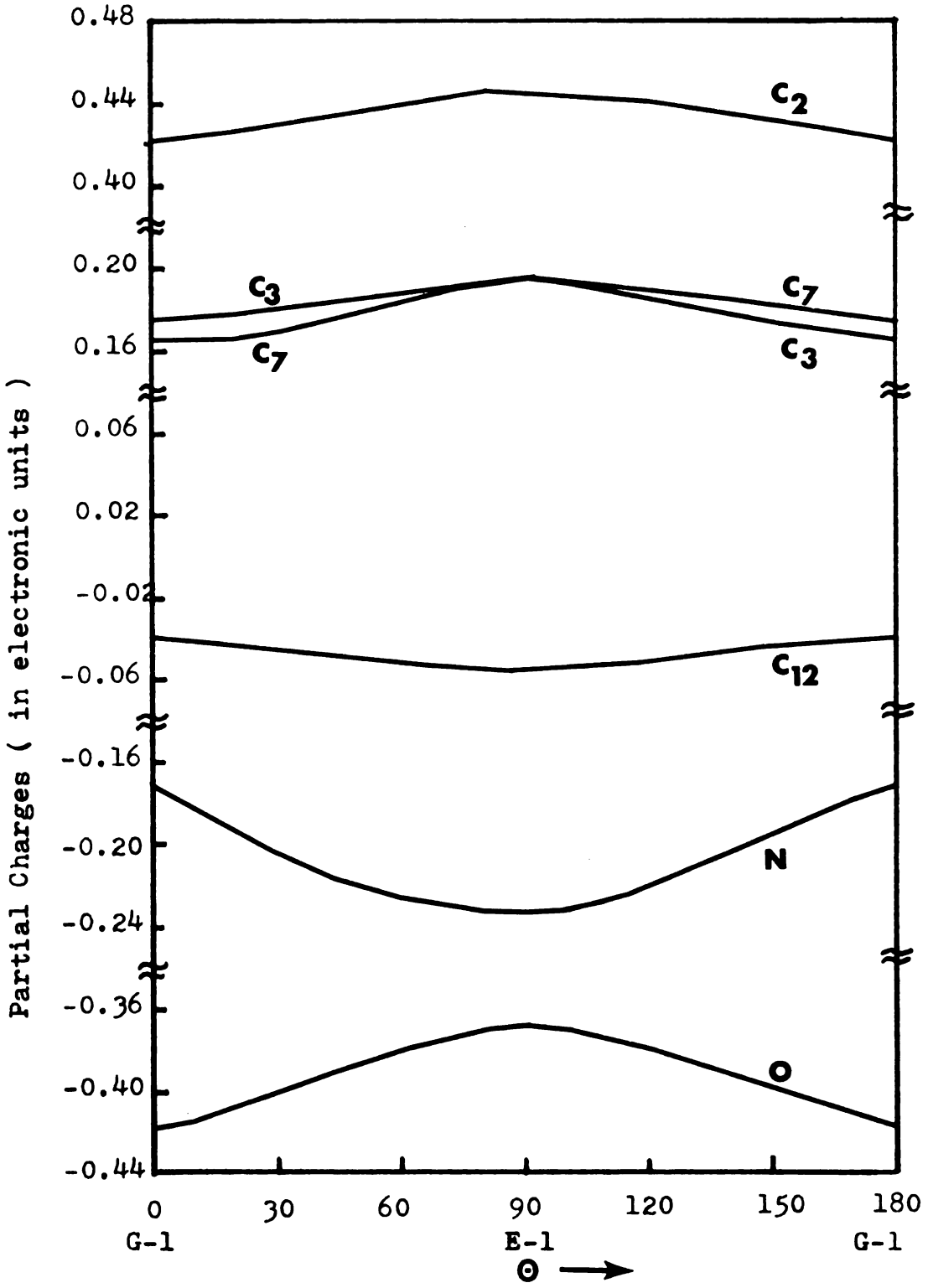

Figure 98. Variation with θ of the partial charges on the atoms of N,N-dimethylacetamide.

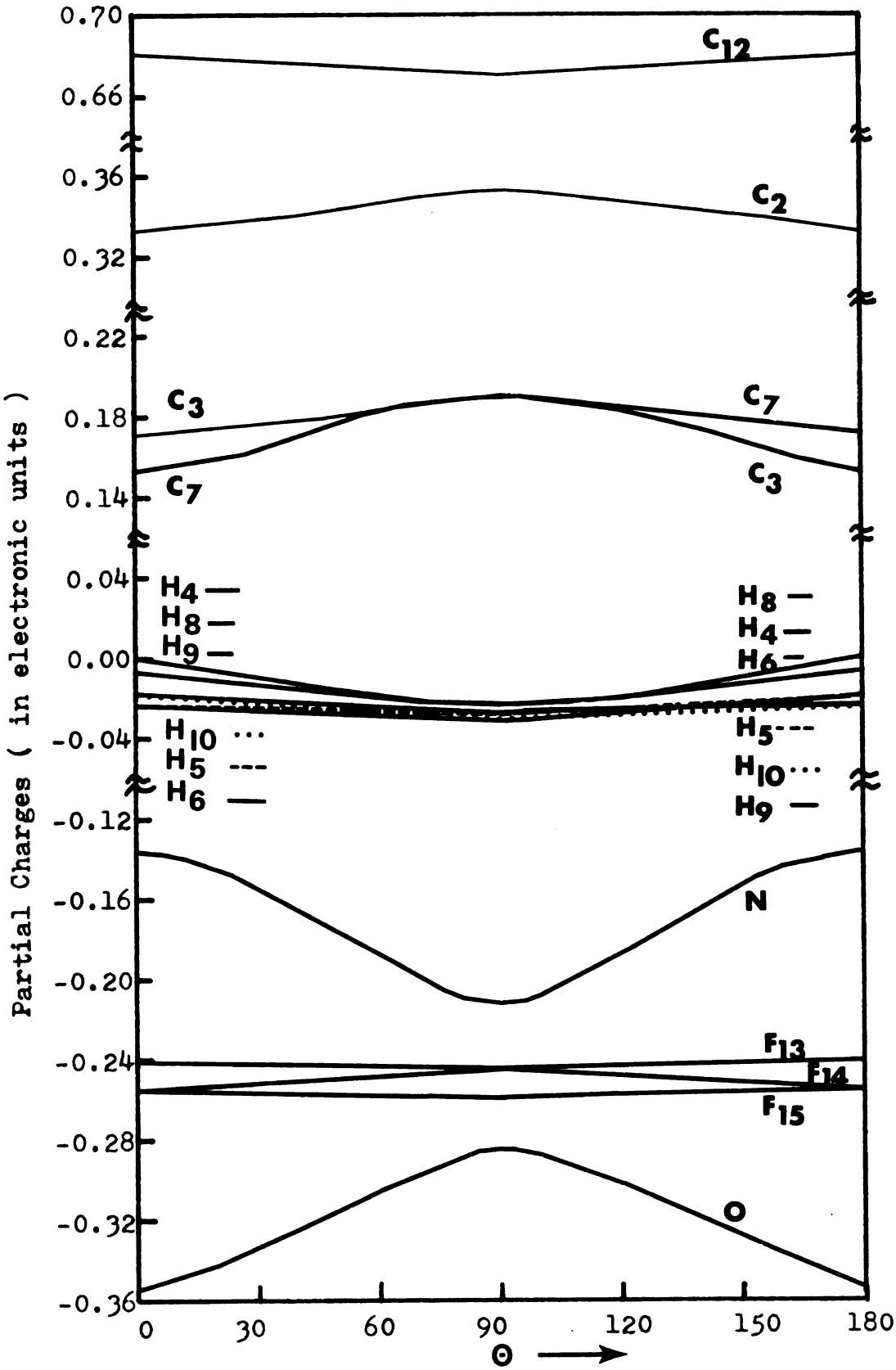

Figure 99. Variation with θ of the partial charges on the atoms of the peptide bond in N,N-dimethyltrifluoroacetamide.

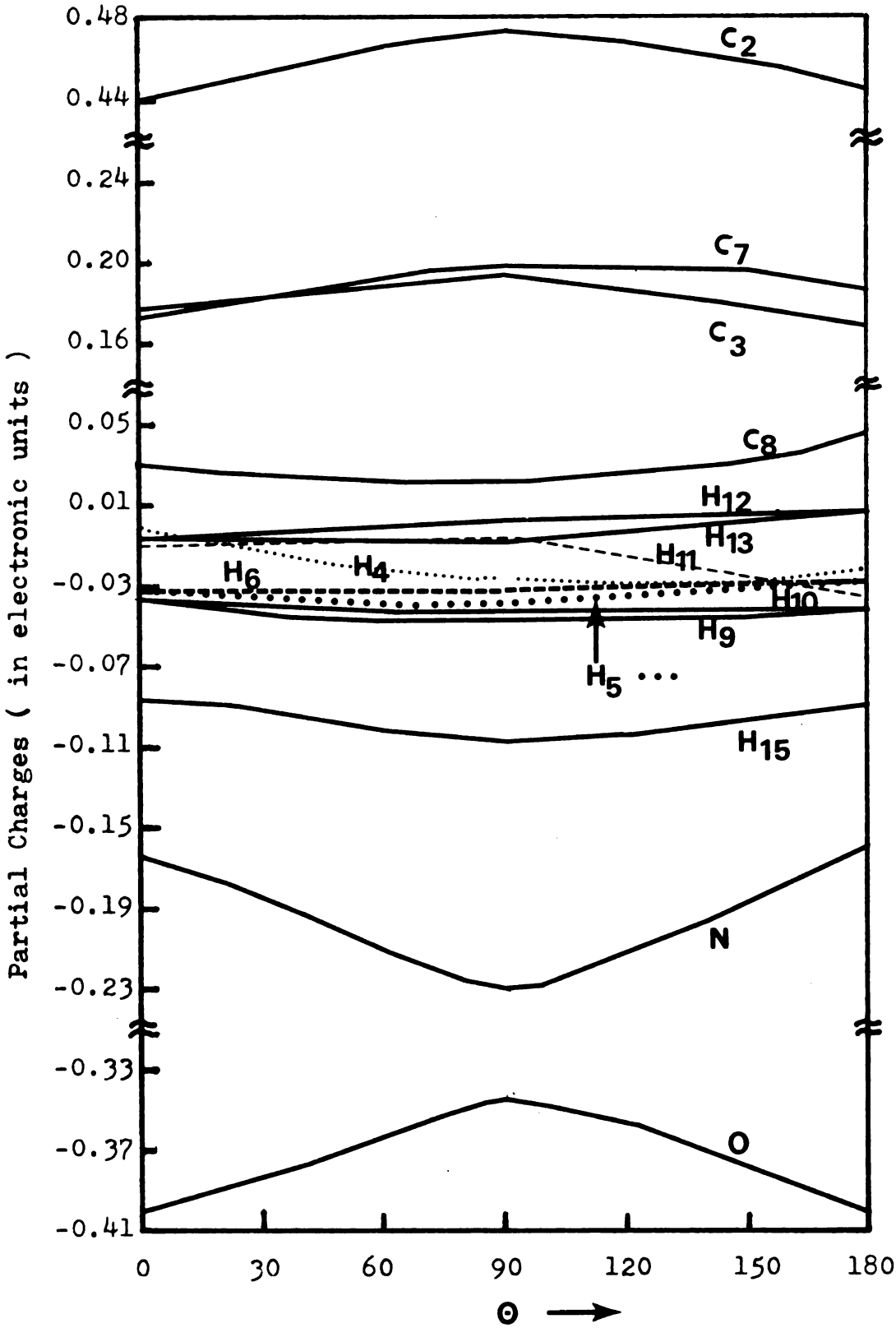

Figure 100. Variation with θ of the partial charges on the atoms of the peptide bond of N-methyl-N-ethyl-formamide.

the Theoretical section of this part of the thesis). In resonance theory it is predicted that in the ground state geometry structures I and II contribute about equally, while in the transition state geometry any contribution of structure II is impossible since the fragment RCO is perpendicular to the fragment NR_2. Therefore, compared with the ground state, the charges on oxygen and carbon will be decreased in the transition state while the charge on nitrogen will be increased.

Assuming that a hydrogen bond is to be formed, we will find that a departure of angle θ from 0° or 180° toward 90° will lead to a weaker hydrogen bond. Expressed in another way, we will find that a hydrogen bond will stabilize the energy of the ground state more than that of the transition state, since there is more charge on oxygen in the ground state. Hence the energy for rotation about the N-C(O) bond will be increased as the hydrogen bond is formed.

D. Variation of charges with respect to the dihedral angles ø

The variation of the partial charges with respect to ø, the dihedral angle for rotation of the methyl about the bond to the methyl carbon (or the ethyl group about the $N-CH_2$ bond), in DMF, DMA, DMTFA, N-methylformamide, N-methylacetamide, N-ethylformamide, and N-ethylacetamide is shown in Figures 101-115. The variation of the partial

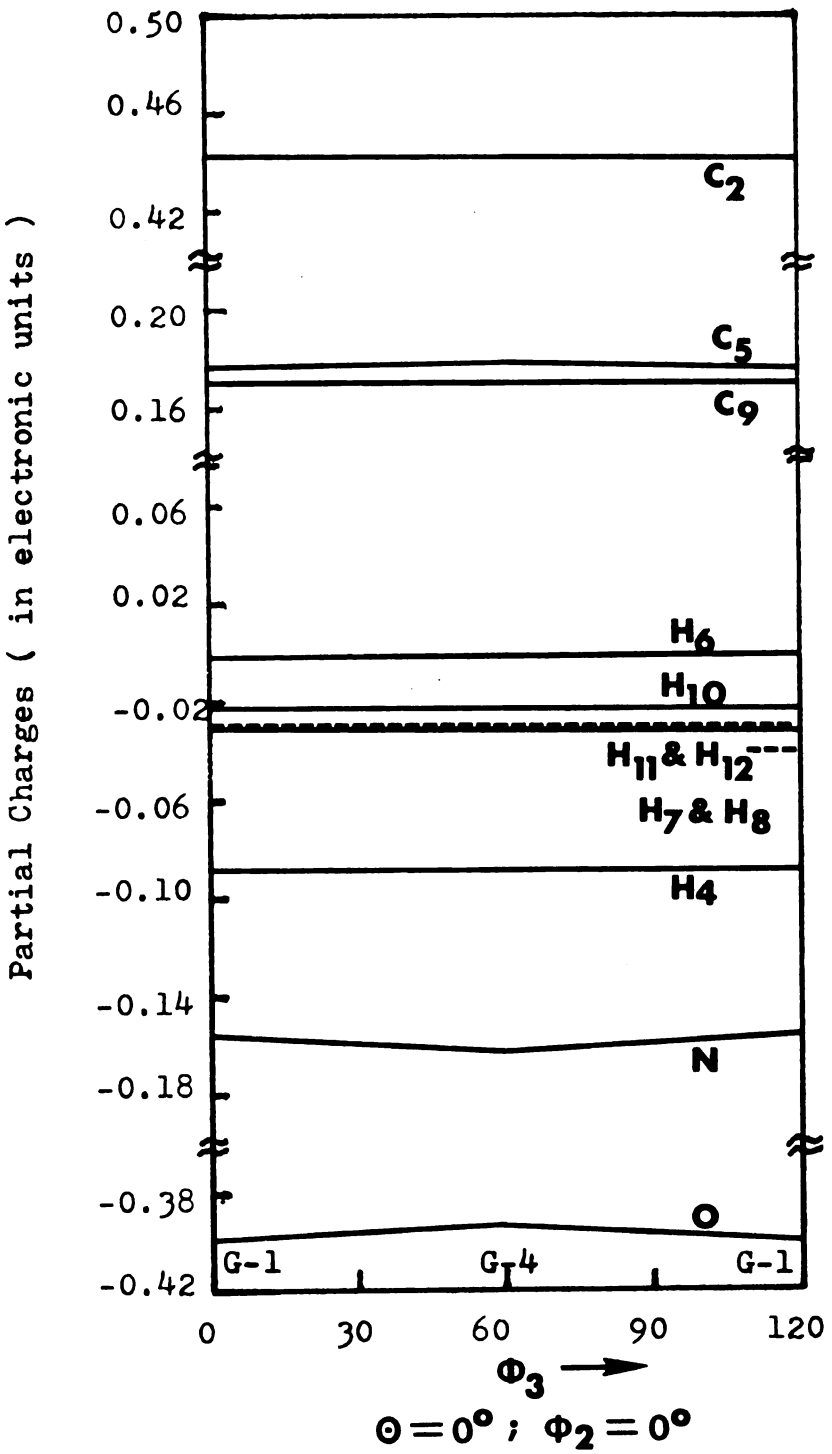

Figure 101. Variation with ϕ_3 of the partial charges on the atoms of the N-CH_3 group of N,N-dimethylformamide. The notations G-1, G-4 given at the bottom of the figure refer to choices of dihedral angles listed in Table 45.

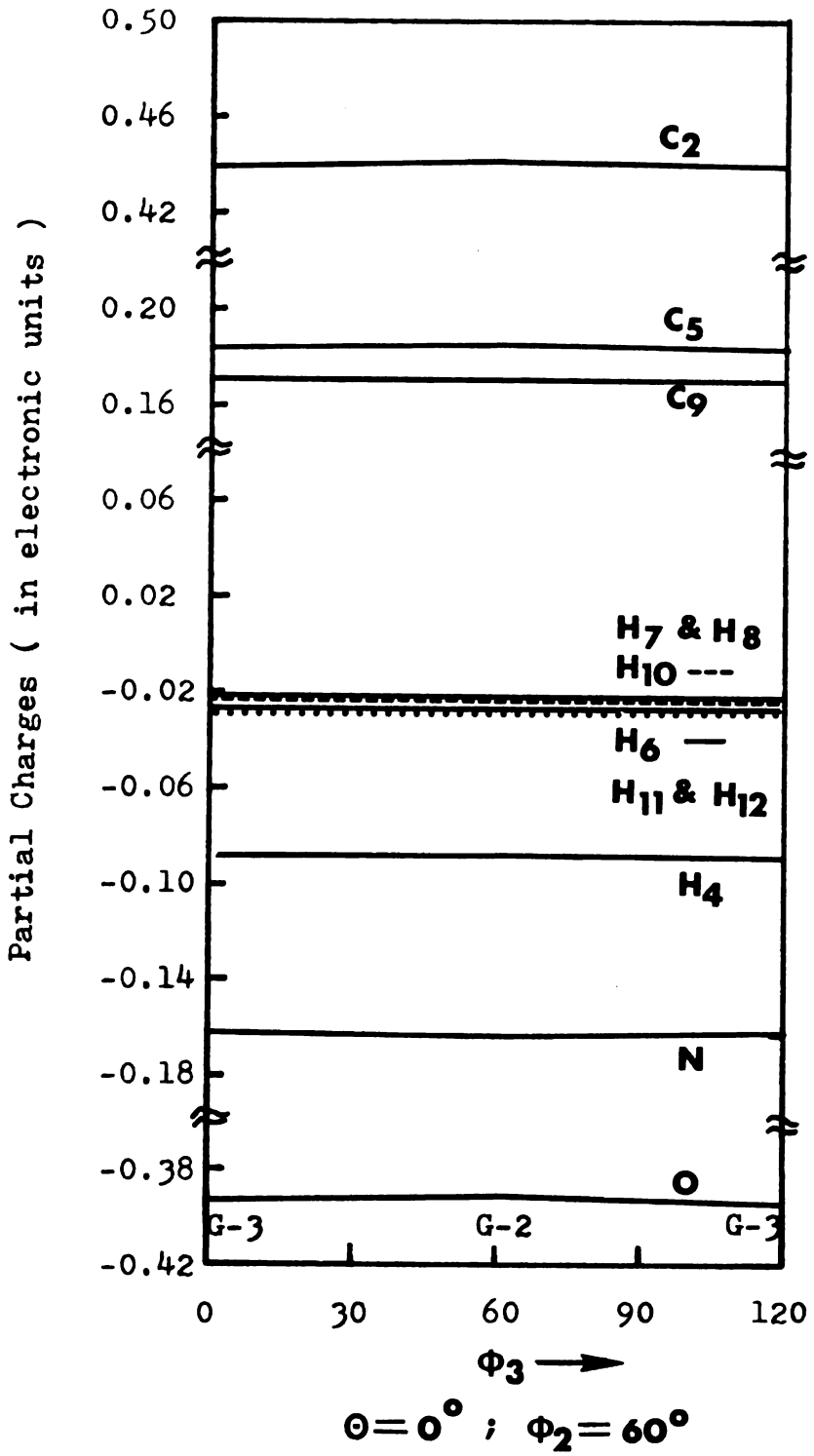

Figure 102. Variation with ϕ_3 of the partial charges on the atoms of the N-methyl group of N,N-dimethylformamide.

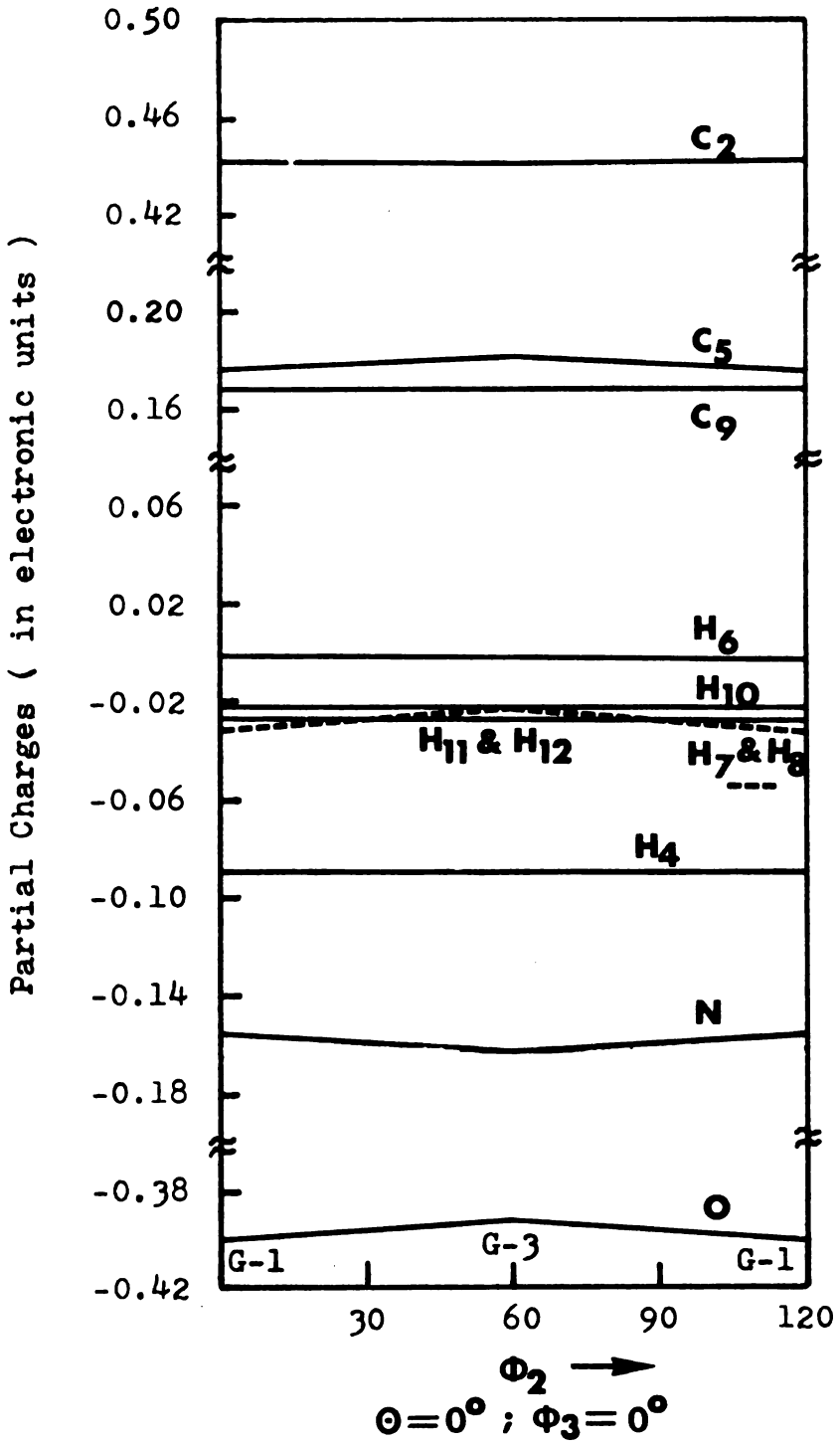

Figure 103. Variation with ϕ_2 of the partial charges on the atoms of the N-methyl group of N,N-dimethylformamide.

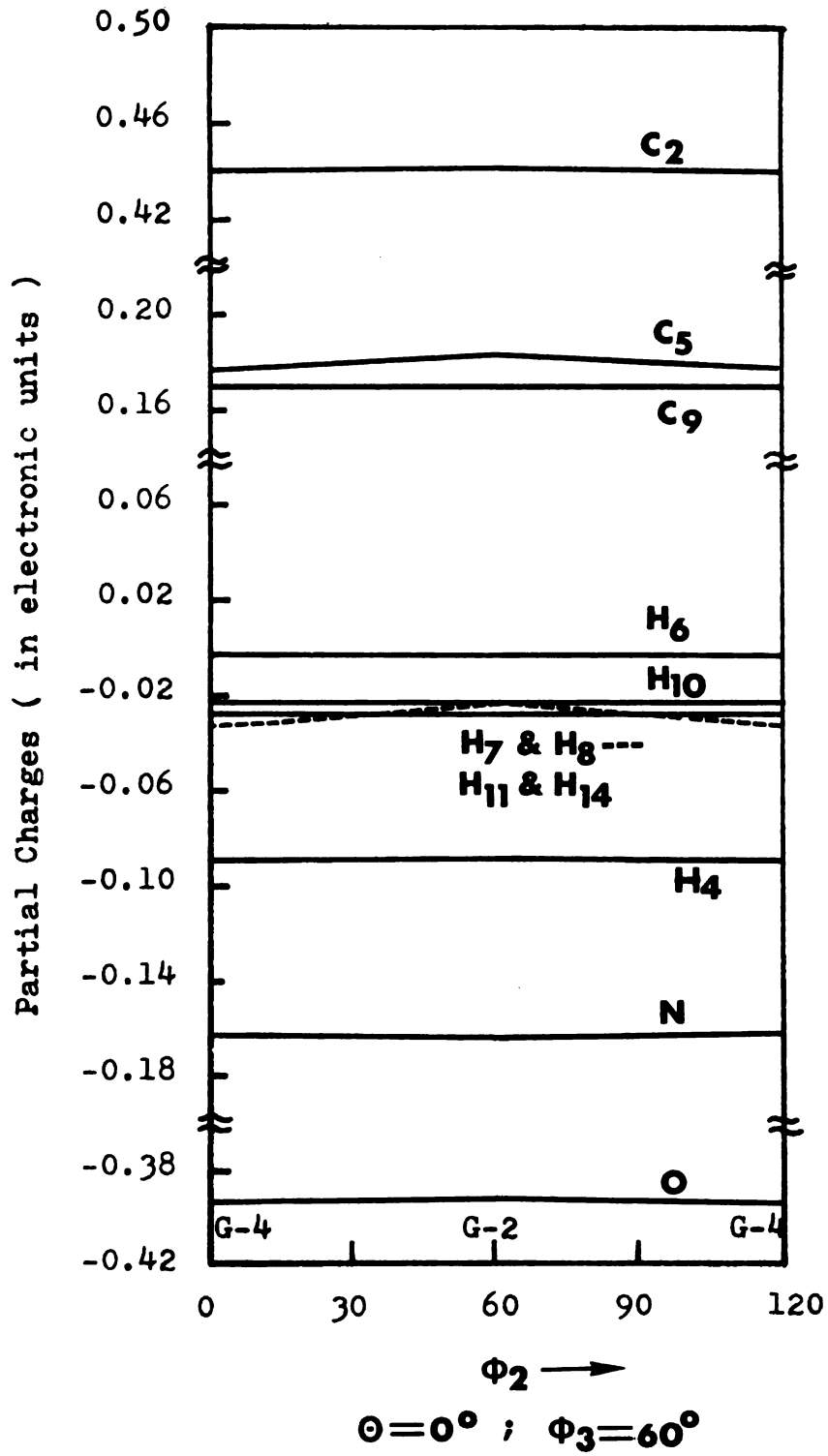

Figure 104. Variation with ϕ_2 of the partial charges on the atoms of the N-methyl group of N,N-dimethylformamide.

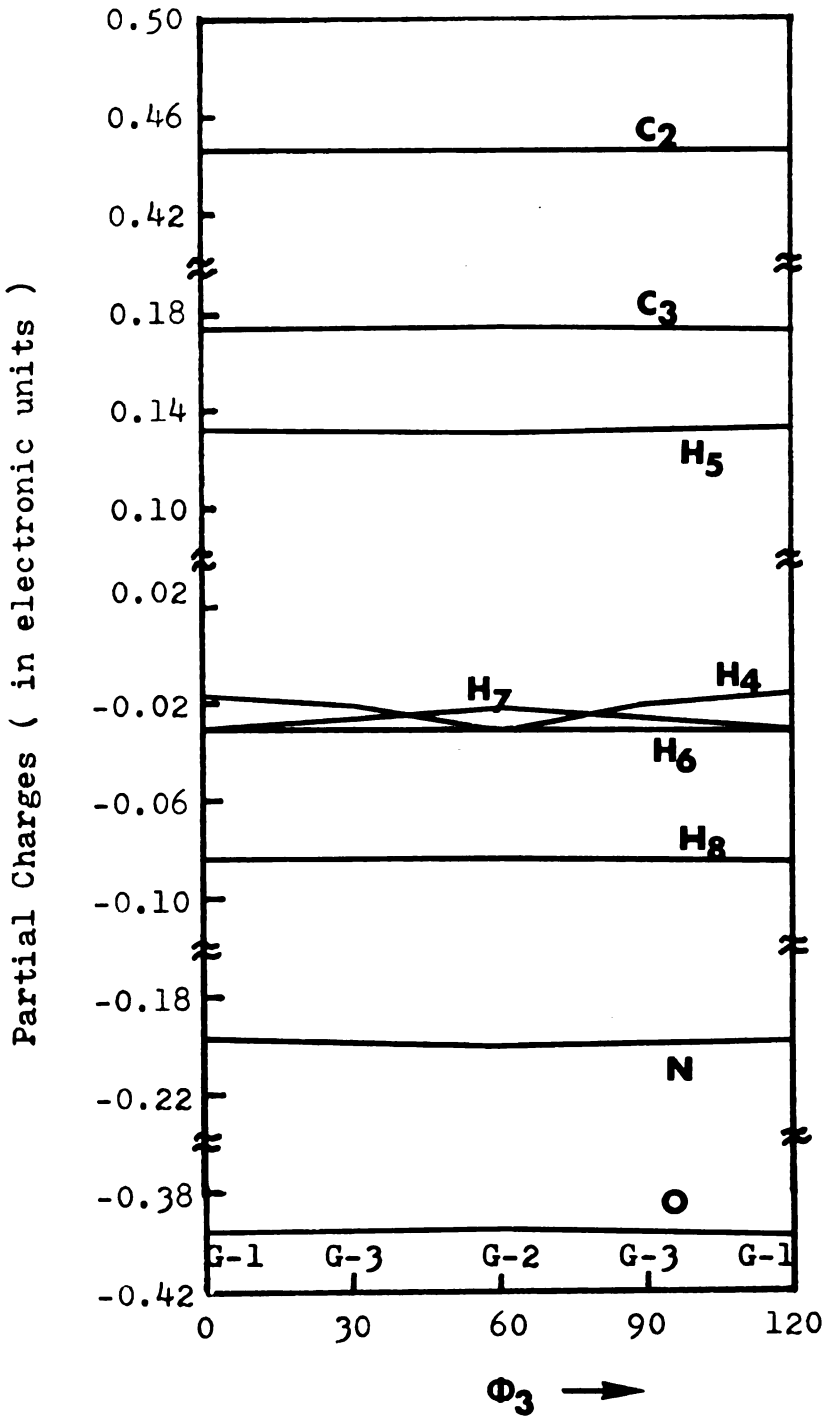

Figure 105. Variation with ϕ_3 of the partial charges on the atoms of the N-methyl group of N-methylformamide.

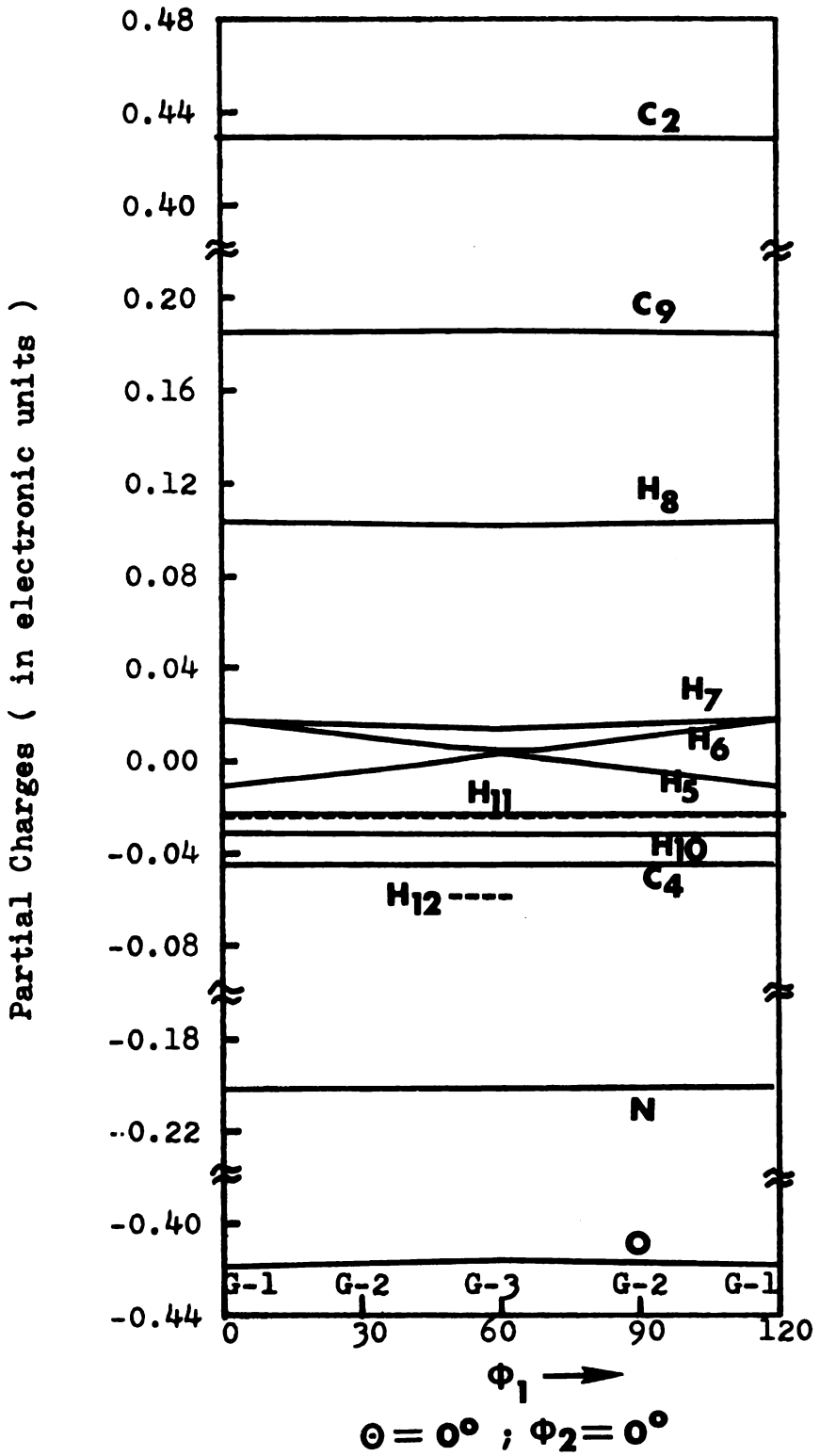

Figure 106. Variation with ϕ_1 of the partial charges on the atoms of the carbonyl-methyl group of N-methylacetamide.

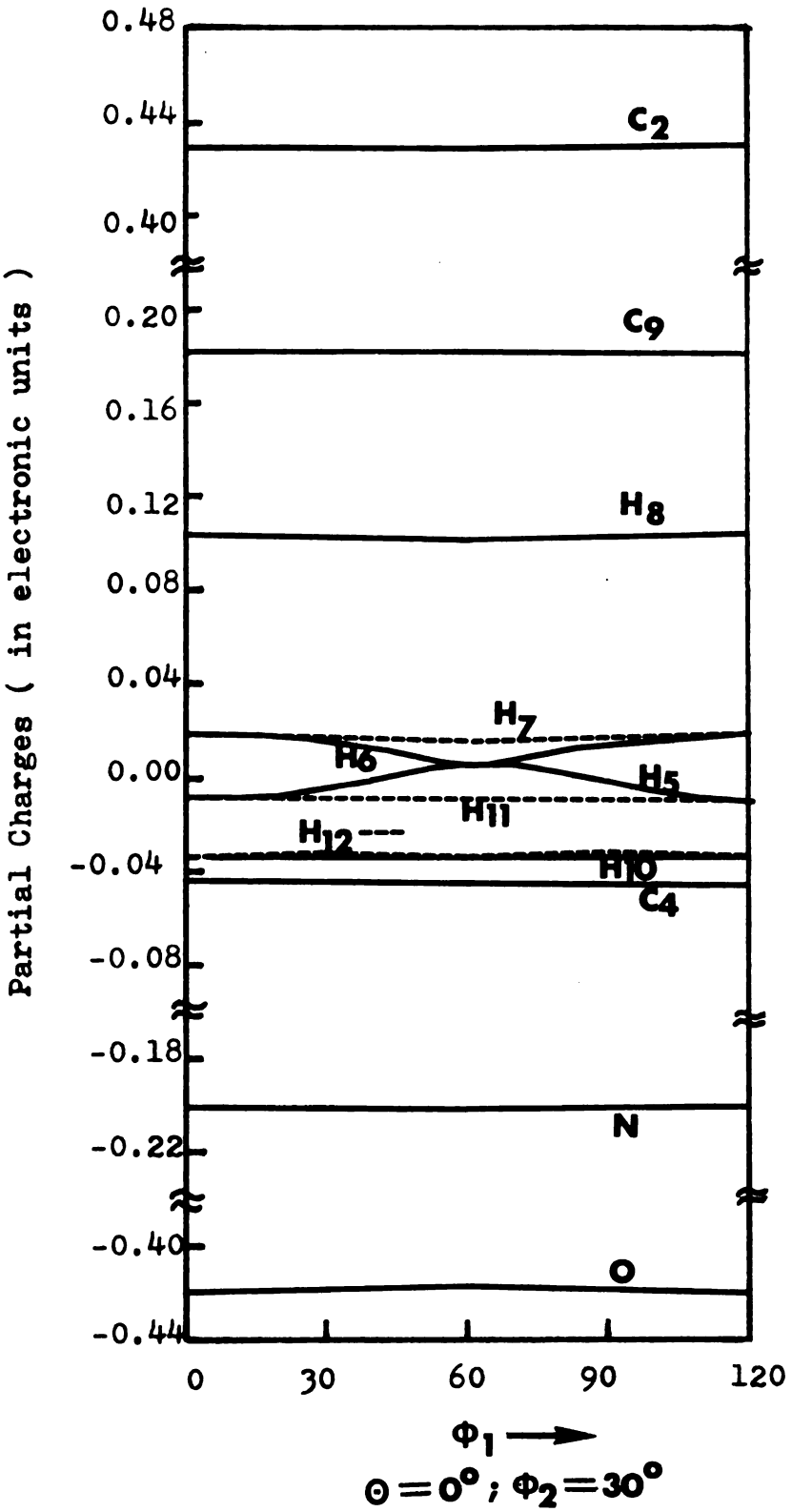

Figure 107. Variation with ϕ_1 of the partial charges on the atoms of the carbonyl-methyl group of N-methylacetamide.

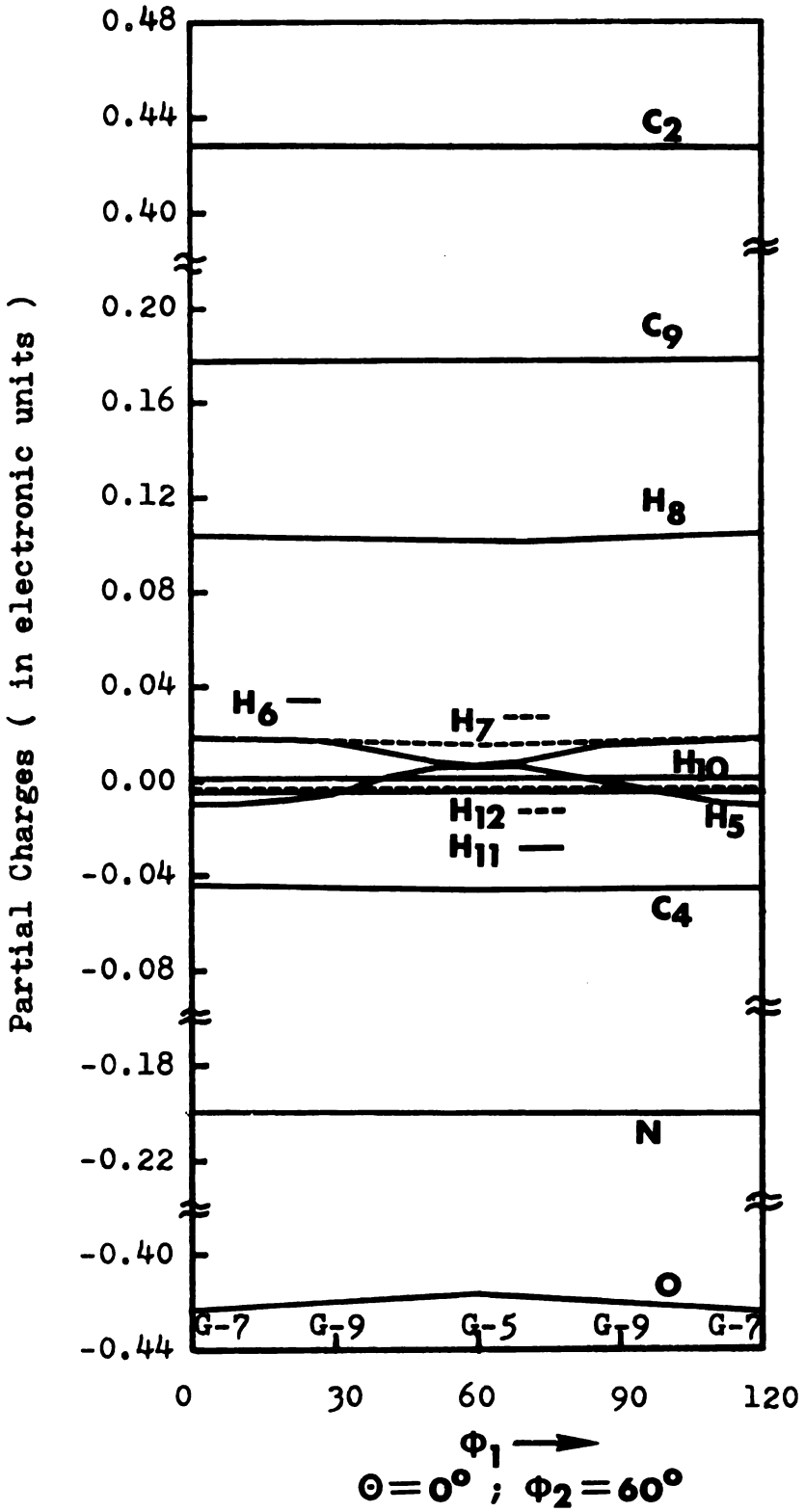

Figure 108. Variation with ϕ_1 of the partial charges on the atoms of the carbonyl-methyl group of N-methylacetamide.

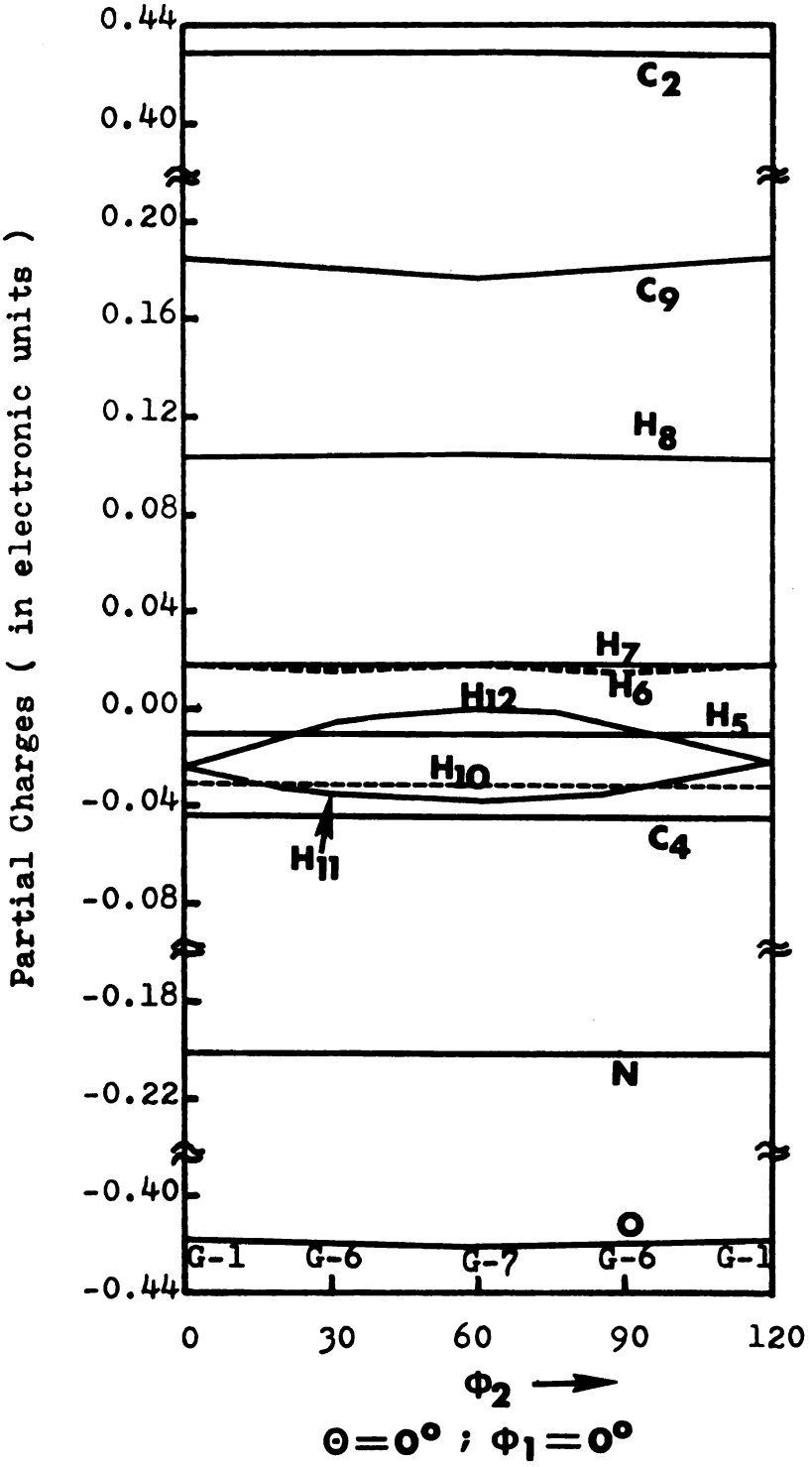

Figure 109. Variation with ϕ_2 of the partial charges on the atoms of the N-methyl group of N-methylacetamide.

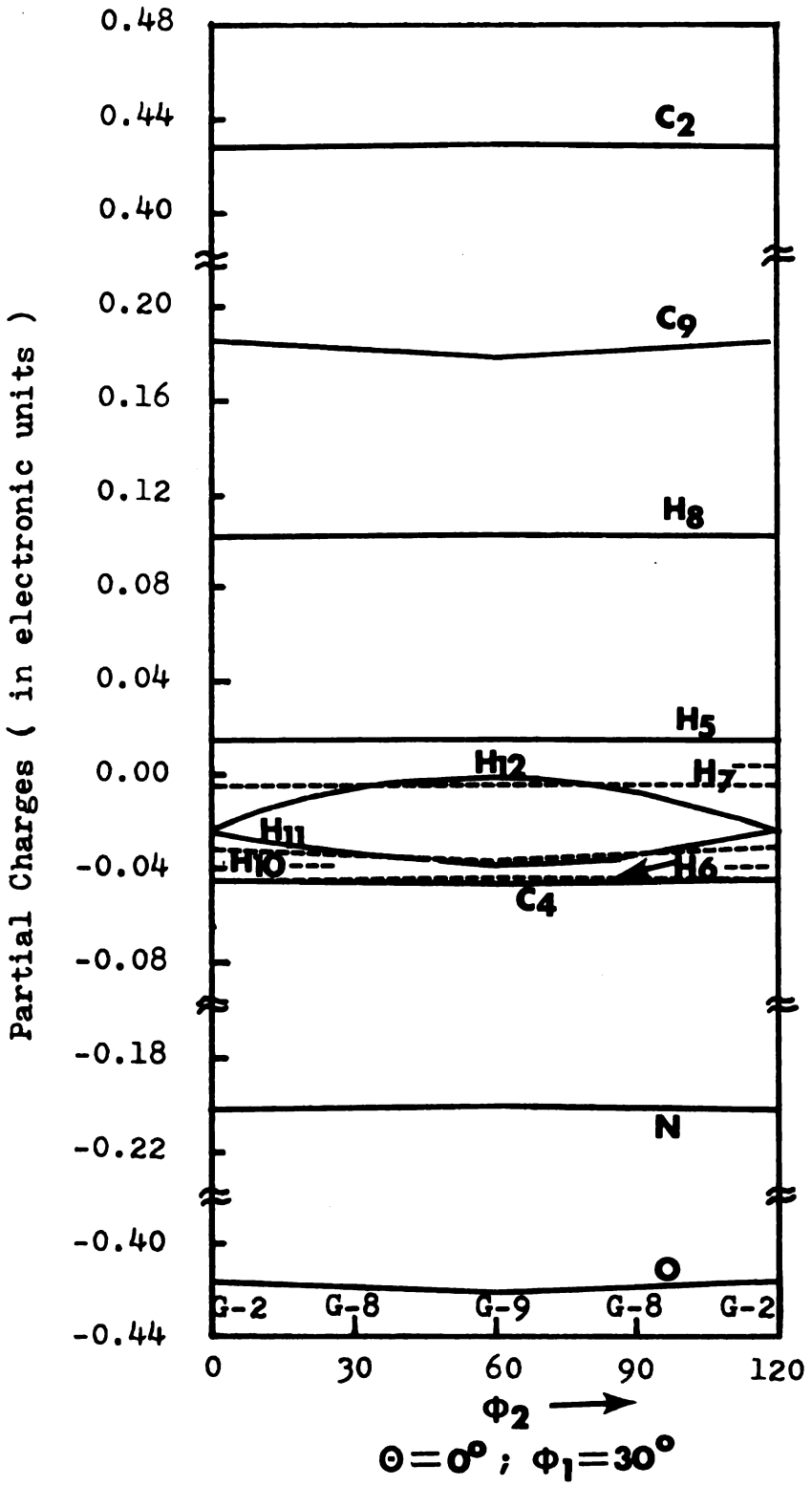

Figure 110. Variation with ϕ_2 of the partial charges on the atoms of the N-methyl group of N-methylacetamide.

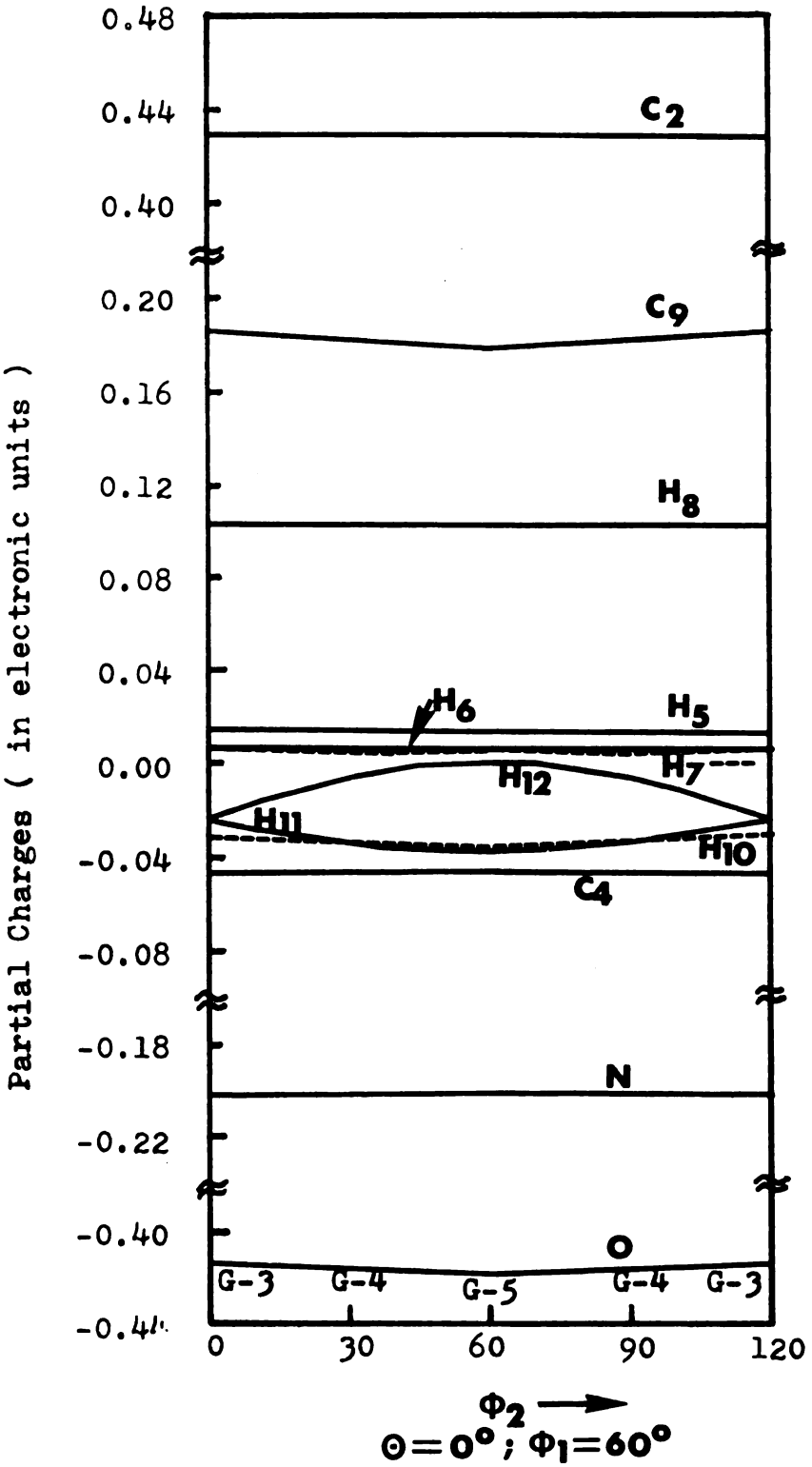

Figure 111. Variation with ϕ_2 of the partial charges on the atoms of the N-methyl group of N-methylacetamide.

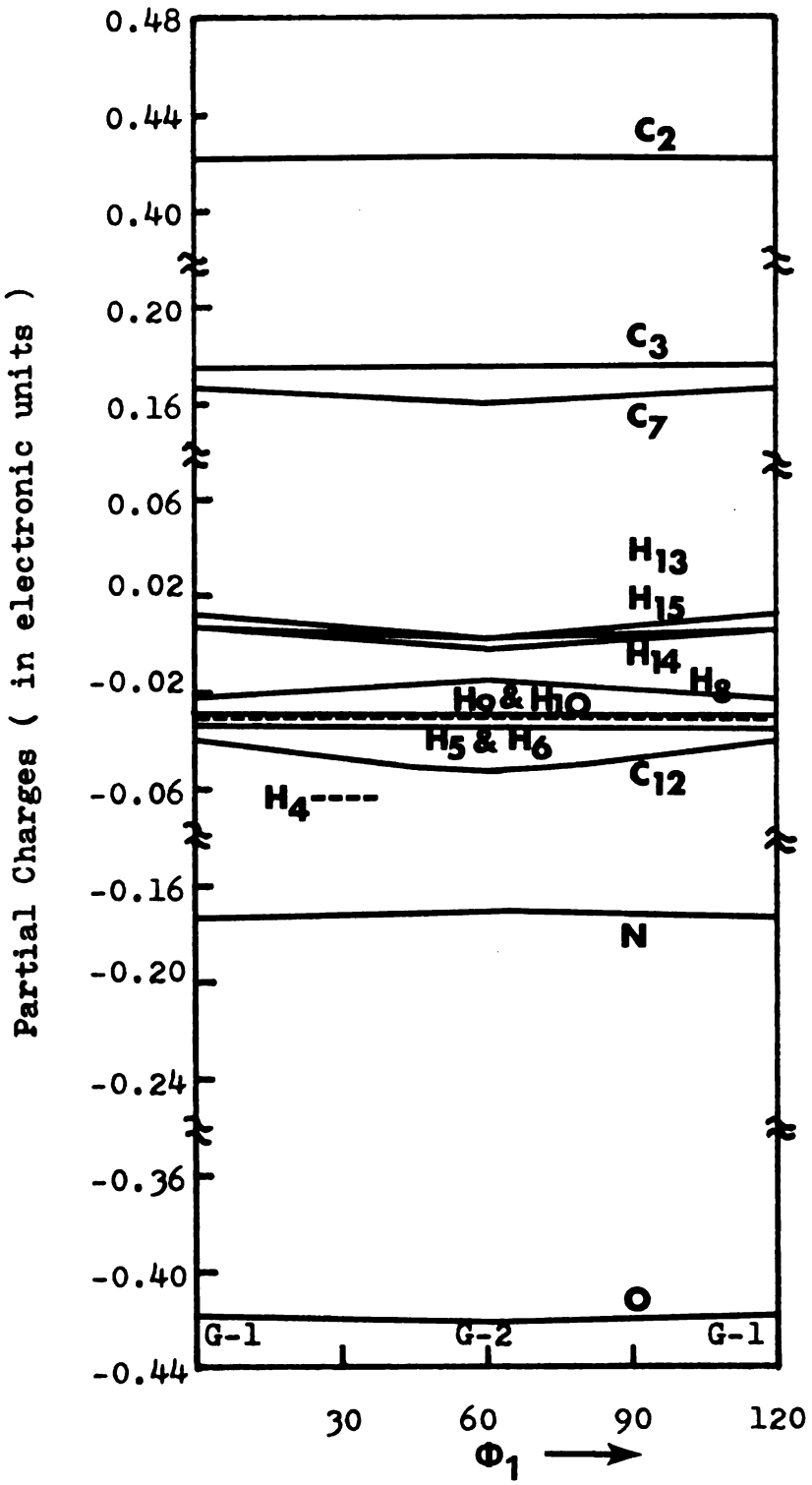

Figure 112. Variation with ϕ_1 of the partial charges on the atoms of the carbonyl-methyl group of N,N-dimethylacetamide.

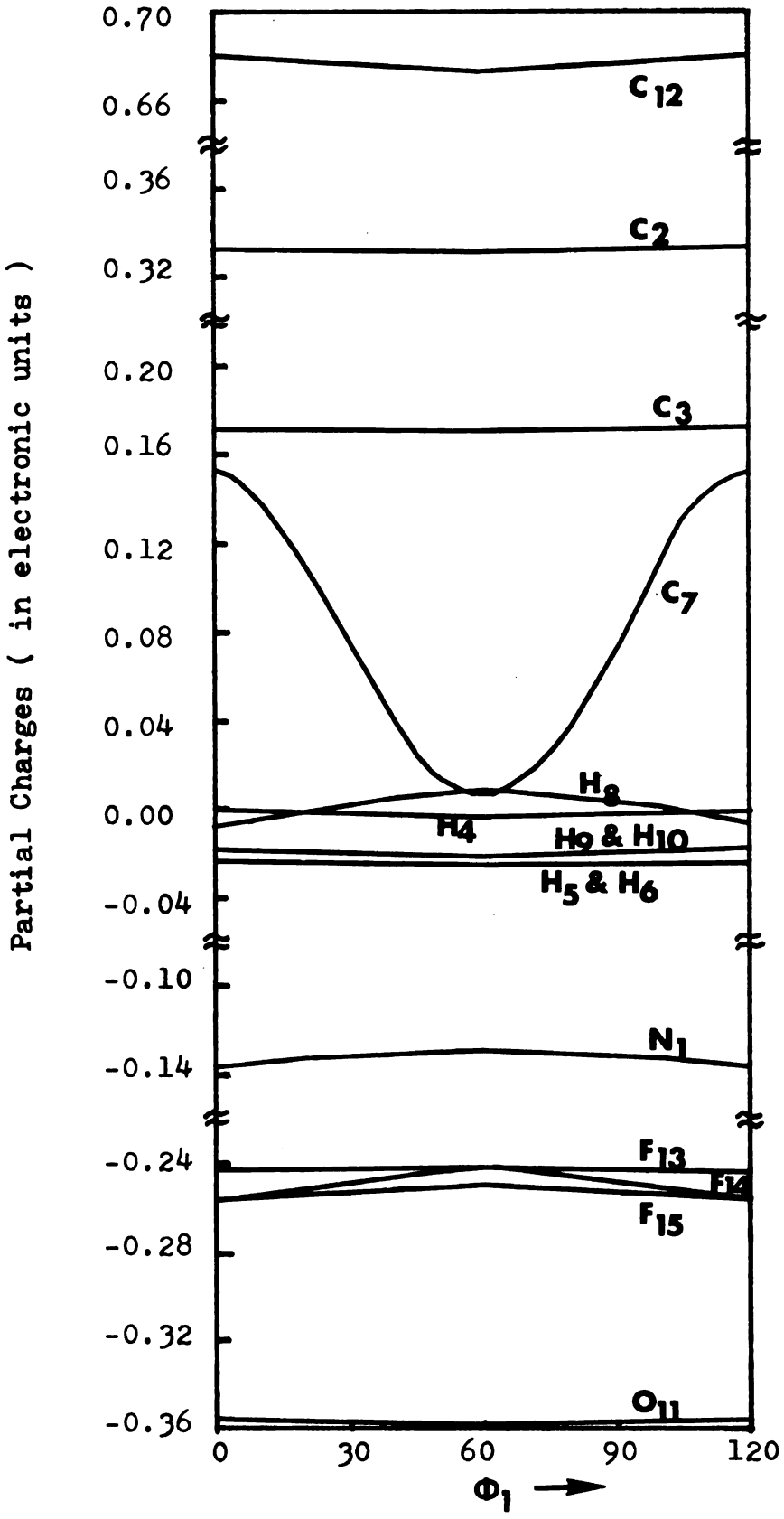

Figure 113. Variation with ϕ_1 of the partial charges on the atoms of the carbonyl-CF_3 group of N,N-dimethyltrifluoroacetamide.

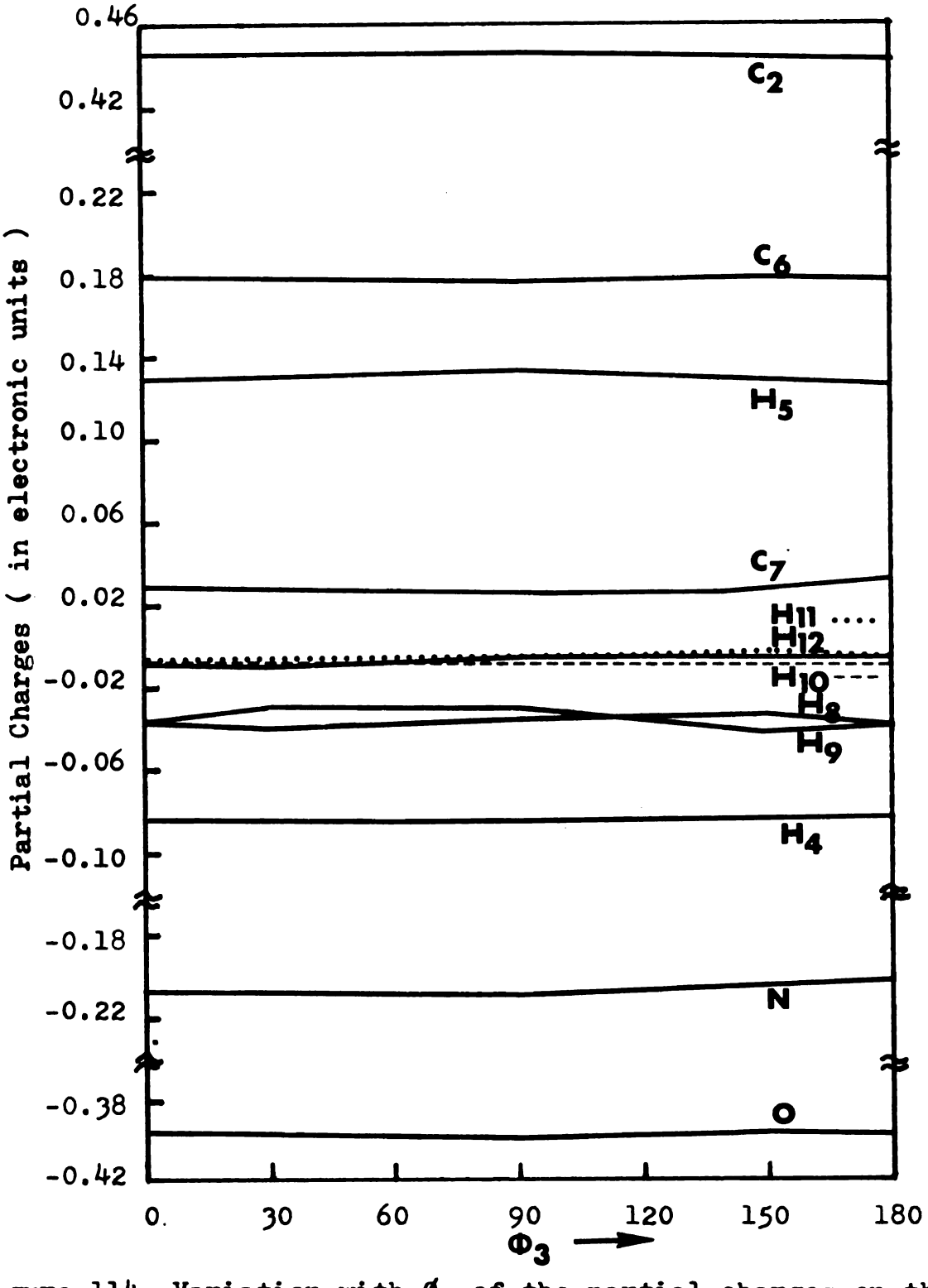

Figure 114. Variation with ϕ_3 of the partial charges on the atoms of the N-ethyl group of <u>trans</u>-N-ethyl-formamide.

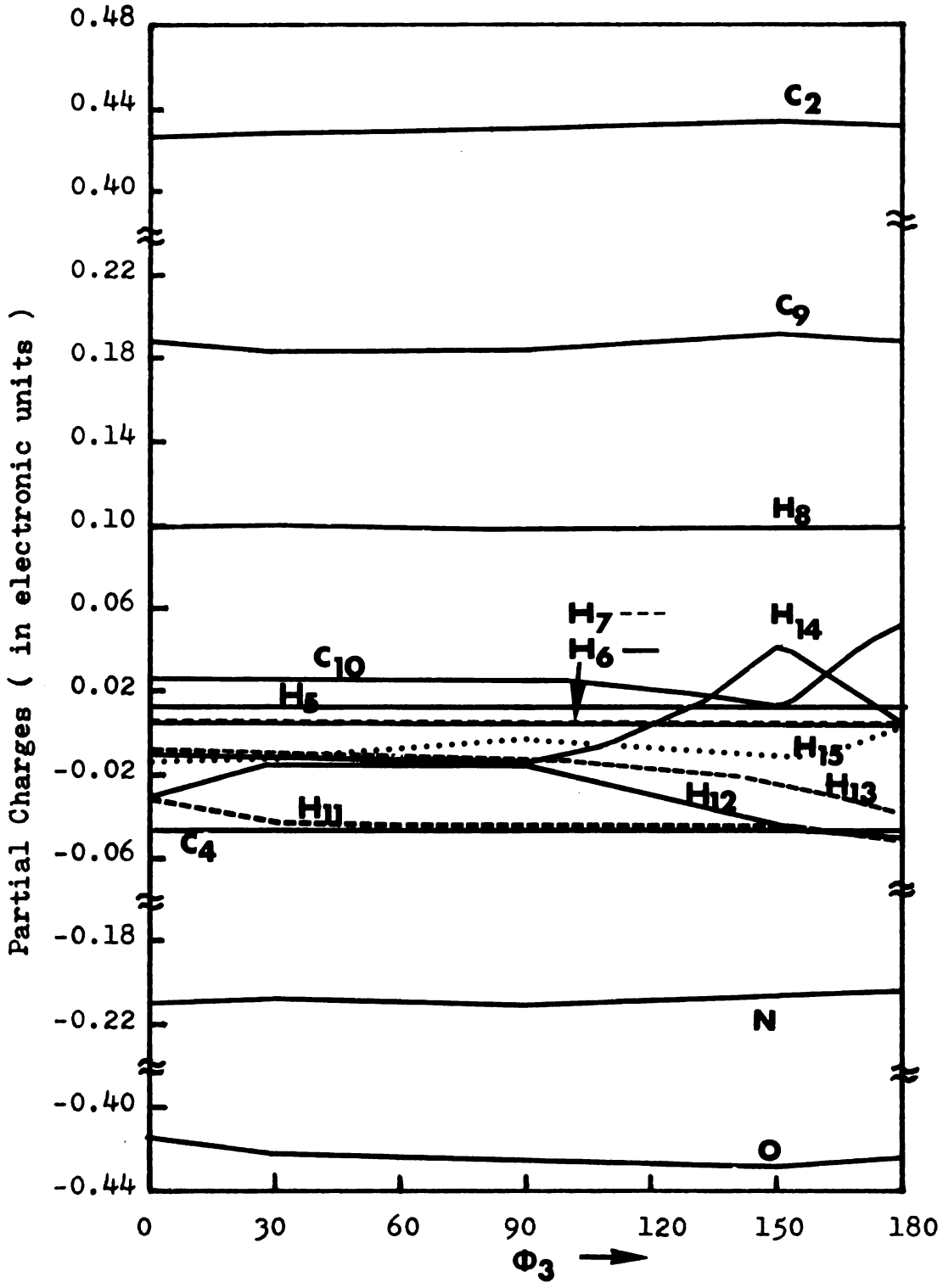

Figure 115. Variation with ϕ_3 of the partial charges on the atoms of the N-ethyl group of <u>cis</u>-N-ethyl-acetamide.

charges on the hydrogens of the methyl groups is usually very small in the ground state. Comparing Figures 101-103 for N,N-dimethylformamide, we find that when the configuration of the methyl group is changed from the stable one to a less stable one, the charge on oxygen is decreased and that on nitrogen is increased, although the change is small. Comparing Figures 101, 103, 104 with Figure 102, we see that the charge on H_6 is less when this hydrogen is eclipsed with oxygen.

In N-methylformamide, Figure 105, the change in the charges on oxygen and nitrogen shows the same tendency as was found for DMF when the N-methyl group was twisted from the stable configuration to a less stable one. In N-methylacetamide the reverse behavior is observed for the charges on oxygen and nitrogen when the N-methyl group goes from a stable configuration to a less stable one, Figures 106 to 109 and Table 45. The charge variation of either methyl group is also nearly independent of the configuration of the other methyl group in N-methylacetamide since the carbonyl-methyl and N-methyl groups are <u>trans</u> to each other.

One especially interesting pair of amides is DMA and DMTFA. Comparing Figures 112 and 113, we find that the charge on C_7 is very strongly dependent on the $-CF_3$ configuration. This may account for the high rotational energy of the $-CF_3$ group. The partial charge on C_{12} is also greatly decreased when the protons in the $-CH_3$ group

are all replaced by fluorine, as seen in Figures 112 and 113. This reduction in charge is mainly attributed to the high electronegativity of fluorine. The variation of charges on oxygen and nitrogen shows the same trend found for N-methylacetamide, as the configuration of $-CH_3$ or $-CF_3$ is varied from a stable one to a less stable one. The charge variations for the atoms of N-ethylformamide and N-ethylacetamide, Figures 114 and 115, are unsymmetrical since the electronic environments are completely changed when the N-ethyl group is rotated from one configuration to the other. This effect is especially enhanced in N-ethylacetamide and there is no apparent order to the variation of the charges on oxygen and nitrogen.

The information we have obtained so far from energy barriers and charges is consistent with a simple molecular orbital description of the peptide bond. In order to explain some spectral characteristics, the following qualitative description of the energy levels for the ground state and the transition state is given.

Assume that the π system of a C = O group interacts with a lone pair on the nitrogen of a neighboring amino group. If there is no interaction, or equivalently when the amino group - NRR' is twisted 90° out of the plane of the -CR = O group, the orbitals of the non-interacting system are shown at the left of Figure 116. In order of increasing energy, the energy levels are: a π_{CO} orbital

of the C = O group, which is lowest due to the large contribution of the electronegativity of oxygen, the lone pair of carbonyl oxygen, n_O; the lone pair of nitrogen, n_N, assumed to be pure 2p; and a π^*_{CO} orbital, which (in contrast to π_{CO}) is concentrated at the carbon atom.

When there is an interaction, the C = O group and the -NRR' group conjugate with each other. According to perturbation theory, the orbital energies and wavefunctions are modified as follows by the interaction:

$$E_n = E_n^{(o)} + \sum_{n' \neq n} \frac{H_{nn'}^{(1)\ 2}}{E_n - E_{n'}}$$

$$\phi_n = \phi_n^{(o)} + \sum_{n' \neq n} \frac{H_{nn'}^{(1)}}{E_n^{(o)} - E_{n'}^{(o)}} \phi_n \ .$$

Some rules govern the interaction: (1) Orbital interactions are pairwise additive, (2) Energy levels repel each other, (3) The interaction strength between two levels is dependent on the overlap and inversely proportional to the separation of the energy levels, and (4) The interaction of two orbitals will result in the mixing of their wavefunctions. The lower energy level mixes with the upper one in a bonding way, while the upper one mixes with the lower one in an antibonding manner.

According to these rules, we obtain the energy levels for the ground state shown at the right side of Figure 116. Again, in order of increasing energy, the

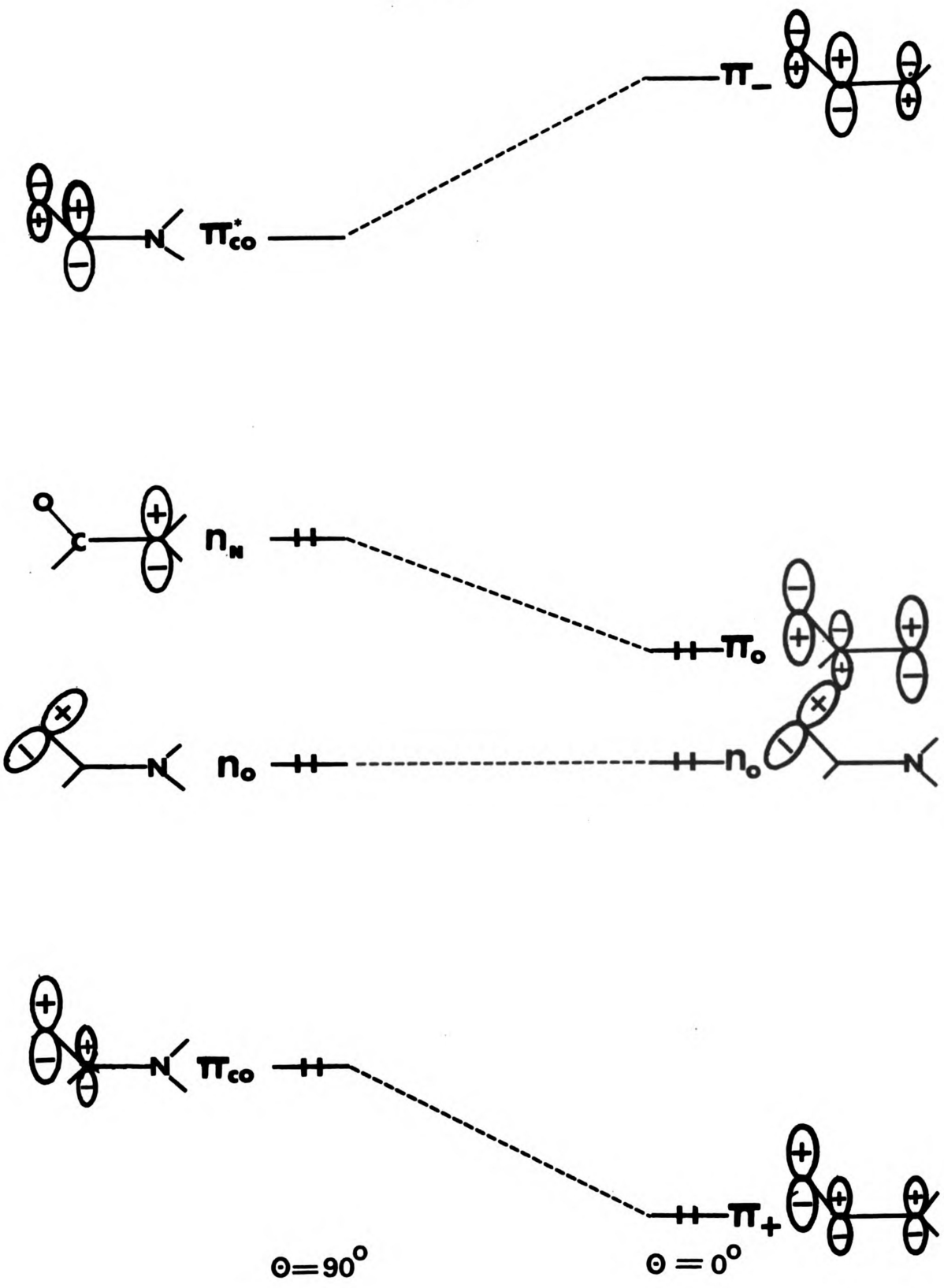

Figure 116. Qualitative description of the energy levels of a typical peptide bond in the conjugated and unconjugated geometries.

lowest energy level is π_+, which results from π_{CO} mixing with n_N stabilizing its energy in a bonding way. The second lowest one is n_O, which lies in the nodal plane of the π orbitals and is unaffected by the interaction. Then comes the π_O, which is due to the interaction of n_N with π_{CO} and π^*_{CO}. The interaction strength is given by the equation,

$$n'_N = \pi_O = n_N + c_1 \pi^*_{CO} - c_2 \pi_{CO},$$

where c_1 and c_2 are the mixing coefficients. It has been proved that the nodal plane is between C and N, implying that $c_2 > c_1$ and hence that n_N is stabilized as a consequence of the interaction. The highest energy level is π_-, which is due to the mixing of π^*_{CO} with n_N, destabilizing it in an antibonding way.

From the qualitative energy levels so obtained, one can explain some of the experimental results:

(1) There is an energy barrier hindering rotation of the $-NR_2$ group out of conjugation with the -CR" = O group. This can be seen from the increase of energy for π_+ and π_O as they become π_{CO} and n_N.

(2) When the -NRR' group rotates out of the plane of the -CR" = O group, the charge on nitrogen is increased while that on the oxygen and carbon atoms of the C = O group is decreased. This is a consequence of the strong interaction between the n_N (donor) and π^*_{CO} (acceptor) orbitals.

In the ground state ($\theta = 0°$), the two electrons in π_O are mostly on N, but with a significant fraction in the carbonyl group. In the transition state, the two electrons in n_N are all on N.

(3) As the -NRR' group rotates out of the plane of the -CR" = O group, there should occur a red shift and an intensity diminution of the $\pi_O \rightarrow \pi_-$ electronic transition (1700-1950 A). This energy shift can be seen from the behavior of the levels shown in Figure 116. There is another peptide electronic transition, $n_O \rightarrow \pi_-$, at about 2200 A, which should also be shifted to lower energy on twisting, but by a smaller amount. All these phenomena have been observed experimentally.

SUMMARY

Theoretical energy barriers for rotation about the central C-N bond in some selected amides have been calculated by the INDO method along with the bond orders for the C-N bond. The variation of the partial charges on each atom in going from the ground equilibrium geometry to the transition state geometry was also studied. From the variation of the charges on the nitrogen and oxygen atoms, the observed decrease of the energy barrier resulting from the formation of hydrogen bonds to the carbonyl oxygen can be accounted for reasonably. The results obtained here for substituted amides using the INDO method are similar to those reported previously using the CNDO/2 method.

REFERENCES

REFERENCES

1. J.W. Emsley, J. Feeney, and L.H. Sutcliffe, "High Resolution NMR Spectroscopy," Chapter 2, Pergamon Press, Oxford (1965).

2. E.L. Hahn, Phys. Rev. 80, 580 (1950).

3. F. Bloch, Phys. Rev. 70, 460 (1946).

4. R.K. Wangness and F. Bloch, Phys. Rev. 81, 728 (1958).

5. T.C. Farrar and E.D. Becker, "Pulse and Fourier Transform NMR, An Introduction to Theory and Methods," Academic Press, New York (1971).

6. H. Margenau and G.M. Murphy, "The Mathematics of Physics and Chemistry," Van Nostrand, Princeton, N.J., Chapter 8 (1943).

7. I.J. Lowe and R.E. Norberg, Phys. Rev. 107, 46 (1957).

8. A. Abragam, "The Principles of Nuclear Magnetism," pp. 32, 114, Clarendon Press, Oxford (1961).

9. R.R. Ernst and W.A. Anderson, Rev. Sci. Instrum. 37, 93 (1966); R.R. Ernst, Chimia 26, 53 (1972).

10. R.B. Blackman and J.W. Tukey, "The Measurement of Power Spectra," Dover, New York (1958).

11. S. Goldman, "Information Theory," Prentice-Hall, Englewood Cliffs, N.J. (1953).

12. "Fast Fourier Transform Data Handling System for NMR," Nicolet Instrument Corp., Madison, Wisconsin, p. 2 (1970).

13. J.W. Cooley and J.W. Tukey, Math. Comput. 19, 296 (1965).

14. R. Klahn and R.R. Shinely, Electronics 124 (1968).

15. R.R. Ernst, Adv. Mag. Res. 2, 1 (1968).

16. J.S. Waugh, J. Mol. Spectrosc. 35, 298 (1970).

17. R.L. Streever and H.Y. Carr, Phys. Rev. 121, 20 (1961).

18. E.D. Becker, J.A. Ferretti, and T.C. Farrar, J. Am. Chem. Soc. 91, 7784 (1969).

19. A. Allerhand, D.W. Cochran, and T.C. Farrar, J. Am. Chem. Soc. 92, 4482 (1970).

20. P. Fellgett, Thesis, University of Cambridge (1951).

21. P.L. Richards in D.H. Martin, Ed., "Spectroscopic Techniques," North Holland Publishers, Amsterdam (1967).

22. N.F. Ramsey, Phys. Rev. 78, 699 (1950); 86, 243 (1952).

23. M. Karplus and J.A. Pople, J. Chem. Phys. 38, 2803 (1963).

24. J.A. Pople, J. Chem. Phys. 37, 53, 60 (1962).

25. J.A. Pople, Mol. Phys. 7, 301 (1964).

26. D.M. Grant and E.G. Paul, J. Amer. Chem. Soc. 86, 2984 (1964); D.M. Dalling and D.M. Grant, J. Am. Chem. Soc. 89, 6612 (1967); D.M. Grant and B.V. Cheney, J. Am. Chem. Soc. 89, 5315 (1967).

27. T. Schaefer, W.F. Reynolds, and T. Yonemoto, Can. J. Chem. 41, 2969 (1963).

28. T.T. Nakashima and G.E. Maciel, Org. Magn. Reson. 4, 321 (1972); T.T. Nakashima and G.E. Maciel, Org. Magn. Reson. 5, 9 (1973).

29. K.G.R. Pachler, J. Magn. Reson. 7, 442 (1972).

30. A.W. Overhauser, Phys. Rev. 92, 411 (1953).

31. I. Solomon and N. Bloembergen, J. Chem. Phys. 25, 261 (1956).

32. R. Kaiser, J. Chem. Phys. 39, 2435 (1963).

33. S. Forsén and R.A. Hoffman, J. Chem. Phys. 39, 2892 (1963).

34. J. Noggle, J. Chem. Phys. 43, 3304 (1965).

35. I. Solomon, Phys. Rev. 99, 559 (1955).

36. D. Doddrell, V. Glushko, and A. Allerhand, J. Chem. Phys. 56, 3683 (1972).

37. K.F. Kuhlmann and D.M. Grant, J. Am. Chem. Soc. 90, 7355 (1968).

38. K.F. Kuhlmann, D.M. Grant, and R.K. Harris, J. Chem. Phys. 52, 3439 (1970).

39. W.T. Huntress, Jr., Adv. Magn. Res. 4, 1 (1970).

40. D.E. Woessner, J. Chem. Phys. 36, 1 (1962).

41. A. Allerhand, D. Doddrell, and R. Komoroski, J. Chem. Phys. 55, 189 (1971).

42. A. Abragam, "The Principles of Nuclear Magnetism," Chapter 8, Oxford University Press, London (1961).

43. T.C. Farrar, S.J. Druck, R.R. Shoup, and E.D. Becker, J. Am. Chem. Soc. 94, 699 (1972).

44. A. Carrington, and A.D. McLachlan, "Introduction to Magnetic Resonance," Chapter 11, Harper and Row, New York (1967).

45. S.K. Green, and J.G. Powles, Proc. Phys. Soc. Lond. 85, 87 (1965).

46. C. Deverall, Mol. Phys. 18, 319 (1970).

47. G.C. Levy, J.D. Cargioli and F.A.L. Anet, J. Am. Chem. Soc. 95, 1527 (1973).

48. T.D. Alger and D.M. Grant, J. Phys. Chem. 75, 2538 (1971).

49. J.R. Lyerla, Jr., D.M. Grant, and R.K. Harris, J. Phys. Chem. 75, 585 (1971).

50. T.D. Alger, D.M. Grant, and J.R. Lyerla, Jr., J. Phys. Chem. 75, 2539 (1971).

51. C.H. Wang, D.M. Grant, and J.R. Lyerla, Jr., J. Chem. Phys. 55, 4674 (1971).

52. J.R. Lyerla, D.M. Grant, and C.H. Wang, J. Chem. Phys. 55, 4676 (1971).

53. T.D. Alger, S.W. Collins, and D.M. Grant, J. Chem. Phys. 54, 2820 (1971).

54. D. Wallach and W.T. Huntress, Jr., J. Chem. Phys. 50, 1219 (1969).

55. J.R. Lyerla, Jr., Ph.D. Thesis, University of Utah (1971).

56. K.T. Gillen, M. Schwartz, and J.H. Noggle, Mol. Phys. 20, 899 (1971).

57. L.R. Lyerla, Jr., and D.M. Grant, "MTP International Review of Science-Magnetic Resonance," Phys. Chem. Series I, Vol. 4, p. 201 (1972).

58. G.C. Levy and G.L. Nelson, J. Am. Chem. Soc. 94, 4897 (1972).

59. D.D. Giannini, I.M. Armitage, H. Pearson, D.M. Grant, and J.D. Roberts, J. Am. Chem. Soc. 97, 3416 (1975).

60. Dreizler and G. Dendl, Z. Naturforsch. 20a, 1431 (1965).

61. W. Gordy, and R.L. Cook, "Techniques of Organic Chemistry," Vol. IX, p. 477, Interscience, New York (1970).

62. J.D. Swalen and C.C. Costain, J. Chem. Phys. 31, 1562 (1959).

63. G.C. Levy, D.M. White and F.A.L. Anet, J. Magn. Reson. 6, 453 (1972).

64. D.W. Vidrine and P.E. Peterson, Anal. Chem. 48, 1301 (1976).

65. R.L. Vold, J.S. Waugh, M.P. Klein, and D.E. Phelps, J. Chem. Phys. 48, 3831 (1968).

66. R.K. Harris and R.H. Newman, J. Magn. Reson. 24, 449 (1976).

67. J.L. Markley and W.H. Horsley, J. Chem. Phys. 55, 3604 (1971).

68. G.G. McDonald and J.S. Leigh, Jr., J. Magn. Reson. 9, 358 (1973).

69. R. Freeman and H.D.W. Hill, J. Chem. Phys. 54, 3367 (1971).

70. R.K. Gupta, J. Magn. Reson. 25, 231 (1977).

71. R. Freeman and H.D.W. Hill, J. Magn. Reson. 4, 366 (1971).

72. V.A. Nicely and J.L. Dye, J. Chem. Educ. 48, 443 (1971).

73. S.J. Opella, D.J. Nelson, and O. Jardetzky, J. Chem. Phys. 64, 2533 (1976).

74. D. Canet, J. Magn. Reson. 23, 361 (1976).

75. D.A. Wright, Ph.D. Thesis, Michigan State University(1974).

76. A.F. Meiners, C. Bolze, A.I. Scherer, and F.V. Morriss J. Org. Chem. 23, 1122 (1958).

77. S.M. McElvain and C.L. Stevens, J. Am. Chem. Soc. 69, 2667 (1947).

78. L.A. Laplanche, Ph.D. Thesis, Michigan State University (1960).

79. Varian Associates, Palo Alto, California, CFT-20 Operating Manual 87-144-200, 1975.

80. K. Sato and A. Nishioka, Bull. Chem. Soc. J. 44, 52 (1971).

81. K. Sato and A. Nishioka, Bull. Chem. Soc. J. 44, 2931 (1971).

82. D.E. Woessner, J. Chem. Phys. 40, 2341 (1964).

83. H. Shimizu, J. Chem. Phys. 40, 754 (1964).

84. D.E. Woessner, B.S. Snowden, Jr., and G.H. Meyer, J. Chem. Phys. 50, 719 (1969).

85. K.F. Kuhlman and D.M. Grant, J. Phys. Chem. 55, 2998 (1971).

86. G.C. Levy, Tetrahedron Lett. 35, 3709 (1972).

87. G.C. Levy, J. Chem. Soc., Chem. Commun. 47 (1972).

88. G.C. Levy, J. Am. Chem. Soc. 6, 161 (1973).

89. J.A. Pople and D.L. Beveridge, "Approximate Molecular Orbital Theory," McGraw-Hill, New York (1970).

90. J.F. Yan, F.A. Momany, R. Hoffmann, and H.A. Scheraga, J. Phys. Chem. 74, 420 (1970).

91. W.H. Flygare and J.T. Lowe, J. Chem. Phys. 43, 3645 (1965).

92. W.J. Moore, "Physical Chemistry," 4th Ed., p. 945, Prentice-Hall, Inc., Englewood Cliffs, N.J. (1972).

93. L.A. Laplanche and M.T. Rogers, J. Am. Chem. Soc. 86, 337 (1964).

94. R.H. Barker and G.J. Boudreaux, Spectrochim. Acta, Part A 23, 727 (1967).

95. L.A. Laplanche and M.T. Rogers, J. Am. Chem. Soc. 85, 3728 (1963).

96. D.M. Grant and B.V. Cheney, J. Am. Chem. Soc. 89, 5315 (1967).

97. H. Fritz, P. Hug, H. Sauter, and T. Winkler, Org. Magn. Reson. 9, 108 (1977).

98. D. Doddrell and A. Allerhand, J. Am. Chem. Soc. 93, 1558 (1971).

99. (a) L. Guibé and E.A.C. Lucken, C.R. Acad. Sci., Paris, 263 , 815 (1966).
(b) Dinesh and M.T. Rogers, J. Magn. Reson. 7, 30 (1972).

100. Y. Abe, Y. Kamishiwa and S. Kojima, J. Phys. Soc. Jpn. 21, 2083 (1966).

101. R. Ikeda, S. Noda, D. Nakamura, and M. Kubo, J. Magn. Reson. 5, 54 (1971).

102. M. Davis and D.K. Thomas, J. Phys. Chem. 60, 767 (1956).

103. I.M. Klotz and J.S. Franzen, J. Am. Chem. Soc. 73, 5414 (1951).

104. E. Breitmaier, K-H Spohn and S. Berger, Angew. Chem. Int. Ed. Engl. 14, 144 (1975).

105. M. Imanari, M. Ohuchi, and K. Ishizu, J. Magn. Reson. 14, 374 (1974).

106. R.F.C. Brown, L. Radom, S. Sternhell, and I.D. Rae, Can. J. Chem. 46, 2577 (1968).

107. R.E. Carter, Acta Chem. Scand. 21, 75 (1967).

108. B.F. Pedersen and B. Pedersen, Tetrahedron Lett. 2995 (1965).

109. J.A. Weil, A. Blum, A.H. Heiss, and J.K. Kinnaird, J. Chem. Phys. 46, 3132 (1967).

110. T.H. Siddall, III, and R.H. Garner, Can. J. Chem. 44, 2387 (1966).

111. T.H. Siddall, III, and C.A. Prohaska, J. Am. Chem. Soc. 88, 1172 (1966).

112. Sadtler Carbon-13 NMR Spectra, 1638C and 1028C.

113. H. Spiesecke and W.G. Schneider, J. Chem. Phys. 35, 731 (1961).

114. W.T. Huntress, J. Chem. Phys. 48, 3524 (1968).

115. P. Hampson and A. Mathias, Mol. Phys. 11, 541 (1966).

116. T.H. Siddall, III, W.E. Stewart, and F.D. Knight, J. Phys. Chem. 74, 3580 (1970).

117. G.J. Martin, J.P. Gouesnard, J. Dorie, C. Rabiller, and L. Martin, J. Am. Chem. Soc. 99, 1381 (1977).

118. A. Saika and C.P. Slichter, J. Chem. Phys. 22, 26 (1954).

119. M. Witanowski and G.A. Webb, "Nitrogen-NMR," p. 165, Plenum Press, New York (1973).

120. E.D. Becker, R.B. Bradley, and T. Axenrod, J. Magn. Reson. 4, 136 (1971).

121. D. Herbison-Evans, and R.E. Richards, Mol. Phys. 8, 19 (1964).

122. G. Fraenkel and C. Franconi, J. Am. Chem. Soc. 82, 4478 (1960).

123. M. Witanowski, J. Am. Chem. Soc. 90, 5683 (1968).

124. C.C. Costain, and J.M. Dowling, J. Chem. Phys. 32, 158 (1960).

125. T.T. Drakenberg, K-I. Dahlqvist, and S. Forsén, J. Phys. Chem. 76, 2178 (1972).

126. J.I. Kroschwitz, M. Winokur, H.J. Reich, and J.D. Roberts, J. Am. Chem. Soc., 91, 5927 (1969).

127. S.H. Grover, J.P. Guthrie, J.B. Stothers and C.T. Tan, J. Magn. Reson. 10, 227 (1973).

128. J.G. Batchelor, J. Magn. Reson. 18, 212 (1975).

129. M.T. Rogers and J.C. Woodbrey, J. Phys. Chem. 32, 158 (1962).

130. H.S. Gutowsky and C.H. Holm, J. Chem. Phys. 25, 1228 (1956).

131. L.R. Isbrandt, Ph.D. Thesis, Michigan State University (1972).

132. B. Sunners, L. Piette and W.G. Schneider, Can. J. Chem. 38, 681 (1960).

133. H. Eyring, T. Ree, D.M. Grant and R.C. Hirst, Z. Elektrochem. 64, 146 (1960).

134. F. Conti and W. von Phillipsborn, Helv. Chim. Acta. 50, 603 (1965).

135. C.W. Freyer, F. Conti, and C. Franconi, Ric. Sic. 35 (II-A), 788 (1965).

136. D.G. Gehring, W.A. Mosher, and G.S. Reddy, J. Org. Chem. 31, 3436 (1966).

137. R.C. Neuman, Jr. and Violet Jonas, J. Am. Chem. Soc. 90, 1970 (1968).

138. R.M. Hammaker and B.A. Gugler, J. Mol. Spectrosc. 17, 356 (1965).

139. B. Birdsall, N.J.M. Birdsall, and J. Feeney, J. Chem. Soc., Chem. Commun. 316 (1972).

140. G. Jikeli, W. Herrig, and H. Günther, J. Am. Chem. Soc. 96, 323 (1974).

141. R.R. Ernst, J. Chem. Phys. 45, 3845 (1966).

142. P.H. McCabe and C.R. Nelson, J. Magn. Reson. 22, 183 (1976).

143. Y.N. Luzikov, N.M. Sergeyev, and Y.A. Ustynyuk, J. Magn. Reson. 18, 406 (1975).

144. G.A. Gray, Anal. Chem. 47, 546A (1975).

145. H. Günther and M. Görlitz, Org. Magn. Reson. 6, 384 (1974).

146. J.C. MacDonald and M. Mazurek, J. Magn. Reson. 19, 51 (1975).

147. S. Sørenson, M. Hansen, and H.J. Jakobsen, J. Magn. Reson. 12, 340 (1973).

148. F.W. Wehrli, Adv. Mol. Relaxation Processes 6, 384 (1974).

149. N.J.M. Birdsall, A.G. Lee, Y.K. Levine, J.C. Metcalfe, P. Partington, and G.C.K. Roberts, J. Chem. Soc., Chem. Commun. 757 (1973).

150. C. Chachaty, Z. Wolkowski, F. Piriou, and G. Lukacs, J. Chem. Soc., Chem. Commun. 951 (1973).

151. W.D. Phillips, J. Chem. Soc. 23, 1363 (1955).

152. H.S. Gutowsky, Discuss. Faraday Soc. 19, 247 (1955).

153. M. Rabinovitz and A. Pines, J. Chem. Soc. B1110 (1968).

154. T. Yonezawa and I. Morishima, Bull. Chem. Soc. Jpn. 39, 2346 (1966).

155. T. Yonezawa, I. Morishima, and K. Takeuchi, Bull. Chem. Soc. Jpn. 40, 1807 (1967).

156. A. Fratiello, Mol. Phys. 7, 565 (1964).

157. R.C. Neuman, Jr., W. Snider, and V. Jonas, J. Phys. Chem. 72, 2469 (1968).

158. L.L. Graham and M.R. Miller, Org. Magn. Reson. 4, 327 (1972).

159. R.C. Neuman, Jr., W.R. Woolfenden, and V. Jonas, J. Phys. Chem. 73, 3177 (1969).

160. M. Rabinovitz and A. Pines, J. Am. Chem. Soc. 91, 1585 (1969).

161. A.A. Sandoval, J. Phys. Chem. 70, 1203 (1966).

162. J.C. Woodbrey and M.T. Rogers, J. Am. Chem. Soc. 84, 13 (1962).

163. R. Radeglia, Ber. Bunsenges. Phys. Chem. 71, 1145 (1967).

164. R.M. Moriarty, J. Org. Chem. 28, 1296 (1963).

165. A.A. Sandoval and M.W. Hanna, J. Phys. Chem. 70, 1203 (1966).

166. T. Matsuo, Can. J. Chem. 45, 1829 (1967).

167. D. Bryce-Smith and M.A. Hens, J. Chem. Soc. B812 (1968).

168. I. Ando, N. Jinno, and A. Nishika, Bull. Chem. Soc. Jpn. 48, 2639 (1975).

169. R.C. Neuman, Jr. and L.B. Young, J. Phys. Chem. 69, 2570 (1965).

170. G. Briegleb, "Electronen Donator-Acceptor Komplex," Springer-Verlag, Berlin (1961).

171. L.J. Andrews, Chem. Rev. 54, 713 (1954).

172. S.P. McGlynn, Chem. Rev. 58, 1113 (1958).

173. J.V. Hatton and R.E. Richards, Mol. Phys. 5, 139; ibid. 5 153 (1962).

174. M.W. Hanna and A.L. Ashbraugh, J. Phys. Chem. 68, 811 (1964).

175. N. Bloembergen and L.O. Morgan, J. Chem. Phys. 34, 842 (1961).

176. Z. Luz and S. Meiboom, J. Chem. Phys. 40, 1058 (1964).

177. Z. Luz and S. Meiboom, J. Chem. Phys. 40, 1060 (1964).

178. A.S. Mildvan and M. Cohn, Adv. Enzymol. 33, 1 (1970).

179. M. Cohn, Q. Rev. Biophys. 3, 61 (1970).

180. A.S. Mildvan and J.L. Engle, Methods Enzymol. 26, 654 (1972).

181. C.H. Fung, A.S. Mildvan, A. Mildvan, R. Komoroski, and M.C. Scrutton, Biochemistry 12, 620 (1973).

182. Y.-F. Lam, G.P.P. Kuntz, and G. Katowycz, J. Am. Chem. Soc. 96, 1834 (1974).

183. J.J. Led and D.M. Grant, J. Am. Chem. Soc. 97, 6963 (1975).

184. J.J. Led and D.M. Grant, J. Am. Chem. Soc. 99, 5845 (1977).

185. A.F. Crockerill, G.L.O. Davies, R.C. Harden and D.M. Rackham, Chem. Rev. 73, 553 (1973).

186. C.D. Barry, R.J.P. Williams, and A.V. Xarrir, J. Mol. Biol. 84, 471 (1974).

187. B.R. McCarvey, Transition Met. Chem. 3, 89 (1966).

188. M. Tinkham, R. Weinstein and A.F. Kip, Phys. Rev. 84, 848 (1951).

189. R.S. Codrington and N. Bloembergen, J. Chem. Phys. 29, 600 (1958).

190. Z. Luz and R.G. Shulman, J. Chem. Phys. 43, 3750 (1965).

191. A.R. Peacock, R.E. Richards, and B. Sheard, Mol. Phys. 16, 177 (1969).

192. J.A. McMillan, "Electron Paramagnetism," Reinhold, New York, p. 27 (1968).

193. N. Bloembergen, J. Chem. Phys. 27, 572 (1957).

194. J. Reuben, G.H. Reed, and M. Cohn, J. Chem. Phys. 52, 1617 (1970).

195. A.R. Peacock, R.E. Richards, and B. Sheard, Mol. Phys. 16, 177 (1969).

196. We use interchangedly several expressions for the solvent molecules in the first coordination shell, e.g., solvation shell, coordination sphere, and ligand molecules.

197. T.R. Stengle and C.H. Langford, Coord. Chem. Rev. 2, 349 (1967).

198. M. Eigen and R.G. Wilkins, Adv. Chem. Ser. 49, 55 (1965).

199. M. Rubinstein, A. Baram, and Z. Luz, Mol. Phys. 20, 67 (1971).

200. H. Eyring, Chem. Rev. 17, 65 (1935).

201. Z. Luz and S. Meiboom, J. Chem. Phys. 40, 2686 (1964).

202. T.J. Swift and R.E. Connick, J. Chem. Phys. 37, 307 (1962).

203. R.H. Henson, Ph.D. Thesis, Oxford (1972).

204. F.F. Brown, I.D. Campbell, R.H. Henson, C.W.J. Hirst, and R.E. Richards, cited in R.A. Dwek, "Nuclear Magnetic Resonance in Biochemistry," Clarendon Press, Oxford, p. 206 (1973).

205. A.W. Nolle and L.O. Morgan, J. Chem. Phys. 36, 378 (1962).

206. C.C. Hinckley and D.B. Chesnut, J. Chem. Phys. 28, 107 (1958).

207. H.M. McConnell and D.B. Chesnut, J. Chem. Phys. 28, 107 (1958).

208. L. Pauling, "The Nature of the Chemical Bond," 3rd Ed., Cornell University Press, Ithaca, New York, p. 281 (1960).

209. A. Julg and P. Carles, Theoret. Chim. Acta 1, 140 (1963).

210. A. Julg and P. Carles, Theoret. Chim. Acta 7, 103 (1967).

211. D.H. Christensen and R.N. Kortzeborn, J. Chem. Phys. 53, 3912 (1970).

212. F.A. Momany, R.F. McGuire, J.F. Yan, and H.A. Scheraga, J. Phys. Chem. 74, 2424 (1970).

213. J.E. Del Bene, J. Chem. Phys. 62, 1961 (1975).

214. J.C. Evans, J. Chem. Phys. 22, 1228 (1954).

215. P.G. Puranik and K.V. Ramiah, J. Mol. Spectrosc. 3, 486 (1959).

216. T. Suzuki, Bull. Chem. Soc. Jpn. 33, 1359 (1960).

217. H. Bash, M.B. Robin, and N.A. Kuebler, J. Chem. Phys. 47, 1201 (1967).

218. M.A. Robb and I.G. Csizmadia, Theoret. Chim. Acta. 10, 269 (1968).

219. H. Basch, M.B. Robin and N.A. Kuebler, J. Chem. Phys. 49, 5007 (1968).

220. R. Mulliken, J. Chem. Phys. 23, 1833, 1841, 2338, 2343 (1955).

221. J.A. Pople and M. Gordon, J. Am. Chem. Soc. 89, 4253 (1967).

222. C.C. Costain and J.M. Dowling, J. Chem. Phys. 32, 158 (1960).

223. A. Pullmann and H. Buthod, Theoret. Chim. Acta 10, 461 (1968).

224. J. Ladell and B. Post, Acta Crystallogr. 7, 559 (1954).

225. R.G. Kurland and E.B. Wilson, J. Chem. Phys. 27, 585 (1957).

226. T. Ooi, R.A. Schott, G. Vanderkooi, and H.A. Scheraga, J. Chem. Phys. 46, 4410 (1967).

227. J.N. Murrell, "The Theory of the Electronic Spectra of Organic Molecules," John Wiley and Sons, Inc., New York, New York (1963).

228. D.A. Brant, W.G. Miller, and P.J. Flory, J. Mol. Biol. 23, 47 (1967).

229. J.A. Schellman and P. Oriel, J. Chem. Phys. 37, 2114 (1962).

230. P.N. Skancke and I. Aanesland, Acta Chem. Scand. 26, 2614 (1972).

231. T. Drakenberg and S. Forsén, J. Phys. Chem. 74, 1 (1970).

232. L.W. Reeves, R.C. Shaddick and K.N. Shaw, Can. J. Chem. 49, 3683 (1971).

233. L. Isbrandt, W.C. Tung and M.T. Rogers, J. Magn. Reson. 9, 461 (1973).

234. L.L. Graham and R.E. Diel, J. Phys. Chem. 73, 2696 (1969).

235. T. Drakenberg and S. Forsén, J. Chem. Soc., Chem. Commun. 1404 (1971).

236. R.Hoffmann, J. Chem. Phys. 39, 1397 (1963); 40, 2474, 2480, 2745 (1964).

237. H. Kamei, Bull. Chem. Soc. Jpn. 41, 2269 (1968).

238. E. Tannenbaum, R.J. Myers, and W.D. Gwinn, J. Chem. Phys. 25, 42 (1956).

239. W.M. Tolles, E.T. Handelman, and W.D. Gwinn, J. Chem. Phys. 43, 3019 (1965).

240. R.E. Naylor and E.B. Wilson, J. Chem. Phys. 26, 1057 (1957).

241. H.D. Rudolph and M. Seiler, Z. Naturforsch. 20, 1682 (1965).

242. W. Walter, E. Schaumann, and H. Rose, Org. Magn. Reson. 4, 191 (1973).

243. H.F. Schaefer, III, "The Electronic Structure of Atoms and Molecules," Addison-Wesley Publishing Co., Reading, Mass. (1972).

244. J.N. Murrell and A.J. Harget, "Semi-empirical SCF Molecular Orbital Theory of Molecules," Wiley-Interscience, New York (1972).

245. A. Streitwieser, "Molecular Orbital Theory for Organic Chemists," John Wiley and Sons, New York (1961).

246. Program MBLD written by Dr. W.G. Waller, Michigan State University.

247. Program CNINDO written by Prof. J.F. Harrison, Michigan State University.